# GPR Investigations of the Sedimentary Architecture of Jökulhlaup Eskers: Skeiðarárjökull, Iceland and Bering Glacier, Alaska

Matthew J. Burke

Ph.D.

2008

# GPR Investigations of the Sedimentary Architecture of Jökulhlaup Eskers: Skeiðarárjökull, Iceland and Bering Glacier, Alaska

Matthew J. Burke

A thesis submitted in partial fulfilment
of the requirements of the
University of Northumbria at Newcastle
for the degree of
Doctor of Philosophy

Research undertaken in the School of Applied Sciences and
in collaboration with Newcastle University

November 2008

# Abstract

Eskers are ridges of stratified glaciofluvial material deposited in englacial, subglacial or supraglacial channels and ice-walled canyons. Eskers have been used to infer the dynamics and palaeo-hydrology of large ice sheets, despite observations of palaeo-esker sedimentary architecture lacking rigorous constraints on depositional timescale. This research aims to identify the hydrological, glaciological and sedimentary controls on the sedimentary architecture of single event outburst flood (jökulhlaup) eskers at Skeiðarárjökull and Bering Glacier. These eskers formed during monitored outbursts, providing time constraints on the depositional events, thereby making the eskers ideal analogues for palaeo-eskers. GPR data was collected using a pulseEKKO Pro 1100 system at Skeiðarárjökull and Bering Glacier during field seasons in 2006 and 2007. At Skeiðarárjökull grids of 100 MHz GPR lines were collected on the glacier surface and 200 MHz GPR grids were collected on all workable sections of an esker and ice-walled canyon fill generated by a jökulhlaup in November 1996. At Bering Glacier 200 MHz GPR grids were collected on workable sections of an ice-walled canyon fill and esker generated during outbursts in July-August and October 1994, respectively. Examination of the GPR data has allowed development of site-specific models for esker and ice-walled canyon fill deposition, providing the first detailed insight into the sedimentary architecture of single event jökulhlaup eskers. These models show that single high-magnitude jökulhlaups can generate eskers with complexities previously unexpected for single events. The englacial position of an esker is controlled by the presence of structural weaknesses within the ice and the jökulhlaup release mechanism. Esker sedimentary architecture, on the other hand, is controlled by a complex interaction between hydrological, glaciological and sedimentary factors. The most fundamental control on jökulhlaup esker sedimentary architecture is conduit geometry, which determines the type of macroform from which the esker is composed. Thus, eskers deposited during jökulhlaups should be made up of both wide ridges as composite macroforms in areas of conduit expansion and narrow ridges composed of upper-stage plane beds in constricted conduits. The smaller scale sedimentary features, which include antidunes and boulder clusters, as well as the frequency of erosional structures, are controlled by interactions between the flow conditions and sediment supply. The eskers generated during the 1996 Skeiðarárhlaup and 1994 Bering Glacier outburst flood demonstrate sedimentary architectures that are similar to those identified in many palaeo-eskers described from previous studies. The research suggests that jökulhlaups may have had a greater role in palaeo-esker sedimentary architecture than previously hypothesised.

# Table of Contents

## Section II: Methodological Approach



## Section III: Results and Interpretations

## Section IV: Discussion and Conclusions

# List of Figures

**Chapter 2**

# List of Tables

# Abbreviations

| | |
|---|---|
| a.s.l. | *above sea level* |
| BP | *before present* |
| CMP | *common mid-point* |
| CO | *common offset* |
| DGPS | *differential global positioning system* |
| DEM | *digital elevation model* |
| EM | *electromagnetic* |
| ENSO | *El Niño Southern Oscillation* |
| GPR | *ground-penetrating radar* |
| GPS | *global positioning system* |
| HF | *high-cut frequency* |
| LF | *low-cut frequency* |
| LGM | *Last Glacial Maximum* |
| LIA | *Little Ice Age* |
| LP | *lower plateau* |
| Pe | *effective pressure* |
| Pi | *ice overburden pressure* |
| Pw | *water pressure* |
| Q | *discharge* |
| RE | *radar element* |
| RES | *radio-echo sounding* |
| RF | *radar facies* |
| SHR | *sub-horizontal reflection* |
| TWTT | *two-way travel time* |
| UP | *upper plateau* |
| USPB | *upper-stage plane beds* |
| yr | *year* |

# Acknowledgements

I would firstly like to thank my principal supervisor, Dr John Woodward, and external advisor Dr Andy Russell (Newcastle University), for their support and inspiration throughout my postgraduate studies, without which, the production of this thesis would not have been possible. Their patience (even after my constant harassment) and encouragement over the past three years has kept both this work and me on track, and I owe them a debt of gratitude which, I hope is partially repaid by the production of this thesis and the associated publications (both current and future).

Fieldwork for this research was funded by the School of Applied Sciences, Northumbria University and the Earthwatch Insititute. I am indebted to Jay Fleisher and Palmer Bailey for their invaluable support during field seasons at Skeiðarárjökull and Bering Glacier, as well as words of advice and encouragement throughout this research. I would also like to thank David Blauvelt, Andrew Gregory, Timothy Harris, Andrew Large, Nigel Mountney, Eric Natel, Jayne Soulsby, Ruth Tinsley and all 'Icelandic and Alaskan Glaciers' Earthwatch volunteers during 2006 and 2007 for assistance during fieldwork at Skeiðarárjökull and Bering Glacier. Thanks must also go to Ragnar Frank Kristjánsson for supporting research in Skaftafell National Park and to Prince William Sound Science Center and Chugach National Forest Office for logistical assistance during fieldwork at Bering Glacier.

Thanks to all in the department who have helped out and shown a pastoral interest in my work, especially Terry Douglas for an enjoyable and constructive mid-point progression meeting. I wish to thank my office mates Atiek, Komal, James, as well as all members of the Disaster and Development Centre and Centre for Environmental and Spatial Analysis, for providing a pleasant working environment and putting up with my frequent outbursts of anger and frustration over the past three years! Thanks also go to my external examiner Doug Benn and internal examiner Jane Entwistle for a very enjoyable viva.

Special thanks must go to my Newcastle University colleagues, David Blauvelt and Andrew Gregory for their camaraderie in and out of the field, as well as willingness to listen to my (sometimes absurd) ponderings about my research. I also owe thanks to a number of friends, namely Dave, Paul, Stew and Rob for their encouragement and uncanny ability to take my mind off my work and help me remain (relatively) sane.

Finally, I would like to thank my mum, dad and grandparents for their love and encouragement over the past three years. Without their support I would not have been able to start, never mind finish, this research project.

# Declaration

I declare that the work contained in this thesis has not been submitted for any other award and that it is all my own work.

Name: Matthew J. Burke

Signature: 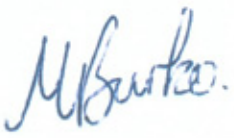

Date: 3rd November 2008

# SECTION I
# Introduction and Background

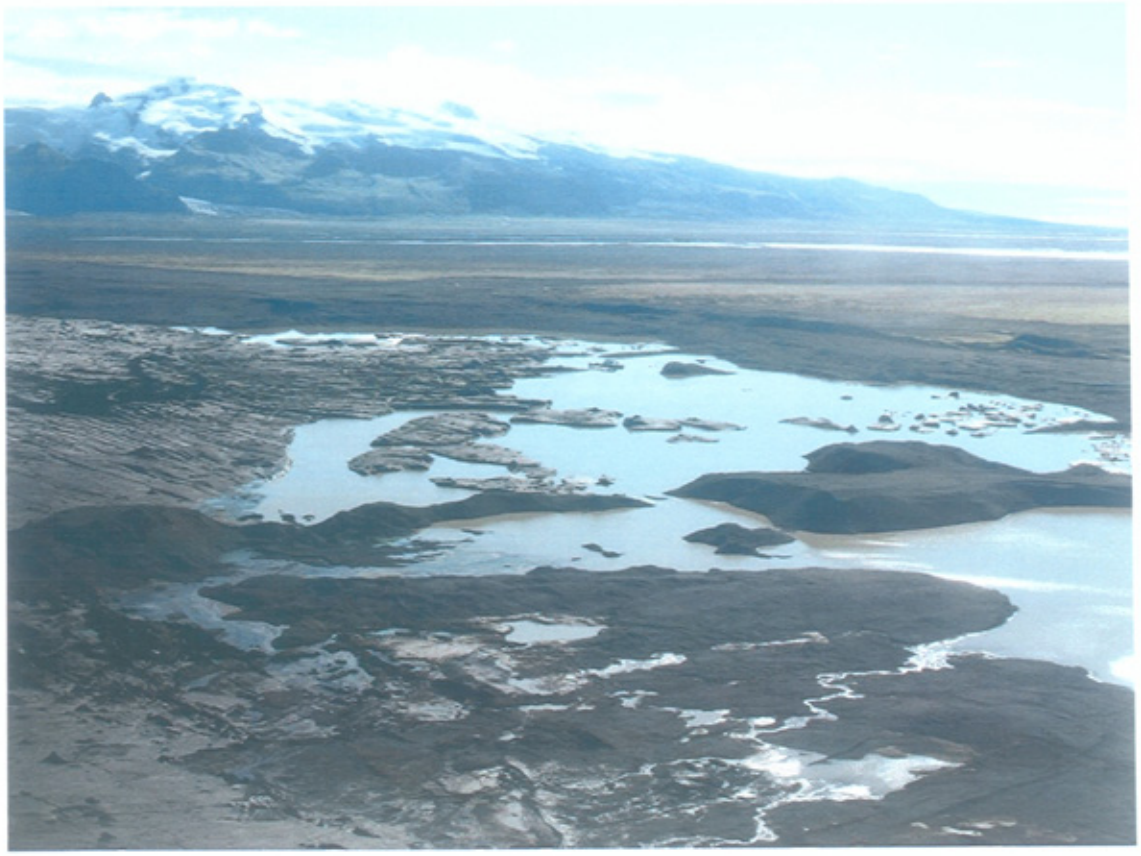

*"eskers resemble one another only in their irregularity"*

Flint (1930)

*The esker and ice-walled canyon fill at Skeiðarárjökull (courtesy of Andrew Gregory, 2006).*

# Chapter 1

## Introduction and Aims

### 1.1 Introduction

Reconstruction of palaeo-glacial environments and dynamics requires detailed interpretation of glacial landsystems and deposits (Evans *et al.*, 2005). Former glacier dynamics can be inferred from the analysis of sedimentary landform assemblages such as eskers (e.g. Brennand and Sharpe, 1993; Warren and Ashley, 1994; Lundqvist, 1999a, 1999b; Brennand, 2000, Delaney, 2001; Boulton *et al.*, 2007a, 2007b, Hooke and Fastook, 2007), crevasse fill ridges (e.g. Gravenor and Kupsch, 1959; Sharp, 1985a, 1985b; Woodward *et al.*, 2003a), drumlins (e.g. Boulton, 1987; Aylsworth and Shilts, 1989), flutings (e.g. Clark, 1993), thrusts (e.g. Bennett *et al.*, 1996; Hambrey *et al.*, 1996; Glasser *et al.*, 1998), hummocky moraines (e.g. Benn and Lukas, 2006) and folded moraines (e.g. Hambrey *et al.*, 1999). Eskers, in particular, have been used to infer details of deglacial conditions of former ice sheets in North America (e.g. Brennand and Sharpe, 1993; Brennand and Shaw, 1996) and Europe (e.g. Warren and Ashley, 1994; Punkari, 1997, Delaney, 2001). The general understanding of esker depositional processes, therefore, can be directly applied to the reconstruction of palaeo-glacial dynamics and palaeo-hydrology of Quaternary ice sheets.

Typically, eskers are sinuous glaciofluvial ridges deposited in an ice-contact environment. Eskers record deposition in subglacial (e.g. Flint, 1928; Stokes, 1958; Gorrell and Shaw, 1991; Auton, 1992; Brennand, 1994; Clark and Walder, 1994; Brennand, 2000; Fiore *et al.*, 2002), englacial (e.g. Shulmeister, 1989; Knudsen, 1995) or supraglacial drainage networks (e.g. Hebrand and Åmark, 1989; Huddart *et al.*, 1999; Russell *et al.*, 2001a), though the term has also been applied simply to ice contact deposition (c.f. Warren and Ashley, 1994). Eskers are generally surmised to be the casts of subglacial or englacial conduits incised into the overlying ice (Flint, 1928), maintained by a balance between frictional melting of the conduit walls and conduit closure due to deformation of the ice (Hooke, 1989; Warren and Ashley, 1994). The term esker, however, in its broadest sense, can cover a multitude of glaciofluvial environments and depositional settings and eskers have also been inferred to have been deposited by transient events associated with jökulhlaups (c.f. Shulmesiter, 1989; Russell *et al.*, 2001a; Fiore *et al.*, 2002; Fleisher *et al.*, 2007).

Jökulhlaups or outburst floods are the discharge of a substantial volume of water from a glacier or moraine-dammed lake, resulting in significant increases in outlet river discharge over a period of minutes to several weeks (Roberts, 2005). Jökulhlaups are a recurrent hazard in modern glaciated terrains creating rapid geomorphological change and in some cases widespread damage to infrastructure (Roberts *et al.*, 2000a). The source of jökulhlaups can be traced to subglacial lakes, subglacial volcanic eruptions, marginal ice- or sediment-dammed lakes (Björnsson, 1992; Benn and Evans, 1998) as well as outbursts associated with the termination of glacier surges[1] (c.f. Kamb *et al.*, 1985; Fleisher *et al.*, 1998). During Quaternary glaciations, it is known that numerous jökulhlaups drained from beneath the North American and Siberian ice sheets (e.g. Baker, 1973; Carling *et al.*, 2002; Teller *et al.*, 2002; Clague *et al.*, 2003). Recent observation of contemporary jökulhlaups have produced an increasing knowledge of flood initiation (e.g. Clarke, 1982; Björnsson, 2002), jökulhlaup dynamics (e.g. Spring and Hutter, 1981; Clarke, 1982, 2003; Björnsson, 1992) and landform associations (e.g. Fleisher *et al.*, 1998; Russell and Knudsen, 1999a, 1999b; Roberts *et al.*, 2000a, 2001; Russell *et al.*, 2001b; Roberts *et al.*, 2005; Russell *et al.*, 2005, 2006, 2007a, 2007b).

### 1.2 Research Gap

The traditional view of esker genesis is that they are formed within a subglacial conduit (e.g. Flint, 1928; Shulmeister, 1989; Gorrell and Shaw, 1991; Brennand, 1994; Brennand and Shaw, 1996; Fiore *et al.*, 2002) and are generally inferred to be deposited over several events associated with ablation controlled discharge or multiple episodes of transience. In very few cases have eskers been suggested to have been deposited via jökulhlaups (e.g. Shulmeister, 1989; Russell *et al.*, 2001a; Fiore *et al.*, 2002; Russell *et al.*, 2006) and in even fewer examples, such as the recent work of Russell *et al.* (2001a; 2006), Evans *et al.* (2006) and Fleisher *et al.* (2007) are they suggested to have formed via a single event. Currently, there are few suitable contemporary analogues for esker sedimentation during previous glaciations and although palaeo-eskers have been studied extensively, only a handful of detailed depositional models have been presented (e.g. Brennand, 1994; Brennand and Shaw, 1996; Brennand, 2000; Fiore *et al.*, 2002; Mäkinen, 2003), which by their nature lack rigorous constraints on depositional timescale. There

[1] Some glaciers demonstrate periodic fluctuations in velocity, during which they undergo changes in morphology and behaviour (Benn and Evans, 1998). These glaciers are known as 'surge-type glaciers'. They oscillate between long periods of virtually stagnant flow (quiescent phase) and comparatively short periods of abruptly accelerated flow (active phase) (Paterson, 1994; Jiskoot, 1999). Surface velocities during quiescence are typically one tenth to one hundredth of those during the active phase (Meier and Post, 1969; Kamb *et al.*, 1985). It has long been recognized that glacier surging is associated with high water pressures at the glacier bed (e.g. Kamb *et al.*, 1985; Kamb, 1987; Björnsson, 1998; Fleisher *et al.*, 1998) and that jökulhlaups may occur concomitant to surge cessation in the contemporary environment (Kamb *et al.*, 1985; Humphrey *et al.*, 1986; Kamb, 1987; Humphrey and Raymond, 1994; van Dijk, 2002).

are insufficient studies of the controls on the sedimentary architecture of jökulhlaup eskers, with studies of esker morphology and/or sedimentology often being site specific. Consequently, most studies are not concerned with characterising the large-scale sedimentary architecture of specific esker types. Where evidence of transience has been identified within esker macroforms (e.g. Gorrell and Shaw, 1991; Brennand, 1994, 2000), the lack of rigorous constraints on depositional timescale and detailed understanding of sedimentation processes within jökulhlaup conduits, have made it difficult to infer the depositional process.

Although it is known that variations in macroform type present within eskers can be directly linked to variations in conduit geometry (e.g. Brennand, 1994; Brennand and Shaw, 1996; Brennand, 2000), the inferred controls on conduit development and geometry are often based upon traditional glacial hydrological theory (Shreve, 1985; Syverson *et al.*, 1994; Hooke and Fastook, 2007), which can only be applied to steady-state scenarios. Recent investigations of englacial hydrology, however, have demonstrated increasing evidence that pre-existing englacial structure can play a significant role on conduit location and development during both steady-state and transient conditions (Fountain and Walder, 1998; Roberts *et al.*, 2000a, 2000b, 2001; Russell *et al.*, 2001a; Waller *et al.*, 2001; Roberts *et al.*, 2002; Fountain *et al.*, 2005a, 2005b; Gulley and Benn, 2007). Indeed, Gulley and Benn (2007) showed that waters can be initially discharged through fractures filled with porous debris, before conduits develop due to a combination of melting and mechanical excavation of the surrounding glacier ice that had been weakened by the presence of the englacial structure. Consequently, the flow path of a shallow englacial conduit may be dominantly influenced by pre-existing lines of high hydraulic conductivity rather than cryostatically determined potential gradients (Gulley and Benn, 2007). This brings into question some of the fundamental assumptions applied to theories of conduit development in which palaeo-eskers were deposited, particularly during transient events.

This study will investigate the three-dimensional sedimentary architecture of eskers at Skeiðarárjökull, Iceland and Bering Glacier, Alaska that were deposited during single, well-documented jökulhlaups. This is the first detailed study of contemporary eskers, where the knowledge of depositional timescale is relatively well constrained and will provide an insight into the rates and processes of eskers deposited during jökulhlaups. This study will also assess the controls on esker sedimentary architecture during jökulhlaups with englacial GPR investigations at Skeiðarárjökull providing evidence for the controls on conduit location and development during the 1996 Skeiðarárhlaup[2].

[2] For brevity when referring to a specific Icelandic jökulhlaup it is usually abbreviated to glacier name followed by *hlaup*. Consequently, the 1996 Skeiðarárjökull jökulhlaup is referred to as the 1996 Skeiðarárhlaup.

### 1.3 Project Aim and Objectives

The overall aim of this research is to identify the hydrological, glaciological and sedimentary controls on the sedimentary architecture of single event eskers, produced during high-magnitude jökulhlaups. In order to fulfil this aim, a number of research objectives have been identified.

**Objective 1:** ***To establish the controls on conduit location and geometry during the November 1996 Skeiðarárhlaup***

*Specific objectives*

- To identify if englacial structure and the esker are visible in the ice of Skeiðarárjökull using GPR.
- To map englacial structure at Skeiðarárjökull that can be observed using GPR.
- To assess the role of pre-existing structural weaknesses on the location of the jökulhlaup conduit in which the esker was deposited.

**Objective 2:** ***To identify the controls on the sedimentary architecture of the November 1996 Skeiðarárhlaup esker and ice-walled canyon fill***

*Specific objectives*

- To develop a radar facies scheme that can be used to classify major GPR reflection types that are representative of sedimentological structure within the November 1996 Skeiðarárhlaup esker and ice-walled canyon fill.
- To identify the major radar elements within the esker and ice-walled canyon fill and to classify these radar elements using the radar facies scheme.
- To develop an evolutionary model for the controls on the sedimentary architecture of the esker and ice-walled canyon fill during the 1996 Skeiðarárhlaup.
- To estimate the depositional timescale for the esker and ice-walled canyon fills on both a radar element and landform scale.

**Objective 3:** ***To identify the controls on the sedimentary architecture of the July-August and October 1994 Bering Glacier outburst floods, ice-walled canyon fill and esker***

*Specific objectives*

- To develop a radar facies scheme that can be used to classify major GPR reflection types that are representative of sedimentological structure within the 1994 Bering Glacier outburst flood, ice-walled canyon fill and esker.
- To identify the major radar elements within the ice-walled canyon fill and esker and to classify these radar elements using the radar facies scheme.

- To develop evolutionary models for the controls on the sedimentary architecture of the esker and ice-walled canyon fill during the 1994 Bering Glacier outburst floods.
- To estimate the depositional timescale for the esker and ice-walled canyon fills on both a radar element and landform scale.

**Objective 4:** ***To compare the sedimentary architecture and depositional history of the 1996 Skeiðarárhlaup and 1994 Bering Glacier outburst flood eskers and ice-walled canyon fills***

*Specific objectives*

- To compare the known/inferred hydrology of the November 1996 Skeiðarárhlaup and 1994 Bering Glacier outburst floods.
- To compare the sedimentary architecture of the Skeiðarárjökull and Bering Glacier jökulhlaup eskers and ice-walled canyon fills.
- To compare the controls on the sedimentary architecture of the esker and ice-walled canyon fills at Skeiðarárjökull and Bering Glacier.
- To assess the preservation potential of the eskers and ice-walled canyon fills at Skeiðarárjökull and Bering Glacier.

**Objective 5:** ***To identify diagnostic criteria for identifying palaeo-eskers generated by high-magnitude jökulhlaups***

*Specific objectives*

- To assess the controls on the sedimentary architecture of eskers deposited during high-magnitude jökulhlaups.
- To compare the sedimentary architecture of single event jökulhlaup eskers to potential sedimentary architecture of eskers deposited within ablation-controlled perennial conduits.
- To assess the broader applicability of the findings of this research to the study of palaeo-eskers.

Achieving the objectives outlined above will allow the controls on the sedimentary architecture of single event jökulhlaup eskers to be identified, fulfilling the overall aim of this thesis. Each data set will first be considered separately to identify site specific controls on esker and ice-walled canyon fill sedimentary architecture. Consideration of the flow conditions associated with the depositional events and glacial hydrology will identify the hydrological controls on esker sedimentary architecture. Comparing the results of englacial GPR investigations at Skeiðarárjökull with recent observations of the controls on englacial hydrology will allow the potential glaciological controls on esker sedimentary architecture, through conduit location and geometry to be assessed.

Consideration of sediment supply will allow the sedimentological controls on esker architecture to be established. In addition to determining the key factors that control the sedimentary architecture of jökulhlaup eskers, direct comparison of the data sets from Skeiðarárjökull and Bering Glacier will allow diagnostic criteria to be identified that can be used to identify the signature of jökulhlaup conditions during the deposition of palaeo-eskers. Whilst previously, site specific studies of contemporary esker sedimentation have been rejected as analogues for palaeo-esker genesis, the synthesis of the Skeiðarárjökull and Bering Glacier data sets will give an insight into the processes and rates of esker sedimentation during jökulhlaups, providing well constrained analogues for esker deposition during previous glaciations. This research will add to the current understanding of esker deposition, as well as provide a basis for future studies of palaeo-esker genesis.

This research suggests that high-magnitude jökulhlaups can generate eskers with complex sedimentary architectures on a landform scale and that such events may have had a greater significance upon palaeo-esker genesis than previously hypothesised. Furthermore, it is shown that the current assumptions surrounding the development of conduits in which eskers were deposited cannot be applied to high-magnitude jökulhlaups and consequently, ice sheet models based upon these assumptions are likely to be flawed. Consequently, care must be taken when basing models of ice sheet hydrology on esker morphology, as the assumption of an ablation-controlled scenario is unlikely for all eskers. The role of jökulhlaups in esker formation needs to be considered, as this has major implications for the glaciological and hydrological processes responsible for esker genesis.

### 1.4 Thesis Structure

The structure of this thesis is summarized below:

**SECTION I:** Relevant background for the thesis will be summarised. *Chapter 2* will review our current understanding of glacial hydrological theory as well as eskers and the processes that lead to their deposition. Particular emphasis will be placed upon the few detailed models of esker sedimentation presented in the literature. *Chapter 3* will give detailed field site descriptions of Skeiðarárjökull and Bering Glacier, paying particular emphasis to the esker forming events and their dynamic history.

**SECTION II:** This section will introduce the techniques used for this research and detail the field methodology. *Chapter 4* introduces the relevant background theory to ground-penetrating radar and data processing, before detailing the field methodology and the data processing techniques employed for this investigation.

**SECTION III:** This section will present the results and interpretations of data collected at Skeiðarárjökull and Bering Glacier. *Chapter 5* will present and interpret ground-

penetrating radar data collected on the ice surface of Skeiðarárjökull. The controls on the development and location of the conduit in which the esker was deposited will be discussed as will its wider significance. *Chapter 6* will present and interpret ground-penetrating radar data collected on the esker and ice-walled canyon fill at Skeiðarárjökull. An evolutionary model will be developed for the controls on esker sedimentary architecture during the November 1996 Skeiðarárhlaup and the depositional timescale will be discussed. *Chapter 7* will present and interpret ground-penetrating radar data collected on the esker and ice-walled canyon fill at Bering Glacier. Evolutionary models will be developed for the controls on the sedimentary architecture of the esker and ice-walled canyon fill during the 1994 outburst floods at Bering Glacier and the depositional timescales will be discussed.

**SECTION IV:** This section will discuss the major findings of this study and synthesise the interpretations presented and discussed in section III. *Chapter 8* will compare the sedimentary architecture of the Skeiðarárjökull and Bering Glacier eskers, as well as the models presented for their development. This comparison will be made in order to establish the controls on the sedimentary architecture of eskers deposited during high-magnitude jökulhlaups. In addition, diagnostic criteria will be identified that can be used in future esker studies to identify the signature of jökulhlaups in palaeo-eskers. The wider significance of the findings of this research will then be discussed, with specific reference to the potential for the influence of jökulhlaups during palaeo-esker deposition. *Chapter 9* will then summarise the key findings and conclusions of the thesis. Finally, suggestions for further work will be made to help clarify the major conclusions and questions raised by the thesis.

# Chapter 2

## Water Movement through Glaciers and Esker Sedimentary Architecture

### 2.1 Introduction

One of the earliest descriptions of an esker was made in Ireland by Richard Prior in 1699 (Davies, 1970; Delaney, 2007). His observation that the ridge was composed of sand and gravels, distinct from surrounding lithology, coupled with the size of the ridge, led him to suggest that the landform was deposited by "some violent motion of waters", though its glaciofluvial origin was not identified (Davies, 1970). The term 'esker' is an English rendering of a Gaelic word *eiscar*, that literally translates to 'ridge', and is now used as reference to elongate, sinuous ridges of stratified sand and gravel (Warren and Ashley, 1994). During early work into the form of such ridges, however, the term was loose, and in Ireland, referred to all mound- or ridge-like structures of stratified deposits. It was not until American investigators widely attributed the term to glaciofluvial ridge deposits that it fixed as a reference to such a landform (Flint, 1930). Eskers can be broadly defined as ridges of stratified glaciofluvial materials that were deposited within ice-walled river channels (Warren and Ashley, 1994; Brennand, 2000; Benn and Evans, 1998) that may or may not be confined by ice on all sides (Banerjee and McDonald, 1975). Consequently, they may record deposition in subglacial (e.g. Flint, 1928; Stokes, 1958; Gorrell and Shaw, 1991; Auton, 1992; Brennand, 1994; Clark and Walder, 1994; Gray, 1997; Brennand, 2000; Fiore *et al.*, 2002), englacial (e.g. Shulmeister, 1989; Knudsen, 1995) or supraglacial drainage networks (e.g. Hebrand and Åmark, 1989; Huddart *et al.*, 1999; Russell *et al.*, 2001a) and ice walled channels (e.g. Brennand and Sharpe, 1993). The formation processes for esker and ice-walled channel fills have been described from many modern (e.g. Flint, 1928; Lewis, 1949; Stokes, 1958; Price, 1966, 1969; Russell and Knudsen, 1999a; Russell *et al.*, 2001a; Cassidy *et al.*, 2003) and palaeosubglacial environments (e.g. Flint, 1928; Allen, 1971; Banerjee and McDonald, 1975; Gorrell and Shaw, 1991; Brennand, 1994; Clark and Walder, 1994; Warren and Ashley, 1994; Brennand, 2000; Fiore *et al.*, 2002; Mäkinen, 2003; Hooke and Fastook, 2007).

Before it is possible to interpret the depositional history of eskers, understanding the mechanisms and dynamics of glacial hydrology is important. In *Section 2.2* an overview of our current understanding of water flow through glaciers will be presented, focusing upon englacial and subglacial discharge, as well as structural controls on water routing and the hydrology of jökulhlaups. The chapter will then focus upon relevant

background to the current understanding of eskers and their depositional mechanisms (*Section 2.3*), before a current understanding of the controls on esker sedimentary architecture (*Section 2.4*) and a chapter summary (*Section 2.5*) are presented.

## 2.2 Movement of Water through Glaciers

Although an overview of the current glacial hydrology literature will be presented, it must be noted that much of this literature is only applicable to a steady-state scenario, where water pressure within a conduit balances ice overburden pressure. This is unlikely for prolonged periods and cannot be applied to jökulhlaup conditions, which are not constrained by much of the theory below. Within steady-state theory water flow through a glacier is controlled by variations in hydraulic potential, which are dependent upon both elevation and water pressure (Shreve, 1972). These variations in hydraulic potential can be represented by equipotential surfaces within a glacier that dip up-ice at an angle approximately eleven times the surface slope of the ice mass (Shreve, 1972; Hooke, 1989) (Figure 2.1). In the traditional view of glacial hydrology, under steady-state conditions, the direction of water routing within a glacier will be normal to these surfaces (Figure 2.1), and thus, in some cases, may flow against the bed slope (Shreve, 1972; Shreve, 1985). Shreve's (1972) theories, however, are based upon the assumption that the water pressure within a sub or englacial conduit is balanced by the cryostatic pressure, which is not always the case, even under steady-state conditions (Röthlisberger, 1972; Lliboutry, 1983). Röthlisberger (1972) argued that the geometry of an englacial or subglacial conduit is controlled by the balance between frictional melting of the conduit walls by the flowing water and conduit closure due to viscous deformation of the ice (Figure 2.2). Spatial increases or decreases in discharge result in increased or decreased rates of energy expenditure via frictional melting and consequently, conduit expansion or contraction, respectively (Röthlisberger, 1972). This predicts that water pressures should be higher where discharge is lower and vice versa (Röthlisberger, 1972). Consequently, at areas of higher pressure, because water flows from areas of high to low hydraulic potential, efficient low pressure conduits tend to capture discharge from neighbouring higher-pressure conduits (Shreve, 1972; Hooke, 1989; Hubbard and Nienow, 1997). This is conducive to the development of an arborescent network of conduits where pressure reduces (and discharge increases) down-flow (Shreve, 1972; Hooke, 1989; Hock and Hooke, 1993; Hubbard and Nienow, 1997), evidence for which can come from the morphologies of some esker systems (c.f. Shreve, 1985; Brennand, 2000; Boulton *et al.*, 2007a, 2007b). As conduit size is largely dependent upon the water flux through the system, they tend to be smallest during the early spring after closure due to viscous deformation (Hooke *et al.*, 1985). Consequently, water pressures are highest during the early melt season, when the small conduits cannot respond immediately to the

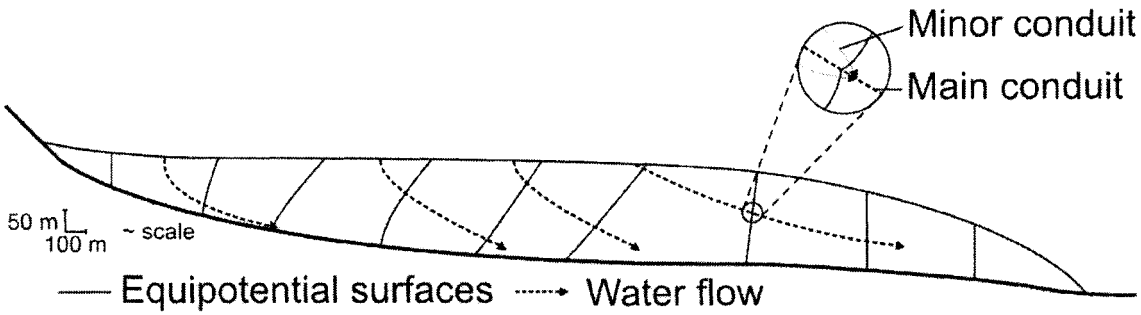


**Figure 2.1.** Longitudinal cross-section of a glacier, showing up-glacier dipping equipotential surfaces and their theoretical influence on the direction of englacial water flow. Inset shows the dimpling effect of main conduits on the equipotential surfaces. This consequently diverts the flow in smaller conduits towards the main conduit (from Hooke, 1989).

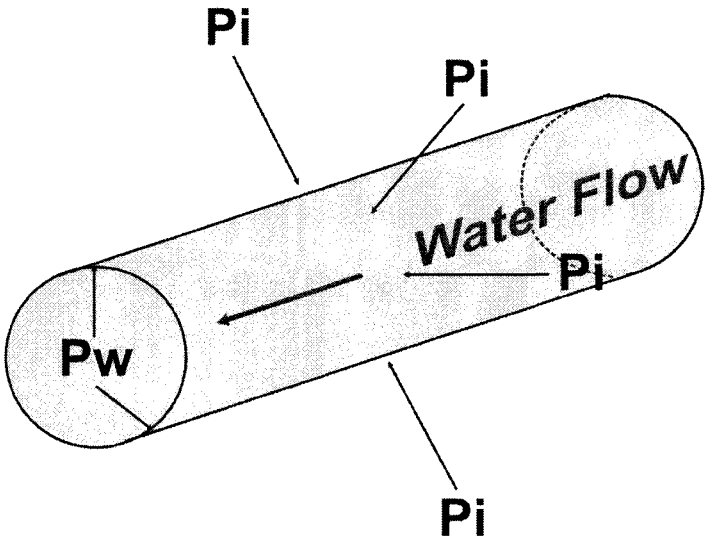


**Figure 2.2.** Schematic representation of the forces controlling the geometry of a Röthlisberger channel (after Röthlisberger, 1972). The channel tends to close by creep of the surrounding glacier ice at overburden pressure (Pi), but is opened by frictional melting as the flowing water (Pw) dissipates energy.

influx of supraglacial meltwater into the system (Hooke *et al.*, 1985). During the height of the melt season, an anabranched network of conduits is developed, with individual conduits likely to be braided (Hock and Hooke, 1993).

It is believed that ablation-controlled conditions, perennial streams can develop due to increases in meltwater discharge from the glacier surface to the bed, with the frequency of these outlets increasing as the glacier advances (Boulton *et al.*, 2007a, 2007b). During the winter months, these perennial streams remain open due to the input of basal melwaters, meaning channels can remain stable for prolonged periods of time where there is a high meltwater flux (Boulton *et al.*, 2007a, 2007b). During the summer, the perennial conduits are fed by groundwater flow, when the glacier rests upon an unconsolidated bed of sediments, though ephemeral conduits can develop if the water pressure within the sediments exceeds the rate at which the major conduits can discharge it (c.f. Boulton *et al.*, 2007a, 2007b).

Such theory assumes that conduits are at full-pipe conditions, but it is known that the rate of conduit enlargement by frictional melting exceeds that of conduit closure by ice deformation (Lliboutry, 1983; Hooke, 1984, 1989), particularly when large amounts of water originate at the glacier surface (Benn and Evans, 1998). Following periods of high discharge, when conduits are able to expand, the associated low discharge result in water exiting from the system at a greater rate than conduits can contract due to viscous deformation of the ice (Hooke, 1984; Hooke *et al.*, 1985, 1990). Consequently, water pressures will be at or close to atmospheric (Lliboutry, 1983; Hooke, 1984; Hooke *et al.*, 1985, 1990), evidence for which may come from the sedimentary architecture of some eskers (c.f. Banerjee and MacDonald, 1975). This, however, can also depend on the conduit position, with closure rates tending to be higher in deep ice sections, where conduits will be full for greater periods of time (Hooke, 1984). Due to the largely inaccessible nature of the subglacial drainage system, field observations are largely restricted to ice marginal areas (Hubbard and Nienow, 1997), where the likelihood of open conduits being present is greatly increased.

The subglacial drainage system is largely governed by the principles set out above and the system may be composed of either an *arborescent* (discrete) or *non-arborescent* (distributed) drainage network (Hubbard and Nienow, 1997), largely fed by supraglacial meltwaters through crevasses and moulins (Stenborg, 1969; Lliboutry, 1983; Holmlund and Hooke, 1983; Hooke, 1989; Fountain and Walder, 1998).

### *2.2.1 Arborescent drainage networks*

Meltwaters within an arborescent network are discharged through large, hydraulically efficient channels that cover a relatively small part of the bed (Hubbard and

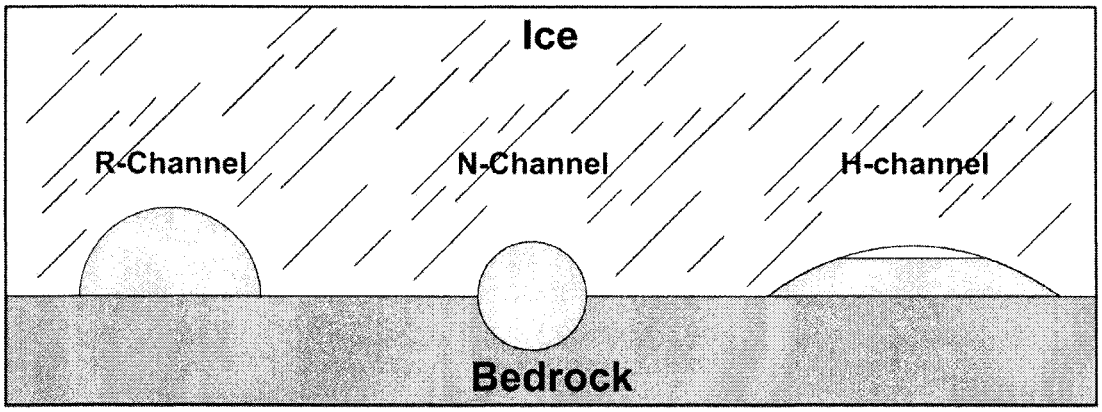


**Figure 2.3.** Schematic representation of the three main subglacial channel types described within the literature. *R-channels* are semi-circular conduits incised upwards into the overlying ice (Röthlisberger, 1972), whilst *N-channels* are conduits incised into the bedrock (Nye, 1973), and *H-channels* are broad and low conduits incised upwards into the overlying ice, which may be at atmospheric pressure for significant periods (Hooke, 1984).

Nienow, 1997). In such a system, three main channel types (Figure 2.3) have been proposed (Hubbard and Nienow, 1997):

1. *R-channels* are semi-circular subglacial tunnels incised upwards from the glacier bed into the overlying ice (Röthlisberger, 1972). It was theorised by Röthlisberger (1972) that the pressure gradient within these channels is scaled inversely withsteady-state water flux, where an increase in discharge results in conduit growth and consequently a reduction in pressure. As discharge decreases and the conduit narrows due to viscous deformation the pressure will increase (Röthlisberger, 1972; Shreve, 1972). Consequently, large low-pressure R-channels can capture flow from smaller, higher pressure conduits, developing an arborescent drainage network (Hubbard and Nienow, 1997). Although it is presumed that such conduits occur at full-pipe flows, it has been shown that their geometry would require they were at atmospheric pressure much of the time (Hooke, 1984, 1989; Hook *et al.*, 1985; Hock and Hooke, 1993; Hooke *et al.*, 1990).
2. *N-channels* are subglacial tunnels incised downwards into the substrate, rather than into the overlying ice (Nye, 1973). These are often observed on exposed bedrock surfaces and their formation requires long-term channel stability (Hubbard and Nienow, 1997).
3. *H-channels* are broad and low, subglacial conduits incised into the overlying ice (Hooke, 1984). It is argued by Hooke (1984, 1989) that R-channels are not often observed, as subglacial conduits do not remain perennially water filled, which is the fundamental assumption behind the Röthlisberger (1972) and Shreve (1972) theories. It has been suggested that a steady state, during which viscous closure of the conduit balances melting of its walls, does not exist (Lliboutry, 1983). For the majority of the year, subglacial conduits will remain at atmospheric pressure. Only during flood conditions do full-pipe conditions prevail (Lliboutry, 1983). During periods when the conduit is at atmospheric pressure, melting is concentrated on the tunnel walls, rather than the ceiling, producing a broad and low cross-section (Hooke, 1984, 1989). It was further theorised that the closure rate of broad and low conduits would be greater, suggesting pressurised water flow could occur for longer period than within R-channels (Hooke *et al.*, 1985, 1990).

### *2.2.2 Non-arborescent drainage networks*

Non-arborescent or distributed drainage systems drain extensive areas of the glacier bed, transporting meltwaters more slowly and at higher pressures than within their arborescent and channelized counterparts (Hubbard and Nienow, 1997). In such systems

meltwaters are drained through more tortuous and resistive flow paths that cover a relatively large proportion of the bed. Furthermore, water pressures scale positively with discharge, preventing the development of an arborescent conduit system (Hubbard and Nienow, 1997). Four major subglacial flow configurations have been proposed for a non-arborescent system:

1. *Film* discharge is associated with the processes of regelation, which involves the melting and refreezing around small bedrock hummocks (Weertman, 1957, 1964). Where the glacier flows over a rigid and impermeable bed, a thin film (a few millimetres in thickness) will discharge the bulk of the subglacial drainage (Weertman, 1972). Walder (1982), however, subsequently argued that such a drainage mechanism is unstable and any sheet flow would collapse into channelized drainage due to variations in the meltwater input.
2. *Linked cavities* develop due to collection of meltwater in the lee of bedrock hummocks (Lliboutry, 1968). Such cavities may be connected by orifices formed from striations or joints in the bedrock (Hooke, 1989), to form a complex anabranching subglacial network of cavities (Lliboutry, 1968; Figure 2.4). Such cavity networks have been linked to glacier surging (e.g. Kamb *et al.*, 1985; Björnsson, 1998; Bennett *et al.*, 2000), with Kamb *et al.* (1985) arguing that during a glacier surge the arborescent drainage system will become unstable and collapse into a linked-cavity network. Furthermore, the presence of cavities due to an irregular bed profile would tend to capture significant amounts of meltwater, further limiting the extent of water sheets (Walder, 1982). In the development of a linked cavity network, melting is of secondary importance to glacier sliding as an enlargement process (Walder, 1986) and the geometry of interconnected cavities with water will largely be controlled by water pressure effects (Kamb *et al*, 1985; Walder, 1986; Hooke, 1989). In addition, water will tend to flow in a direction oblique to ice movement, avoiding regions of the bed where the normal stress exerted by the ice is large (Walder, 1986).
3. *Canals* have been inferred for drainage over a saturated, deformable bed (Walder and Fowler, 1994; King *et al.*, 2004). Such a drainage mechanism involves the development of an anabranching network that develops due to a positive relationship between discharge and water pressure (Hubbard and Nienow, 1997). Furthermore, Walder and Fowler (1994) suggest that canals can coexist with an arborescent network of conduits beneath a glacier.
4. *Groundwater flow* can take place where a glacier overlies a bed of unconsolidated sediments (e.g. Lliboutry, 1983; Fountain, 1994; Boulton *et al.*, 1996, 2007a, 2007b). Where large meltwater influxes occur, however, such a mechanism is incapable of discharging all basal waters and consequently, waters may become

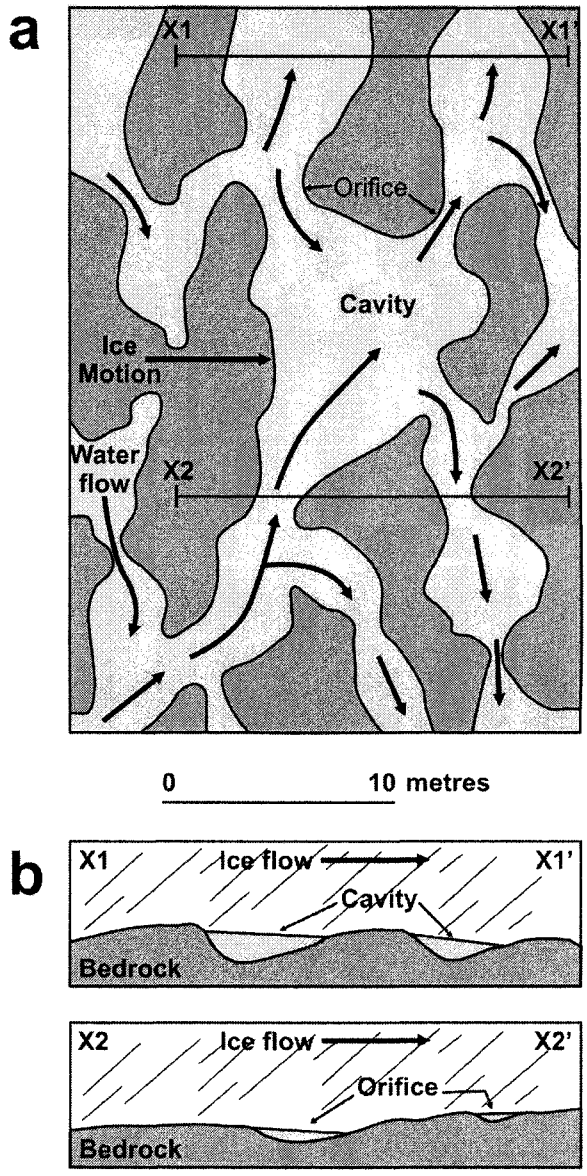


**Figure 2.4.** Idealised subglacial cavity network in (a) plan view and (b) cross section (from Kamb, 1987). The darker shaded areas are regions of ice-rock contact, whilst the lighter shading represents regions of ice-rock separation (cavities). The cavities are linked by constricted orifices between them, with water flow direction being indicated by the arrows.

focused within a system of high-capacity subglacial conduits or channels (c.f. Boulton *et al.*, 1996, 2007a, 2007b).

Whilst arborescent and non-arborescent drainage systems have been defined seperately, it is known that both can coexist (Walder, 1986; Hooke, 1989; Fountain and Walder, 1998). As long as glacier movement is controlled by basal sliding, linked cavities are likely to be present, as the overriding ice will separate from the bed on the lee of any obstacles that are there (Hooke, 1989). It is likely, however, that distributed drainage systems transfer meltwaters from wider areas of the bed into arborescent networks of high-capacity conduits (Hubbard and Nienow, 1997; Boulton *et al.*, 2007a, 2007b), with the primary mode of subglacial drainage varying temporally (Hubbard and Nienow, 1997; Fountain and Walder, 1998). For example, during the winter months the rate of meltwater input into the subglacial system is low and consequently it is likely that waters are discharged through a distributed system (Hooke *et al.*, 1985; Hubbard and Nienow, 1997). During the spring, when the meltwater input increases, this distributed system may destabilise into a discrete network of R- or H-channels (Hooke *et al.*, 1985; Hubbard and Nienow, 1997), which migrate up-glacier through the summer as the meltwater influx increases (Hubbard and Nienow, 1997; Fountain and Walder, 1998). When a linked cavity system is present and water pressure rises there will be a reduction in bed roughness and consequently an increase in basal sliding (Walder, 1986). During such scenarios, it has been argued that flow through the interconnected cavities would be captured by growing R-channels, which develop into an arborescent system (Walder, 1986). The meltwater input from the glacier surface is fundamental to conduit development (Shreve, 1985). In the autumn, the dramatic reduction in supraglacial meltwater results in destabilisation of the channel system and a return to a distributed network (Hubbard and Nienow, 1997).

### *2.2.3 Englacial hydrology*

It was first theorised by Nye and Frank (1973) that water will flow through veins present along intersections between ice crystals, forming a network of capillary sized tubes through which waters can flow englacially. It has been subsequently suggested that intergranular drainage is negligible (Hooke, 1989; Fountain and Walder, 1998) and instead water will enter the englacial system from supraglacial streams that plunge into the glacier via crevasses and moulins (Stenborg, 1973; Holmlund and Hooke, 1983; Hooke, 1989; Fountain and Walder, 1998). Water descending from the crevasses through veins or ice structures (Fountain and Walder, 1998) will dissipate energy into the surrounding ice and enlarge into a conduit that can accommodate all the meltwater influx (Hooke, 1989). Moulins may persist for several melt seasons, until another crevasse

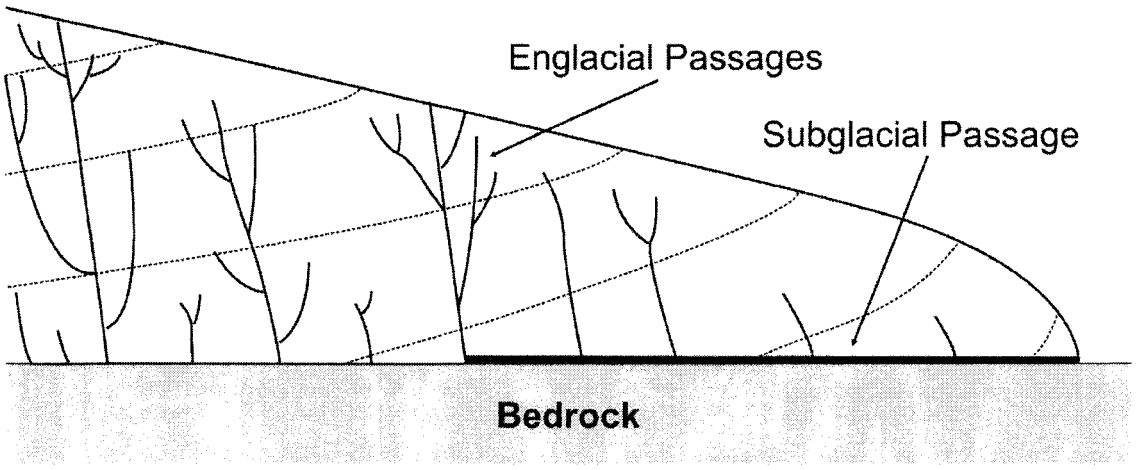


**Figure 2.5.** Theoretical equipotential surfaces (Dashed lines) and a hypothetical upward-branching network of arborescent englacial channels (from Shreve, 1985).

opens farther up-glacier and captures the water flowing to it (Holmlund and Hooke, 1983; Hooke, 1989). Shreve (1972) argues that the englacial hydrological system should form an upward branching arborescent network, with the flow direction being determined by equipotential surfaces within the ice mass (Figure 2.5). This traditional theory of englacial drainage has been challenged by observations made at Storglaciären (Sweden), however, where englacial conduits had a tendency to be gently inclined, rather than near vertical (Fountain and Walder, 1998). It is suggested that such near-horizontal conduits form by water flow along the base of crevasses, which may flow through either steeply dipping, enlarged veins or will enter the microfractures that connect to other crevasses and were created during crevasse formation (Fountain and Walder, 1998). This is consistent with the observation of Hooke (1989) that meltwaters from the base of moulins tend to follow a path trending in the direction of the crevasse in which the moulin formed. Fountain and Walder (1998) suggested that as the crevasse bottom stream melts down into the glacier, ice creep will close the crevasse above to create an isolated englacial conduit (Figure 2.6). Observations of the englacial hydrological system suggest it is dynamic, with abandonment and reoccupation of conduits taking place within a melt season (Irvine-Fynn *et al.*, 2006). It was shown by the work of Nienow *et al.* (1996) that at Glacier d'Arolla, Switzerland, englacial conduits acted as overflow channels during periods of high discharge, subsequently being abandoned when discharges were low.

Whilst subglacial and englacial hydrology has here been discussed separately, the interconnections between them (Figure 2.7) suggest they should be regarded as a system (Hooke, 1989; Fountain and Walder, 1998). Water typically enters the system through crevasses and moulins where water enters englacial passages comprising a complex combination of steeply inclined conduits formed from the enlargement of veins, and near-horizontal passages developed along the base of crevasses (Fountain and Walder, 1998). In general, these englacial conduits will supply supraglacial meltwaters into larger subglacial channels (Figure 2.7), except where the bed is overdeepened (Lliboutry, 1983; Hooke *et al.*, 1988; Hooke, 1989; Pohjola, 1994; Kirkbride and Spedding, 1996; Fountain and Walder, 1998). It is argued that the adverse bed slope associated with overdeepened basins results in the inability of stable subglacial conduits to develop due to meltwater refreezing (Hooke, 1989; Fountain and Walder, 1989). Consequently, it has been suggested that waters are discharged through englacial conduits (Hooke *et al.*, 1988; Hooke, 1989; Fountain and Walder, 1998) or in subglacial tunnels that discharge waters around the overdeepening (Lliboutry, 1983; Hock and Hooke, 1993; Fountain and Walder, 1998). Again, however, these interpretations are based upon steady-state theory and based upon indirect observations and subglacial drainage can in actuality take place in overdeepened basins (e.g. Meier *et al.*, 1994; Vieli *et al.*, 2004).

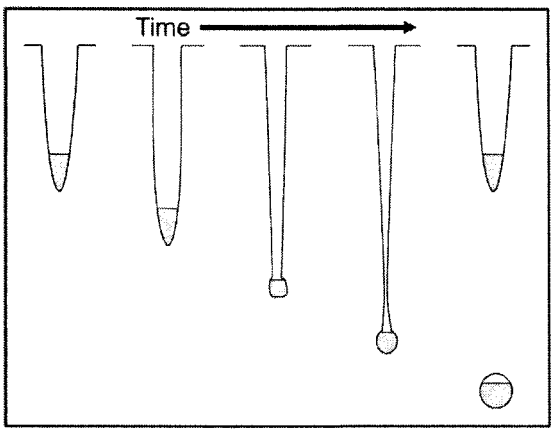


**Figure 2.6.** Qualitative depiction of the proposed evolution of an englacial conduit from a crevasse (from Fountain and Walder, 1998). Flow of water at the base of a crevasse results in melting of the ice with which the water is in contact. This results in downcutting of the stream, which becomes isolated from the crevasse due to its closure by ice creep.

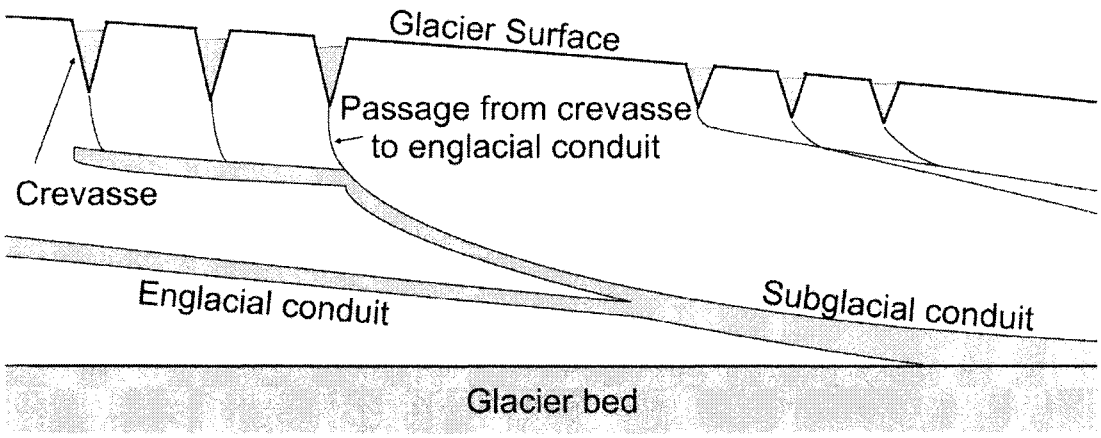


**Figure 2.7.** The geometry of a hypothetical englacial drainage system, comprising gently dipping conduits derived from crevasse-bottom streams, and steeply plunging englacial passages (from Fountain and Walder, 1998). These englacial conduits feed meltwaters into a subglacial conduit.

*2.2.4 The role of structure on water routing*

In recent works, increasing evidence is being presented for the significant role pre-existing structure can play on glacial hydrology during both steady-state and transient conditions (Pohjola, 1994; Fountain and Walder, 1998; Roberts *et al.* 2000a, 2000b, 2001; Russell *et al.*, 2001a; Waller *et al.*, 2001; Roberts *et al.*, 2002; Fountain *et al.* 2005a, 2005b; Gulley and Benn, 2007). Although it has long been known that the routing of water to the bed via moulins is controlled by the presence of crevasses (Stenborg, 1968, 1972; Holmlund and Hooke, 1983), it was assumed that the englacial hydrological system would be composed of a near-vertical arborescent system of conduits that feed into major subglacial conduits (Shreve, 1972, 1985; Hooke, 1989). Conduits have been observed in areas of structure previously (c.f. Stokes, 1958), but it was first shown by Pohjola (1994) that englacial drainage was commonly associated with crevasses and associated blue ice structures. Later Fountain and Walder (1998) suggested that englacial conduits could be created by the flow of water through the base of near-surface crevasses, which then become encased by the ice as the upper crevasse closes. Further studies by Fountain *et al.* (2005a, 2005b) and Fountain (2007) showed that the traditional view of a circular, high discharge englacial conduit could only be directly identified where the water flux is great enough to initiate shear heating and melting of fracture walls. More commonly identified was low velocity convection of water through interlinked fracture networks.

More recently, Gulley and Benn (2007) mapped englacial conduits through which supraglacial lakes had been drained. Evidence here again pointed to the typical presence of structure at the location of the conduit. Gulley and Benn (2007) suggested that waters were initially discharged through fractures filled with porous debris, before conduits developed due to a combination of melting and mechanical excavation of the surrounding glacier ice that was weakened by the presence of significant structure (Figure 2.8). This suggests that for shallow englacial drainage the flow path is dominantly influenced by pre-existing lines of high hydraulic conductivity rather than cryostatically determined potential gradients (Gulley and Benn, 2007).

*2.2.5 Water flow during jökulhlaups*

In glaciated environments, stored water may be released suddenly as a jökulhlaup. The traditional understanding of jökulhlaup dynamics assumes that a single subglacial conduit links a pressure-coupled reservoir of meltwater to the glacier terminus, the geometry of which is balanced by frictional melting of the conduit walls and their closure due to viscous deformation of the ice (e.g. Nye, 1976; Spring and Hutter, 1981; Clarke, 1982; Szilder and Lozowski, 1997; Fowler, 1999). The 1996 Skeiðarárhlaup demonstrated that such assumptions cannot be applied to a linearly rising jökulhlaup, as waters cannot be solely discharged by perennial outlets alone and instead new outlets

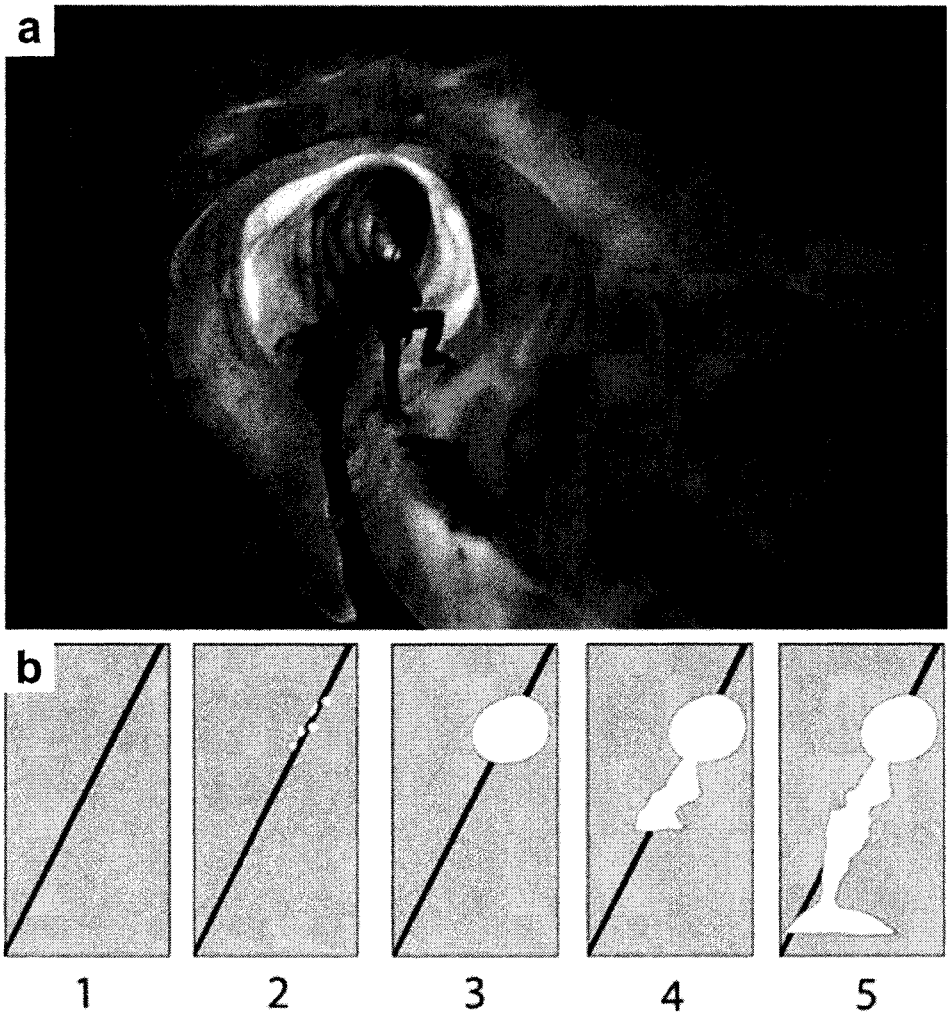


**Figure 2.8.** a) Photograph of a structurally controlled englacial conduit at Ngozumpa Glacier, Nepal. b) Conceptual model of conduit evolution. 1: debris-filled crevasse trace; 2: water flow along the crevasse trace creates a network of proto-conduits; 3: elliptical phreatic tube is created; 4: vadose incision of conduit floor towards the local base level; 5: incision becomes independent of parent structure and passage floor stabilizes at base level (from Gulley and Benn, 2007).

must be rapidly created (Roberts, 2005). During the 1996 Skeiðarárhlaup, floodwaters were forced to high elevations within the ice column via hydraulic jacking and hydrofracturing of the overlying ice (c.f. Roberts *et al.*, 2000a, 2000b, 2001, 2002; Russell *et al.*, 2005, 2006, 2007a). This resulted in discharge through dense networks of supraglacial fracture outlets, which then developed into primary conduit outlets and supraglacial embayments, the geometry of which are believed to have been significantly influenced by flood generated hydrofracturing (c.f. Roberts *et al.*, 2000a, 2000b, 2001, 2002; Russell *et al.*, 2005, 2006, 2007a). Such drainage of jökulhlaups through supraglacial outlets is common (Theakstone, 2001). Roberts *et al.* (2000b, 2002) showed that the rate of pressure increase during a jökulhlaup determines the type of embayment that is created at the glacier surface (Roberts *et al.*, 2000b, 2002). Very rapid increases in pressure forces diffuse fracturing at the near surface, allowing deeply incised embayment development through collapse and excavation of the weakened ice roof (Roberts *et al.*, 2002). In contrast, when the rate of pressure increase is lower, the propensity for diffuse hydrofracturing is lessened, resulting in the gradual removal of collapsed ice blocks due to undermining by the exiting floodwaters (c.f. Roberts *et al.*, 2002). During exponentially rising jökulhlaups, when pressure increase is gradual, however, the likelihood of supraglacial outlet development is much lower and subglacial discharge is typically an efficient means of expelling all floodwater input (Roberts *et al.*, 2000b).

These relatively recent observations of linearly rising jökulhlaups contrast with the traditional view of jökulhlaup hydrology, where it has been presumed that melting is the most important control upon the development of conduits (e.g. Nye, 1976; Clarke, 2003). It is known, however, that when discharge rises rapidly, the low effective pressures are affiliated with intense fracturing of the surrounding glacier and ice fragmentation can exceed the volume of flood-induced melt from conduits (Roberts, 2005). This suggests mechanical excavation of ice is commonplace during jökulhlaups that demonstrate a very rapid rise to peak discharge (Tweed and Russell, 1999). The traditional understanding of jökulhlaup dynamics can only be applied to typical exponentially rising jökulhlaups, and their linearly rising counterparts are a separate event, in which steady-state theory is no longer valid.

### 2.3 Eskers

Eskers are generally surmised to be the casts of subglacial or englacial conduits incised into the overlying ice (Flint, 1928; Clark and Walder, 1994), maintained by a balance between frictional melting of the conduit walls and conduit closure due to viscous deformation of the ice (Hooke, 1989; Syverson *et al.*, 1994; Warren and Ashley, 1994; Boulton *et al.*, 2007a, 2007b; Fountain, 2007; Hooke, 2007). Increases or decreases in discharge result in increased or decreased rates of energy expenditure via frictional

melting and consequently, conduit expansion or contraction, respectively (Röthlisberger, 1972). The typical esker size of tens to hundreds of metres in width and height is believed by Clark and Walder (1994) to be an unrealistic representation of R-channel geometry, even during jökulhlaups, as it was stated by Nye (1976) that subglacial channels during Grímsvötn drainage events would have been no more than approximately ten metres in diameter. They, therefore, conclude that eskers with these characteristics developed over several years, with annual sedimentation and upward as well as lateral melting of the conduit walls (Clarke and Walder, 1994; Warren and Ashley, 1994; Hooke, 2007).

Eskers commonly have steep sides and a single-crested ridge, usually being elongate, sinuous deposits of glaciofluvial sand and gravel (Flint, 1928; Warren and Ashley, 1994), though double crested ridges have also been reported (e.g. Shilts, 1984; Brennand and Sharpe, 1993, Brennand, 2000). Within the landscape they may form prominent sinuous ridges of variable size and morphology (Price, 1966; Brennand, 2000, 2007), but can also be buried (Brennand, 2007; Jol *et al.*, 2007), perhaps accounting for the lack of observed eskers in parts of North America (Brennand, 2000). Eskers can be up to tens of metres in height, hundreds of metres in width, and kilometres in length, sometimes including gaps of non-deposition or erosion along their path (Banerjee and McDonald, 1975; Saunderson, 1977; Brennand, 1994). In North America, they are typically found south of ~72°N, suggesting that temperate glaciers provide the hydrological conditions required for esker development (Banerjee and McDonald, 1975). Furthermore, Clark and Walder (1994), suggest that North American eskers are commonly located on areas of rigid bedrock rather than sedimentary basins, arguing their distribution is controlled by bed rheology, with rigid beds being favourable for channelized discharge. Boulton *et al.* (1996), on the other hand, predicted that esker development is largely controlled by the permeability of the substrate and the meltwater flux. Areas with low permeability beds will allow the development of channelized subglacial drainage and consequently esker deposition on both rigid beds and within some sedimentary basins (c.f. Brennand, 2000; Grasby and Chen, 2005). This has been subsequently applied to esker development in Canada, where it predicts esker distribution quite well (c.f. Grasby and Chen, 2005).

The mode of esker deposition, however, is varied with sedimentation associated with seasonal ablation patterns (e.g. Banerjee and McDonald, 1975; Shreve, 1985; Brennand, 1994; Clark and Walder, 1994; Warren and Ashley, 1994; Lundqvist, 1999a, 1999b; Brennand, 2000; Boulton *et al.*, 2007a, 2007b; Hooke, 2007; Hooke and Fastook, 2007) or jökulhlaups (e.g. Shulmeister, 1989; Delaney, 2001; Russell *et al.*, 2001a; Delaney, 2002; Mokhtari Fard, 2002) being inferred and eskers can be morphologically controlled by glacier surges (c.f. Knudsen, 1995; Evans and Rea, 1999). It was stated in the seminal paper by Banerjee and McDonald (1975) that "beyond the general

acceptance of eskers as ice-contact glaciofluvial features, little consensus exits with respect to theories of origin." As such, eskers appear to be a polygenetic landform (c.f. Flint, 1928; Banerjee and McDonald, 1975; Warren and Ashley, 1994; Brennand, 2000; Bennett and Huddart, 2007), and no single model can account for all processes of esker deposition (Warren and Ashley, 1994).

Warren and Ashley (1994) investigated the morphology and sedimentary architecture of Irish eskers on a regional scale, making inferences to the mode of deglaciation. A number of esker types were identified, though they typically formed in an orientation that is perpendicular to the ice margin and are continuous or segmented in character, showing variations in height and width along their length (Warren and Ashley, 1994; Delaney, 2001). This polygenetic nature of eskers can also be seen in those of North America (c.f. Banerjee and McDonald, Brennand, 2000), with eskers displaying various morphologies and depositional environment (e.g. Banerjee and McDonald, 1975; Brennand, 1994, 2000, 2007).

### *2.3.1 Esker sedimentary architecture*

Although eskers are suggested to be a polygenetic landform (c.f. Flint, 1928; Banerjee and McDonald, 1975; Warren and Ashley, 1994; Brennand, 2000) and it is argued generalizations of esker sedimentology are difficult to make (Mäkinen, 2003), the sedimentary architecture of esker systems can display some similarities (c.f. Banerjee and MacDonald, 1975; Warren and Ashley, 1994; Brennand, 2000). This suggests that some commonality exists, concerning the processes controlling esker sedimentary architecture. Eskers can be composed of a range of sedimentary facies, dominantly composed of sands, gravels, silts, clays and boulders (Figure 2.9). Disparities in sedimentary facies present within different eskers can be partly explained by the esker types observed across North America (c.f. Banerjee and McDonald, 1975; Brennand, 2000) and Europe (e.g. Warren and Ashley, 1994; Evans *et al.*, 2006) (Figure 2.10):

- **Long continuous eskers (*Type I*)** are deposited in single conduits or dendritic networks that demonstrate periodic highs and lows along their length. They are typically composed of sand to boulder-sized materials that are deposited from both a traction carpet and suspension (Brennand, 1994), and are typically well rounded due to long transport distances (Brennand, 1994; Brennand and Shaw, 1996; Brennand, 2000, 2007) or multiple cycles of movement by meltwater (c.f. Price, 1966, 1969). An esker core is often identified that may be composed of extensive units of unstratified gravel to boulder-sized material (Saunderson, 1975; Gorrell and Shaw, 1991; Warren and Ashley, 1994; Thomas and Montague, 1997; Mokhtari Fard, 2002; Mokhtari Fard and Gruszka, 2007), horizontal bedding (Delaney, 2001), or diamicton (Mokhtari Fard,

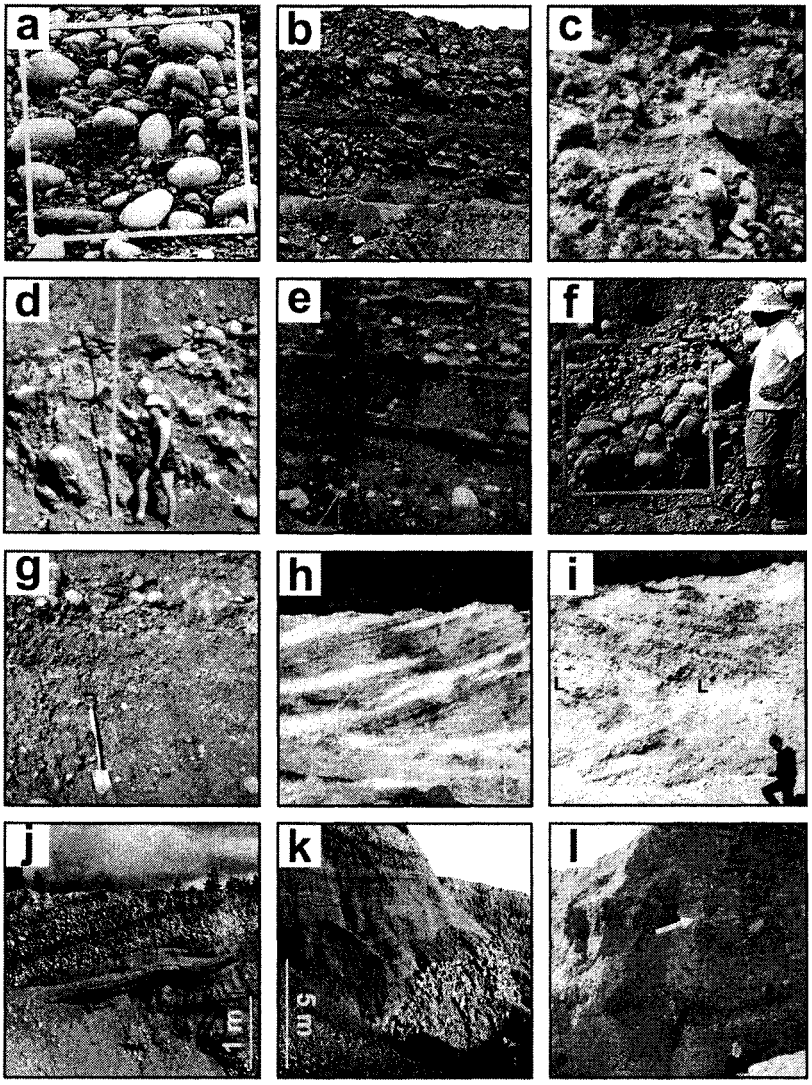


**Figure 2.9.** Examples of sedimentary facies observed in Quaternary and contemporary eskers. a) Heterogeneous, unstratified gravel with imbricate clast clusters (Grid is 1 $m^2$), Albiti esker (Brennand and Shaw, 1996). b) Massive, imbricate, clast-supported gravel alternating with sand, Tweed esker, Ontario (Brennand, 1994). c) Boulder rich gravel of a subglacial esker in Sweden (Mokhtari Fard, 2001). d) Chaotically bedded gravel in the Köyliönjärvi-Säkylänharju esker, Finland (Mäkinen, 2003). e) Coarse grained rhythmites in the 1996 Skeiðarárhlaup ice-walled canyon fill (Russell and Knudsen, 1999b). f) Cross-bedded gravel (Grid is 1 $m^2$), Albiti esker, North America (Brennand, 2000). g) Horizontally bedded cobble and pebble gravel in the Ballymahon esker, Ireland (Delaney, 2001). h) Backset beds observed in the Joux Valley eskers, Switzerland. The section is ~3 m in height (Fiore *et al.*, 2002.). i) Foreset beds overlying an erosional surface (L) in the Joux Valley eskers, Switzerland (Fiore *et al.*, 2002). j) Pseudo-anticlinal bedding within the Pålmalm esker, Sweden (Mokhtari Fard, 2002). k) Boulder-rich esker core, overlain by stratified sand and gravels (Mokhtari Fard, 2002). l) Sub-vertical, inverse fault caused by buried ice melting or post-depositional compaction (Fiore *et al.*, 2002).

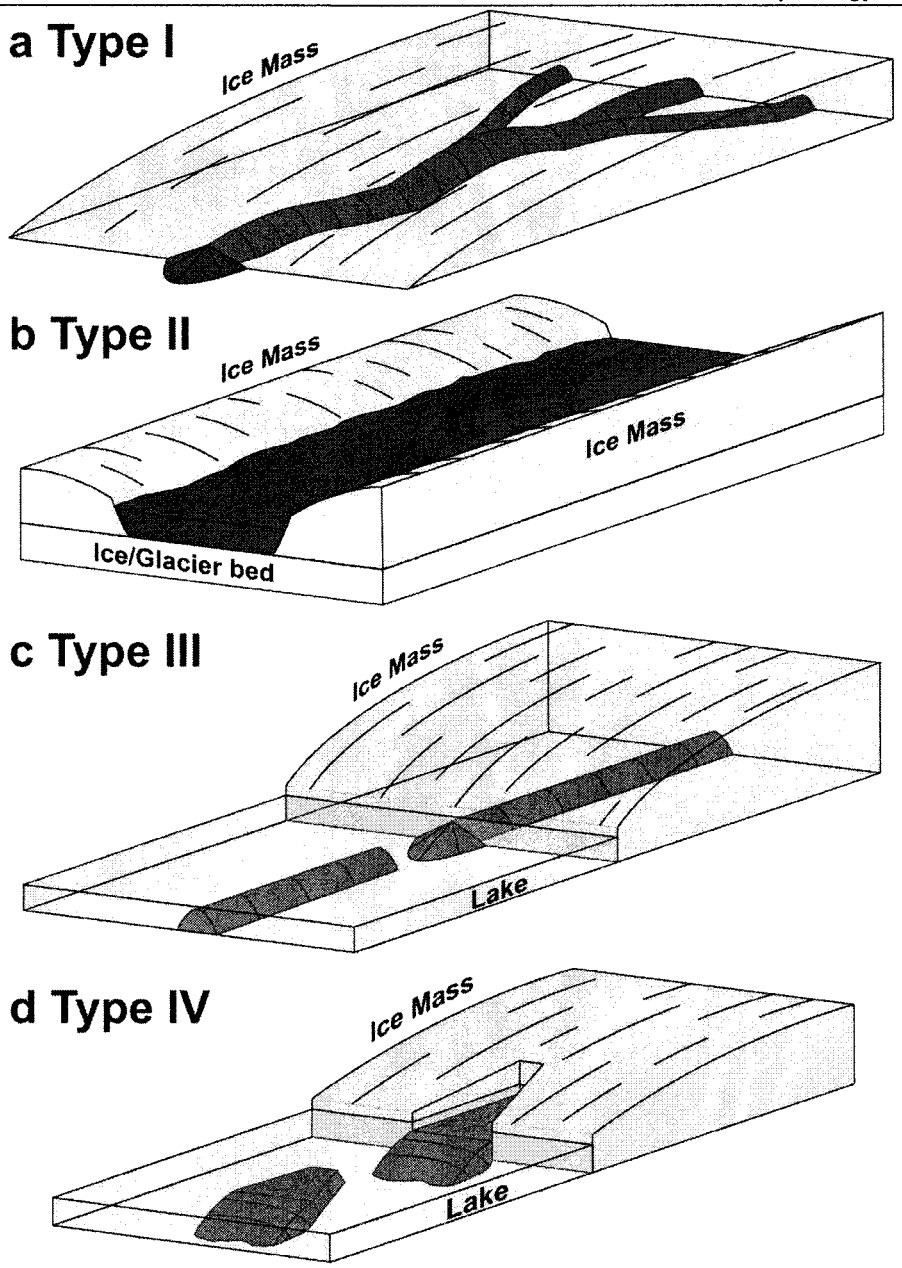


**Figure 2.10.** Diagrammatic sketches showing the depositional environment of the four main esker types described within the literature (after Warren and Ashley, 1994). a) Continuous ridge (Type I), deposited synchronously within a continuous conduit and/or dendritic network of conduits. b) Continuous ice-walled channel fill (Type II), deposited subaerially between walls of supporting ice. c) Long segmented eskers (Type III) are deposited within ice-marginal tunnels that exit into an ice-marginal water body. Retreat of the ice mass results in time-transgressive deposition of esker segments in an up-glacier direction. d) Short 'beaded' ridges (Type IV) are deposited within an ice-marginal water body and partly confined by walls of supporting ice at the proximal end. Ice-marginal retreat results in time-transgressive deposition of 'beads' in an up-glacier direction.

2002; Brennand, 2007; Sjogren *et al.*, 2007) that may indicate conduit closure and sediment deformation (Brennand, 2007). Overlying sediments are arranged into dominant units of heterogeneous, unstratified gravel, trough cross-bedding, horizontal bedding, backset bedding and foreset bedding (Shulmeister, 1989; Brennand and Sharpe, 1993; Brennand, 1994; Warren and Ashley, 1994; Brennand, 2000; Delaney, 2002; Brennand, 2007; Mäkinen and Artimo, 2007), typically arranged into rhythmic sequences (Saunderson, 1975; Shulmeister, 1989; Brennand and Sharpe, 1993; Brennand and Shaw, 1996). On a larger scale, however, gravel facies are typically arranged into ridge scale macroforms, controlled by conduit geometry (c.f. Brennand, 1994; Brennand and Shaw, 1996; Brennand, 2000; Delaney, 2002; Fiore *et al.*, 2002; Mokhtari Fard, 2002; Brennand, 2007; Sjogren *et al.*, 2007).

- **Ice-walled channel fills (*Type II*)** are deposited subaerially between confining ice walls, but are less frequently identified within the literature (e.g. Warren and Ashley, 1994; Russell and Knudsen, 1999b; Russell *et al.*, 2001a; Thomas *et al.*, 2007) and in some cases may be associated with ice-marginal reentrants (Delaney, 2001). They may develop on the glacier surface, thus resting directly upon an ice base (c.f. Shaw, 1972; Russell and Knudsen, 1999b; Russell *et al.*, 2001a), between retreating ice lobes (c.f. Warren and Ashley, 1994) or within ice-marginal reentrants (c.f. Cheel, 1982; Delaney, 2001). Typically, they can contain a core of boulder gravel, representing initial deposition within a conduit before deposition within a subaerial channel. The presence of widespread distortion within core materials of some Irish eskers is seen as evidence for initial deposition within an englacial conduit (Delaney, 2001). Conduit deposits (where present) are draped by subaerial deposits including plane beds, cross-beds, foreset beds and scour-and-fill structures (Saunderson, 1975; Warren and Ashley, 1994; Delaney, 2001; Bennett and Huddart, 2007; Thomas *et al.*, 2007). In addition, structures can also be arranged into numerous rhythmic sequences deposited by high magnitude jökulhlaup flow (Russell and Knudsen, 1999b).
- **Segmented eskers (*Type III*)** are deposited in short ice-marginal tunnels and are largely composed of gravel facies with low palaeo-flow variability (Banerjee and McDonald, 1975). Internal clasts are typically less well rounded than in *Type I* eskers, due to shorter transport distances (c.f. Brennand, 1994, 2000). Like long, continuous eskers, they are composed of a series of bedforms, including dunes, antidunes and prograding gravel bars (Banerjee and McDonald, 1975; Mäkinen, 2003), though sedimentation is argued to have taken place within a rapidly retreating ice margin (Warren and Ashley, 1994; Delaney, 2002; Mäkinen, 2003). Like continuous eskers, segmented eskers can also be composed of core gravel materials that are arranged into horizontal beds (Hebrand and Åmark, 1989; Delaney, 2001). Although the

presence of antidunes has been used to indicate the presence of a free water surface (Banerjee and McDonald, 1975), it has been subsequently argued that this is not necessarily the case (Brennand, 1994, 2000). Consequently, deposition may have taken place under either open or closed pipe conditions.

- **Short 'beaded' eskers (*Type IV*)** are deposited in ice-contact lakes and typically show high palaeo-flow variability (Banerjee and McDonald, 1975; Warren and Ashley, 1994) and rapid downstream fining (Banerjee and McDonald, 1975; Delaney, 2002; Thomas and Chiverrell, 2006; Brennand, 2007). Where 'beads' have been identified, they typically have greater sedimentary complexity than associated major esker ridge(s) (Gorrell and Shaw, 1991; Warren and Ashley, 1994). Beads are associated with terminal subaqueous fans that are largely composed of massive, plane bedded, cross-bedded and draped sand, silt and clay, including flame and water escape structures (Henderson, 1988; Delaney, 2002; Brennand, 2007), foreset beds and flow tills (Henderson, 1988; Mokhtari Fard and Ringberg, 2001; Thomas and Chiverrell, 2006). In addition, they may onlap and be connected to esker tunnel fill deposits, proximally (Thomas and Montague, 1997).

In two eskers in Ontario and Quebec, Banerjee and McDonald (1975) observed that although they differed in morphology and depositional environment, both planar bedding and cross-bedding were common. The ridges were composed of a series of bedforms including, dune trains, prograding bar fronts (foreset beds) and antidunes (backset beds) (Banerjee and McDonald, 1975). The presence of backset beds was interpreted to represent antidunes, indicating open channel flow, allowing deposition at atmospheric pressure to be distinguished from pressurised conduit deposition (Banerjee and McDonald, 1975), which has been associated with a sliding bed facies (Saunderson, 1977). The assumption that backset beds and antidunes are indicative of a free water surface, is based upon laboratory simulations of closed pipe deposition (c.f. Kennedy, 1963). This assumption, however, may be flawed, as large-scale backset bed deposition has been shown to have taken place within pressurised conduits (c.f. Brennand, 1994; Brennand and Shaw, 1996; Brennand, 2000; Delaney, 2001, 2002; Fiore *et al.*, 2002; Mäkinen, 2003; Brennand, 2007; Fleisher *et al.*, 2007; Mokhtari Fard and Gruszka, 2007), associated with migrating hydraulic jumps (Delaney, 2001; Fiore *et al.*, 2002; Delaney, 2002; Mäkinen, 2003). Furthermore, laboratory studies of closed-pipe conditions are based upon a uniform conduit, which by its nature is unable to account for flow characteristics created by non-uniform conduit geometries and it is known that antidunes may develop at a range of density interfaces (c.f. Brennand, 2000). As the logic linking the sliding bed facies to its hydraulic interpretation lacks detail, Brennand (2000) suggests that sedimentary facies are not good diagnostic indicators of depositional environment,

despite having to be consistent with it. Furthermore, studies of esker facies composition and sedimentary architecture at Victoria Island, Canada could not discriminate between depositions within pressurised or open conduits (Brennand and Sharpe, 1993).

Brennand (1994, 2000, 2007) showed that the sedimentary architecture of continuous ridge eskers (Type I) may be complex. In south-central Ontario, esker sediments show little palaeo-flow variability, consequent of the relatively constricted flow conditions (Gorrell and Shaw, 1991; Brennand, 1994). Although the eskers are composed of predominantly plane-bedded and cross-bedded sediments, they can also contain in-phase wave structures and gravel facies are commonly arranged into ridge scale bedforms (macroforms, see *Section 2.3.4*), controlled by conduit geometry (Brennand, 1994; Brennand and Shaw, 1996; Brennand, 2000, 2007; Sjogren *et al.*, 2007). Such complexities were also observed by Warren and Ashley (1994), who suggest that long eskers in Ireland show downstream variations in morphology analogous to a chute-and-pool system, which is a notion also suggested for some eskers in Switzerland (Fiore *et al.*, 2002). Delaney (2001) also documents close association between esker ridge morphology and the associated sedimentary architecture for eskers in Ireland. The sedimentary architecture of the Irish eskers includes large-scale bedforms associated with conduit geometry, likely in the form of macroforms (Delaney, 2002). This association of esker morphology and internal composition appears to be apparent in most continuous eskers, with Hebrand and Åmark (1989), suggesting that Swedish eskers are typically composed of coarse gravels where they are wider, whilst narrow segments are primarily composed of finer sands. Furthermore, a pseudoanticlinal structure has also been identified in eskers in Sweden (c.f. Mokhtari Fard, 2002) and Ireland (c.f. Thomas and Chiverrell, 2006), as well as a contemporary englacial esker in Alaska (c.f. Syverson *et al.*, 1994).

In some eskers, vertically stacked gravel-sand couplets can be observed, which display a downstream transition into varves, adding credibility to the notion that esker sedimentation occurred over several years and was controlled by supraglacial meltwater input (Gorrell and Shaw, 1991; Brennand and Sharpe, 1993; Brennand, 1994; Warren and Ashley, 1994; Brennand and Shaw, 1996; Brennand, 2000). Structural and textural variations, such as the presence of gravel-sand couplets and fines within distal fans, has been used as evidence of unsteady discharge associated with seasonal meltwater patterns and transient events such as supraglacial lake drainage (Brennand, 2000). Bimodal, matrix-supported gravels have been associated with high discharge jökulhlaup deposition (c.f. Saunderson, 1977; Lindström, 1985; Shulmeister, 1989), as have units of massive cobble and pebble gravels (Delaney, 2001, 2002). Open-framework gravels, however, may indicate winnowed (e.g. Lundqvist, 1979) or waning stage jökulhlaup (e.g. Shulmeister, 1989) deposits. Whilst depositional timescales are difficult to infer, the

complex nature of esker sedimentary architecture is often used as evidence of multi-event deposition (e.g. Gorrell and Shaw, 1991; Brennand and Sharpe, 1993; Brennand, 1994; Clark and Walder, 1994; Syverson *et al.*, 1994; Brennand and Shaw, 1996; Brennand, 2000), which has been supported by observations of some contemporary eskers, where the limited observation of bedding has been attributed to the possibility of single event deposition (c.f. Syverson *et al.*, 1994).

Esker sediments are often arranged into a series of fining upwards rhythmites (Shulmeister, 1989; Gorrell and Shaw, 1991; Brennand and Sharpe, 1993; Brennand, 1994; Warren and Ashley, 1994; Russell and Knudsen, 1999b; Delaney, 2001; Mokhtari Fard and Ringberg, 2001; Fleisher *et al.*, 2007; Grimm and Auton, 2007; Mokhtari Fard and Gruszka, 2007). These are typically inferred to represent the waning stage of multiple events (c.f. Shulmeister, 1989; Brennand and Sharpe, 1993; Brennand, 1994), though it has also been shown that such sequences can be deposited very rapidly (c.f. Allen, 1971) during flood stages (c.f. Delaney, 2001, 2002) and during a single event (Russell and Knudsen, 1999b). Thin clay beds can separate individual rhythmites, the presence of which has been argued to represent a complete shutdown in conduit discharge (c.f. Saunderson, 1975; Gorrell and Shaw, 1991; Brennand and Sharpe, 1993; Warren and Ashley, 1994). Absence of clay indicates subdued meltwater flow and flushing of fine material from the conduit (Shulmeister, 1989). Where clays are present within esker deposits, this is generally interpreted as an indicator of seasonally controlled deposition, typically from the input of supraglacial meltwater (Hebrand and Åmark, 1989; Brennand and Sharpe, 1993; Brennand, 1994; Warren and Ashley, 1994), though high discharge events have also been inferred (c.f. Gorrell and Shaw, 1991). Furthermore, rhythmites within major eskers have been argued to represent only the greatest discharge, whilst those within 'beaded' deposits may additionally include diurnally controlled rainfall events and jökulhlaups (c.f. Gorrell and Shaw, 1991; Brennand and Sharpe, 1993).

### *2.3.2 Depositional timescale and associated ice dynamics*

Although it is generally accepted that eskers are associated with ice recession (e.g. Price, 1966, 1969; Henderson, 1988), the main disparity within the literature is associated with the time scale of deposition for long eskers or '*esker trains*' (c.f. Lundqvist, 1999a, 1999b), which is suggested as either synchronous (e.g. Shulmeister, 1989; Gorrell and Shaw, 1991; Brennand, 1994; Knudsen, 1995; Brennand and Shaw, 1996; Gray, 1997; Evans *et al.*, 1999; Huddart *et al.*, 1999; Russell *et al.*, 2001a; Fiore *et al.*, 2002) or time-transgressive (e.g. Banerjee and McDonald, 1975; Ringberg, 1984; Hebrand and Åmark, 1989; Lundqvist, 1999a, 1999b; Delaney, 2001; Mäkinen, 2003; Hooke, 2007; Kehew *et al.*, 2007). Synchronous deposition usually refers to elongate sinuous ridges

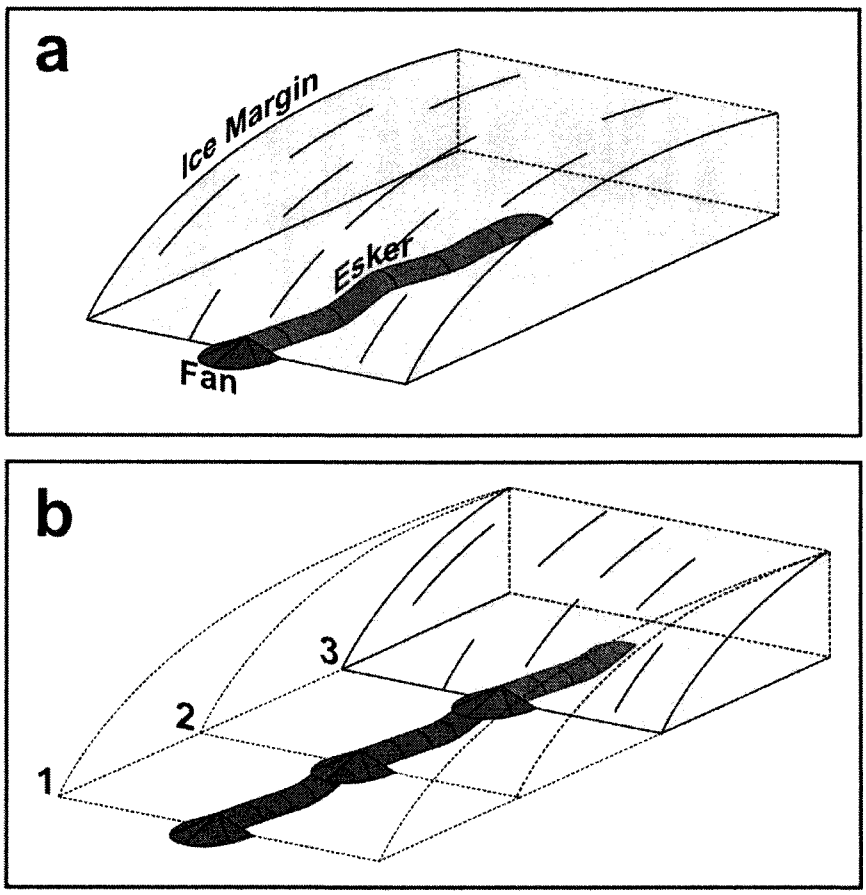


**Figure 2.11.** Schematic model representing generalized modes of esker system development. a) Synchronous deposition of an esker through a continuous conduit that may extend for tens to hundreds of kilometres from the ice margin. The esker may be continuous for its entire length, though may also include gaps of either non-deposition or post depositional erosion. Subaerial fans are found at the distal end of the ridge system, only. b) Deposition of eskers within short conduits that extend for hundreds of metres to a few kilometres from the ice margin. Rapid retreat of the ice-margin results in time-transgressive development of esker segments that form a sequential sequence of esker ridges, separated by gaps and/or subearial fans (1-3).

(that are largely continuous), with all main and tributary deposits being generated by the same events (Brennand, 2000), thus relating to a single ice-marginal position (Delaney, 2001). Time-transgressive formation refers to esker segments that are arranged sequentially,being deposited in ice-marginal locations only (Figure 2.11). The presence of gaps along esker ridges is used as evidence of time-transgressive deposition (e.g. Banerjee and McDonald, 1975; Delaney, 2001), though these gaps may equally represent non-deposition within a continuous conduit (Saunderson, 1977; Brennand and Shaw, 1996; Brennand, 2000) or syn-/post-depositional erosion (Price, 1969; Saunderson, 1977; Brennand and Shaw, 1996; Brennand, 2000; Fiore *et al.*, 2002). Under time-transgressive theory, each segment records the location of the ice margin at a point in time during deglaciation (Brennand, 2000; Delaney, 2001), perhaps showing annual rates of retreat (Mäkinen, 2003), or more prolonged periods of deposition (Hooke, 2007). Interestingly, esker morphology and size variations in Sweden have been linked to one year, three year and eleven year cycles of deposition associated with variations in meltwater input due to a single season, El Niño Southern Oscillation (ENSO) and sunspot cycles, respectively (Lundqvist, 1999a, 1999b). This, however, assumes esker sedimentation is uniform and time-transgressive, which may be rather speculative with the study being based solely on esker morphology and lacking detailed sedimentological investigations.

Further distinctions drawn by the literature are associated with ice dynamics, either being deposited within a stagnant (e.g. Flint, 1930; Price, 1966; Shaw, 1972; Shulmesiter, 1989; Brennand and Sharpe, 1993; Brennand, 1994; Brennand and Shaw, 1994, 1996; Brennand, 2000; Fiore *et al.*, 2002; Kehew *et al.*, 2007) or active (e.g. Banerjee and McDonald, 1975; Warren and Ashley, 1994; Knudsen, 1995; Mokhtari Fard and Ringberg, 2001; Mäkinen, 2003; Boulton *et al.*, 2007a, 2007b) ice mass. The traditional view is that esker deposition takes place within stagnant ice (Horne, 1923; Flint, 1928, 1930), the lack of erosion and deformation within deposits being used as evidence for the disintegration of the ice mass *in situ* (Flint, 1930). Warren and Ashley (1994), however, concluded that the sinuous tunnel-fill eskers in Ireland formed under active ice conditions, as ice closure by viscous deformation would be greater and may therefore account for the relatively narrow ridge shapes (Warren and Ashley, 1994).

In North America, like Ireland, eskers have been formed both time-transgressively and synchronously, though long sinuous eskers are typically attributed to synchronous deposition (Gorrell and Shaw, 1991; Brennand, 1994; Brennand and Shaw, 1996; Brennand, 2000). Unlike the views of Warren and Ashley (1994) for the Irish eskers, however, it is argued that within an active ice mass, R-channels would have a tendency to change their position, suggesting active ice would not be conducive in preserving intricate dendritic systems that required R-channel stability for many years (Brennand, 2000). It was demonstrated by Boulton *et al.* (2007a, 2007b), however, that perennial meltwater

streams at Breiðamerkurjökull, Iceland, remained in constant positions for at least one hundred years despite the ice being active. This is based upon the location of these perennial outlets corresponding to the major esker systems observed in the forefield (Price, 1969; Boulton *et al.*, 2007a, 2007b).

Mäkinen (2003) studied an esker segment in Finland that was part of a complex of a similar scale to those of North America, formed beneath the Fenoscandian ice sheet. Mäkinen (2003) argues, unlike most research into the eskers of North America (c.f. Shulmeister, 1989; Gorrell and Shaw, 1991; Brennand and Shaw, 1994), that the Lake Köyliönjarvi-Säkylänharju esker formed time-transgressively at a retreating interlobate, grounding-line margin. Furthermore, unlike traditional ideas of esker genesis beneath stagnant ice (c.f. Flint, 1930; Shulmeister, 1989; Fiore *et al.* 2002), it is suggested by Mäkinen (2003) that the Köyliönjarvi-Säkylänharju esker was deposited beneath active ice. It is argued by Krüger (1983), however, that the Scandinavian ice sheet, at least in Denmark, underwent retreat of an active ice margin in some localities, whilst in others the ice stagnated. Consequently, the eskers of Denmark likely formed within areas of both active and stagnant ice, rather than being restricted to an individual form of ice recession.

Hebrand and Åmark (1989) argue that time-transgressive esker deposition in Sweden was associated with both active and stagnant ice simultaneously. During esker deposition, the ice margin underwent "stagnation zone retreat" (c.f. Koteff, 1974), where a largely active ice mass is bordered by a thin marginal zone of stagnant ice (Hebrand and Åmark, 1989, Lundqvist, 1999a, 1999b). This has also been inferred for deglaciation of ice sheets in parts of North America (Koteff, 1974) and Ireland (c.f. Delaney, 2001). Hebrand and Åmark (1989) suggest that eskers in Southern Sweden were deposited sequentially upstream, with ridge deposits being representative of conduit sedimentation, with the hummocky extended materials being deposited on the surface of a thin stagnant ice zone. Koteff (1974), however, suggested some North American eskers were deposited on the surface of the stagnant zone, whilst Delaney (2001) argues for deposition beneath a stagnant ice margin.

Whilst certain esker characteristics can be used to distinguish between time-transgressive and synchronous deposition (Table 2.1), differentiating between sedimentation within active and stagnant ice is more difficult. The traditional view is that eskers are indicative of stagnant ice conditions (Horne, 1923; Flint, 1928, 1930), though arguments for an active ice scenario have subsequently been made (e.g. Banerjee and McDonald, 1975; Warren and Ashley, 1994; Mäkinen, 2003). Studies of contemporary eskers have shown that deposition takes place within an active ice margin (c.f. Lewis, 1949; Stokes, 1958; Russell and Knudsen, 1999a, 1999b; Russell *et al.*, 2001a, 2005, 2006; Boulton *et al.*, 2007a, 2007b; Fleisher *et al.*, 2007; Russell *et al.*, 2007a), though the

| | Synchronous Deposition | Time-transgressive Deposition |
|---|---|---|
| *Morphology* | • Relatively continuous ridge with 'gaps' resulting from non-deposition or post-depositional erosion within a continuous conduit<br>• Whilst lateral fans may occur, subaerial fans are only found at the most distal end of the ridge | • Relatively short ridges, punctuated by fans/deltas<br>• Typically with a beaded morphologic expression |
| *Sedimentology* | • Typically composed of coarse materials with little palaeo-flow variability<br>• Clast roundness is dependent upon transport distance.<br>• Gravel facies are arranged into ridge-scale macrofoms | • Segmental trends in sediment structure and texture, consistent with flow deceleration or entry into standing water, with high palaeo-flow variability<br>• Clast roundness is typically low<br>• Sedimentary architecture will be consistent with decelerating flow on entry into a standing water body |

**Table 2.1.** Diagnostic morpho-sedimentary criteria for determining the timescale of long dendritic esker system genesis (from Brennand and Shaw, 1996; Brennand, 2000).

suitability of modern eskers as analogous for Quaternary esker deposition has been questioned (c.f. Mokhtari Fard, 2002; Mokhtari Fard and Gruszka, 2007). It appears likely that eskers are not restricted to either active or stagnant ice conditions (Krüger, 1983; Brennand, 2000).

### *2.3.3 Transient controls on esker development*

The general consensus within the literature is that esker materials are accumulated within a channel over time (e.g. Flint, 1928, 1930; Shulmeister, 1989; Gorrell and Shaw, 1991; Brennand and Sharpe, 1993; Brennand, 1994; Warren and Ashley, 1994; Brennand, 2000; Mäkinen, 2003; Boulton *et al.*, 2007a, 2007b; Hooke, 2007; Kehew *et al.*, 2007). Eskers are typically surmised to be deposited over prolonged periods constrained by seasonal drainage patterns, which control the melting of the conduit walls, from where the esker sediments are primarily sourced (e.g. Allen, 1971; Banerjee and McDonald, 1975; Shilts, 1984; Shreve, 1985; Gorrell and Shaw, 1991; Brennand, 1994; Warren and Ashley, 1994, Boulton *et al.*, 2007a, 2007b; Fountain, 2007; Hooke, 2007; Hooke and Fastook, 2007). During the relatively short summer period, the majority of meltwater is supplied from the glacier surface via moulins and crevasses (Shreve, 1985; Boulton *et al.*, 2007a, 2007b; Hooke and Fastook, 2007), during which time the esker materials are deposited (Boulton *et al.*, 2007a, 2007b). In winter, the main source of meltwater is derived by basal ice melt, which allows the long-term development of perennial streams and continued esker growth during the following summer (Boulton *et al.*, 2007a, 2007b). Whilst steady-state theories of esker development are commonplace (e.g. Shreve, 1985; Hooke, 2007; Hooke and Fastook, 2007), in some studies, evidence has been presented to suggest that deposition took place from high energy, possibly jökulhlaup flows (e.g. Saunderson, 1977; Shulmeister, 1989; Gorrell and Shaw, 1991; Russell, 1994; Delaney, 2001; Mokhtari Fard, 2001; Russell *et al.*, 2001a; Delaney, 2002; Mokhtari Fard, 2002; Russell *et al.*, 2005, 2006, 2007a).

Evidence for high energy deposition largely comes from the presence of units composed of coarse and boulder sized materials (e.g. Shulmeister, 1989; Gorrell and Shaw, 1991; Thomas *et al.*, 2007), as well as poorly stratified units of massive pebble to cobble gravels interpreted to represent rapid deposition from hyperconcentrated flows (e.g. Saunderson, 1977; Delaney, 2001, 2002; Mokhtari Fard, 2002; Delaney, 2007). The notion of high energy deposition within eskers is substantiated by the presence of beads along some eskers in North America, which is suggestive of the ice being close to flotation (c.f. Gorrell and Shaw, 1991; Brennand, 1994).

Eskers in North America are often found within tunnel channels (c.f. Brennand and Sharpe, 1993; Brennand and Shaw, 1994; Fisher *et al.*, 2005; Kehew *et al.*, 2007; Sjogren *et al.*, 2007) that may have formed during catastrophic drainage events (c.f. Brennand and

Sharpe, 1993; Brennand and Shaw, 1994; Fisher *et al.*, 2005; Russell *et al.*, 2007a). Shulmeister (1989) carried out a study of several exposures along the Tweed esker in southern Ontario (also located in a tunnel channel), and concluded that the sedimentary sequences in the deposits formed via fluviatile sedimentation that is suggested to have taken place during several "catastrophic" flood events occurring throughout the deglaciation of a regionally stagnant ice mass. This argument suggests that a single jökulhlaup would have deposited a single sedimentary unit, with multiple events thus resulting in esker build up. This is supported by Brennand (1994), who suggests that most deposition will take place during the waning-stage of a jökulhlaup where individual gravel-sand couplets may indicate a single jökulhlaup.

The significance of jökulhlaups during esker deposition is further supported by the work of Gorrell and Shaw (1991) from eskers in Southern Ontario. The presence of morphological widenings, termed 'beads', along the length of the esker, coupled with their sedimentary architecture are interpreted as evidence of deposition during high water pressure events when the ice is locally close to flotation (Figure 2.12). Although Brennand (2000) is in agreement that the presence of 'beads' along the length of long, continuous eskers is indicative of jökulhlaup deposition, it is suggested that the major form of an esker is driven by variations in seasonal melt patterns, though jökulhlaups from supraglacial lakes may have deposited some gravel-sand couplets. The unsteadiness in meltwater discharge is linked to variations in subglacial water pressure and results in the formation of 'beads' close to the ice margin during transient conditions (Gorrell and Shaw, 1991; Brennand, 2000), typically along bends in the esker path, where water pressure is higher (Gorrell and Shaw, 1991; Brennand and Sharpe, 1993). When discharge reduces, these marginal cavities become cut off due to reformation of a pressurised seal at the conduit margin (Gorrell and Shaw, 1991; Brennand, 1994). These cavities may consequently remain water-filled and form points of weaknesses that become reactivated during subsequent jökulhlaups, allowing rhythmically bedded deposits to be generated over multiple jökulhlaups (Brennand, 1994). For an esker system in Southern Ontario, it was shown that 'beads' contain the most complex sedimentary sequences, with deposition being associated with hydraulic jumps created by flow into standing water bodies.

For Quaternary eskers, however, even when jökulhlaups have been inferred as the mechanism of esker deposition, the complex sedimentary architectures often observed (e.g. multiple units separated by numerous unconformities), have been used as evidence of multiple event deposition (c.f. Shulmeister, 1989; Gorrell and Shaw, 1991; Brennand, 1994). The study of contemporary eskers have recently shown that eskers, bearing structural resemblance to Quaternary eskers, can be deposited during a single high-magnitude jökulhlaup (Russell and Knudsen, 1999a, 1999b; Russell *et al.*, 2001a, 2005,

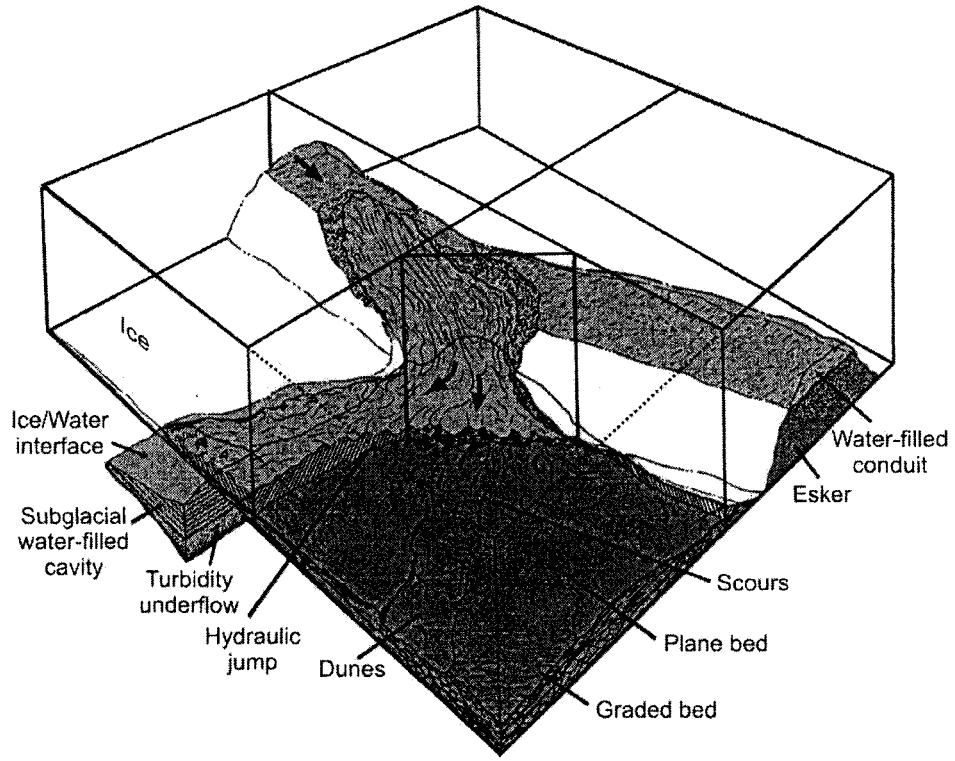


**Figure 2.12.** Near to a grounding line that is close to flotation, transient increases in subglacial water pressure result in hydraulic lifting and the formation of lateral subglacial fans (from Brennand, 2000, after Gorrell and Shaw, 1991).

2006; Fleisher *et al.*, 2007; Russell *et al.*, 2007a). Whilst single events have been cautiously inferred for some Quaternary eskers in Sweden (c.f. Mokhtari Fard, 2001, 2002), lending support to the significance of jökulhlaups in esker deposition, the lack of direct observations mean depositional timescales can only be inferred. Consequently, in most cases rhythmically bedded deposits of jökulhlaup origin are interpreted as the product of multiple events (c.f. Shulmeister, 1989; Brennand and Sharpe, 1993; Brennand, 1994), though Allen (1971) showed that individual beds may be deposited over a period of hours to tens of hours, consistent with timescales for rhythmite deposition during a single jökulhlaup (c.f. Russell and Knudsen, 1999b).

It appears that no diagnostic criteria exist that can distinguish between jökulhlaup deposition and sedimentation controlled by seasonal drainage patterns. This is exemplified by Brennand and Shaw's (1994) suggestion that eskers in southern Ontario may represent a return to seasonally controlled subglacial drainage (R-channels) within tunnel channels following the large jökulhlaup (the Algonquin event) that eroded them (Brennand and Shaw, 1994). In contrast, the works of Shulmeister (1989), and Gorrell and Shaw (1991) argue these eskers are generated by multiple jökulhlaups. Similarly, Warren and Ashley (1994) suggest seasonally controlled drainage patterns are responsible for Irish esker deposition, whilst Delaney (2001, 2002) argue that the Irish eskers display a sedimentary architecture more consistent with deposition during jökulhlaup flows. From our current understanding and lack of suitable contemporary analogues, however, it is difficult to refute either hypothesis.

### *2.3.4 Models of esker deposition*

Whilst the sedimentary architectures of eskers are widely documented, the processes controlling the sedimentary environment during rapid deglaciation are not fully understood (Mokhtari Fard, 2002). Only a handful of sedimentological models have been put forward for esker genesis (Banerjee and McDonald, 1975; Brennand, 1994; Brennand and Shaw, 1996; Brennand, 2000; Fiore *et al.*, 2002). It has been argued, however, that no universally applicable model exists for the origin of eskers (Mokhtari Fard and Gruszka, 2007). In their seminal paper, Banerjee and McDonald (1975) proposed three models of esker sedimentation (Figure 2.13):

1. Open channel, where sedimentation takes place at atmospheric pressure allowing the deposition of antidunes. In addition, depositional units would be lenticular in transverse section and more tabular in longitudinal profile;
2. Pressurised subglacial tunnel where deposits consist of tabular and relatively continuous units of planar or cross-bedded sediments. There is also a distinct lack of fine material or major variations in palaeo-current direction.

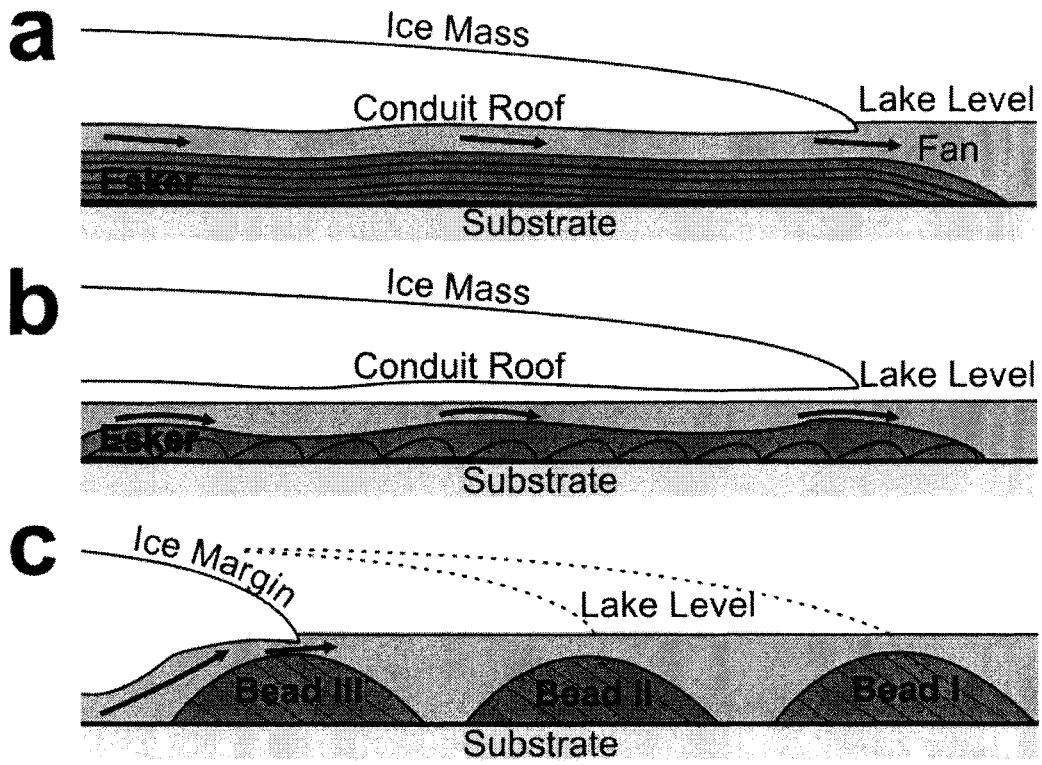


**Figure 2.13.** Schematic representation of the three esker depositional models, put forward by Banerjee and McDonald (1975). a) Sedimentation within a pressurised conduit (full-pipe) results in the deposition of relatively planar and cross-bedded sediments. b) Sedimentation within an open-pipe takes place at atmospheric pressure, allowing the deposition of antidunes that are in-phase with the water surface. c) The deltaic model involves time-transgressive deposition of individual beads that may or may not overlap to form a continuous ridge. Discharge from a conduit feeder into stagnant water results in the deposition of deltaic deposits that show rapid downstream fining and high palaeo-flow variability.

3. Deltaic eskers are typically beaded in character, with rapid downstream facies changes from proximal gravels, to lacustrine silts and clays. Additionally, palaeo-current directions show great variability.

These models distinguish between pressurised deposition, sedimentation at atmospheric pressure and sedimentation from a conduit into an ice-marginal water body. The work of Brennand (1994, 2000) and Brennand and Shaw (1996) suggests that sedimentary architectures of conduit fills are more variable than is suggested by the Banerjee and McDonald (1975) triple model approach. Three models of esker sedimentation have been proposed (Figure 2.14), based upon the study of large subglacial esker systems deposited by the Laurentide ice sheet (c.f. Brennand, 1994; Brennand and Shaw, 1996; Brennand, 2000):

1. Composite macroforms (Figure 2.14a) are depositionally complex and are composed of stacked gravel and sand facies. They develop by deposition in zones of flow expansion at the point of conduit widening. Due to lower flow velocities within the expansion environment, low-angled backset beds (5°-10°) are deposited at the proximal end of the cavity, sediments become finer downstream and the lee-side of the bedform may demonstrate higher-angled down-flow dipping beds. Rapid sedimentation is simultaneous with upward and lateral melting of the conduit walls as the macroforms develop. The location and sedimentary architecture of composite macroforms was initially controlled by conduit geometry and sediment supply, and later by the interaction between the macroform and conduit geometry. Lateral faulting can be associated with removal of the supporting ice walls either subsequent to esker deposition, or due to rapid enlargement of the conduit.
2. Oblique accretion avalanche bed macroforms (Figure 2.14b) demonstrate high-angle, inclined surfaces and occur at zones of slight expansion along relatively continuous, narrow conduits. Bedforms associated with these deposits demonstrate crest lines oblique to the predominant flow direction. It is suggested, therefore, that these macroforms develop by the deposition of migrating alternating bars that climb over pre-existing deposits resulting in net accretion. This macroform is analogous to alternating bars within braided stream deposits, though can be distinguished as a conduit deposit due to the presence of a steep avalanche face at the forward margin of the oblique bars.
3. Pseudoanticlinal macroforms (Figure 2.14c) develop by sedimentation in a geometrically narrow and uniform conduit, with the esker displaying slightly arched or anticlinal bedding in cross-section. The downflow sediment fabric demonstrates crest-convergent flow associated with secondary currents or vortices within the uniform conduit. They are typically observed along ridges with a geometrically uniform conduit

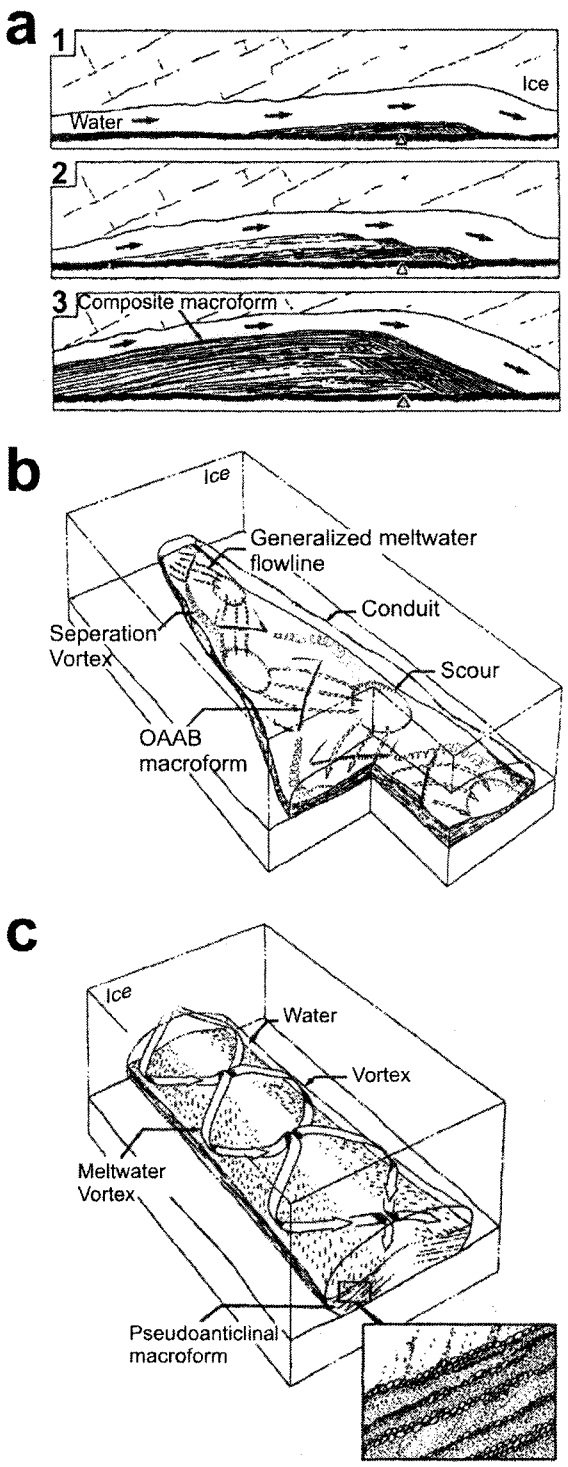


**Figure 2.14.** Models for macroform development in long, continuous (*Type I*) eskers (from Brennand and Shaw, 1996; Brennand, 2000). a) Incremental formation (1-3) of a composite macroform, within a conduit enlargement. b) Formation of an oblique-accretion, avalanche bed (OAAB) macroform. These macroforms are related to the combined effects of separation vortices at the bedform lee and convergence scours. These are expected where macroforms migrate into conduit enlargements. c) Deposition of pseudoanticlinal macroforms related to paired vortices of similar power in a uniform conduit.

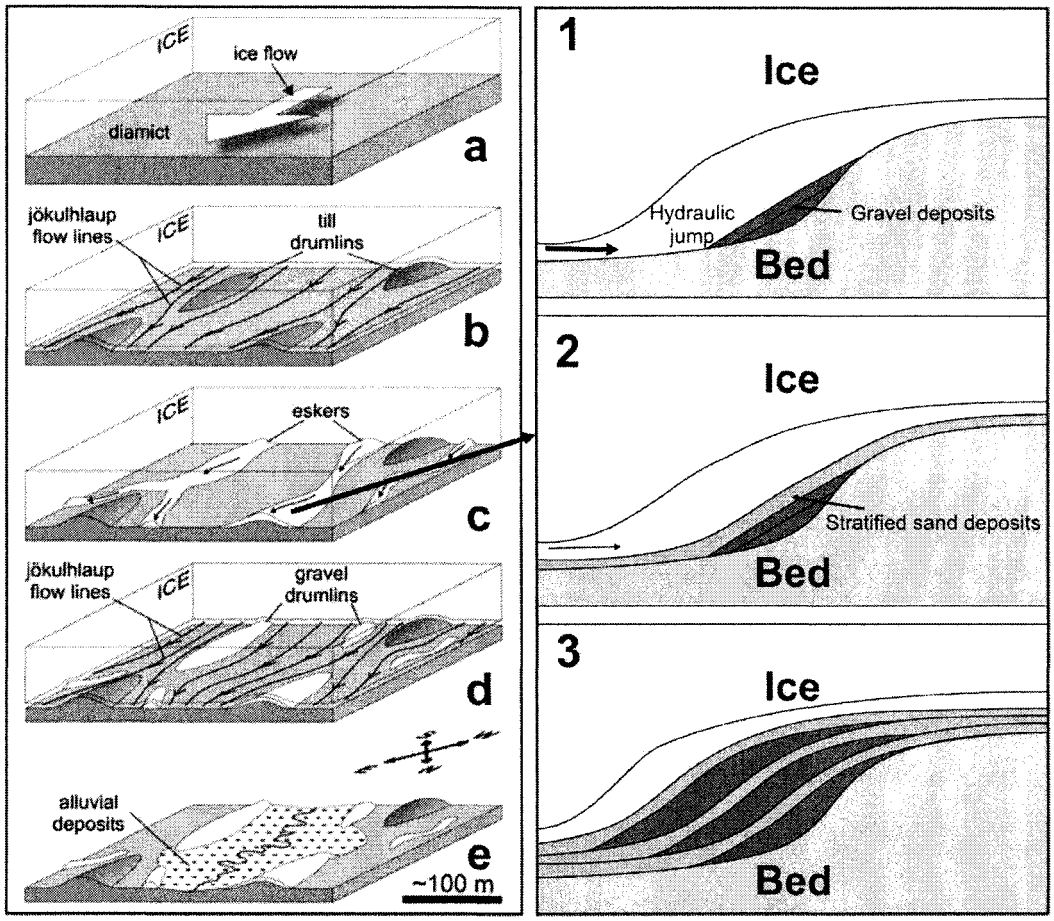


**Figure 2.15.** Schematic model showing the development of Joux Valley eskers (from Fiore *et al.*, 2002). a) Till deposition by flowing ice. b) Jökulhlaup sheet flow resulted in till drumlin formation. c) Esker deposition subsequently took place within stagnant ice: 1) High flow energy into a hydraulic jump resulting from a conduit enlargement resulted in the deposition of gravel backset beds; 2) Reduced flow energies resulted in the deposition of sand dominated backset beds; 3) Deposition of gravel and sand backsets took place concomitant to conduit growth and upstream migration of the hydraulic jump. d) A further jökulhlaup(s) partially eroded the eskers, leading to the formation of gravel drumlins. e) Subsequent to ice retreat, alluvial sediments were deposited within the valley by the current river.

that do not vertically or laterally narrow or widen, and were deposited by powerful flows.

Fiore *et al.* (2002) identified a sedimentary architecture associated with composite macroform development within esker deposits in Joux valley, Switzerland. Fiore *et al.* (2002) argue that esker ridge deposition took place in a 'chute-and-pool' system (Figure 2.15), with backset beds being deposited within conduit enlargements (pools) and planar deposition taking place in the shallower, connecting conduits (chutes). Similar chute-and-pool conditions have been suggested for continuous eskers in Ireland (Warren and Ashley, 1994) and based upon the morpho-sedimentary descriptions of eskers in both North America and Europe, it is possible that macroforms will be a widespread phenomenon (e.g. Hebrand and Åmark, 1989; Shulmeister, 1989; Gorrell and Shaw, 1991; Lindström, 1993; Delaney, 2001, 2002; Mokhtari Fard, 2002).

Although the models presented by Banerjee and McDonald (1975), Brennand (1994), Brennand and Shaw (1996), Brennand (2000) and Fiore *et al.* (2002) were based upon detailed sedimentological investigations, they are unable to specify the timescale for deposition. Mäkinen (2003) presented a depositional model for an esker in Finland where deposition was proposed to be time-transgressive at the juxtaposition of retreating ice streams. Each conduit fill is proposed to represent rapid, steady state ice-marginal sedimentation associated with seasonal melt patterns linked to deglaciation (Mäkinen, 2003). It is suggested here, that the interlobate system developed time-transgressively, via the deposition of summer (gravels), winter (silts and clays) and spring (sand) lithofacies as a single segment of the overlapping ice-marginal deposits (Mäkinen, 2003). As the ice margin retreated, further segments were developed annually, onlapping and eroding older deposits to form the continuous esker ridge (Figure 2.16). The correspondence of the size of the segments and annual retreat rates of the ice margin, allowed the presentation of a time-transgressive model that can be directly linked to seasonal melt patterns associated with the rapid retreat of the European ice sheet in Scandinavia (Mäkinen, 2003).

### 2.4 Controls on Esker Sedimentary Architecture

Table 2.2 provides a summary of the current understanding of controls on the sedimentary architecture of ablation controlled and transient controlled eskers. Although eskers have been studied extensively, no single model of esker deposition is universally applicable to esker genesis. Consequently, esker sedimentation has been linked to both seasonal ablation patterns (e.g. Banerjee and McDonald, 1975; Boulton *et al.*, 2007a, 2007b) and multiple jökulhlaups (e.g. Shulmeister, 1989; Gorrell and Shaw, 1991). Although Mäkinen (2003) suggested generalisations of esker sedimentology are difficult to make, Brennand (1994), Brennand and Shaw (1996) and Brennand (2000) identified a

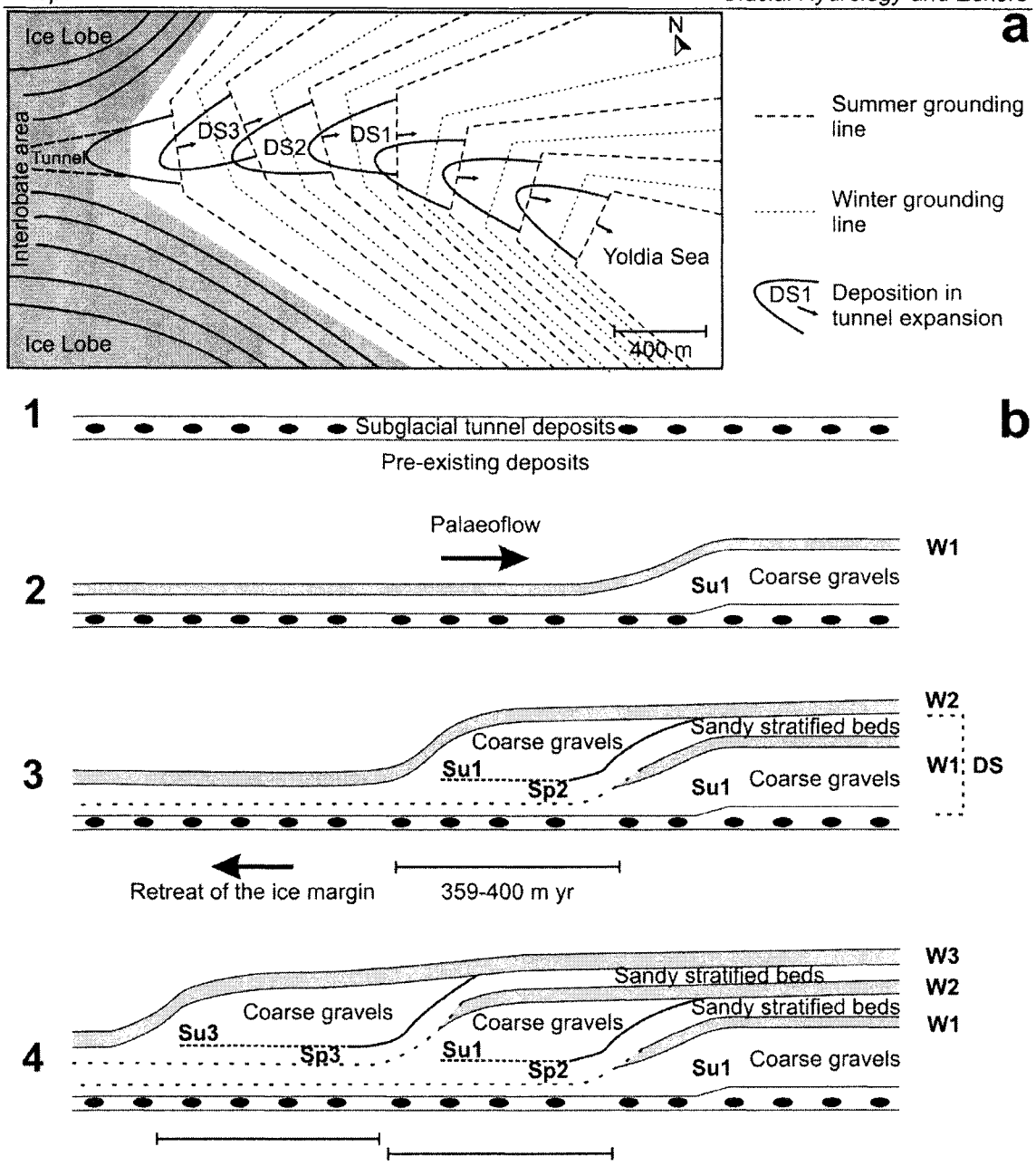


**Su1-3** = Summer deposits. Material fining from proximal cobble-boulder to medial gravelly sands

**W1-3** = Winter deposits. Material fining from proximal medium-coarse sand to medial-distal fines

**Sp2-3** = Spring deposits. Material fining from proximal cobble-boulder gravel to medial sands

**DS** = Depositional sequence

**Figure 2.16.** Schematic model for the development of the Köyliönjärvi-Sakylänharju esker segment (from Mäkinen, 2003). a) Diagram demonstrating the time-transgressive pattern of depositional sequences within the interlobate esker. b) A simplified model for the deposition of the esker segment (DS1-3 in (a)). The model shows the time-transgressive deposition of the seasonally controlled lithofacies associations: 1) synchronous deposition of subglacial closed conduit deposits; 2) deposition of coarse gravels (summer), draped by fines (winter) at the tunnel expansion, associated with the grounding line of the ice mass; 3) Rapid glacier retreat results in headward migration of the grounding, resulting in upstream deposition of the lithofacies associations; 4) continued ice-marginal retreat results in time-transgressive deposition of the lithofacies associations on a seasonal time-scale (DS1-3 in (a)).

| | | Ablation Controlled | | Jökulhlaup Controlled | | Product of control |
|---|---|---|---|---|---|---|
| | *Mechanism* | *Observations* | *Limitations* | *Observations* | *Limitations* | |
| **Conduit Geometry** | Conduit Closure | Fundamental in ablation controlled esker literature (e.g. Shreve, 1985; Hooke and Fastook, 2007) | Assume constant steady-state full-pipe conditions , which is unlikely (Hooke, 1984) | Important in jökulhlaup models (e.g. Nye, 1976; Flowers *et al.*, 2004) | Jökulhlaup conduit diameter is less than esker cross-sectional area (Clarke & Walder, 1994) | Macroform type |
| | Frictional Melting | | | | | |
| | Ice Flotation | | | Negative *Pe* near glacier margin locally floats ice | Mechanism restricted to ice-marginal sections | |
| | Drainage Confluence | • Conduit widening linked to presence of moulin (Brennand, 2000)<br>• Esker enlargement linked to converging eskers (Lindström, 1993) | Lack direct control and are based upon esker morphology and are based upon glacial hydrology observed at valley glaciers | | | |
| **Flow Conditions** | Mode of sediment transport | Bedload transport (Brennand, 1994, 2000) | Lacking rigorous constraints on flow conditions during deposition | Transport in suspension (e.g. Saunderson, 1977; Mokhtari Fard, 2002) | Could occur at lower flow regimes, if the dominant clast size is small | Depostional style (i.e. traction carpet, lag boulders, hyperconcentrated flow) |
| **Sediment Supply** | Sediment availability | Local variations in the size of an esker (Brennand and Sharpe, 1993) | Lack of control on esker formation | | | Esker size |
| | Sediment size | Units composed of silts and clays used as evidence of winter deposition (e.g. Warren & Ashley, 1994; Mäkinen, 2003) | • Lack of depositional timescale<br>• Supply limitations have not been considered | Clay identified as waning stage deposit (Gorrell & Shaw, 1991) | Lack of direct knowledge of depositional events (Gorrell & Shaw, 1991) | Esker size and dominant clast size |

**Table 2.2.** Summary of possible controls on the sedimentary architecture of ablation and transient-controlled eskers, based upon the current understanding from the esker literature. Observations linking to the controlling mechanisms are given, as are the limitations of the observations. The product of control can be linked to the linked to the mechanism.

number of ridge scale macroforms that can be observed in North American eskers suggesting they are fundamentally controlled by conduit geometry, which is primarily governed by the water flux through the conduit (Röthlisberger, 1972; Shreve, 1972). Within the esker literature four fundamental mechanisms that govern conduit geometry have been investigated:

1. *Conduit closure* is determined by the rate of ice deformation into the conduit (Röthlisberger, 1972; Shreve, 1972). This is typically less than the rate of conduit growth due to frictional melting (see below) and so is most likely to be influential during winter (Hooke, 1984). It has been noted that the core of some esker may display deformation, assumed to be associated with conduit closure (Brennand, 2007). Although Nye (1976) modelled exponentially rising jökulhlaups from Grímsvötn, including conduit closure rate, it is unclear to what extent this will effect conduit geometry over the relatively short timescales of a jökulhlaup.
2. *Frictional melting* is determined by the rate of water flow through the conduit (Röthlisberger, 1972; Shreve, 1972). This is the most fundamental factor governing the geometry of a conduit (e.g. Brennand, 2000; Boulton *et al.*, 2007a, 2007b; Hooke and Fastook, 2007) and is also important in the enlargement of conduits during exponentially rising jökulhlaups (Nye, 1976).
3. *Ice flotation* was shown by Gorrell and Shaw (1991) to be influential in creating local variations in conduit geometry. Although it has not been applied to ablation controlled eskers, Gorrell and Shaw (1991) and Brennand (1994) argued that during a jökulhlaup the low effective pressures result in localized flotation of marginal ice forcing deposition in a conduit widening.
4. *Drainage confluences*, including input from moulins (e.g. Brennand, 2000) and from branches of dendritic esker networks (e.g. Lindström, 1993). This can result in morphological widenings along eskers ridges during ablation controlled discharge, though this has not been investigated for transient controlled eskers.

On a smaller scale, esker sedimentary architecture is controlled by meltwater flow conditions, identified by variations in bedload or suspension transport (Brennand, 1994, 2000), though this has received less attention than conduit geometry. This is due to the lack of rigorous constraints on depositional timescales or detailed insight into the processes responsible for esker sedimentation during jökulhlaups. The identification of hyperconcentrated flow deposits within eskers has been used to infer sediment transportation in suspension (e.g. Saunderson, 1977). It has been suggested that such deposits are indicative of jökulhlaup controls during esker deposition (e.g. Delaney, 2001, 2002; Mokhtari Fard, 2002), though finer grained materials could be transported in suspension by lower flow regimes and this has not been considered.

Although receiving less attention than conduit geometry, sediment supply has also been suggested to play a role in the sedimentary architecture of both ablation and transient controlled eskers (e.g. Gorrell and Shaw, 1991; Brennand and Sharpe, 1993; Warren and Ashley, 1994; Mäkinen, 2003), through two mechanisms:

1. *Sediment availability* was used as an explanation for local variations in the size of eskers by Brennand and Sharpe (1993). This study, however, was based upon morphology rather than sedimentology and so, the depositional environment was not considered.
2. *Sediment size* within depositional units has been used to infer the mode of esker genesis. Where eskers contain units of silts and clays, a number of studies have inferred this represents deposition during winter (e.g. warren and Ashley, 1994; Mäkinen, 2003), though Gorrell and Shaw (1991) suggested that silts and clays could be deposited on the waning stage of jökulhlaups. Unfortunately, the lack of a depositional timescale makes it difficult to refute either hypothesis and sediment supply limitations have not been considered.

Although eskers have been studied extensively, few have attempted to characterize the large-scale sedimentary architecture of specific esker types. Consequently, the controls on esker sedimentary architecture for both ablation- and transient controlled eskers are not fully understood. This is exemplified by the significant gaps and lack of detail concerning the controls on esker sedimentary architecture, which are summarized in Table 2.2.

## 2.5 Summary

The sub- or englacial conduits in which many eskers were deposited are assumed to be maintained by a balance between frictional melting of the conduit walls and conduit closure due to viscous deformation (Rötjlisberger, 1972; Shreve, 1972). Under steady-state theory, which is inapplicable to jökulhlaups, variations in discharge through the conduits result in variations in conduit geometry, with the direction of flow being normal to equipotential surfaces within the ice (Shreve, 1972). The subglacial hydrological system can be classified as either arborescent or non-arborescent (Hubbard and Nienow, 1997). The arborescent system may be composed of R-channels, N-channels or H-channels, whilst the non-arborescent system includes water films, linked cavities, canals or groundwater flow. The traditional view of the englacial drainage system is that supraglacial meltwater plunges into the glacier through open crevasses and moulins, forming an upward branching arborescent network of englacial conduits that feed into subglacial conduits, discharging meltwater to the glacier margin (Shreve, 1985). More recent observations from alpine glaciers has shown that englacial conduits are often

gently inclined, with water flowing along the base of interconnected crevasses (Fountain *et al.*, 2005a, 2005b) and it is known that where the glacier bed is overdeepened, meltwaters will be discharged through englacial, rather than subglacial conduits (e.g. Kirkbride and Spedding, 1996). These observations, however, have only been applied to steady-state conditions and more recently, Gulley and Benn (2007) observed that englacial conduits that drained supraglacial lakes were located along areas of englacial structural weakness. The conduits developed from initial discharge along debris-filled structure, with conduit enlargements being linked to gravitational collapse and mechanical excavation of highly weakened glacier ice (Gulley and Benn, 2007). Although traditional glacial hydrological theory is applied to steady-state scenarios, it is known that such scenarios are often not the norm and transient events can be common at some glaciers, with stored water being released as jökulhlaups. The traditional view of jökulhlaup hydrology assumes that conduits are controlled by a balance between frictional melting and conduit closure (e.g. Nye, 1976). This, however, is only applicable to jökulhlaups that display a gradual rise in discharge and events with short rising stages cannot be expelled by perennial conduits alone (Roberts, 2005). During such events, the effective pressure is negative and water can be forced to high elevations within the ice column via hydraulic jacking, hydrofracturing and retorfeeding of open crevasses and moulins (e.g. Roberts *et al.*, 2000a, 2000b, 2001). High capacity conduits (primary conduits) and supraglacial ice-walled canyons later develop due to predominantly mechanical excavation of glacier ice, which is associated with significant ice-block release (e.g. Tweed and Russell, 1999).

Whilst eskers have been formed during both ablation controlled (e.g. Shreve, 1985; Boulton *et al.*, 2007a, 2007b) and transient controlled (e.g. Shulmeister, 1989; Gorrell and Shaw, 1991) conditions, the general consensus is that they were deposited over multiple events (e.g. Clark and Walder, 1994; Brennand, 1994; Boulton *et al.*, 2007a, 2007b) and no single model can account for all modes of esker deposition (Mäkinen, 2003). Eskers can, however, be broadly grouped into four main types: long continuous eskers (type I), ice-walled channel fills (type II), segmented eskers (type III), or short 'beaded' eskers (Type IV). They are dominantly composed of clays, silts, sands, gravels and boulders that can be arranged into trough-cross beds, antidunes, horizontal beds, backset beds, foreset beds, or units completely lacking stratification (e.g. Brennand, 2000). Whilst it is generally accepted that eskers are deposited during glacier recession (e.g. Henderson, 1988), the timescale of deposition is contentious, with some eskers being argued to have been deposited synchronously (entire esker systems deposited by the same events) or time-transgressively (esker segment deposited separately as the ice margin retreats). It is likely that neither scenario is applicable to all eskers (Brennand, 2000) and morpho-sedimentary criteria have been put forward to distinguish between the two esker forms during field studies (c.f. Brennand and Shaw, 1996; Brennand, 2000). As

yet, however, such criteria are not available to distinguish between ablation controlled and transient controlled eskers. Although the sedimentary architecture of eskers is widely documented, only a handful of sedimentological models have been presented (e.g. Banerjee and McDonald, 1975; Brennand, 1994; Brennand and Shaw, 1996; Brennand, 2000; Fiore *et al.*, 2002; Mäkinen, 2003). These models, though based upon detailed sedimentological investigations, are founded upon the study of Quaternary eskers and consequently, lack rigorous constraints on depositional timescale and may be site specific. The most useful models to broader studies of esker sedimentary architecture, perhaps, are those presented by Brennand (1994), Brennand and Shaw (1996) and Brennand (2000), which suggest eskers can be arranged into ridge scale macroforms that vary with conduit geometry and concomitant flow conditions: composite and oblique accretion avalanche bed macroforms develop at conduit enlargements, and pseudoanticlinal macroforms develop in narrow conduits and zones of more constricted flow. Although these models are based upon esker observations in North America, similar macroforms have also been identified in Europe (e.g. Fiore *et al.*, 2002).

The most fundamental control on esker sedimentary architecture for both ablation- and transient controlled eskers, is conduit geometry. Variations in conduit geometry govern the large-scale (ridge scale) sedimentary architecture of an esker and is dependent upon: rates of frictional melting and conduit closure, localized ice flotation and drainage confluences. On a smaller scale, esker sedimentary architecture can be controlled by flow conditions and sediment supply, though these have received less attention than conduit geometry.

This thesis will attempt to address the significance of the potential controls on jökulhlaup esker sedimentary architecture identified here (Table 2.2), by comparing the sedimentary architecture of eskers generated during jökulhlaups at Skeiðarárjökull and Bering Glacier. The identification of criteria diagnostic of jökulhlaup deposition in eskers will provide a basis for establishing the significance of transient events in palaeo-esker deposition. It can be seen in Table 2.2 how there are a number of areas of the controls on esker sedimentary architecture that need further investigation. Only through the analysis of eskers that have well constrained depositional timescales can this be achieved.

# Chapter 3

# Field Site Description

### 3.1 Introduction and Site Selection

Despite being located in distinctly different geologic settings, Skeiðarárjökull and Bering Glacier share a similar history of glacial events and display unique characteristics uncommon to most other glacial systems (Fleisher *et al.*, 2004). Both are temperate, surge-type glaciers, occupying overdeepened basins and are the outlet source of periodic jökulhlaups (Fleisher *et al.*, 1998, 2004; Russell *et al.*, 2006). At both glaciers high-pressure jökulhlaup discharge has created a distinctive suite of landforms and deposits consisting of sediment-filled hydrofractures, eskers, supraglacial ice-walled canyon fills as well as ice-contact outwash deposits displaying ice block obstacle marks and kettle holes (Fay, 2002a, 2002b; Russell and Knudsen, 1999a, 1999b; Fleisher *et al.*, 2004, 2007). Eskers are currently melting out at the margins of Skeiðarárjökull, Iceland and Bering Glacier, Alaska that were deposited during single jökulhlaups (c.f. Fleisher *et al.*, 2004; Russell *et al.*, 2005, 2006; Fleisher *et al.*, 2006a, 2007; Russell *et al.*, 2007a).

This chapter will discuss relevant background information to both Skeiðarárjökull (*Section 3.2*) and Bering Glacier (*Section 3.3*). As well as briefly describing the glacial history at both field sites (*Sections 3.2.1 and 3.3.1*), attention will be given to surge (*Sections 3.2.2 and 3.3.2*) and jökulhlaup (*Sections 3.2.3 and 3.3.3*) history. The field sites at Skeiðarárjökull (*Section 3.2.4*) and Bering Glacier (*Section 3.3.4*) will be then be discussed.

### 3.2 Skeiðarárjökull, Iceland

At present, approximately 11 % of Iceland is glaciated (Guðmundsson, 2005), made up of a small ice cap (Drangajökull) and cirque glaciers in the North, and larger ice caps including Eyafjalljökull, Mýrdalsjökull and Vatnajökull, in the south (Björnsson, 1980). The Vatnajökull ice cap (8, 300 $km^2$) accounts for over 70% of Iceland's glacier cover and although its average thickness is approximately 420 m, it can reach up to 1.1 km in places and is the largest ice cap in Europe (Björnsson, 1980). Some of Iceland's most active glaciers can be found on the southern slopes of Vatnajökull as a result of large accumulation rates (Björnsson, 1980).

Skeiðarárjökull, a temperate piedmont glacier, is one of the largest outlets (1, 370 $km^2$) of Vatnajökull (Roberts, *et al.*, 2000b; Russell, *et al.*, 2006) (Figure 3.1) and it's most

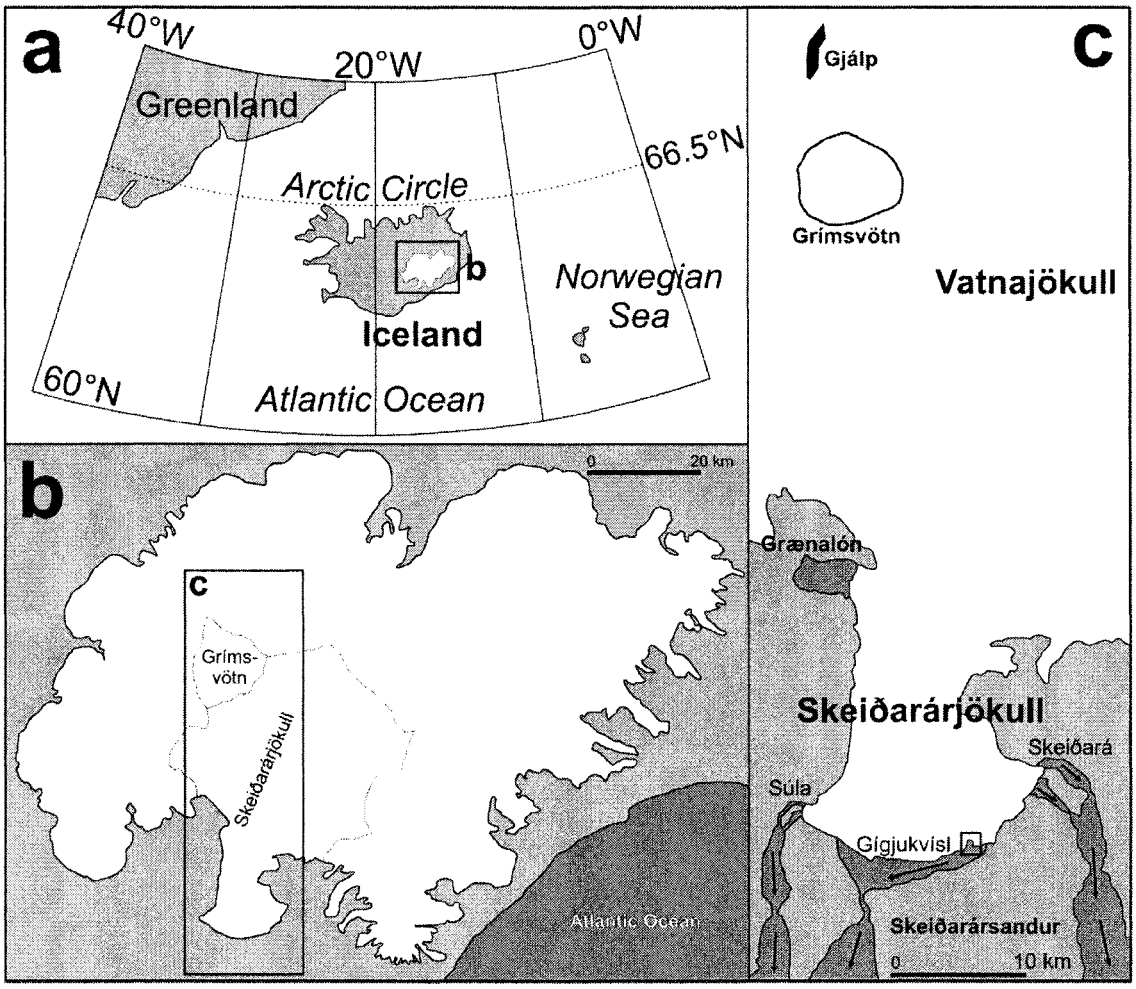


**Figure 3.1.** a) Location of Iceland; b) Vatnajökull Ice Cap, showing the location of Skeiðarárjökull and Grímsvötn; c) Skeiðarárjökull, showing the location of ice-marginal lake Grænalón, subglacial lake Grímsvötn, the 1996 eruption site (Gjálp) and peak flood routing (darker shading with arrows) from the main outlets. The box indicates the location of the ice-walled canyon (Figure 3.4) excavated during the 1996 Skeiðarárhlaup and the field site of this research (from Russell *et al.*, 2006).

hydrologically active (Flowers *et al.*, 2003). It is composed of three ice streams (van Dijk, 2002), expanding from a 10-15 km wide upland valley into a 22 km lobe (Figure 3.1), where they front onto Skeiðarársandur, the world's largest, active proglacial outwash plain (>1000 $km^2$). Skeiðarárjökull is drained by three main rivers (Figure 3.1c) that discharge 20 km across Skeiðarársandur to the coast (Guðmundsson *et al.*, 2003). The West is drained by the Súla, the central-west by the Gígjukvísl and the east by the Skeiðará (Guðmundsson *et al.*, 2003).

In addition to being of surge-type, the high precipitation, frequent subglacial volcanic eruptions and enhanced geothermal heat flux of Iceland, result in Skeiðarárjökull being a frequent outlet source of jökulhlaups (Russell, *et al.*, 2006). Both surging and jökulhlaups at Skeiðarárjökull have been responsible for the genesis of ice-marginal landforms (c.f. Russell, *et al.*, 2001b; Russell, *et al.*, 2006), though Skeiðarársandur is dominantly composed of jökulhlaup deposits (Björnsson, 1980; Guðmundsson *et al.*, 2003; Cassidy *et al.*, 2003).

### *3.2.1 Icelandic glacier fluctuations*

Icelandic glaciers are highly responsive to climate changes (Björnsson, 1980). The Last Glacial Maximum (LGM) in Iceland was reached at around 21 k yr BP (Hubbard *et al.*, 2006) when it was mantled by ice masses that stretched to the continental shelf and neighbouring islands (Figure 3.2) (Björnsson, 1980; Hubbard *et al.*, 2006; Hubbard, 2006). Models show that the LGM Icelandic ice sheet had an average thickness of 940 m and a maximum plateau elevation of ~2, 000 m (Hubbard *et al.*, 2006). Its retreat began prior to 13 k yr BP (Gudmundsson, 1997), though recession was temporarily halted by re-advances taking place around 12.5-12 k yr BP (Older Dryas) and 11-10 k yr BP (Younger Dryas) (Björnsson, 1980; Ingólfsson *et al.*, 1997).

During the Younger Dryas, re-advances resulted in the ice sheet reaching close to or beyond the present shoreline (Ingólfsson *et al.*, 1997). Although rapid retreat ensued with the onset of the Holocene, around 10 k yr BP (Björnsson, 1980), a short-lived early Preboreal advance temporarily halted deglaciation, dated at around 9.7 k yr BP (Ingólfsson *et al.*, 1997). Subsequently, retreat continued and by ~8 k yr BP all ice had disappeared from the area at which it was thickest during the Pleistocene (Björnsson, 1980). By ~2.5 k yr BP the remainder of Pleistocene ice had diminished, to leave only small ice caps on the highest mountains, such as Öræfajökull (Björnsson, 1980; Ingólfson *et al.*, 1997).

Three major advances of Icelandic glaciers have taken place over the past 5 k yr (Björnsson, 1980; Gudmundsson, 1997). The first began at ~2.5 k yr BP, consequent of climate cooling and increased precipitation, when the few remaining glaciers expanded over the highland plateau to form the contemporary ice caps such as Vatnajökull

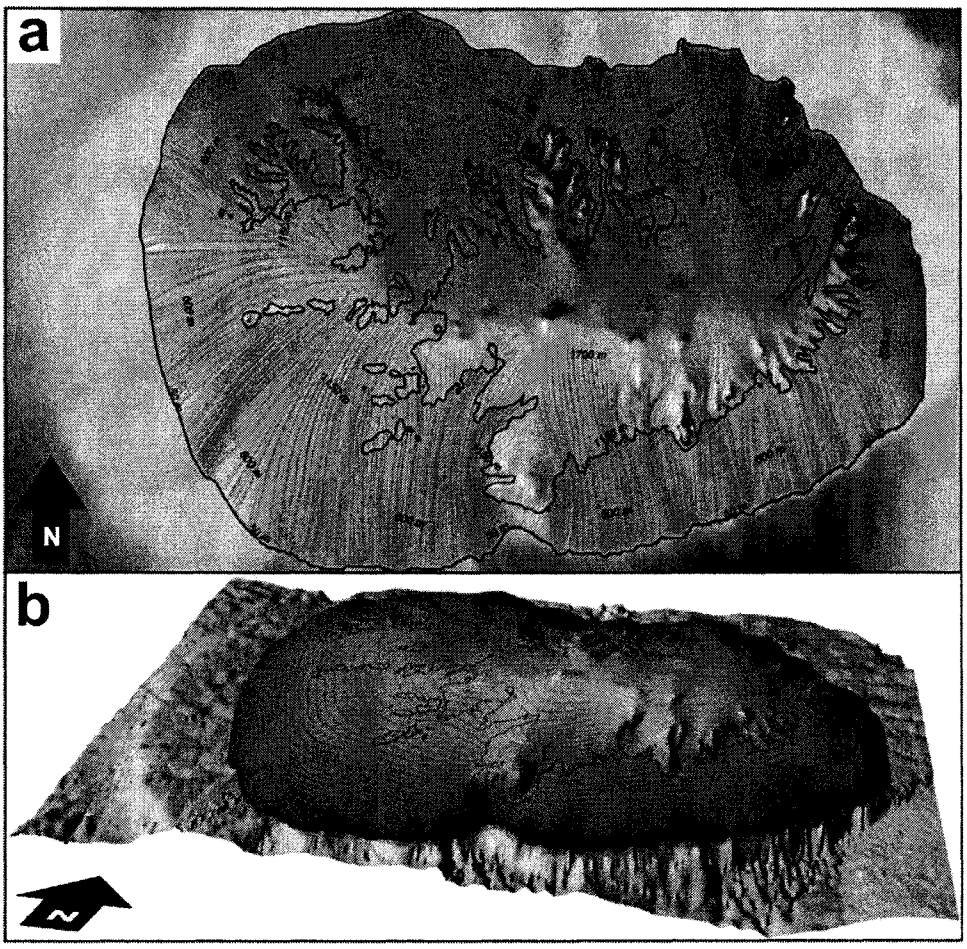


**Figure 3.2.** a) Model of the LGM Icelandic Ice sheet, with the lines indicating the modelled flow regime. The ice has a maximum thickness of ~2, 000 m and it extends beyond the modern day coastline (Fig. 5 of Hubbard *et al.*, 2006). b) Three-dimensional view of the LGM Icelandic ice sheet (a) from the south, contoured at 50 m intervals. The domed ice sheet topography is punctuated by numerous nunataks and the ice sheet extends to the edge of the continental shelf at its southern margin (Fig. 6 of Hubbard *et al.*, 2006).

(Björnsson, 1980). The second stage of advance occurred during the early Medieval period and corresponded to Northern Hemisphere glacial advance (Gudmundsson, 1997). Subsequent retreat forced Icelandic glacier recession through the 'Medieval Optimum' before climatic deterioration, beginning around ~700 yr BP, culminated in the 'Little Ice Age' (LIA) between ~400 to ~100 yr BP (Björnsson, 1980). Through the LIA, Icelandic glaciers greatly increased in mass and extent prior to ~300 yr BP, with a more slowed advance continuing until around ~100 yr BP, when glaciers had typically reached their maximum LIA extent (Sigurðsson, 2005). The exact timing of LIA maximum, however, varied with glacier type, with steep glaciers reaching their LIA maximum at ~250 yr BP, and piedmont outlets reaching their LIA maximum at ~150 yr BP (Björnsson, 1980; Sigurðsson, 2005).

By the 20th century all glaciers began a slow retreat that continued until 1930 when recession quickened markedly, with some glaciers having receeded to their pre-18th century extent prior to 1950 (Sigurðsson, 2005). A climatic decay in the period 1965-1985 provided a respite to general retreat, with distinct glacier advance throughout Iceland. This was short lived, however, and a warming climate post-1995 has resulted in a return to retreat of all monitored Icelandic glaciers (Sigurðsson, 2005) and over the past ~115 years the volume of the Vatnajökull ice cap has decreased by ~5-10 % (Björnsson, 1980).

*3.2.1.1 Skeiðarárjökull fluctuations*

Skeiðarárjökull reached its neoglacial maximum terminal position in the 18th (Sigurdðsson, 2005) or 19th century (Guðmunddson *et al.*, 2003) and fluctuated around that point until 1890, which is marked by a moraine ridge at the western margin that is 1700 m forward of its 1904 position (Þórarinsson, 1943). Although Skeiðarárjökull exhibits climate induced variations similar to those of Icelandic glaciers generally, its recent terminal position is largely influenced by surge activity. This results in sudden advances and subsequent periods of prolonged retreat and the surge of 1929 may have extended some parts of the terminus beyond its LIA maximum (van Dijk, 2002).

*3.2.2 Surge activity*

Skeiðarárjökull is known to have surged in 1929, 1985/86 and most recently in 1991 (Russell, *et al.*, 2001b; van Dijk, 2002; Björnsson *et al.*, 2003), resulting in advances of 350 m, 450 m and 1 km, respectively (Russell *et al.*, 2001b; van Dijk, 2002), though an advance of 1 km is typical (Björnsson *et al.*, 2003). The most recent surge at Skeiðarárjökull began in March 1991 when abundant new crevasses formed on the glacier surface (Björnsson, 1992), proceeded by the arrival of a 50 m high surge front at the eastern terminus in early May. The surge culminated in a 450 m advance of the eastern terminus, ending in mid-July (Björnsson 1998). The 1 km advance of the western

terminus began in late September, coincident to expansion of crevassing up-glacier until the end of October, before surge cessation in early November (Björnsson, 1992).

### 3.2.3 Jökulhlaups

Skeiðarárjökull is affected by jökulhlaup drainage originating ice-marginally from Grænalón and subglacially from Grímsvötn (Figure 3.1c):

- ***Grænalón*** (5 x $10^8$ $m^3$) is a subaerial lake, dammed by the western flank of Skeiðarárjökull, with unstable drainage having resulted in forty-five jökulhlaups at the western snout of Skeiðarárjökull during the 20th Century (Roberts *et al.*, 2005). The styles of outburst from this source, however, have evolved from low-frequency, high-magnitude events to higher-frequency, but lower magnitude (involving ~1 % of the lake volume) outbursts (Roberts *et al.*, 2005).
- ***Grímsvötn*** is the most volcanically active centre beneath Vatnajökull (Björnsson, 1992) and is the largest subglacial lake in Iceland (Björnsson, 2002). Its waters are sealed within a caldera, where processes associated with the intense geothermal activity of the area have resulted in basal melting of the blanketing ice and the development of a depression directly above the site (Nye, 1976; Björnsson, 1992) that is 10 km wide and 300 m deep (Björnsson, 2002). Under steady-state conditions, local ice and meltwater flow into the centre of the depression resulting in lake growth until a critical point for drainage is reached (Nye, 1976). Under such conditions Skeiðarárhlaups are instigated every 1-10 years in the Skeiðará River at the eastern margin, 50 km down-glacier from Grímsvötn (Björnsson, 1992; Björnsson, 1998; Björnsson, 2002). Grímsvötn jökulhlaups are typically triggered before the lake reaches a level at which it can float the ice dam, suggesting some other process habitually breaks the seal (Björnsson, 2002).

#### 3.2.3.1 Grímsvötn jökulhlaups

Two jökulhlaups from Grímsvötn occurred during the 1991 surge of Skeiðarárjökull (Björnsson, 1998). The first of these began on 16th September reaching a peak discharge of ~320 $m^3s^{-1}$ on the 2nd October (Björnsson, 1998). The jökulhlaup terminated after only 25% of Grímsvötn's total volume had been drained, which is not typical of Grímsvötn jökulhlaups (Björnsson, 1998). The second jökulhlaup began towards the end of the surge in late October with drainage resulting in a 60 m drop in the level of Grímsvötn (Björnsson, 1998). The floodwaters burst from the Skeiðará outlet on 27th October reaching a peak discharge of ~2, 145 $m^3s^{-1}$ after twenty-six days and waning five days later (Björnsson, 1998).

It is argued that the variation in jökulhlaup propagation between these 1991 events is due to differences in the drainage network associated with the ongoing surge

(Björnsson, 1998). During the first jökulhlaup floodwaters were slowed by the presence of a reorganised drainage system, i.e. a linked-cavity network (c.f. Kamb *et al.*, 1985), whilst the second jökulhlaup took place towards the end of the surge and, thus, floodwaters were discharged through a tunnel network, typical of most observed Grímsvötn jökulhlaups (Björnsson, 1998). Björnsson (1998) argues that reduced sliding towards the end of the surge (consequent of a flattened surface slope) allowed the development of a 'tunnel' network through which the floodwaters could be efficiently drained.

Jökulhlaup discharge associated with steady-state subglacial hydrothermal systems ('typical' Grímsvötn outbursts) are a lower-magnitude form of jökulhlaup typically discharged through the Skeiðará outlet alone (Björnsson, 2002). Not all jökulhlaups from Grímsvötn are solely discharged through the Skeiðará outlet, with occasional high-magnitude jökulhlaups discharging from outlets across the entire glacier margin (c.f. Roberts *et al.*, 2000b; Russell *et al.*, 2006). Some of the most violent and destructive jökulhlaups are the result of subglacial volcanic eruptions (Björnsson, 1992; Björnsson, 2002).

*3.2.3.2 The November 1996 Skeiðarárhlaup*

The last major jökulhlaup to affect Skeiðarárjökull from Grímsvötn occurred due to a volcanic eruption beneath Vatnajökull, beginning on September 30$^{th}$, 1996 (Russell and Knudsen, 1999a; Russell *et al.*, 2006, 2007b). Over the following month ~3.8 km$^3$ of meltwater flowed subglacially into Lake Grímsvötn, until the critical level for drainage was reached and for the first time in historical observations, the ice dam was floated off the glacier bed, with the ensuing floodwaters exceeding the ice overburden and lifting the glacier from the bed along its flow path (Björnsson, 2002).

The resulting jökulhlaup began in the easterly river draining Skeiðarárjökull (Skeiðará) on the 5th November, reaching a peak discharge of >45, 000 m$^3$s$^{-1}$ after fourteen hours (Figure 3.3), almost totally flooding Skeiðarársandur (Russell *et al.*, 2001a; Russell *et al.*, 2006, 2007b) and washing blocks of ice over the vast outwash plain (Fay, 2002a, 2002b; Björnsson, 2002). Subsequently, water burst from multiple ice-roofed vents and fractures that perforated the entire 22 km wide margin (Figure 3.4a), before becoming increasingly focused upon the Gígjukvísl outlet, which had the lowest hydraulic potential across the glacier margin (Russell *et al.*, 2006). Here, supraglacial drainage continued into the late-rising, peak and early waning stage of the jökulhlaup, with flows exiting from a supraglacial fracture network (Roberts *et al.*, 2000b). By the following day (~17 hours later) these fracture outlets defined the headwalls of a large (extending >700 m from the active glacier margin) supraglacial ice-walled canyon, often termed the Double Embayment (Figure 3.4b), via the excavation of ~5 x 10$^6$ m$^3$ of glacier ice (Russell *et al.*,

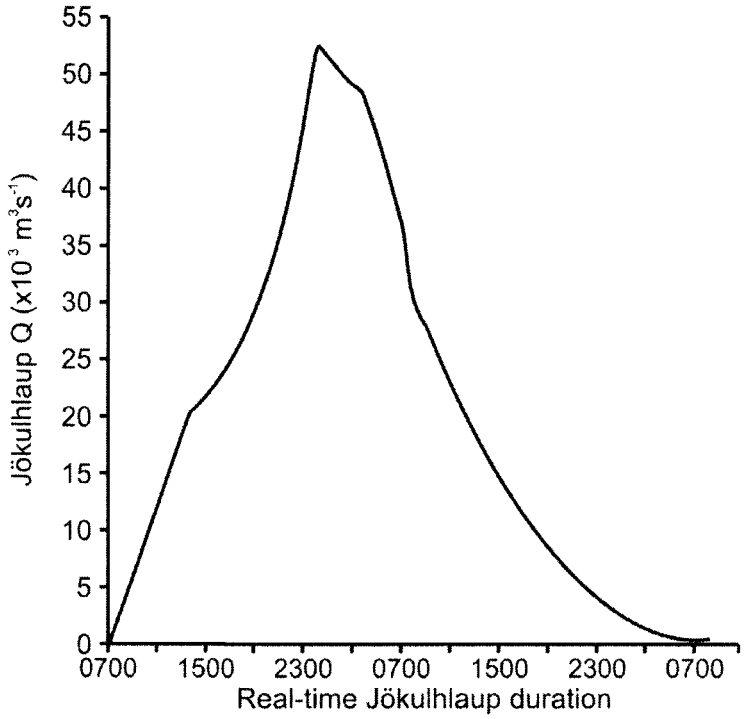


**Figure 3.3.** The November 1996 jökulhlaup hydrograph at Skeiðarárjökull, showing total discharge (after Snorasson *et al.*, 2002). The event rises linearly to its peak over a period of approximately 14 hours, before waning more steadily for up to 32 hours.

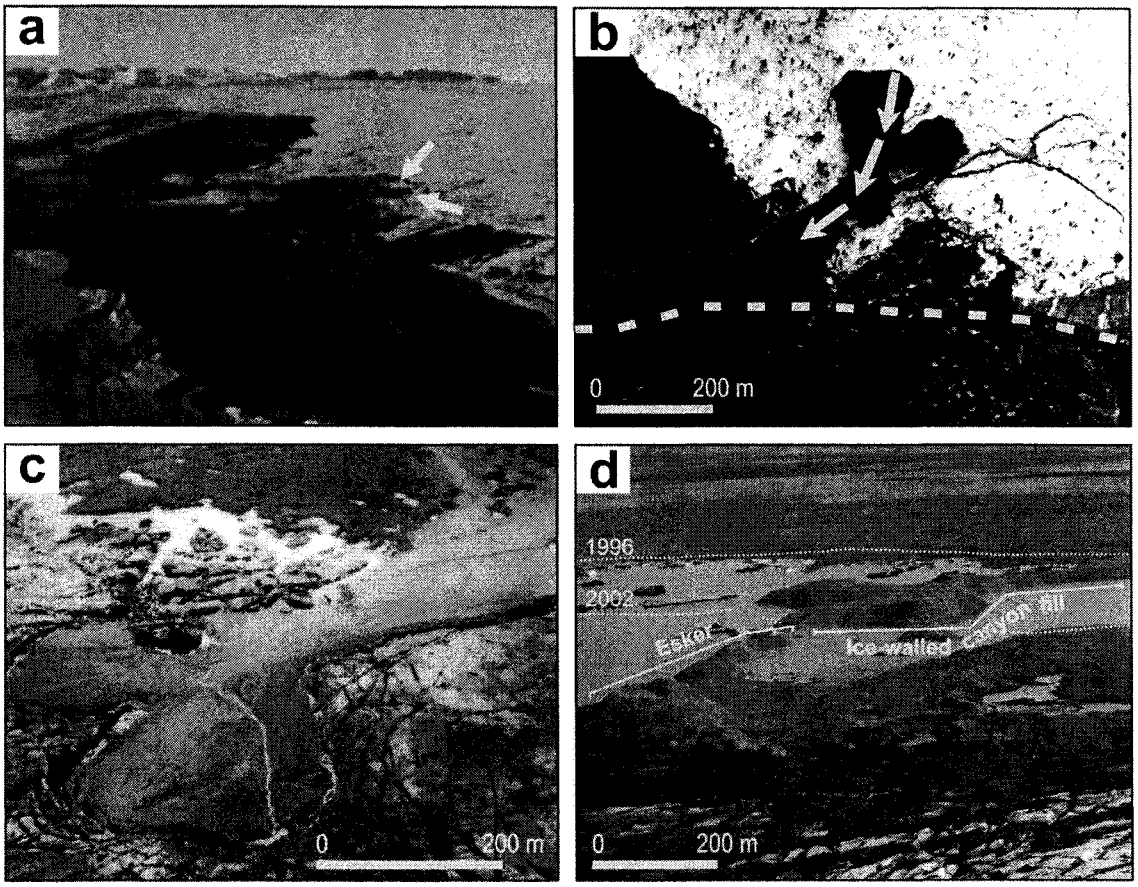


**Figure 3.4.** a) Supraglacial discharge of floodwater during the early-rising stage of the 1996 Skeiðarárhlaup. The arrows indicate the location of the outlet points from which the Double Embayment was later excavated. b) An aerial photograph of the Double Embayment and ice-walled canyon taken at c. 12:00h on 6th November, 1996. The arrows indicate the flow direction of the floodwaters through the canyon from a point outlet at the head of the western chamber. The dashed line indicates the pre-jökulhlaup ice-margin (after Russell *et al.*, 2001a). c) An oblique aerial photograph taken in 1997 (post jökulhlaup) showing the sediments that were deposited within the confining ice walls of the canyon by the 1996 floodwaters (after Russell *et al.*, 2001a). d) An oblique aerial photograph taken in 2007, illustrating how both the ice-walled canyon sediments and the connecting esker have been released by the retreating margin (courtesy of Andrew J. Russell). The esker connects directly to the point where waning-stage floodwaters were observed discharging into the Double Embayment. The approximate positions of the glacier margin in 1996 and 2002 are indicated by the labelled dashed lines.

2001a, 2006). Floodwaters then deposited thick sedimentary sequences in the Double Embayment (Figure 3.4c) (Russell and Knudsen, 1999a, 1999b; Russell *et al.*, 2001a; Cassidy *et al.*, 2003; Russell *et al.*, 2005, 2006). The floodwaters transported boulder-sized clasts in suspension through the conduit and subaerial ice-walled canyon (Russell and Knudsen, 1999a).

### *3.2.4 Field sites*

Subsequent to the November 1996 jökulhlaup, Skeiðarárjökull has been retreating at a rate of ~10 m/yr at the central-western margin (Russell *et al.*, 2006). This has released both the sediments deposited within the Double Embayment (ice-walled canyon) and an esker, from the supporting ice (Figure 3.4d). The distal end of this esker matches the discharge point for waning stage floodwaters into the Double Embayment (Figure 3.4d). As no major portal was located in this area prior to the November 1996 jökulhlaup, the esker must have been generated entirely during the 1996 Skeiðarárhlaup synchronous to the Double Embayment (Russell *et al.*, 2005, 2006).

The current (August 2006), exposed section of the esker extends continuously from the ice margin towards the ice-walled canyon fill for a distance of >700 m, having a maximum width of ~40 m and height of <30 m (Figure 3.4d). The esker is largely continuous for its entire length and is slightly sinuous in morphology (Figure 3.5a). Its surface topography is, in places, irregular, with a tendency towards greater elevations on the western side and it has a double-crested appearance in places (Figure 3.5b-c). Buried ice can be observed at the flanks of the esker (Figure 3.5d and 6.1) and ice-walled canyon fill and consequently the margins of the landforms are relatively unstable, with collapse of material occurring regularly in places.

The esker and ice-walled canyon fill landforms are the focus of data collection at Skeiðarárjökull. Ground-penetrating radar (GPR) grids have been collected in a near-continuous succession along the esker and onto the ice-walled canyon fill (*Section 4.2.2*). In addition, GPR grids were collected on the surface of Skeiðarárjökull, just up-glacier from the point at which the esker is being released by the retreating ice (*Section 4.2.1*).

## 3.3 Bering Glacier, Alaska

Approximately 5 % (74, 705 $km^2$) of Alaska is currently ice-covered, with 50% of this being located in the Kenai, Chugach and St. Elias Mountains in south-central Alaska (Calkin *et al.*, 2001) (Figure 3.6a). This area is one of the most tectonically active coastlines in the world, with mountains exceeding 5, 000 m in elevation being located <15 km from the Gulf of Alaska coast (Sauber and Molnia, 2004). Subsequent high precipitation rates (>2-3 m yr) have led to the formation of a temperate glacier setting (Jaeger *et al.*, 1998), hosting the most extensive ice fields on the North American

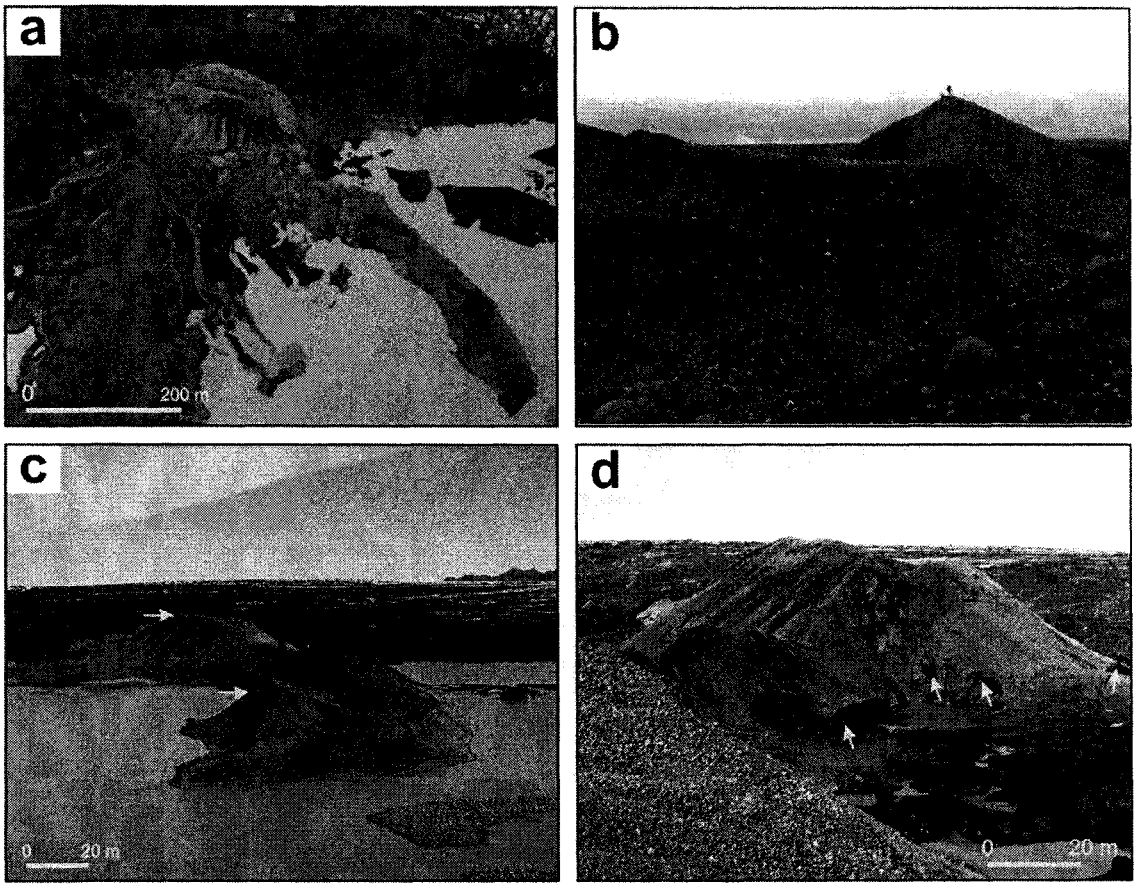


**Figure 3.5.** Photographs of the esker that has been progressively released from the margin of Skeiðarárjökull since 2002: a) aerial photograph (2006) of the esker, showing its continuous and sinuous morphology, with the ridge narrowing down-flow of an enlargement at the head of the exposed esker (courtesy of Andrew J. Russell); b) a down-flow view of a ridge enlargement at the most up-flow section of the emerged esker (persons for scale on right-hand ridge). Here, the ridge has an irregular cross-section, with an almost double-crested morphology, though is at its greatest elevation at the western flank (right); c) an up-flow view of the esker, taken from the head of the ice-walled canyon fill (courtesy of Palmer K. Bailey). The esker has an irregular morphology and the arrows indicate topographic highs located at the western flank of the landform; d) an up-flow view of the esker enlargement. The arrows indicate the presence of buried ice at the flanks of the landform.

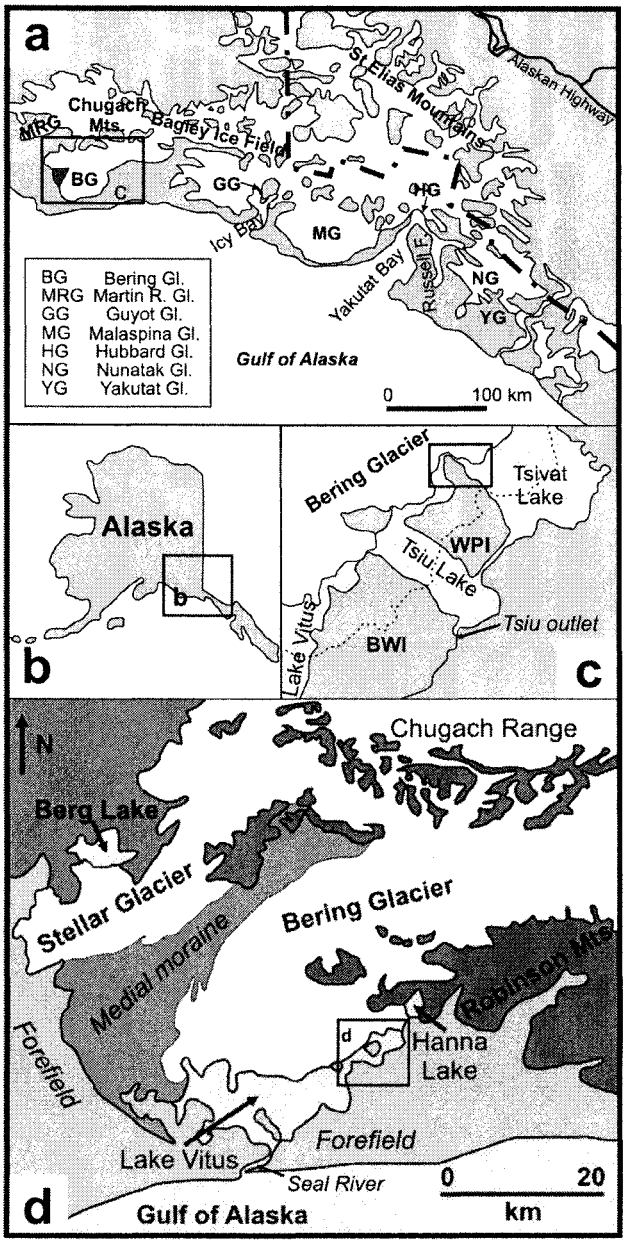


**Figure 3.6.** a) South-central Alaska, showing the location of major Glaciers. The box indicates the location of Bering Glacier and (d). b) location of Alaska, with (a) being indicated by the box. c) Zoomed view of the eastern forefield sector of Bering Glacier (WPI: Weeping Peat Island; BWI: Bentwood Island). The position of the ice-margin shown is that in 1993 (pre-surge), whilst the dashed line indicates the ice-marginal position in 1995 (post-surge). The box indicates the area at which the esker and ice-walled canyon fill can be located. d) Map of Bering Glacier piedmont lobe. The box indicates the location of the field site (c).

continent (Post, 1972). The Bagley Ice Field is one of the largest, flowing 200 km from the Canadian border through the Chugach Range (Figure 3.6a) in south-central Alaska (Muller and Fleisher, 1995), following a 7.5-12 km wide trough (Herzfeld and Mayer, 1997). It feeds outlet glaciers on both its North and South margins, though the southern side has much larger glacier systems (Figure 3.6a), being the product of its high latitude and maritime proximity (Meigs and Sauber, 2000). The Bering Glacier is the largest outlet glacier of the Bagley Ice Field (Muller and Fleisher, 1995), accounting for more than 6% of Alaska's ice-covered area (Molnia, 2005). It descends from its source as a 10 km wide trunk glacier (Fleisher *et al.*, 2004) before coalescing with the Stellar Glacier to form a 50 km wide piedmont lobe (Figure 3.6d) (Muller and Fleisher, 1995; Wiles *et al.*, 1999; Fleisher *et al.*, 2003).

### *3.3.1 Alaskan glacier fluctuations*

The last major glaciation of Alaska corresponds to LGM fluctuations of the Laurentide Ice Sheet, commencing ~24k yr BP and reaching a maximum extent at ~18k yr BP (Sauber and Molnia, 2004). Retreat from the adjacent continental shelf began ~16k-14k yr BP, and was complete by approximately 10k yr BP (Sauber and Molnia, 2004). During the subsequent Holocene period, Alaskan coastal glaciers experienced numerous fluctuations in their terminal extent, associated with climatic variability. The first occurred during dramatic climatic cooling, coupled with an increase in precipitation ~3.5k yr BP (Calkin *et al.*, 2001). Following a period of recession ~2k yr BP further glacial advances occurred between 1.5k and 1.3k yr BP (Calkin *et al.*, 2001). Glacier recession until ~800 yr BP (Medieval Optimum), was followed by land-based glacier expansions associated with the LIA occurring around 800 yr BP to 100 yr BP (Calkin *et al.*, 2001). During the LIA glacier coverage was at least 10% greater than at present (Sauber and Molnia, 2004), with the onset of retreat commencing around 200-250 yr BP in all areas of south-eastern Alaska, except the Chugach/St. Elias range where it began ~150 yr BP (Sauber and Molnia, 2004). Glaciers in the area have been receding rapidly over the last century (Meigs and Sauber, 2000), with more than 95% of glaciers that extend below 1, 500 m currently undergoing thinning, retreat, and/or stagnation (Sauber and Molnia, 2004). Alaskan glaciers have been retreating since the mid-1950s, though the rate of retreat has increased since the mid-1990s (Arendt *et al.*, 2002).

#### *3.3.1.2 Bering Glacier fluctuations*

Bering Glacier fluctuations over the past two millennia have been consistent with that described above (Wiles *et al.*, 1999; Calkin *et al.*, 2001). Evidence presented by Fleisher *et al.* (1999) suggests that prior to the Holocene the Bering Glacier system had combined with the Martin River glacial system (Figure 3.6a). During the Holocene gradual

expansion may have taken place due to climatic cooling as early as 6, 000 yr BP (Muller and Fleisher, 1995) and it is argued that further ice advances took place around 1, 500 yr BP and 920 yr BP (Wiles *et al.*, 1999). Subsequent retreat prevailed until ~400 yr BP, after which the Bering lobe re-advanced to within a few kilometres of its neoglacial moraine (Wiles *et al.*, 1999). Since ~120 yr BP, the Bering Glacier has retreated (Molnia *et al.*, 1996; Wiles *et al.*, 1999; Calkin *et al.*, 2001) with periodic surges producing readvances since the turn of the 20$^{th}$ century (Molnia *et al.*, 1996; Wiles *et al.*, 1999). Currently, the rate of retreat for the Bering lobe is around 50-75 m/year, where the ice terminates on land (Fleisher *et al.*, 2005; Miller *et al.*, 2006). Between 1995 and 2003 the Bering piedmont lobe experienced maximum thinning of >100 m and had retreated by up to 6.5 km where it terminates in deep lakes (Sauber and Molnia, 2004).

### *3.3.2 Surge activity*

Bering Glacier is one of more than two hundred temperate glaciers in Alaska and north-western Canada known to surge (Molnia, 1993), and is argued by Wiles *et al.* (1999) to be the largest surge-type glacier in the world. The debris bands and tightly folded medial moraines of the central and eastern sectors are contended by Post (1972) to be generated by lateral spreading and compression of the moraines by periodic surge movement of the Bering branch past the non-surging Stellar Glacier (Post, 1972; Muller and Fleisher, 1995). Muller and Fleisher (1995) argue that the spacing and amplitude of the folds suggest notable surge cyclicity over the past few centuries. Bering Glacier surged in ca. 1837 (Lingle *et al.*, 1993; Muller and Fleisher, 1995), 1900, 1920, 1940, 1965-1967 and most recently in 1993-1995 (Post, 1972; Molnia *et al.*, 1993; Muller and Fleisher, 1995; Wiles *et al.*, 1999).

The general downwasting of the Bering lobe that had been occurring since 1968 was interrupted in 1993 when accelerated flow was observed to be spreading from the Bering trunk into the piedmont lobe (Fleisher *et al.*, 1993). Although the exact location of surge onset is unknown, it is believed to have been situated below the equilibrium line (Lingle *et al.*, 1993), and observations of SAR imagery have led Roush *et al.* (2003) to suggest it to have been in an area north of the Grindle Hills. Following initiation, the surge front propagated down-glacier at a rate of ~100 m $d^{-1}$, with accelerated flow and crevasses spreading up-glacier at a rate of ~200-500 m $d^{-1}$ (Fatland and Lingle, 1998), affecting part of the Bagley Ice Field (Herzfeld and Mayer, 1997; Fatland and Lingle, 1998; Arcone, 2002). The eastern margin began to advance in July 1993, at rates ranging from 1.0 to 7.4 m $d^{-1}$ (Fleisher *et al.*, 1998; 2006b), though in western and central parts of the glacier rates were greater at 10-20 m $d^{-1}$ (Figure 3.7) (Fatland and Lingle, 1998; Roush *et al.*, 2003). In the central section where the glacier terminated into Lake Vitus, rates of movement were greater at 19 m $d^{-1}$, culminating in a total advance of up to 9 km during

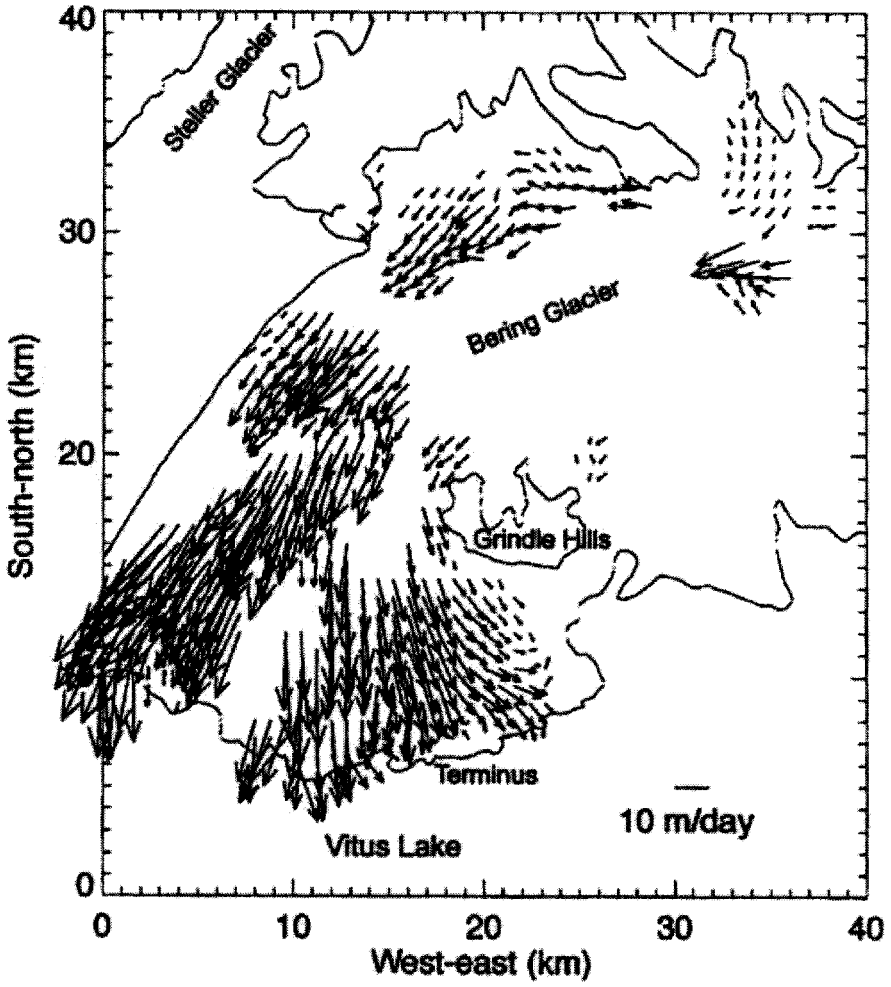


**Figure 3.7.** Velocity vectors (m $d^{-1}$) on Bering Glacier (9 August-13$^{th}$ September 1993). The velocity is spatially variable, with the highest measurements located in the central and western terminus (fronting in Lake Vitus). Lower velocities dominate the eastern sector (from Roush *et al.*, 2003).

the first phase of the surge (Merrand and Hallet, 1996). Phase one of the 1993-1995 surge was associated with the presence of significant volumes of stored water at the glacier bed, with the thickness of a water layer being estimated at ~0.3-0.5 m, pervading the entire surge-affected area (~2, 500 $km^2$) (Merrand and Hallet, 1996). Termination of this first phase occurred abruptly on 27$^{th}$ July 1994 as an outburst flood discharged into Tsivat lake basin (*Section 3.3.3.1*) (Fleisher *et al.*, 1998; Roush *et al.*, 2003), with subsequent rates of retreat being measured at 0.3 m $d^{-1}$ (Fleisher *et al.*, 1998).

A second smaller advance phase began in the spring of 1995, though forward advance was sporadic, fluctuating between 1-2 m/day, resulting in a relatively small terminal advance (Fleisher *et al.*, 1998; 2003). InSAR uplift measurements suggest that through both phases of the surge, migrating pockets of subglacial water produced accelerated motion that began 110 km from the Bering Glacier margin (Fatland and Lingle, 1998). This invokes the possibility that, like the 1991 surge at Skeiðarárjökull (c.f. Björnsson, 1998), the 1993-1995 event at Bering Glacier involved a major reorganisation of the subglacial hydrological system. This idea can be further substantiated by the occurrence of a six fold increase in sedimentation within eastern sector lakes, during the surge, indicating the subglacial hydrological system had increased access to subglacial sediment (Fleisher *et al.*, 2003). Fleisher *et al.* (2003) argue that this was the result of the closing of subglacial conduits and the development of a distributed drainage network, though some evidence suggests that the glacier bed was deforming in the eastern sector (Fleisher *et al.*, 2002, 2006c).

Following each of the last four surges, Bering Glacier has undergone decadal periods of rapid retreat, the rate of which has been variable (Molnia, 2005). Prior to the 1965-1967 surge, the ice margin had retreated between 2-5 km from its 1940 surge limit (Muller and Fleisher, 1995). In the twenty-five year quiescent phase prior to the 1993-1995 surge, the glacier retreated a total of 10.7 km (Molnia, 2005). Following the 1993-1995 surge the glacier margin has retreated >6 km (Molnia, 2005).

### *3.3.3 Outburst floods*

Bering Glacier has been the outlet of periodic outburst floods that have coincided with the termination of at least the two most recent surges in 1966 and 1994 (Fleisher *et al.*, 1998; 2006a; 2006c). 'Boulder zones', several metres thick, bounded above and below by conventional outwash can be observed in the forefield stratigraphy of Bering Glacier and are suggested by Fleisher *et al.* (2006a) to have characteristics attributable to high discharge events and may provide evidence of periodic, neoglacial outburst floods from the margin of Bering Glacier. The outburst floods following both the 1966 and 1994 surge phases resulted in the development of ice-walled canyons at similar locations along the glacier margin (Fleisher *et al.*, 2006a). It has been suggested that hydraulic potentials

are controlled by subglacial topography, which forced the development of a conduit system in a similar location during the July-August 1994 outburst flood (Fleisher *et al.*, 1998, 2006a).

*3.3.3.1 The 1994 Bering Glacier outburst floods*

The 1993-1995 surge was broken into two phases by an outburst flood that commenced on 27th July 1994, discharging floodwaters into Tsivat lake basin (Figure 3.8) (Fleisher *et al.*, 1998, 2003). In the days following the outburst, both sediment and ice were expelled from outlets (Fleisher *et al.*, 1998), where they rapidly aggraded into a delta in Tsivat lake basin (Fleisher *et al.*, 2003) (Figure 3.9). Like the 1996 Skeiðarárhlaup, the July-August 1994 outburst flood at Bering Glacier resulted in the genesis of an ice-walled canyon (Figure 3.8) that eroded into the ice margin at a rate of approximately 150-200 m/day (Fleisher *et al.*, 1998). The final geometry of the canyon, measured in October 1994 showed it to be approximately 130 m wide at its up-flow extent, 250 m wide at its distal end, and 1 km long (Fleisher *et al.*, 1998). The canyon extended into the ice with a north-westerly trend for approximately 600 m before abruptly shifting orientation to the south-west as it continued for a further 400 m (Fleisher *et al.*, 1998). The outburst flood lasted ~10 days, reaching its peak discharge of ~3, 000 $m^3s^{-1}$ (Fleisher *pers. comm.*, 2008) after approximately five days (Figure 3.10). During its waning stage, reduced flood conditions persisted, transporting ice blocks over the surface of the aggrading delta in Tsivat Lake basin (Fleisher *et al.*, 2003). Data collected by Merrand and Hallet (1996) at the Lake Vitus outlet (Seal River) during the summer of 1994 captured the signature of this event (Figure 3.10), though this was attenuated due to filtering of the outburst flood by the presence of a proglacial lake complex. Consequently, the increased discharge was not observed at Seal River (Figure 3.6d) until 31st July, peaking on the 5th August and ending around 9th August (Figure 3.10) (Merrand and Hallet, 1996). A second outburst flood cut across Weeping Peat Island between 7th September and 20th October 1994, to form two new sandar that graded into Tsiu lake basin (Figure 3.8d) (Fleisher *et al.*, 1998, 2003). The second phase of surge advance then completely closed the ice-walled canyon (Fleisher *et al.*, 1998).

*3.3.4 Field sites*

The eastern sector forefield of the Bering lobe (north of Lake Vitus), comprises an area of approximately 100 $km^2$, including both islands (rarely exceeding 30 m in relief) and a proglacial lake complex (Fleisher *et al.*, 1998), including, Tsivat, Tsiu and Vitus lakes (Figure 3.6c). Lake Vitus is the largest, being 24 km long, 8 km wide and >165 m below sea-level at its deepest point (Molnia *et al.*, 1996). The lake is composed of four bedrock

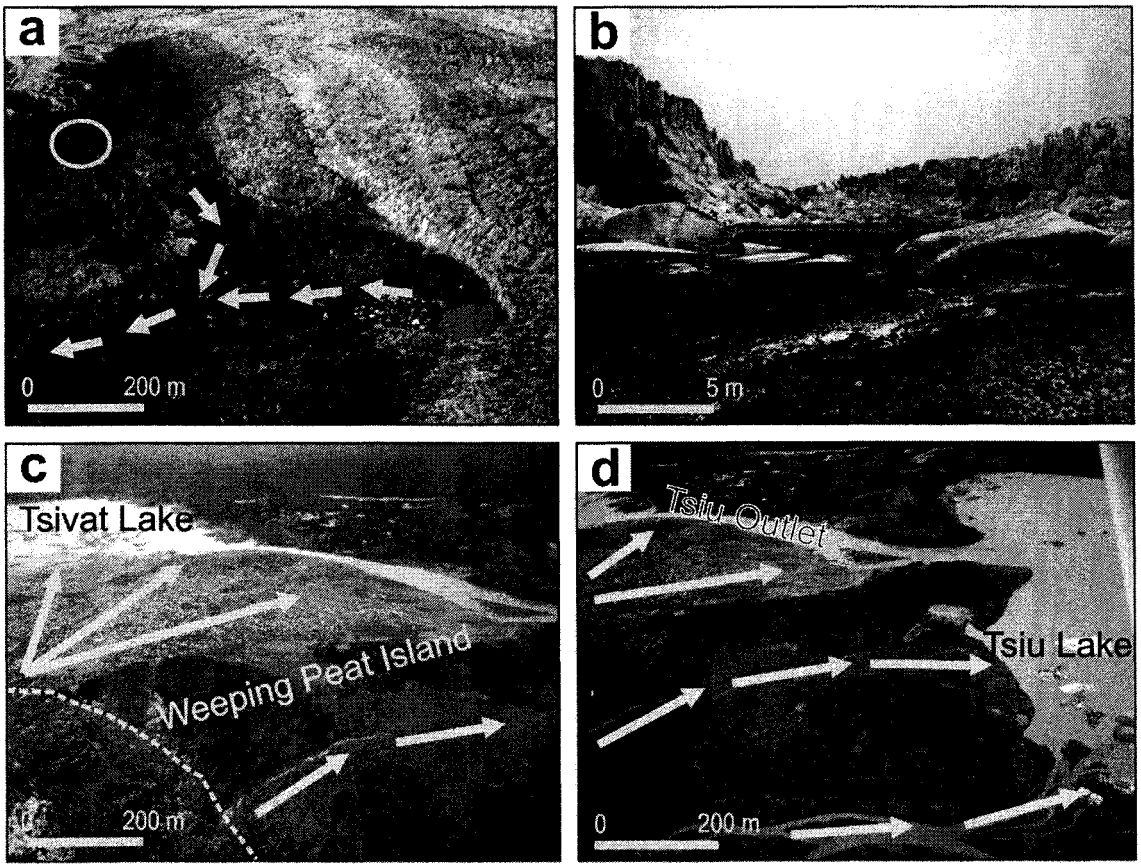


**Figure 3.8.** a) Aerial Photograph of the Ice-walled canyon formed during the July-August 1994 outburst flood. The arrows indicate the approximate flow direction during the outburst, whilst the circle indicates the approximate outlet location of the October 1994 outburst flood. Sediments infilled the canyon and a number of ice-blocks were deposited in the outwash. b) Photograph looking up-flow within the western extension of the ice-walled canyon fill (focus of ice-walled canyon data collection). Two ice blocks can be seen in the centre of the photograph. c) Aerial photograph of Weeping Peat Island and the ice margin (dashed line), which fronted onto the Island in October 1994. The arrows indicate the direction of floodwaters during the July-August 1994 (top left) and October 1994 (bottom left) outburst floods. The outwash fans that were rapidly aggraded during the events can also be seen, with that associated with the July-August outburst flood being littered with ice-blocks up to 30 m in diameter. d) The south-eastern part of Weeping Peat Island following the 1994 outburst floods. The arrows indicate the flow direction of both events, with those cutting across Weeping Peat Island into Tsiu Lake being associated with the October outburst flood (photographs courtesy of Palmer K. Bailey).

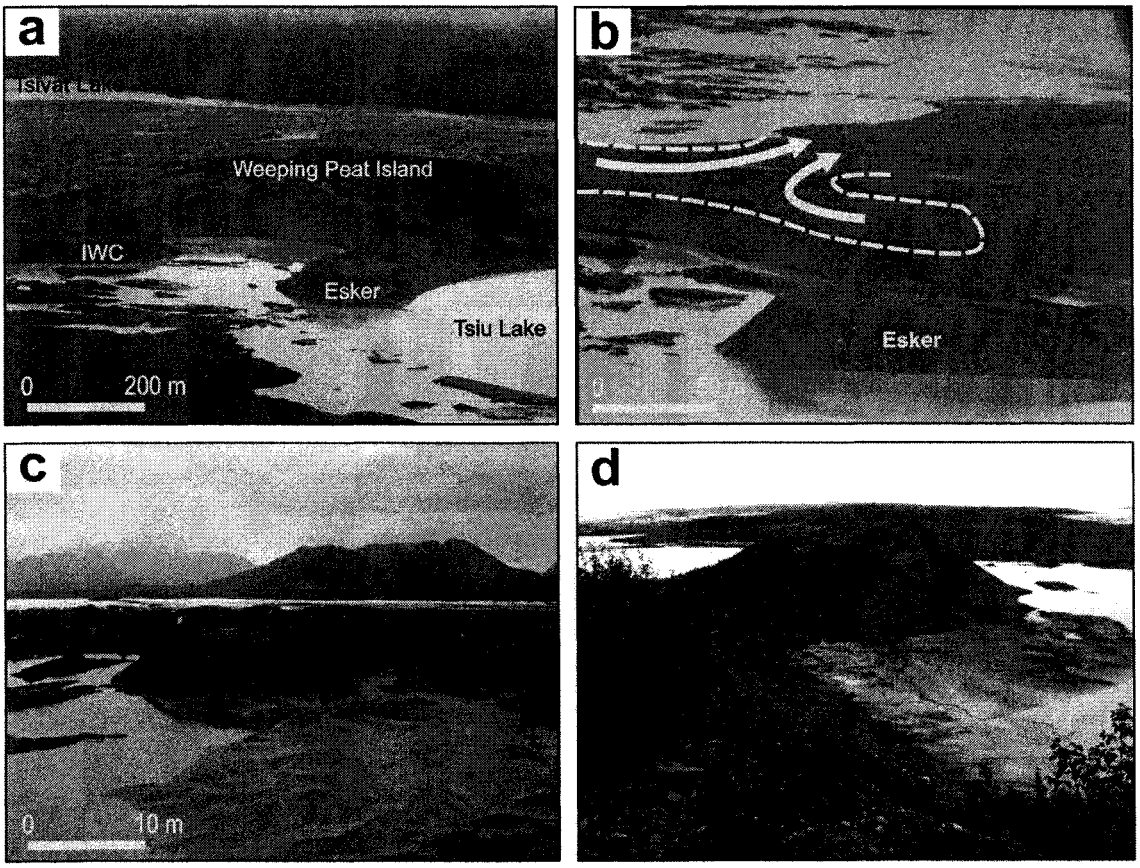


**Figure 3.9.** a) Aerial photograph looking approximately southwest to northeast across Weeping Peat Island. The locations of the esker and ice-walled canyon (IWC) are indicated, as are Tsivat and Tsiu Lakes (courtesy of Palmer K. Bailey). b) Aerial photograph of the esker and ice-walled canyon fill (dashed lines) in June 2006 (courtesy of Palmer K. Bailey). The dashed line and arrows indicate the approximate position of the ice-walls and flow direction, respectively, during the July-August 1994 outburst flood. c) Photograph of the western extension of the ice-walled canyon fill that is the focus of data collection on this landform. The photograph is looking approximately down-flow. d) Photograph of the esker (orientated up-flow). The irregular cross-section of the esker can be observed, with a greater elevation on its northern side (right).

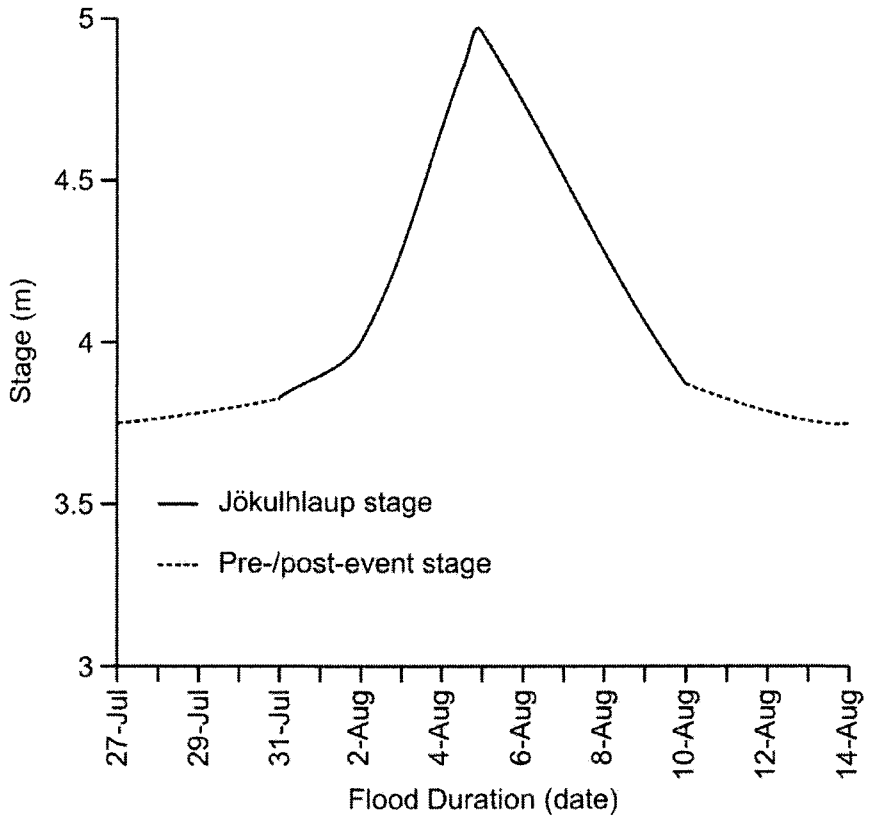


**Figure 3.10.** Stage record of the July-August 1994 jökulhlaup, recorded at Seal River (outlet of Lake Vitus). The tidal response has been removed. Although the jökulhlaup began on 27th July, the presence of a significant forefield lake complex resulted in a delayed arrival of discharge at Seal River and an attenuation of the signature (after Merrand and Hallet, 1996).

basins within which the maximum basal sediment thickness is 100 m and the current sedimentation rate more than 10 m $yr^{-1}$ (Molnia *et al.*, 1996).

The peripheral drainage system of the eastern sector is dynamic, responding to ice advance and retreat due to surge activity. It is fed by waters from the Grindle Hills to the North and glacier melt that flows through Tsivat and Tsiu lakes prior to entering Lake Vitus to the south-west (Fleisher *et al.*, 1993). This drainage system is interspersed by the presence of foreland Islands over which the ice has periodically advanced and retreated (Figure 3.6c), with Weeping Peat Island being exposed during marginal retreat following 1965-1967 surge (Fleisher *et al.*, 1993).

During the ~6 km of backwasting since the 1993-1995 surge the ice-walled canyon fill (associated with the July-August 1994 outburst flood) and an esker that corresponds to a position up-glacier from the October 1994 outburst flood outlet have melted out (Figures 3.8 and 3.9). As the esker was not observed in this area prior to readvance of the ice during the 1993-1995 surge (Fleisher *pers. comm.*, 2007) and there was no major outlet at the site following the October 1994 outburst flood, it must have been generated entirely during the October 1994 outburst. The ice-walled canyon fill has an irregular surface topography, with kettle holes and areas of collapse, associated with the melting of supporting ice walls and/or buried ice. Buried ice has been identified beneath primary bedded sediments at the flanks of the landform (Fleisher *pers. comm.*, 2007).

The esker is located ~150 m to the south-west of the ice-walled canyon fill (Figure 3.9a). This esker has a linear orientation from ~north-west to ~south-east, being roughly >20 m wide and ~380 m long, lacking any sinuosity (Figure 3.9). The esker has an irregular cross-section, with its northern flank being at a greater elevation (Figure 3.9d). Subsequent to its exposure from the glacier margin the esker has been partially eroded by drainage through an outlet from Tsivat Lake into Tsiu Lake. Since its exposure, the esker has been partially colonised by vegetation (alder), constraining GPR surveys to locations free from Alder.

The esker and ice-walled canyon fills are the focus of data collection at Bering Glacier. GPR grids have been collected on all workable sections of the esker and western extension of the ice-walled canyon fill, in order to identify their three-dimensional sedimentary architecture (*Section 4.2.3*).

# SECTION II
# Methodological Approach

*"…studies of glacial deposits along the margin of the glacier* [Vatnajökull], *for comparison with similar deposits of the Pleistocene ice sheets, will give a clue to many problems connected with the latter."*

Hakon Wadell (1935)

*pulseEkko Pro 1100 GPR system at Bentwood Island, Eastern Sector Forefield, Bering Glacier, Alaska.*

# Chapter 4

# Ground-penetrating radar: Background, Field Methodology and Processing

## 4.1 Introduction to Ground-penetrating Radar

Ground-penetrating radar (GPR) is a popular technique for imaging and interpreting sedimentary architecture (Davis and Annan, 1989; Neal, 2004) and is commonly employed in periglacial, glacial and glaciofluvial environments (Woodward and Burke, 2007). GPR surveys emit high-frequency electromagnetic (EM) waves (50-1000 MHz) from a surface transmitter. These EM waves pass through the underlying medium and are partially reflected by subsurface features that exhibit electrical properties contrasting with those from the surrounding matrix (Davis and Annan, 1989; Neal, 2004). An example of materials of contrasting dielectric permittivities would be a water-filled conduit within glacier ice (Figure 4.1a-b). As the matrix (the ice) has different electrical properties to the anomaly (the conduit), a proportion of the reflecting EM wave is reflected back towards the surface from the ice/water interface (Davis and Annan, 1989). This reflected signal is then detected by the receiver, which amplifies, digitises and stores the data ready for processing (Woodward *et al.*, 2003b). Typical plots of GPR data display signal amplitude (mV) against two-way travel time (TWTT) in ns (Daniels *et al.*, 1988; Davis and Annan, 1989; Neal, 2004).

Geophysical techniques were first developed in the 1950's when radio echo soundings (RES) were conducted in Greenland and Antarctica to determine ice sheet thickness (Steenson, 1951; Cook, 1960; Harrison, 1970). It was not until the 1970's that the applications of geophysical techniques grew through the development of ground-based surveys for aiding mineral exploration, mine detection for the military, moon exploration on the Apollo lunar missions (c.f. Annan, 2002) and in the field of glaciology (e.g. Davis *et al.*, 1973; Watts and England, 1976). In the 1980's the reliability of radar techniques was advanced, allowing the development of modern, commercial GPR units, including SIR (GSSI, USA), pulseEKKO (Sensors and Software, Canada) and RAMAC (Malå, Sweden) (Woodward and Burke, 2007), with more recent advancements in methodology, processing and interpretation increasing the reliability of GPR to a level comparable with more established geophysical techniques (Annan, 2002; Woodward and Burke, 2007).

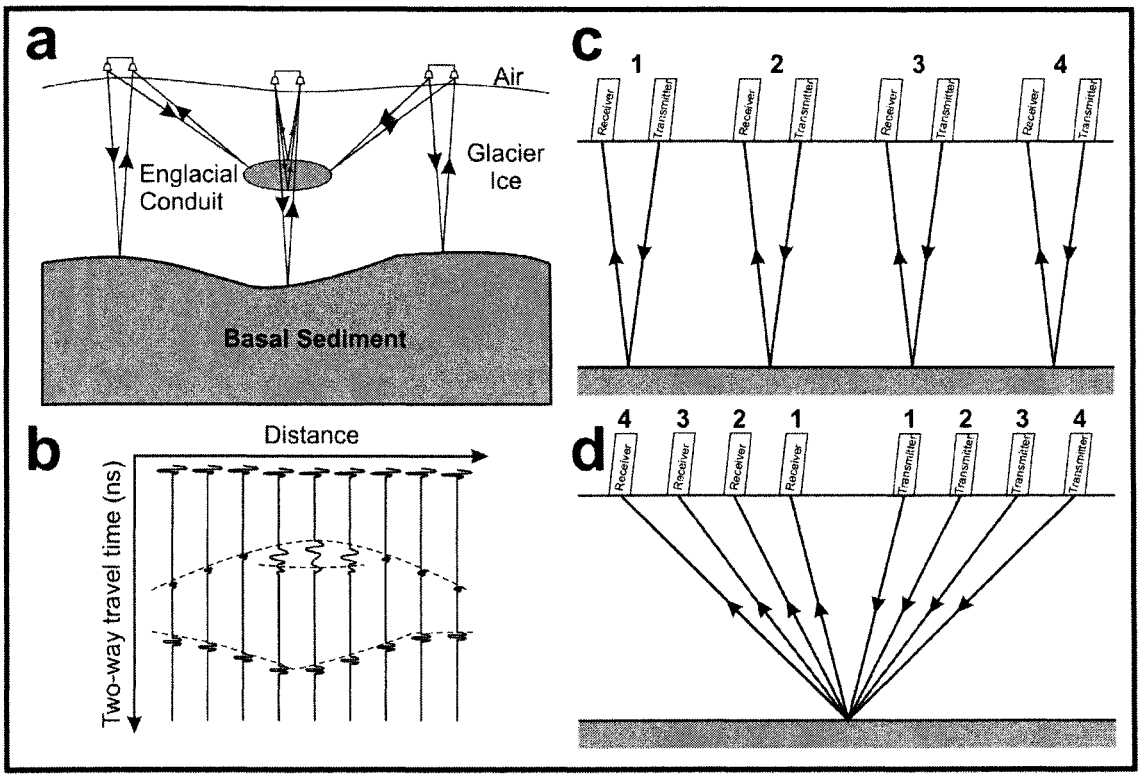


**Figure 4.1.** a) Conceptual illustration of GPR usage in the reflection mode on glacier ice with a sediment bed. A water-filled englacial conduit is also imaged. b) resulting radar record along the profile. Offline reflections are created by the conduit to produce a hyperbolic reflection pattern. A second reflection indicates the position of the ice/basal sediment interface (after Davis and Annan, 1989). Antennae configuration during: a) Common offset survey (CO), when data are collected by moving the antennae as a pair (with a fixed distance between them) along the survey line; b) Common mid-point survey (CMP), when the antennae are moved progressively apart at equal offset from a central survey point (from Woodward, 1999).

Comprehensive summaries of GPR background, methodology, field use, data processing and interpretation are available in the literature (e.g. Daniels *et al.* 1988; Davis and Annan, 1989; Daniels, 1996; Jol and Bristow, 2003; Woodward *et al.* 2003b; Neal, 2004; Hubbard and Glasser, 2005; Woodward and Burke, 2007). The remainder of this section will document important concepts for the interpretation of GPR data at Skeiðarárjökull and Bering Glacier, as well as briefly summarise the current use of GPR in glaciology of relevance to this research.

*4.1.1 Types of survey and EM wave propagation*

The most common form of survey is known as common-offset (CO) surveying and involves the synchronised movement of the antennae along a transect, with the transmitter and receiver being kept at a constant distance of separation (Figure 4.1c) (Woodward, 1999; Neal, 2004). In conventional surveys, the antennae are orientated perpendicular to the survey line (Neal, 2004). The outputs of such surveys display distance along the transect versus two-way travel-time (TWTT), on the x- and y-axis, respectively (Davis and Annan, 1989). In order to convert TWTT into real depth, common mid-point (CMP) surveys are often employed (Davis and Annan, 1989; Woodward, 1999). CMP surveying involves moving the antennae sequentially in opposite directions along the transect from a shared central point (Figure 4.1d). The consequent increases in TWTT with distance from the centre can be used to calculate average radar signal velocity through the substrate (Davis and Annan, 1989; Woodward, 1999; Neal, 2004). During CO surveying, data can be collected either continuously or via step-mode. Continuous surveying involves dragging the antennae along the surface with data being recorded continuously, whilst during step-mode data is collected at set intervals along the transect (Neal, 2004). Step-mode can generate more coherent and higher amplitude reflections, as antennae are stationary during data collection. Furthermore, antennae-ground coupling is more consistent, with the additional benefit of improved trace stacking (Neal, 2004). It is argued by Woodward *et al.* (2003b) that when data is collected continuously it can be more difficult to tie surface structure to reflections and makes some processing steps, such as migration (*Section 4.3.6*) and topographic correction (*Section 4.3.8*), problematical.

The propagation of a radar signal is dependent upon the high frequency electrical properties of the ground. The propagation of radio waves in the ground can be described by both velocity and attenuation, which are dependent upon the dielectric and conductivity properties of the materials (Davis and Annan, 1989). Typical velocity and dielectric permittivity ($\varepsilon$) value for common materials within the glacial environment are given in Table 4.1.

| Material | Velocity (m/ns) | Dielectric Permittivity |
|---|---|---|
| Air | 0.300 | 1 |
| Dry snow | 0.194-0.252 | 1.2-2.0 |
| Wet snow | 0.194-0.252 | 1.5-3.3 |
| Cold Ice | 0.167-0.170 | 3-4 |
| Temperate Ice | 0.140-0.160 | 1.9-2.1 |
| Water | 0.033 | 80 |
| Sediment-rich Ice | 0.122 | 6 |
| Permafrost | 0.120-0.150 | 4-6.3 |
| Till | 0.071-0.087 | 12-18 |
| Shales and Mudstones | 0.077-0.134 | 5-15 |
| Unsaturated sand | 0.1-0.2 | 2.5-7.5 |
| Saturated sand | 0.05-0.08 | 20-31.6 |
| Unsaturated sand and gravel | 0.09-0.13 | 3.5-6.5 |
| Saturated sand and gravel | 0.071-0.076 | 15.5-17.5 |
| Unsaturated clay | 0.09-0.12 | 2.5-5 |
| Saturated clay | 0.05-0.07 | 15-40 |

**Table 4.1.** Velocity and dielectric permittivity ($\varepsilon$) values for materials common within the glacial environment (from Murray *et al.*, 2000a).

Changes in ε through the medium create reflections on a GPR profile (Daniels *et al.*, 1988). In sediments, changes in the amount and type of fluid occupying pore spaces, minor changes in porosity, changes in grain shape, orientation and packing all give significant reflections (Neal, 2004). GPR survey polarity is determined from the polarity of the airwave. The polarity of a GPR wavelet is dependent upon the ε of the materials on either side of the reflection interface (Figure 4.2) (Murray *et al.*, 2000a). If the material beneath the interface demonstrates a decrease in ε (hence an increase in velocity) relative to the negative-positive-negative (-+-) transmitted wavelet then the reflection appears negative-positive-negative (-+-). If the material present beneath the interface has a higher ε (decrease in velocity) the phase of the wavelet will invert, becoming positive-negative positive (+-+) (Murray *et al.*, 2000a). This may allow the interpretation of the nature of subsurface reflections, such as sediment-filled hydrofractures within ice (*Section 5.2.1*).

When designing a GPR survey, there is a compromise between the desired depth of penetration and resolution. Resolution is the ability of the system to distinguish two signals that are close to each other in TWTT and this is dependent upon the centre frequency of the antennae (Neal, 2004). As the frequency is increased, the resolution increases, whilst the depth of penetration is reduced and vice versa (Davis and Annan, 1989), with the resolution typically being one quarter of the GPR wavelength (Woodward *et al.*, 2003b; Neal, 2004). Penetration depth is largely controlled by system performance, attenuation in the ground and the reflection properties at a boundary where the electrical properties vary (Davis and Annan, 1989; Neal, 2004). Signal amplitude is reduced by scattering from thin layers, point-objects like boulders, and the contrast in electrical properties at the reflector (Davis and Annan, 1989).

### *4.1.2 Uses of radar in glacial research*

This section will review the current applications of GPR to englacial surveys and the study of glacial and glaciofluvial landforms. A more extensive review of the application of GPR to glacial and frozen materials can be found in Woodward and Burke (2007).

#### *4.1.2.1 Crevasses and shear zones*

GPR has been commonly used in englacial investigations to map crevasses (e.g. Glover and Rees, 1992; Retzlaff and Bentley, 1993; Clarke and Bentley, 1994) and shear zones (e.g. Nobes, 1994; Goodsell *et al.*, 2002). Glover and Rees (1992) were able to distinguish between crevasses found in relatively shallow new firn and those characterised by hyperbolic scattering found in mature firn or glacier ice. Similar crevasses were also identified in the ice of the Whillans Ice Stream, Antarctica by Clarke and Bentley (1994). Due to assessment of accumulation rates and depth of burial, it was

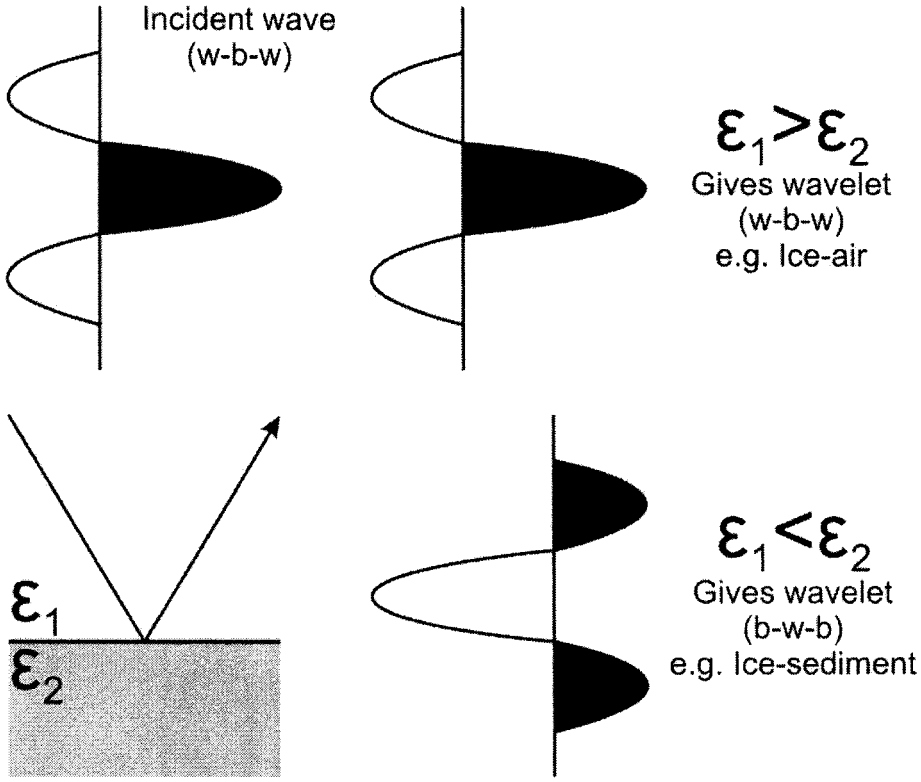


**Figure 4.2.** GPR wavelet polarity resulting from a subsurface reflection between materials of contrasting dielectric permittivities (ε) (Table 4.1), with an incident wave polarity of negative-positive-negative (w-b-w) (after Murray *et al.*, 2000a).

suggested the crevasses were formed at the current zone of ice stream onset and it was calculated that this zone has been stable for the last ~210 years (Clarke and Bentley, 1994). In contrast, based upon similar principles, at the Kamb Ice Stream the depth to crevasses was used to identify details of ice stream stagnation, which propagated up-flow taking >100 years for the entire ice stream to stagnate (Retzlaff and Bentley, 1993).

In addition to crevasse identification, shear zones within the ice matrix have also been observed in GPR profiles of glacier ice. By correlating angled zones of up-glacier dipping hyperbolic reflections to zones of dark ogive bands on the glacier surface, Goodsell *et al.* (2002) were able to identify shear zones at the base of an ice fall at Bas Glacier d'Arolla, Switzerland. A further example comes from the Tasman Glacier, where Nobes (1994) inferred zones of shear associated with extensional flow of ice into a proglacial lake.

#### *4.1.2.2 Englacial sedimentary structure*

Sediment can be incorporated into ice by various processes and GPR has been used to infer various mechanisms, including medial moraine formation (e.g. Glasser *et al.*, 2006), basal ice formation (e.g. Arcone *et al.*, 1995; Murray *et al.*, 1997, 2000a), thrusting (e.g. Glasser *et al.*, 2003) and crevasse filling (e.g. Woodward *et al.*, 2002, 2003a). The imaging of near surface englacial features, such as thrusts and crevasse fills, is often linked to sedimentary outcrops on the glacier surface, aiding interpretation of the GPR profiles (Murray *et al.*, 1997, 2000a; Glasser *et al.*, 2003; Woodward *et al.*, 2003a).

#### *4.1.2.3 Glacial and glaciofluvial landforms*

GPR has been utilized to investigate the internal structure of both glacial and glaciofluvial landforms in the contemporary (e.g. Lønne and Lauritsen, 1996; Russell *et al.*, 2001a; Cassidy *et al.*, 2003; Carrivick *et al.*, 2007) and palaeo-glacial environment (e.g. Busby and Merritt, 1999; Lønne *et al.*, 2001; Fiore *et al.*, 2002; Jacobsen and Overgaard, 2002; Bakker and Van der Meer, 2003). At the margin of Turnerbreen, Svalbard, GPR identified the presence of both buried ice and thrust faulting within the sediments of a contemporary push-moraine (Lønne and Lauritsen, 1996). This provided an analogue applied to the evolution of palaeo-glacial landscapes such as the extensive push-moraine complex near Arnhem, in the Netherlands (Bakker and Van der Meer, 2003). Here, GPR revealed the importance of thrusting in push-moraine formation through the identification of imbricate thrusts that dip towards the former glacier. GPR studies have identified similar compressional folding in ice-push ridges at Denmark (Jakobsen and Overgaard, 2002) and in the U.K. (Busby and Merritt, 1999), though GPR data sets also suggest that the deformational structures imaged in the push moraine complexes differ from those in marine ice-contact systems (Lønne *et al.*, 2001). Faulting

of sediments, as well as being associated with the formation of glacial landforms, can be associated with paraglacial reworking of glaciofluvial sediments (c.f. Woodward *et al.*, 2008).

In the Joux Valley, Switzerland Fiore *et al.* (2002) combined geomorphological, sedimentological and GPR data to interpret the formation of drumlinoid deposits within subglacial conduits prior to a jökulhlaup that eroded the landforms into their current morphology. This study identified the presence of subglacial macroforms that have been identified in Quaternary eskers through sedimentological (Brennand, 1994; Brennand and Shaw, 1996; Brennand, 2000) and GPR data (Sjogren *et al.*, 2007).

In Iceland, proglacial areas are dominated by coarse sedimentary sequences, making them ideal GPR environments (Woodward and Burke, 2007). Russell *et al.* (2001a) and Cassidy *et al.* (2003) investigated the sedimentary architecture of a large, supraglacial ice-walled canyon fill that was deposited during the November 1996 Skeiðarárhlaup. These studies have given an insight into the sedimentary architecture and rates of deposition of glaciofluvial landforms during high-magnitude jökulhlaups (Russell *et al.*, 2001a; Cassidy *et al.*, 2003).

In palaeo-glacial environments, GPR has been an important tool for the identification of glaciofluvial deposits (e.g. Fisher *et al.*, 2005). Due to the lack of sedimentary exposures, Fisher *et al.* (2005) utilized GPR as part of a wider research project reassessing the landscape associated with the Saginaw Lobe of the Laurentide Ice Sheet. By coupling GPR data with other methods, such as the analysis of digital elevation models (DEMs), they suggested that most of the lowland valleys in the study area are tunnel channels and argued that meltwater plays an important role in the evolution of glaciated landscapes (Fisher *et al.*, 2005).

### 4.2 Field Methodology

All GPR data were collected using a pulseEKKO Pro 1100 system (Sensors and Software Inc., Canada), the specifications of which are given in Table 4.2. Three field seasons have been undertaken at Skeiðarárjökull, Iceland, through 2006 and 2007, with englacial structure being investigated in April 2006 and landform sedimentary architecture investigated in July-August 2006, as well as April 2007. A single field season was conducted at Bering Glacier in June 2006, investigating landform sedimentary architecture. All CO GPR data was collected with a 1 m antennae separation in stop-and-collect mode. A number of CMP profiles were collected in order to estimate the rate of EM pulse propagation through the subsurface, allowing depth correction to CO profiles. The remainder of this section will describe the field methodology employed to investigate

| GPR SPECIFICATIONS | |
|---|---|
| Manufacturer | Sensors and Software Inc., Canada |
| System | PulseEKKO Pro 1100 |
| Maximum system performance | 186 dB |
| Programmable time window | 500 ps to 200,000 ns |
| Programmable sampling interval | Any multiple of 50 ps |
| Hardware stacking | $2^n - 1$ to 32,768 |
| Transmitter output voltage | 1000 V |
| Antennae Frequency | 100-200 MHz |

**Table 4.2.** Specifications of the pulseEKKO Pro 1100 GPR System (from sensors and Software Inc., Canada).

englacial structure at Skeiðarárjökull (*Section 4.2.1*), as well as landform sedimentary architecture at Skeiðarárjökull (*Section 4.2.2*) and Bering Glacier (*Section 4.2.3*).

### *4.2.1 Englacial structure, Skeiðarárjökull*

In April 2006, two grids of GPR CO line (2, 595 m) were collected on the surface of Skeiðarárjökull, just up-glacier from an area in which the esker is melting from the margin (*Section 3.2.4*). Grid 1 was collected using a nominal frequency of 100 MHz and a trace spacing of 0.5 m. Lines were orientated oblique to the ice margin and spaced every 50 m, with the grid extending up-glacier for ~250 m (Figure 4.3). Due to the topographical constraints of an incised stream channel, the central lines could not be extended continuously for 400 m resulting in a gap between lines C and H, as well as D and G. The aim of this grid was to identify if the esker deposit(s) could be observed englacially. Subsequently, Grid 2 was collected with X- and Y-lines parallel and perpendicular to Grid 1 lines, respectively. GPR lines here were collected at a nominal frequency of 100 MHz and a trace spacing of 0.2 m. X-lines were spaced every 10 m between lines A and B (Grid 1), whilst Y-lines were spaced every 20 m (Figure 4.3). In addition, two CMP profiles were collected on Grid 2 (*Section 4.3.5*). A summary of GPR line collected to investigate englacial structure at Skeiðarárjökull is given in Table 4.3. Topographical information for all lines was collected using a differential global positioning system (DGPS) and major supraglacial structure within the grids was mapped using a global positioning system (GPS).

### *4.2.2 Sedimentary architecture of the landforms at Skeiðarárjökull*

In July-August 2006 and April 2007 (Survey 2), five grids of CO GPR line (3, 764 m) were collected on all workable sections of the exposed esker with three grids collected on the portal proximal and central sections of the Ice-walled canyon fill. All grids were collected at a step size of 0.1 m using 200 MHz antennae, with lines spaced every 5 m (Figure 4.4). Flow-parallel GPR lines were run between grids, wherever possible, to allow down-flow radar element continuity to be identified, and one ground control line was collected above a sedimentary section along the esker (Figure 4.4). To allow conversion of TWTT into depth (*Section 4.3.8*) and for migration (*Section 4.3.6*), three sets of CMP profiles were collected within the grids (Figure 4.4). Each line was surveyed using either DGPS or a total station to allow for topographic correction during data processing.

### *4.2.3 Sedimentary architecture of the landforms at Bering Glacier*

In June 2006 (Survey 3), two grids of CO GPR line (812 m) were collected on workable areas of the esker with one grid on the western extension of the ice-walled

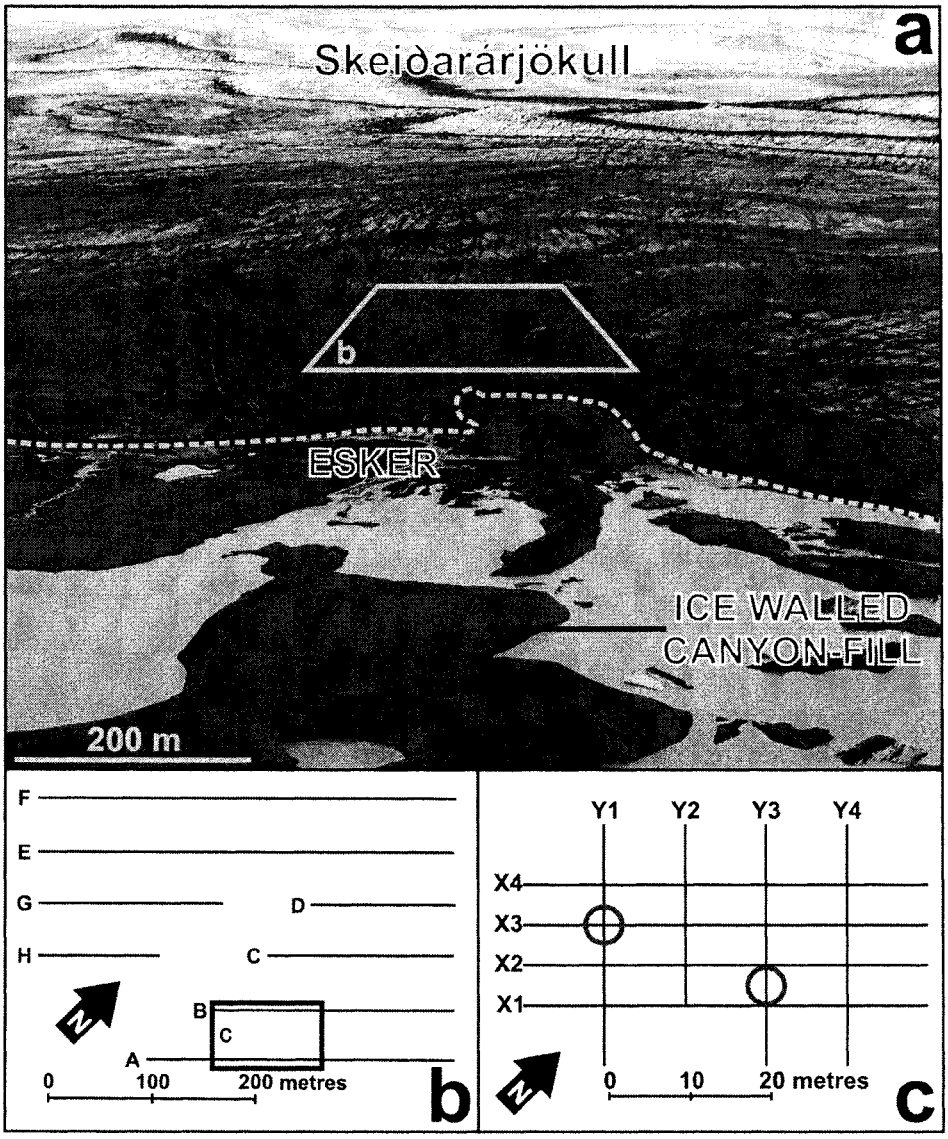


**Figure 4.3.** a) The margin of Skeiðarárjökull (July 2006) in the area of the November 1996 Skeiðarárhlaup esker and ice-walled canyon fill. The location of GPR Grid 1 is indicated by the box. The dashed line highlights the ice margin. b) CO GPR lines collected as part of Grid 1. The box indicates the location of Grid 2. c) CO GPR lines collected as part of Grid 2. The circles indicate the location of CMP profile mid-points.

| Survey | Grid | Landform | Total Lines (m) | Total length (m) | Line Spacing (m) | Freq. (MHz) | Trace spacing (m) |
|---|---|---|---|---|---|---|---|
| Skeiðarárjökull Englacial (Apr 06) | 1 | Englacial Esker | 8 | 1, 960 | 50 | 100 | 0.5 |
| | 2 | | 8 | 635 | 20 x 10 | | 0.2 |
| Skeiðarárjökull Sediments (Jul-Aug 06, Apr 07) | 1 | Esker | 10 | 220 | 5 | 200 | 0.1 |
| | 2 | | 21 | 717 | | | |
| | 3a | | 15 | 505 | | | |
| | 3b | | 7 | 101 | 5 x 3 | | |
| | 3c | | 18 | 505 | 5 | | |
| | 4a | Ice-walled canyon fill | 26 | 930 | | | |
| | 4b | | 16 | 586 | | | |
| | 5 | | 10 | 200 | | | |
| Bering Glacier Sediments (Jun 06) | 1 | Esker | 13 | 322 | | | 0.2 |
| | 2 | | 12 | 280 | | | |
| | 3 | Ice-walled canyon | 9 | 210 | | | |

**Table 4.3.** Summary of CO GPR data collection at Skeiðarárjökull and Bering Glacier.

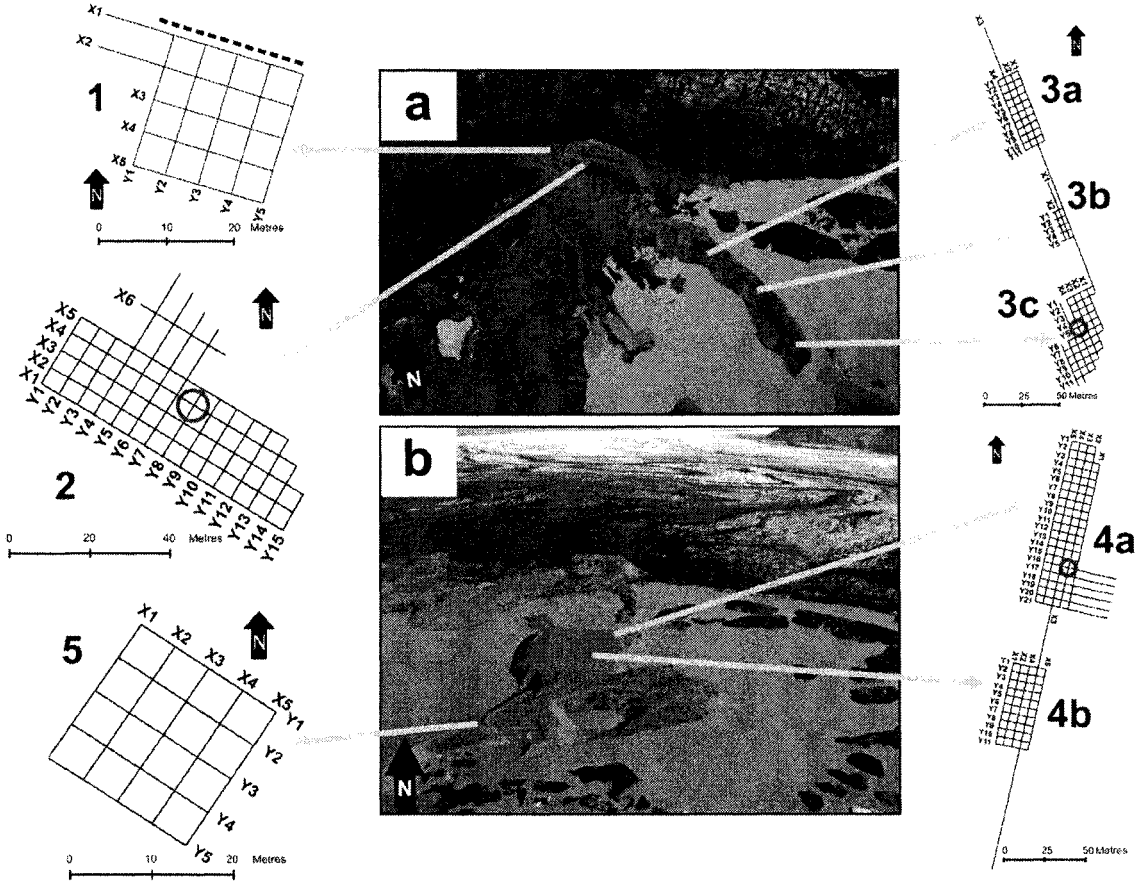


**Figure 4.4.** The location and orientation of GPR grids (1-5) collected along all workable sections of the esker and part of the ice-walled canyon fill during field seasons in 2006 and 2007 (photographs courtesy of Andrew J. Russell and Andrew Gregory). The mid-points of CMP profiles are circled on the relevant grids (2, 3c, 4a). The locations of the sedimentary exposure (Ground control line) is indicated by a dashed line.

canyon fill. All grids were collected at a trace spacing of 0.2 m using 200 MHz antennae, with lines spaced every 5 m where possible (Figure 4.5). In addition two common-mid point (CMP) profiles were collected at Grids 1 and 2 (Figure 4.5) to allow conversion of TWTT into depth (*Section 4.3.8*) and for migration (*Section 4.3.6*). Topographical information for each line was collected using an engineering level. Subsequent to data collection, sedimentary sections were eroded into the esker and ice-walled canyon landforms due to ice-marginal lake drainage in August 2006 (Fleisher *pers. comm.*, 2007). The sections were photographed, providing ground control for the GPR data collected on the landforms (photographs courtesy of P. Jay Fleisher and Palmer K. Bailey; *Section 7.4*).

## 4.3 Data Processing

The basic aim of processing GPR data is to improve the signal to noise ratio (Woodward *et al.*, 2003b) by overcoming the limitations of raw data, resulting in a more realistic cross-section of subsurface electrical properties (Neal, 2004). Some limitations, however, are inherent from site characteristics and the system configuration during data collection (e.g. penetration depth, resolution, step size) and, therefore, cannot be remedied via processing (Neal, 2004).

All data were processed using REFLEXW version 4.2 (Sandmeier, 2006). This section will explain the processing steps used, whilst exploring those available within the REFLEXW package that are relevant to processing of these data sets. For each data set (*Sections 4.2.1-4.2.3*) processing steps and parameters were tested on a single profile, in order to identify the optimal processing protocol for each. For each processing step a number of varying parameter inputs were tested and that which optimized the data most (judged by analysis of CO profiles), without affecting data around the centre frequency (judged by analysis of the spectral plot, e.g. Figure 4.6) was chosen. Examples of parameter testing will be discussed for each processing step, based upon that carried out for sedimentary architecture data sets collected at Skeiðarárjökull. The remainder of the section will present the processing protocols applied to the data sets.

### *4.3.1 Gain function*

The amplitude of a reflected signal reduces with time because of dielectric absorption, geometrical spreading, partial reflection, and scattering (Davis and Annan, 1989; Woodward *et al.*, 2003b; Neal, 2004; Woodward and Burke, 2007). Consequently, it is usually necessary to increase the strength of reflections with increasing TWTT and thus enhance the signal amplitude via the use of a gain function (Woodward *et al.*, 2003b; Neal, 2004). A gain is a time-variant scaling function (Neal, 2004) and REFLEXW supports several functions (Figure 4.6). For englacial surveys at Skeiðarárjökull the most

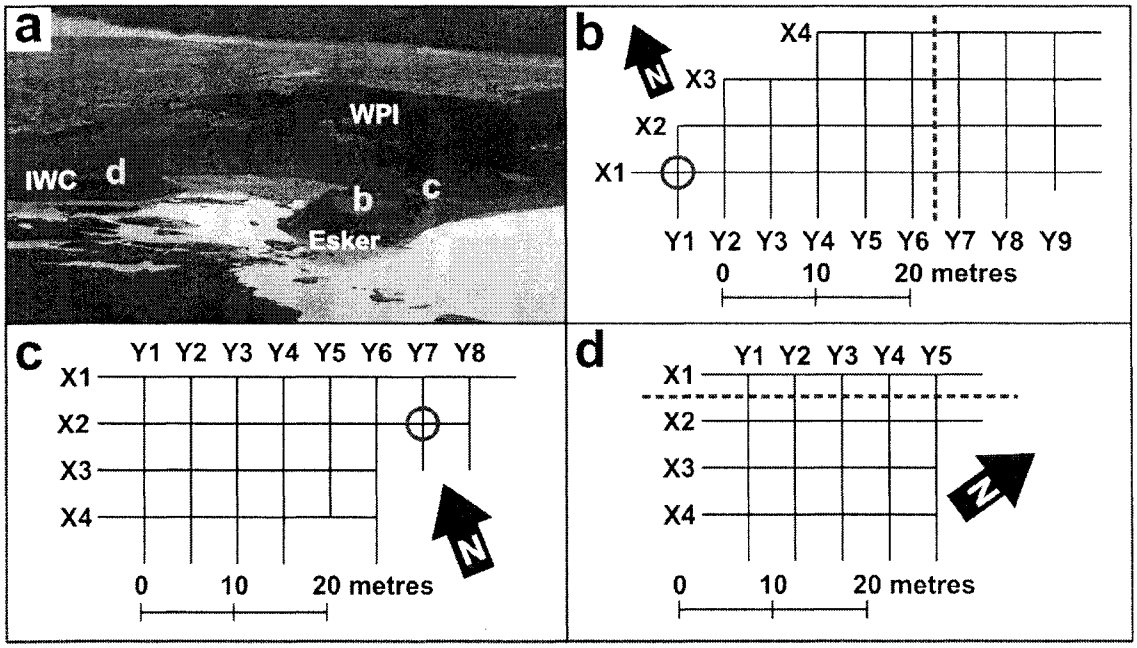


**Figure 4.5.** a) Aerial photograph (courtesy of Palmer K. Bailey) looking approximately southwest to northeast across Weeping Peat Island (WPI). The locations of the esker and ice-walled canyon fill (IWC) are indicated, as are the locations of GPR grids 1-3 (b-d). b) CO GPR lines collected as Grid 1. The circle highlights the mid-point of a CMP profile, whilst the dashed line indicates the approximate location of a sedimentary section that was eroded subsequent to data collection (materials were eroded to left of dashed line). c) CO GPR lines collected as part of Grid 2. The circle highlights the mid-point location of a CMP profile. d) CO GPR lines collected as part of Grid 3. The dashed line indicates the approximate location of a sedimentary section that was eroded into the landform subsequent to data collection (materials were eroded above the dashed line).

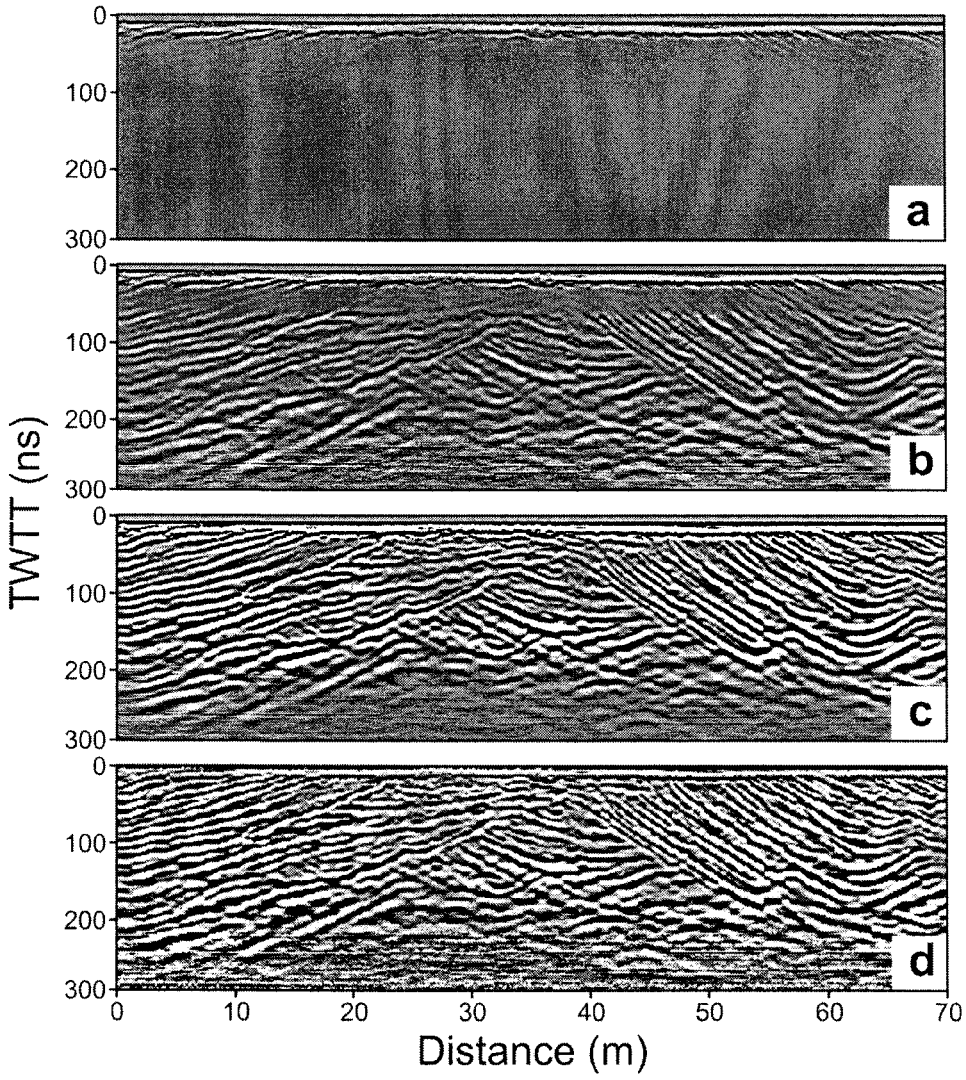


**Figure 4.6.** Effect of different gain functions upon line X1 of Grid 2 (Survey 2): a) Prior to the application of a gain function; b) Following application of an 'AGC gain' with a window length of 70 and a scaling value of 1. Data are not equally amplified down trace; c) After application of 'gain function' with linear and exponential values of 1 and 2.6, respectively, at a maximum gain value of 7000, applied over the entire time range. Again, data is not equally amplified down trace; d) subsequent to the application of an 'energy decay' gain with scaling value of 2. This was found to be the most optimal gain function for sedimentary architecture data sets as it equally amplifies reflections down trace.

optimal was found to be a '*Gain Function*', which multiplies each data point by a chosen linear (0.08) and exponential value (0.02), beginning at a chosen start time (0 ns) and applying a gain up to the chosen maximum value (1000). This function was inappropriate for sedimentary architecture data sets, however, as the '*gain function*' failed to equalize gain down the profile (Figure 4.6c). Instead an '*Energy Decay*' was utilized, which divides every data point down trace by values associated with the automatically calculated decay curve. Next, all data points are multiplied by a chosen 'scaling value', with the most optimal for sedimentary architecture data sets being 2. These gain functions were chosen as they result in consistent reflection amplitudes with increasing TWTT.

*4.3.2 Time-zero correction*

During GPR data collection the first wave-form to arrive at the receiver from the transmitter is the airwave (Woodward *et al.*, 2003b). There is a delay, however, in the onset time of this first arrival on the graphical output, consequent of the length of the fibre optic cables connecting the antennae and the console (Woodward *et al.*, 2003b). This does not remain constant throughout the survey as the unit must warm-up to its ambient operating temperature, thus creating a drift in the arrival time. Use of a damaged optic cable and problems with the internal electronics of the transmitter and receiver units can also result in drift (Woodward *et al.*, 2003b). Not only can this drift be created for the first break, but primary and secondary reflections in the lower profile can also become distorted (Neal, 2004). This is corrected by aligning the airwave arrival at zero on the graphical output.

*4.3.3 Dewow filtering*

GPR data often have a low frequency noise component within the trace, obscuring real data at higher frequencies due to its greater amplitude (Woodward *et al.*, 2003b). This is a consequence of saturation of the system electronics due to the short interval between arrivals of the airwave, ground wave and near-surface reflections (Neal, 2004). The frequency of this noise is dependent upon antennae separation, antennae-ground-coupling and the electrical state of the near surface medium (Woodward, 1999). Dewow is a high-pass filter (Neal, 2004) that suppresses the low frequency 'wow', but allows the spectral peak to remain.

REFLEXW supports one type of 'Dewow' filter: '*Subtract-mean (Dewow)*'. For each data point of each trace, a mean is calculated over a specified time window and then subtracted from the central data value. This time window is moved down the trace by one point and the process is repeated. Various time window lengths were tested on each data set, the results of which for sedimentary architecture data from Skeiðarárjökull can be seen in Figure 4.7. The most suitable time window for sedimentary architecture data sets

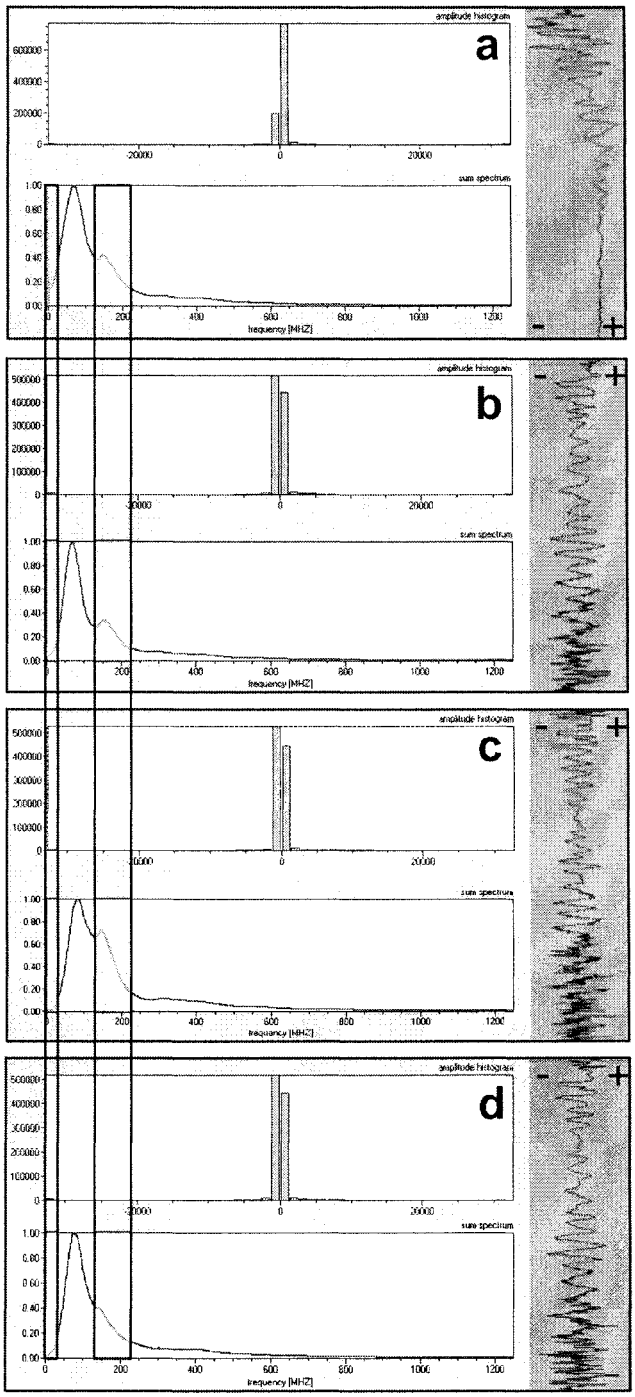


**Figure 4.7.** Effects of the application of a 'dewow' filter to the amplitude histogram (top), spectral plot (bottom) and an example wiggle trace (right) of line X1 of Grid 2 (sedimentary architecture, Skeiðarárjökull). The boxes highlight the key areas of the spectral plot affected by the filters. The left boxes highlight the 'wow', whilst the right boxes highlight the plot around the nominal frequency: a) raw data, showing a 'wow' peak in the spectral plot, as well as low frequency noise in the wiggle trace; b) After application of a dewow filter with a time window of 20 ns. Most 'wow' has been removed but the main peak of the spectral plot has been affected, with the peak being shifted and tightened; c) after application of a dewow filter with a time window of 10 ns. Most 'wow' has been removed but the main peak of the spectral plot has been affected by increasing the high frequency component; d) after application of a dewow filter with a time window of 13.5 ns (optimal for sedimentary architecture data sets). This removes the majority of 'wow' without greatly affecting the main spectral peak.

from Skeiðarárjökull and Bering Glacier was 13.5 ns (Figure 4.7a), whilst a shorter window length of 10 ns was applied to englacial data. Greater time windows, although removing the majority of the low-frequency noise, have a greater effect upon the main peak, and thus the 'real' data (Figure 4.7b). Lower time windows, on the other hand, remove virtually all of the low-frequency noise, but appear to have the greatest impact upon the frequency range around the centre frequency (Figure 4.7c). The optimal time windows remove the majority of the 'wow' peak from the spectral plot whilst having minimal impact on the centre frequency.

### *4.3.4 Bandpass filtering*

Bandpass filtering allows the removal of noise at both the high and low end of the amplitude spectrum (Woodward *et al.*, 2003b). For this study the most optimal bandpass filter supported by REFLEXW is a '*Bandpass Frequency*' filter. '*Bandpass Butterworth*' filters were inappropriate as these created significant background noise within the GPR profile (Figure 4.8). A '*Bandpass Frequency*' filter requires the input of four parameters: 1) low-cut frequency (LF); 2) lower plateau (LP); 3) upper plateau (UP); 4) high-cut frequency (HF). During parameter testing it was ensured that frequency value pairs were kept at an octave (a doubling of frequency, i.e. 20-40-300-600), as steep tapered sections can result in pervasive ringing within GPR data (Woodward *et al.*, 2003b). The most successful parameters (LF-LP-UP-HF) were found to be 15-30-250-500 and 15-30-225-450 for sedimentary architecture data sets collected at Skeiðarárjökull and Bering Glacier, respectively. For englacial data a lower parameter configuration was chosen (30-60-150-300). The most optimal configurations remove most high- and remaining low-frequency noise, whilst having a minimal impact upon the main spectral peak (Figure 4.8).

### *4.3.5 Velocity analysis*

In order to correctly migrate a CO profile (*Section 4.3.6*) a knowledge of the velocity of propagation of the EM pulse in the subsurface is necessary. Furthermore, knowledge of velocity allows better calculation of the depth of reflections in the profile. A number of CMP surveys were collected at Skeiðarárjökull and Bering Glacier, the results of which can be seen in Table 4.4. For CMP surveys, the first arrivals are the air and ground waves below which there are hyperbolic reflections from horizons at depth within the profile (Woodward *et al.*, 2003).

#### *Semblance velocity analysis*

In REFLEXW semblance analysis of CMP profiles can be undertaken to calculate velocities within the substrate. Semblance is a measure of the coherence of hyperbolic reflection energy at a particular normal move-out velocity (Murray *et al.*, 2000a), which are

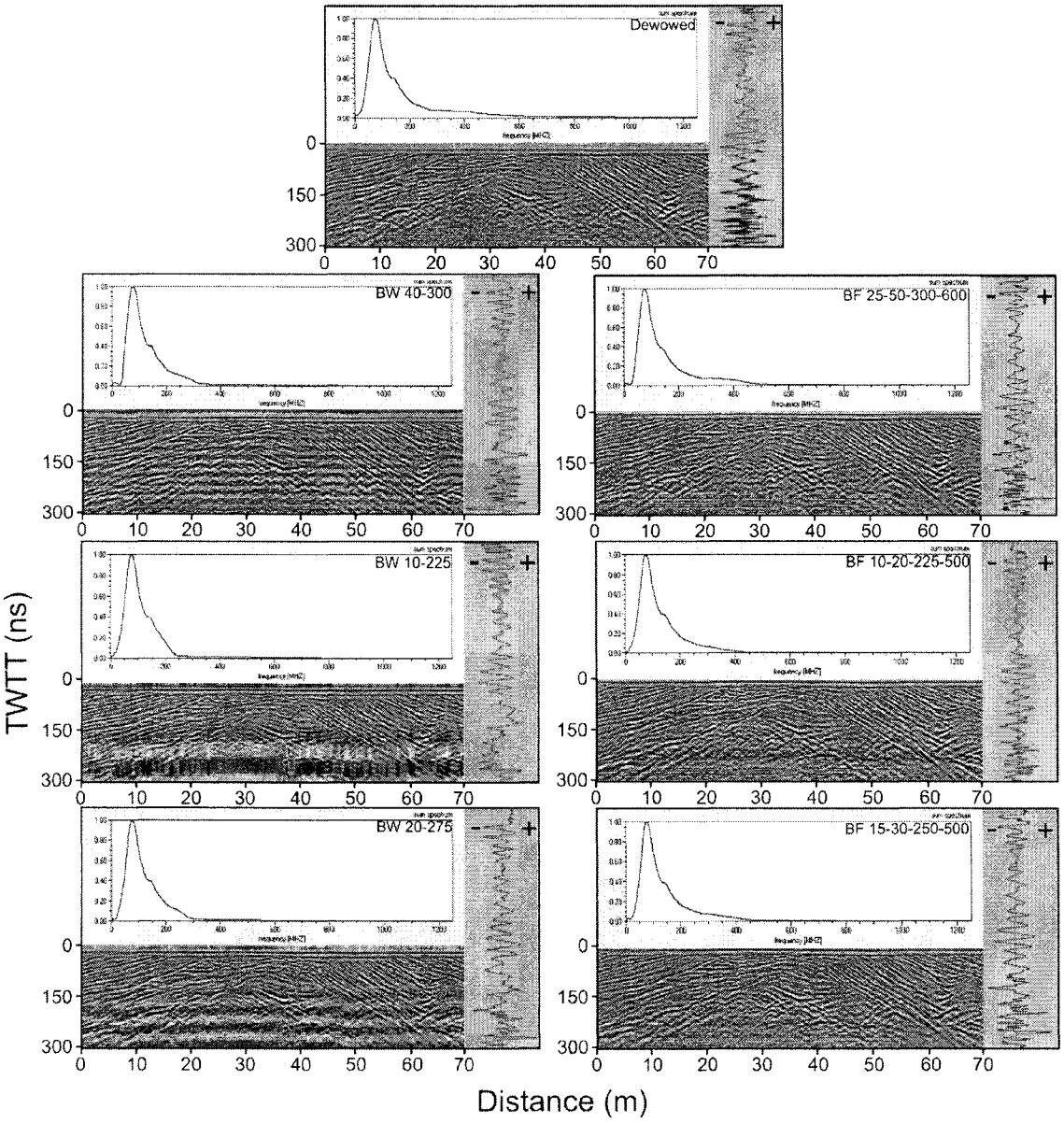


**Figure 4.8.** Effect of applying bandpass filters (all data has been dewowed prior to bandpass filtering) of varying parameters on line X1 of Grid 2 (sedimentary architecture, Skeiðarárjökull). Bandpass butterworth (BW) parameters (left) are in the format, LF-HF. Bandpass frequency (BF) parameters (right) are in the format LF-LP-UP-HF. Although a BW filter can be effective at removing a significant proportion of both the low- and high-frequency component, ringing can be quite pervasive and background noise is also created. Ringing and background noise are less apparent within the data when a BF filter is applied. The optimal filter is found to be BF with parameters of 15-30-250-500 for sedimentary architecture (Skeiðarárjökull) data. This reduces or removes a significant part of both the low- and high frequency component, whilst having a minimal impact upon the main peak of the spectral plot. Higher cut-off parameters (top right) do not improve upon the amount of low-frequency removed from the data and are less effective at removing high-frequency noise. Furthermore, the main peak of the spectral plot is shifted slightly. Lower cut-off values (middle-right), on the other hand, are less effective at removing the low-frequency component and, although removing greater amounts of high-frequency noise, tighten and slightly shift the main peak of the spectral plot.

| Survey | Grid | CMP | Layer | Velocity (m/ns) | CMP mean velocity (m/ns) | Landform mean velocity (m/ns) |
|---|---|---|---|---|---|---|
| Skeiðarárjökull Englacial | 2 | 1 | 1 | 0.150 | 0.135 ± 0.010 | 0.137 ± 0.009 |
| | | | 2 | 0.128 | | |
| | | | 3 | 0.228 | | |
| | | | 4 | 0.034 | | |
| | | | 5 | 0.135 | | |
| | | | 6 | 0.125 | | |
| | | 2 | 1 | 0.150 | 0.139 ± 0.008 | |
| | | | 2 | 0.131 | | |
| | | | 3 | 0.093 | | |
| | | | 4 | 0.136 | | |
| | | | 5 | 0.138 | | |
| Skeiðarárjökull Sediments | 3c | 1 | 1 | 0.083 | 0.084 ± 0.001 | 0.082 ± 0.001 |
| | | | 2 | 0.085 | | |
| | | 2 | 1 | 0.081 | 0.081 | |
| | | | 2 | 0.081 | | |
| | 2 | 3 | 1 | 0.081 | 0.081 | |
| | | 4 | 1 | 0.083 | 0.082 ± 0.001 | |
| | | | 2 | 0.082 | | |
| | 4a | 5 | 1 | 0.080 | 0.080 | 0.078 ± 0.003 |
| | | | 2 | 0.042 | | |
| | | 6 | 1 | 0.076 | 0.076 | |
| | | | 2 | 0.108 | | |
| Bering Glacier Sediments | 1 | 1 | 1 | 0.081 | 0.078 ± 0.004 | 0.079 ± 0.011 |
| | | | 2 | 0.074 | | |
| | | | 3 | 0.079 | | |
| | | | 4 | 0.062 | | |
| | | | 5 | 0.130 | | |
| | 2 | 2 | 1 | 0.069 | 0.080 ± 0.015 | |
| | | | 2 | 0.099 | | |
| | | | 3 | 0.044 | | |
| | | | 4 | 0.120 | | |
| | | | 5 | 0.083 | | |
| | | | 6 | 0.068 | | |

**Table 4.4.** Results of semblance velocity analysis of CMP profiles collected as part of the GPR surveys (Figure 4.9-4.11). An average velocity has been taken for each survey or landform. This average has been used in migration algorithms and for the conversion of TWTT into a depth scale. Those layer velocities which have been highlighted have not been used in average velocity calculations as these are deemed to be unrealistic velocities and are probably created by offline reflectors.

converted to interval velocities within REFLEXW. For a given velocity range and velocity increment a semblance (i.e. the normalised output-to-input energy ratio) is calculated over a given trace range. Once calculated the quantities are displayed as a contoured semblance plot on a grid of TWTT (y-axis) against velocity (x-axis). The plots show 'bullseyes' representing semblance velocities ('bullseyes' are the brightest points in Figures 4.9-4.11), from which the velocity estimates can be manually picked (Figures 4.9-4.11), and a layer velocity can be calculated. Although a number of 'bullseyes' are created from each CMP, only those with the highest semblance values (brightest contours) and fit a major hyperbola within the CMP profile were picked, as these represent the most coherent reflections. The results of the semblance velocity analysis are shown in Table 4.4 and the average for each data set is given. Table 4.1 shows typical velocities for materials common within the glacial environment. For englacial data, the velocity shows significant variations with depth and between CMP profiles (Figure 4.9). The average velocity of 0.137 ± 0.009 m/ns is lower than expected for temperate ice (Table 4.1) and is considerably lower than that calculated for Falljökull (0.149-0.167 m/ns) (c.f. Murray *et al.*, 2000b), which is a temperate glacier ~20 km to the east of Skeiðarárjökull in Iceland.

For sedimentary architecture data from Skeiðarárjökull, CMP mean velocities range from 0.076 m/ns to 0.084 m/ns (Figure 4.10), with the esker and Ice-walled canyon fill averages being 0.082 ± 0.001 m/ns and 0.078 ± 0.003 m/ns, respectively. For sedimentary architecture data from Bering Glacier, the CMP velocities show variation between profiles and with depth (Figure 4.11). The average velocity is 0.079 ± 0.011 m/ns, which is similar to sedimentary architecture data collected at Skeiðarárjökull. The velocity estimates for all sedimentary architecture data sets, however, are consistent with that expected for sands and gravels (Table 4.1). The mean velocities presented in Table 4.4 and used for migration and depth conversion are best estimates (Figures 4.9-4.11). A single average velocity value was used rather than creating a 2D velocity profile as velocity variation with depth was not consistent on each CMP gather. Consequently, a 2D velocity profile may have been affective at one location, but not at another. Furthermore, the use of a single velocity was based on an average of all velocity values for each data set and could be applied to multiple GPR lines, significantly reducing computation time. The calculated average velocity values were relatively consistent with that expected for the materials on which the GPR surveys were conducted (Table 4.1).

### *4.3.6 Migration*

Point and dipping reflectors can create hyperbolic patterns within GPR data, due to the antennae transmitting and receiving an electromagnetic wave that has the form of a complex three-dimensional cone (Neal, 2004), therefore imaging off-line reflections.

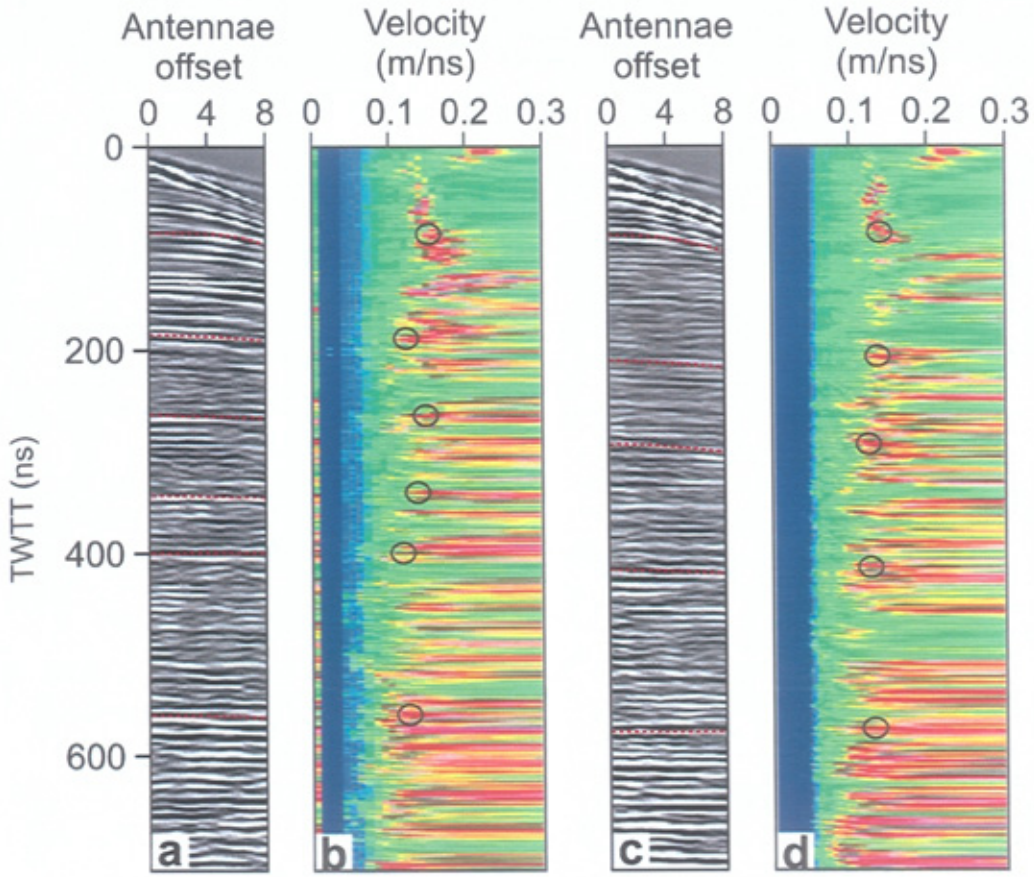


**Figure 4.9.** The results of semblance velocity analyses of CMP profiles collected as part of englacial data collection at Skeiðarárjökull. The CMP profile collected on line Y1 of Grid 2 is shown in a) and the semblance plot is given in (b). c) CMP profile collected on line Y3 of Grid 2, with the semblance plot shown in (d). The semblance peaks or 'bulls-eyes' (circled) are associated with a coherent reflection at depth within the profile (dashed red lines). See *Section 4.3.5* for a full discussion.

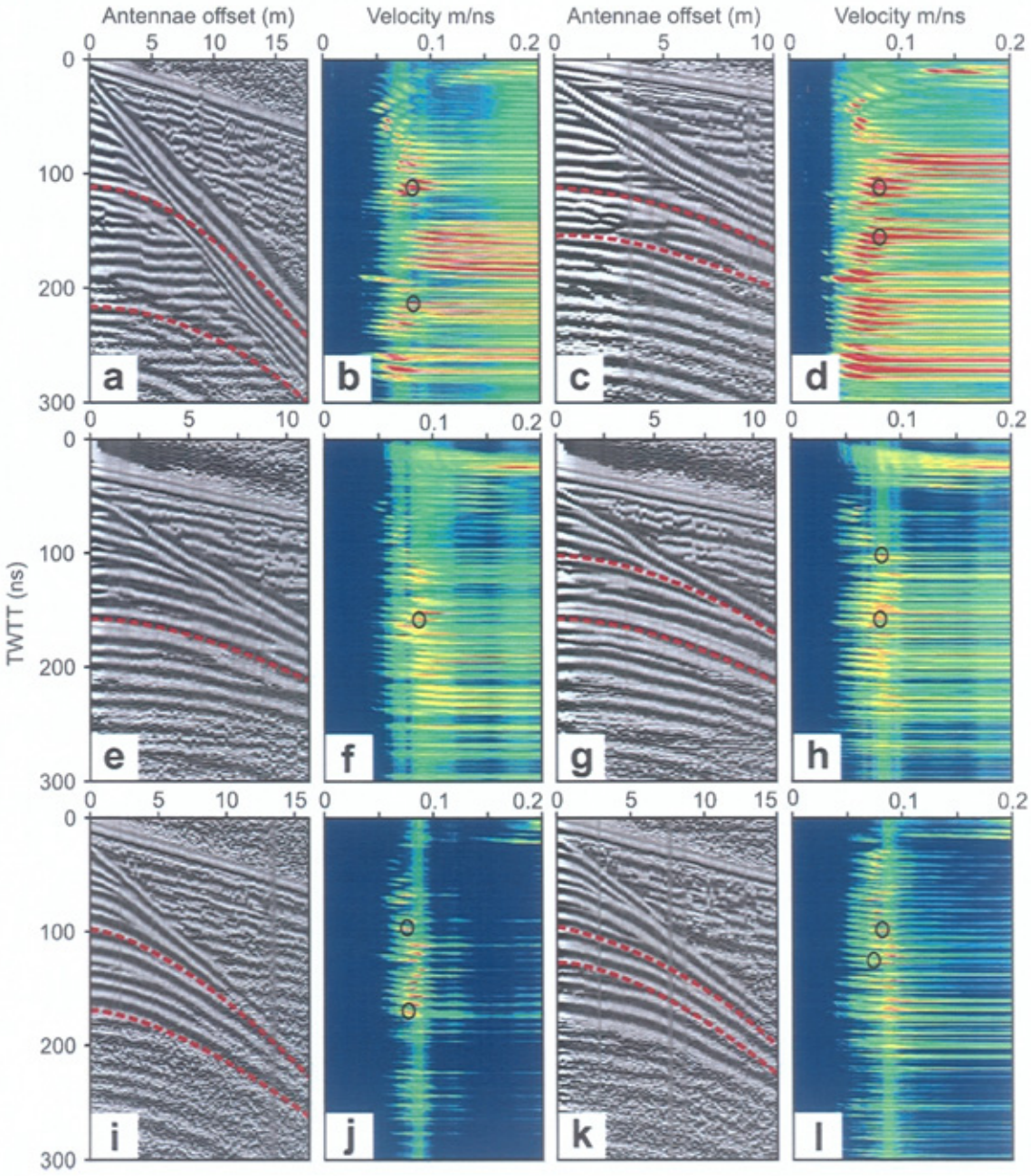


**Figure 4.10.** CMP profiles collected as part of sedimentary architecture data collected at Skeiðarárjökull. The CMP profiles (left) and semblance plots (right) are arranged into pairs collected on Grid 3c (a, b and c, d), Grid 2 (e, f and g, h) and Grid 4a (i, j and k, l). The semblance peaks or 'bulls-eyes' (circled) are associated with a coherent reflection at depth within the profile (dashed red line). See *Section 4.3.5* for a full discussion.

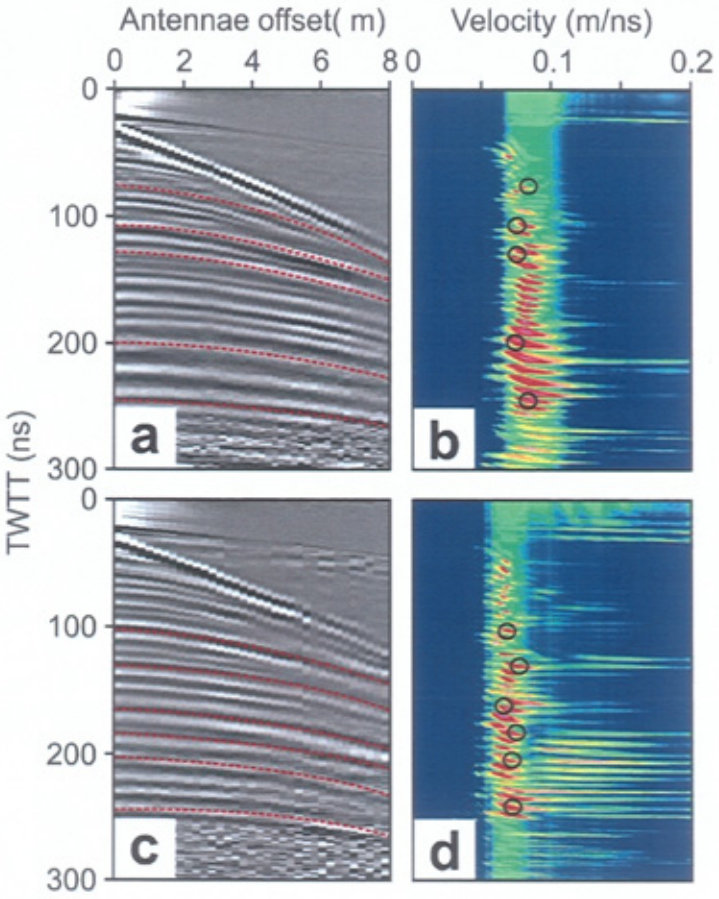


**Figure 4.11.** CMP profiles collected as part of sedimentary architecture data collected at Bering Glacier. The CMP profiles and semblance plots collected on Grid 1 (a and b: line Y1) and Grid 2 (c and d: line Y7) are shown. The semblance peaks or 'bulls-eyes' (circled) are associated with a coherent reflection at depth within the profile (dashed red line). For the CMP gather collected at line Y7, an offset reflection can be identified (c), which will create a problem in velocity calculation. See *Section 4.3.5* for a full discussion.

Migration is applied in order to collapse such reflections back to their original source and to position dipping reflections correctly (Woodward *et al.*, 2003b; Neal, 2004). A migration algorithm assumes that all echoes arise from reflections that are in line with the two-dimensional plane of the survey (Woodward, 1999; Neal, 2004). As an estimate of radar wave velocity is required during application of the processing step, if the source of a hyperbola is off-line the data may become over-migrated producing noise and 'migration smiles' in the data. REFLEXW supports a number of migration algorithms (Figure 4.12). The optimal algorithm for sedimentary architecture data sets was found to be '*Diffraction Stack*', which sums each data point over a chosen summation width, the required size of which is dependent upon the width of the largest hyperbolae. A constant velocity is also specified (mean velocity calculated from CMP profiles) and the algorithm can be applied over a specified time range. For Skeiðarárjökull and Bering Glacier sedimentary architecture data, the optimal summation widths were found to be 75 and 25 traces, respectively (Figure 4.12b) applied over a time window of 30 ns-*end of trace*. For englacial data, however, this algorithm was inappropriate as noise is enhanced within the data set and the spectral plot is significantly affected. Instead, the most optimal algorithm was found to be an '*Fk Migration*', which is applied to the frequency-wavenumber (fk) range. Within this range the migration is performed based upon a specified constant velocity (calculated from CMP profiles) and a scaling value (1). Following application of the algorithm within the fk-range, the data is then transformed back into the distance-time range. For each data set the chosen optimal configurations were deemed to have successfully collapsed hyperbolae that could be identified within the CO profiles, as well as created only minimal noise within the profile (Figure 4.12).

### *4.3.7 Background removal*

Background noise is produced by a slight ringing in the antennae, being a repetitive signal represented by coherent banding within the GPR data that is parallel to the surface wave (Woodard *et al.*, 2003b). Background removal eliminates this banding without degrading useful information within the trace (Woodward, 2003b). A background filter calculates an average (reference) trace over a chosen distance range, subsequently subtracting this mean from every trace within the profile. Woodward *et al.* (2003b) suggest care must be taken in this process not to remove real linear events, such as the surface wave.

A number of parameters for background removal were tested on data that had been migrated (Figure 4.13). The optimal for all data sets was found to be a background removal utilising all traces within the profile (for calculation of the mean trace), and applied over a time range beginning at 50 ns for sedimentary architecture data (Figure 4.13c) and 30 ns for englacial data. These remove a significant amount of background noise from

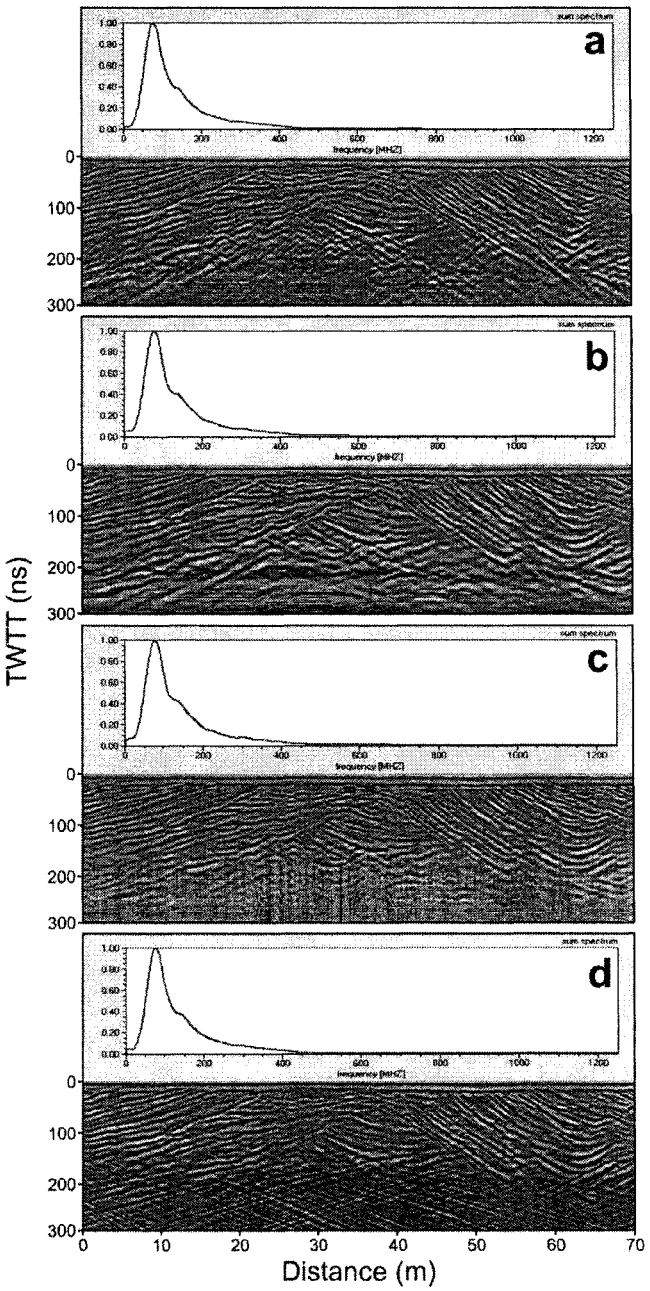


**Figure 4.12.** Effect of migration algorithms on line X1 of Grid 2 (sedimentary architecture, Skeiðarárjökull). For all tests shown a velocity of 0.082 m/ns has been used. a) Pre-migration; the profile has been time-zero corrected, dewowed and bandpass filtered. A number of hyperbolae can be observed within the profile, particularly at greater TWTTs. b) After application of a 'diffraction stack' migration with a summation width of 75 traces and a time window of 30-300 ns. This was found to be the most optimal algorithm for sedimentary architecture data from Skeiðarárjökull, as most hyperbolae have been correctly collapsed, whilst noise is kept at a minimum. Background noise, however, is apparent in the lower profile. Any under-migrated hyperbolae remaining in the profile are deemed to be off-line. c) After application of 'kirchhoff migration' with a summation width of 75 traces and a time window of 30-300 ns. A significant proportion of hyperbolae have been correctly collapsed, though noise is relatively pervasive in the lower profile. d) Following application of 'Fk migration' with a scaling value of 5 and a time window of 0-300 ns. Extremely pervasive noise has been created in the lower profile making it difficult to assess its effectiveness at collapsing hyperbolae.

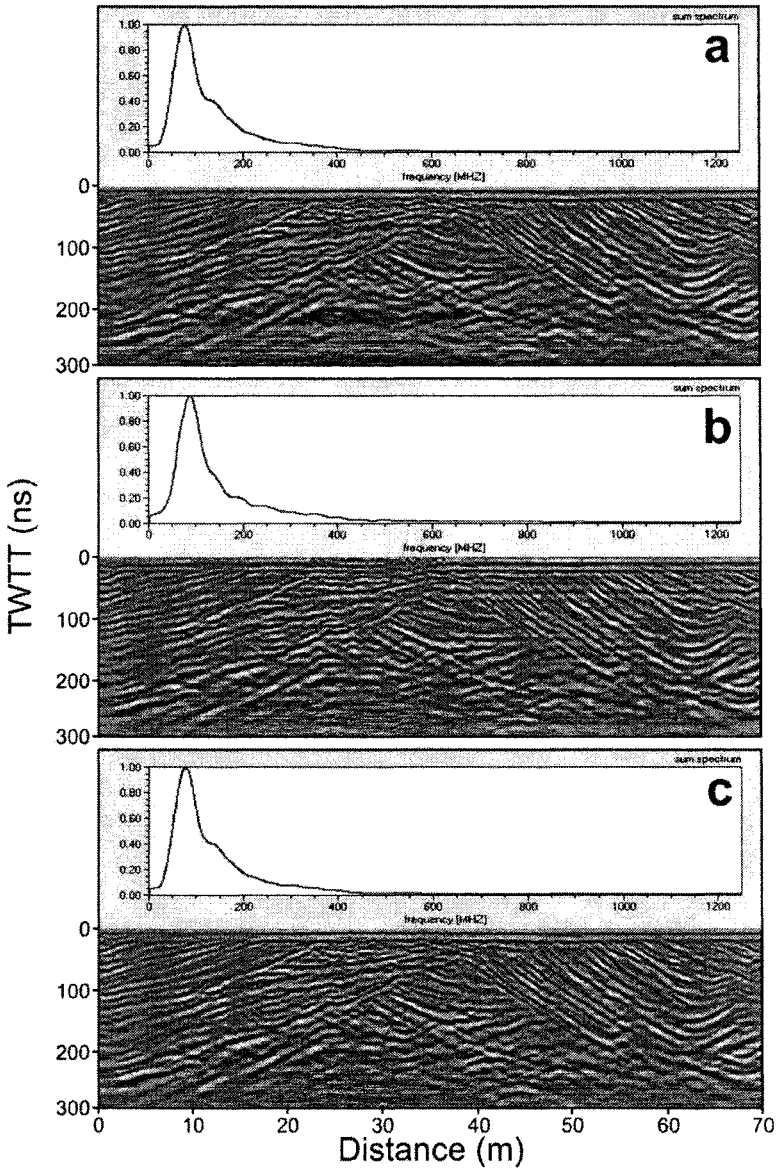


**Figure 4.13.** Effects of background removal filters on line X1 of Grid 2 (sedimentary architecture, Skeiðarárjökull). a) Time-zero corrected, dewowed, bandpass filtered and migrated. Migration has produced background noise within the lower profile. b) After the application of a background removal filter using traces between 30 m and 35 m and a time window of 0-585.6 ns. Most background noise has been eradicated, but the surface wave has been removed in places and the spectral plot has been slightly widened. Furthermore, lower-amplitude background noise is produced throughout the profile, particularly at 50 ns. c) Optimal background removal filter for all data sets, with all traces of the profile used over a time window of 50 ns-end of trace. The majority of background has been removed from the profile without affecting the surface wave or spectral plot.

the profile without affecting 'real' reflections or the frequency spectrum. Lower start times such as 0 or 20 ns, are effective at eliminating background noise, but can degrade the surface wave and affect the spectral plot (Figure 4.13b). When applied over short distance ranges (trace windows) (e.g. 30-35 m) background noise created by the migration algorithm is reduced, but lower-frequency background beginning at a time of approximately 50 ns is created (Figure 4.13b). For the chosen distance range, however, noise was not created.

*4.3.8 Topographic and depth correction*

GPR data must be corrected to take into account topographic variations along the survey transect. By converting relative elevation changes from a base point (greatest elevation) into a value of TWTT (the average velocity of the medium must be known) traces can be shifted up or down by this value, thus displaying the topographic variation of the line (Neal, 2004). In addition, TWTT can be converted into real depth based upon the mean velocity values calculated from CMP semblance analysis (Table 4.4).

*4.3.9 Processing sequence*

The processing sequence for CO lines on each Survey, were tested on an example profile (in a manner similar to that presented in Figures 4.6-4.8, 4.12-4.13) and then applied to all lines within the relevant grids of each data set. Figures 4.14-4.16 summarize the details of the optimal processing sequences applied to all data sets, which are similar to that used by Woodward *et al.* (2003a, 2003b). Although the order of processing remains the same for each data set (Figures 4.14-4.16), the detailed parameters for each step vary and are summarized in Table 4.5. The GPR data will be displayed in this thesis as grayscale plots, where the average amplitude for a certain depth down the trace is taken and assigned a grey-shade value relative to the other amplitude values in the profile. To a lesser extent, wiggle plots will also be presented where appropriate, with the actual waveform displayed and half shaded (on the positive side of the axis).

**4.4 Summary**

A total of 7,171 m of CO GPR line have been collected at Skeiðarárjökull, Iceland and Bering Glacier Alaska. During englacial data collection, two grids of 100 MHz GPR line were collected on the surface of Skeiðarárjökull, just up-glacier from an esker that is being exposed by ice-marginal retreat. During field seasons in 2006 and 2007 (sedimentary architecture data collection at Skeiðarárjökull), eight grids of 200 MHz GPR line were collected on all workable sections of the esker and part of the Ice-walled canyon fill. Sedimentary architecture investigations were conducted at Bering Glacier in June

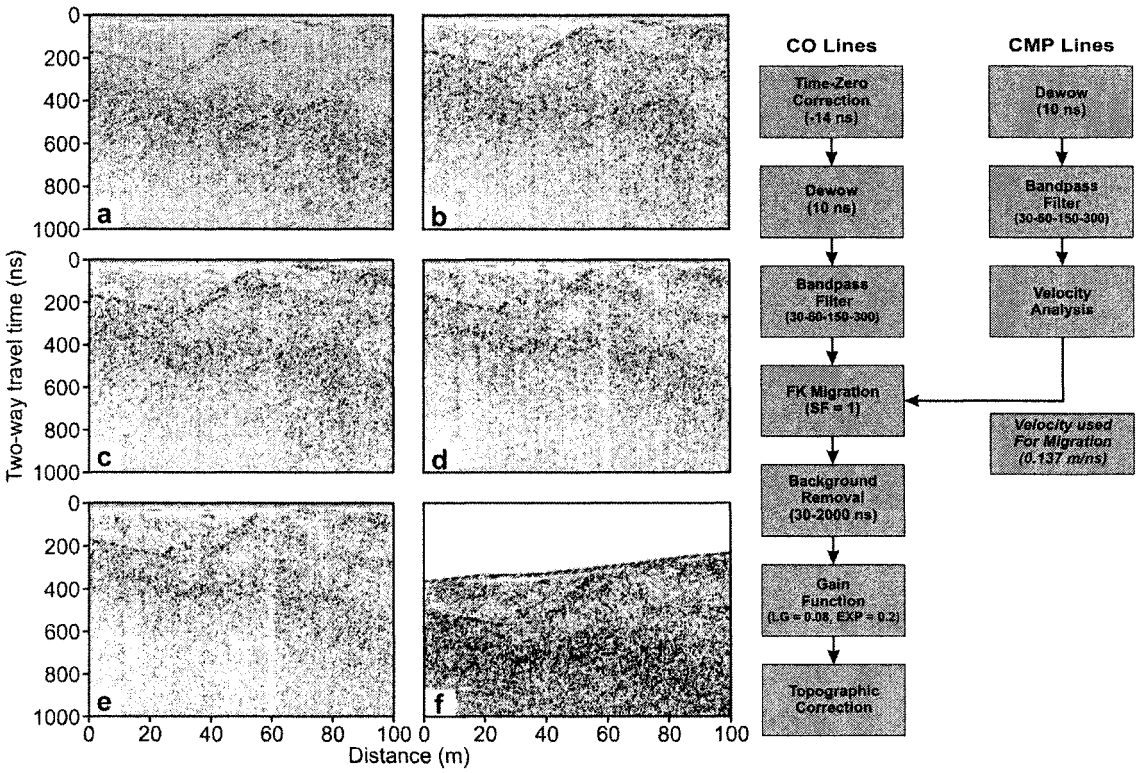


**Figure 4.14.** The optimal processing sequence (right) applied to englacial data collected at Skeiðarárjökull. The profile used for parameter testing was line A of Grid 1. The effects of each processing step upon 0-100 m (line distance) of Line A are shown (a-f): a) raw data after time-zero correction; b) after 'dewow' filtering; c) after the application of a bandpass frequency filter; d) after migration using the appropriate velocity estimated from CMP semblance analysis; e) after background removal; f) after the application of a gain function and topographic correction.

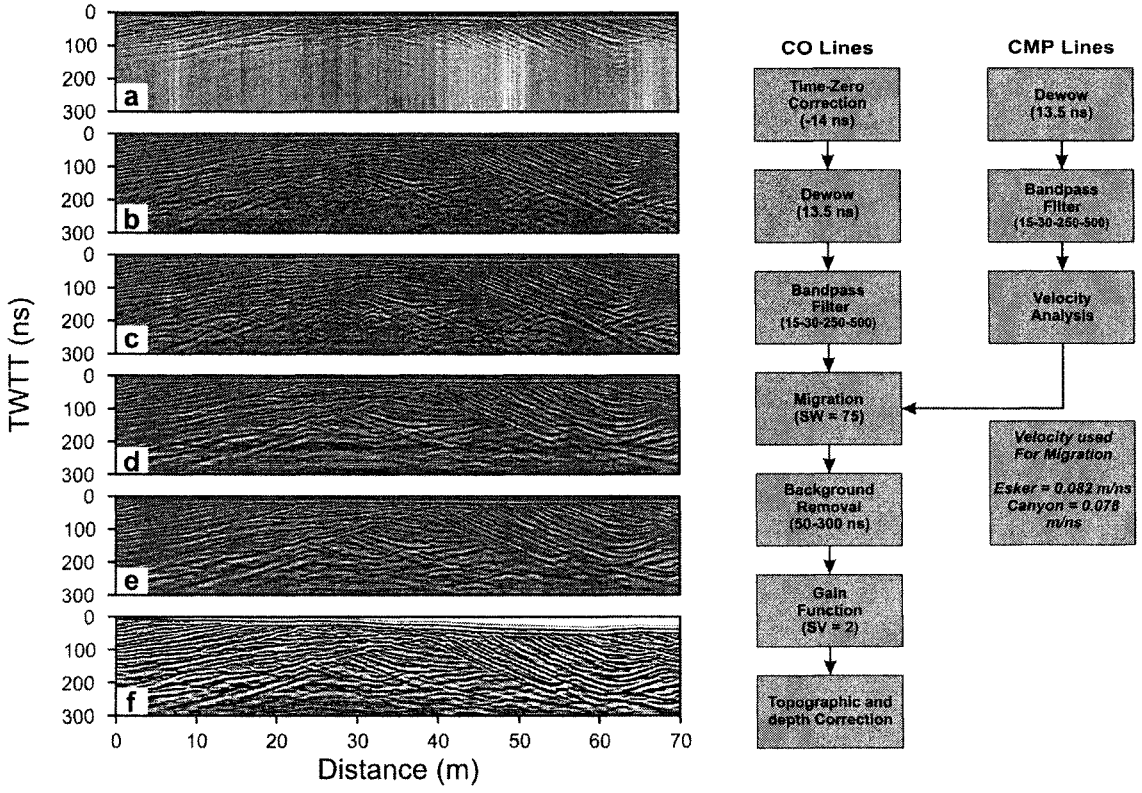


**Figure 4.15.** The optimal processing sequence (right) applied to sedimentary architecture data collected at Skeiðarárjökull. The profile used for parameter testing was line X1 of Grid 2. The effects of each processing step upon Line X1 are shown (a-f): a) raw data after time-zero correction; b) after 'dewow' filtering; c) after the application of a bandpass frequency filter; d) after migration using the appropriate velocity estimates from CMP semblance analysis; e) after background removal; f) after the application of a gain function and topographic correction.

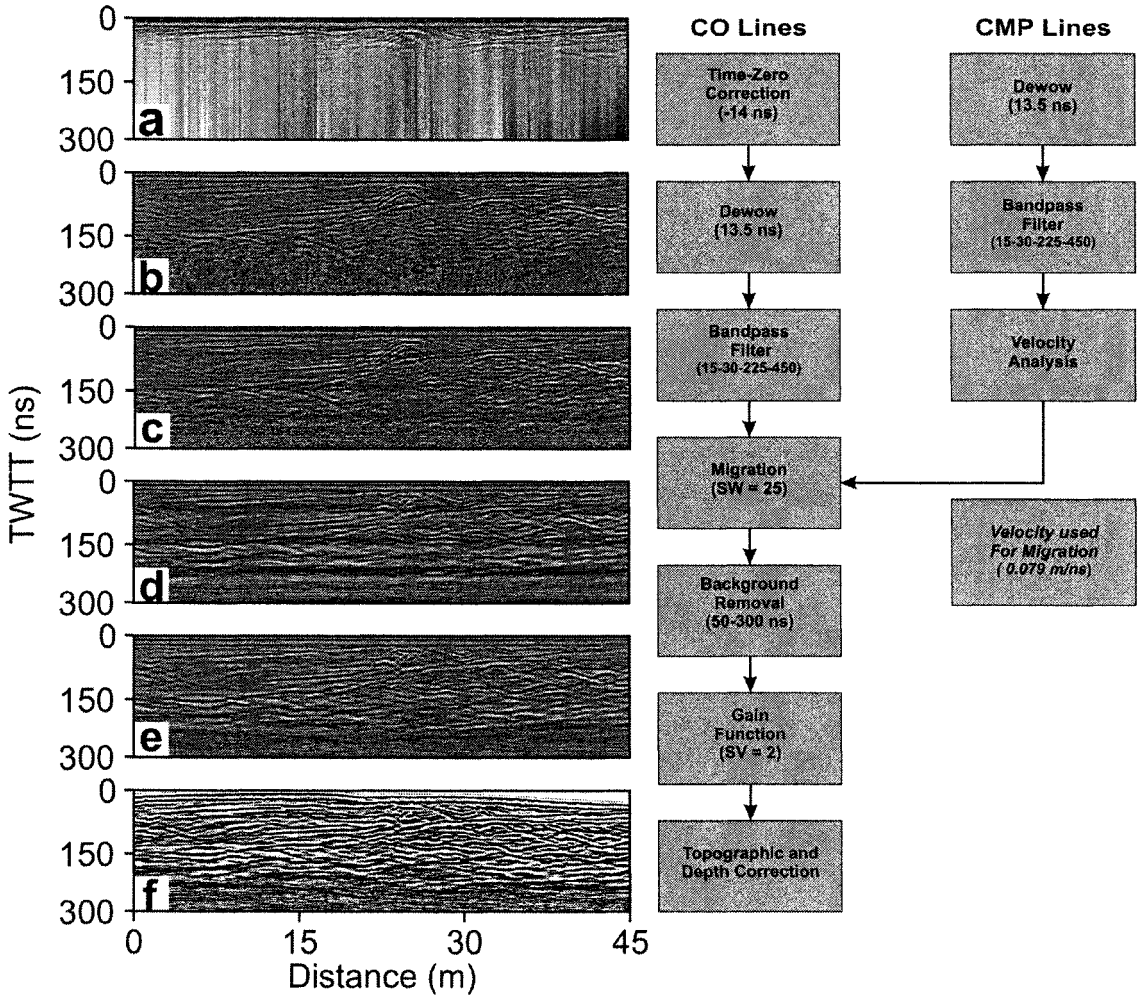


**Figure 4.16.** The optimal processing sequence (right) applied to sedimentary architecture data collected at Bering Glacier. The profile used for parameter testing was line X2 of Grid 1. The effects of each processing step upon Line X2 are shown (a-f): a) raw data after time-zero correction; b) after 'dewow' filtering; c) after the application of a bandpass frequency filter; d) after migration using the appropriate velocity estimates from CMP semblance analysis; e) after background removal; f) after the application of a gain function and topographic correction.

| Processing | Skeiðarárjökull Englacial | Skeiðarárjökull Sediments | Bering Glacier Sediments |
|---|---|---|---|
| *Frequency* | 100 MHz | 200 MHz | |
| *Stacks* | 32 | | |
| *TZC* | -14 ns | | |
| *Dewow* | 10 ns | 13.5 ns | |
| *Bandpass filter* | 30-60-150-300 | 15-30-250-500 | 15-30-225-450 |
| *Velocity (migration/depth conversion)* | 0.140 m/ns | Esker: 0.082 m/ns<br>IWCF: 0.079 m/ns | 0.076 m/ns |
| *Migration* | (Fk)<br>Scaling factor: 1 | (Diffraction Stack)<br>Summation width: 75 | (Diffraction Stack)<br>Summation width: 75 |
| *Background removal* | 30-2000 ns | 50-300 ns | |
| *Gain Function* | (Gain Function)<br>LG: 0.08, EXP: 0.2 | (Energy Decay)<br>Scaling value: 2 | |

**Table 4.5.** Specifics of the optimal processing different data sets (TZC: time-zero correction; IWCF: Ice-walled canyon fill; steps (Figures 4.14-4.16) for LG: linear gain; EXP: exponent).

2006, where three grids of 200 MHz GPR line were collected on workable sections of the esker and western extension of the ice-walled canyon fill. In addition a number of CMP profiles were collected during all data collections and for sedimentary architecture data sets, lines were tied to sedimentary exposures where possible. All GPR line were surveyed for topographic variation and major ground surface structure (to assist with data interpretation).

Following tests on sample profiles from each data set, the acquired optimal processing sequence was applied to all data collected as part of each survey. Both a 'dewow' and bandpass filter were applied to remove low and high frequency noise, respectively, and application of a migration algorithm, using mean velocities calculated from semblance analysis of CMP profiles, have moved dipping reflections to their 'true' subsurface position, as well as collapsed hyperbolic reflections associated with offline reflectors. Background removal was used to eradicate horizontal banding from the data, before a gain function was applied and profiles were topographically corrected.

# SECTION III
# Results and Interpretations

*"…it should seem probable that this Ridge of Pebble and Sand was brought from some remote places by some violent motion of Waters, and dispos'd into the form it now remains in, which induc'd the Author several times to say, he believ'd it to be the effects of Noah's Flood, the Consideration whereof he refers to better judgements."*

Richard Prior's 1699 description of an Irish esker

*Sediment section along an esker segment deposited during the November 1996 Skeiðarárhlaup (palaeo-flow direction is from right to left).*

# Chapter 5

## Structural Controls on Englacial Esker Sedimentation: Skeiðarárjökull, Iceland

### 5.1 Introduction

Two grids of ground-penetrating radar data were collected on the surface of Skeiðarárjökull, approximately thirty metres up-glacier from the point at which the esker has been partially exposed from the glacier margin (Figure 4.3). Both grids of CO GPR line were collected at a nominal frequency of 100 MHz. Grid 1 extends up- and across-glacier for 250 m and 400 m, respectively. Grid 2 was collected at finer trace spacing and in an area where englacial reflections were identified on Grid 1 lines. In addition, two CMP profiles were collected on Grid 2 to gain an estimate of subsurface EM wave velocity. This chapter will present the results and then interpretations of structure imaged on the GPR lines. A summary of this chapter has been submitted for peer-review to the *Annals of Glaciology*.

### 5.2 Description and quantification of GPR grids

In general, the pervasiveness of near-surface tephra bands, hydrofractures and shear planes, coupled with the temperate ice environment made for poor radar conditions. Some reflections, however, could be identified on Grids 1 and 2, which will be described below. All seven GPR lines collected as part of Grid 1 are presented as separate figures (Figures 5.1-5.8), whilst Grid 2 lines are shown collectively (Figure 5.11). Enlarged Grid 2 GPR lines and interpretations are presented in *Appendix 2*.

#### *5.2.1 Grid 1*

In all GPR lines, structure can be identified to a maximum depth of approximately seventy metres, below which the signal rapidly attenuates. Several major reflections can be identified within Grid 1 GPR profiles (Figures 5.1-5.8):

- Within Grid 1, eight near surface zones of scattering (labelled 'S') can be identified (Figures 5.1-5.4, 5.7-5.8).
- On all Grid 1 GPR lines two suites of dipping englacial reflections can be traced from the glacier surface to varying depths within the profile. The first suite of englacial reflections, labelled T (and numbered in Figures 5.1-5.2 to aid descriptions), typically dip at angles from 1-10° in an orientation that is oblique to the ice margin. Most reflections can only be traced in the near surface for distances of <20 m, though in line

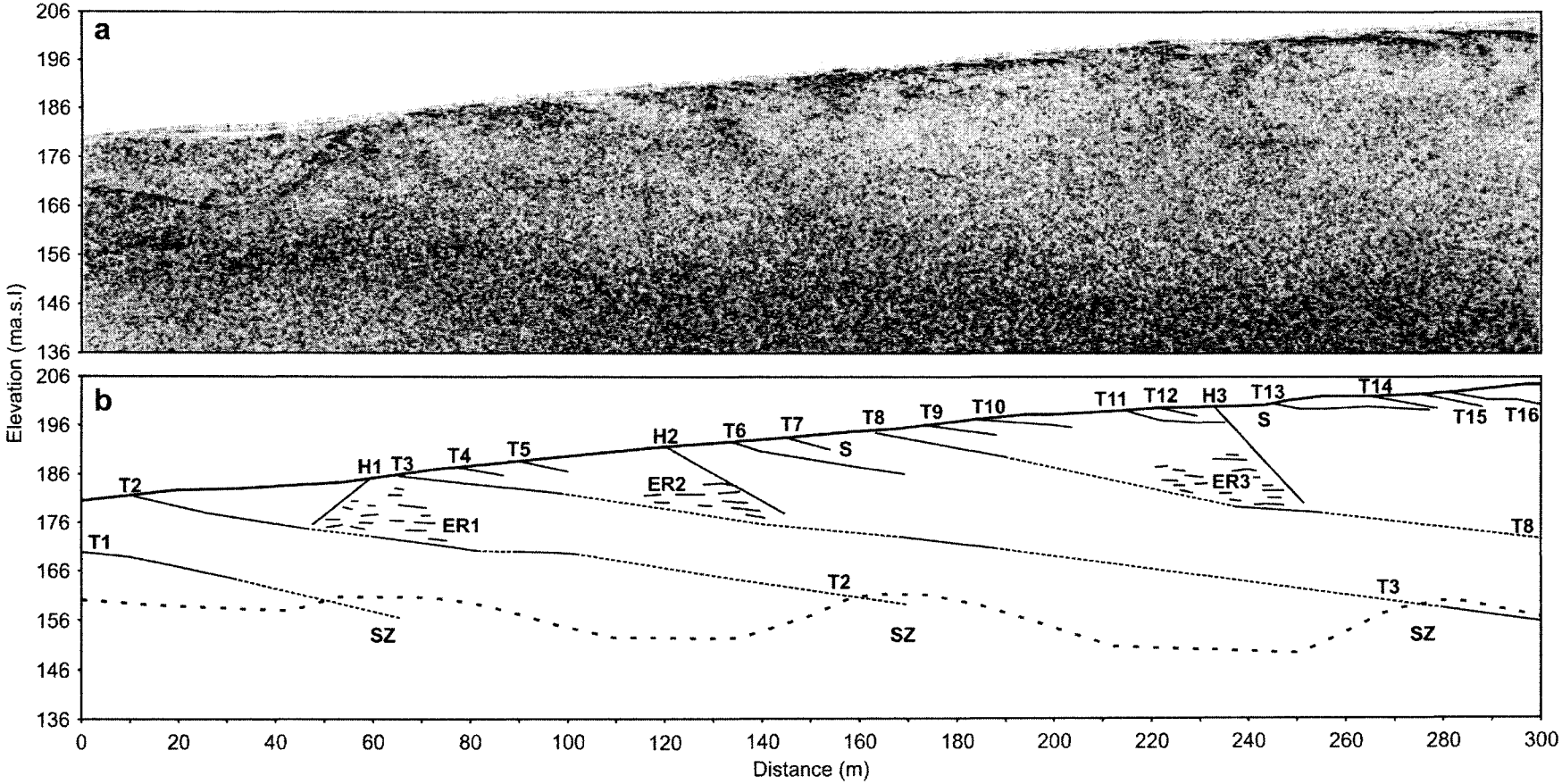


**Figure 5.1.** a) Line A after the application of the optimal processing sequence presented in Figure 4.14. b) Interpretation of Line A: The wide dashed line represents the approximate position of a transition to a zone of englacial scattering (SZ). At the near surface, two suites of dipping reflections can be identified and are labelled 'T' and 'H' (they are numbered in order to identify those that can be traced through Grid 2, Figure 5.11). Three areas of englacial reflections (ER) are identified (individual lines denoting ER1-3 are representative and do not indicate all reflections). The bases of the ER are defined by englacial dipping reflections (T), the amplitude of which vary along the line, with weaker amplitude sections being indicated by a narrow dashed line. Two near surface zones of scattering can be identified and correlated to supraglacial streams (S) at the time of data collection.

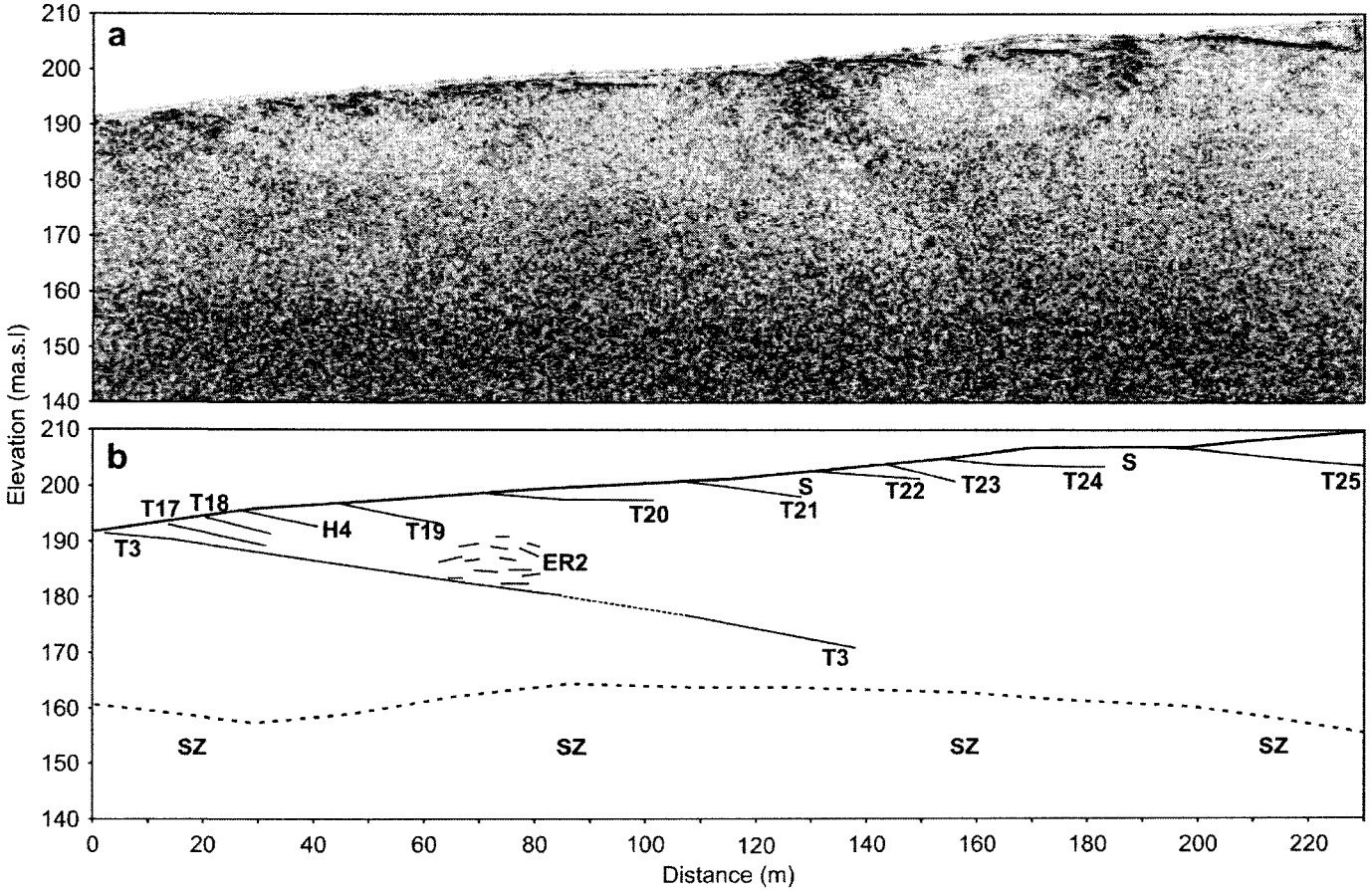


**Figure 5.2.** a) Line B after the application of the optimal processing sequence presented in Figure 4.14. b) Interpretation of Line B: The wide dashed line represents the approximate position of a transition to a zone of englacial scattering (SZ). At the near surface, one suite of dipping reflections can be identified and are labelled 'T' (they are numbered in order to identify those that can be traced through Grid 2, Figure 5.11). One area of englacial reflections (ER2) is identified (individual lines denoting ER2 are representative and do not indicate all reflections). The base ER2 are defined by englacial dipping reflections (T), the amplitude of which vary along the line, with weaker amplitude sections being indicated by a narrow dashed line. Two near surface zones of scattering can be identified and correlated to supraglacial streams (S) at the time of data collection.

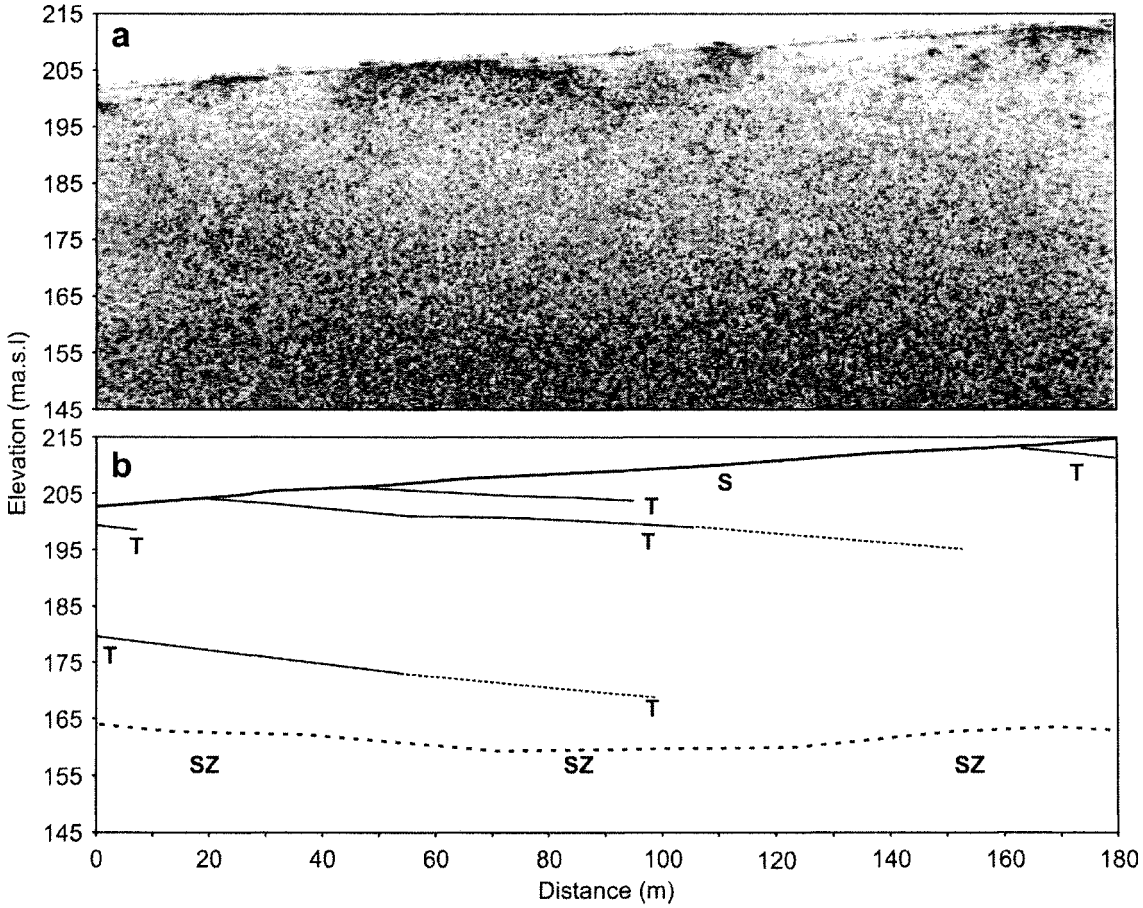


**Figure 5.3.** a) Line C after the application of the optimal processing sequence presented in Figure 4.14. b) Interpretation of Line C: The wide dashed line represents the approximate position of a transition to a zone of englacial scattering (SZ). At the near surface, one suite of dipping reflections can be identified and are labelled 'T', the amplitude of which vary along the line, with weaker amplitude sections being indicated by a narrow dashed line. One near surface zone of scattering can be identified and correlated to a supraglacial stream (S) at the time of data collection.

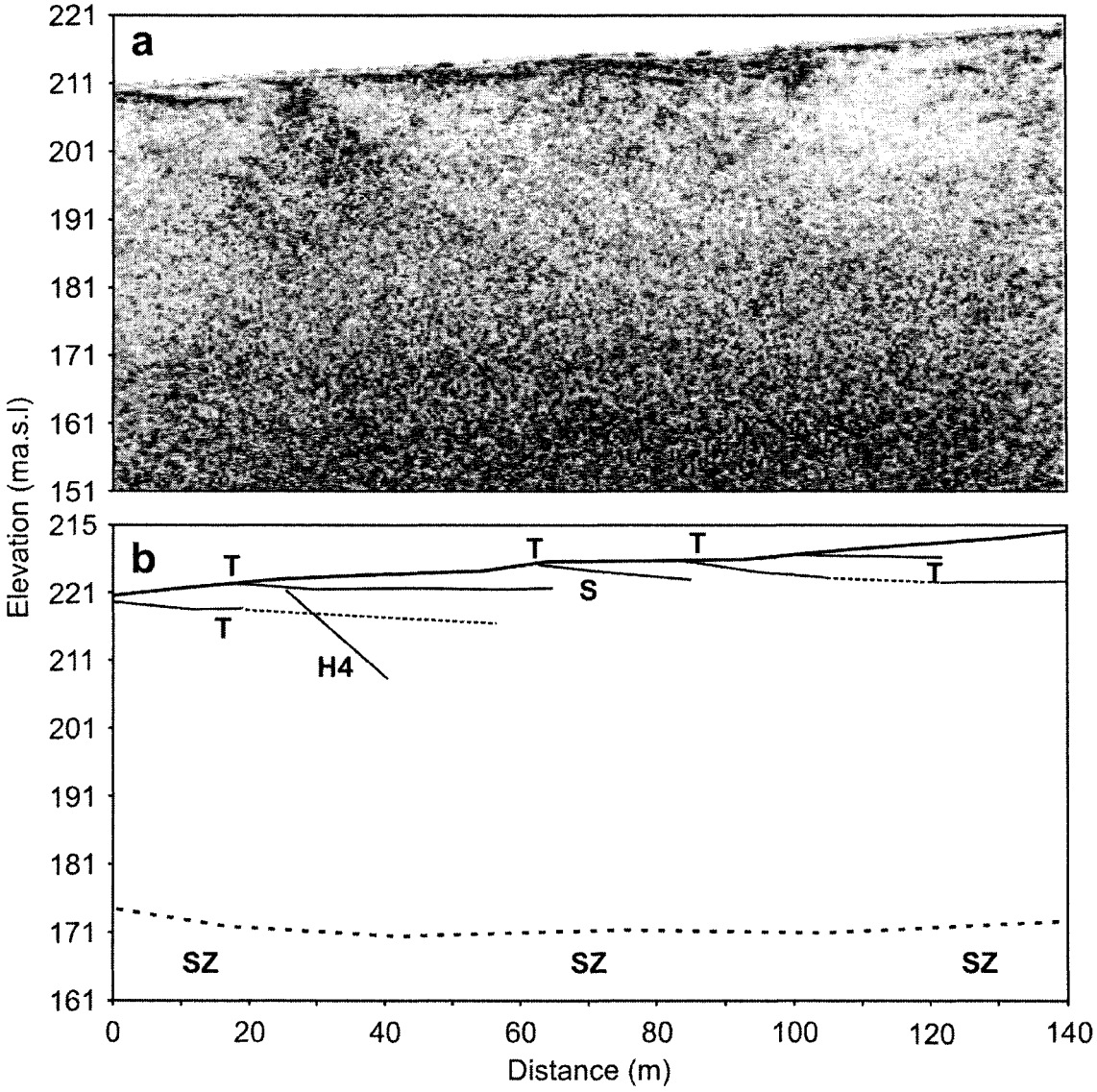


**Figure 5.4.** a) Line D after the application of the optimal processing sequence presented in Figure 4.14. b) Interpretation of Line D: The wide dashed line represents the approximate position of a transition to a zone of englacial scattering (SZ). At the near surface, two suites of dipping reflections can be identified and are labelled 'T' and 'H'. The amplitude of T which vary along the line, with weaker amplitude sections being indicated by a narrow dashed line. One near surface zone of scattering can be identified and correlated to a supraglacial stream (S) at the time of data collection.

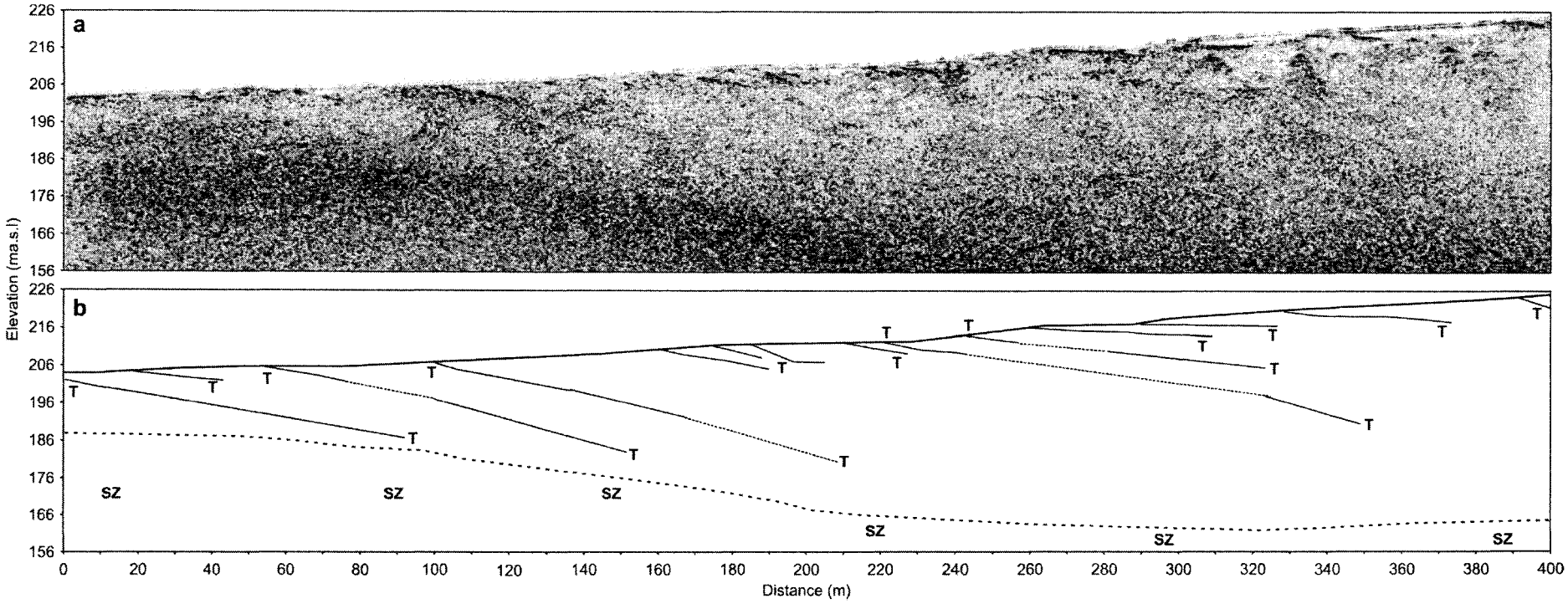


**Figure 5.5.** a) Line E after the application of the optimal processing sequence presented in Figure 4.14. b) Interpretation of Line E: The wide dashed line represents the approximate position of a transition to a zone of englacial scattering (SZ). At the near surface, one suite of dipping reflections can be identified and are labelled 'T', the amplitude of which vary along the line, with weaker amplitude sections being indicated by a narrow dashed line.

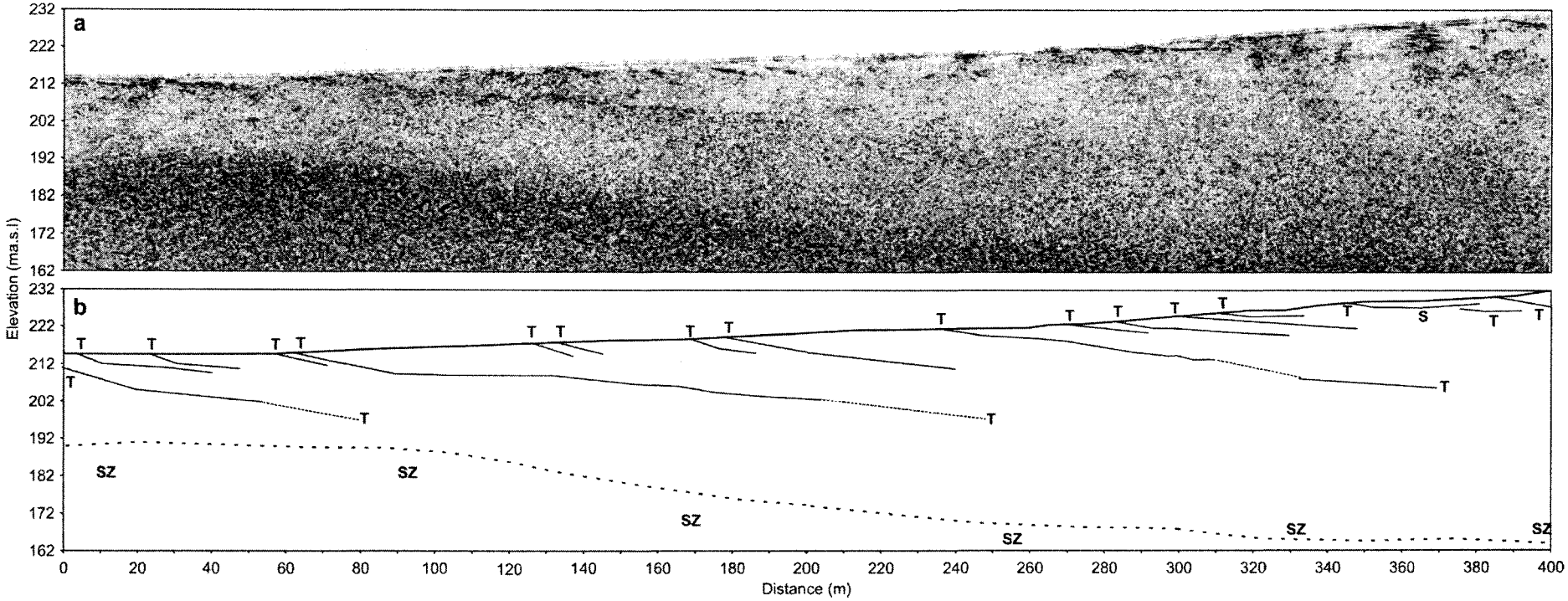


**Figure 5.6.** a) Line F after the application of the optimal processing sequence presented in Figure 4.14. b) Interpretation of Line F: The wide dashed line represents the approximate position of a transition to a zone of englacial scattering (SZ). At the near surface, one suite of dipping reflections can be identified and are labelled 'T', the amplitude of which vary along the line, with weaker amplitude sections being indicated by a narrow dashed line. One near surface zone of scattering can be identified and correlated to a supraglacial stream (S) at the time of data collection.

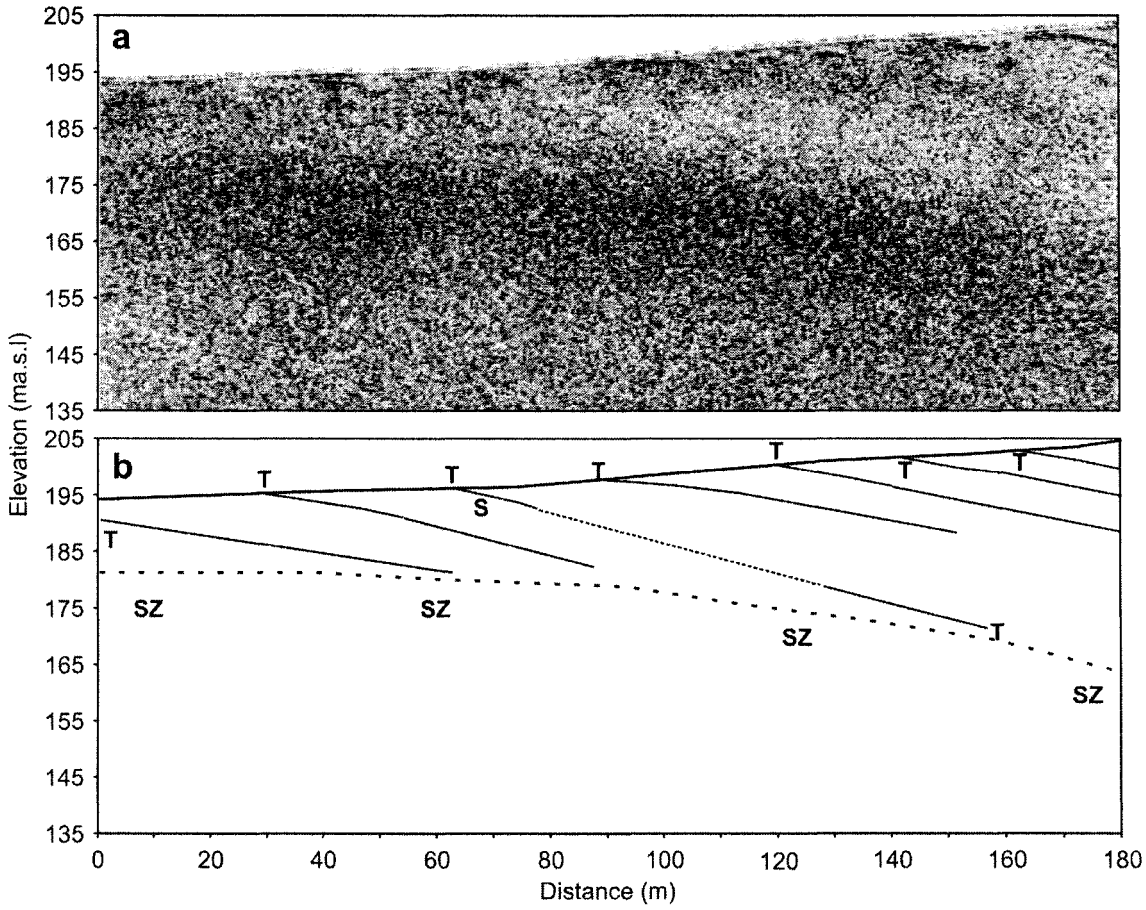


**Figure 5.7.** a) Line G after the application of the optimal processing sequence presented in Figure 4.14. b) Interpretation of Line G: The wide dashed line represents the approximate position of a transition to a zone of englacial scattering (SZ). At the near surface, one suite of dipping reflections can be identified and are labelled 'T', the amplitude of which vary along the line, with weaker amplitude sections being indicated by a narrow dashed line. One near surface zone of scattering can be identified and correlated to a supraglacial stream (S) at the time of data collection.

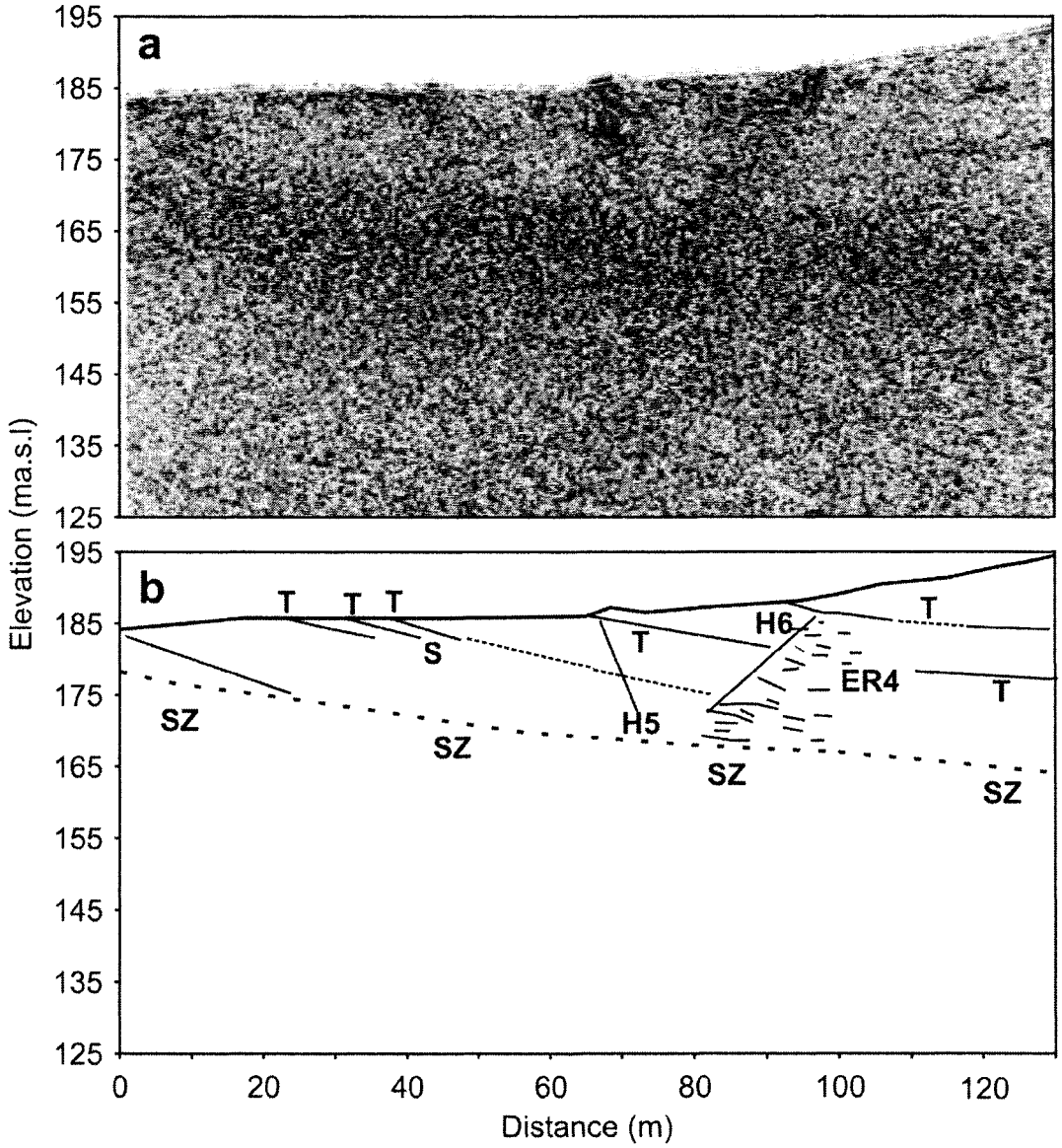


**Figure 5.8.** a) Line H after the application of the optimal processing sequence presented in Figure 4.14. b) Interpretation of Line H: The wide dashed line represents the approximate position of a transition to a zone of englacial scattering (SZ). At the near surface, two suites of dipping reflections can be identified and are labelled 'T' and 'H', tough the amplitude of T vary along the line, with weaker amplitude sections being indicated by a narrow dashed line. One area of englacial reflections (ER4) is identified (individual lines denoting ER4 are representative and do not indicate all reflections), which is in close association with H6. One near surface zone of scattering can be identified and correlated to a supraglacial stream (S) at the time of data collection.

A (Figure 5.1) three of the structures, at 12 m (T2), 65 m (T3) and 165 m (T8), can be traced for distances >150 m before the extent of signal scatter within the profile prevents further tracing of the reflections. The reflection amplitude along the reflection is variable with the solid line interpretations (Figures 5.1-5.8) corresponding to high amplitude reflections within the GPR profile (e.g. T3 between 170-190 m), whilst the narrow dashed line interpretations correspond to low amplitude reflections (e.g. T3 between 100-170 m, Figure 5.1). The second suite of englacial reflections, labelled H, dip at angles from 30-50° in varying orientations. On Line A (Figure 5.1), reflections can be traced for ~20 m from the glacier surface at 58 m (H1), 125 m (H2) and 235 m (H3) as continuous high amplitude reflections.

- Three areas of englacial reflections (ER) can also be identified on Line A (Figure 5.1), at distances of 50-70 m (ER1), 115-140 m (ER2) and 220-240 m (ER3), which are composed of reflections of varying amplitude, often showing little lateral continuity (Figure 5.1). In Figure 5.1 ER1-3 are located directly above T2, T3 and T8, respectively and ER2 can be traced to Line B (Figure 5.2). The steeply inclined dipping reflections H1, H2 and H3 are found in close association with the lateral margins of ER1-3 (Figure 5.1). A fourth area of englacial reflections (ER4) can be identified at a distance of 80-100 m on line H. Like on line A, ER4 is in close association with a steeply inclined dipping reflection H6.
- The basal part of each line displays an increase in englacial scattering with depth, which results in rapid GPR signal attenuation below 156 m a.s.l (figures 5.1-5.8). In Figures 5.1-5.8 this zones of increased scatter is broadly indicated by the wide dashed line labelled 'SZ'. SZ can be traced through the grid (Figures 5.1-5.9) increasing slightly in elevation at the western part of the grid (e.g. ~0-200 m on line F: Figure 5.6 and 5.9), though the depth of SZ is irregular across each GPR line.

Examination of the waveform of the dipping reflections and ER on Figure 5.10 (lines A and H) can give some indication of the type of materials associated with the reflections. The phase polarity sequence of a reflected wavelet depends on that of the transmitted wavelet and of the reflection coefficient (Figure 4.2). Examination of CMP surveys show that the airwave appears positive-negative-positive (+-+), whilst the waveform of the ice wave has an opposite phase polarity, appearing negative-positive-negative (-+-). Reflections from interfaces where the dielectric coefficient decreases (velocity increases) will not be phase shifted relative to the ice wave and will appear -+- (Murray *et al.*, 2000a). If the dielectric constant increases (velocity decreases) downward across the reflection interface then the phase polarity of the transmitted wavelet will invert (+-+) relative to the ice wave (Murray *et al.*, 2000a). The wavelets of near surface and englacial dipping reflections (T), as well

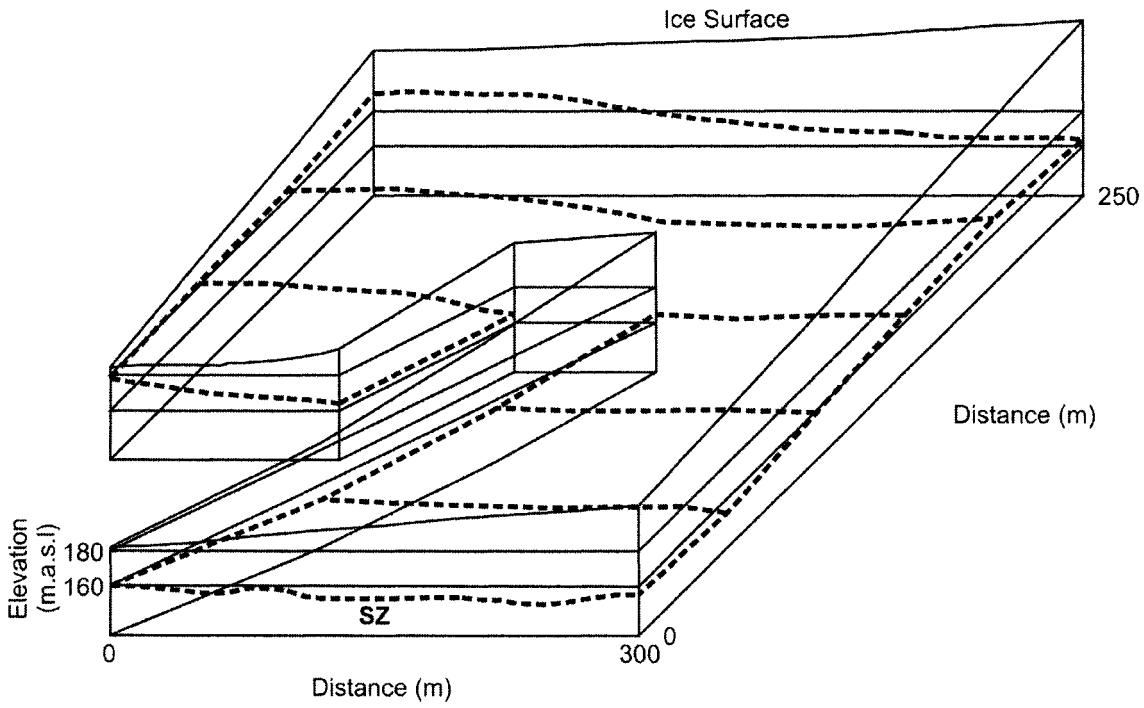


**Figure 5.9.** Psuedo-three-dimensional structure of SZ, as imaged in Grid 1. Although interconnection of all lines was not possible due to the presence of a supraglacial canyon running through the survey site, SZ is at a greater elevation in the southwest of the grid. At the eastern part of the grid, SZ is comparatively uniform and remains at a relatively consistent elevation.

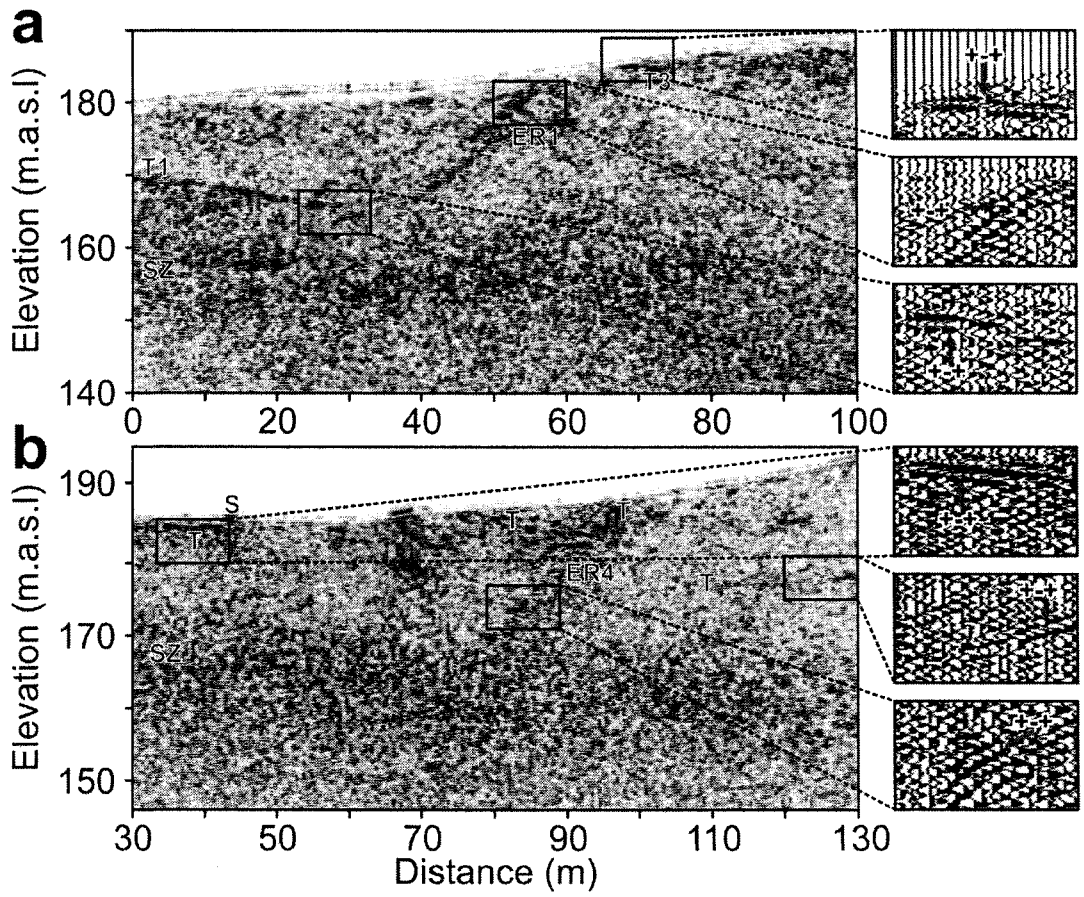


**Figure 5.10.** GPR sections from Lines A (a) and H (b) of Grid 1. S, supraglacial stream; T, near surface dipping reflections; ER, englacial reflections. The enlargements (right) show wiggle plots in order to identify the wavelet polarity of the major reflection types identified. In all cases a positive-negative-positive (+-+) reflection is produced, as a result of an increase in the dielectric coefficient and consequently a decrease in velocity (Figure 4.2 and Table 4.1).

as ER2 and ER4 give a positive-negative-positive (+-+) reflection, suggesting an increase in the dielectric coefficient (decrease in velocity). This is consistent with a transition from temperate ice to either sediment-rich ice or ice containing greater water content (Table 4.1).

*5.2.2 Grid 2*

This higher resolution grid of GPR line has allowed a pseudo-three-dimensional visualisation of structure within the area immediately up-glacier of the emerging esker sediments (Figure 5.11):

- On line X1 of Figure 5.11, a near surface zone of scatter (labelled 'S') can be identified at 160 m.
- Like on Grid 1, at the near surface, two suites of dipping reflections can also be discerned (Figure 5.11). The first suite of englacial reflections (T) typically dip at angles of 1-10° (southwest-northeast) and 1-5° (southeast-northwest), in an orientation oblique to the ice margin. As in Figures 5.1-5.8, these near surface dipping reflections can commonly be traced for <20 m, though the more continuous T3, which could be traced from the glacier surface on Line A, can also be traced through Grid 2. This reflection forms an undulating surface across the grid, with an overall dip from southwest to northeast at an angle of ~10° (Figure 5.11e). Although variations in reflection amplitude (Figure 5.11) result in a slightly discontinuous presence to the reflection, it can be traced through most of the grid, with solid line interpretations corresponding to higher amplitude reflections within the GPR profiles and lower amplitude sections being indicated by the narrow dashed line (Figure 5.11). The second suite of englacial reflections are less common, typically dipping at angles of 20-30° (northwest-south east) and 30-70° (southwest-northeast), dipping down-glacier (H). As in Grid 1, H can be traced from the glacier surface for distances up to 20 m and in some cases crosscut T (Figure 5.11).
- ER2 identified and described from line A of Grid 1 (Figure 5.1) can be traced through Grid 2, forming a large englacial feature, the imaged part of which is ~10 m in height, ~20 m wide and ~60 m long (Figure 5.11d). Reflections within ER2 are typically discontinuous and irregular and a number of hyperbolae can be identified. T3 defines the base of ER2 throughout the grid (Figure 5.11). In some places (e.g. distance 100 m on line X2 and 55 m on line Y2) the upper englacial reflections appear to have a close association with other near surface dipping reflections. The maximum elevation of ER2 corresponds to the position of a series of near surface dipping reflections and the western flank of ER2 appears to be defined by a steeply inclined reflection labelled H3 (Figure 5.11).

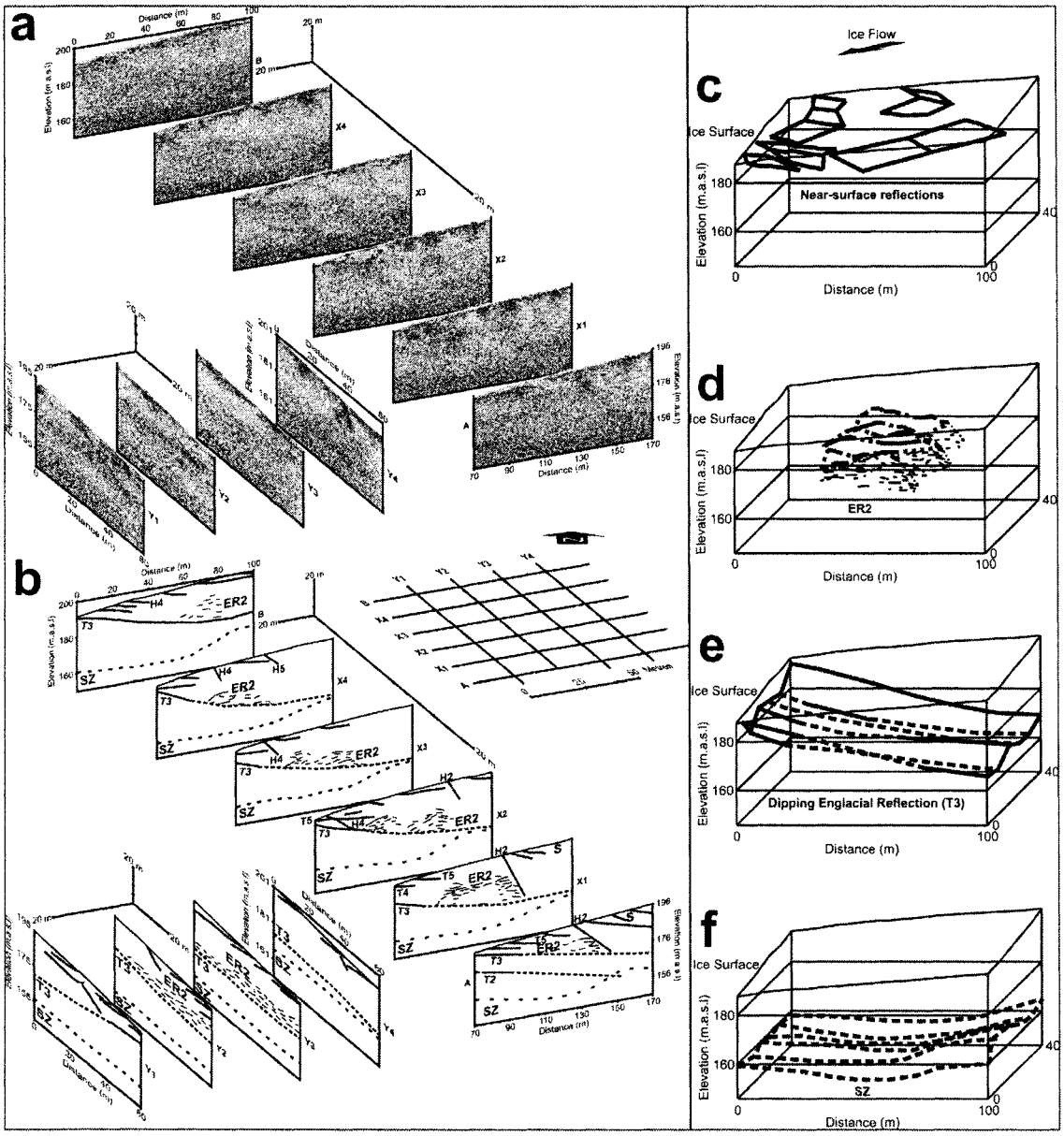


**Figure 5.11.** a) Fence diagram of processed Grid 2 GPR lines and (b) subsequent interpretation. The basal scatter zone (SZ), dipping englacial reflection labelled T3 (sections represented by narrow dashed line are lower amplitude reflections) and the englacial reflections (ER2) can be traced across significant parts of the grid (individual lines denoting ER2 are representative and do not indicate all reflections) and can be visualised pseudo-three-dimensionally (c-f). Two suites of englacial dipping reflections are identified and labelled T and H; c) near surface dipping reflections; d) englacial reflections (ER2). The upper surface (bold) and some deeper ER are plotted; e) continuous dipping englacial reflection (T3). The reflection amplitude varies and weaker signals are indicated by the dashed lines; f) the approximate position of the transition from reflection poor ice to a zone of scattering (SZ).

- Each Grid 2 GPR line shows an increase in englacial scattering with depth, which results in rapid attenuation at depths below 156 m a.s.l. In Figure 5.11, the transition to this zone of increased scatter is approximately indicated by the wide dashed line labelled 'SZ'. The depth of SZ is irregular along the GPR lines, but has a consistent pattern through the grid (Figure 5.11f).

### 5.3 Results from the CMP surveys

Two CMP profiles were collected on lines Y1 and Y3, respectively and within the resolution of the technique, some velocity anisotropy was identified (Figure 5.12). The velocity varies not only vertically, but also laterally between the lines. Semblance analysis was used on both CMP profiles to determine the normal move-out velocities of reflections at different depths within the profile. Semblance measures the coherence of hyperbolic reflection energy at a particular normal move-out velocity (Murray *et al.*, 2000a). Velocities are then picked from bulls-eyes in the semblance plot (Figure 5.12). The average velocity for the two CMP profiles is calculated as 0.137 ± 0.009 m/ns consistent with that for temperate, sediment rich ice. At points where there are few reflections the velocity is greater at 0.150 m/ns (e.g. Layers 1 in CMP 1 and 2), which is consistent with the middle range expected in temperate ice (Table 4.1). There are a number of key velocity changes at depth within the CMP profiles (Figure 5.12):

*CMP1 (0.135 ± 0.01 m/ns)*

A reflection at a TWTT of 555 ns (Layer 5) is associated with a velocity of 0.135 m/ns. This reflection is consistent with the location of the transitional boundary represented by SZ.

*CMP2 (0.139 ± 0.008 m/ns)*

- At a TWTT of 207 ns (Layer 2) the velocity reduces to 0.131 m/ns, corresponding to ER2.
- At a TWTT of 413 ns (Layer 4) a velocity value of 0.136 m/ns is obtained, corresponding to the location of T3.
- At a TWTT of 573 ns (Layer 5) a velocity value of 0.138 m/ns is obtained, corresponding to where SZ can be observed.

These velocity values are lower than would be expected for temperate ice and are more consistent with the presence of sediment bodies within the ice matrix (Table 4.1). Indeed the average velocity of CMP1 is lower than both the average for this study and temperate ice generally (Table 4.1). The lateral variation in velocity (between CMP1 and CMP2) is likely to be a direct result of variations in sediment content.

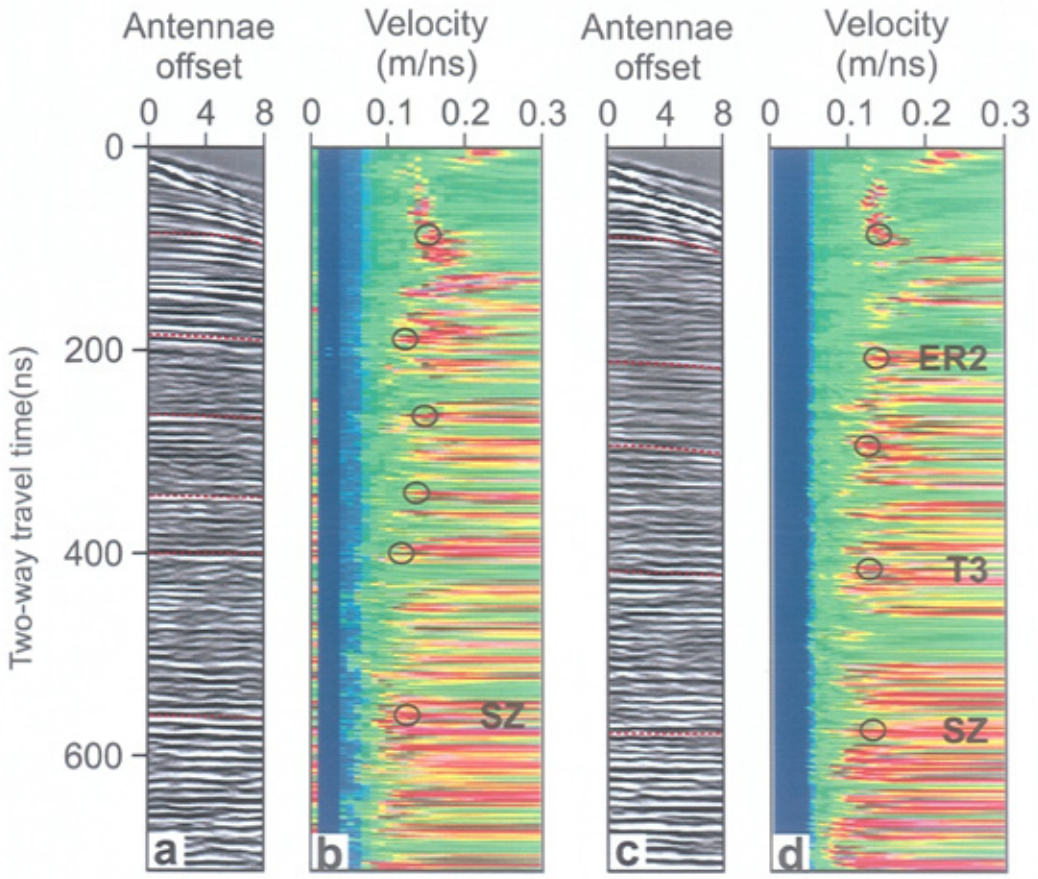


**Figure 5.12** CMP profiles and semblance plots collected on lines Y1 (a and b) and Y3 (c and d) of Grid 2. The semblance peaks or 'bullseyes' picked are associated with points at which a coherent event is present. There are major variations in the velocity with depth. These can be linked to reflections associated with SZ, T3 and ER2.

## 5.4 Interpretation

*Basal transition to increased scatter (SZ)*

The basal zone of scatter can be interpreted to represent either basal ice or an increase in water inclusions. As the survey was conducted in April, there was relatively little supraglacial melting, suggesting that this basal zone of scattering is likely caused by the peizometric surface, with its characteristics being similar to that reported from other temperate glaciers (e.g. Murray *et al.*, 2000b). Local variations in the height of the peizometric surface are likely caused by water that has infiltrated the glacier through englacial debris filled structure.

*Low angle dipping reflections (T)*

Low angle dipping reflections could be identified within all GPR lines, with many occurring at similar angles and orientations (typically around 10°). The tracing of some reflections to tephra bands outcropping on the glacier surface at the time of data collection that have similar orientations to the dipping reflections, combined with a waveform consistent with an increase in dielectric permittivity and a layer velocity reduction suggest that the reflections represent tephra bands within the ice. The extent to which these tephra bands can be traced into the ice, as well as reflection amplitude are variable across both Grids and are likely to be linked to variations in layer thickness and/or chemical composition. The thickness of a tephra band is controlled by the amount of tephra deposited (dependent upon the size of the eruption and the distance from the eruption site) and ice flow rate and characteristics. Where tephra bands are thicker, a high amplitude reflection is produced that can be traced for considerable distances from the glacier surface.

*High angle dipping reflections (H)*

High angle dipping reflections could be identified within all GPR lines, showing variable angles of dip and orientation. Some of these reflections could be traced to sediment filled hydrofractures outcropping on the glacier surface. Furthermore, waveform and CMP analysis are consistent with a velocity reduction at the interface i.e. a change from ice to sediment, suggesting these reflections represent hydrofracture fills generated during the November 1996 jökulhlaup.

*Englacial reflections (ER)*

Although the radar signal at depth within the profiles is weak, due to dielectric absorption by near surface structure and water bodies, the areas of englacial reflections identified on Lines A (Figure 5.1) and B (Figure 5.2) of Grid 1 and in Grid 2 (ER2) are interpreted to represent the englacial continuation of the jökulhlaup esker for three

reasons: 1) the anomalous areas of reflections are relatively consistent through Grid 2; 2) the irregular upper surface of the englacial reflections identified from pseudo-three-dimensional surveys (Figure 5.11d) are consistent with the morphology of the exposed section of the esker (Figure 3.5); 3) these areas of englacial reflections are located just up-glacier from the position where the esker is emerging from the glacier margin (Figure 4.3). As the base of all esker materials are defined by tephra bands T2, T3 and T8, the conduit probably developed along these planes. Furthermore, the esker materials show close association with the steeply inclined reflections representing the hydrofracture fills (H).

*Near surface scatters (S)*

Nine near-surface zones of scattering can be identified in Grids 1 and 2. Although the extent of supraglacial melting was relatively low during data collection, a number of supraglacial streams flowed across the glacier surface at the field area. The near surface scatter zones labelled as 'S' correspond to the position of such streams and are consequently interpreted as supraglacial streams, consistent with interpretations at other glaciers (e.g. Murray *et al.*, 2000b; Woodward *et al.*, 2003).

## 5.5 Discussion

This research has identified a suite of englacial structure at Skeiðarárjökull that enable the controls on the development of conduits during high-magnitude jökulhlaups to be identified:

1. During the early rising stage of the November 1996 Skeiðarárhlaup pre-existing conduits could not respond rapidly enough to the transient input of floodwaters and consequently new outlets had to be created (c.f. Roberts and others, 2001) and the November 1996 Skeiðarárhlaup appears to have flowed englacially for some distance towards the margin. The routing of the 1996 Skeiðarárhlaup waters was probably controlled by pre-existing tephra bands, filled with porous sediments, which provided the most direct route to the glacier margin, as suggested by Gulley and Benn (2007) for englacial drainage within debris covered glaciers.
2. The rate of discharge increase during the November 1996 Skeiðarárhlaup exceeded the rate at which floodwaters could be expelled along these pre-existing lines of weakness. Consequently, hydrofractures were developed from these flow paths, before being infilled with glaciofluvial sediment through accretion of sediment-laden supercooled water.
3. As the jökulhlaup progressed, floodwaters became focused upon preferential flow paths, where englacial conduits developed through the mechanical excavation of the surrounding ice. During the waning stages of the flood these englacial conduits were

infilled by glaciofluvial sediments to form the englacial esker. Although a structural control on conduit positioning is not new (e.g. Fountain and Walder, 1998; Fountain *et al.*, 2005a, 2005b; Gulley and Benn, 2007) this is the first direct observation of structurally controlled conduits during a linearly rising jökulhlaup.

Although a structural control on conduit positioning is not a new concept (c.f. Fountain and Walder, 1998; Fountain *et al.*, 2005a, 2005b; Gulley and Benn, 2007) this is the first observation of structural control upon conduits and an esker formed during a high-magnitude jökulhlaup. In all models of jökulhlaup discharge to date, the basic assumption of conduit growth and decay is that this is controlled by the balance between frictional melting and creep closure (e.g. Flowers *et al.*, 2004) and that flow paths are determined by potential gradients within the ice. The findings of this research suggest that these factors may be less influential than previously thought and it is likely that pre-existing lines of weakness are more influential than hydraulic potential gradients within the ice. Furthermore, the location of esker sediments in ice weakened by englacial structure, coupled with the suggestion that ice fragmentation exceeded the volume of flood induced melting during the November 1996 Skeiðarárhlaup (Roberts, 2005), suggest mechanical removal of a weakened ice roof plays a greater role in conduit development than frictional melting over the short time scales associated with high-magnitude jökulhlaups. Despite the acknowledgement that structure can influence outlet development during linearly rising jökulhlaups (c.f. Roberts *et al.*, 2001; Russell *et al.*, 2001a), this study provides the first evidence for the importance of structure for primary conduit positioning during a high-magnitude jökulhlaup. Understanding and quantifying the nature of structural controls may be crucial to successfully simulating a linearly rising jökulhlaup, as well as predicting flood routing and outlet development.

### 5.6 Summary

Over 2.5 km of GPR line were collected at Skeiðarárjökull, up-glacier from an englacial esker that is emerging from the glacier margin. In general, the pervasiveness of near-surface debris filled structure, coupled with the temperate ice environment made for poor radar conditions. In lines closest to where the esker is emerging from the glacier margin, however, 'zones' of englacial reflections could be identified. These englacial reflections are interpreted as esker material, the base of which is defined by a sub-horizontal reflection that is interpreted as a sediment-filled planar surface, possibly associated with a tephra band. Jökulhlaup waters were probably discharged along this pre-existing structure to form an englacial conduit. This study provides the first observation of the importance of structure for the development of primary conduit outlets during a jökulhlaup. Results presented in this chapter and the paper submitted to *Annals*

*of Glaciology*, have shown the importance of structural weaknesses for both the development and location of conduits and, consequently, englacial esker deposition during a single high-magnitude jökulhlaup.

# Chapter 6

## The Sedimentary Architecture of the Skeiðarárjökull Esker and Ice-walled Canyon Fill

### 6.1 Introduction

Eight grids of ground-penetrating radar (GPR) line were collected on the esker and ice-walled canyon fill at Skeiðarárjökull. All grids of CO GPR line were collected at a nominal frequency of 200 MHz, covering all workable areas of the esker, as well as portal proximal and central sections of the ice-walled canyon fill. Wherever possible, long GPR lines were run between grids to allow down-flow continuity of radar elements to be identified. A summary of this chapter has been accepted for publication in *Quaternary Science Reviews*.

The results of the GPR investigations are described in *Section 6.2* and *Section 6.3*. *Section 6.2* describes and interprets each radar facies identified on the GPR lines, before the radar elements are described for each grid in *Section 6.3*. The radar facies and element pattern will be summarized in *Section 6.4*, before, the distribution of radar facies and radar elements is interpreted in *Section 6.5*. The discussion in *Section 6.6* will focus upon conduit evolution during the 1996 jökulhlaup at Skeiðarárjökull, as well as the depositional timescales of the associated landforms. The chapter will then be summarized in *Section 6.7*.

### 6.2 Classification and interpretation of radar facies

GPR profiles from the esker and ice-walled canyon fill grids are interpreted using a radar facies (RF) classification scheme (Figure 6.1) developed to identify distinct radar elements. Radar element (RE) bounding surfaces were identified as the highest amplitude reflections that could be traced pseudo-three-dimensionally across grids for significant distances. The control line collected at Grid 1, shows relatively good correlation between depositional units and the radar bounding surfaces that were picked in the data (Figure 6.2). The upper and lower bounding surfaces of RE-D (SHR1 and SHR2 in Figure 6.2c, respectively) correspond to depositional boundaries identified in the section, occurring at a similar angle and orientation (Figure 6.3a). Although the section was too degraded to confirm most radar facies interpretations, the occurrence of boulder clusters in the section (Figure 6.2a) correspond to the presence of quasi hyperbolic reflections in the GPR data (Figure 6.2b) interpreted as boulder clusters at ~18 m in RE-F (Figure 6.2c). Boulder clusters between 10-20 m in RE-D (Figure 6.2c) and observed at

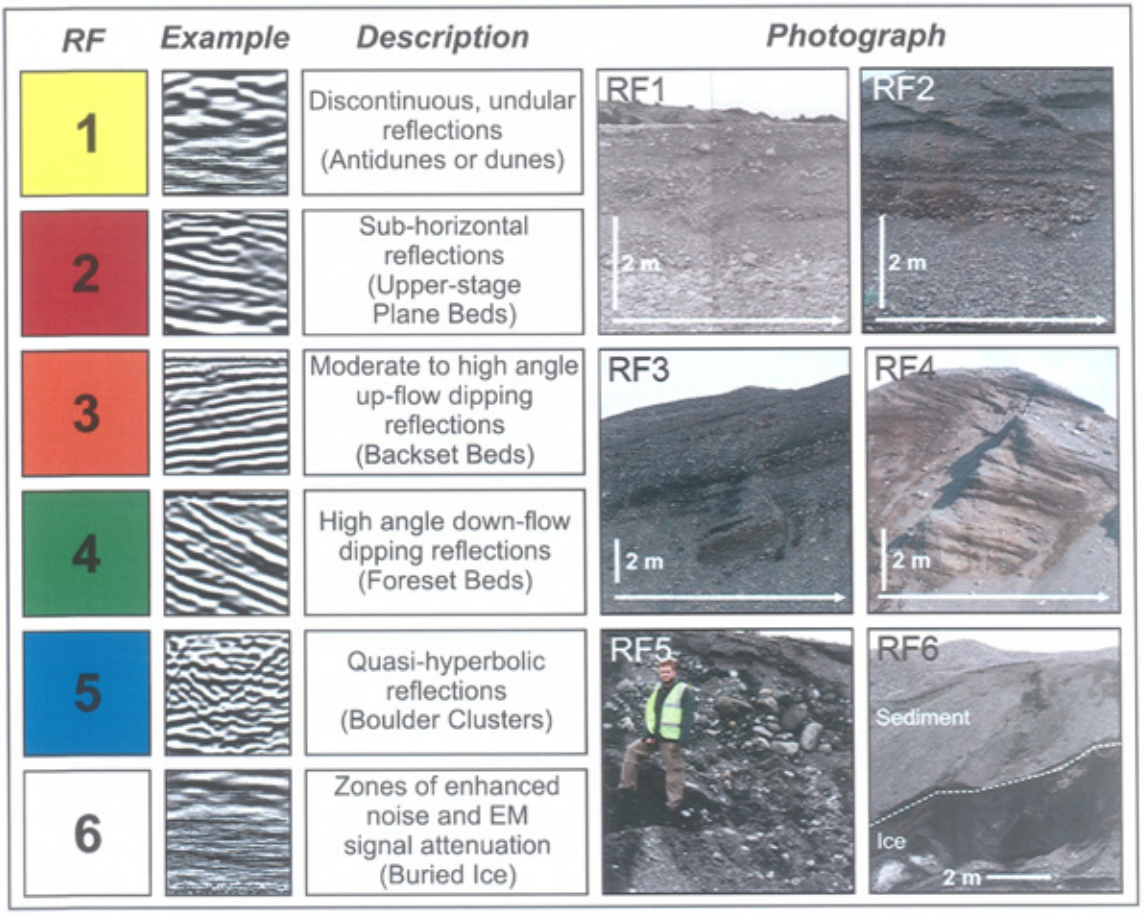


**Figure 6.1.** Generalised radar facies (RF) used to describe and interpret the processed GPR profiles. The radar facies descriptions and sedimentological interpretations (in brackets) of the radar facies are indicated, and photographs of comparable sedimentary structures exposed at the field site are presented (arrows indicate flow direction where appropriate).

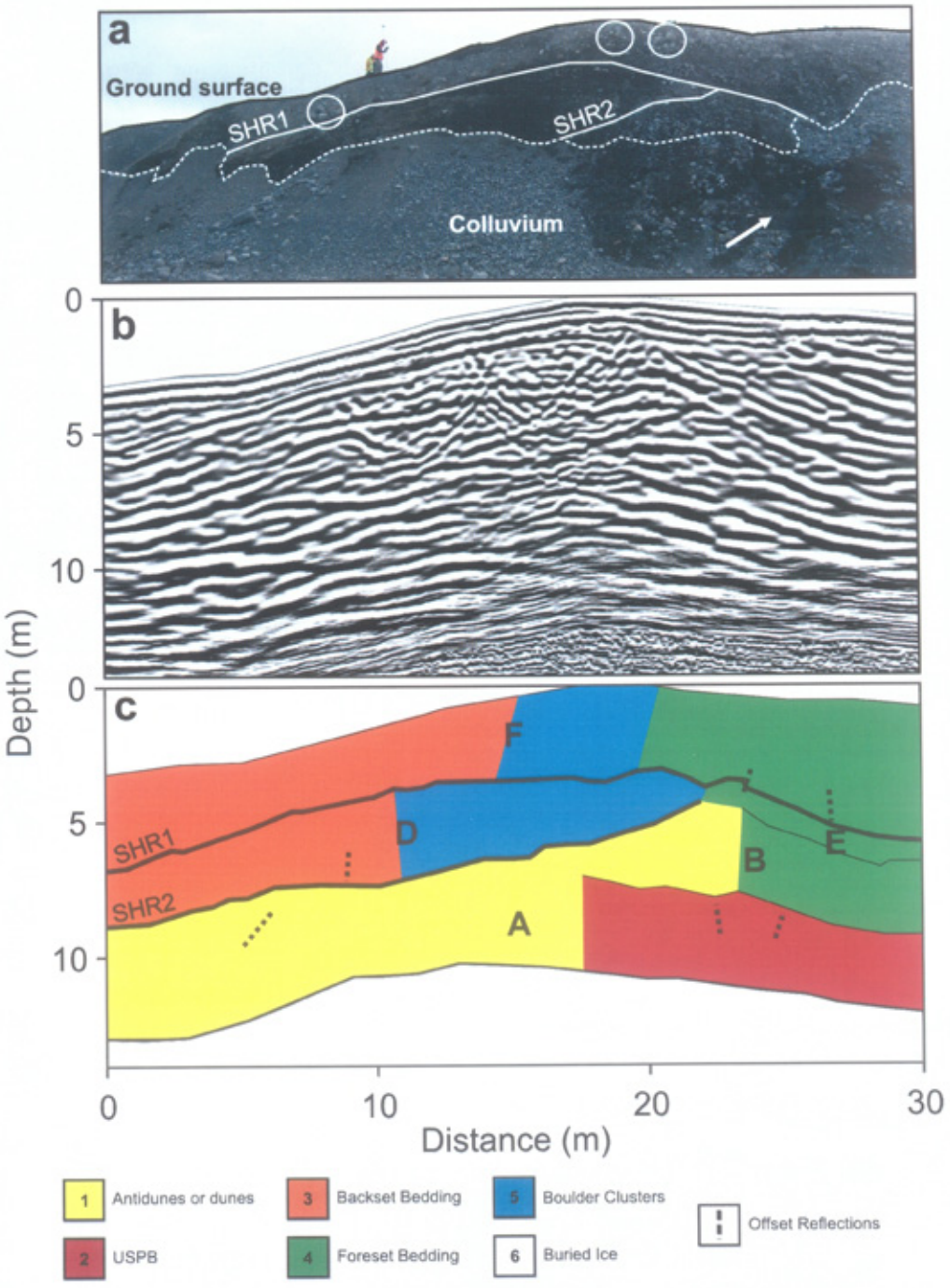


**Figure 6.2.** a) Sediment section located at Grid 1 (Figure 6.3). Depositional contacts (SHR1-2) correspond to radar bounding surfaces identified in the corresponding GPR profile (c). The circles indicate the approximate position of boulder clusters, whilst the arrow highlights the position of buried ice. b) The processed GPR line that corresponds to the location of this section. c) Whilst the section was too degraded to confirm some facies interpretation, the major radar element bounding surfaces correspond to major depositinal units. Furthermore, some boulder clusters identified in the GPR line correspond to boulders in the section. Although the buried ice identified in the section is located within the colluvium (and hence does not rest beneath primary bedded sediments), its position corresponds to buried ice identified in the GPR line.

the left side of the section (Figure 6.2a), however, do not directly correlate. This is likely due to the offline nature of these reflectors. The GPR line was positioned ~1-2 m from the section (being slightly oblique to it) and it is probable that the boulder clusters identified in the section, but not in the data, are too far offline to be imaged. Equally, the quasi hyperbolic reflections interpreted as boulder clusters in RE-D of Figure 6.2c are likely to have not been exposed in the section, being positioned deeper into the landform. Despite the discrepancies in RF interpretation, the good correspondence between RE bounding surfaces and depositional units, as well as some correlation to RF interpretations give confidence to the subsequent interpretations. For each GPR line, the main depositional elements were identified and classified (Figures 6.3-6.4, 6.6-6.8, 6.10-6.12), based upon the radar facies scheme detailed below (Figure 6.1).

*Radar facies 1: Discontinuous, undular reflections*

Radar facies 1 (RF1) is composed of sets of undular or trough-shaped reflections that range from individual troughs ~2 m across, to sub-horizontal discontinuous reflections<12 m across, e.g. RE-A, at ~18-30 m on line X2 of Grid 2 (Figure 6.4). These sets of reflections can extend laterally for up to ~70 m and be up to ~5 m in thickness, e.g. RE-A, sub-grid 3a (Figure 6.6). They can also grade into more continuous reflection sets. RF1 is interpreted to represent cross bedding associated with the development of antidune or dune sets. Sambrook Smith *et al.* (2006) interpreted similar reflection sets to be trough-cross stratification associated with dune migration. This requires subcritical conditions, which would be unlikely during the 1996 Skeiðarárhlaup. The distinction between flow regimes (subcritical or supercritical) is drawn by a dimensionless number, the Froude number (*Fr*), which is given by the ratio of inertial to gravitational forces in the flow (Collinson *et al.*, 2006):

$$Fr = \sqrt{gd}$$

Where $v$ = mean flow velocity (m $s^{-1}$), $d$ = flow depth (m) and $g$ = gravitational acceleration (9.81 $ms^2$). For $Fr > 1$, the flow regime is supercritical and flows are rapid, whilst $Fr < 1$ are associated with a subcritical flow regime where flows are tranquil. Although a dune interpretation cannot be ruled out from the GPR data, an antidune interpretation is favoured for two reasons: 1) deposition during the jökulhlaup is likely to have been under supercritical flow conditions; 2) major troughs can only be identified in flow-parallel lines, where reflections are typically more irregular, than in flow-transverse lines. Antidunes form in supercritical conditions and individual troughs can only be identified in lines normal to flow direction, if the antidune is a 2-D form (Alexander *et al.*, 2001; Duller *pers. comm.*,

2007). The variations in concavity of bedform troughs are likely to be a consequence of GPR line orientation with respect to bedform crest line.

*Radar facies 2: Sub-horizontal reflections*

Radar facies 2 (RF2) consists of sets of sub-horizontal reflections with an angle of dip <10° from horizontal. They can be arranged as horizontal or dipping sets that tend to be sub-parallel to the bed slope. These sets can extend laterally as individual units for up to ~95 m, e.g. RE-F, line X4, sub-grid 4b (Figure 6.11) and have a maximum thickness of ~10 m, e.g. RE-F, line X4, sub-grid 4b (Figure 6.11), in some cases grading into or from discontinuous or inclined reflections (dipping up or downstream). The incidence of less distinct reflections is common suggesting that set thickness is often less than EM wavelength. RF2 is interpreted to represent deposition of upper-stage plane beds during critical to supercritical flow conditions (Carling, 1999; Alexander *et al.*, 2001).

*Radar facies 3: Up flow dipping moderate to high-angle inclined reflections*

Radar facies 3 (RF3) consists of sets of reflections that dip upstream at an angle of 10° to 25° from horizontal, with angles closer to 10° being more common. This facies can be quite extensive, ranging in lateral coverage from ~2 m to ~100 m down and across a grid, e.g. 0-80 m on sub-grid 4a X-lines (Figure 6.10). Units of RF3 are typically bounded by strong reflections at their base. There are also strong reflections that cut through these sets, likely representing boundaries between distinct radar elements, the thickness of which can range from ~4 m to ~6 m. RF3 is interpreted as backset bedding that is typically deposited at a hydraulic jump associated with a switch from supercritical to subcritical flow conditions (e.g. Jopling and Richardson, 1966; Alexander *et al.*, 2001). This is consistent with interpretations made by Fiore *et al.* (2002) who identified backset bedding in eskers in the Joux Valley, Switzerland using GPR, and by Brennand and Shaw (1996) in North American eskers. In some instances, however, the bedding follows surface and bed slopes that are consistent with backset angles of >10°, but are associated with planar deposition, e.g. RE-B-C, RE-E-G and RE-H at ~50-80 m, Line X3, Grid 3a (Figure 6.6).

*Radar facies 4: Down flow dipping high-angle inclined reflections*

Radar facies 4 (RF4) consists of sets of reflections that dip downstream at an angle of 15° to 30° from horizontal. These can be extensive, ranging in lateral coverage from ~10 m to ~40 m, e.g. RE-F, G, I at ~20-60 m, line X5, Grid 2 (Figure 6.4), though strong, continuous reflections interpreted to represent the bounding surfaces between distinct radar elements, may subdivide the sets, which can be up to ~2-6 m in thickness. RF4 is interpreted to record foreset bedding. This is consistent with interpretations made

by Fiore *et al.* (2002) who identified downstream dipping reflections at comparable angles in the Joux Valley eskers and classified these as foreset beds. In some instances, however, the reflections follow bounding surface slopes that are consistent with foreset angles of >15°, but are associated with planar deposition, e.g. RE-B, C, E at ~120-150 m on line X3 of sub-grid 3a (Figure 6.6).

*Radar facies 5: Quasi-hyperbolic reflections*

Radar facies 5 (RF5) consists of collections of quasi-hyperbolic reflections, associated with strong, point source reflectors. RF5 has been identified within radar elements, extending laterally for up to ~4 m with a maximum thickness of ~3 m in Grid 1 (Figure 6.3) and Sub-grid 3c (Figure 6.8), only. This facies can only be identified within RE-D-F and in similar cross-sectional locations, e.g. within RE-E and RE-F between ~22-26 m on line X4 of Grid 1 (Figure 6.3). A sedimentary exposure running parallel to the axis of GPR Grid 1 allowed observation of boulder clusters in locations corresponding to the observed incidence of RF5 (Figure 6.2). This facies, therefore, is interpreted as boulder clustering associated with deposition during the later stages of esker development. This is consistent with the interpretations of Cassidy *et al.* (2003) who identified similar reflections that corresponded to boulders within sedimentary exposures in distal ice-walled canyon deposits at Skeiðarárjökull. The isolated occurrence of this facies is likely controlled by sediment supply.

*Radar facies 6: zones of enhanced noise and EM signal attenuation*

Radar facies 6 (RF6) incorporates a zone of noise and enhanced attenuation of EM signals, bounded on its upper surface by a relatively continuous reflection. Though the signal-to-noise ratio is usually low within this facies, structure can still be observed (to some extent) below the bounding reflection. In all cases, RF6 is located at the base of the profile, below all other radar facies and, when observable, can usually be traced over significant parts of a grid (Figures 6.3-6.4, 6.6-6.7, 6.10-6.12). RF6 is interpreted to represent buried ice, with its extensive coverage across a grid suggesting it represents the base of the conduit/channel in which the esker and ice-walled canyon sediments were deposited. This would be consistent with observations of buried ice along the margins of the esker (Figure 6.1). Furthermore, the relative position of RF6 in Grid 1 (Figure 6.3) corresponds to an exposure of buried ice in Section 1 (Figure 6.2).

*Offset reflections*

In some places distinct offsets are observed within and/or between radar elements and facies. This offsetting is observable in at least some profiles of each grid, but can be more pervasive within some grids, e.g. sub-grid 4a (Figure 6.10). The angle and

orientation of this offset is highly variable, and on sub-grid 4a (Figure 6.10), some offsetting can be linked to normal faulting observed on the surface of the ice-walled canyon fill. Consequently, offsets are interpreted to record structural collapse of the sediments associated with normal faulting (c.f. McDonald and Shilts, 1975) of the assemblage due to melting of supporting ice walls and/or buried ice (Woodward *et al.*, 2008).

## 6.3 Description and Quantification of Radar Elements

In order to establish the frequency of each radar facies throughout the GPR grids the individual coverage of each was calculated for all lines of every grid. From this, the total percentage occurrence of each facies for individual lines and grids could be calculated. The distribution by each grid can be used to identify down-flow trends (Figure 6.14), whilst examining individual X- and Y-lines highlights within grid trends (enlarged GPR lines are presented in *Appendix 3*), on an individual grid basis (Figures 6.3-6.4, 6.6-6.8, 6.10-6.12). GPR grids are described in turn starting with the most up-flow and working down-flow (grids are presented in Figures 6.3-6.4, 6.6-6.8, 6.10-6.12). The major bounding surfaces have also been visualized for each grid (Figures 6.5, 6.9 and 6.13).

### *6.3.1 Grid 1*

The esker here is constructed from a series of radar elements (minimum of six), some of which are sheet-like in morphology, whilst others are more lenticular and truncated (Figure 6.3). RF6 (buried ice) is identified at a maximum depth of ~10 m and is continuous across the majority of the grid. The upper surface of RF6 is crudely parallel to the esker surface (Figure 6.5a), having a general dip upstream at an angle of approximately 5°-12°. Resting directly on this surface is a pervasive element (RE-A)predominantly classified as RF1 (cross bedding), though the unit can grade into RF2 (upper-stage plane beds) or from RF3 (backset beds). The largest bedforms (RF1) appear to have a maximum crest height of ~2.4 m and length of <8 m in flow-parallel lines, though internal structure is largely unidentifiable.

Truncating the basal radar element (RE-A) are crosscutting elements (RE-B-E), but RE-F is more laterally continuous. Upstream these radar elements are composed of up-flow dipping or backset beds, which are replaced by down-flow dipping or foreset beds distally. This backset-foreset transition is not consistent across the entire grid, as there appears to be no similar downstream transition at the southern side of the grid, with backset beds only becoming sub-horizontal (RF2) down-flow at ~15-20 m on lines X4 and X5 (Figure 6.3).

Within RE-D-F at distances of approximately 15-20 m, boulder clusters (RF5) have been identified. These can only be observed on profiles X1, X2, X4 and Y2-Y4 (Figure

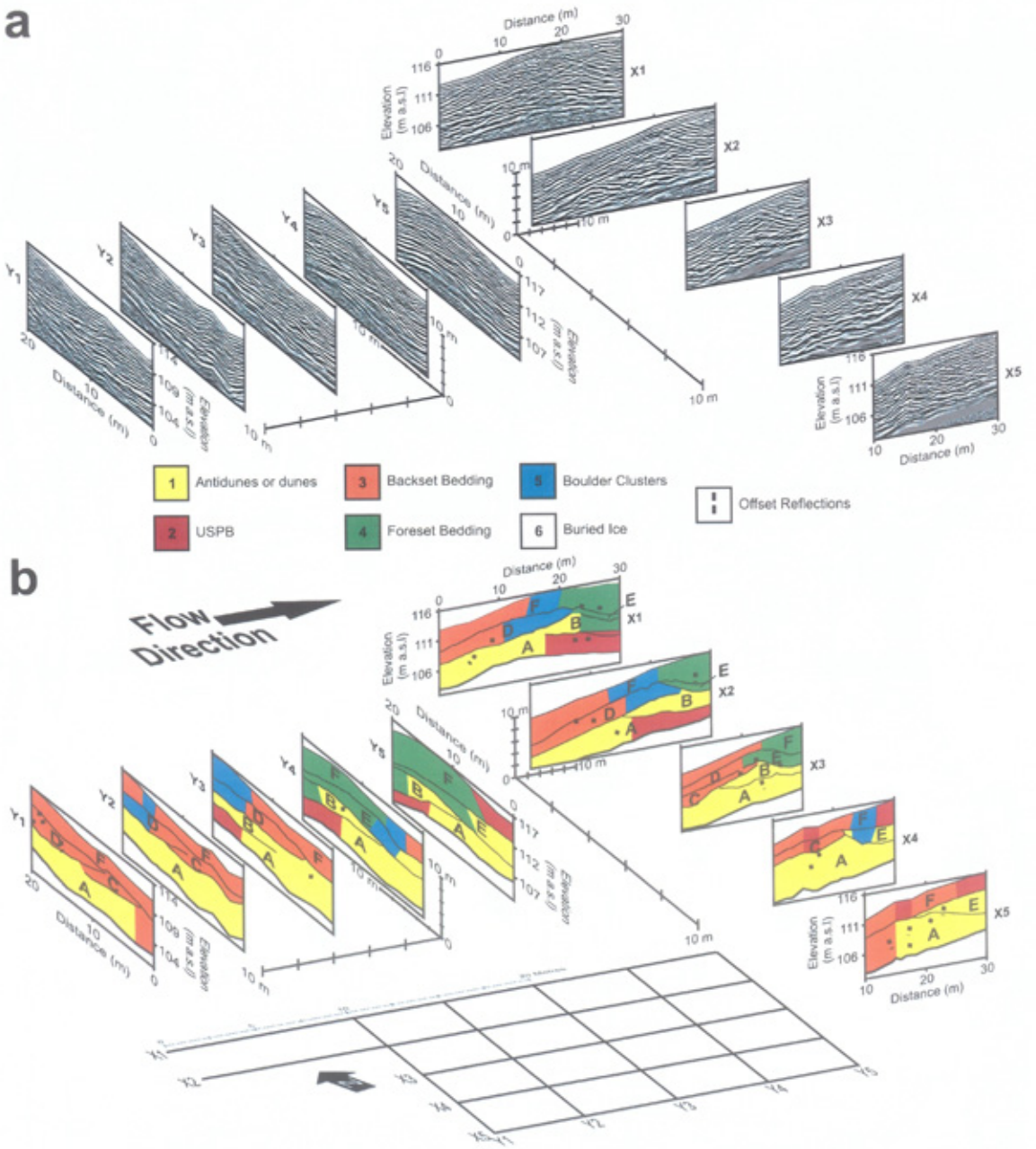


**Figure 6.3.** a) Fence diagram of Grid 1 GPR profiles and b) subsequent interpretation (distance ticks are at 10 m intervals). Each profile has been processed using the protocol identified in Figure 4.15. The grid map at the bottom of the figure shows the true line orientation. All elevations are relative to sea level and recorded by DGPS. Each radar facies has been colour coded to allow identification of trends (see Figure 6.1 for radar facies descriptions and interpretations). Radar elements have been labelled with letters in order of deposition. Buried ice defines the base of the landform across much of the grid. There is a general downstream transition from backset to foreset bedded sediments, though boulder clusters are also identified (see text for full interpretation of the grid).

6.3). For each radar element in which RF5 is identified, the radar facies are deposited in similar cross-sectional positions in both flow-parallel and flow transverse profiles, e.g. RF5 in RE-F is located above and in line with RF5 in RE-D (Figure 6.3).

Some offset reflections can be observed within the grid and in all radar facies, though the sediments do not appear to be highly distorted and offsetting is more readily identified in downstream profiles. Offsetting is typically discerned within a marginal location and reflections are offset by <1 m.

*6.3.2 Grid 2*

The esker architecture here bears some similarity to that in Grid 1, though is composed of more radar elements (a minimum of nine) with greater cross-cutting bounding surfaces (Figures 6.4, 6.5b). RF6 (buried ice) is identified at a maximum depth of ~12 m and is continuous across the majority of the grid (Figure 6.5b). Overlying the buried ice (RF6) is a relatively continuous radar element (RE-A) composed predominantly of backset beds (RF3) up-flow and cross-beds (RF1) down-flow, with a maximum bedform crest height of ~3 m and length of <12 m in flow parallel profiles. RE-A, although continuous across most of the grid, is absent from the most northerly area. Here on line X6, and from the ~25 m point of lines Y4-Y7, RE-B lies directly on the bounding surface of RF6 (Figure 6.4).

Truncating RE-A at a distance of ~0-40 m down-grid are RE-B-E that in some cases are bounded by well-defined unconformities (Figure 6.5b). RE-B-E are varied in their classification, though are typically classified as RF3 up-flow and either RF1 or RF2 centrally. Down-flow (from an X-line distance of ~30-40 m), RE-F, G and RE-I are deeply incised into RE-A-C (Figures 6.4, 6.5b). Although RE-F-G and RE-I can grade from RF2 into RF4, they are predominantly classified as RF4 (foreset beds). Some offset reflections can be observed across the entirety of the grid, though are more prevalent in the up-flow half and distal end of the grid. In general, however, sediments are not greatly distorted; reflection offsets are <1 m.

*6.3.3 Grid 3*

Radar Grid 3 is composed of three sub-grids that are linked by a long flow-parallel GPR line (Figure 4.4; X3 Sub-grid 3a), allowing identification of continuous radar elements along the ridge. In total for all three sub-grids a minimum of nine radar elements can be discerned (Figures 6.6-6.8).

*6.3.3.1 Sub-grid 3a*

The esker here is composed of at least nine radar elements (RE-A-I) that are relatively continuous for considerable distances down- and across the sub-grid. RF6

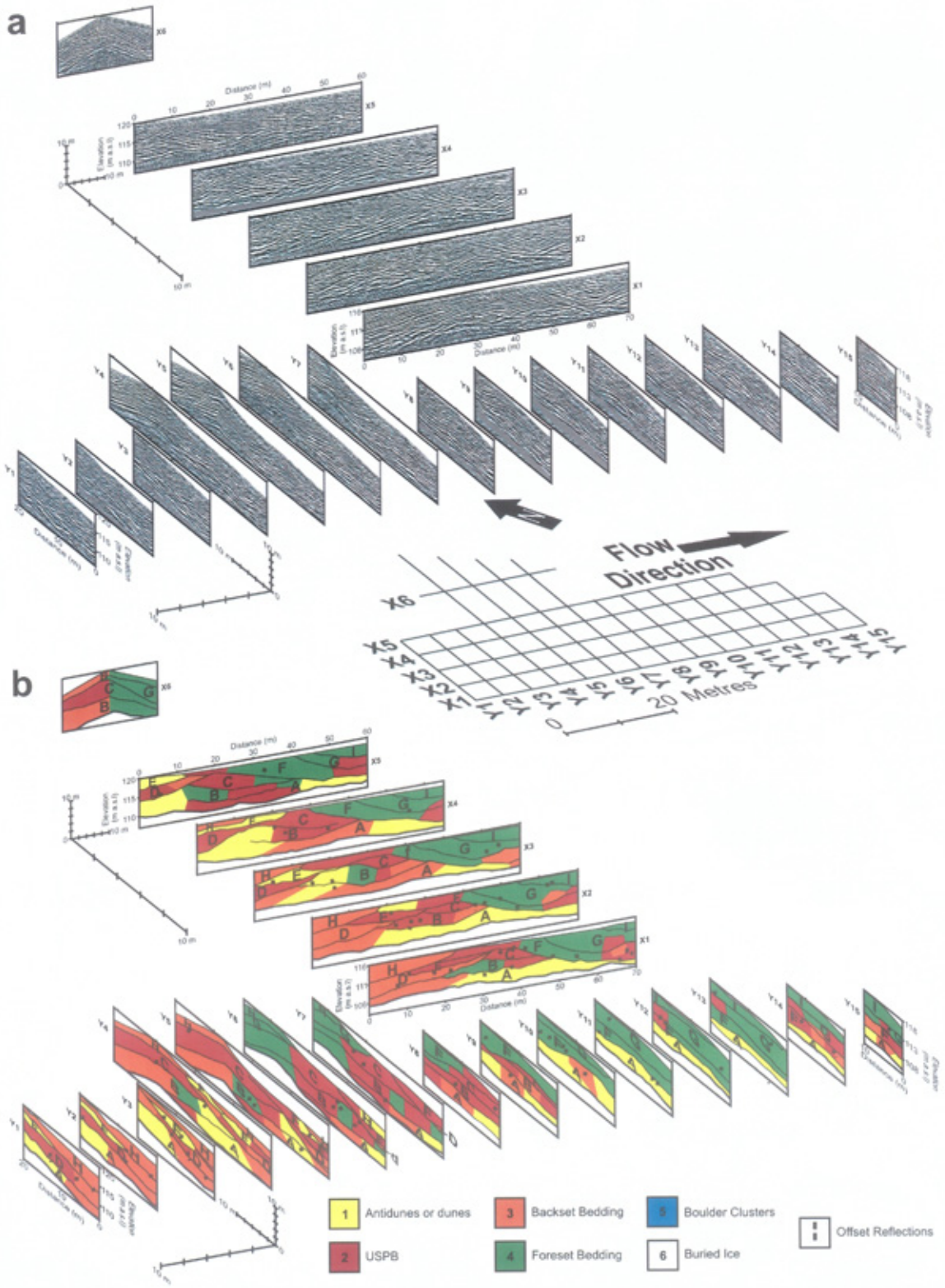


**Figure 6.4.** a) Fence diagram of Grid 2 GPR profiles and b) subsequent interpretation, following protocols and layout described in Figure 6.3. Buried ice defines the base of the landform across much of the grid. Although deposition was complex, there is a general downstream transition from backset to foreset bedded sediments (see text for full interpretation of the grid).

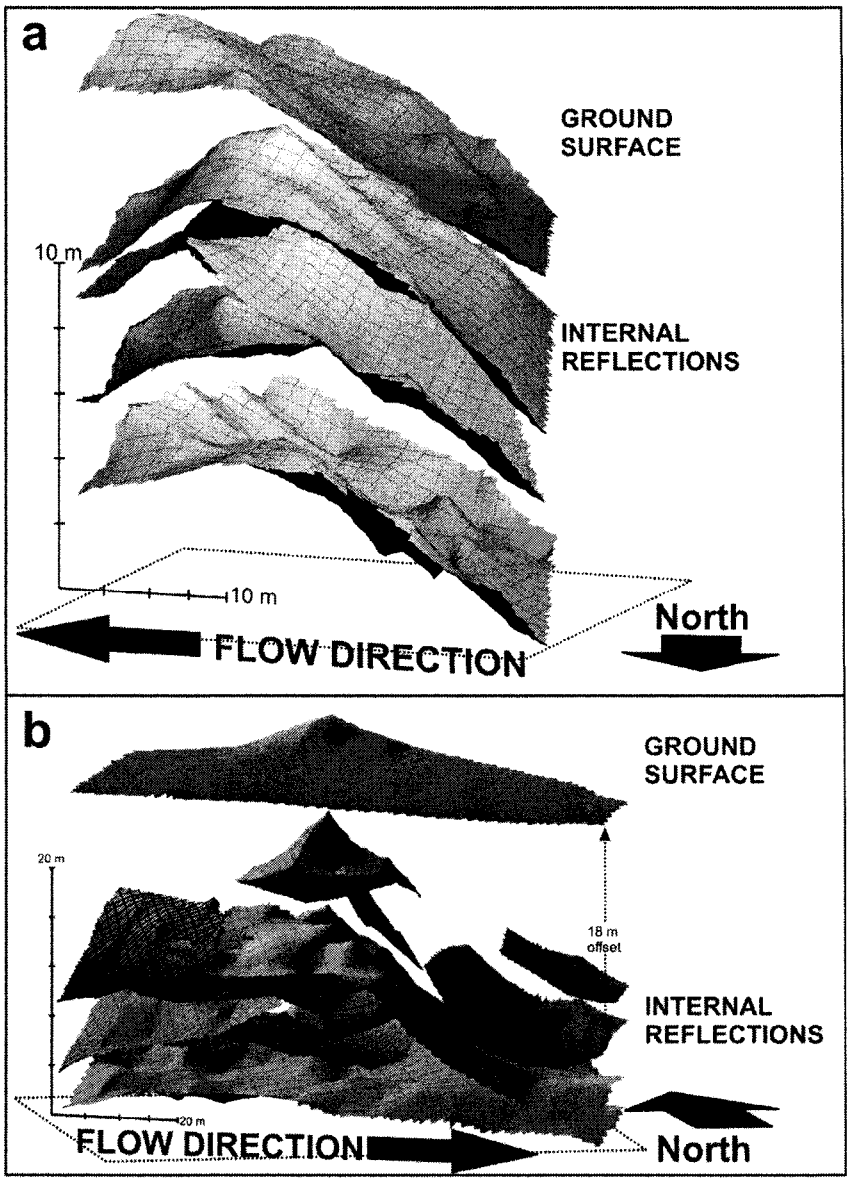


**Figure 6.5.** Pseudo-three-dimensional visualisation of radar element bounding surfaces within up-flow esker grids (with a two times vertical exaggeration). The lowest bounding surfaces define RF6 and consequently the base of the esker. The upper most surface represents the landform surface: a) Grid 1 bounding surfaces (Figure 6.3), with flow direction from right to left. At the down-flow end of the grid the bounding surfaces dip down-stream at an angle that is oblique to the esker surface. b) Grid 2 bounding surfaces (Figure 6.4), with flow direction from left to right. The ground surface is offset from its true vertical elevation by ~18 m to allow internal reflections to be identified more clearly. Internal reflections dip up-flow at the western end of the grid, whilst those at the eastern end dip down-flow.

(buried ice) can be identified at a maximum depth of ~12.5 m and is continuous across much of the sub-grid (Figures 6.6, 6.9a). At the eastern side of the sub-grid, the surface drops in elevation and has an irregular topography (Figure 6.9a). RE-A can only be identified on line X3 from a distance of ~70-150 m and is truncated by RE-B on its up-flow side. RE-A is classified as RF1 (cross-bedded), though individual bedforms are difficult to distinguish. Instead, the reflections are characteristically discontinuous, suggesting individual bedforms are below the resolution of the GPR configurations used in this study, or the line is oblique to the direction of bedform migration. Up-flow from RE-A, RE-B-E rest directly upon the buried ice (at a distance of ~0-70 m on X-lines).

RE-B-H are dominated by upper-stage plane beds (RF2), but where there is a rise or fall in the bed slope these have been classified as dipping beds (RF3 and RF4). Although RE-B-H are relatively continuous across much of the sub-grid, an area of truncation can be discerned from ~70-82 m on line X3 (bounding surface of RE-I).

Some offset reflections can be discerned across the sub-grid, though they tend to be in marginal locations and along the narrowest sections of the ridge (~60-115 m on line X3), where reflections are offset by <1 m.

#### *6.3.3.2 Sub-grid 3b*

The esker here is composed of at least five radar elements (RE-A-C, E, G) that are continuous throughout the sub-grid (Figure 6.7). RF6 (buried ice) can be traced across the sub-grid at a maximum depth of ~9 m (Figure 6.9b). RE-A lies directly on the buried ice and is composed of cross-bedded sediments (RF1), consistent with the development of antidune or dune sets with a maximum crest height of ~2.5 m and length of <8 m in flow parallel profiles. The upper bounding surface of this unit appears abrupt in places, with individual bedforms being truncated.

There is a distinct change between RE-A and RE-B-E, G, which are dominantly classified as upper-stage plane beds (RF2), only being classified as foreset bedding from ~32-40 m on line X1 and the cross-cutting Y-lines (RE-G).

Some offset reflections can be identified on the western side of the sub-grid, where they dip towards the periphery of the deposit. Individual reflections are typically offset by <1 m.

#### *6.3.3.3 Sub-grid 3c*

The esker here is composed of at least 5 radar elements (RE-A-B, RE-E-F, RE-H) that are relatively continuous across the sub-grid (Figures 6.8, 6.9c). RE-A is composed of upper-stage plane beds (RF2) or down-flow dipping beds (RF4) and is relatively continuous across the sub-grid, with a down-flow dipping upper bounding surface.

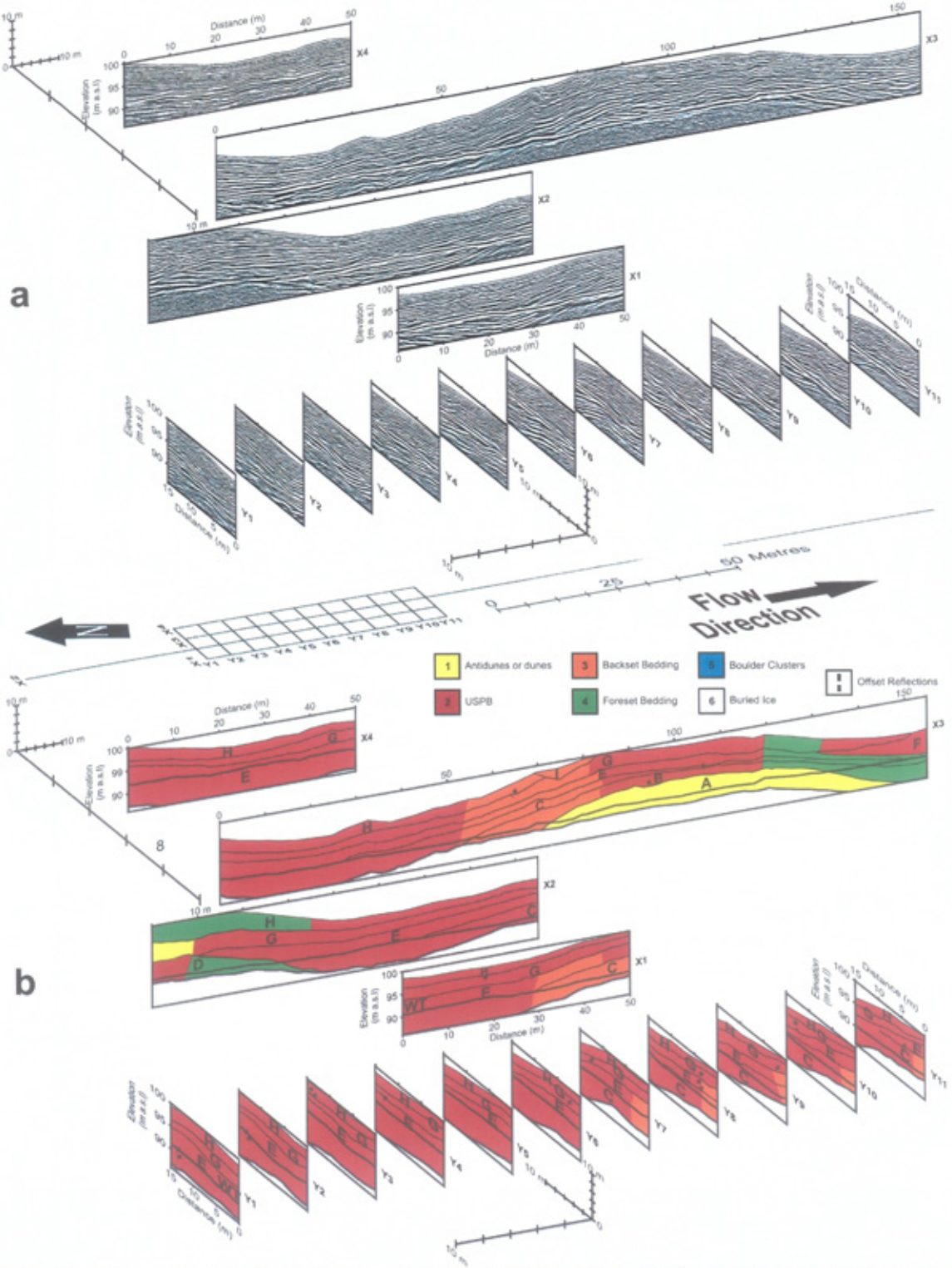


**Figure 6.6.** a) Fence diagram of Sub-grid 3a GPR profiles and b) subsequent interpretation (distance ticks are at 5 m intervals on Y-lines), following protocols and layout described in Figure 6.3. As the sub-grid was connected to Sub-grids 3b and c, radar element lettering refers to depositional ordering through each of these grids. Buried ice defines the base of the landform, which is composed of predominantly upper-stage plane beds (USPB). The water table (WT) is highlighted on line X1 and Y1 (bold lines) and can be traced through the grid (see text for full interpretation of the grid).

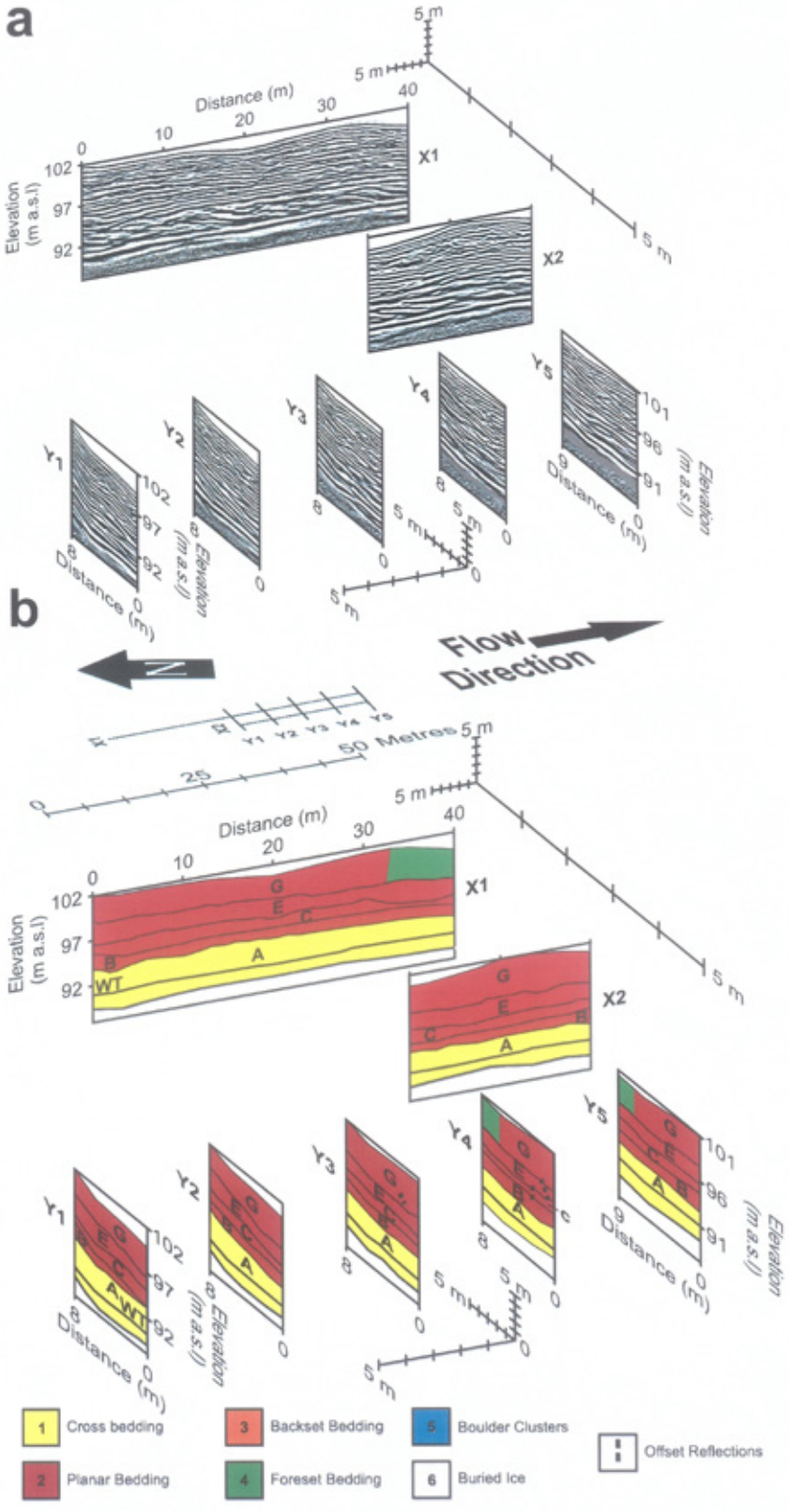


**Figure 6.7.** a) Fence diagram of Sub-grid 3b GPR profiles and b) subsequent interpretation, following protocols and layout described in Figure 6.3. As the Sub-grid was connected to sub-grids 3a and c, radar element lettering refers to depositional ordering through each of these grids. Buried ice defines the base of the landform, which is composed of predominantly upper-stage plane beds (USPB). The linear reflection at an elevation of ~92 m represents the water table (WT), which is highlighted on line X1 and Y1 (bold lines) and can be traced through the grid (see text for full interpretation of the grid).

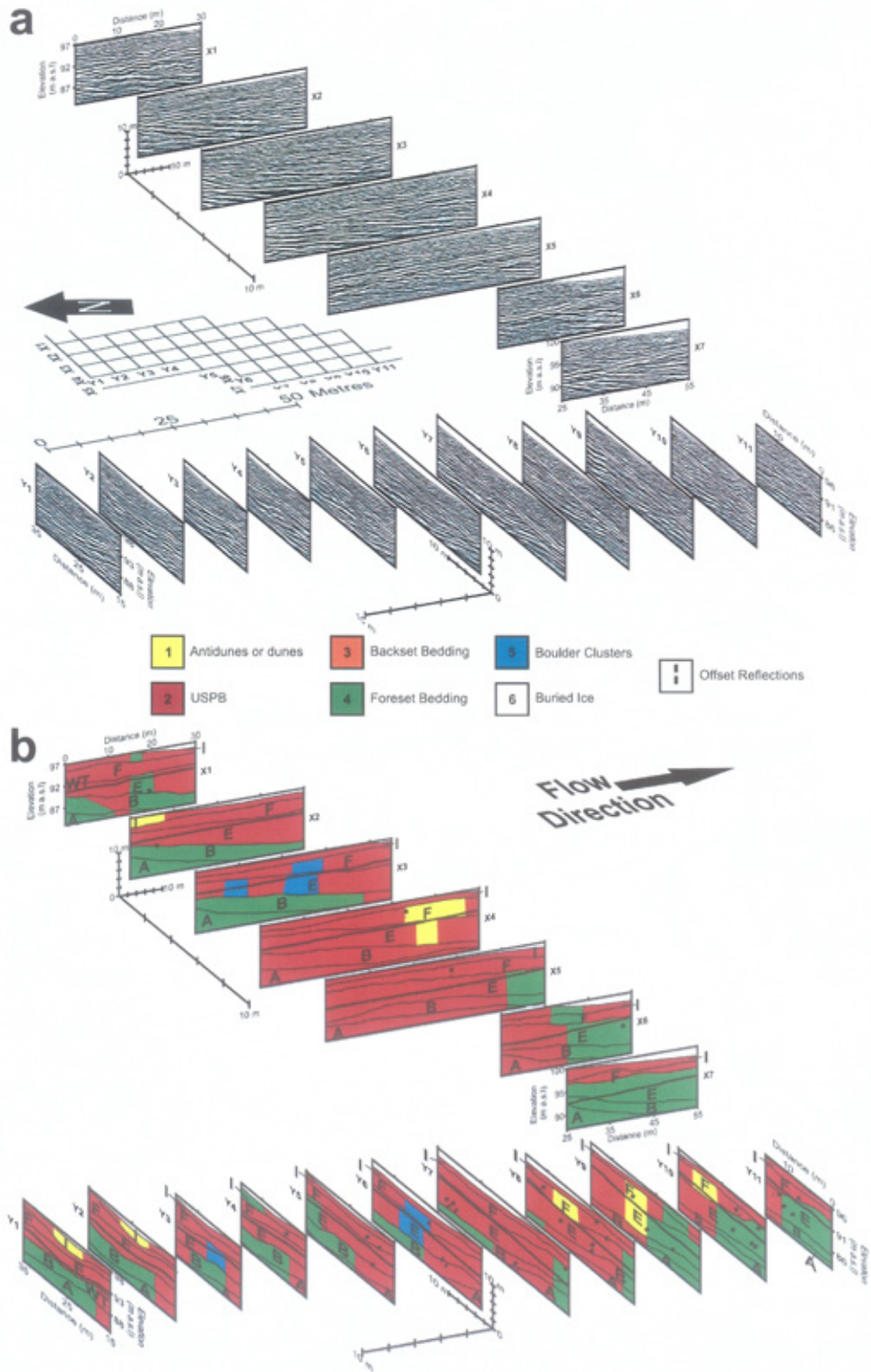


**Figure 6.8.** a) Fence diagram of Sub-grid 3c GPR profiles and b) subsequent interpretation, following protocols and layout described in Figure 6.3. As the Sub-grid was connected to sub-grids 3a and b, radar element lettering refers to depositional ordering through each of these grids. The landform here is composed of predominantly upper-stage plane beds (USPB) and boulder clusters can also be observed. The linear reflection at an elevation of ~92 m represents the water table (WT), which is highlighted on line X1 and Y1 (bold lines) and can be traced through the grid (see text for full interpretation of the grid).

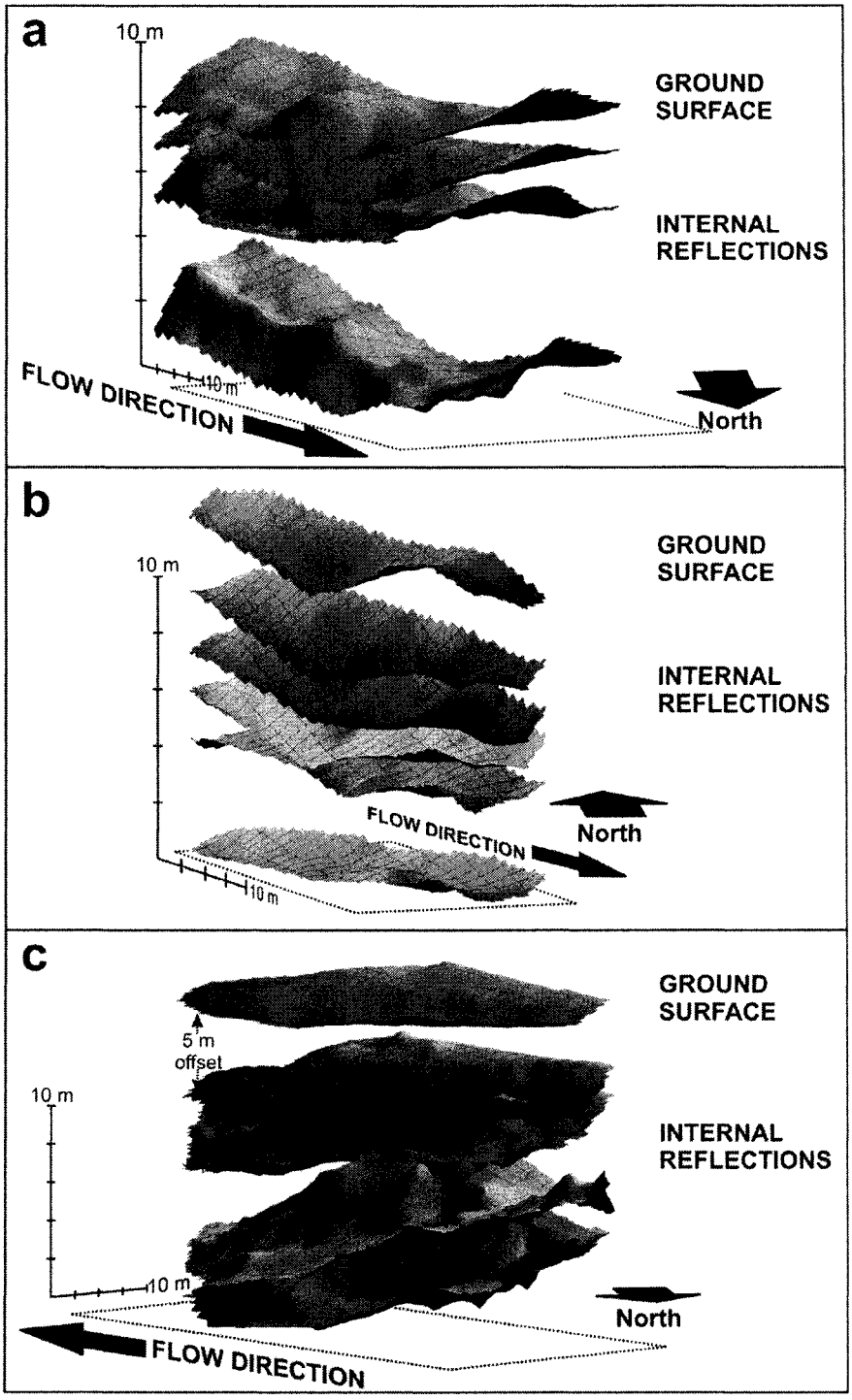


**Figure 6.9.** Pseudo-three-dimensional visualisation (two times vertical exaggeration) of radar element bounding surfaces within: a) sub-grid 3a (Figure 6.6). The lowest surface represents the upper boundary of RF6 and so defines the base of the esker at this location. Internal reflections are typically sub-horizontal, though slightly arching, and are parallel to the esker surface; b) Sub-grid 3b (Figure 6.7). The lowest surface represents the upper bounding surface of RF6 and consequently the base of the esker. Internal reflections are typically sub-horizontal and parallel to the esker surface, though dip to the south-west; c) Sub-grid 3c (Figure 6.8). The highest surface has been offset from its true vertical position by ~5 m to allow internal reflections to be identified more clearly. Internal reflections typically dip-down flow at a low angle.

RE-B, E-F and RE-H are dominated by upper-stage plane beds (RF2), though can in some cases, grade to or from foreset (RF4) or cross-bedded (RF1) deposits. The location of foreset bedding, however, is non-random, with this occurring both in RE-A and also dominantly at the western (at a distance of between ~25 m and ~55 m on lines X6-7) and eastern (at a distance of ~0-40 m on lines X1-3) margins of the esker (Figure 6.9c).

Boulder clusters (RF5) can be identified within RE-E-F, between a depth (from the surface) of ~2-9 m at a distance of ~6-28 m. For each radar element in which RF5 is identified, the radar facies are deposited in similar cross-sectional positions in both flow-parallel and flow transverse profiles, e.g. RF5 in RE-E is located above and in line with RF5 in RE-F (Figure 6.8).

The morphology of RE-H is trough-like towards the centre of the grid (Figures 6.8, 6.9c). In some places (particularly at a distance of between ~0-10 m where the trough is the deepest) this truncates lower deposits.

Offset reflections can be observed within the deposits, though these are more frequent at down-flow and marginal locations. Individual reflections are typically offset by <1 m.

### *6.3.4 Grid 4*

Grid 4 is located on the portal-proximal part of the ice-walled canyon fill and is composed of two sub grids that are connected by a flow-parallel line (Figure 4.4), to allow the tracing of individual radar elements and facies down-flow. In total a minimum of eleven radar elements are identified in Grid 4 (Figures 6.10-6.11). For sub-grid 4a all X-lines are presented, as well as line Y16 (Figure 6.10) (Not all Y-lines are shown as they add little additional information to that shown in the X-lines).

#### *6.3.4.1 Sub-grid 4a*

The ice-walled canyon fill here is composed of at least eight radar elements (RE-B, C, F-K) that are continuous across much of the sub-grid (Figures 6.10, 6.13a). RF6 (buried ice) can be traced across the sub-grid at a maximum depth of ~10 m, with this surface being crudely parallel to the land surface topography (Figures 6.10, 6.13a). At the eastern side of the sub-grid, however, the buried ice (RF6) drops in elevation, e.g. at a distance of ~25-45 m on Line Y16 (Figure 6.10). RE-B and RE-C are only discernable at the distal end of the sub-grid (~60-100 m), where sediments are classified as cross-bedded (RF1). These radar elements are composed of antidunes or dunes, with a maximum crest height of ~2 m and length of <6 m in flow parallel profiles.

RE-B and RE-C are truncated on the upstream side by five radar elements (RE-F-J) classified as backset beds (RF3). Backset beds (RF3) dominate the sub-grid profiles between ~0-70 m in the down-flow direction. These radar elements and the internal

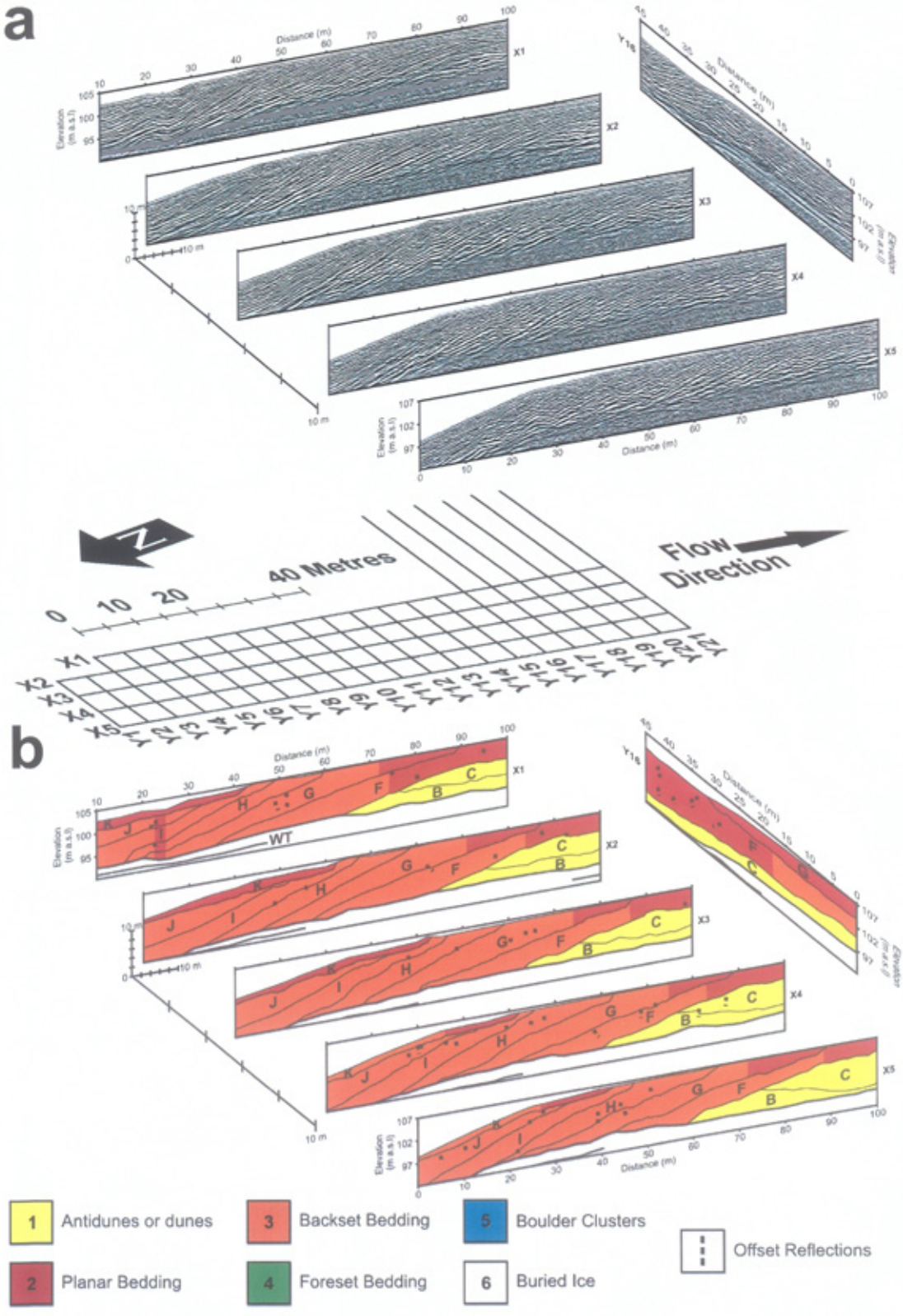


**Figure 6.10.** a) Fence diagram of Sub-grid 4a GPR profiles and b) subsequent interpretation, following protocols and layout described in Figure 6.3. As the Sub-grid was connected to sub-grid 4b, radar element lettering refers to depositional ordering through each of these grids. Buried ice defines the base of the landform, which is predominantly composed of sequentially stacked backset bedded radar elements. The water table (WT) is highlighted on line X1 (bold line) and can be traced through some lines of the grid (see text for a full interpretation of the grid).

reflections are steeply inclined (~10-20°) with the steepest located at the up-flow end of the sub-grid (Figure 6.13a). These backset beds (RF3) grade into upper-stage plane beds (RF2) towards the down-flow end of the sub-grid at a distance of ~70-100 m on X-lines (Figure 6.10), where they overlie RE-B and RE-C that mainly contain cross-bedding (RF1).

Some offset reflections can be identified (reflections are typically offset by <1 m). These are more frequent at the up-flow end of the X-lines and are most pronounced at the eastern end of Y-lines, e.g. Line Y16 at a distance of ~25-45 m (Figure 6.10). The most pronounced offsets correspond to where the lines crosscut faults on the land surface of the western chamber of the ice-walled canyon fill. This corresponds to a distinct drop in buried ice elevation (Figure 6.10).

*6.3.4.2 Sub-grid 4b*

The ice-walled canyon fill here is composed of at least seven radar elements (RE-A-G) that are relatively continuous at the up-flow end of the sub-grid and become more lenticular at the down-flow end of the sub-grid (Figures 6.11, 6.13b). RF6 (buried ice) is continuous across the sub-grid at a maximum depth of ~12 m. Although the upper bounding surface of RF6 is crudely parallel to the landform surface, it has a non-uniform and slightly undulating topography. RE-A and RE-B rest directly upon the buried ice and are dominantly classified as RF1 (cross-beds), though upper-stage plane beds are also present (RF2), typically down-flow. These sediments have been deposited as antidunes or dunes with a maximum crest height of ~2.5 m and length of <6.5 m in flow parallel profiles.

RE-A and RE-B are overlain by cross-cutting radar elements (RE-C-G) (Figure 6.13b) that contain mainly upper-stage plane beds (RF2). These upper-stage plane beds (RF2) may grade to or from foreset (RF4) or backset (RF3) deposits in lines parallel to flow direction. On inspection of flow-perpendicular profiles, however, continuous radar elements are composed of small-scale climbing bedforms (<1 m width) that appear as undular reflections (likely due to their dimensions being less than GPR resolution in this study). Offset reflections can be discerned randomly through the sub-grid, with individual reflections typically being offset by <1 m.

*6.3.5 Grid 5*

Grid 5 is located in the central part of the ice-walled canyon fill and contains at least four radar elements (RE-A-D) that are continuous across the grid (Figures 6.12, 6.13c). RF6 (buried ice) is continuous across the grid at a maximum depth of ~12 m. This surface is relatively horizontal, but does display some undulation (Figure 6.13c). RE-A and RE-B mainly contain foreset (RF4), cross-bedded (RF1) or upper-stage plane

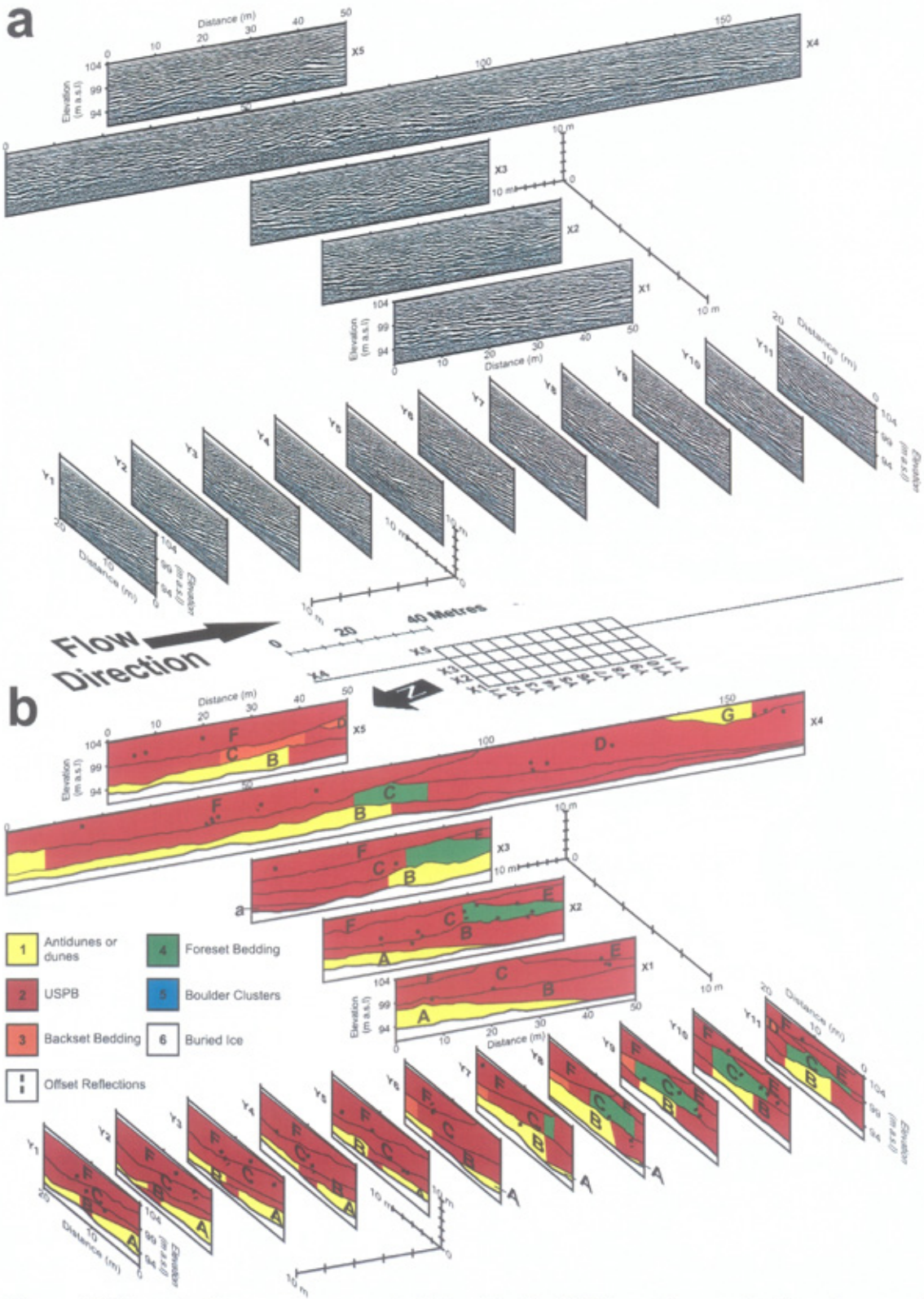


**Figure 6.11.** a) Fence diagram of Sub-grid 4b GPR profiles and b) subsequent interpretation, following protocols and layout described in Figure 6.3. As the Sub-grid was connected to sub-grid 4a, radar element lettering refers to depositional ordering through each of these grids. Buried ice defines the base of the landform, which is predominantly composed of upper-stage plane beds (USPB) (see text for a full interpretation of the grid).

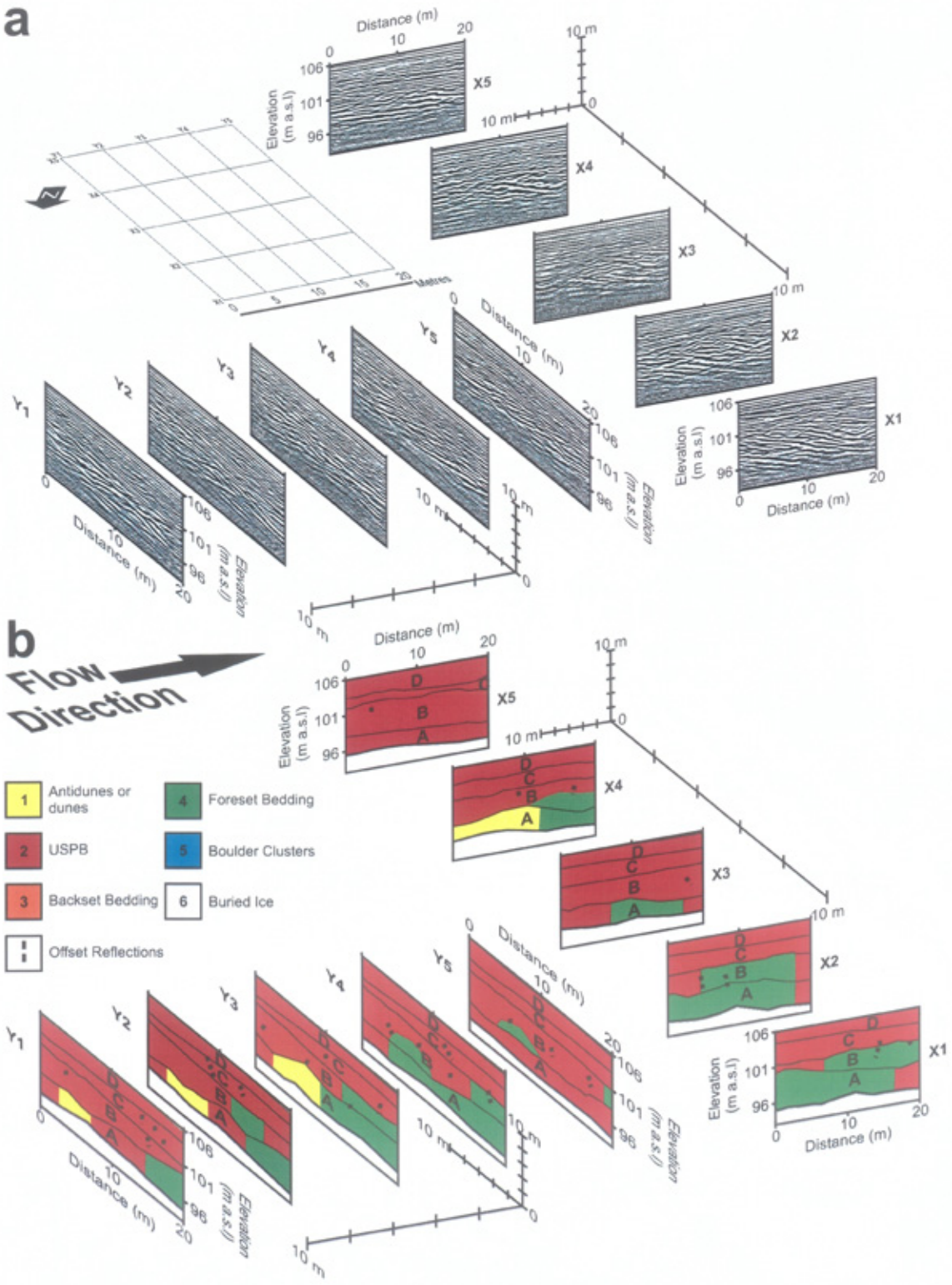


**Figure 6.12.** a) Fence diagram of Grid 5 GPR profiles and b) subsequent interpretation, following protocols and layout described in Figure 6.3. Buried ice defines the base of the landform, which is predominantly composed of upper-stage plane beds (USPB). An armoured layer was also deposited, defined by the lower bounding surface of RE-C (see text for a full interpretation of the grid).

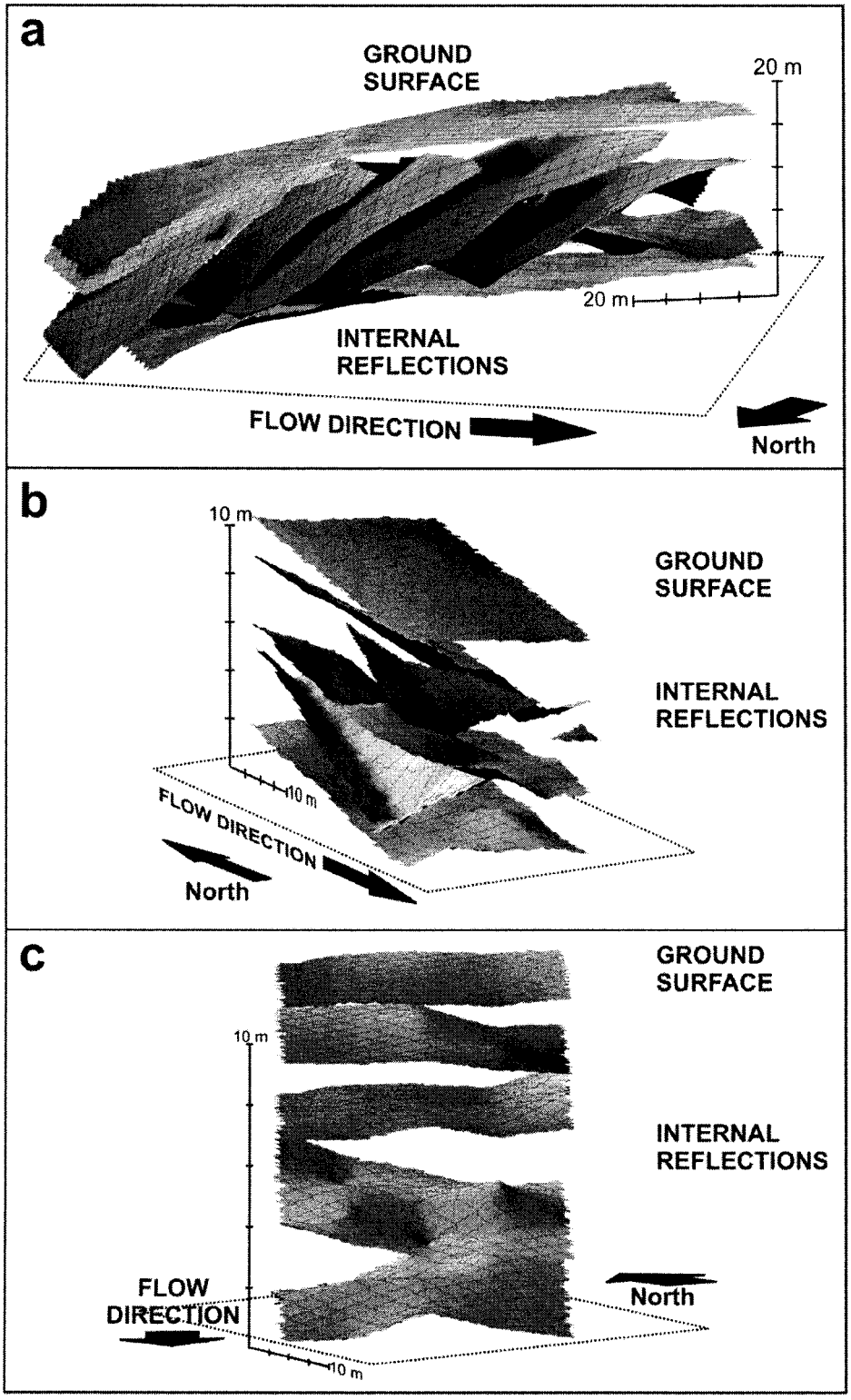


**Figure 6.13.** Pseudo-three-dimensional visualisations of radar element bounding surfaces within ice-walled canyon fill grids, with a two times vertical exaggeration. The most upper surfaces represent the landform surface, whilst the lowest surfaces represent the base of the landform (RF6): a) Sub-grid 4a (Figure 6.10). Internal reflections typically dip up-flow at an angle that is oblique to the landform surface; b) Sub-grid 4b (Figure 6.11). Internal reflections typically dip towards either margin of the Grid; c) Grid 5 (Figure 6.12). Internal reflections are typically sub-parallel to the landform surface, though do display some irregularities.

bedded (RF2) sediments. RE-A and RE-B appear to have been deposited as antidunes or dunes (RF1) with a maximum crest height of ~2.5 m and length of <6 m in flow parallel profiles.

The upper bounding surface of RE-B truncates the reflection sets within it and is represented by a sub-horizontal reflection (Figure 6.13c), above which the radar facies is distinct (Figure 6.12). RE-C-D are entirely classified as upper-stage plane beds (RF2), with individual beds being relatively continuous across the grid. Offset reflections are identified throughout the grid, becmoing more frequent towards the north-west. Individual reflections are typically offset by <1 m.

### 6.4 Radar Facies and Element Pattern

Development and application of a radar facies model to the data collected at Skeiðarárjökull shows distinct variations in sedimentary architecture. Figure 6.14 shows the percentage occurrence of each facies type for each grid. It is clear from this figure and the observations described above that the landform can be divided into four key areas:

1. Up-flow esker (Grids 1 and 2) – A significant percentage of this area has been classified as backset and foreset bedded sediments (41 % combined). Figures 6.3-6.4 show that backset beds generally dominate the stoss side of the ridge scale undulation, whereas foreset progradation is relatively localised to the lee slope of the undulation.
2. Down-flow esker (Grid 3) – Planar bedding is dominant (64 %) throughout this section of the esker, although some foreset bedding does occur distally.
3. Portal-proximal ice-walled canyon (sub-grid 4a) – A significant percentage of this area has been classified as backset beds (46 %), deposited as steeply inclined and stacked Radar elements. These truncate basal RE-B-C of antidunes (or dunes) at the down-flow end of the grid (Figures 6.10, 6.13a).
4. Central ice-walled canyon (sub-grid 4b and Grid 5) – Planar bedding is the dominant mode of deposition (66 %), and typically rest upon a basal radar element of antidunes (or dunes) (Figures 6.11-6.12).

### 6.5 Macroforms and Landforms

Sedimentation within the esker was complex due to within-event conduit evolution that resulted in alternating periods of erosion and aggradation evidenced by unconformities between radar elements. The identification of an ice-contact surface, defining the base of the landform through most the system (Grids 1-3b, 4a-5), suggests that the landform was initially generated within an englacial conduit that enlarged to become supraglacial at its distal end.

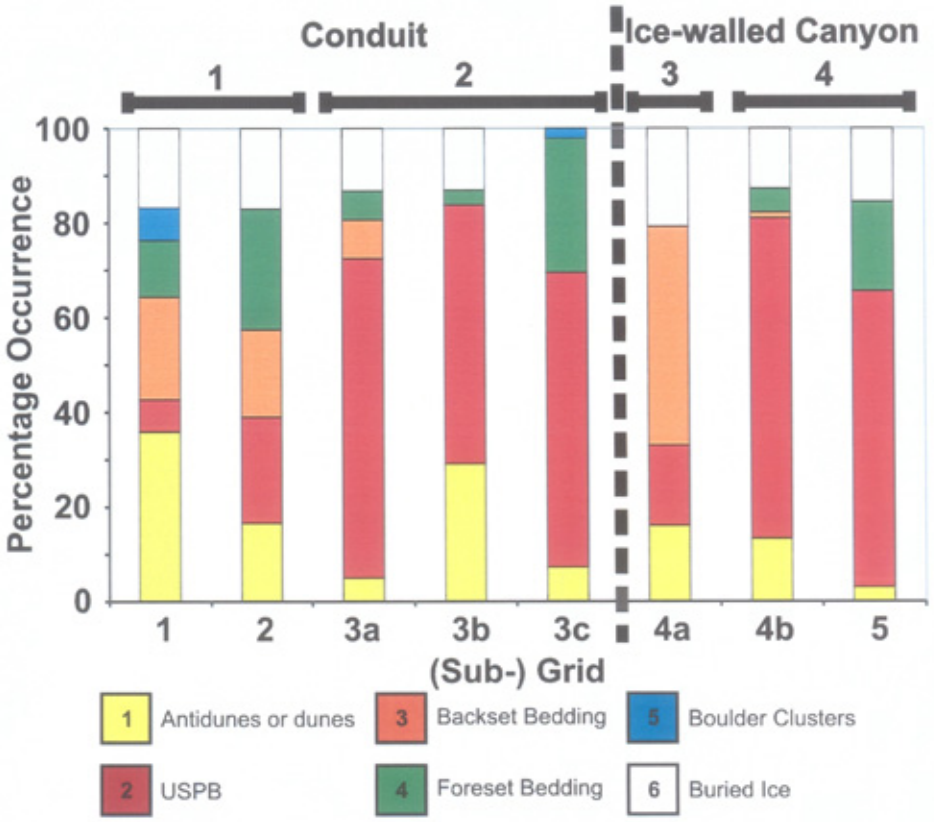


**Figure 6.14.** Graph showing the percentage occurrence of each radar facies type within each (sub-) grid. Each radar facies has been colour coded (see key), with radar facies type descriptions and colour keys following those presented in Figure 6.1. The sedimentary architecture of the landform can be split into four depositional environments: 1) composite macroform development within a conduit enlargement; 2) Dominance of upper-stage plane beds (USPB) indicating deposition within constricted flow; 3) Deposition of backset beds at an upstream migrating hydraulic jump, which was a consequence of a switch from pressurised deposition within an englacial conduit to deposition at atmospheric pressure within the ice-walled canyon; 4) Upper-stage plane beds indicate deposition took place in shallower flows.

RE-A and RE-B can be identified in almost all grids in the form of antidune (or dune) aggradation. These radar elements demonstrate an EM signature that is distinct from the radar elements overlying them. The occurrence of antidunes coupled with relatively consistent bedform dimensions, suggest that flow depths were relatively low (<3 m), Froude numbers were >0.84 (Carling, 1999) and that these conditions would have been relatively constant through each grid. This radar element, however, is absent in some locales, such as the up-flow end of sub-grid 3a, e.g. at a distance of ~0-70 m (Figure 6.6). The simplest explanation for its absence is that these are areas of non-deposition (c.f. Saunderson, 1977; Brennand, 1994), though the unconformities typically defining its upper bounding surface here suggest that it must have been at least partly eroded.

At Grids 1 and 2 RE-B-I show a downstream transition from backset to foreset bedded sediments, which is consistent with that of a composite macroform (c.f. Brennand, 1994; Brennand and Shaw, 1996; Brennand, 2000) and a significant increase in flow depth. At the eastern side of Grid 1 the lack of RE-A suggests that the conduit position was not stable, and composite macroform development was synchronous with conduit growth (c.f. Brennand, 1994; Brennand and Shaw, 1996; Brennand, 2000) and migration. Down-flow from the composite macroform (Grids 3) RE-B-I are more continuous through the grids and mainly contain upper-stage plane beds (RF2), suggesting Froude numbers would be >0.84 (Carling, 1999) and flow depths would have been lower (e.g. Alexander *et al.*, 2001).

The orientations of RE-F-J at the portal-proximal ice-walled canyon fill demonstrate upstream aggradation of backset beds (Figures 6.10, 6.13a), which took place suabaerially within a supraglacial ice-walled canyon (c.f. Russell and Knudsen, 1999a, 1999b; Russell *et al.*, 2001a; Cassidy, *et al.*, 2003; Russell, *et al.*, 2005, 2006). The contrast in sedimentary architecture between conduit and ice-walled canyon deposits is due to the occurrence of a hydraulic jump (c.f. Jopling and Richardson, 1966; Fiore *et al.*, 2002), which is associated with the sudden discharge of floodwaters into an expansion environment, likely due to a switch from pressurized floodwaters to deposition at atmospheric pressure. The stacked nature of backset units could be due to pulsation of floodwaters and/or upstream migration of the hydraulic jump, though the steep angles of backsetting (~25°) and the upstream-dipping bounding surfaces suggest the latter is more probable.

Down-flow at the central ice-walled canyon fill (Sub-grid 4b and Grid 5) radar elements are characterised by antidune (or dune) aggradation, which is consistent with the observations of upstream migrating standing waves during the jökulhlaup and post-flood GPR surveys conducted by Cassidy *et al.* (2003). RE-C-G are dominantly planar bedded, indicating lower flow depths and supercritical conditions. In addition, at the most

distal grid (5) of this study, an armoured layer was deposited (c.f. Cassidy *et al.*, 2003), which is not observed in up-flow radar profiles (Grids 1-4b).

## 6.6 Discussion

### *6.6.1 Conduit evolution*

The observations described above form the basis of an evolutionary model for the controls on the sedimentary architecture of the 1996 Skeiðarárhlaup esker (Figures 6.15-6.16). The stages of this model can be linked to the conceptual hydrograph of a linearly-rising jökulhlaup (Figure 6.17b).

The onset of conduit development (Stage 1, Figures 6.15-6.16) likely took place during stage B of the hydrograph, when low effective pressures resulted in the development of supraglacial outlets (B, Figure 6.17b). During the earliest phase of conduit development cavities were excavated along the primary floodwater path (Stage 1, Figures 6.15-6.16), due to mechanical excavation of surrounding glacier ice that was extensively fractured by passage of the flood wave and/or hydraulic jacking (Roberts *et al.*, 2000b). Supercritical flow conditions resulted in cavity infilling by antidune (or dune) sets (Stage 2, Figures 6.15-6.16). The development of cavities and deposition along the flood path took place within a pressurised system.

During stage C of the jökulhlaup (C, Figure 6.17b), the effective pressure increased and floodwaters focussed along the path (Stage 3, Figures 6.15-6.16), resulting in the connection of cavities to form a relatively efficient englacial conduit. Ice excavation and cavity generation, however, were non-uniform and a conduit enlargement was excavated at the up-flow end of the exposed system. Vertical conduit growth towards the supraglacial outlet resulted in conduit unroofing by removal of the fractured and weakened ice roof near the ice margin (Roberts *et al.*, 2000b). Consequently, the sudden switch from pressurised deposition to deposition at atmospheric pressure within an expansion environment resulted in the creation of a hydraulic jump.

Within the up-flow conduit enlargement, flow depths were increased and backset beds aggraded onto the stoss-side of the deposit, with foresets subsequently prograding within the flow separation on the lee-side. During stage C of the hydrograph discharge continued to rise (C, Figure 6.17b) and the conduit, as well as having expanded vertically into the ice, enlarged due to upstream and downstream expansion as well as lateral migration. Downstream, where flow depths were lower and velocities were higher, predominantly upper-stage plane beds were deposited (c.f. Allen, 1992). In geometrically narrow and uniform conduits high velocity flows might be expected to produce pseudo-anticlinal macroforms, represented by broad, low-angled, arched or anticlinal beds (Brennand, 1994, 2000). These are not observed throughout the down-flow esker, but the GPR line coverage was partially restricted due to topographical constraints at the ridge

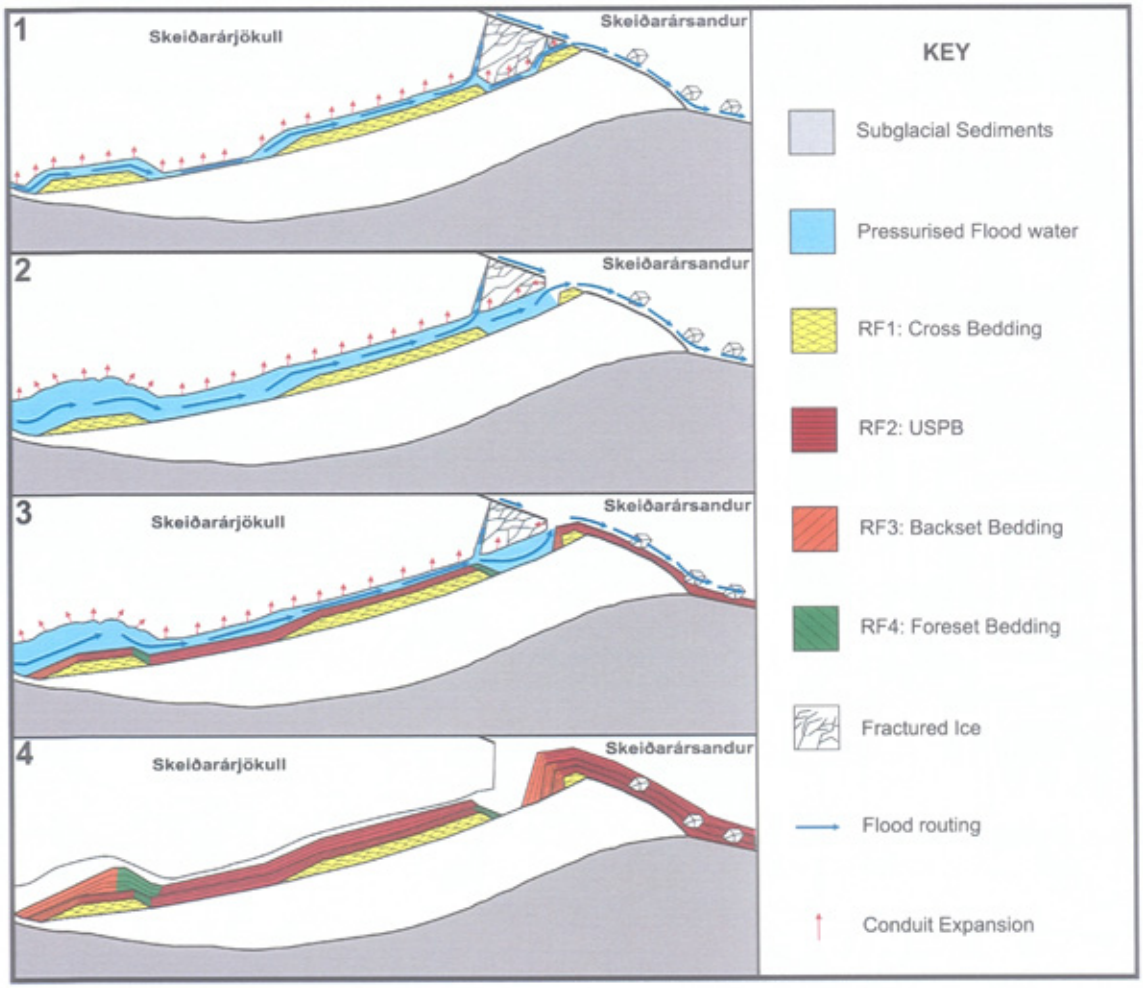


**Figure 6.15.** Two-dimensional model for the development of the 1996 jökulhlaup esker at Skeiðarárjökull, Iceland: 1) Cavity generation due to pressure variations along flood paths created accommodation space allowing the deposition of antidune or dune sets, within a pressurised englacial position. 2) As floodwaters became focused along primary outlets, further ice excavation resulted in conduit development due to connection of cavities. Enhanced ice excavation in the proximal conduit created a 'conduit enlargement'. Distal conduit unroofing created a hydraulic jump due to a switch from pressurised to atmospheric pressure discharge, which partially eroded older sediments. 3) Variations in conduit geometry resulted in the deposition of a varying sedimentary architecture along the length of the system. 4) Within the conduit enlargement, the sedimentary architecture is consistent with composite macroform development. Downstream, upper-stage pane beds dominated due to the reduction in flow depths. Upstream migration of the hydraulic jump resulted in headward excavation of the ice-walled canyon and deposition of sequentially stacked backset bedded units.

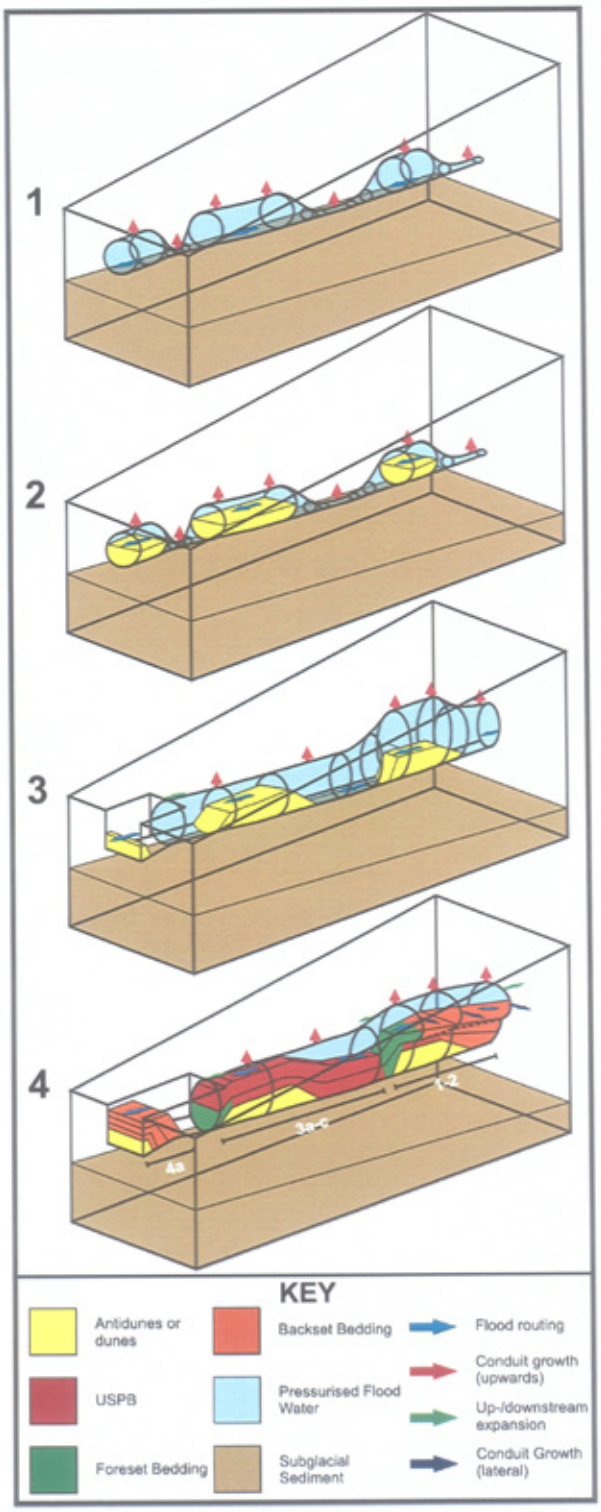


**Figure 6.16**. Three-dimensional model for conduit development and consequent controls on esker sedimentary architecture during the 1996 Skeiðarárhlaup. There are four major stages of conduit development: 1) Pressurised englacial flood discharge resulted in localised ice excavation and cavity generation. 2) Early deposition took place englacially within the newly created accommodation space. 3) Focusing of floodwaters resulted in further cavity generation and conduit development. The up-flow conduit became locally expanded. Downstream the conduit grew upwards into the ice, resulting in conduit unroofing at the distal end and the creation of an ice-walled canyon at the margin. 4) As the conduit became infilled, it grew. At the enlarged conduit, growth occurred vertically, upstream, downstream and laterally.

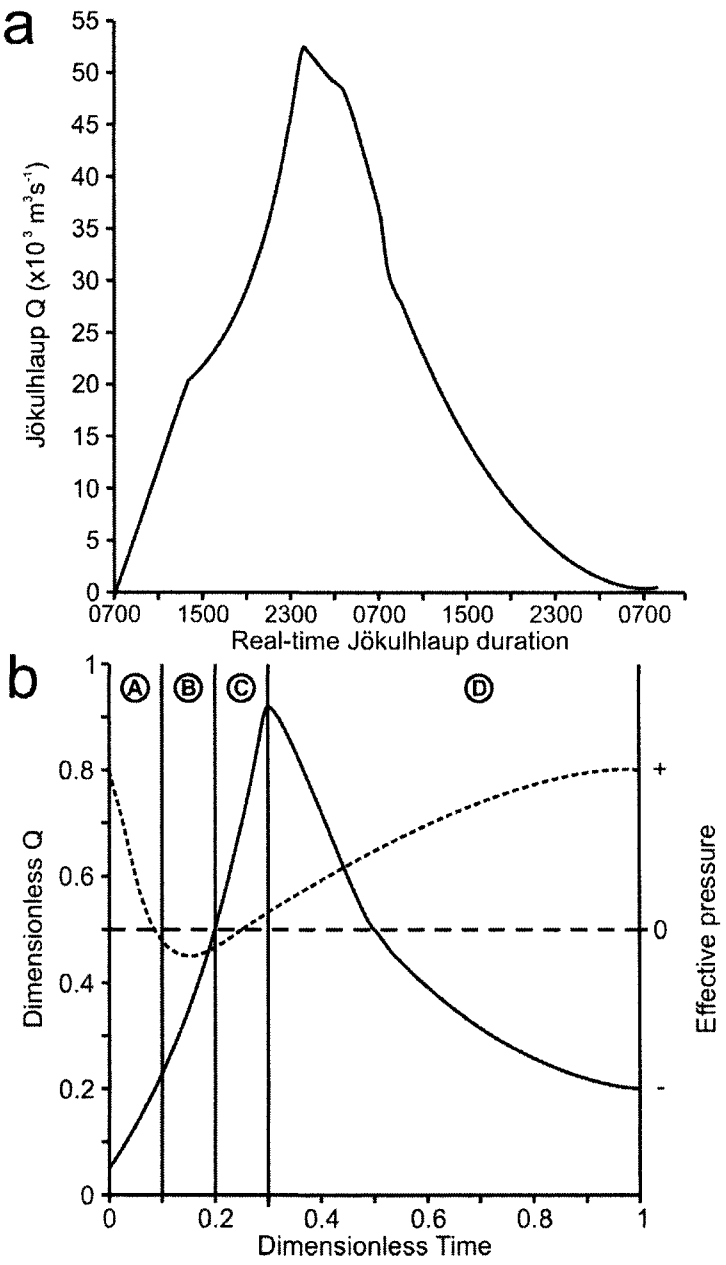


**Figure 6.17**. a) The November 1996 jökulhlaup hydrograph at Skeiðarárjökull, showing total discharge (after Snorasson *et al.*, 2002). The event rises linearly to its peak discharge over a period of approximately 14 hours, before waning more steadily for up to 32 hours. b) Conceptual hydrograph (solid line) of a linearly rising jökulhlaup and concomitant effective pressure (dashed line) (after Roberts, 2005): A) Propagation of the flood wave results in reduction of effective pressure and routing of floodwater into the glacier; B) continued spread of the flood wave and development of supraglacial outlets. In the wake of the flood wave, floodwater travels through a system of conduits; C) Primary conduit outlets develop, though discharge continues to rise despite an increase in effective pressure; D) waning-stage floodwaters are conveyed through relatively few conduits.

margins (Figures 6.6-6.8). Continued conduit unroofing at the down-flow end of the conduit resulted in upstream migration of the hydraulic jump and deposition of sequentially stacked backset units within the newly created accommodation space (Stage 4, Figures 6.15-6.16).

*6.6.2 Depositional timescale*

Based upon the assumptions of outlet development during a linearly rising jökulhlaup (Figure 6.17b), estimates can be made as to the timing of esker development during the November 1996 jökulhlaup at Skeiðarárjökull. Approximately three hours (*c.* 10:15h) after the initial outburst, at the eastern Skeiðará outlet, supraglacial fracture outlets developed at the head of the Gígjukvísl catchment (Roberts *et al.*, 2000b). By *c.* 17:00h (~10 hours after jökulhlaup onset) all supraglacial outlets had ceased except for increasing discharge through two isolated fractures located within the Gígjukvísl catchment (site of the ice-walled canyon) (Roberts *et al.*, 2000b). Conduit development must have begun within approximately three and ten hours of flood onset, supporting the time scale of outlet development for an idealised linearly rising jökulhlaup (see *Section 6.6.1* and Roberts, 2005). Approximately seventeen hours later (*c.* 10:00h on the 6$^{th}$ November) the ice-walled canyon had been excavated into the margin of Skeiðarárjökull, with its most headward extent matching the uppermost fracture through which floodwaters discharged (Roberts *et al.*, 2000b). As the conduit and ice-walled canyon assemblages were deposited synchronously, it is likely they were generated within a period of between approximately seventeen and twenty-four hours. Although the jökulhlaup did not wane until the 7th November (Figure 6.17a), little evidence can be identified for late-waning stage reworking of the esker (such as erosion of rising-stage deposits, or deposition of fine materials), further supporting a development phase beginning and ending during the mid-rising and mid-waning stages, respectively.

The maximum number of radar elements identified in the esker and ice-walled canyon deposits is eleven, all of which were deposited over a maximum period of twenty-four hours. If a uniform sedimentation rate is assumed, individual units were generated in approximately two hours. This, however, is likely an overestimate, as erosive periods and variations in sedimentation rate cannot be taken into account. Sedimentation rates, however, were high and individual units had to be deposited over a period of minutes to hours, which is consistent with estimates made by Russell and Knudsen (1999a) that lamina were deposited within seconds to minutes and depositional units within minutes to hours. These estimates were based upon the quantification of slack water sediments within the eastern chamber of the ice-walled canyon fill (Russell and Knudsen, 1999a).

Although some studies have inferred rapid sedimentation rates for eskers (e.g. Allen, 1971; Brennand, 1994; Mokhtari Fard, 2001; Fiore *et al.*, 2002; Mäkinen, 2003), a

depositional timescale cannot be rigorously applied to the controls on palaeo-esker sedimentary architecture. This study, therefore, adds to recent work in the contemporary environment that demonstrates the significant role jökulhlaups can exert upon landform genesis (e.g. Russell, 1994; Russell and Knudsen, 1999a, 1999b; Roberts *et al.*, 2000b, 2001, Russell *et al.*, 2001; Cassidy *et al.*, 2003; Roberts, 2005; Russell *et al.*, 2005, 2006).

### 6.7 Summary

This chapter and the paper accepted for publication in *Quaternary Science Reviews* provide the first detailed model of the controls on englacial esker sedimentary architecture, during a well documented, high-magnitude jökulhlaup within a contemporary glacier setting. This linearly rising jökulhlaup was associated with high water pressures allowing floodwaters to be discharged through englacial and supraglacial outlets. Sudden cavity generation and ice excavation resulted in rapid conduit development and the consequent sedimentation rates were high. As the conduit developed quickly in response to swiftly rising discharge the depositional environment evolved rapidly to accommodate the increasing discharge through primary outlets, which were developed due to an exponential input of floodwaters (c.f. Roberts, 2005). Consequently, conduit geometry was a fundamental control on the sedimentary architecture of the esker (Brennand, 1994; Brennand and Shaw,1996; Brennand, 2000; Fiore *et al.*, 2002), with the system being divided into four key areas:

1. *Up-flow esker* where sedimentation took place within a conduit enlargement.
2. *Down-flow esker* where deposition was within relatively constricted flows.
3. *Portal-proximal supraglacial ice-walled canyon* where sedimentary architecture was controlled by headward conduit unroofing due to conduit growth.
4. *Central supraglacial ice-walled canyon* where sediments were deposited within an ice-walled canyon excavated due to ice block removal from intensely fractured ice.

Esker genesis took place during the mid-rising to mid-waning stages of the jökulhlaup. This constrains esker sedimentation into a very short period of time (17-24 hours) resulting from the rapid hydrological response to exponential floodwater input. During the rise to peak discharge the glacial hydrological system was forced to create new outlets in response to a discharge that could not be accommodated by perennial outlets alone. Although rapid sedimentation rates have been inferred for some eskers deposited during previous glaciations (e.g. Allen, 1971; Brennand, 1994; Mokhtari Fard, 2001; Fiore *et al.*, 2002; Mäkinen, 2003), this is the first study of an esker that can be well constrained to a depositional timescale of less than twenty-four hours.

# Chapter 7

# The Sedimentary Architecture of the Bering Glacier Esker and Ice-walled Canyon Fill

## 7.1 Introduction

Two grids of ground-penetrating radar (GPR) line were collected on the esker, and one grid on the ice-walled canyon fill at the eastern sector forefield of Bering Glacier, Alaska. All grids of CO GPR line were collected at a nominal frequency of 200 MHz, covering all workable areas of the esker and ice-walled canyon fill. Each of the GPR profiles collected on the esker and ice-walled canyon fill can be broken down into a number of radar facies and radar elements. Subsequent to data collection, an outburst flood at Bering Glacier has created new sections through both landforms that have aided interpretation of the GPR data sets.

This chapter presents the results of GPR surveys and interprets the sedimentary architecture as imaged by the GPR. The results of the GPR investigations are described in *Section 7.2* and *Section 7.3*. *Section 7.2* describes and interprets each radar facies identified on the GPR lines, before the radar elements are described for each grid in *Section 7.3*. The distribution of radar facies and radar elements will be interpreted in *Section 7.4*. The discussion in *Section 7.5* focuses upon conduit evolution during the 1994 outburst floods at Bering Glacier, and discusses the depositional timescales of the associated landforms. The chapter will then be summarized in *Section 7.6*.

## 7.2 Classification and interpretation of radar facies

GPR profiles from the esker and ice-walled canyon fill are interpreted using a radar facies classification scheme (Figure 7.1) developed to identify distinct radar elements. Radar element (RE) bounding surfaces were identified as the highest amplitude reflections that could be traced pseudo-three-dimensionally across grids for significant distances. For each GPR line, the main depositional elements were identified and classified (Figures 7.2-7.3, 7.5-7.6), based upon the radar facies scheme detailed below (Figure 7.1).

*Radar facies 1: Discontinuous undular reflections*

Radar facies 1 (RF1) is composed of sets of undular or trough-shaped reflections that range from individual troughs ~4 m in diameter, to more horizontal, discontinuous reflections, e.g. RE-B at ~39-43 m on line X2 of Grid 1 (Figure 7.3). In some cases the

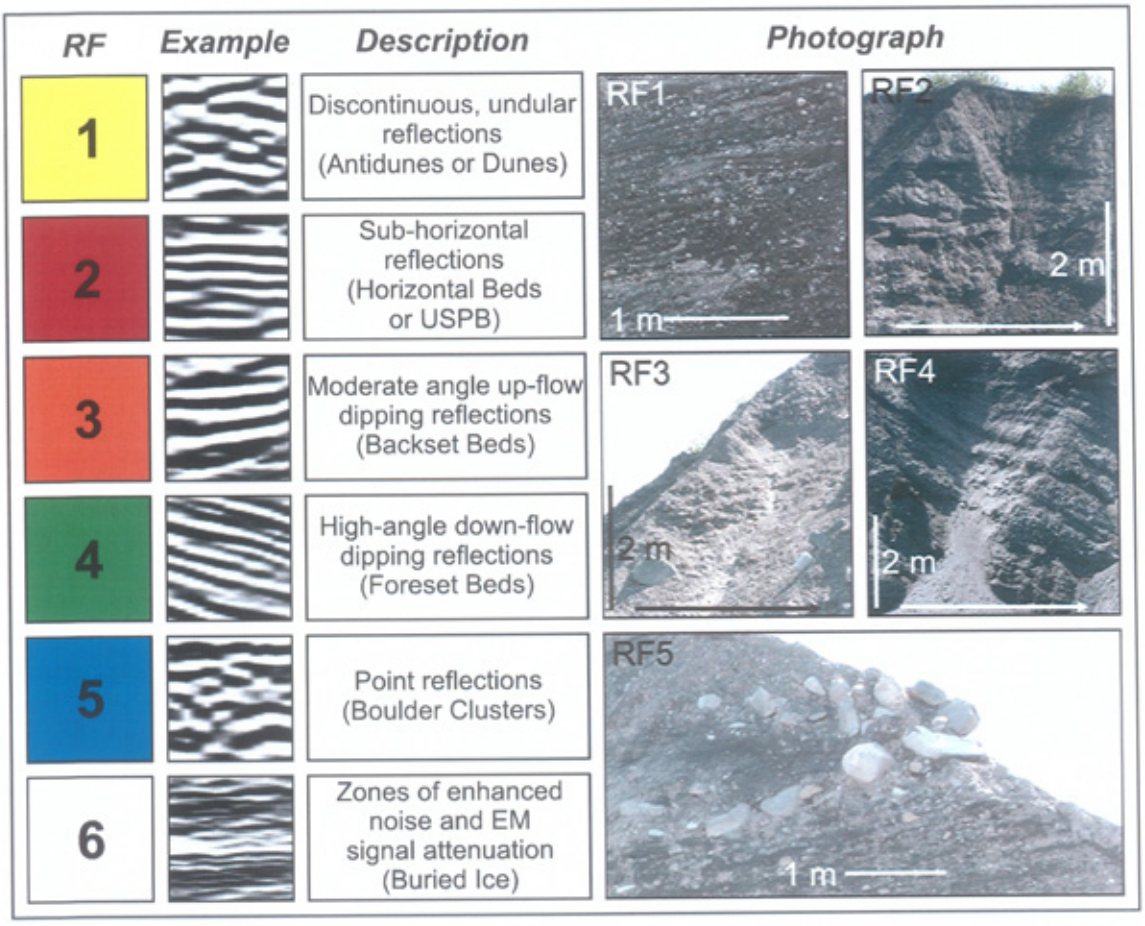


**Figure 7.1.** Generalised radar facies used to describe and interpret the processed GPR profiles (USPB: upper-stage plane beds). The sedimentological descriptions and interpretations (in brackets) of the radar facies are indicated and photographs of comparable sedimentary structures are presented (arrows indicate flow direction where appropriate).

largest examples may have a maximum crest height of up to ~2 m and contain an internal structure of discontinous reflections, e.g. RE-C at ~8 m on line X4 of Grid 3 (Figure 7.6). These reflections can extend laterally for a maximum of ~50 m, with radar elements having a maximum thickness of ~4 m, e.g. RE-B on line X1 0f Grid 1 (Figure 7.3). They can also grade to or from more continuous reflection sets, e.g. RE-B on line X2 of Grid 1 (Figure 7.3). RF1 is interpreted to represent cross-bedding associated with the development of antidune or dune sets (*Section 6.2*). Although a dune interpretation cannot be ruled out by evidence within the GPR data, for reasons given in *Section 6.2*, an antidune interpretation is preferred.

*Radar facies 2: Sub-horizontal reflections*

Radar facies 2 (RF2) consists of sets of sub-horizontal reflections with an angle of dip <5° from horizontal. They can be arranged as horizontal or dipping sets that tend to be sub-parallel to the bed slope. When bed thickness is less than the EM wavelength, less distinct reflections are produced (Davis and Annan, 1989; Neal, 2004) representing internal layer structure that is below the resolution of the GPR. Radar elements containing sub-horizontal reflections can extend laterally for up to ~40 m, having a maximum thickness of <5 m, e.g. RE-C on line X3 of Grid 2 (Figure 7.5). In some cases these reflections can grade into or from discontinuous or inclined reflections, e.g. RE-E on X-lines of Grid 1 (Figure 7.3) and radar elements are commonly divided by unconformities, e.g. RE-C at ~0-15 m on line X1 of Grid 1 (Figure 7.3). In Grid 3, sub-horizontal reflections are located within RE-G that can be correlated to deformation materials (Figure 7.10). RF2 is interpreted as horizontal beds or upper-stage plane beds, though as in *Section 6.2*, an upper-stage plane bed interpretation is preferred in most cases for two reasons: 1) often sub-horizontal reflections can be correlated to primarily deposited plane beds exposed at the margins of the landforms (Figures 7.1 and RE-G in Figure 7.10); 2) upper-stage plane beds are deposited during critical to supercritical flow conditions which are likely during the outburst floods (Carling, 1999; Alexander *et al.*, 2001). Where other interpretations are likely, this will be discussed accordingly.

*Radar facies 3: Up-flow dipping low to moderate-angle inclined reflections*

Radar facies 3 (RF3) consists of sets of reflections that dip up-flow at an angle of 5-10° from horizontal, with angles closer to 5° being more common. This facies can only be identified on Grid 1, where individual radar elements have a maximum lateral coverage of <20 m and a maximum thickness of ~3 m, e.g. RE-C on line X3 of Grid 1 (Figure 7.3). Individual reflections within radar elements containing RF3 are generally discontinuous, perhaps indicating the deposition of climbing bedforms by turbulent flows. As in *Section 6.2,* RF3 is interpreted as backset bedding that is typically deposited at a hydraulic jump

associated with a switch from supercritical to subcritical flow conditions (Jopling and Richardson, 1966; Alexander *et al.*, 2001).

*Radar facies 4: Down-flow dipping high-angle inclined reflections*

Radar facies 4 (RF4) consists of sets of reflections that dip downstream at angles ranging from 10-20° from horizontal, with angles of ~15° being more common. Although not restricted to, they are most extensive in Grid 3 deposits, with a maximum lateral extent and thickness of ~20 m and ~5 m, respectively, e.g. RE-E and RE-F on line X2 of Grid 3 (Figure 7.6). They may grade to or from other facies types, typically being identified in down-flow grid sections (Figure 7.6). As in *Section 6.2*, RF4 is interpreted to represent foreset bedding deposited at a point of flow separation by turbulent flows (c.f. Jopling, 1965).

*Radar facies 5: Point reflections*

Radar facies 5 (RF5) consists of point and irregular reflections associated with point source reflectors that have been successfully collapsed from small hyperbolae (that can be seen in the raw data) during migration (*Section 4.3.6*), e.g. RE-C at a distance of ~22-27 m on line X2 of Grid 1 (Figure 7.3). In some cases, however, these hyperbolae have been under-migrated, suggesting the reflectors are offline, e.g. radar element 5 at a distance of ~18 m on line X1 of Grid 2 (Figure 7.5). RF5 has been identified within radar elements extending laterally for up to ~6 m with a maximum thickness of ~2 m in Grids 1 (Figure 7.3) and 2 (Figure 7.5), only. This facies is in all cases, located within near land surface radar elements and in similar cross-sectional locations, e.g. within RE-D and RE-E between ~22-29 m on line X1 of Grid 2 (Figure 7.5). An exposure running approximately perpendicular to the axis of GPR Grid 1 allowed observation of boulder clusters in locations corresponding to the observed incidence of RF5 (Figure 7.8). RF5, therefore, is interpreted as boulder clusters that have been deposited during later stages of deposition, or lag deposits of erosive events within the outburst flood (Fleisher *et al.*, 2007). The isolated occurrence of RF5 is likely testament to sediment supply constraints, with there being a limited availability of large clasts.

*Radar facies 6: zones of enhanced noise and EM signal attenuation*

Radar facies 6 (RF6) incorporates a zone of noise and enhanced attenuation of EM signals, bounded on its upper surface by a relatively continuous reflection. Though the signal-to-noise ratio is usually low within this facies, structure can still be observed (to some extent) below the bounding reflection. This facies can only be identified on Grid 3 lines, where it is identified at the base of the GPR profiles across the grid (Figure 7.6). RF6 is interpreted to represent buried ice, with its extensive coverage across a grid

suggesting it represents the base of the channel in which the ice-walled canyon sediments were deposited. The presence of this facies in Grid 3 is consistent with buried ice observed at sections within the ice-walled canyon fill (Fleisher *pers. comm.*, 2007).

*Offset reflections*

In some places distinct offsets are observed within and/or between radar elements and facies. This offsetting is observable in at least some profiles of each grid, but can be more pervasive within some grids, e.g. Grid 3 (Figure 7.6), with variable angles and orientations. Consequently this offsetting is interpreted as structural collapse of the sediments associated with normal faulting (c.f. McDonald and Shilts, 1975) of the landform due to melting of the supporting ice walls and/or buried ice (Woodward *et al.*, 2008).

## 7.3 Description and Quantification of Radar Elements

For each GPR line the main depositional units were identified and classified, based upon the facies scheme detailed above (see Figure 7.2 for example), using the same approach adopted for data interpretation in *Chapter 6*. In order to establish the frequency of each radar facies throughout the GPR grids the individual coverage of each was calculated for all lines of every grid. From this, the total percentage occurrence of each facies for individual lines and grids could be calculated. The distribution by each grid can be used to identify down-flow trends, whilst examining individual X- and Y-lines highlights within grid trends (See *Appendix 4* for enlarged GPR lines and interpretations). Each GPR grid is described in turn starting with the most up-flow and working down-flow on the esker, before the grid on the ice-walled canyon fill is described.

### *7.3.1 Grid 1*

The esker here is relatively complex being composed of at least five radar elements (Figure 7.3) that are relatively continuous across the grid. A continuous, though slightly irregular (Figure 7.4a), high-amplitude sub-horizontal reflection can be identified at a maximum depth of ~8 m and traced across the entire grid. Although the EM signal rapidly attenuates below this strong sub-horizontal reflection, reflections are classified as RF2 (upper-stage plane beds). Identified directly above this reflection are RE-A and RE-B predominantly classified as cross-beds (RF1), which may grade to or from upper-stage plane beds (RF2). The largest bedforms (RF1) appear to have a maximum crest height of ~1.5 m and length of <4 m in flow parallel lines, though internal structure is typically unidentifiable. RE-A-B represent a significant area of the esker (~45-50%; Figure 7.7) and have an up-flow dipping (at ~5°) upper bounding surface that truncates the internal reflections of RE-B (Figure 7.3). Within RE-B (line X2) at an elevation of ~30 m and

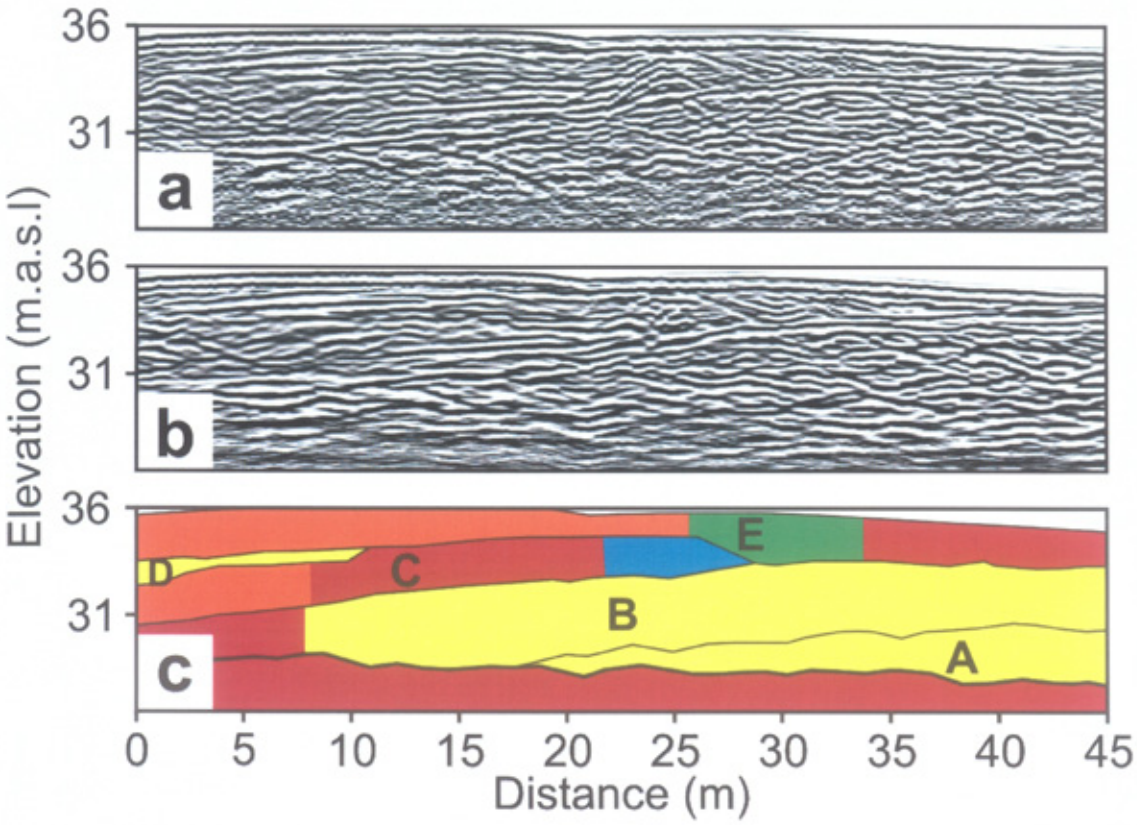


**Figure 7.2.** Figure showing line X2 (Grid 1), with palaeo-flow direction being from left to right. a) The processed line following the sequence presented in Figure 4.16, without the application of a migration algorithm. b) The processed line following application of the optimal processing sequence presented in Figure 4.16, including the application of a migration algorithm. c) Interpretation based upon the radar facies scheme presented in Figure 7.1. A continuous, but non-uniform reflection defines the base of the assemblage, below which the radar facies classification is different to radar elements resting upon it. RE-A and RE-B are predominantly cross-bedded sediments that rest directly upon non-related planar beds. RE-C-E show more complexity, with erosional contacts being identified, including a cut-and-fill structure at the ice-proximal end of the line (RE-D). Boulders can be identified at the centre of the line, within RE-C, though RE-C and RE-E are dominated by backset beds upstream, grading into forests centrally and planar beds distally.

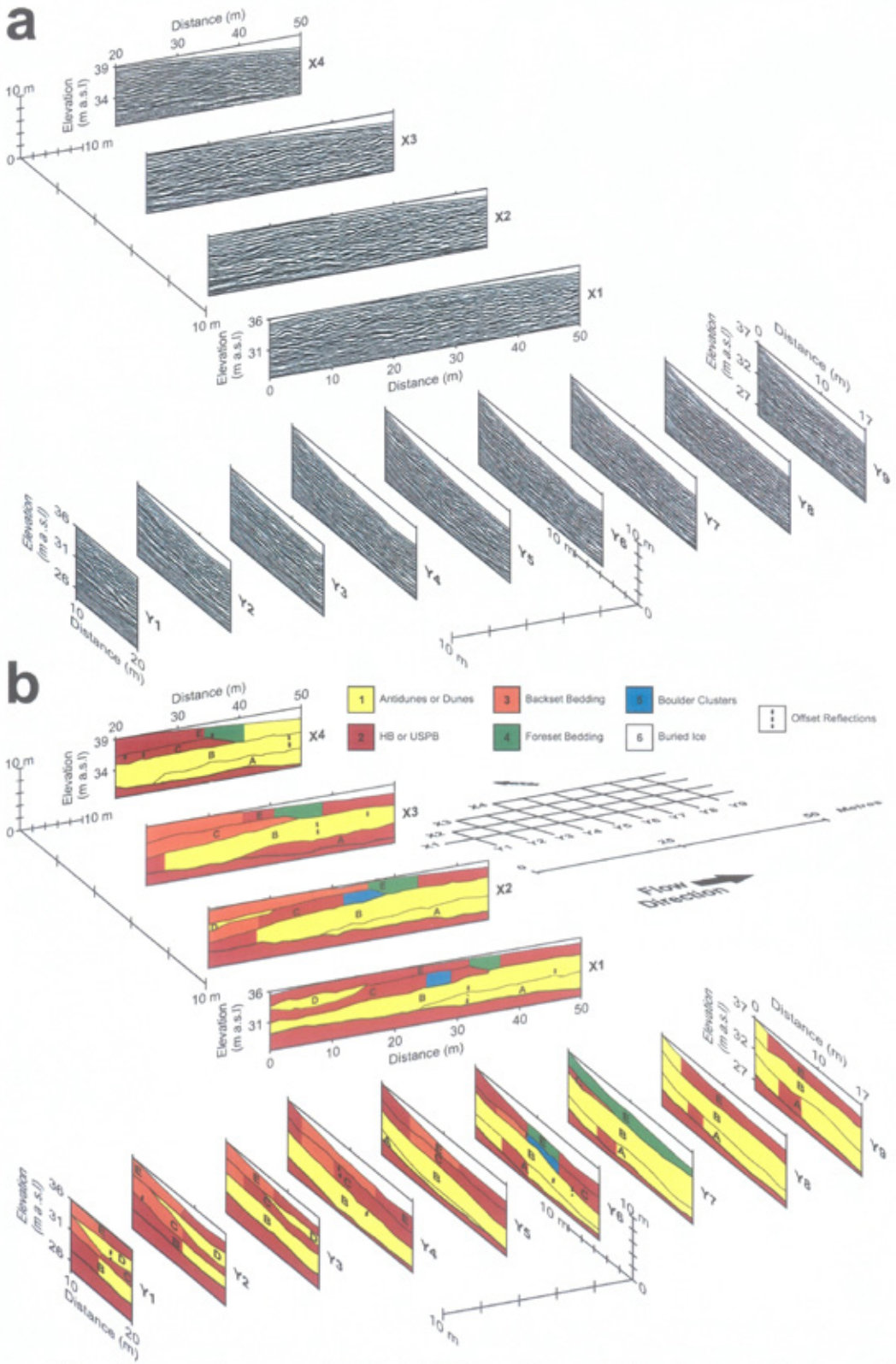


**Figure 7.3.** a) Fence diagram of Grid 1 GPR profiles and b) subsequent interpretation (distance ticks are at 10 m intervals). Each profile has been processed using the sequence identified in Figure 4.16. The grid map in the centre of the figure shows the true line orientation. Each facies has been colour coded to allow identification of trends (see Figure 7.1 for facies descriptions). Sedimentation here is complex, with units showing major lateral and vertical variations in architecture (HB: horizontal beds, USPB: upper-stage plane beds).

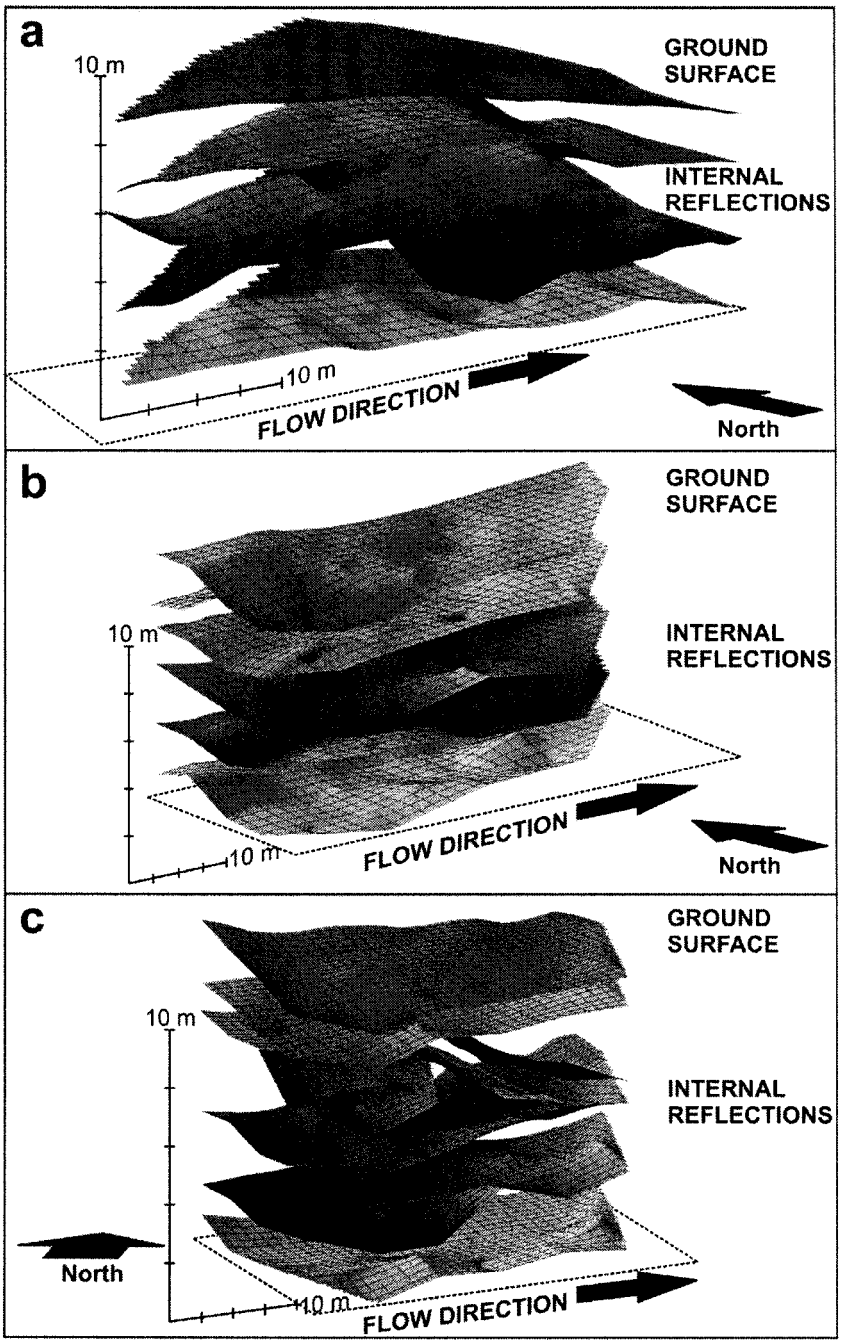


**Figure 7.4.** Pseudo-three-dimensional visualization of radar element bounding surfaces (with a two-times vertical exaggeration): a) Grid 1 bounding surfaces (Figure 7.3), including both the ground surface and internal reflections. The bounding surfaces at the up-flow part of the grid dip up-flow at a low angle; b) Grid 2 bounding surfaces (Figure 7.5), including both the ground surface and internal reflections, which are typically sub-horizontal; c) Grid 3 bounding surfaces (Figure 7.6), including both the ground surface and internal reflections. The internal reflections show major vertical variations in geometry. Those up-flow are typically sub-horizontal, but are truncated by high-angle down-flow dipping reflections at the down-flow end of the grid.

distance of ~2-20 m a large hyperbolae can be identified (Figure 7.2a), which after migration is collapsed into a strong coherent reflection within the upper part of RE-B.

The bounding surfaces of RE-C-E are typically associated with unconformities, though the internal reflections are generally more continuous, relative to those within RE-A-B. Internal reflections within these elements (RE-C-E) have a variable radar facies classification. Radar elements at the up-flow end of the grid (at ~0-25 m) typically contain backset beds (RF3) in central (lines X2-3) and upper-stage plane beds (RF2) in lateral lines (X1 and X4). This is due to the low angles associated with backset deposition here. Those lines classified as RF2 are still dipping up-flow, but at an angle lower than the cut-off used to distinguish RF3. Within RE-C, boulder clusters can be identified at the down-flow end of the radar element, where the upper bounding surface dips down flow at a high-angle (~20°) This central (relative to the grid) down-flow dipping unconformity corresponds to the location of foreset beds (RF4) within RE-E, which typically grade into upper-stage plane beds down-flow (Figure 7.3). As well as containing a high diversity of radar facies, a small (~10 m by ~10 m) concave-up unconformity defines the base of RE-D (Figure 7.4a), with internal reflections being classified as RF1 (cross-bedding). RE-C-E account for ~40-50 % of esker materials.

Some offset reflections can be observed in the grid, though the reflections do not appear to be highly distorted. Offset reflections are randomly distributed across the grid and individual reflections are typically offset by <1 m.

*7.3.2 Grid 2*

The GPR lines here (Figure 7.5) are of relatively less complexity than is described for Grid 1 radar elements, though are composed of at least 6 radar elements. The maximum depth of penetration achieved by the GPR is ~11 m, below which the EM signal rapidly attenuates. RF2 (upper-stage plane beds) are the dominant radar facies, accounting for ~94% coverage of the total facies distribution in this area (Figure 7.7).

RE-C-E have relatively uniform bounding surfaces that are sub-parallel to the land surface topography. The upper bounding surfaces of RE-A-B, however, display some irregularities (Figure 7.4b), particularly at the south-western side of the grid. Internal reflections of RE-A-B are continuous through much of the radar element, and are of greater amplitude. In contrast, reflections within RE-C-F are less continuous through the radar elements and of lower amplitude. In addition, reflections are in some areas, e.g. at a distance of ~0-12 m on line X1 (Figure 7.5), classified as cross-bedding (RF1), being composed of irregular and discontinuous reflections, within which individual bedforms cannot be identified. Within RE-D-E boulder clusters (RF5) are discerned, though in general these are confined to the north-eastern and south-western margins of the grid, e.g. lines Y3, Y5, Y7 (Figure 7.5).

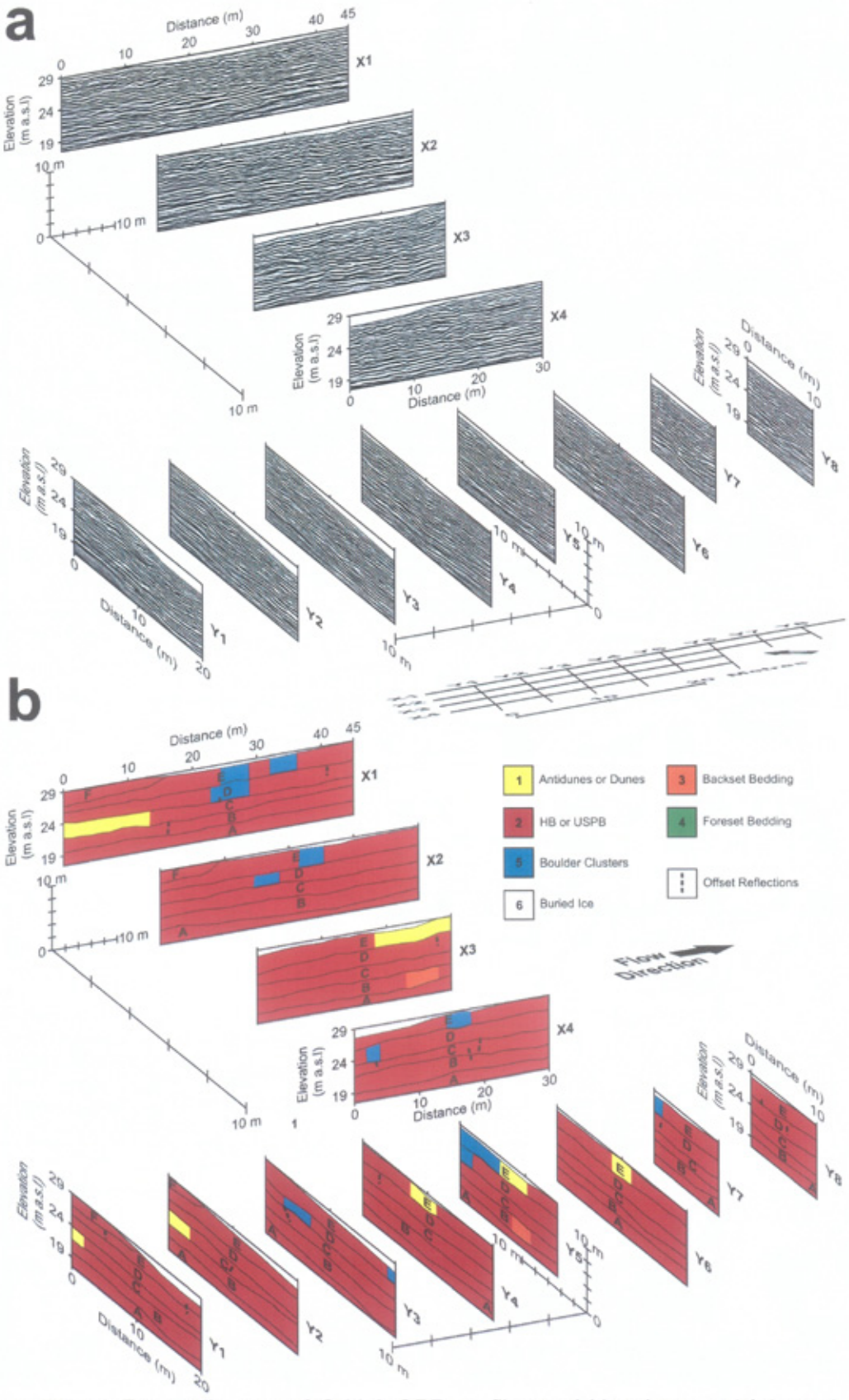


**Figure 7.5.** a) Fence diagram of Grid 2 GPR profiles and b) subsequent interpretation, following protocols and layout described in Figure 7.3. Sedimentation here is less complex than for Grid 1, with upper-stage plane beds (USPB) being dominant. At the northern end of the grid is a dipping radar element (RE-F), the lower contact of which truncates reflections below it (HB: horizontal beds, USPB: upper-stage plane beds).

RE-F is confined to the northern end of the grid on lines X1-2 and Y1-2 (Figure 7.5). Its lower bounding surface is an unconformity that dips up-flow and across-flow (south-west to north-east) at angles of ~5° and ~4°, respectively. RE-F is an irregular element (relative to RE-A-E) that is entirely composed of upper-stage plane beds (RF2). In addition, RE-F corresponds to an area of increased land surface elevation (Figure 7.4b).

Some offset reflections can be identified within the grid, though the reflections do not appear to be highly distorted. Offset reflections are randomly distributed across the grid and individual reflections are typically offset by <1 m.

*7.3.3 Grid 3*

The ice-walled canyon fill here is composed of at least seven radar elements that are typically divided by relatively irregular bounding surfaces (Figure 7.6). RF6 (buried ice) is identified at a maximum depth of ~11.5 m and is continuous across the grid. The upper bounding surface of RF6 (buried ice) is relatively irregular (e.g. line X1 and Figure 7.4c). Resting directly upon this surface are two pervasive radar elements (RE-A-B) predominantly classified as upper-stage plane beds (RF2), though plane beds in RE-B may grade from cross beds (RF1). The largest bedforms have a maximum crest height of ~1.6 m and length of ~5 m, with internal structure largely being below the resolution of the employed GPR configuration. The upper bounding surfaces of RE-A-B are sub-parallel to the bounding surface of RF6, though become irregular towards the margins of the grid (Figure 7.4c).

RE-C-D are identified at the up-flow end of the grid, predominantly containing RF1 (cross-bedding), with individual bedforms that have a maximum crest height of ~2 m and length of ~6 m. The upper bounding surfaces of RE-C-D are defined by an unconformity, with the lower bounding surface of RE-E dipping downstream at a high-angle (~15-25°). RE-E-F typically contain foreset beds (RF4), though some cross beds (RF1) are identified in RE-F, e.g. lines X3-4 (Figure 7.6).

RE-G contains relatively continuous reflections RF2 (horizontal beds) and has a lower bounding surface that is sub-parallel to the land surface topography (Figure 7.4c). This radar element has a maximum thickness of ~2.5 m with its lower bounding surface truncating the internal reflections of RE-D-F.

Some offset reflections can be identified within the grid, though are generally confined to the up-flow part of the grid (lines Y1 and Y2). Offset reflections are more pervasive than for Grids 1 and 2 and individual reflections are typically offset by <1 m.

## 7.4 Macroforms and Landforms

In August 2006, subsequent to GPR data collection at Bering Glacier in June 2006, Tsivat and Tsiu lakes drained into Lake Vitus (Fleisher *pers. comm.*, 2006) eroding

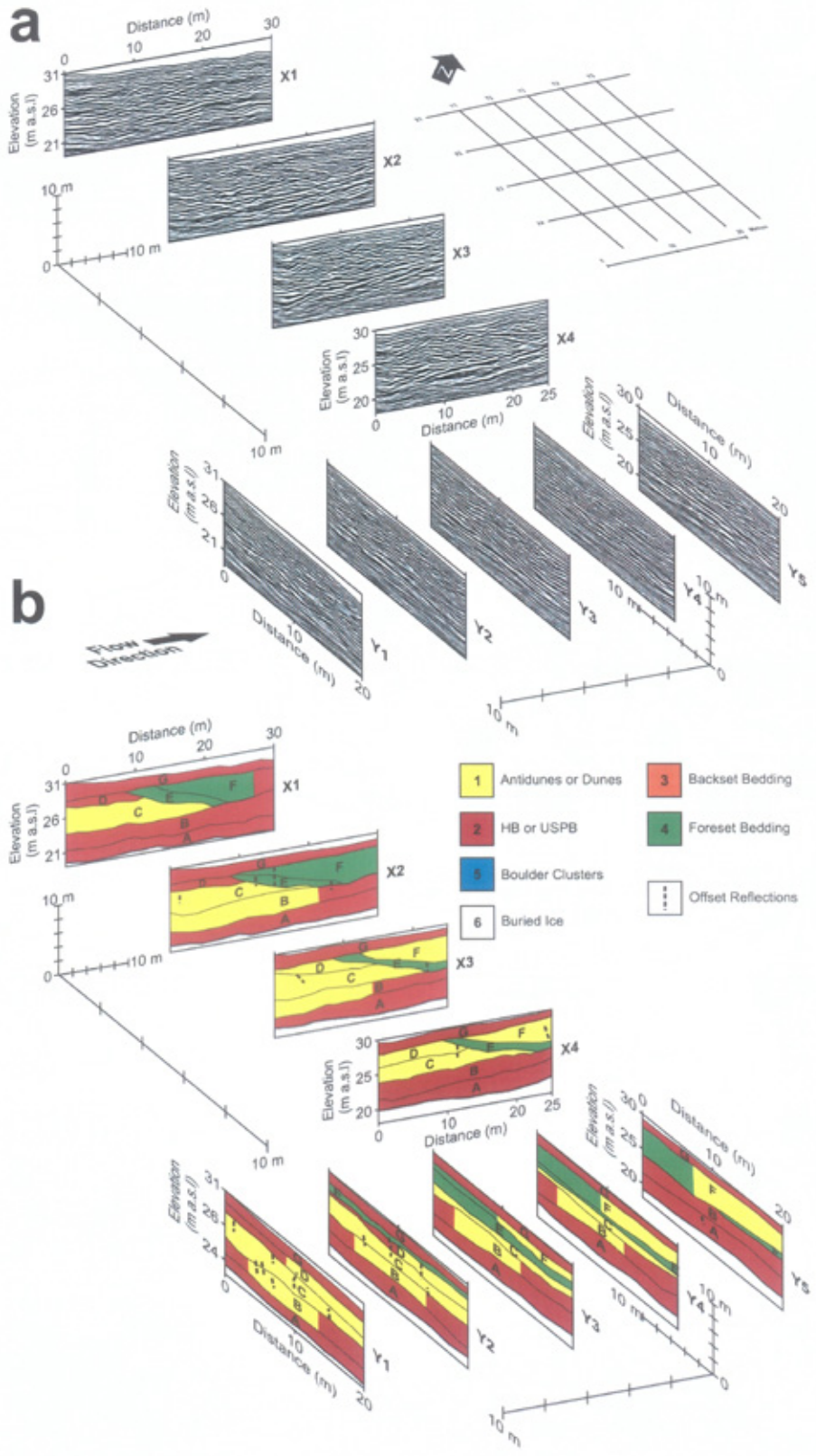


**Figure 7.6.** a) Fence diagram of Grid 3 GPR profiles and b) subsequent interpretation, following protocols and layout described in Figure 7.3. Sedimentation here is relatively complex. The base of the assemblage is defined by an ice-contact. Upper-stage plane beds (USPB) dominate early deposits, with overlying units being dominantly classified as cross- or foreset bedded. A uniform radar element (RE-G) of horizontal reflections that truncate deeper radar elements can be discerned across the entire grid (HB: horizontal beds, USPB: upper-stage plane beds).

section 1 into the esker and section 2 into the ice-walled canyon fill. These have been used as ground control for the GPR data sets (Figures 7.8 and 7.10), as well as to aid discussion of esker sedimentary architecture.

*7.4.1 Esker sedimentary architecture*

The lower bounding surface of RE-A (SHR2 on Figure 7.8c) corresponds to an unconformity within section 1, below which the sediments contrast to those within the radar elements above. Sediments below RE-A appear more consistent with pre-surge foreland strata, observed elsewhere on Weeping Peat Island (Figure 7.9a), suggesting this unconformity (SHR2) corresponds to the base of the esker. Consequently, the esker was generated within a subglacial conduit and the limited extent of post-depositional disturbance supports the evidence used to interpret palaeo-eskers as subglacial (e.g. Flint, 1928; Banerjee and McDonald, 1975; Gorrell and Shaw, 1991; Brennand, 1994, 2000).

Sedimentation within the esker was relatively complex, which is evidenced by erosional bounding surfaces that divide the radar elements, the presence of scour-and-fill structures (RE-D of Grid 1; Figure 7.3), as well as changing depositional conditions through time. RE-A-B are dominated by antidune sets that suggest flow depths were relatively low (<2 m) and that Froude numbers were >0.84 (Carling, 1999). Common characteristics between RE-A and RE-B suggest limited lateral variability of flow conditions during esker aggradation and vertical conduit growth into the ice. The presence of antidune sets within RE-A-B is suggestive of a period of very rapid aggradation in order to allow bedform preservation (Alexander and Fielding, 1997). The up-flow dipping and stacked nature of RE-A and RE-B suggests that as well as growing upwards into the ice, the conduit also enlarged in an up-flow direction.

A large hyperbolic reflection could be identified in an unmigrated GPR line within RE-B (Figure 7.2a). The source of this reflection is too large to be associated with a boulder and is perhaps more consistent with the presence of a buried ice block. This is similar to observations made by Cassidy *et al.* (2003) of ice blocks in glaciofluvial sediments at Skeiðarárjökull and would be consistent with forefield observations made at the Bering Glacier (Fleisher *pers. comm.*, 2007). Figure 7.9b shows a large ice block within proglacial outburst flood deposits at the Bering Glacier, testament to the release of ice blocks from outburst flood outlets. The presence of kettle holes on the esker and ice-walled canyon assemblages substantiate the presence of buried ice at depth.

The upper bounding surface of RE-B is an up-flow dipping unconformity that corresponds to an erosional boundary (SHR1) in section 1 (Figure 7.8). The change in reflection characteristics above this unconformity (RE-C-E) also corresponds to a change in sediment characteristics in section 1 (Figure 7.8a). Within RE-C and along the upper

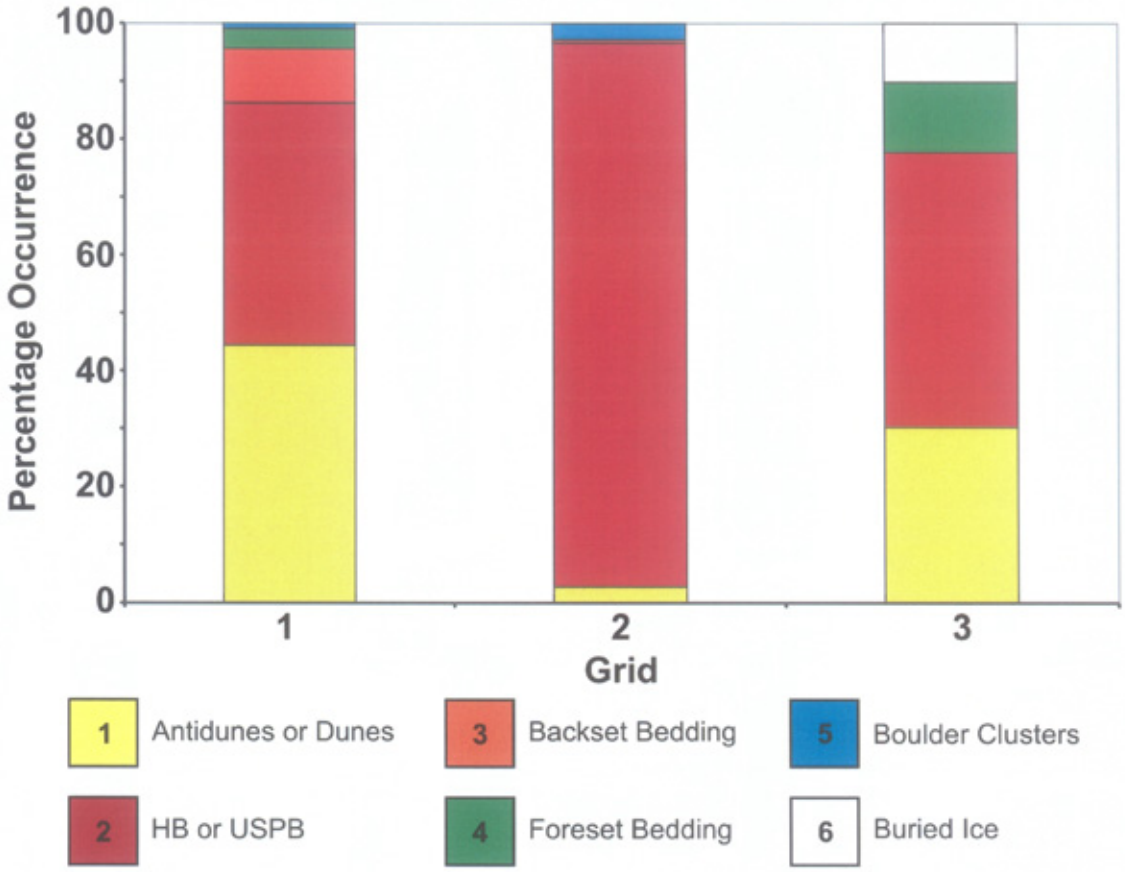


**Figure 7.7.** Graph showing the percentage occurrence of each facies type within Grids 1-3. Each facies has been colour coded (see key), with facies type descriptions and colour keys following those presented in Figure 7.1 (HB: horizontal beds, USPB: upper-stage plane beds).

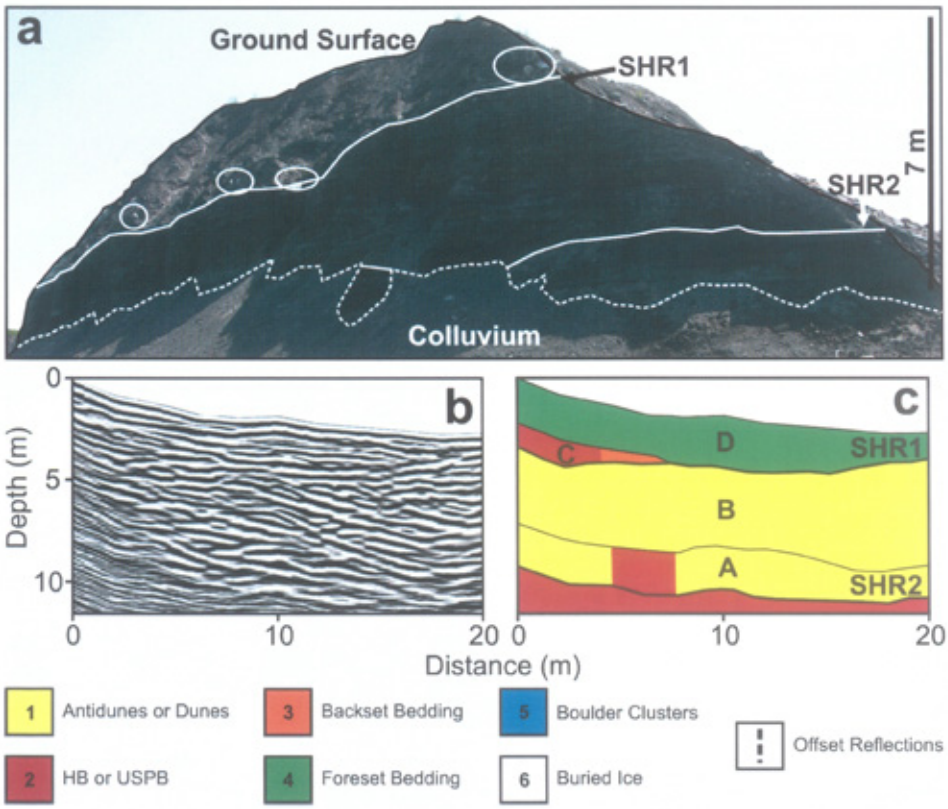


**Figure 7.8.** a) Section 1 created due to erosion of the esker by ice-marginal lake drainage subsequent to GPR data collection (photograph courtesy of Palmer K. Bailey). A distinct basal reflection (SHR2) represents a major change in material characteristics that are consistent with pre-surge foreland strata (Figure 7.9a). SHR1 represents an erosional contact above which sediment characteristics change once again and along which boulder clusters can be identified (circled). The location of this section corresponds roughly to the position of line Y7 of Grid 1 (b) and both SHR1 and SHR2 of the section correspond to the location of contacts that define major changes in the sedimentary architecture (c). Radar facies classifications are based upon those for flow-parallel lines and so consequently, there are some irregularities in radar facies classification within RE-A and RE-C (HB: horizontal beds, USPB: upper-stage plane beds).

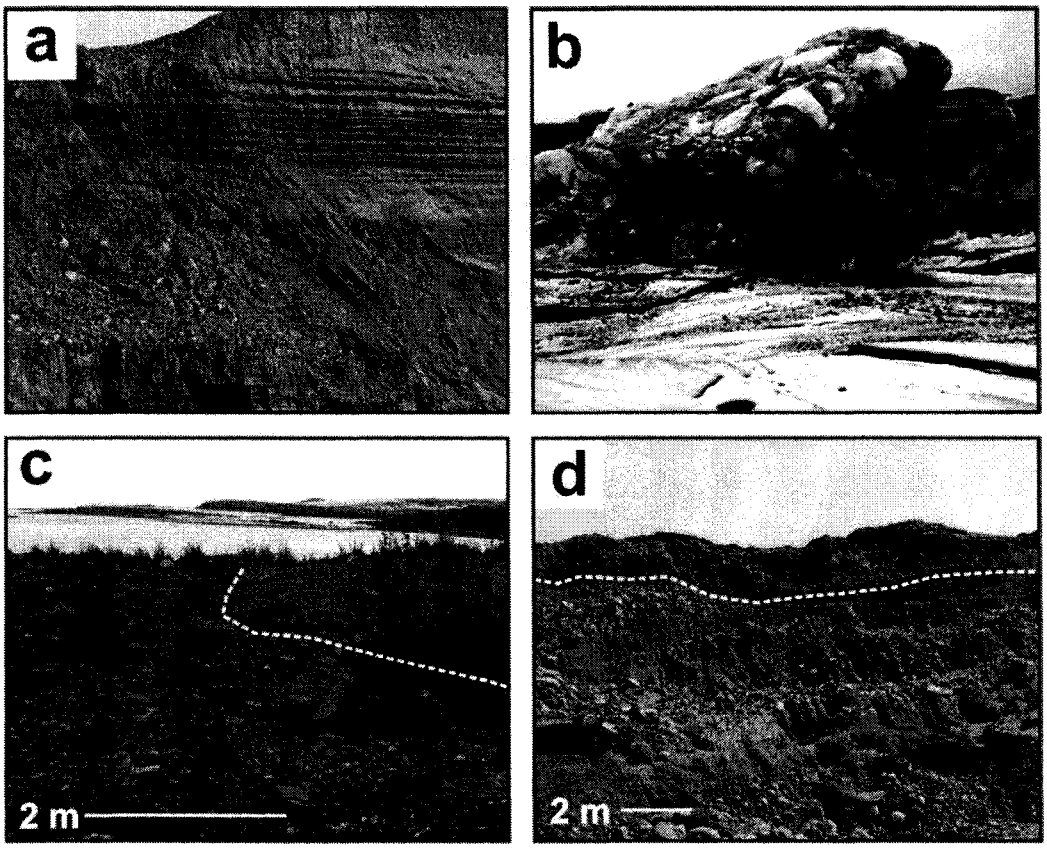


**Figure 7.9.** a) photograph showing the characteristics of pre-surge foreland strata at Weeping Peat Island (photograph courtesy of Palmer K. Bailey). b) An ice block (which is a breccia of angular ice blocks) transported and deposited during an outburst at the Bering Glacier in 1994 (note persons for scale) (photograph courtesy of P. Jay Fleisher). c) At the site of the October 1994 outburst flood on Weeping Peat Island there is a distinct transition (dashed line) from open-framework gravels (right) to much more angular materials (left). d) A section exposed on the ice-walled canyon sediments. The dashed line indicates a contact separating material deformed by overriding ice (above) and bedded sediments (below) (photograph courtesy of P. Jay Fleisher).

bounding surface of RE-B, boulder clusters are identified within the GPR data. This is consistent with boulders observed along the unconformity (SHR1) in section 1 (Figure 7.8a). The presence of boulders along this bounding surface are likely to be either lag boulders (c.f. Fleisher *et al.*, 2007) or traction deposits along the erosional contact. Given that no boulder clusters can be identified within RE-A-B, the latter interpretation is more likely. The transportation of boulder materials during the deposition of RE-C-E are also testament to the change in flow conditions from the deposition of RE-A-B. Although boulder clusters are not identified in Figure 7.8c despite their occurrence in section 1, this is likely due to them being offline. Section 1 is located between lines Y6 and Y7 (Figure 4.5b) and although the boulder clusters here are not imaged in line Y7, they can be identified in a stratigraphic position in line Y6 (Figure 7.3b) that corresponds to section 1.

The overall sedimentary architecture of RE-C-E shows a down-flow transition from backset to foreset beds, which is consistent with the sedimentary architecture of a composite macroform, within a conduit enlargement (c.f. Brennand, 1994; Brennand and Shaw, 1996; Brennand, 2000; Fiore *et al.*, 2002), associated with a significant increase in flow depth. Down-flow, RE-E is dominated by upper-stage plane beds, deposited when Froude numbers would be >0.84 (Carling, 1999). This indicates that flow depths were relatively low (e.g. Alexander *et al.*, 2001) associated with a relatively constricted conduit. RE-F of Grid 2 (Figure 7.5) corresponds to an abrupt transition that can be seen on the ground surface from predominantly well-rounded, open-framework gravel to angular and less-well rounded material (Figure 7.9c). Although no interconnection could be made between Grids 1 and 2, RE-F is interpreted to represent esker materials at the up-flow end of Grid 2 deposited simultaneously with corresponding RE-E in Grid 1.

### *7.4.2 Ice-walled canyon sedimentary architecture*

The sedimentary architecture of the ice-walled canyon is complex, which is shown by erosional unconformities that divide the radar elements within the landform, as well as the varying radar facies classifications with depth, most of which correspond to observations within section 2 (Figure 7.10). The identification of an ice contact surface, defining the base of the landform demonstrates that it was generated within a supraglacial or englacial conduit/channel. Although buried ice cannot be identified within section 2 (Figure 7.10), its presence within the GPR profiles is consistent with previous field observations (Fleisher *pers. comm.*, 2007) and the reported supraglacial position of the ice-walled canyon (Fleisher *et al.*, 1998). The melting of this buried ice and/or supporting ice walls has resulted in collapse of the sediments, indicated by the increased frequency of structural collapse (Figure 7.6) relative to that within the subglacial esker materials, e.g. Grid 1 (Figure 7.3).

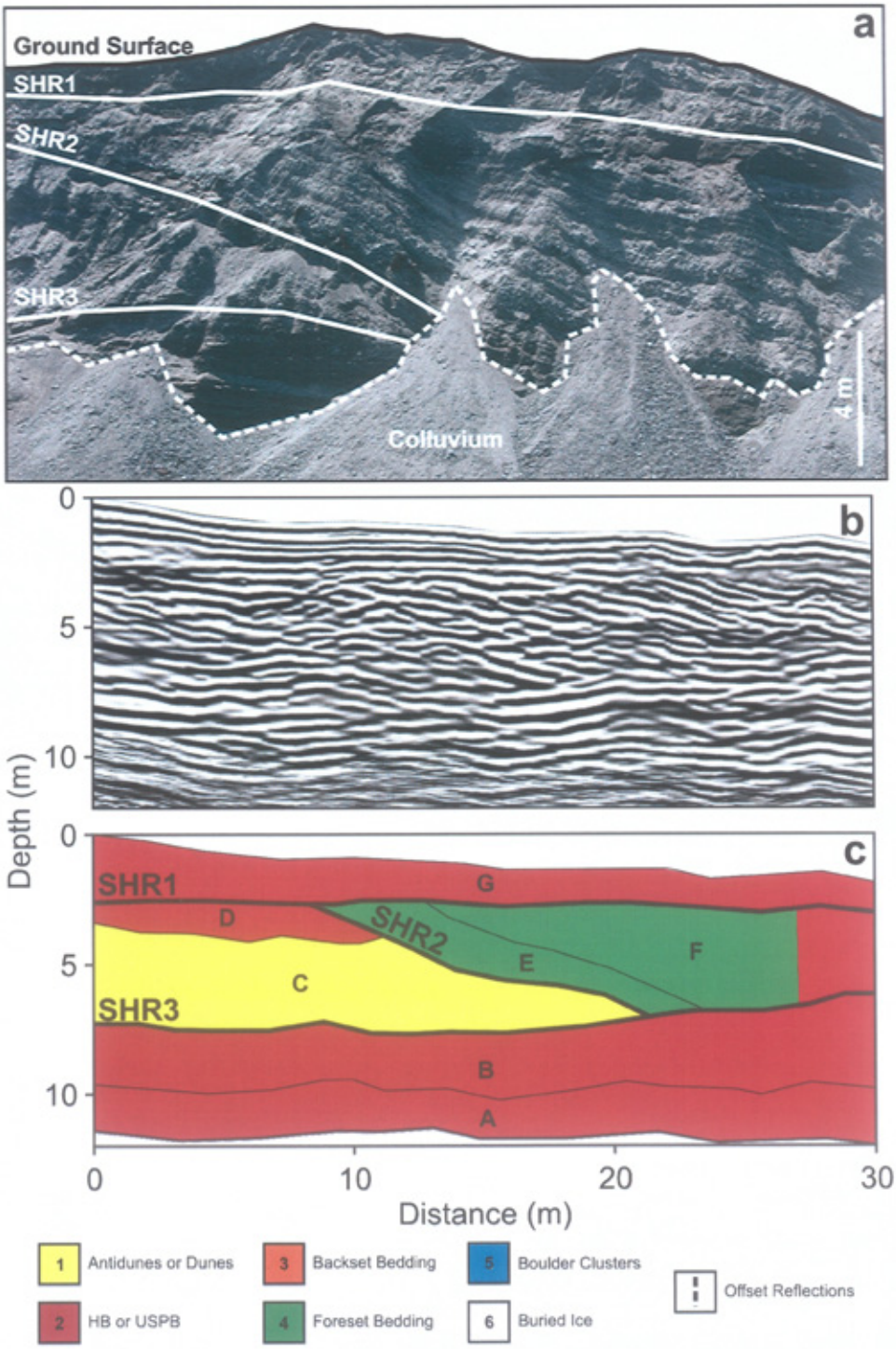


**Figure 7.10.** a) Section 2 created due to erosion of the assemblage by ice-marginal lake drainage, subsequent to GPR data collection (photograph courtesy of P. Jay Fleisher). Sub-horizontal reflections (SHR1-3) correspond to major radar element bounding surfaces identified in the GPR line (c). The location of this section corresponds roughly to the position of line Y7 of Grid 1 (b). Furthermore, the orientations of bedding match that of reflections in the GPR profile (b) and are consistent with sedimentary facies classifications (c). Sediments above SHR1 (a) are consistent with deformed material identified elsewhere in surge-related deposits (Figure 7.9d).

RE-A-B are distinct from RE-E-G, with the presence of upper-stage plane beds (RE-A-B), and antidunes (RE-B) similar to those within RE-A-B of the esker deposits, suggesting that flow depths were relatively low (<2 m) and Froude numbers were >0.84 (Carling, 1999). Furthermore, the similarity of bedforms between RE-A-B within the ice-walled canyon and RE-A-B within the esker, suggest that RE-A-B within the ice-walled canyon fill were deposited by similar flow conditions. Bedform dimensions within RE-B are lower than those within RE-C, suggesting flow depths were greater at the time of RE-C deposition. The unconformity that divides RE-B from RE-C corresponds to an erosional surface that can be identified in section 2, below which plane beds can be discerned (Figure 7.10a), again corresponding to upper-stage plane beds (RF2) identified within the GPR profiles (Figure 7.10b-c).

The upper bounding surface of RE-C is an unconformity that truncates the internal structure of the radar element (Figure 7.6). This unconformity dips down-flow at a high-angle (~15-25°), which corresponds to an erosional contact (SHR2) in section 2 (Figure 7.10a). The foreset beds identified above SHR2 in section 2 (Figure 7.10a) are consistent with the internal structure of foreset beds within RE-E-F identified within the GPR profiles. The presence of foreset beds that offlap the upper bounding surface of RE-C indicate the presence of a flow separation (c.f. Jopling, 1965). This could represent the deposition of a prograding bar-form.

RE-G corresponds to an abrupt change in material characteristics (SHR1) that can be observed in section 2 (Figure 7.10a). The characteristics of this radar element (composed of horizontal beds) are consistent with deformed sediments (Figure 7.9d), which is a product of surge advance and the creation of a deformation till (c.f. Fleisher *et al.*, 2006c), subsequent to the deposition of the landform. Advance of the ice over the sediments deposited during the outburst flood, resulted in their near surface deformation.

Unfortunately, the extent of GPR data collection was limited due to large kettle holes and collapse features, such as steep slopes, on the landform surface. Consequently, data could not be collected up- or downstream of this grid and thus distal variations in architecture could not be explored.

## 7.5 Discussion

### *7.5.1 Conduit evolution*

The data described in *Section 7.3.2* and *Section 7.4.1* form the basis of evolutionary models for the controls on the sedimentary architecture of the esker and ice-walled canyon fill deposited during the 1994 Bering Glacier outburst floods (Figures 7.11-7.12). Although based upon jökulhlaups from Iceland, the theoretical considerations of Roberts (2005) concerning the development of an exponentially rising jökulhlaup, can be used to infer a more constrained depositional timescale. The esker generated by the

October 1994 Bering Glacier outburst flood was developed over four main stages (Figure 7.11):

1. Initial conduit development likely took place during the mid to late rising stage of the outburst flood (Roberts, 2005). During this period the erosional potential of the waters was greatest and effective pressures were likely to have been negative, which resulted in localised cavity generation along the flow path. The deposition of fragmented breccias of angular ice blocks (Figure 7.9b) from the outlet is testament to the erosive nature of the outburst flood. It is likely that mechanical excavation of ice blocks was fundamental to the rapid development of conduits (Roberts *et al.*, 2001; Russell *et al.*, 2001a; Roberts *et al.*, 2002; Roberts, 2005; Russell *et al.*, 2005, 2006). This rapidly created accommodation space in which antidune sets were aggraded by the supercritical floodwaters as the conduit enlarged due to vertical growth into the ice and expansion up-glacier.
2. As the conduit enlarged, further floodwaters were focused along this flow path, resulting in increased discharge and transport capacity through the outlet. This partially eroded the antidune sets, as well as eroded the conduit roof through mechanical processes. Consequently, a conduit enlargement was created at the up-flow end of the esker, whilst the conduit down-flow of the enlargement remained relatively narrow.
3. The flow of waters into an enlarged cavity was associated with an increase in flow depth, creating a hydraulic jump. Backset beds were deposited at the point of the jump, concomitant to further conduit growth both upstream and vertically.
4. As discharge continued to rise the conduit enlarged vertically and upstream simultaneous to esker deposition at the hydraulic jump. This created a flow separation on the lee-side of the backset units, resulting in foreset progradation on the lee of the bedform (c.f. Jopling, 1965) and the development of a composite macroform. Downstream, the flow depth reduced within a relatively narrow conduit and flows deposited predominantly upper-stage plane beds (c.f. Allen, 1992).

Although the outburst flood that resulted in the development of the ice-walled canyon fill was in a similar area to that of the esker, the resulting landform was different. The data described in *Section 7.3.3* and interpreted in *Section 7.4.2* have allowed an evolutionary model for the controls on ice-walled canyon fill sedimentary architecture during the July-August 1994 Bering Glacier outburst flood to be developed (Figure 7.12):

1. Initial conduit development likely took place during the mid to late rising stage of the outburst flood (Roberts, 2005), as the major outlet shifted to the southwest (c.f. Fleisher *et al.*, 1998). Floodwaters were discharged within a relatively narrow, pressurised englacial conduit, the location of which may have been controlled by

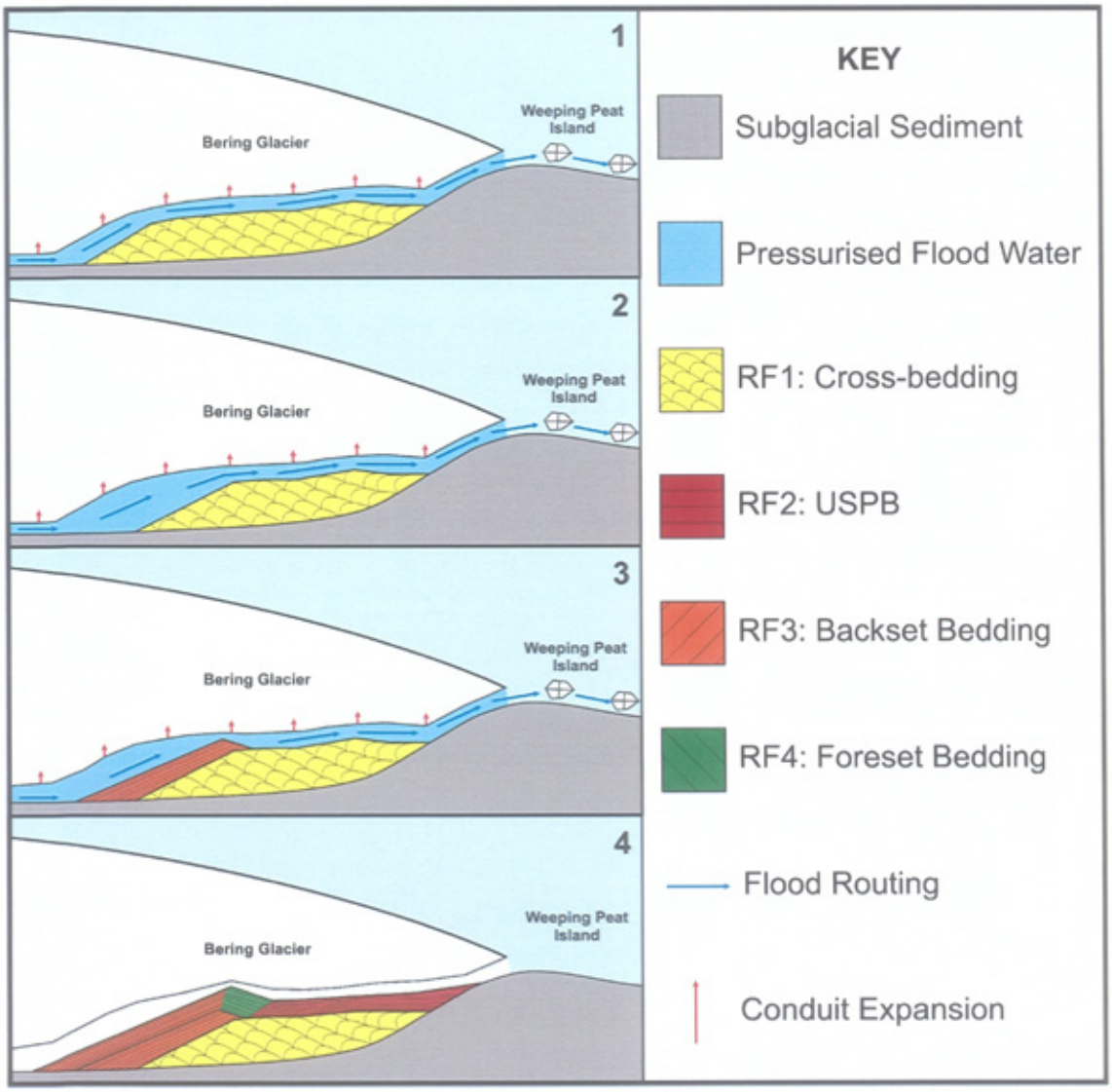


**Figure 7.11.** A two-dimensional model for the development of the October 1994 outburst flood esker at Bering Glacier, Alaska: 1) Localised cavity generation due to pressure variations along the flood path created accommodation space in which the supercritical outburst flood waters could rapidly deposit antidune sets; 2) An erosional phase partially excavated early deposits and heightened the conduit roof to create a conduit enlargement at the upstream end of the cavity; 3) The increased flow depths were associated with a sudden velocity reduction, resulting in backset deposition; 4) A composite macroform developed within the conduit enlargement due to backset aggradation and subsequent foreset progradation on their lee-side. Downstream, a reduced conduit cross-sectional area increased the flow velocity, which was conducive to the deposition of predominantly upper-stage plane beds.

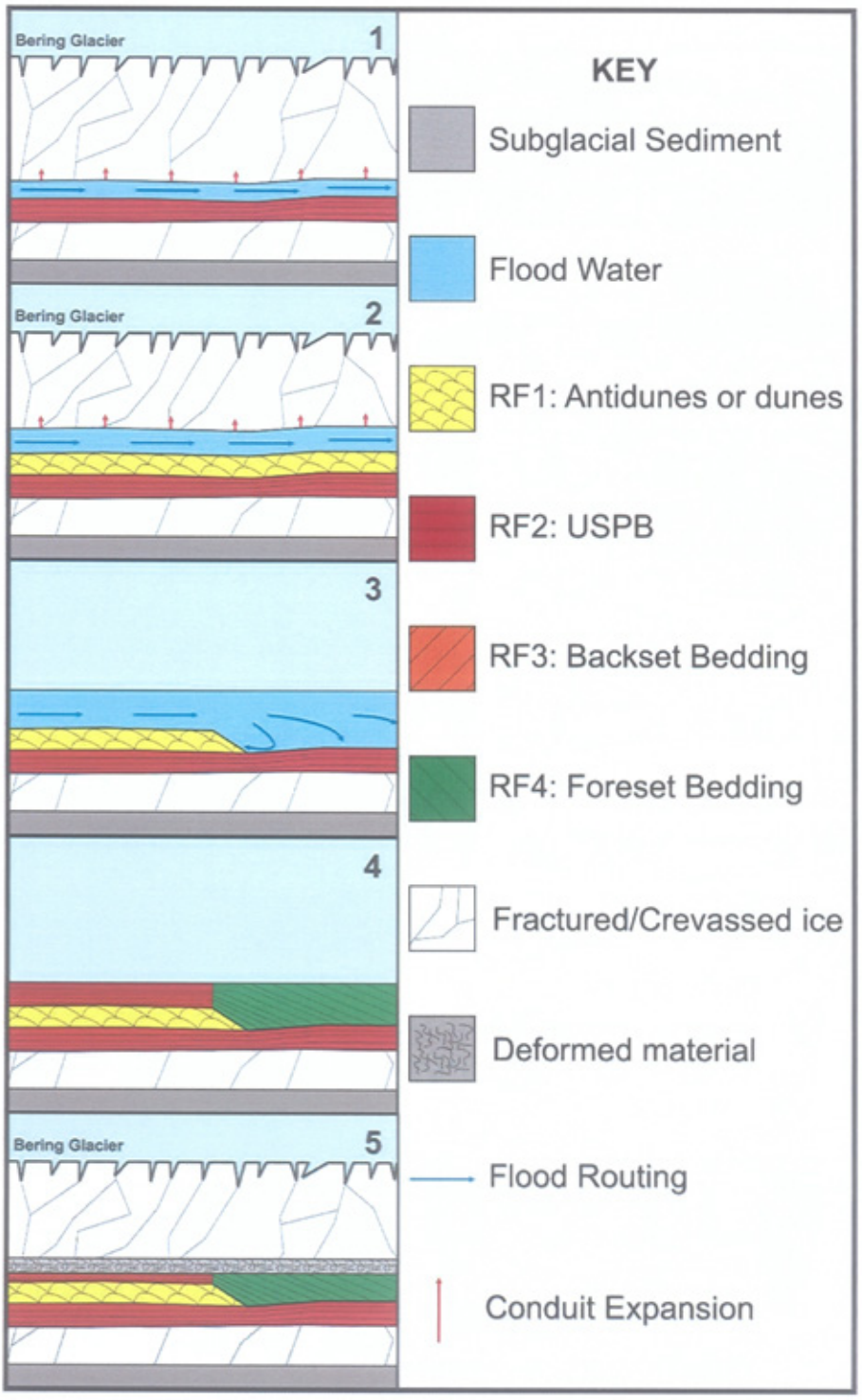


**Figure 7.12.** A two-dimensional model for the development of the July 1994 outburst flood ice-walled canyon fill at Bering Glacier, Alaska: 1) Flows through a relatively shallow conduit resulted in the deposition of upper-stage plane beds (USPB); 2) Conduit growth increased flow depth and antidune sets were deposited within the supercritical floodwaters; 3) Vertical conduit growth resulted in its unroofing and partial scouring of the antidune sets, creating a non-uniform bed profile; 4) The increased flow depth distally, is conducive to the deposition of foreset beds, analogous to a prograding fan. 5) Continued surge activity, following the outburst flood, completely closed the ice-walled canyon, with the ice advance deforming an upper layer of the glaciofluvial material.

surge induced structural weaknesses. The relatively constricted flow conditions were associated with the deposition of upper-stage plane beds (c.f. Allen, 1992).

3. Focusing of floodwaters through the outlet resulted in increased discharge and vertical conduit growth, which increased the flow depth in which the supercitical floodwaters deposited antidune sets.Continued discharge of outburst flood waters through this outlet corresponded to growth of the englacial conduit, which became subaerial due to headward conduit unroofing (Fleisher *et al.*, 1998). The creation of an expansion environment was associated with partial scouring of the antidune sets at the down-flow end of the grid.
4. The consequent increase in flow depth down-flow created a flow separation eddy that was conducive to foreset bed deposition, analogous to a prograding bar-form (c.f. Jopling, 1965).
5. Subsequent to outburst flood cessation, surge advance was resumed, with ice advance completely closing the ice-walled canyon (Fleisher *et al.*, 1998). Advance of the surging ice over the ice-walled canyon assemblage deformed the shallowest radar elements, creating a mantle of deformed glaciofluvial material.

*7.5.2 Depositional timescale*

Although esker and ice-walled canyon fill genesis cannot be linked to specific times within the outburst flood events, it is known they were generated entirely within these single events (Fleisher *et al.*, 1998, 2007), based upon pre-surge field observations that showed no landforms in the current locations of the esker (Fleisher *et al.*, 2007). Whilst the July-August 1994 outburst flood was directly observed and some measurements taken (c.f. Merrand and Hallet, 1996; Fleisher *et al.*, 1998), the October 1994 outburst flood was not observed. Subsequent fieldwork suggests it was of a lesser intensity than the earlier event (Fleisher *et al.*, 1998). Although the earliest outburst flood began on 27$^{th}$ July it did not reach the Lake Vitus outlet until 31$^{st}$ July (Merrand and Hallet, 1996). This is due to filtering of the floodwaters and signal attenuation through the proglacial lake system at the eastern sector of Bering Glacier (Merrand and Hallet, 1996). Nevertheless, the timing of the outburst can be discerned in the stage record from Seal River (Figure 7.13). The outburst flood lasted approximately ten days, reaching its peak after approximately five days (Merrand and Hallet, 1996). Conduit development would have taken place through the rising stage of the outburst flood when basal water pressures were high, resulting in mass ice block excavation to create the accommodation space in which the ice-walled canyon sediments were deposited. If ice-walled canyon sediments were deposited concomitant to conduit growth, it is likely that deposition began during the mid-rising stage of the outburst flood and continued through the late-rising and waning stage of the event. Consequently, ice-walled canyon sediments would have been

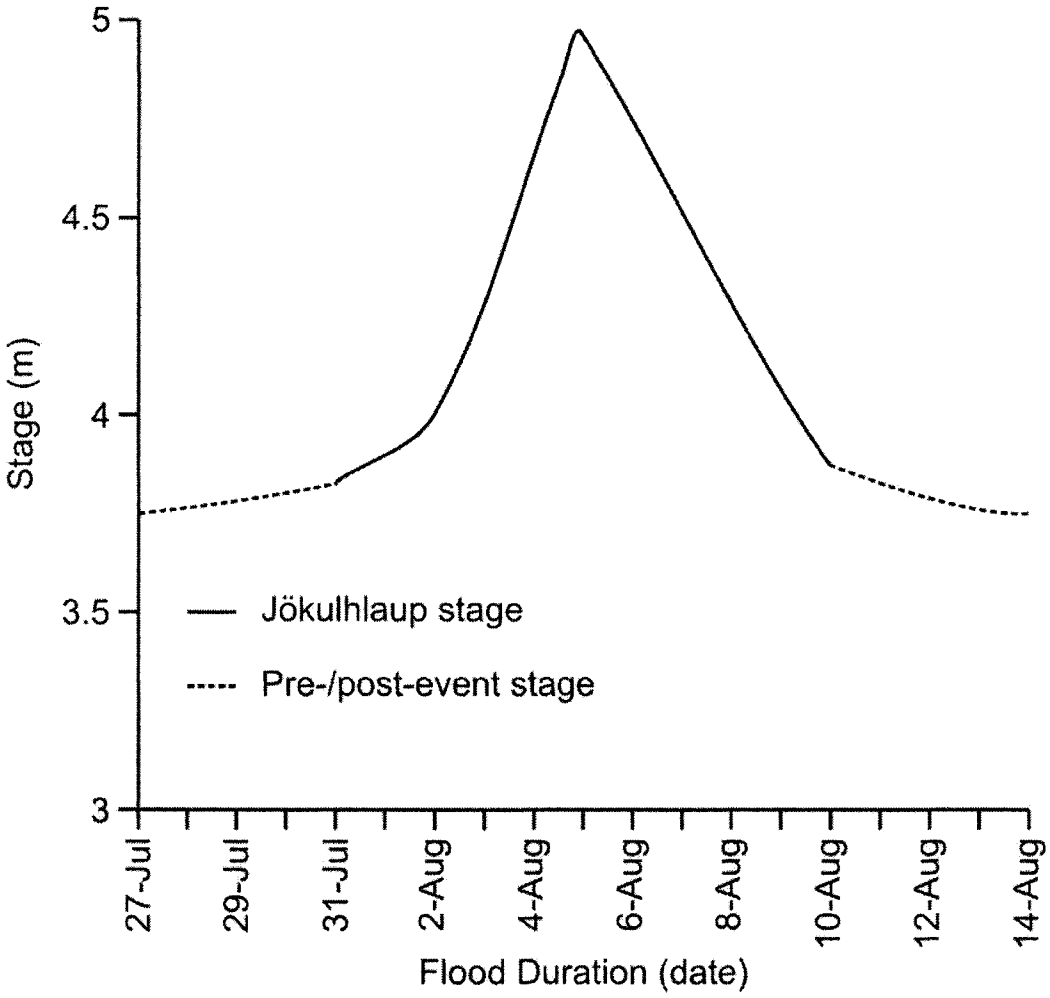


**Figure 7.13.** Stage record of the July-August 1994 outburst flood, as recorded at Seal River (outlet to Lake Vitus). This plot does not include values associated with the high and low tide. Although the outburst flood was reported to have begun on 27$^{th}$ July, the presence of a significant forefield lake complex resulted in a delayed arrival of discharge at Seal River and significant attenuation of the signature (after Merrand and Hallet, 1996).

deposited within a maximum period of ~7-8 days, though the majority of deposition likely took place concomitant to conduit growth during the rising stage of ~2-3 days. As there were no direct observations of the October 1994 outburst flood it is impossible to suggest a depositional timescale.

The maximum number of radar elements identified within the surveyed ice-walled canyon fill is six, not including RE-G (deformation material). These were deposited over a maximum period of 8 days (~190 hours) and if a uniform sedimentation rate is presumed over the entire depositional period, then individual units would have been deposited in approximately thirty hours. This, however, is likely an overestimate, as erosive periods and variations in sedimentation rates cannot be taken into account.

### 7.6 Summary

Three grids of GPR lines were collected at the eastern sector forefield of Bering Glacier, Alaska. Six main radar facies were identified: 1) discontinuous, undular reflections, interpreted as cross-beds, associated with the deposition of antidune (or dune) sequences; 2) sub-horizontal reflections (dip <5°), associated with deposition of upper stage plane beds; 3) up-flow dipping moderate to high-angle (>5°) inclined reflections, interpreted as backset accretion associated with large-scale bedform development; 4) down-flow dipping high-angle (>10°) inclined reflections, interpreted as foreset accretion associated with macroform progradation; 5) point reflections, interpreted as zones of boulder clustering; and 6) zones of enhanced noise and EM signal attenuation. Classification of radar elements within the GPR grids has allowed the controls on the sedimentary architecture of conduit fill and ice-walled canyon fill eskers to be investigated. The October 1994 outburst flood discharged from a subglacial vent across Weeping Peat Island. The high pressures associated with passage of the aggressive outburst flood waters locally enlarged the conduit, which became infilled with antidune sets deposited by the supercritical floodwaters. Subsequent, partial erosion of these antidune sets created an enlarged conduit at the proximal end of the cavity. This became infilled with backset and foreset bedded sediments, analogous to composite macroform development identified in eskers deposited in North America and Europe during the last glaciation. Down-flow the conduit was narrower and upper-stage plane beds were deposited by the constricted flows. In contrast, the ice-walled canyon fill was generated during a documented outburst flood in July-August 1994. Sedimentation initially took place within a pressurised englacial conduit, which gradually unroofed due to conduit growth, becoming a supraglacial ice-walled canyon. The final stages of deposition took place subaerially and were analogous to the development of a prograding bar-form, but closure of the canyon during the second phase of the 1993-1995 surge has deformed the upper units of this assemblage. The esker and ice-walled canyon fill were likely to have been generated rapidly (<8 days).

# SECTION IV
# Discussion and Conclusions

*"The discussion of the origin of eskers seems to have subsided almost as completely as the glacial streams by which, it is universally conceded they were formed..."*

Crosby (1902)

*A down-flow view of the November 1996 Skeiðarárhlaup esker and ice-walled canyon fill, taken from the up-flow esker*

# Chapter 8

# Discussion

## 8.1 Introduction

This thesis has examined the development of the sedimentary architecture of eskers and ice-walled canyon fills that were deposited during the November 1996 jökulhlaup at Skeiðarárjökull, Iceland and the July-August and October 1994 outburst floods at Bering Glacier, Alaska. The pseudo-three-dimensional sedimentary architecture was documented using GPR on esker and ice-walled canyon fill segments released from the supporting ice walls of Skeiðarárjökull and Bering Glacier, as well as direct GPR surveys on the ice surface of Skeiðarárjökull. The thesis so far has focused upon objectives 1, 2 and 3, namely the controls on conduit location and geometry during a high magnitude jökulhlaup have been established and the controls on the sedimentary architecture of the November 1996 Skeiðarárhlaup and 1994 Bering Glacier outburst floods, eskers and ice-walled canyon fills have been identified.

This chapter will focus upon objectives 4 and 5 (*Section 1.3*) by comparing the sedimentary architecture and depositional history of the 1996 Skeiðarárhlaup and 1994 Bering Glacier outburst floods, eskers and ice-walled canyon fills (*Section 8.2*) and identifying diagnostic criteria for identifying palaeo-eskers generated by high-magnitude jökulhlaups (*Section 8.6*). This will allow the hydrological, glaciological and sedimentary controls on the sedimentary architecture of single event eskers, generated during high-magnitude jökulhlaups to be investigated (*Section 8.5*).

## 8.2 Comparison of the 1996 Skeiðarárhlaup and 1994 Bering Glacier Outburst Floods

The esker and ice-walled canyon fill at Skeiðarárjökull were deposited entirely during the November 1996 jökulhlaup within a maximum period of twenty-four hours. Similarly, both an esker and ice-walled canyon fill were deposited at the Bering Glacier, though these were generated by separate outburst floods in July-August 1994 and October 1994, respectively. Ice-walled canyon fill deposition likely took place within a maximum period of eight days, whilst a timescale for esker genesis could not be rigorously applied. Although the 1996 Skeiðarárhlaup and 1994 Bering Glacier outburst flood generated similar assemblages, the jökulhlaups demonstrated some disparities.

The 1996 Skeiðarárhlaup rapidly rose to its peak discharge of >40,000 $m^3s^{-1}$ within fourteen hours, with peak discharge through the Double Embayment being estimated at

~20,000 $m^3s^{-1}$ (Roberts *et al.*, 2000b; Russell *et al.* 2001a, 2005, 2006). This rapid rise in discharge was a consequence of a greater rate of floodwater entering Skeiðarárjökull than could escape through pre-existing drainage outlets, resulting in increased basal water pressures and fracturing of the overlying ice (Roberts *et al.*, 2000b). In contrast, the July 1994 Bering Glacier outburst flood rose steadily to a peak discharge of ~3, 000 $m^3s^{-1}$ within approximately five days (Fleisher *pers. comm.*, 2008). This outburst was located at the site of an ice surface depression associated with a subglacial trench believed to control the position of a subglacial conduit system through which outburst floods have been discharged at least at the termination of the two most recent surges (Fleisher *et al.*, 1998). The October 1994 Bering Glacier outburst flood discharged through an outlet to the southwest, again in a location corresponding to a subglacial depression associated with another hydrologically isolated basin (Fleisher *et al.*, 1998), reaching a discharge of ~1, 500 $m^3s^{-1}$ (Fleisher *pers. comm.*, 2008).

Jökulhlaup outlets at Bering Glacier and Skeiðarárjökull can be linked to the presence of subglacial depressions (Fleisher *et al.*, 1998; Roberts *et al.*, 2000b). The 1996 Skeiðarárhlaup and July-August 1994 Bering Glacier outburst flood, however, resulted in discharge through supraglacial outlets and the development of supraglacial ice-walled canyons, whilst the October 1994 Bering Glacier outburst flood was discharged subglacially. The 1996 Skeiðarárhlaup was believed to be associated with the development of outlets through hydrofracturing and retro-feeding of moulins and crevasses (e.g. Roberts *et al.*, 2000b, 2001, 2002; Russell *et al.*, 2005, 2006). Although the July-August 1994 Bering Glacier outburst flood was discharged supraglacially, the location of these outbursts was relatively restricted in comparison to those during the 1996 Skeiðarárhlaup (Fleisher *et al.*, 1998). In contrast, discharge during the October 1994 Bering Glacier outburst flood was through a pre-existing conduit system that could develop at a pace consistent with the rate of floodwater input.

## 8.3 Comparison of the Skeiðarárjökull and Bering Glacier Eskers and Ice-walled Canyon Fills

Although the radar facies schemes developed for interpretation of Skeiðarárjökull and Bering Glacier GPR lines are very similar, comparison of the data sets shows some major variations in landform sedimentary architecture and morphology. Through comparison of the data sets from Skeiðarárjökull and Bering Glacier, objective 4 (*Section 1.3*) will be achieved. It is only through direct comparison of these data sets that commonality between the field sites can be identified, which will provide the basis for identifying the controls on esker sedimentary architecture during jökulhlaups, as well as allow establishment of diagnostic criteria for jökulhlaup deposition (objective 5). A summary of this comparison can be seen in Table 8.1.

| | SKEIÐARÁR ESKER | BERING ESKER | SKEIÐARÁR IWCF | BERING IWCF |
|---|---|---|---|---|
| ***Morphology*** | Slightly sinuous | Straight | Slightly sinuous | Straight |
| ***Conduit Position*** | Englacial | Subglacial | Englacial/Supraglacial | Englacial/Supraglacial |
| ***Control on Position*** | Structural | Not Observed | Structural | Not Observed |
| ***Length*** | ~700 m | ~350 m | ~500 m | ~400 m |
| ***Width*** | ~40 m | ~30 m | <200 m | ~100 m |
| ***Maximum Thickness*** | ~12 m | ~8 m | ~12 m | ~11 m |
| ***Cross-sectional Area*** | ~480 $m^2$ | ~240 $m^2$ | ~2400 $m^2$ | ~1100 $m^2$ |
| ***Number of Depositional Phases*** | 2 | 2 | 2 | 3 |
| ***Deepest Deposits*** | Antidune sets | Antidune sets | Antidune sets | Upper-stage plane beds |
| ***Max. Bedform Dimensions*** | ~3 m (H), ~12 m (L) | ~1.5 m (H), ~4 m (L) | ~2.5 m (H), ~6.5 m (L) | ~2 m (H), ~6 m (L) |
| ***Shallow Deposits*** | Composite Macroform, USPB | Composite Macroform, USPB | Expansion Bar | Prograding Bar-form |
| ***Minimum no. Units*** | 7 | 5 | 8 | 6 |
| ***Macroform Length/Width*** | ~70 m (L), ~25 m (W) | ~40 m (L), ~20 m (W) | NA | NA |
| ***Depositional Timescale*** | <24 hours | ? | <24 hours | <8 days |

**Table 8.1.** A comparison of the key structural and morphological elements of the esker and ice-walled canyon fills (IWCF) at Skeiðarárjökull, Iceland and Bering Glacier, Alaska.

*8.3.1 The morphology and sedimentary architecture of the eskers*

The current exposed section of the esker (August 2006) deposited during the November 1996 Skeiðarárhlaup is ~700 m in length, has a maximum cross-sectional area of ~480 $m^2$ and is slightly sinuous in morphology. The exposed section of the esker deposited during the October 1994 outburst at Bering Glacier (June 2006) is ~350 m in length, with a maximum cross-sectional area of ~240 $m^2$ and a straight morphology. Internal sedimentary architectures identified from GPR surveys on both landforms are similar, though the style of deposition is varied:

- Radar elements within both the Bering Glacier esker and Skeiðarárjökull esker are divided by some unconformities, but the patterns of erosion and deposition vary. The Skeiðarárjökull esker is composed of at least eleven radar elements that become more continuous through the landform down-flow and have an average maximum thickness of ~5 m. At its up-flow section, the cross-cutting radar elements are typically lenticular, with the order of deposition alternating between each side of the landform. Down-flow radar elements are tabular and deposition is consistent across the conduit, though radar element bounding surfaces arch slightly towards the margins of the landform. In contrast, the Bering Glacier esker is composed of at least five radar elements that have an average maximum thickness of ~3 m. Radar elements here are typically tabular, continuous through the landform, and their bounding surfaces are generally sub-horizontal to the ground surface in flow perpendicular cross-sections. In flow-parallel lines, however, radar element bounding surfaces are generally inclined up-flow.
- For the conduit fill eskers at Skeiðarárjökull and Bering Glacier the sedimentary architectures demonstrate a similar evolution. The deepest radar elements, representing the first phases of sedimentation, are typically composed of discontinuous and undular reflections, likely to be associated with the deposition of antidune sets (*Sections 6.2 and 7.2*), suggesting that Froude numbers were between ~0.7 and 1.7 and flows were supercritical (Carling, 1999; Carling and Shvidechenko, 2002; Duller *et al.*, 2007). The maximum crest heights of the largest bedforms at Skeiðarárjökull are ~3 m, whilst at Bering Glacier the largest bedforms have a smaller crest height of ~1.5 m. This suggests that flow depths during the earliest depositional phase were greater at Skeiðarárjökull. The upper bounding surfaces of these radar elements are typically defined by unconformities associated with reactivation surfaces. Relative to the maximum cross-sectional area of the conduit, the antidune sets within the Skeiðarárjökull esker account for a lesser proportion of the total landform, relative to those within the Bering Glacier esker.
- Resting upon the deepest radar elements composed of antidunes, are radar elements made up of reflections that are more continuous. Although, the radar facies

classification of these reflections is varied, their more continuous characteristics indicate lower velocities at the time of deposition and perhaps less turbulent flows (Carling, 1999). The pattern of down-flow changes in radar facies within these radar elements, are similar within the eskers at Skeiðarárjökull and Bering Glacier. Within both eskers, up-flow sections of the landform show a general downstream transition from backset to foreset bedded sediments, though their angle of dip is typically lower within the Bering Glacier esker. This is consistent with the development of composite macroforms within conduit enlargements (Brennand, 1994; Brennand and Shaw, 1996; Brennand, 2000; Fiore *et al.*, 2002) at both field sites. The composite macroform within the Skeiðarárjökull esker is composed of eight radar elements, the bounding surfaces of which are defined by up-flow and down-flow dipping unconformities. In contrast, the composite macroform within the Bering Glacier esker is composed of three radar elements that have bounding surfaces, which are more regular and continuous through the landform. Down-flow from the composite macroforms, however, both landforms are dominated by upper-stage plane beds that suggest flow depths were lower and consequently flow velocities were greater (Allen, 1992; Alexander *et al.*, 2001). The bounding surfaces of these radar elements are typically more continuous through the landform at both field sites, suggesting a more regular depositional pattern.

*8.3.2 The morphology and sedimentary architecture of the ice-walled canyon fills*

At Skeiðarárjökull, the ice-walled canyon fill is connected to the esker at its up-flow end, but when considered separately, is ~500 m in length with a maximum cross-sectional area of ~2, 400 $m^2$ and has a slightly sinuous morphology. The southwestern extension of the ice-walled canyon fill at Bering Glacier extends for ~400 m with a maximum cross-sectional area of ~1, 100 $m^2$ and is slightly sinuous in morphology. Internal sedimentary architecture of these landforms, identified from GPR surveys is varied:

- Radar elements within both ice-walled canyon fills are divided by bounding surfaces that are represented by unconformities. The Skeiðarárjökull ice-walled canyon fill is composed of at least eleven radar elements that are relatively continuous through the landform and have an average maximum thickness of ~5 m. The ice-walled canyon fill at Bering Glacier, however, is composed of at least seven radar elements that are typically divided by unconformities and have a maximum average thickness of ~3 m. The patterns of classification of radar elements at both field sites are contrasting, however.
- The deepest radar elements within the ice-walled canyon fill at Skeiðarárjökull are composed of discontinuous and undular reflections, likely to be associated with the deposition of antidunes (*Section 6.2*). Although the deepest deposits within the Bering

Glacier ice-walled canyon fill are dominated by upper-stage plane beds, these evolve into less continuous and undular reflections likely to be associated with antidunes (*Section 7.2*). The presence of antidunes suggests that deposition took place within supercritical flows, with Froude numbers >0.84 (Carling, 1999; Carling and Shvidechenko, 2002), though flow depths were slightly greater at Skeiðarárjökull, with the maximum bedform crest height being ~2.5 m, compared to a crest height of ~2 m at Bering Glacier. The upper bounding surfaces of these early radar elements are typically defined by unconformities that represent reactivation surfaces.

- The final phase of sedimentation within the Skeiðarárjökull and Bering Glacier ice-walled canyon fills are very different, despite reflections within both landforms typically being more continuous. The up-flow end of the Skeiðarárjökull ice-walled canyon fill is typically composed of radar elements that dip up-flow at high angles (~25°) and are typically divided by unconformities. These radar elements are dominantly classified as backset beds that indicate deposition within an expansion environment (Jopling and Richardson, 1966; Alexander *et al.*, 2001). Down-flow radar elements are cross-cutting with deposition typically switching from left to right within the canyon. These radar elements are classified as predominantly upper-stage plane beds, though cut-and-fill structures may contain antidune (or dune) sets. In contrast, the ice-walled canyon fill at the Bering Glacier is composed of radar elements that are continuous through the landform in flow perpendicular cross-sections. These are generally classified as foreset beds, associated with deposition within a flow separation eddy (Jopling, 1965).

### *8.3.3 The controls on esker sedimentary architecture*

The esker at Skeiðarárjökull was generated within a pressurised englacial conduit, the geometry and position of which was controlled by pre-existing structural weaknesses within the ice. During the earliest stage of a linearly rising jökulhlaup (Figure 8.1a) the inability of pre-existing outlets to respond to the rapid input of floodwaters means that effective pressures became negative and waters were forced into high elevations within the ice column (Roberts *et al.*, 2000b; Clarke, 2003). At Skeiðarárjökull, this was along a pre-existing englacial structure filled with porous debris (similar to Gulley and Benn, 2007). Contrastingly, the Bering Glacier esker was deposited within a pressurised subglacial conduit the position of which was likely to have been controlled by subglacial topography (Fleisher *et al.*, 1998). During the early part of the rising stage of an exponentially rising jökulhlaup (Figure 8.1b) the gradual input of floodwaters allows the pre-existing drainage systems to respond to increases in discharge (Clague and Matthews, 1973; Roberts *et al.*, 2000b; Roberts, 2005). The erosive nature of the floodwaters, however, allows undermining of the weakened conduit roof.

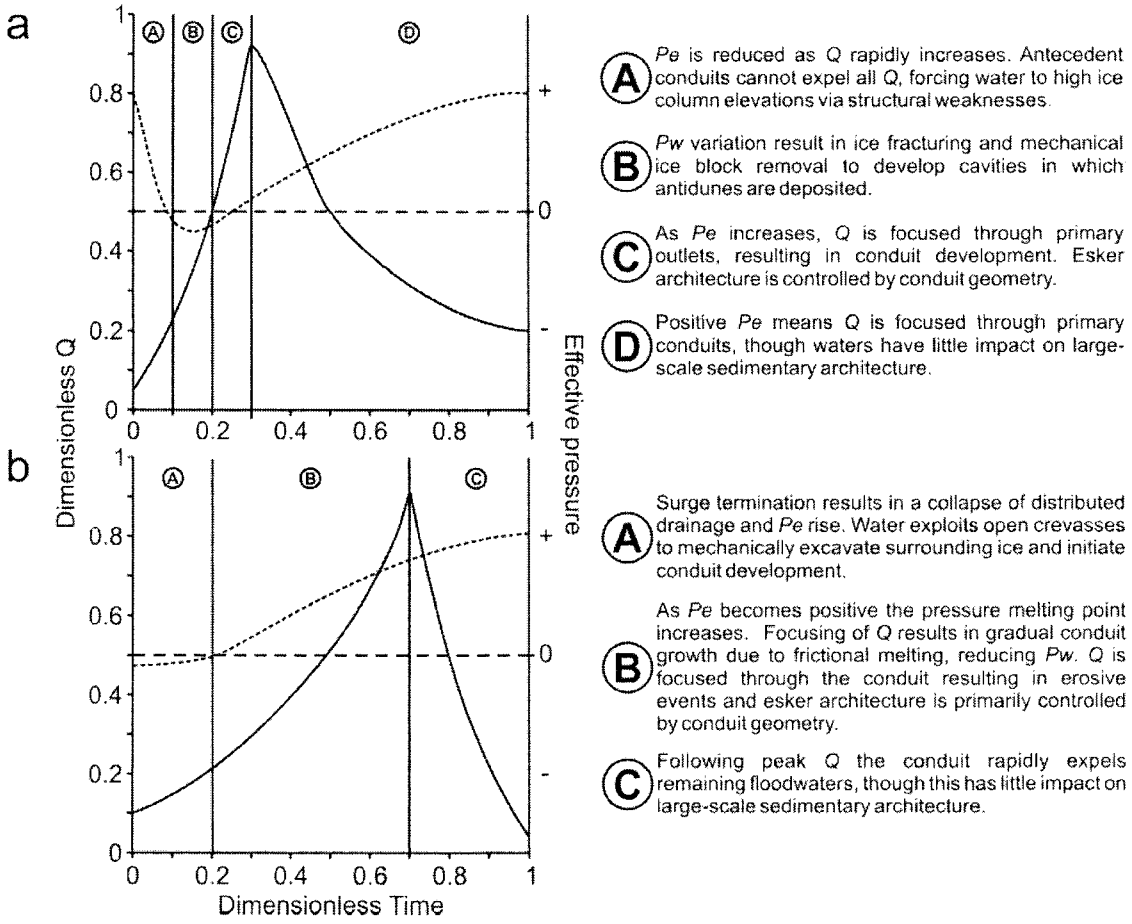


**Figure 8.1.** Conceptualised hydrographs (solid lines) for a) linearly rising and b) exponentially rising jökulhlaups (after Roberts, 2005). Changes in effective pressure are shown (dashed line) and both jökulhlaup types are divided into stages associated with conduit and esker development (*Q* = discharge, *Pw* = water pressure, *Pe* = effective pressure).

At Skeiðarárjökull, negative effective pressures resulted in localised hydraulic jacking and cavity generation (Roberts *et al.*, 2000a, 2000b, 2001, 2002; Roberts, 2005) along the flow path. Indirect evidence of hydraulic jacking may come from the observation of concentric linear fractures on the surface of Skeiðarárjökull along the path of the esker (Roberts, 2002). These fractures denote an area of ice surface collapse (Roberts, 2002) that may have developed because of locally buoyed ice. At Skeiðarárjökull and Bering Glacier, the negative effective pressures, rapid creation of accommodation space, turbulent flows, and relatively high velocities, resulted in the deposition of antidunes within the transitional to supercritical flow conditions (Carling, 1999; Alexander *et al.*, 2001; Duller *et al.*, 2007) (Figure 8.1). The largest antidunes within the Skeiðarárjökull esker are greater than those within the Bering Glacier esker. This suggests flow depths and conduit size were slightly greater at the time of deposition (c.f. Carling, 1999; Alexander *et al.*, 2001; Duller *et al.*, 2007).

On a ridge-scale, within the up-flow sections of the esker at Skeiðarárjökull and the Bering Glacier esker, the sedimentary architecture suggests the development of a composite macroform within a conduit enlargement, analogous to similar forms identified in Quaternary eskers (c.f. Brennand, 1994; Brennand and Shaw, 1996; Brennand, 2000; Fiore *et al.*, 2002). Within both eskers, erosion of earlier deposits and the surrounding glacier ice created the conduit enlargement. It is suggested by Gulley and Benn (2007) that limestone karst caves are analogous to the near-surface glacial hydrological system in debris covered glaciers. Widenings (or 'rooms') are often found along limestone caves and these are typically associated with a confluence of several passages or at an area of more vigorous solution (White, 1988). If the glacial hydrological system behaves in a similar manner to limestone caves (c.f. Gulley and Benn, 2007), it is likely that the conduit enlargements in which composite macroforms were deposited may have developed due to a confluence of drainage, roof collapse, or at a site of enhanced ice excavation. In the englacial conduits mapped by Gulley and Benn (2007), enlarged conduits were located in sections of ice containing numerous structural weaknesses and this may explain the presence of a conduit widening at both field sites. In addition, the observation of three eskers within the ice of Skeiðarárjökull (Figure 5.1), up-glacier from the exposed single esker, may be used as indirect evidence for a confluence of drainage. The creation of a conduit widening is associated with a consequent increase in flow depth and a significant decrease in flow velocity, which forces the deposition of backset beds within the widened conduit. The composite macroform develops by vertical and up-glacier conduit growth in which up-flow dipping radar elements are deposited in an up-glacier direction from supercritical flows with Froude numbers between 1.1 and 1.77 (Duller *et al.*, 2007) that discharge into subcritical flow. As this macroform enlarges a flow separation is created on

the lee side (c.f. Jopling, 1965; Allen, 1984) where foreset beds are deposited within the separation eddy (c.f. Brennand, 1994; Brennand and Shaw, 1996; Brennand, 2000).

Down-flow of the composite macroforms, deposition was dominated by upper-stage plane beds at both Skeiðarárjökull and Bering Glacier, indicating that sedimentation took place within flows of lower depth and velocity (Allen, 1992; Alexander *et al.*, 2001; Collinson *et al.*, 2006). This would have taken place within a constricted conduit (c.f. Brennand, 1994; Brennand and Shaw, 1996; Brennand, 2000), though pseudo-anticlinal macroforms were not directly identified.

*8.3.4 The controls on ice-walled canyon fill sedimentary architecture*

The ice-walled canyon fill at Skeiðarárjökull was deposited within a pressurised englacial conduit at its proximal end, which then unroofed up-flow due to conduit growth to become a supraglacial ice-walled canyon. This corresponds to previous interpretations of headward excavation of the Embayment region of the canyon (Cassidy *et al.*, 2003). Similarly, the Bering Glacier ice-walled canyon fill was deposited within a pressurised englacial conduit, which became a supraglacial ice-walled canyon due to headward unroofing of the conduit (Fleisher *et al.*, 1998), consequent of vertical conduit growth or collapse of the weakened ice roof.

The ice-walled canyon fill at Skeiðarárjökull is connected to the esker at its proximal end, and its geometry corresponds to the position of supraglacial outlets during the jökulhlaup rising stage (Roberts *et al.*, 2001). This suggests that its supraglacial location is structurally controlled, as has been identified for the esker. Similarly, although no direct observations of a structural control have been made as part of this data set, the position of the Bering Glacier ice-walled canyon corresponded to a crevasse or shear plane (perpendicular to the direction of ice flow) visible on aerial photographs (see Figure 3.8a). This suggests (though tentatively) that structure may have played some role in the positioning of the assemblage. During the surge, such structure may have formed due to tectonic process towards the compressional zone at the glacier margin where basal crevasses and thrust planes may have developed, elevating subglacial sediments into the ice column (Sharp, 1985b, 1988). In addition, crevasses-fills may be formed during a surge when the opening of extensional crevasses forces pressurised bed material to be injected into them, or immediately following a surge when the stagnating, but crevassed ice sinks into its soft bed (Clarke *et al.*, 1984; Sharp, 1985a; Murray *et al.*, 1997; Evans and Rae, 1999; Woodward *et al.*, 2003a). At Bering Glacier, the presence of such a debris-filled structure may have provided a weakness along which floodwaters were initially discharged (similar to Gulley and Benn, 2007) prior to conduit and ice-walled canyon development during the outburst flood.

The first phase of deposition within the Skeiðarárjökull ice-walled canyon fill was of antidunes within the pressurised englacial conduit. Although initial deposition during the July-August Bering Glacier outburst flood also took place within an englacial conduit, upper-stage plane beds characterize the deepest radar elements. This suggests that flow velocities were higher at Skeiðarárjökull, though the deposition of antidunes within the conduit at Bering Glacier subsequent to upper-stage plane beds shows velocities increased, probably as discharge became focused upon this outlet (Fleisher *et al.*, 1998). At Skeiðarárjökull, conduit unroofing was rapid, resulting in discharge into a flow expansion environment where the antidune sets would have been partially eroded and backset beds were deposited at the hydraulic jump. Deposition was analogous to that of an expansion bar (c.f. Baker, 1973) that migrated upstream due to rapid headward conduit unroofing. This bedform was deposited rapidly in relatively shallow flows, directly from suspension. In contrast, at Bering Glacier, as the conduit unroofed predominantly foreset beds were deposited, analogous to the development of a prograding bar-form in relatively deep flows (Jopling, 1965).

### *8.3.5 Summary*

Although the eskers and ice-walled canyon fills at Skeiðarárjökull and Bering Glacier were deposited during single events, the sedimentary architectures display some differences, despite containing similar radar facies. The landforms at Skeiðarárjökull are typically composed of less continuous radar elements divided by unconformities representing reactivation surfaces. In contrast, the radar elements that make up the Bering Glacier landforms are typically more continuous through the landforms and the presence of reactivation surfaces is minimal in comparison to those within the Skeiðarárjökull landforms. On a ridge scale, however, the eskers display a similar evolutionary pattern. The initial phase of deposition is dominated by antidunes, which are testament to the supercritical conditions during their deposition. The later phases of deposition are dominated by composite macroforms at up-flow sections of the eskers, indicating the presence of conduit widening. At down flow sections of both eskers the conduit geometry must have been smaller, allowing the deposition of upper-stage plane beds. These similarities, however, cannot be extended to the ice-walled canyon fills, with that at Skeiðarárjökull being deposited as an expansion bar, which contrasts to the deposition of a prograding bar-form at the Bering Glacier. The identification of similar evolutionary patterns and ridge-scale macroforms within the eskers, however, suggests some commonailty exists between the jökulhlaup eskers. Smaller scale, sedimentary architecture, however, is varied.

## 8.4 The Preservation Potential of the Skeiðarárjökull and Bering Glacier Landforms

It is important to assess the preservation potential of the eskers and ice-walled canyon fills at Skeiðarárjökull and Bering Glacier, as this may determine whether the models of their formation can be directly applied as analogues for Quaternary esker deposition. Both Skeiðarárjökull and Bering Glacier are dynamic environments, being subject to surges (c.f. Post, 1972; Fleisher *et al.*, 1998; Björnsson, 1998; Russell *et al.*, 2001b) and frequent jökulhlaups (c.f. Björnsson, 1992; Fleisher *et al.*, 1998), both of which can lead to the modification of previously deposited materials (c.f. Russell *et al.*, 2001b, 2006). In addition, buried ice is present across the immediate forefield of Skeiðarárjökull and Bering Glacier, evidenced by the formation of kettle holes and collapse structures in outwash sediments.

### *8.4.1 Buried ice melt*

The esker and ice-walled canyon fill at Skeiðarárjökull were deposited within an englacial conduit and supraglacial ice-walled canyon, respectively. Likewise, the ice-walled canyon fill at Bering Glacier was deposited within a supraglacial position. Consequently, the landforms rest upon buried ice, the thickness of which could not be directly measured. The lack of post-depositional disturbance within Quaternary eskers has lead to the interpretation that many were deposited within subglacial conduits and that englacial deposition would have a low preservation potential (e.g. Banarjee and McDonald, 1975; Brennand, 1994). Furthermore, in the interpretation of some esker systems, the presence of kame and kettle topography has been used as evidence of disturbance of esker material deposited within englacial or supraglacial positions (Hebbrand and Åmark, 1989; Thomas and Montague, 1997; Huddart and Bennett, 1997). In a study by Price (1969), however, it was observed that englacial or supraglacial eskers could be lowered onto the substrate, due to melting of 2-15 m of buried ice, without significant disturbance of the landform. The extent of buried ice beneath the eskers at Skeiðarárjökull and Bering Glacier is unknown, however. At Skeiðarárjökull, significant amounts of buried ice are present across Skeiðarársandur, some of which is believed to have survived for at least two hundred years (Everest and Bradwell, 2003). Buried ice here, has been estimated to melt out at an average rate of between 0.6-1 mm yr (Everest and Bradwell, 2003). Consequently, forefield landforms are still undergoing 'secondary glaciation' (Everest and Bradwell, 2003) and the final form of the esker remains to be seen. Even if the thickness of buried ice upon which the esker directly rests was known, the presence of buried ice beneath lower englacial/subglacial sediments negates the ability to assess the impact of buried ice melt out. Currently, the normal faulting observed in the esker and ice-walled canyon fill landforms appears to be largely due to removal of

the supporting ice walls, rather than more complex faulting patterns associated with buried ice melt (c.f. Woodward *et al.*, 2008).

The esker at the Bering Glacier was generated within a subglacial conduit and so was deposited directly onto the substrate. Consequently, the landform does not directly rest upon a significant body of buried ice, though a slight kettled surface suggests that some disturbance may take place due to the melting of individual ice blocks within the landform. For the Bering Glacier esker, the melting of buried ice may not result in major post-depositional disturbance, though as was identified for southern Icelandic glaciers (Everest and Bradwell, 2003), buried ice of unknown quantity may survive beneath forefield sediments for several decades or centuries.

### *8.4.2 Jökulhlaups*

It was argued by Smith *et al.* (2006) that the geomorphic affect of the November 1996 Skeiðarárhlaup has been removed within the ten years following deposition. The esker and ice-walled canyon fill, however, are located outside of Smith *et al.*'s (2006) field area and survived because they are not located at a site of a major perennial meltwater outlet. Consequently, erosion by seasonally controlled drainage has not taken place. The potential for jökulhlaup activity and changes in meltwater routing due to retreat into overdeepened basins (Marren, 2005), however, may provide a potential problem for the preservation of the eskers and ice-walled canyon fills. At the Bering Glacier, retreat of the ice margin since 1995 has resulted in the re-opening of an outlet between Tsivat and Tsiu lakes along the ice margin. At the time of data collection in June 2006, this had resulted in partial erosion of the up-flow end of the esker due to undermining by the waters flowing through the outlet. In August 2006, an outburst flood occurred that resulted in partial drainage of Tsivat and Tsiu lakes into Lake Vitus (Fleisher *pers. comm.*, 2006). This has partially scoured the ice-walled canyon fill and the esker has been eroded at the up-flow end to reduce its length by ~40 m (Fleisher *pers. comm.*, 2007) (Figure 8.2). Based upon the recent activity it is unlikely that the esker and ice-walled canyon fill will be preserved in their current form, though to what extent they will be maintained remains unclear.

Since exposure of the esker and release of the Skeiðarárjökull ice-walled canyon fill from the supporting ice walls, the ice-walled canyon fill has retreated significantly with materials being redeposited into the surrounding lake. This disturbance has largely came from normal faulting of marginal materials due to removal of the supporting ice and melting of buried ice that has been exposed in sections along the flanks of the feature. Since the November 1996 jökulhlaup Skeiðarárjökull has retreated (>10 m $yr^{-1}$) into an overdeepened basin, which has resulted in the development of an interconnected lake

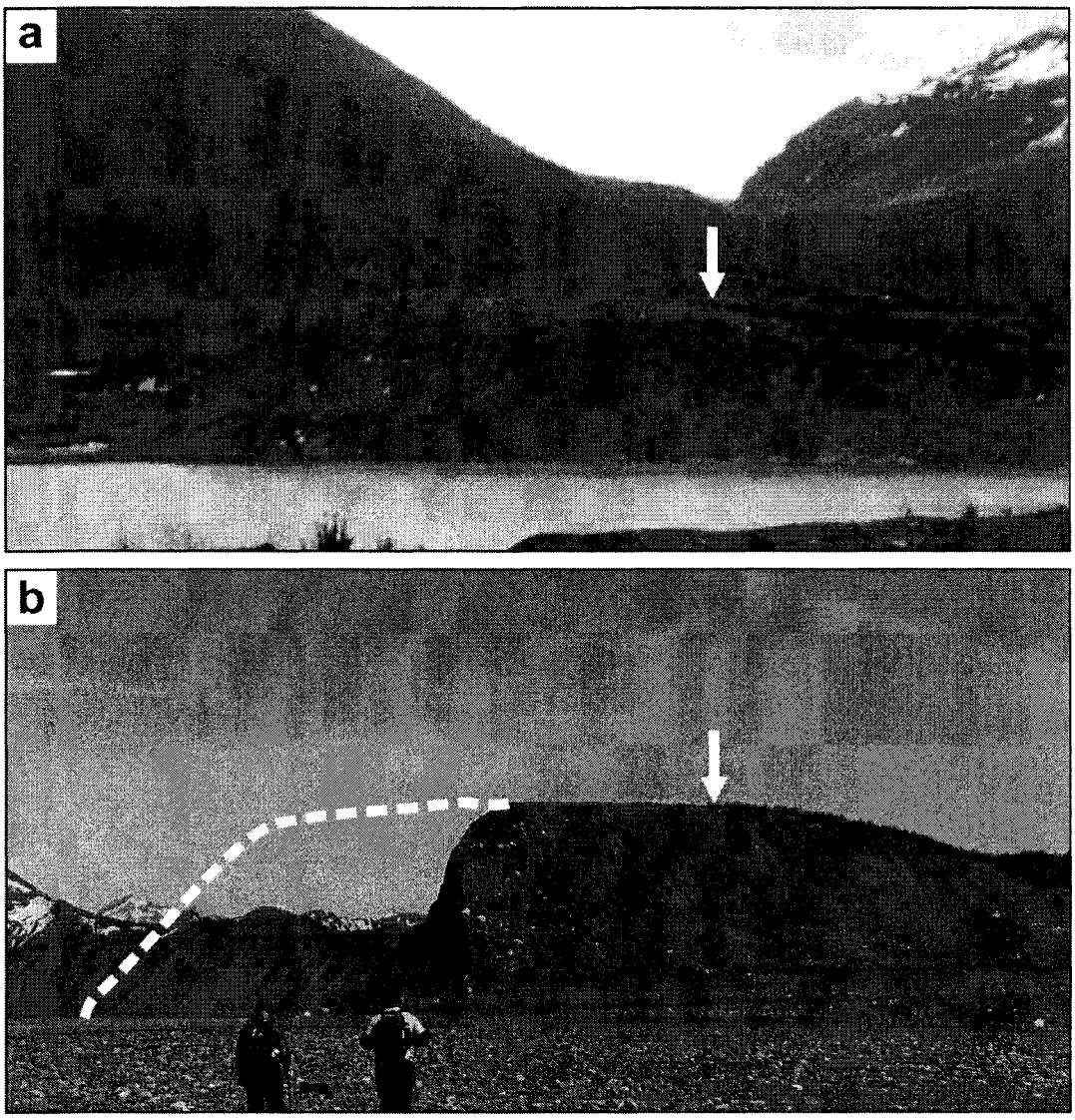


**Figure 8.2.** a) photograph of the esker at the Bering Glacier in June 2006. b) Photograph of the esker at Bering Glacier in June 2007. In August 2006, drainage of Tsivat and Tsiu lakes into Lake Vitus undermined the esker and eroded a significant amount of the landform. The position of the arrow corresponds to that in a). The dashed line highlights the approximate extent of the esker in June 2006.

complex in the area surrounding the esker and ice-walled canyon fill. If the current rates of retreat continue, eventually drainage of typical Grímsvötnhlaups from the Skeiðará outlet will be diverted along the glacier margin towards the Gígjukvísl. The lakes may consequently act as sediment traps and the esker and ice-walled canyon fill may become buried in lacustrine sediment. Once the buried ice beneath the landform melts out, their position may be marked by an area of negative topography.

In contrast, when a jökulhlaup on the scale of the November 1996 event takes place, the erosive nature of the floodwaters may erode the esker and ice-walled canyon fill landforms. It was suggested by Everest and Bradwell (2003), that buried ice can survive beneath insulating sediments for several decades. Fay (2002a, 2002b) stated that the November 1996 Skeiðarárhlaup entrained buried ice bodies that had became detached from the glacier margin. Should the buried ice beneath the esker and ice-walled canyon fills at Skeiðarárjökull survive until the next large jökulhlaup, the presence of entrainable ice beneath the landforms may aid their destruction.

### *8.4.3 Surge activity*

Both Skeiðarárjökull and Bering Glacier are subject to surge activity and may potentially be subject to reworking associated with such events. Surges of the Bering Glacier have a return cycle of approximately 25 years, whilst a surge return period has not been identified for Skeiðarárjökull. In theory, the advance of an ice margin may destroy older landforms and this was used as an explanation for a lack of eskers older than the most recent surges at Brúarjökull, Iceland (Knudsen, 1995). Both the esker and ice-walled canyon, were modified through subglacial sediment deformation when they were overrun by the second phase of the 1993-1995 surge. This, however, did not destroy the large scale sedimentary landforms, suggesting that a surge may not have a major impact upon the architecture. Furthermore, the most recent surges of Skeiðarárjökull and Bering Glacier have only temporarily halted the general retreat, with surge maxima also retreating (Fleisher *et al.*, 1998; Molnia *et al.*, 1996). Consequently, if this trend continues, the eskers and ice-walled canyon fills may be located at a position that is not within the next surge maximum and, consequently, would not be overrun by the advancing ice.

### *8.4.4 Summary*

From current observations at both field sites it is unclear to what extent the landforms will be preserved. Consequently, only tentative inferences of preservation potential can be made and only time will show the final form of the eskers and ice-walled canyon fills. Therefore, the potential for the models presented in *Chapters 6* and *7* to provide direct analogues to Quaternary eskers cannot be established.

## 8.5 Controls on Jökulhlaup Esker Sedimentary Architecture

The aim of this thesis is to identify the hydrological, glaciological and sedimentary controls on the sedimentary architecture of single event eskers, produced during high-magnitude jökulhlaups. In order to fulfil this aim, this chapter has so far compared the sedimentary architecture of the eskers deposited during jökulhlaups at Skeiðarárjökull and Bering Glacier. This section will address the potential controls on the sedimentary architecture of jökulhlaup eskers. The eskers and ice-walled canyon fills at Skeiðarárjökull and Bering Glacier were deposited in different positions within the glacier, with the 1996 Skeiðarárhlaup esker and ice-walled canyon fill being deposited englacially and supraglacially, respectively. The 1994 Bering Glacier outbursts, however, deposited the ice-walled canyon fill supraglacially and the esker subglacially. Consequently, prior to identifying the controls on the sedimentary architecture of jökulhlaup eskers, the controls on conduit position during jökulhlaups will be discussed.

### *8.5.1 Conduit position*

The position of the major jökulhlaup outlets across the margins of Skeiðarárjökull and Bering Glacier seems to be primarily controlled by subglacial topography. At both Skeiðarárjökull and Bering Glacier, major jökulhlaup outlets were focused along subglacial depressions or overdeepenings (Björnsson, 1998; Björnsson *et al.*, 1999; Roberts *et al.*, 2000b; Carlson *et al.*, 1993; Merrand and Hallet, 1996; Fleisher *et al.*, 1998). Whilst the November 1996 Skeiðarárhlaup and July-August 1994 Bering Glacier outburst flood, eskers and ice-walled canyon fills were initially deposited within englacial conduits, the October 1994 Bering Glacier outburst flood esker was deposited within a subglacial conduit. Although it has been previously hypothesised that subglacial drainage is negligible through an overdeepening (e.g. Hodge, 1976; Hooke *et al.*, 1988; Kirkbride and Spedding, 1996), this research shows that during a jökulhlaup, the presence of a subglacial overdeepening does not control the englacial or subglacial position of a major outlet. The jökulhlaups at both field sites were subglacial for at least some of their flow paths and it is likely jökulhlaup dynamics fundamentally controlled conduit position.

The dynamics of a jökulhlaup are governed by the release mechanism (c.f. Tweed and Russell, 1999). If floodwaters are released rapidly and associated with a sudden increase in water pressure, antecedent drainage routes cannot effectively respond to the increase in discharge (Roberts *et al.*, 2000b). Consequently, floodwaters are forced into high elevations within the ice column and discharged englacially. In contrast, when floodwaters are released exponentially, existing drainage systems can maintain the increasing discharge and the outlet position is more likely to be subglacial and remain static (Clague and Matthews, 1973; Roberts *et al.*, 2000b; Roberts, 2005). For the November 1996 Skeiðarárhlaup and the July-August 1994 outburst flood at Bering

Glacier, effective pressures were negative and consequently, waters were forced into an englacial position (Roberts *et al.*, 2000b; Roberts, 2005), which was controlled by the presence or absence of englacial structural weaknesses. In contrast, during the October 1994 outburst flood at Bering Glacier the basal water pressure remained below that of ice overburden and discharge remained subglacial, perhaps also being governed by an absence of a major englacial structural weakness in this area.

### *8.5.2 Conduit geometry*

In palaeo-esker studies, conduit geometry has often been speculated as the most fundamental factor governing the large-scale sedimentary architecture of an esker (e.g. Brennand, 1994, 2000; Delaney, 2001; Fiore *et al.*, 2002). Conduit geometry is also identified as the most influential factor governing the sedimentary architecture of jökulhlaup eskers on a ridge scale, as identified at both Skeiðarárjökull and Bering Glacier.

During a jökulhlaup, the conduit geometry is non-uniform rapidly changing down-flow (within a few tens of metres) from widened (composite macroforms) to more uniform and constricted conduits (upper-stage plane beds), which was observed at both Skeiðarárjökull and Bering Glacier. Conduit widenings were identified by Gulley and Benn (2007) at locations corresponding to significant structural weaknesses within the surrounding glacier ice and it was argued their development was consequent on gravitational collapse and enhanced erosion of the weakened ice. During the November 1996 Skeiðarárhlaup localised hydraulic jacking of the overlying ice was observed, rapidly lifting the overlying ice by several metres. If this process takes place along a major floodwater path, it could create a localised conduit widening, which is associated with an increase in flow depth that is conducive to the sudden reduction in flow velocity that is required for composite macroform sedimentation. Locally enhanced conduit growth may also be linked to a confluence of drainage, with the increased discharge, enlarging the conduit at the site of the confluence.

Areas lacking structural weaknesses, a confluence of drainage or the negative effective pressures required for hydraulic jacking, would not provide the conditions required to create a localised conduit enlargement. Consequently, the conduit will remain geometrically narrow and uniform, conducive to the deposition of predominantly upper-stage plane beds, which were identified at down-flow sections of the Skeiðarárjökull and Bering Glacier eskers.

### *8.5.3 Jökulhlaup flow conditions*

Although the eskers and ice-walled canyon fills at Skeiðarárjökull and Bering Glacier were both generated during single jökulhlaups and their large-scale sedimentary

architectures have similar characteristics, small-scale sedimentary architecture shows significant contrast. The peak discharge through the esker conduit and ice-walled canyon at Skeiðarárjökull was an order of magnitude greater than the 1994 outburst floods at Bering Glacier. The maximum cross-sectional areas of the esker and ice-walled canyon fills at both field sites, however, are within the same order of magnitude (Table 8.1). Baker and Costa (1987) state that the geomorphic effectiveness of a flood is linked directly, not to its magnitude, "but to shear stress and stream power per unit boundary". Stream power and boundary shear stress are both measures of the erosional potential of a flow and its sediment carrying capacity, with greater discharges, flow velocities and channel depths being conducive to higher stream power and boundary shear stress values (Baker and Costa, 1987). The greater values of boundary shear stress and stream power that would have prevailed during the 1996 Skeiðarárhlaup, compared to the 1994 Bering Glacier outburst floods, correspond to greater number of radar element bounding surfaces that are defined by unconformities. These unconformities represent reactivation surfaces that are testament to the greater erosional potential of the 1996 jökulhlaup waters at Skeiðarárjökull and suggest pulsating flow. In contrast, the Bering Glacier esker contains fewer unconformities and the flow would have had a lower erosional potential than the 1996 Skeiðarárhlaup.

Froude numbers have been calculated for the main stages of esker development at Skeiðarárjökull (see *Section 6.2* for calculation), providing an insight into the flow regime at Skeiðarárjökull. Although Froude values cannot be calculated for the Bering Glacier outburst floods (as flow velocity is unknown), those for Skeiðarárjökull ranged from 1.43 to 1.01 through the jökulhlaup, suggesting flows were supercritical throughout the deposition of the esker. These Froude values must be used with caution, however, as they are based upon average velocity estimates for ice-walled canyon flows during the waning stage of the jökulhlaup (Russell *et al.*, 2001a). Furthermore, the flow depth was assumed to equate to radar element thickness, rather than bedform height, which is likely an overestimate.

During the initial phase of esker development, a Froude value of 1.43 was calculated. This suggests that the flows were supercritical and falls within the range at which antidunes are deposited, supporting the antidune interpretation for radar elements deposited during this period (Carling, 1999; Carling and Shvidchenko, 2002; Duller *et al.*, 2007). The lower Froude number (1.01) calculated for the second main phase of esker is consistent with the presence of more continuous upper-stage plane beds that suggest supercritical flows, but that flow depths were greater and consequently velocities would have been lower (c.f. Carling, 1999; Carling and Shvidchenko, 2002; Duller *et al.*, 2007). Unfortunately, although the estimated Froude values for initial jökulhlaup deposition are consistent with the regime required for antidune sedimentation, the current lack of

knowledge about the processes and hydraulics required for antidune deposition in full-pipe flows make it difficult to assess the conditions prevalent during this phase of deposition.

Although jökulhlaup eskers display similar large-scale sedimentary architecture, the small-scale variability is controlled, not by the discharge of the event, but by the associated values of boundary shear stress and stream powers. Higher magnitude events are associated with higher boundary shear stress and stream power values, which is conducive to a higher erosional potential. This results in the development of radar element bounding surfaces that are defined by reactivation surfaces. Variations in boundary shear stress and stream power may provide a control for the size of the esker, with higher erosional potential resulting in greater excavation of older deposits, consequently, limiting the final size of the jökulhlaup esker. This, however, can also be explained by variations in sediment supply.

*8.5.4 Sediment supply*

Sediment supply is fundamental to esker development, controlling the size range of material available to the jökulhlaup waters. When coupled with a knowledge of shear stress and stream power, this will govern the sedimentary architecture of the esker and ice-walled canyon fill. Consequently, a knowledge of the sediment supply during the November 1996 Skeiðarárhlaup and 1994 Bering Glacier outburst floods, may help to explain variations in the sedimentary architecture of the eskers and ice-walled canyon fills. Higher values of boundary shear stress and stream power, when coupled with a limited sediment supply would be conducive to greater erosional potential once available sediment had been exhausted. If sediments are exhausted prior to the termination of a jökulhlaup, the final size of the esker may be limited due to reworking of older materials deposited within the conduit.

Due to the residence time of volcanic meltwaters in Grímsvötn, prior to the November 1996 Skeiðarárhlaup, no primary eruption material were detected in floodwaters from Skeiðarárjökull (Maria *et al.*, 2000). In addition, the likelihood of esker sediments being composed of material melted out from an englacial position is highly improbable and consequently, sediments were derived from unconsolidated materials at the glacier bed, suggesting the conduit was subglacial at some position up-glacier (Russell *et al.*, 2006). It has been estimated that the November 1996 Skeiðarárhlaup resulted in a total of 0.3 m of subglacial erosion of areas presumed to be affected by the event (Smith *et al.*, 2000; Russell *et al.*, 2006), though observations during the jökulhlaup suggested that sediments began to be exhausted approximately twenty hours after flood onset (Snorrason *et al.*, 2002).

Similarly, at the Bering Glacier, it is unlikely that esker materials were derived from englacial sediment and field evidence suggests there was significant erosion of the glacier bed (c.f. Fleisher *et al.*, 2007). The largest clasts identified within deposits at both field sites were boulders with diameters <1 m. It was estimated by Russell *et al.* (2001a) that boulders with a diameter of up to 20 cm could be carried as suspended load, but these observations were based upon ice-walled canyon data. The boundary shear stress and stream powers within the conduit are likely to have been much greater as a consequence of more constricted flow and higher velocities, enabling clasts of much greater size to have been transported in suspension. The ability of the November 1996 Skeiðarárhlaup to transport large clasts in suspension, however, appears to have been limited by sediment supply. Whilst the flood waters had the potential to transport large clasts, the relatively low identification of boulder clusters is testament to the limited supply of large clasts. The Bering Glacier had shear stress and stream power values that were less than those for the November 1996 Skeiðarárhlaup. The limited supply of larger clasts at Skeiðarárjökull, however, has resulted in a similar maximum clast diameter. The difference, between the form of deposition, however, is that at Skeiðarárjökull these clasts are likely to have been transported as suspended load, whilst those at the Bering Glacier were transported as bedload. This is represented by the position of boulder clusters within radar elements. At Skeiðarárjökull boulder clusters are deposited within a matrix of finer materials, whilst at Bering Glacier boulder clusters are commonly located at the base of radar elements (Fleisher *et al.*, 2007; Figures 6.2 and 7.8).

### *8.5.5 Summary of the controls on jökulhlaup esker sedimentary architecture*

The comparison of the sedimentary architectures of the eskers at Skeiðarárjökull and Bering Glacier, has allowed assessment of the controls on the sedimentary architecture of eskers deposited during high-magnitude jökulhlaups. This has added significantly to the understanding of the controls on the sedimentary architecture of transient generated eskers from current literature that was summarized in Table 2.2 (Table 8.2). The most fundamental control on large-scale (ridge scale) sedimentary architecture is conduit geometry. Jökulhlaup eskers display complex down-flow changes in sedimentary architecture, consequent of rapid (within a few tens of metres) changes in conduit geometry. There are a number of factors that may influence conduit geometry during a jökulhlaup (a number of which have not been previously considered in esker studies):

1. *Conduit closure*, whilst fundamental to ablation-controlled scenarios, is unlikely to affect conduit geometry over the relatively short timescale associated with a high-magnitude jökulhlaup.

| | | Ablation Controlled | | Jökulhlaup Controlled | | Product of Control |
|---|---|---|---|---|---|---|
| | *Mechanism* | *Observations* | *Limitations* | *Observations* | *Limitations* | |
| **Conduit Geometry** | Conduit Closure | Fundamental in ablation controlled esker literature[1, 2] | Assume constant steady-state full-pipe conditions , which is unlikely[3] | Unlikely to impact conduit geometry over short timescales | Rates have not been calculated for the 1996 Skeiðarárhlaup or 1994 Bering Glacier outburst floods | Macroform type |
| | Frictional Melting | | | Likely to be occurring [4], but negligible as a control[5] | | |
| | Mechanical Excavation | Not considered in current esker literature[6] | Difficult to assess without direct observation of esker formation | Significant ice block release from outlets – fundamental over short timescales[7] | Cannot be quantified | |
| | Hydraulic Jacking | Only observed during jökulhlaups | | Negative *Pe* associated with jökulhlaups locally buoys ice [5] | *Pe* variations along the conduit are unknown | |
| | Ice Flotation | | | | | |
| | Structural Weaknesses | Not considered in steady-state esker scenarios[1, 6] | Difficult to assess without direct observation of esker formation | Strong structural control at Skeiðarárjökull similar to Gulley & Benn[8] | Site specific and may not be present in the ice of some glaciers | |
| | Drainage Confluence | • Conduit widening linked to presence of moulins[6]<br>• Esker enlargement linked to converging eskers[9] | Lack direct control and are based upon esker morphology and glacial hydrology observed in valley glaciers | Englacial GPR from Skeiðarárjökull show a possible confluence of drainage up-flow of composite macroform | The converging eskers yet to be directly linked to exposed esker | |
| **Flow Conditions** | Mode of sediment transport | Bedload transport[6, 10] | Lack of control on deposition | • Transport in suspension[11, 12]<br>• Boulders in suspension at Skeiðarárjökull and traction at Bering Glacier | Could occur at lower flow regimes, if the dominant clast size is small | Depostional style (i.e. traction carpet, lag boulders, hyperconcentrated flow) |
| | Shear stress/Stream power | | | Higher jökulhlaup Q has greater shear stress/stream power = greater transport and erosional potential | Lack of required information to calculate stream power and shear stress | • Frequency of erosional structures (complexity)<br>• Esker size |
| | Flow regime | Likely to be subcritical (calculated from data presented by Boulton *et al.*[13, 14]) | Is based upon data from a contemporary glacier – is this applicable to the Laurentide? | Supercritical throughout esker deposition at Skeiðarárjökull | • Data used for calculations are likely an underestimate<br>• Could not be calculated for Bering Glacier | Bedform type (e.g. supercritical = antidune, subcritical = dune) |
| **Sediment Supply** | Sediment availability | Local variations in the size of an esker[15] | Lack of control on the processes of esker formation | Sediment exhaustion at Skeiðarárjökull resulted in erosion | Observation of sediment exhaustion based on proglacial rather than conduit measurements[16] | • Frequency of erosional surfaces (complexity)<br>• Esker size |
| | Sediment size | Units composed of silts and clays used as evidence of winter deposition[17, 18] | • Lack of depositional timescale<br>• Supply limitations have not been considered | • Clay identified as waning stage deposit [19]<br>• Boulder clusters observed at Skeiðarárjökull and Bering Glacier | • Lack of direct knowledge of depositional events[19]<br>• Clast analysis not undertaken as part of this study<br>• Skeiðarárjökull and Bering Glacier landforms had similar maximum clast size despite varying carrying capacity | Esker size and dominant clast size |

2. *Frictional melting* is likely to be taking place during a high-magnitude jökulhlaup (e.g. Clarke, 2003), but is expected to be negligible as a control on conduit geometry during a linearly rising jökulhlaup (Roberts, 2005).
3. *Mechanical excavation* is a significant factor that controls conduit growth during a high-magnitude jökulhlaup. Ice-block release from outlets at both the Bering Glacier during the 1994 outbursts and the 1996 Skeiðarárhlaup was vast and this can exceed the rate of conduit melting during such events (e.g. Tweed and Russell, 1999).
4. *Ice flotation and Hydraulic jacking* will be significant to local variations in conduit geometry during a high-magnitude jökulhlaup, due to the negative effective pressures usually associated with them. Gorrell and Shaw (1991) originally suggested that the seal surrounding subglacial conduits could be floated to create morphological widening, termed beads. This mechanism, however, was restricted towards ice-marginal locations, where the ice is thinner. Roberts *et al.* (2000a, 2000b) and Roberts (2005) noted that during the 1996 Skeiðarárhlaup ice was uplifted locally via the process of hydraulic jacking, even in relatively deep ice sections.
5. *Structural weaknesses* within the ice are not only fundamental to the position of englacial conduits during transient events (as observed by Gulley and Benn, 2007 and in this study), but can also result in the weakening of glacier ice that forces localised conduit enlargement (Gulley and Benn, 2007). Observations from Skeiðarárjökull suggest strong structural controls on the conduit in which the esker was deposited. The influence of structure during ablation-controlled scenarios, however, has not been considered in esker studies and so it is difficult to assess the influence this could play under such conditions.
6. A *drainage confluence* has been previously identified as influential in creating morphological widenings along esker ridges for ablation-controlled scenarios (e.g. Lindström, 1993; Brennand, 2000). Englacial GPR surveys at Skeiðarárjökull identified a potential drainage confluence, up-glacier from the composite macroform identified in sedimentary architecture surveys. This suggests, although tentatively, that such a scenario may also be influential to the creation of conduit widening during a high-magnitude jökulhlaup.

**Table 8.2.** (*Previous page*) Revised summary of possible controls on the sedimentary architecture of ablation and jökulhlaup-controlled eskers, incorporating the findings of this research. Observations linking to the controlling mechanisms are given, as are the limitations of the observations. The product of control can be linked to the mechanism. Boxes are highlighted to indicate new observations/controls (red) and revised concepts (yellow). Superscript numbers are in reference to the following: [1]Shreve,1985; [2]Hooke and Fastook, 2007; [3]Hooke, 1984; [4]Clarke, 2003; [5]Roberts, 2005; [6]Brennand, 2000; [7]Tweed and Russell, 1999; [8]Gulley and Benn, 2007; [9]Lindström, 1993; [10]Brennand, 1994; [11]Saunderson, 1977; [12]Mokhtari Fard, 2002; [13]Boulton *et al.* 2007a, [14]2007b; [15]Brennand and Sharpe, 1993; [16]Snorasson *et al.*, 2002; [17]Warren and Ashley, 1994; [18]Mäkinen, 2003; [19]Gorrell and Shaw, 1991.

Any of the above mechanisms can individually, or more likely, in combination result in local variations in conduit geometry, which controls the macroforms deposited within the esker system. For example, enhanced mechanical excavation due to the presence of significant structural weaknesses and a confluence of drainage would result in a sudden increase in flow depth and reduction in flow velocity, which is conducive to composite macroform development. In areas lacking these mechanisms, the conduit remains geometrically narrow and uniform. The relatively shallow and high velocity flows are favourable to the deposition of slightly arched upper-stage plane beds as the conduit grows vertically into the ice.

On a smaller scale, a complex interaction between the flow conditions and sediment supply are more influential, controlling dominant clast size, the frequency of erosional structures and the size of the esker. There are three mechanisms that can influence variations in the flow conditions:

1. The *mode of sediment transport* has been previously used to distinguish between ablation and transient-controlled conditions, with bedload transport suggesting ablation controls (e.g. Brennand, 1994, 2000) and suspension deposits indicating transience (e.g. Saunderson, 1977; Mokhtari Fard, 2002). These studies, however, lacked depositional controls and observations from Skeiðarárjökull suggest materials were carried in suspension, whilst similar sized clasts at the Bering Glacier were transported as bedload. Consequently, both mechanisms of sediment transport can take place during a jökulhlaup, dependent upon the transportational potential.
2. *Shear stress/stream power* are a measure of the transportational and erosional potential of a flow and can influence the frequency of erosional surfaces within an esker, as well as the cross-sectional area of the esker. Higher discharge events are associated with greater shear stress/stream powers and so have a greater transport and erosional potential.
3. The *flow regime* dictates the types of bedform that are deposited. For ablation-controlled systems, the flows are likely to be subcritical (based on calculations of Froude values from data presented by Boulton *et al.*, 2007a, 2007b) (*Section 8.6*). In contrast, during the 1996 Skeiðarárhlaup, the flows were supercritical throughout.

Although flow conditions may be directly influential upon small-scale esker sedimentary architecture, the controls will have a greater impact upon esker size and the frequency of erosional surfaces when combined with variations in sediment supply. Two mechanisms influence sediment supply:

1. Brennand and Sharpe (1993) suggested *sediment availability* could explain local variations in ablation-controlled esker size. This research, however, suggests that exhaustion of sediments prior to termination of a jökulhlaup can increase the erosional

potential of the flow and thus, result in a smaller esker cross-sectional area as compared to a scenario where sediments are available for the entire flood duration.

2. *Sediment size* availability is crucial in determining the dominant clast size within an esker. Although the shear stress/stream power values of the 1996 Skeiðarárhlaup would have been significantly greater than for the 1994 Bering Glacier outburst floods, the maximum clast size within the esker is the same. This suggests that, although the 1996 Skeiðarárhlaup had the potential to transport much larger clasts, these were not available to the flows.

## 8.6 Identification of Criteria Diagnostic of Jökulhlaup Deposition in Eskers

The conduit fill eskers at Skeiðarárjökull and Bering Glacier, despite showing some differences in sedimentary architecture, demonstrate common characteristics that may not be present in ablation-controlled conditions. Assessment of the flow conditions prevalent during ablation-controlled conditions can be directly compared to those expected during a high-magnitude jökulhlaup.

### *8.6.1 The sedimentary architecture of jökulhlaup eskers and ablation controlled eskers*

There are three main components common to the eskers at Skeiðarárjökull and Bering Glacier that may be fundamental to identifying a jökulhlaup control on esker genesis:

1. The initial phase of esker sedimentation during a jökulhlaup involves the deposition of antidune sets. This requires supercritical flow conditions, as well as shallow flow depths and high velocities (c.f. Carling, 1999; Carling and Shvidchenko, 2002; Duller *et al.*, 2007). Although only crude estimates of velocity were obtained for this phase in the development of the Skeiðarárjökull esker, it was shown that conditions were likely to have been supercritical.

   Based upon an average flow depth of ~3.5 m and velocity of ~2.5 m $s^{-1}$ at perennial streams at Breiðamerkurjökull, Iceland (c.f. Boulton *et al.*, 2007a), Froude numbers during peak summer discharge can be estimated at 0.427. If this is taken as an analogue for perennial streams of the southern margin of the Laurentide Ice Sheet, as is suggested by Boulton *et al.* (2007a, 2007b), the calculated Froude numbers would have been subcritical during steady-state seasonally controlled drainage. This would not provide the supercritical conditions required for the deposition of large-scale, coarse-grained antidunes. Such antidunes do not occur at Froude number less than ~0.7 (Carling, 1999; Carling and Shvidchenko, 2002; Duller *et al.*, 2007) and instead the presence of lower-stage plane-beds or dunes would be more likely.
2. Although no direct clast size analysis was undertaken as part of this research, the eskers at Skeiðarárjökull and Bering Glacier are largely composed of sands and

gravels (c.f. Russell *et al.*, 2001a, 2006; Fleisher *et al.*, 2007). In addition, boulder clusters were identified within GPR data collected at both field sites, having been deposited from suspension and as bedload. Data from this research, however, has shown that although values of shear stress and stream power were high during the November 1996 Skeiðarárhlaup, the limited identification of boulder clusters is testament to a limited supply of large clasts. Consequently, although the presence of boulder clusters within an esker may be used to indicate high energy flows, the size of the largest clasts should only be used with caution when attempting to interpret the magnitude of the flow. Furthermore, the relatively good depth of penetration achieved for GPR data collected at both field sites, suggest a lack of fine material (clay) in the landforms (Neal, 2004). This indicates that fine materials are washed through the conduit(s).

3. The large-scale sedimentary architecture of the landforms at both field sites are consistent with the development of composite macroforms. Composite macroforms are associated with deposition within an enlarged conduit (c.f. Brennand, 1994; Brennand and Shaw, 1996; Brennand, 2000) and the presence of a hydraulic jump (Fiore *et al.*, 2002). The creation of a hydraulic jump requires a switch from supercritical to subcritical flow conditions (Allen, 1984; Cassidy *et al.*, 2003; Duller *et al.*, 2007). Again, presuming the measurements of Boulton *et al.* (2007a, 2007b) can be used as an analogue for Quaternary glacier hydrological conditions, the predominantly subcritical conditions identified would not be conducive to the development of a hydraulic jump required for composite macroform development. Consequently, it can be suggested that during a high-magnitude jökulhlaup the high water pressures and erosive nature of the floodwaters result in the rapid development of conduit enlargements, which create significant reductions in flow velocity and consequently allow the deposition of a composite macroform. The presence of numerous reactivation surfaces are testament to the high values of shear stress and stream power calculated for a high-magnitude event. When jökulhlaup discharge is through a subaerial ice-walled canyon fed by an englacial or subglacial conduit, the associated hydraulic jump may result in the deposition of large-scale high-angle backset beds associated with an expansion bar (Baker, 1973).

### *8.6.2 Summary and diagnostic criteria for identifying eskers deposited by high-magnitude jökulhlaups*

The observation of comparable sedimentary architectures between the Skeiðarárjökull and Bering Glacier eskers and assessment of the flow conditions associated with ablation controlled scenarios, has identified some criteria that may be used for the identification of eskers formed by high-magnitude jökulhlaups. This,

therefore, adds to morpho-sedimentary criteria presented by Brennand and Shaw (1996) and Brennand (2000) for determining the mode of genesis of Quaternary eskers originally presented in Table 2.1 (Table 8.3). Eskers that have been deposited during a high-magnitude jökulhlaup should have an irregular morphology composed of both wide and narrow ridge sections. Internally, the morphological widenings are associated with composite macroforms, whilst narrow ridges are associated with upper-stage plane beds. These narrow ridges may also be expected to display a pseudo-anticlinal structure (e.g. Brennand and Shaw, 1996; Brennand, 2000), though this was not observed in GPR data collected at Skeiðarárjökull and Bering Glacier. In addition, the presence of an expansion bar may indicate jökulhlaup deposition in an ice-walled canyon, as such landforms may be diagnostic of high magnitude regimes, having not previously been reported for high-frequency low-magnitude settings. On a smaller scale, jökulhlaup eskers should contain supercritical beforms, namely large-scale, coarse-grained antidunes and upper-stage plane beds, as well as include boulders that, depending upon the flow conditions, were deposited from either suspension or traction load. The lack of boulders, however, should not be used to argue against jökulhlaup deposition, as their absence may be constrained by sediment supply and a lack of available large clasts. At both Skeiðarárjökull and Bering Glacier, there was a distinct lack of fine materials, as evidenced from sedimentary exposures and the good GPR penetration depth. This lack of fine materials could be used as partial evidence of jökulhlaup controls on esker sedimentary architecture and consequently, the presence of significant clay deposits within jökulhlaup eskers, coupled with the lack of large clasts, may be used as an indicator of low magnitude deposition. As esker clast size is influenced by sediment supply, however, interpretations of depositional environment based solely upon the dominant clast size within an esker should be used with caution. Furthermore, the extent to which an individual occurrence of the presented diagnostic criteria for jökulhlaup deposition can be used as sole evidence of jökulhlaup deposition is unclear. In eskers where many or all of the criteria are identified, however, are likely to have been controlled by transient events.

## 8.7 The Applicability of the Models for Single Event Jökulhlaup Eskers to Quaternary Esker Studies

Eskers have been used to identify the deglacial conditions of former ice sheets in North America (e.g. Brennand and Shaw, 1996; Hooke and Fastook, 2007) and Europe (e.g. Warren and Ashley, 1994; Punkari, 1997, Delaney, 2001). Traditional views of esker deposition are based upon the assumption that sedimentation took place within conduits that developed over time due to a balance between frictional melting of the conduit walls and their closure due to viscous deformation (e.g. Shreve, 1985; Warren and Ashley,

| | High-magnitude Jökulhlaup Deposition | Synchronous Deposition | Time-transgressive Deposition |
|---|---|---|---|
| *Morphology* | • An irregular undulating ridge composed of both 'narrow' and 'expanded' sections<br>• Multiple-crested morphology | • Relatively continuous ridge with 'gaps' resulting from non-deposition or post-depositional erosion within a continuous conduit<br>• Whilst lateral fans may occur, subaerial fans are only found at the most distal end of the ridge | • Relatively short ridges, punctuated by fans/deltas<br>• Typically with a beaded morphologic expression |
| *Sedimentology* | • Composed of sands, gravels and boulders<br>• Boulders are arranged into clusters, the frequency of which depend upon sediment supply<br>• A distinct lack of fine deposits (clay & silt)<br>• The presence of supercritical bedforms – large-scale, coarse-grained antidunes, and upper-stage plane beds<br>• Sand and gravel facies are arranged into ridge-scale composite macroforms and expansion bars. | • Typically composed of coarse materials with little palaeo-flow variability<br>• Clast roundness is dependent upon transport distance.<br>• Gravel facies are arranged into ridge-scale macrofoms | • Segmental trends in sediment structure and texture, consistent with flow deceleration or entry into standing water, with high palaeo-flow variability<br>• Clast roundness is typically low<br>• Sedimentary architecture will be consistent with decelerating flow on entry into a standing water body |
| *Esker Type* | 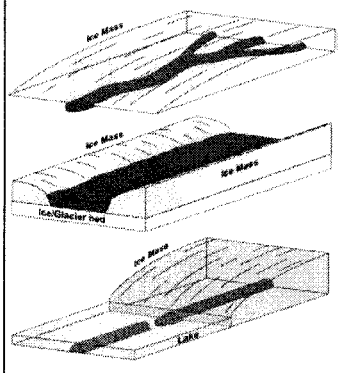 | 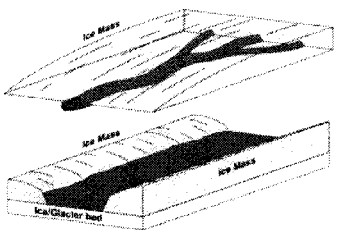 | 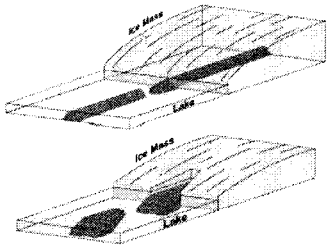 |

**Table 8.3.** Diagnostic morpho-sedimentary criteria to distinguish high-magnitude jökulhlaup, time-transgressive and synchronous deposition in eskers (synchronous and time-transgressive criteria are after Brennand and Shaw, 1996; Brennand, 2000). The esker types refer to those described in *Section 2.3.1* (Figure 2.10).

1994; Hooke and Fastook, 2007). Synthesis of results from GPR surveys presented in *Chapters 5, 6* and *7* has allowed the development of ideas around the controls on esker development and sedimentary architecture during a single jökulhlaup. As well as being of significance for models developed for the deposition of eskers during previous glaciations, this study has major implications for the traditional views of glacial hydrology that have been fundamental to many esker studies and applied to modelling of contemporary jökulhlaups (e.g. Nye, 1976; Clarke, 2003).

### *8.7.1 Glacial hydrology*

The location of primary conduit outlets during the November 1996 Skeiðarárhlaup and 1994 Bering Glacier outburst floods corresponded to overdeepened (c.f. Björnsson *et al.*, 1999; Roberts, 2000b) and/or hydraulically isolated basins (c.f. Merrand and Hallet, 1996; Fleisher *et al.*, 1998). Such a topographic control has also been inferred for the upstream continuation of esker paths during time-transgressive deposition in Ireland (c.f. Delaney, 2001), Finland (Mäkinen and Räsänen, 2003; Mäkinen and Artimo, 2007), Sweden (Hebrand and Åmark, 1989) and North America (Henderson, 1988; Brennand and Shaw, 1994). Although subglacial topography may constrain the position of drainage, as shown by some North American eskers that are located within tunnel channels (Shulmeister, 1989; Brennand and Shaw, 1994; Fisher *et al.*, 2005; Brennand *et al.*, 2006), this research is inconsistent with the theory that subglacial discharge is unlikely to occur at the base of overdeepened basins (Lliboutry, 1983; Hooke *et al.*, 1988; Hooke, 1989; Pohjola, 1994; Kirkbride and Spedding, 1996; Fountain and Walder, 1998; Waller *et al.*, 2001). Instead, the jökulhlaups were discharged subglacially for some distance, before becoming englacial near the glacier margin. This englacial position was controlled by structural weaknesses within the ice, rather than subglacial topography, suggesting pre-existing weaknesses may be more influential in glacial hydrology than previously hypothesised.

### *8.7.2 Quaternary eskers*

Although some studies suggest jökulhlaups may produce a complex architecture over multiple events (e.g. Shulmeister, 1989; Gorrell and Shaw, 1991; Brennand, 1994), Clark and Walder (1994) suggest single events would be incapable of producing an esker on the scale and with the complexity of those observed in North America. This research, however, has shown that a single 'high-magnitude' jökulhlaup can result in the development of a sedimentary architecture and morphology that is consistent with some descriptions of Quaternary eskers (c.f. Brennand, 1994; Brennand and Shaw, 1996; Brennand, 2000; Fiore *et al.*, 2002; Sjögren *et al.*, 2007). Whilst it is likely that eskers are a polygenetic landform (e.g. Flint, 1928; Warren and Ashley, 1994; Brennand, 2000), this

research provides a basis for distinguishing between landforms that were deposited during jökulhlaups and seasonal drainage patterns, with the presence of composite macroforms being likely candidates of transient events.

Composite macroforms have been described from Quaternary eskers in both North America (Brennand, 1994; Brennand and Shaw, 1996; Brennand, 2000) and Europe (Fiore *et al.*, 2002), though their timescales of deposition were previously unconstrained. As composite macroform deposition requires a switch from supercritical to subcritical conditions, it is unlikely they are representative of seasonally controlled drainage patterns and are likely to be representative of flow transience. Although the work of Fiore *et al.* (2002) is the first to directly identify composite macroforms in European eskers, this does not preclude their wider occurrence. Lindström (1993) described morphological enlargements along continuous eskers in Sweden. Although no detailed sedimentological interpretations are presented, it is suggested such enlargements take place at a point where a major hydrological change would be expected. Composite macroforms develop at the site of a major hydrological change (c.f. Brennand, 1994; Brennand and Shaw, 1996; Brennand, 2000; Fiore *et al.*, 2002) and are associated with morphological enlargements within an esker ridge. It is likely that the 'enlargements' described by Lindström (1993) are associated with composite macroforms (Brennand, 2000), indicating that such bedforms are not uncommon in North American and European eskers, with similar 'widenings' being described by Warren and Ashley (1994) and Delaney (2001) for the Irish eskers. The potential widespread occurrence of composite macroforms may be testament to the significance of jökulhlaups upon esker sedimentary architecture.

### *8.7.3 Implications for ice sheet hydrology*

It is known that during the last glaciation, high magnitude jökulhlaups drained the margins of the North American (c.f. Baker, 1973; Teller *et al.*, 2002; Clague *et al.*, 2003), European (c.f. Mokhtari Fard, 2001; Knight, 2002) and Siberian ice sheets (c.f. Carling *et al.*, 2002). Typically, esker sedimentary architecture has been attributed to discharge patterns associated with seasonal variations in supraglacial meltwater input (e.g. Banerjee and McDonald, 1975; Shreve, 1985; Brennand and Shaw, 1994). The potential widespread occurrence of composite macroforms within eskers in North America (Brennand, 1994; Brennand and Shaw, 1996; Brennand, 2000; Sjogren *et al.*, 2007) and Europe (Lindström, 1993; Warren and Ashley, 1994; Delaney, 2001; Fiore *et al.*, 2002) may be testament to the widespread occurrence of jökulhlaups during retreat of the Late Pleistocene ice sheets.

Recent evidence from the Antarctic ice sheets suggest the movement of stored water at the bed of the ice sheets is common (Gray *et al.*, 2005; Wingham *et al.*, 2006;

Fricker *et al.*, 2007; Bell, 2008) and may be discharged as jökulhlaups beneath ice streams (Wingham *et al.*, 2006). In addition, the Greenland ice sheet has extensive areas of surface melting that collect in large supraglacial lakes, the waters from which can be drained into the subglacial hydrologic system and discharged as jökulhlaups (Bell, 2008). These observations have major implications for the movement of water beneath the retreating Laurentide ice sheet.

In Antarctica, >145 subglacial lakes have been identified and it has been recently observed that subglacial water moves in large volumes between some of these lakes (Fricker *et al.*, 2007) and into the ocean as jökulhlaups (Bell, 2008). If such drainage of waters between subglacial lakes took place beneath the Laurentide and European ice sheets, a deranged drainage pattern would have developed. Indeed, for both North American and Irish eskers, such a pattern has been described for some eskers (e.g. Warren and Ashley, 1994; Brennand, 2000). The potential for identifying jökulhlaup eskers in both North America and Europe is high and future esker studies may be able to reassess the controls on esker deposition.

Eskers have been used to reconstruct palaeo-ice sheet surface slopes (Hooke and Fastook, 2007), though this is based upon the assumption of steady state glacial hydrological theory (Röthlisberger, 1972; Shreve, 1972, 1985). Jökulhlaup dynamics are also based upon traditional assumptions of glacial hydrology (Nye, 1976; Clarke, 2003), which can only be applied to steady-state conditions. While it was shown by Roberts *et al.* (2000a, 2000b, 2001, 2002) that structural control plays a role in outlet development, hydrofracturing of the overlying ice is suggested to be most important in floodwater routing. This study, however, has shown that, at least in overdeepened basins, pre-existing structures within the ice can control the route floodwaters take towards the glacier margin, rather than equipotential surfaces within the ice. Consequently, when reconstructing ice surface gradient from esker paths, care must be taken to assess the likelihood of transient controls on esker deposition, as structural weaknesses may be more influential than equipotential gradients within the ice.

Care must also be taken when using eskers, on a regional scale, to interpret the deglacial conditions of former ice sheets. The traditional assumptions of eskers as being controlled by seasonal drainage patterns and thus representing rapid downwasting of regionally stagnant ice (e.g. Flint, 1928; Brennand, 2000) is unlikely to be applicable to all eskers. Although in a study of the Bedshiel Kames, Scotland, Evans *et al.* (2006) suggested the esker (which has an irregular morphology) may have been formed during a single event, such studies are largely neglected when it comes to interpreting Laurentide esker systems. It is likely that eskers are polygenetic landforms, but the importance of high-magnitude jökulhlaups during the development of some eskers needs further investigation.

## 8.8 Summary

Synthesis of the data sets collected at Skeiðarárjökull and Bering Glacier has enabled assessment of the hydrological (conduit geometry, flow conditions), glaciological (jökulhlaup type, subglacial topography, structural wekanesses within the ice) and sedimentary (sediment supply) controls on the sedimentary architecture of eskers deposited during high-magnitude jökulhlaups, thus fulfilling the overall aim of this thesis, set out in *Chapter 1*. This has added considerable information to the previous understanding of the controls on esker sedimentary architecture presented in Table 2.2 (Table 8.2), with new mechanisms being identified, as well as allowing reassement of some previous concepts. In addition, the identification of similar depositional stages and architectures between the eskers at Skeiðarárjökull and Bering Glacier suggest diagnostic criteria that may be used in future palaeo-esker studies to identify eskers that were generated during jökulhlaups (Table 8.3).

# Chapter 9

# Conclusions

## 9.1 Introduction

The overall aim of this research was to identify the hydrological, glaciological and sedimentary controls on the sedimentary architecture of single event eskers, produced during high-magnitude jökulhlaups. To address this aim the project has:

1. Established the controls on conduit location and geometry during the November 1996 Skeiðarárhlaup.
2. Developed an evolutionary model for the controls on the sedimentary architecture of the November 1996 Skeiðarárhlaup esker and ice-walled canyon fill.
3. Developed evolutionary models for the controls on the sedimentary architecture of the July-August and October 1994 Bering Glacier outburst floods ice-walled canyon fill and esker.
4. Compared the sedimentary architecture and depositional history of the 1996 Skeiðarárhlaup and 1994 Bering Glacier outburst flood eskers and ice-walled canyon fills.
5. Identified diagnostic criteria for identifying palaeo-eskers generated by high magnitude jökulhlaups.

This chapter will summarise the key findings of this project related to each of the research objectives above, before suggesting future work (*Section 9.9*), highlighting issues beyond the scope of this project.

## 9.2 Objective 1: Controls on Conduit Location and Geometry during the November 1996 Skeiðarárhlaup

Over 2.5 km of GPR line were collected at Skeiðarárjökull, up-glacier from an englacial esker that is emerging from the glacier margin. In general, the pervasiveness of near-surface debris filled structure, coupled with the temperate ice environment made for poor radar conditions. In lines closest to where the esker is emerging from the glacier margin, however, 'zones' of englacial reflections could be identified. These englacial reflections are interpreted as esker material, the base of which are defined by a sub-horizontal reflection that is interpreted as a sediment-rich planar surface, possibly associated with a 1991 surge-related plane of décollement. Jökulhlaup waters were

discharged along this pre-existing structure to form an englacial conduit. Whilst the importance of structural control upon glacial hydrology is not new, this study provides the first direct observation of the importance of structure for the development of primary conduit outlets during a jökulhlaup. Results from these GPR surveys have shown the importance of structural weaknesses for both the development and location of conduits and, consequently, englacial esker deposition during a single high-magnitude jökulhlaup, through an overdeepened basin.

This adds to the growing body of literature that has presented evidence for the crucial role structure can play upon conduit location and development (e.g. Roberts *et al.*, 2002; Fountain *et al.*, 2005a, 2005b; Gulley and Benn, 2007). This may bring into question the traditional views of the controls on water routing through glaciers that have been used to understand the location and morphology of eskers, as well as reconstruct the surface slope of former ice sheets (Hooke and Fastook 2007). Coupled with the recent acknowledgement that structural control is important in steady state and jökulhlaup scenarios, it is imperative that the significance of structural controls on glacial hydrology be considered when interpreting esker systems generated during previous glaciations.

### 9.3 Objective 2: Controls on the Sedimentary Architecture of the November 1996 Skeiðarárhlaup Esker and Ice-walled Canyon Fill

The linearly rising November 1996 Skeiðarárhlaup was associated with high water pressures, allowing floodwaters to be discharged through englacial and supraglacial outlets. Sudden cavity generation and ice excavation resulted in rapid conduit development and consequent high sedimentation rates. As the conduit developed quickly in response to swiftly rising discharge, the depositional environment evolved rapidly to accommodate the increasing discharge through primary outlets. Consequently, conduit geometry was a fundamental control on the sedimentary architecture of the esker, with the system being divided into four key areas:

1. *Up-flow esker* where sedimentation took place within a conduit enlargement.
2. *Down-flow esker* where deposition was within relatively constricted flows.
3. *Proximal supraglacial ice-walled canyon* where the sedimentary architecture was controlled by headward conduit unroofing due to vertical conduit growth.
4. *Central supraglacial ice-walled canyon* where sediments were deposited within an ice-walled canyon excavated due to ice block removal from intensely fractured ice.

Esker genesis took place during the mid-rising to mid-waning stages of the jökulhlaup. This constrains esker sedimentation into a very short period of time (17-24 hours) resulting from the rapid hydrological response to transient floodwater input. During the

rise to peak discharge the glacial hydrological system was forced to create new outlets in response to a discharge that could not be accommodated by perennial outlets alone. Although rapid sedimentation rates have been inferred for some eskers deposited during previous glaciations (e.g. Allen, 1971; Brennand, 1994; Mokhtari Fard, 2001; Fiore *et al.*, 2002; Mäkinen, 2003), this is the first study of an esker with a well constrained depositional timescale.

## 9.4 Objective 3: Controls on the Sedimentary Architecture of the 1994 Bering Glacier Outburst Floods, Esker and Ice-walled Canyon Fill

The October 1994 outburst flood discharged from a subglacial conduit across Weeping Peat Island. The high pressures associated with passage of the erosive floodwaters locally enlarged the conduit, which became infilled with antidune sets deposited by the supercritical flows. Subsequent partial erosion of these antidune sets and the surrounding glacier ice created an enlarged conduit at the proximal end of the cavity. This became infilled with backset bedded sediments, which aggraded in an up-flow direction before foresets prograded on the lee-side of the macroform, analogous to composite macroform development identified in eskers deposited in North America and Europe during the last glaciation (Brennand, 1994; Brennand and Shaw, 1996; Brennand, 2000; Fiore *et al.*, 2002). Down-flow the conduit was narrower and upper-stage plane beds were deposited by the constricted flows.

The ice-walled canyon fill was generated during a documented outburst flood in July-August 1994. Sedimentation initially took place within a pressurised englacial conduit, which gradually unroofed due to vertical conduit growth, becoming a supraglacial ice-walled canyon. The final stages of deposition took place subaerially and were analogous to the development of a prograding bar-form, but closure of the canyon during the second phase of the 1993-1995 surge has deformed the upper units of this assemblage. The ice-walled canyon fill was likely to have been generated over a period of eight days, whilst the lack of direct observations for the October 1994 outburst flood has not allowed such a constrained timescale to be applied. The results of this study, however, have shown that the eskers were deposited rapidly, suggesting sedimentation rates were high.

## 9.5 Objective 4: Comparison of the Sedimentary Architecture and Depositional History of the 1996 Skeiðarárhlaup and 1994 Bering Glacier Outburst Floods Eskers and Ice-walled Canyon Fills

Previous models of the controls on esker sedimentary architecture have been unable to constrain a timescale of deposition (e.g. Brennand, 2000) and single events

were often not expected to generate a complex sedimentary architecture. This research from Skeiðarárjökull and Bering Glacier, however, has shown that single high-magnitude jökulhlaups can generate eskers with complex sedimentary architectures on a landform scale. The esker at Skeiðarárjökull is an ~700 m long, slightly sinuous ridge with a maximum cross-sectional area of ~480 $m^2$. The smaller Bering Glacier esker is a relatively straight ~350 m long ridge, with a maximum cross-sectional area of ~240 $m^2$. Although radar elements within both eskers are defined by some unconformities, the Skeiðarárjökull esker is composed of eleven radar elements that change from cross-cutting lenticular elements up-flow, to tabular radar elements that are more continuous through the landform down-flow. In contrast, the Bering Glacier esker is composed of five radar elements that remain continuous and tabular throughout the landform. Within both eskers, the deepest radar elements are dominantly composed of antidunes, suggesting supercritical flow conditions. The greater bedform crest height within the Skeiðarárjökull esker, however, indicates a greater flow depth than within its Bering Glacier counterpart. Resting upon the deepest radar elements of both eskers are elements that show similar down-flow changes in dominant radar facies. At up-flow sections of the eskers there is a downstream transition from backset to foreset bedded sediments, though the presence of unconformities is more common within the Skeiðarárjökull deposits. Down-flow the eskers are dominated by upper-stage plane beds.

The Skeiðarárjökull esker was generated within a pressurised englacial conduit, the geometry and position of which was controlled by pre-existing structural weaknesses within the ice. In contrast, the Bering Glacier esker was deposited within a pressurised subglacial conduit, the position of which was likely to have been primarily controlled by subglacial topography. At both field sites the negative effective pressures, rapid creation of accommodation space, turbulent flows, and relatively high discharges, resulted in the deposition of antidunes within the transitional to supercritical flows. Later, the excavation of older materials and surrounding glacier ice resulted in a non-uniform conduit geometry. At up-flow sections the conduits were enlarged, which was conducive to the deposition of composite macroforms. These composite macroforms developed by vertical and up-glacier conduit growth, with the deposition of backset bedded sediments creating a flow separation on the lee-side of the macroform that forced foreset progradation. Down-flow of the composite macroforms the conduits became geometrically narrow, which increased flow velocities, conducive the deposition of upper-stage plane beds. Whilst a depositional timescale cannot be stringently applied to the esker at Bering Glacier, the Skeiðarárjökull esker is at least twice its size and was deposited more rapidly (<24 hours).

The ice-walled canyon fills at Skeiðarárjökull and Bering Glacier are both slightly sinuous, though that at Skeiðarárjökull is slightly larger. The surveyed section of the ice-

walled canyon fill at Skeiðarárjökull is composed of at least eleven radar elements, compared to the seven radar elements that make up the surveyed section of the Bering Glacier ice-walled canyon fill. In addition, the patterns of radar facies classification are differ between the two landforms. The deepest radar elements within the Skeiðarárjökull ice-walled canyon fill are dominated by antidunes. The lowest radar elements within the Bering Glacier ice-walled canyon fill, however, are dominated by upper-stage plane beds, though these evolve into antidunes within the radar elements directly above. The presence of antidunes and/or upper-stage plane beds in both landforms indicates supercritical flow conditions, though the larger bedform crest height within the Skeiðarárjökull ice-walled canyon fill suggest that flow depths were greater at Skeiðarárjökull. The shallowest radar elements at Skeiðarárjökull and Bering Glacier are very different, however. The portal proximal ice-walled canyon fill at Skeiðarárjökull is dominantly composed of continuous radar elements composed of backset beds that indicated deposition at a flow expansion. Down-flow, the landform is composed of cross-cutting radar elements dominantly classified as upper-stage plane beds. In contrast, the Bering Glacier ice-walled canyon fill is dominated by continuous radar elements composed of foreset beds that indicate deposition within a flow separation.

The ice-walled canyon fills at Skeiðarárjökull and Bering Glacier were initially deposited within englacial conduits that then unroofed to become supraglacial ice-walled canyons, the englacial/supraglacial positions of which are likely to have been controlled by structural weaknesses within the ice. At Skeiðarárjökull, however, conduit deposition was dominated by antidunes, whilst at Bering Glacier initial deposition was dominated by upper-stage plane beds. This suggests that whilst the floodwaters were supercritical, flow velocities were initially higher at Skeiðarárjökull, though the later deposition of antidunes indicates that flow velocities increased, probably as floodwaters became focused upon the western outlet at Bering Glacier. The final phases of deposition took place within subaerial environments as the conduits unroofed due to vertical conduit growth at both field sites. At the proximal end of the ice-walled canyon fill at Skeiðarárjökull, backset beds were deposited at a flow expansion, analgous to an up-flow aggrading expansion bar. In contrast, at Bering Glacier, foreset beds were deposited analogous to a prograding bar-form. Although the ice-walled canyon fills show significant contrast in large-scale sedimentary architecture, the eskers display commonality. On a smaller scale, however, the sedimentary architectures are quite different.

## 9.6 Objective 5: Diagnostic Criteria for Identifying Palaeo-eskers Generated by High-magnitude Jökulhlaups

Synthesis of data sets collected at Skeiðarárjökull and Bering Glacier have identified a number of criteria that can be used to identify jökulhlaup controls on palaeo-esker sedimentary architecture. The consistent presence of antidunes and composite macroforms in the eskers at Skeiðarárjökull and Bering Glacier suggest such features may be diagnostic of jökulhlaup conditions. Both require the discharge of supercritical waters, as well as rapid conduit enlargement to create the hydraulic jump required for backset deposition. Such conditions are unlikely for ablation-controlled scenarios and consequently, they may provide diagnostic criteria that could be used as evidence of jökulhlaup deposits within palaeo-eskers. Indeed, the eskers generated during the November 1996 Skeiðarárhlaup and 1994 Bering Glacier outburst floods demonstrate sedimentary architectures that are similar to descriptions of many Quaternary eskers in previous studies.

On a smaller scale, the clast size may be used to infer the likelihood of a jökulhlaup control. During a high-magnitude jökulhlaup the high stream powers may be conducive to the transportation and deposition of boulders, as took place at both Skeiðarárjökull and Bering Glacier. Maximum clast size within an esker should be used with caution to infer the dominant flow conditions, however, as their presence/absence may be limited by sediment supply constraints. At both Skeiðarárjökull and Bering Glacier there was a distinct lack of fine materials within the eskers, suggesting jökulhlaups are not conducive to their deposition and jökulhlaup eskers are unlikely to contain significant amounts of fine materials. Consequently, when boulders are identified within an esker and there is a distinct lack of fine deposits, these observations together could be used as partial evidence of transience during esker deposition. Although deposits diagnostic of ablation-controlled conditions have yet to be identified, the suite of macroforms and deposits that have been recognized in this study, when observed together may provide strong evidence for jökulhlaup controls during the development of the landform.

It is known that high-magnitude jökulhlaups took place following the Last Glacial Maximum. Recent observations from Antarctica (Wingham *et al.*, 2006) suggest that the large scale movement of water beneath palaeo-ice sheets, such as the Laurentide, was likely. Furthermore, some descriptions of palaeo-esker sedimentary architecture within the literature that are consistent with observations in this research, suggests the influence of jökulhlaups on esker sedimentary architecture during the last glaciation may have been previously understated. Further work is required to resolve this issue.

## 9.7 Controls on the sedimentary architecture of eskers deposited during high-magnitude jökulhlaups

During a high-magnitude jökulhlaup esker sedimentary architecture is controlled primarily by conduit geometry, as well as a complex interaction between the flow conditions and sediment supply. In summary, esker sedimentary architecture during a high-magnitude jökulhlaup is controlled by a complex interaction between hydrological, glaciological and sedimentary factors:

- *Hydrological controls*: conduit geometry is the most fundamental factor governing the large-scale (ridge scale) esker sedimentary architecture. On a smaller scale, however, the sedimentary architecture is controlled by variations in the flow conditions, such as boundary shear stress and stream power.
- *Glaciological controls*: the jökulhlaup release mechanism (jökulhlaup type), coupled with subglacial topography and the presence or absence of structural weaknesses within the ice can control both the depositional position of the esker, as well as its sedimentary architecture.
- *Sedimentary controls*: sediment supply, such as the clast sizes available to the jökulhlaup and whether or not the event is sediment supply limited can influence the erosional potential of jökulhlaup waters, as well as constrain the maximum cross-sectional area of an esker.

During a jökulhlaup, the erosive nature of the floodwaters results in the relatively rapid growth of conduits largely through mechanical process. The earliest deposits are dominated by antidune sets that are testament to the supercritical nature of the floodwaters. As the growing conduit infills rapidly, the sedimentary architecture becomes primarily influenced by the geometry of the conduit. If conduit growth takes place rapidly and is locally enhanced, perhaps due to the presence of structural weaknesses, a confluence of drainage, and hydraulic jacking, conduit enlargements may be created that are associated with a suddenly heightened conduit roof and a reduction in flow velocity. This is conducive to the deposition of backset beds at the site of the velocity reduction. As these macroforms enlarge up-flow, a flow separation is created on the lee-side, which allows the progradation of foresets to result in an architecture consistent with that of a composite macroform.

Whilst the englacial position of an esker can be explained by the presence of structural weaknesses within the ice and an overdeepened bed, the finer details of jökulhlaup esker sedimentary architecture are controlled by the flow conditions of the event. Despite the possibility of great variability in the peak discharge of a jökulhlaup, this is not the fundamental control upon esker sedimentary architecture and scale. Instead,

variations in stream power and boundary shear stress, coupled with sediment supply can explain variations in sedimentary architecture. When stream power and boundary shear stress values are high the pervasiveness of unconformities is greater and the potential for the transport of large clasts (>1 m diameter) is increased. The largest clasts observed in eskers, however, must be used with caution when attempting to infer the magnitude of the jökulhlaup, as the lack of large clasts may be controlled by sediment supply rather than the carrying capacity of the flow. In addition, where flows have a significant erosional potential and sediments are exhausted prior to jökulhlaup termination, the esker size may be restricted due to enhanced excavation of older materials.

### 9.8 Limitations of this Research

Although the large scale sedimentary architecture of the eskers and ice-walled canyon fills at Skeiðarárjökull and Bering Glacier has been imaged effectively, there are some limitations inherent within the GPR data collection and in its interpretation:

1. At both Skeiðarárjökull and Bering Glacier, the presence of collapsed and steep terrain resulted in non-continuous collection of GPR grids along the eskers and ice-walled canyon fills. This has meant that downstream continuity in radar elements could not be identified through the entire landforms and only inferences can be made about depositional ordering through the assemblages.
2. At Skeiðarárjökull the limited extent of sedimentary exposures resulted in minimal collection of ground control lines. Consequently, some sedimentological interpretations could not be directly correlated to sedimentary sequences.
3. The vertical resolution of EM radar techniques (ability to determine reflection position in space and time) is proportional to the frequency and the radar wave velocity through the medium (Neal, 2004). This is important for sedimentological interpretations as it will determine the scale of the sedimentary structure that can be observed. For data collected on the esker and ice-walled canyon fills at Skeiðarárjökull and Bering Glacier, the minimum bed thickness that could be imaged with 200 MHz antennae was in the order of ~0.1 m. Consequently, small-scale sedimentary structure could not be identified, which can explain the presence of zones of less distinct reflections, as well as lack of observed internal structure within antidune (or dune) sets.
4. Although this study has given a unique insight into the rates and processes of esker formation during documented jökulhlaups and is the best data set available, the extent of interpretations about timescale and flow conditions is still limited. This is because direct observations of conduit geometry and flow velocity were not made. These limitations make the rates of individual radar element deposition difficult to calculate.

Indeed the presence of unconformities that divide the radar elements is indicative of periods of erosion, for which the timescale is unknown.

5. There are currently few published GPR studies of Quaternary eskers, which makes direct comparison of the data collected from Skeiðarárjökull and Bering Glacier with Quaternary sediments difficult. Furthermore, a significant number of published esker research papers are largely based upon morphological observations that cannot be directly compared to GPR studies of sedimentary architecture.
6. The lack of observation of esker sedimentary processes during ablation-controlled seasonal conditions makes it difficult to fully develop a model that can be used to differentiate between jökulhlaup and seasonal controls in palaeo-eskers.

Although some of these limitations are inherent in the use of GPR to investigate sedimentary architecture, others could be remedied by further research.

### 9.9 Suggestions for Future Work

Although the findings of this research have identified the controls on jökulhlaup esker sedimentary architecture and established diagnostic morpho-sedimentary criteria that may be used as evidence for jökulhlaup controls on palaeo-esker sedimentary architecture, the following research areas need to be addressed:

1. This research has focused upon the sedimentary architecture of contemporary eskers formed at Skeiðarárjökull and Bering Glacier. GPR data needs to be collected at palaeo-eskers in North America and Europe in order to allow direct comparisons to be made between the findings of this research and a suite of Quaternary eskers. This will expand the findings of this research by allowing further assessment of the suitability of the contemporary eskers at Skeiðarárjökull and Bering Glacier as analogues for palaeo-esker deposition. Establishing the distribution of jökulhlaup signatures, such as composite macroforms, is crucial to gauging the role of jökulhlaups in palaeo-esker genesis. In eskers where no criteria for jökulhlaup deposition can be identified, these may be assumed to have been controlled by seasonal drainage patterns. Where this is the case, it may allow the identification of diagnostic criteria for seasonally controlled eskers and the development of a model that can be used to identify the controls on palaeo-esker sedimentary architecture. If jökulhlaup and ablation-controlled eskers can be distinguished and restricted to certain morphological types, regional scale studies may be undertaken to assess the distribution of esker types. It is already known that in North America, individual esker types can be generally found in restricted areas/zones (Brennand, 2000). By understanding their mode of deposition it will be possible to assess/reassess the dynamics of palaeo-ice sheets on a regional scale.

2. Following the early view that antidunes within eskers indicated deposition at atmospheric pressure (Banerjee and McDonald, 1975), it has been argued they can also be deposited under full-pipe conditions (c.f. Brennand, 2000) and this research goes further to suggest their presence in eskers may be indicative of jökulhlaup deposition. Unfortunately, our understanding of the flow conditions required for their formation under full-pipe conditions is limited. Flume experiments and field studies have been restricted to subaerial scenarios and future experiments need to identify the flow conditions required for antidune deposition in a pressurised conduit of irregular geometry. If this issue can be addressed, this may allow further refinement of the initial conditions that take place during the earliest phase of conduit development during high-magnitude jökulhlaups and allow a more detailed insight into esker deposition during such events.
3. In light of the findings of this research it would be beneficial to model jökulhlaup flow conditions in order to correlate critical thresholds of boundary shear stress and stream power with the associated sedimentary architecture. Although this was beyond the scope of the current study, a more detailed knowledge of the flow conditions during high-magnitude jökulhlaups will allow further refinement of the controls on jökulhlaup esker sedimentary environments.
4. The presence of buried ice beneath the esker at Skeiðarárjökull brings into question its preservation potential. Woodward *et al.* (2008) have used GPR to identify structures within the ice-walled canyon fill at Skeiðarárjökull associated with the reworking of these materials through melting of supporting ice walls and/or buried ice. Repeat surveys of GPR lines on the esker and ice-walled canyon fill at Skeiðarárjökull, coupled with airborne and ground-based LIDAR surveys will allow changes in the landforms through time to be identified. Models for the post-depositional development of englacial eskers as the buried ice melts out may be developed, shedding further light on the direct applicability of the esker as an analogue for palaeo-esker genesis.
5. The 200 MHz antennae used in sedimentary architecture investigations for this research, whilst providing a good compromise between resolution and penetration depth, could only image beds of >0.1 m thickness. Repeat surveys of GPR lines on the landforms at a higher frequency (e.g. 450 MHz), whilst reducing penetration depth, would allow sedimentary structures at the lamina scale to be imaged at the near surface. This will give some insight into the small-scale structures within beds that were poorly resolved with the 200 MHz antennae.
6. The lack of ground-truthing has meant some sedimentary interpretations could not be verified. Consequently, future work may focus upon radar facies verification through more detailed sediment section logging and descriptions.

# References


Alexander, J. and Fielding, C. (1997), Gravel antidunes in the tropical Burdekin River, Queensland, Australia, *Sedimentology*, **44**, 327-337.

Alexander, J., Bridge, J.S., Cheel, R.J. and Leclair, S.F. (2001), Bedforms and associated sedimentary structures formed under supercritical water flows over aggrading sand beds, *Sedimentology*, **48**, 133-152.

Allen, J.R.L. (1971), A theoretical and experimental study of climbing-ripple cross-lamination, with a field application to the Uppsala esker, *Geografiska Annaler*, **53A**, 157-187.

Allen, J.R.L. (1984), *Sedimentary Structures: Their Character and Physical Basis*, Vol. 2., Elsevier, Amsterdam.

Allen, J.R.L. (1992), *Principles of Physical Sedimentology*, London, Chapman & Hall.

Annan, A.P. (2002), GPR – history, trends, and future developments. *Subsurface Sensing Technologies and Applications*, **3**(4), 253-270.

Arcone, S.A. (2002), Airborne-radar stratigraphy and electrical structure of temperate firn: Bagley Ice Field, Alaska, U.S.A., *Journal of Glaciology*, **48**(161), 317-334.

Arcone, S.A., Lawson, D.E. and Delaney, A.J. (1995), Short-pulse radar wavelet recovery and resolution of dielectric constrasts within englacial and basal ice of Matanuska Glacier, Alaska, U.S.A. *Journal of Glaciology*, **41**(137), 68-86.

Arendt, A.A., Echelmeyer, K.A., Harrison, W.D., Lingle, C.S. and Valentine, V.B. (2002), Rapid wastage of Alaska Glaciers and their contribution to rising sea level, *Science*, **297**, 382-386.

Auton, C. (1992), Scottish landform examples – 6: The Flemington eskers, *Scottish Geographical magazine*, **108**, 190-196.

Aylsworth, J.M. and Shilts, W.W. (1989), Bedforms of the Keewatin ice sheet, Canada, *Sedimentary Geology*, **62**, 407-428.

Baker, V.R. (1973), Paleohydrology and sedimentology of lake Missoula flooding Eastern Washington, *Geological Society of America*, Special Paper, **144**, 79.

Baker, V.R. and Costa, J.E. (1987), Flood power, *In*: Mayer, L., Nash, D. (Eds.), *Catastrophic Flooding*, Allen and Unwin, London, 1-25

Bakker, M.A.J. and van der Meer, J.J.M. (2003), Structure of a Pleistocene push moraine revealed by GPR: the eastern Veluwe Ridge, The Netherlands: *In*: Ground Penetrating Radar in Sediments, Bristow, C.S. and Jol, H.M. (eds.), *Geological Society of London*, Special Publication, **211**, 143-151.

Banerjee, I. and McDonald, B.C. (1975), Nature of esker sedimentation, *In*: Jopling, A.V., McDonald, B.C., (Eds.), *Glaciofluvial and Glaciolacustrine Sedimentation*. Society of Economic Palaeonologists and Mineralogists. Special Publication, **23**, 304-320.

Bell, R.E. (2008), The role of subglacial water in ice-sheet mass balance, *Nature Geoscience*, **1**, 297-304.

Benn, D.I. and Evans, D.J.A. (1998), *Glaciers and Glaciation*, London, Arnold.

Benn, D.I. and Lukas, S. (2006), Younger Dryas glacial landsystems in North West Scotland: an assessment of modern analogues and palaeoclimatic implications, *Quaternary Science reviews*, **25**, 2390-2408.

Bennett, M.R. and Huddart, D. (2007), Models of esker formation involving supraglacial sandurs: examples from Svalbard and Scotland, *Geological Society of America Abstracts with programs*, **39**(6), 118.

Bennett, M.R., Huddart, D. and Waller, R.I. (2000), Glaciofluvial crevasse and conduit fills as indicators of supraglacial dewatering during a surge, Skeiðarárjökull, Iceland, *Journal of Glaciology*, **46**(152), 25-34.

Bennett, M.R., Hambrey, M.J., Huddard, D. and Ghienne, J.F. (1996), The formation of geometrical ridge networks ('crevasse-fill' ridges), Kongsvegen, Svalbard, *Journal of Quaternary Science*, **11**(6), 437-449.

Björnsson, H. (1980), Glaciers in Iceland, *Jökull*, **29**, 74-80.
Björnsson, H. (1992), Jökulhlaups in Iceland: prediction, characteristics and simulation, *Annals of Glaciology*, **16**, 95-106.
Björnsson, H. (1998), Hydrological characteristics of the drainage system beneath a surging glacier, *Nature*, **395**, 771-774.
Björnsson, H. (2002), Subglacial lakes and jökulhlaups in Iceland, *Global Planetary Change*, **35**, 255-271.
Björnsson, H., Pálsson, F. and Magnússon, E. (1999), Skeiðarárjökull: landslag og rennslisleiðir vatns undir sporði, *Raunvísindastofnun Háskólans*, RH-11-99.
Björnsson, H., Pálsson, F., Sigurðsson, O. and Flowers, G.E. (2003), Surges of glaciers in Iceland, *Annals of Glaciology*, **36**, 82-90.
Boulton, G.S. (1987) A theory of drumlin formation by subglacial sediment deformation, *In*: Menzies, J. and Rose, J. (eds.), *Drumlin Symposium*, Rotterdam, 25-79.
Boulton, G.S., Lunn, R., Vidstrand, P. and Zatsepin, S. (2007a), Subglacial drainage by groundwater-channel coupling, and the origin of esker systems: Part 1 – glaciological observations, *Quaternary Science Reviews*, **26**, 1067-1090.
Boulton, G.S., Lunn, R., Vidstrand, P. and Zatsepin, S. (2007b), Subglacial drainage by groundwater-channel coupling, and the origin of esker systems: Part II – theory and simulation of a modern system, *Quaternary Science Reviews*, **26**, 1091-1105.
Boulton, G.S., Caban, P.E., Gijssel, K. van, Leijnse, A., Punkari, M. and Weert, F.H.A. van (1996), The impact of glaciation on the groundwater regime of Northwest Europe, *Global and Planetary Change*, **12**, 397-413.
Brennand, T.A. (1994), Macroforms, large bedforms and rhythmic sedimentary sequences in subglacial eskers, south-central Ontario: implications for esker genesis and meltwater regime, *Sedimentary Geology*, **91**, 9-55.
Brennand, T.A. (2000), Deglacial meltwater drainage and Glaciodynamics: inferences from Laurentide eskers, Canada, *Geomorphology*, **32**, 263-293.
Brennand, T.A. (2007), Laurentide esker types: their geomorphic elements and sedimentary assemblages, *Geological Society of America Abstracts with Programs*, **39**(6), 116.
Brennand, T.A. and Sharpe, D.R. (1993), Ice-sheet dynamics and subglacial meltwater regime inferred from form and sedimentology of glaciofluvial systems: Victoria Island, District of Franklin, Northwest Territories, *Canadian Journal of Earth Sciences*, **30**, 928-944.
Brennand, T.A. and Shaw, J. (1994), Tunnel Channels and associated landforms, south-central Ontario: their implications for ice-sheet hydrology, *Canadian Journal of Earth Sciences*, **31**, 505-522.
Brennand, T.A. and Shaw, J. (1996), The Harricana glaciofluvial complex, Abiti region, Quebec: its genesis and implications for meltwater regime and ice-sheet dynamics, *Sedimentary Geology*, **102**, 221-262.
Brennand, T.A., Russell, H.A.J. and Sharpe, D.R. (2006), Tunnel channel character and evolution in central southern Ontario, *In*: Knight, P.G. (Ed.), *Glacier Science and Environmental Change*, 37-39.
Busby, J.P. and Merritt, J.W. (1999), Quaternary deformation mapping with ground-penetrating radar, *Journal of Applied Geophysics*, **41**, 75-91.
Calkin, P.E., Wiles, G.C. and Barclay, D.J. (2001), Holocene coastal glaciation of Alaska, *Quaternary Science Reviews*, **20**, 449-461.
Carling, P.A. (1999), Subaqueous gravel dunes, *Journal of Sedimentary Research*, **69**(3), 534-545.
Carling, P.A. and Shvidchenko, A.B. (2002), A consideration of the dune:antidune transition in fine gravel, *Sedimentology*, **49**, 1269-1282.
Carling, P.A., Kirkbride, A.D., Parnachov, S., Borodavko, P.S. and Berger, G.W. (2002), Late Quaternary catastrophic flooding in the Alti Mountains of south-central Siberia: a synoptic overview and an introduction to flood deposit sedimentology, *In*: Martini, I.P., Baker, V.R., Garzón, G. (Eds.), *Flood and Megaflood Processes and Deposits: Recent and Ancient Examples*, Special Publication of the International Association of Sedimentologists, **32**, 17-35.

Carlson, P.R., Molnia, B.F. and Post, A. (1993), Pre-Holocene and Holocene erosional and depositional history of Bering Trough and Vitus lake, Bering Glacier, Alaska, *EOS*, **74**(43), Supplement, 292.

Carrivick, J.L., Pringle, J.K., Russell, A.J. and Cassidy, N.J. (2007), GPR-derived sedimentary architecture of outburst flood sedimentation within a bedrock valley system, Hraundalur, Iceland, *Journal of Environmental and Engineering Geophysics*, **12**(1), 127-143.

Cassidy, N.J., Russell, A.J., Marren, P.M., Fay, H., Knudsen, Ó., Rushmer, E.L. and van Dijk, T.A.G.P. (2003), GPR derived architecture of November 1996 jökulhlaup deposits, Skeiðarársandur, Iceland, *In*: Bristow, C.S. and Jol. H.M. (Eds.), *Ground Penetrating Radar in Sediments*, Geological Society London, Special Publications, **211**, 153-166.

Cheel, R.J. (1982), The depositional history of an esker near Ottawa, Canada, *Canadian Journal of Earth Sciences*, **19**, 1417-1427.

Clague, J.J. and Matthews, W.H. (1973), The magnitude of jökulhlaups, *Journal of Glaciology*, **12**, 501-504.

Clague, J.J., Barendregt, R., Enknin, R.J. and Foit, F.F. (2003), Paleomagnetic and tephra evidence for tens of Missoula floods in southern Washington, *Geology*, **31**, 247-250.

Clark, C.D. (1993) Mega-scale lineations and cross-cutting ice-flow landforms, *Earth Surface Processes and Landforms*, **18**, 1-29.

Clark, P.U. and Walder, J.S. (1994), Subglacial drainage, eskers, and deforming beds beneath the Laurentide and Eurasian ice sheets, *Geological Society of America Bulletin*, **106**, 304-314.

Clarke, G.K.C. (1982), Glacier outburst floods from "Hazard Lake", Yukon Territory, and the problem of flood magnitude and prediction, *Journal of Glaciology*, **28**, 3-21.

Clarke, G.K.C. (2003), Hydraulics of subglacial outburst floods: new insights from the Spring-Hutter formulation, *Journal of Glaciology*, **49**(165), 299-313.

Clarke, T.S. and Bentley, C.R. (1994), High-resolution radar on Ice Stream B2, Antarctica: measurements of electromagnetic wave speed in firn and strain history from buried crevasses, *Annals of Glaciology*, **20**, 153-159.

Clarke, G.K.C., Collins, S.G. and Thompson, D.E. (1984), Flow, thermal structure and subglacial conditions of a surge-type glacier, *Canadian Journal of Earth Science*, **21**, 232-240.

Collinson, J.D., Mountney, N.P. and Thompson, D.B. (2006), *Sedimentary Structures*, Third Edition, Terra Publishing, England.

Cook, J.C. (1960), Proposed mono-cycle very-high-frequency radar for air-borne snow and ice measurement, *Transaction of the American Institution for Electrical Engineering*, **79(1)**, 588-594.

Daniels, D.J. (1996), Surface-penetrating radar, *IEE Radar, Sonar, Navigation and Avionics*, Series **6**.

Daniels, D.J., Guton, D.J. and Scott, H.F. (1988), Introduction to subsurface radar, *IEE Proceedings*, **135**(F4), 278-305.

Davies, G.L. (1970), Richard Prior's 1969 description of an Irish esker, *Journal of Glaciology*, **9**(55), 147-148.

Davis, J.L. and Annan, A.P. (1989), Ground-penetrating radar for high-resolution mapping of soil and rock stratigraphy, *Geophysical Prospecting*, **37**, 531-551.

Davis, J.L., Hallifay, J.S. and Miller, K.J. (1973), Radio echo sounding on a valley glacier in east Greenland, *Journal of Glaciology*, **12**(64), 87-91.

Delaney, C. (2001), Esker formation and the nature of deglaciation: the Ballymohon esker, Central Ireland, *North West Geography*, **1**(2), 23-33.

Delaney, C. (2002), Sedimentology of a glaciofluvial landsystem, Lough Ree area, Central Ireland: implications for ice margin characteristics during Devensian deglaciation, *Sedimentary Geology*, **149**, 111-126.

Delaney, C.A. (2007), Sedimentology of esker systems and associated landforms in the Irish Midlands: processes, controls and implications for facies models, *Geological Society of America Abstracts with programs*, **39**(6), 118.

Duller, R.A., Mountney, N.P., Russell, A.J. and Cassidy, N.C. (2007), Architectural analysis of a volcaniclastic jökulhlaup deposit, southern Iceland: sedimentary evidence for supercritical flow, *Sedimentology*, doi: 10.1111/j.1365-3091.2007.00931.x.

Evans, D.J.A. and Rea, B.R. (1999), Geomorphology and sedimentology of surging glaciers: a land-systems approach, *Annals of Glaciology*, **28**, 75-82.

Evans, D.J.A., Clark, C.D. and Mitchel, W.A. (2005), The last British Ice Sheet: a review of the evidence utilised in the compilation of the Glacial Map of Britain, *Earth-Science Reviews*, **70**, 253-312.

Evans, D.J.A., Lemmen, D.S. and Rea, B.R. (1999), Glacial landsystems of the southwest Laurentide Ice Sheet: modern Icelandic analogues, *Journal of Quaternary Science*, **14**, 673-679.

Evans, D.J.A., Wilson, S.B. and McGregor, D.F. (2006), Scottish landform example 37: 'The Kaims' of Bedshiel, *Scottish Geographical Journal*, **122**(1), 79-83.

Everest, J. and Bradwell, T. (2003), Buried ice in southern Iceland and its wider significance, *Geomorphology*, **52**, 347-358.

Fatland, D.R. and Lingle, C.S. (1998), Analysis of the 1993-95 Bering Glacier (Alaska) surge using differential SAR inferometry, *Journal of Glaciology*, **44**(148), 532-546.

Fay, H. (2002a), Formation of kettle holes following a glacial outburst flood (jökulhlaup) Skeiðarársandur, southern Iceland, *In*: Snorrason, Á. (Ed.), *Extremes of the Extremes: Extraordinary Floods*, Proceedings of a symposium held in Reykjavik, July 2000, International Association of Hydrological Sciences, Special Publication, **271**, 205-210.

Fay, H. (2002b), The formation of ice block obstacle marks during the November 1996 glacier outburst flood (jökulhlaup), Skeiðarársandur, Iceland, *In:* Martini, I.P., Baker, V.R. and Garzon, G. (Eds.), *Flood and Megaflood Deposits: Recent and Ancient*, Special publication of the International Association of Sedimentologists, **32**, 85-97.

Fiore, J., Pugin, A. and Beres, M. (2002), Sedimentological and GPR studies of subglacial deposits in the Joux Valley (Vaud, Switzerland): backset accretion in an esker followed by an erosive jökulhlaup, *Géographie physique et Quaternaire*, **56** (1), 19-32.

Fisher, T.G., Jol. H.M. and Boudreau, A.M. (2005), Saginaw lobe tunnel channels (Laurentide Ice Sheet) and their significance in south-central Michigan, USA, *Quaternary Science Reviews*, **24**, 2375-2391.

Fleisher, P.J., Bailey, P.K. and Cadwell, D.H. (2003), A decade of sedimentation in ice-contact, proglacial lakes, Bering Glacier, AK, *Sedimentary Geology*, **160**, 309-324.

Fleisher, P.J., Cadwell, D.H. and Muller, E.H. (1998), Tsivat Basin conduit system persists through two surges, Bering Piedmont Glacier, Alaska, *Geological Society of America Bulletin*, **110**(7), 877-887.

Fleisher, P.J., Bailey, P.K. and Natel, E.M. (2006a), Outburst floods at Bering Glacier, Alaska, *Geological Society of America Abstracts with Programs*, **38**(2), 17.

Fleisher, P.J., Franz, J.M. and Gardner, J.A. (1993), Bathymetry and sedimentary environment in proglacial lakes at the eastern Bering Piedmont Glacier, Alaska, *Journal of Geological Education*, **41**, 267-274.

Fleisher, P.J., Lachniet, M.S, and Muller, E.H. (2002), 'Substrate deformation attributed to overriding ice, Bering Glacier, Alaska', *Quaternary Stratigraphy and the Glacial Environments: In Honour of Ernest H. Muller*, Denver Annual Meeting (October 27-30, 2002), Colorado Convention Centre, Geological Society of America.

Fleisher, P.J., Lachniet, M.S., Muller, E.H. and Bailey, P.K. (2006c), Subglacial deformation of trees within overridden foreland strata, Bering Glacier, Alaska, *Geomorphology*, **75**, 201-211.

Fleisher, P.J., Muller, E.H., Peteet, D.M. and Lachniet, M.S. (1999), Arctic Enigma: was Alaska's Late Pleistocene Bering Glacier really out of step with its neighbours? New terrestrial evidence suggests otherwise, *Geotimes*, **44**, 16-21.

Fleisher, P.J., Russell, A.J., Bailey, P.K. and Natel, E.S. (2007), An outburst esker, eastern sector, Being Glacier, Alaska, *Geological Society of America Abstracts with Programs*, **39**(6), 117.

Fleisher, P.J., Bailey, P.K., Natel, E.M., Cadwell, D.H., and Muller, E.H. (2006b), Events associated with the 1993-95 surge and outburst floods, Bering Glacier, Alaska, *Geological Society of America Abstracts with Programs*, **38**(5), 72.

Fleisher, P.J., Bailey, P.K., Natel, E.M., Miller, J.R. and Tracy, M.W. (2005), Post-surge field measurements of ablation and retreat, eastern sector, Bering Glacier, Alaska, *Geological Society of America Abstracts with Programs*, **37**(7), 423.

Fleisher, P.J., Russell, A.J., Bailey, P.K., Natel, E.M., Tweed, F.S. and Harris, T.D. (2004), Impacts of glacier surges and jökulhlaups at two large temperate outlet glaciers: Bering glacier, Alaska and Skeiðarárjökull, Iceland, *Geological Society of America Abstracts with Programs*, **36**(5), 67.

Flint, R.F. (1928), Eskers and crevasse fillings, *American Journal of Science*, **15-16**, 410-416.

Flint, R.F. (1930), The origin of the Irish eskers, *Geographical Review*, **20**, 615-630.

Flowers, G.E., Björnsson, H. and Pálsson, F. (2003), New insights into the subglacial and periglacial hydrology of Vatnajökull, Iceland, from a distributed physical model, *Journal of Glaciology*, **49**(165), 257-270.

Flowers, G.E., Björnsson, H., Pálsson, F. and Clarke, G.K.C. (2004), A coupled sheet-conduit mechanism for jökulhlaup propagation, *Geophysical Research Letters*, **31**, LO5401,doi:10.1029/2003GL0198088.

Fountain, A.G. (1994), Borehole water-level variations and implications for the subglacial hydraulics of South Cascade Glacier, Washington State, U.S.A., *Journal of Glaciology*, **40**(135), 293-304.

Fountain, A.G. (2007), Hydraulic processes in subglacial conduits, *Geological Society of America Abstracts with programs*, **39**(6), 116.

Fountain, A.G. and Walder, J.S. (1998), Water flow through temperate glaciers, *Reviews of Geophysics*, **36**, 299-328.

Fountain, A.G., Jacobel, R.W., Schlichting, R. and Jansson, P. (2005a), Fractures as the main pathways of water flow in temperate glaciers, *Nature*, **433**, 618-621.

Fountain, A.G., Schlichting, R.B., Jansson, P. and Jacobel, R.W. (2005b), Observations of englacial water passages: a fracture-dominated system, *Annals of Glaciology*, **40**, 25-30.

Fowler, A.C. (1999), Breaking the seal at Grímsvötn, Iceland, *Journal of Glaciology*, **45**(151), 506-516.

Fricker, H.A., Scambos, T., Bindschadler, R. and Padman, L. (2007), An active subglacial water system in West Antarctica mapped from space, *Science*, **315**, 1544-1548.

Glasser, N., Goodsell, B., Copland, L. and Lawson, W. (2006), Debris characteristics and ice-shelf dynamics in the ablation region of the McMurdo Ice Shelf, Antarctica, *Journal of Glaciology*, **52**(177), 223-234.

Glasser, N., Hambrey, M.J., Crawford, K.R., Bennett, M.R. and Huddart, D. (1998), The structural glaciology of Kongsvegen, Svalbard, and its role in landform genesis, *Journal of Glaciology*, **44**(146), 136-148. (Erratum: **46**(154), 2000, p538)

Glasser, N.F., Hambrey, M.J., Etienne, J.L., Jansson, P. and Pettersson, R. (2003), The origin and significance of debris charged ridges at the surface of Storglaciären, Northern Sweden, *Geofrafiska Annaler* A, **85A**(2), 127-147.

Glover, J.M. and Rees, H.V. (1992), Radar investigations of firn structures and crevasses, *In*: Ground Penetrating Radar, J. Pilon (Ed.), *Geological Survey of Canada*, Paper **90-4**, 75-84.

Goodsell, B., Hambrey, M.J. and Glasser, N.F. (2002), Formation of band and associated structures at Bas Glacier d'Arolla, Valais, Switzerland, *Journal of Glaciology*, **48**(161), 287-299.

Gorrell, G. and Shaw, J. (1991), Deposition in an esker, bead and fan complex, Lanark, Ontario, Canada, *Sedimentary Geology*, **72**, 285-314.

Grasby, S.E. and Chen, Z. (2005), Subglacial recharge into the Western Canada Sedimentary Basin – Impact of Pleistocene glaciation on basin hydrodynamics, *Geological Society of America Bulletin*, **117**(3-4), 500-514.

Gravenor, C.P. and Kupsch, W.O. (1959), Ice disintegration features in western Canada. *Journal of Geology*, **67**, 48-64.

Gray, J.M. (1997), The origin of the Blakeney esker, Norfolk, *Proceedings of the Geologists Association*, **108**, 177-182.

Gray, L., Joughin, I., Tulaczyk, S., Spikes, V.B., Bindschadler, R. and Jezek, K. (2005), Evidence for subglacial water transport in the West Antarctic Ice Sheet through three-dimensional satellite radar interferometry, *Geophysical Research Letters*, **32**, L0351, doi: 10.1029/2004GL021387.

Grimm, R.P. and Auton, W.J. (2007), Constructional lithofacies geometry of a subaqueous esker delta complex as a control on the evolution of sediment body porosity and permeability, *Geological Society of America Abstracts with programs*, **39**(6), 118.

Gudmundsson, H.J. (1997), A review of the Holocene environmental history of Iceland, *Quaternary Science Reviews*, **16**, 81-92.

Guðmundsson, M.T. (2005), Subglacial volcanic activity in Iceland, *In*: Caseldine, C., Russell, A., Harðardóttir, J. and Knudsen, Ó (Eds.), *Iceland – Modern Processes and Past Environments*, Developments in Quaternary Science, **5**, 241-255.

Guðmundsson, M.T., Bonnel, A. and Gunnarsson, K. (2003), Seismic soundings of sediment thickness on Skeiðarársandur, SE-Iceland, *Jökull*, **51**, 53-64.

Gulley, J. and Benn, D.I. (2007), Structural control of englacial drainage systems in Himalayan debris-covered glaciers, *Journal of Glaciology*, **53** (182), 399-412.

Hambrey, M.J., Dowdeswell, J.A., Murray, T. and Porter P.R. (1996), Thrusting and debris entrainment in a surging glacier: Bakaninbreen, Svalbard, *Annals of Glaciology*, **22**, 241-248.

Hambrey, M.J., Bennett, M.R., Dowdeswell, J.A., Glasser, N.F. and Huddard, D. (1999), Debris entrainment and transfer in polythermal valley glaciers, *Journal of Glaciology*, **45**(149), 69-86.

Harrison, C.H. (1970), Reconstruction of subglacial relief from radio echo sounding records, *Geophysics*, **35**(6), 1099-1115.

Hebrand, M. and Åmark, M. (1989), Esker formation and glacier dynamics in eastern Skåne and adjacent areas, southern Sweden, *Boreas*, **18**, 67-81.

Henderson, P.J. (1988), Sedimentation in an esker system influenced by bedrock topography near Kingston, Ontario, *Canadian Journal of Earth Sciences*, **25**, 987-999.

Herzfeld, U.C. and Mayer, H. (1997), Surge of Bering Glacier and Bagley Ice Field, Alaska: an up-date to August 1995 and an interpretation of brittle deformation patterns, *Journal of Glaciology*, **43**(145), 427-434.

Hock, R. and Hooke, R. LeB. (1993), Evolution of the internal drainage system in the lower part of the ablation area of Storglaciären, Sweden, *Geological Society of America Bulletin*, **105**, 537-546.

Hodge, S.M. (1976), Direct measurement of basal water pressures: a pilot study, *Journal of Glaciology*, **16**(74), 205-218.

Holmlund, P. and Hooke, R.L.B. (1983), High water pressure events in moulins, Storglaciären, Sweden, *Geografiska Annaler*, **65A**, 19-25.

Hooke, R. LeB. (1984), On the role of mechanical energy in maintaining subglacial water conduits at atmospheric pressure, *Journal of Glaciology*, **30**, 180-187.

Hooke, R. LeB. (1989), Englacial and subglacial hydrology: a qualitative review, *Arctic and Alpine Research*, **21**, 221-233.

Hooke, R. LeB. (2007), Quantitative analysis, *Geological Society of America Abstracts with programs*, **39**(6), 116.

Hooke, R. LeB. And Fastook, J. (2007), Thermal conditions at the bed of the Laurentide ice sheet in Maine during deglaciation: implications for esker formation, *Journal of Glaciology*, **53**(183), 646-658.

Hooke, R. LeB., Laumann, T. and Kohler, J. (1990), Subglacial water pressures and the shape of subglacial conduits, *Journal of Glaciology*, **36**, 67-71.

Hooke, R., Miller, S.B. and Kohler, J. (1988), Character of the englacial and subglacial drainage system in the upper part of the ablation area of Storglaciären, Sweden, *Journal of Glaciology*, **34**(117), 228-231.

Hooke, R., Wold, B. and Hagen, J.O. (1985), Subglacial hydrology and sediment transport at Bondhusbreen, southwest Norway, *Geological Society of America Bulletin*, **96**(3), 388-397.

Horne, J. (1923), *The Geology of the lower findhorn and lower Strath Nairn*, Memoir of the Geological Society of Great Britain (Scotland), Edinburgh: HMSO.

Hubbard, A. (2006), The validation and sensitivity of a model of the Icelandic ice sheet, *Quaternary Science Reviews*, **25**, 2297-2313.

Hubbard, B. and Glasser, N, (2005), *Field techniques in glaciology and glacial geomorphology*, Wiley, Chichester, UK.

Hubbard, B. and Nienow, P. (1997), Alpine subglacial hydrology, *Quaternary Science Reviews*, **16**, 939-955.

Hubbard, A., Sugden, D. Dugmore, A., Norddahl, H. and Pétursson, C. H.G. (2006), A modelling insight into the Icelandic Last Glacial Maximum ice sheet, *Quaternary Science Reviews*, **25**, 2283-2296.

Huddart, D., Bennett, M.R. and Glasser, N.F. (1999), Morphology and sedimentology of a high arctic eskers system: Vegbreen, Svalbard, *Boreas*, **28**, 253-273.

Humphrey, N.F. and Raymond, C.F. (1994), Hydrology, erosion and sediment production in a surging glacier: Variegated Glacier, Alaska, 1982-83, *Journal of Glaciology*, **40**, 539-552.

Humphrey, N.F., Raymond, C. and Harrison, W. (1986). Discharges of turbid water during mini-surges of Variegated Glacier, Alaska, *Journal of Glaciology*, **32**(111), 195-207.

Ingólfsson, Ó., Björck, S., Haflidason, H. and Rundgren, M. (1997), Glacial and climatic events in Iceland reflecting regional North Atlantic climatic shifts during the Pleistocene-Holocene transition, *Quaternary Science*, **16**, 1135-1144.

Irvine-Fynn, T.D.L., Moorman, B.J., Williams, J.L.M. and Walter, F.S.A. (2006), Seasonal changes in ground-penetrating radar signature observed at a polythermal glacier, Bylot Island, Canada, *Earth Surface Processes and Landforms,* **31**, 892-909.

Jackobsen, P.R. and Overgaard, T. (2002), Georadar facies and glaciotetconic structures in ice marginal deposits, northwest New Zealand, Denmark, *Quaternary Science Reviews*, **21**, 917-927.

Jaeger, J.M., Nittrouer, C., Scott, N.D. and Milliman, J.D. (1998), Sediment accumulation along a glacially impacted mountainous coastline: north-east Gulf of Alaska, *Basin Research*, **10**, 155-173.

Jiskoot, H. (1999), Characteristics of surge-type glaciers, *Ph.D. Thesis*, University of Leeds, U.K.

Jol, M. and Bristow, C.S. (2003), GPR in sediments: advice on data collection, basic processing and interpretation, a good practice guide, *In*: Bristow, C.S. and Jol, H.M. (Eds.), *Ground Penetrating Radar in Sediments*, Geological Society of London, Special Publications, **211**, 9-27.

Jol, H.M., Comas, X., Slater, L., Fisher, T.G. and Reeve, A. (2007), Ground penetrating radar: a noninvasive, high resolution method for the development of facies models in eskers, *Geological Society of America Abstracts with programs*, **39**(6), 117.

Jopling, A.V. (1965), Laboratory study of the distribution of grain sizes in cross-bedded deposits, *In*: Middleton, G.V. (Ed), *Primary Sedimentary Structures and their Hydrodynamic Interpretation*, Special Pubication, **12**, Society of Economic Paleontologists and Mineralogists, 53–65.

Jopling, A.V. and Richardson, E.V. (1966), Backset bedding developed in shooting flow in laboratory experiments, *Journal of Sedimentary Petrology*, **36**(3), 821-825.

Kamb, B. (1987), Glacier surge mechanism based on linked cavity configuration of the basal water conduit system, *Journal of Geophysical research*, **92**, 9083-9100.

Kamb, B., Raymond, C.F., Harrison, W.D., Englehardt, H., Echelmeyer, K.A., Humphrey, N., Brugman, M.M. and Pfeffer, T. (1985), Glacier surge mechanism: 1982-1983 surge of variegated glacier, Alaska, *Science*, **227**, 469-479.

Kehew, A.E., Kozlowski, A.L., Woolever, C.J. and Barnes, N.A. (2007), Subglacial drainage and aquifer potential: Saginaw Lobe, Michigan, *Geological Society of America Abstracts with programs*, **39**(6), 117.

Kennedy, J.F. (1963), The mechanics of dunes and antidunes in erodible-bed channels, *Journal of Fluid Mechanics*, **16**, 521-544.

King, E.C., Woodward, J. and Smith, A.M. (2004), Seismic evidence for a water-filled canal in deforming till beneath Rutford Ice Stream, West Antarctica, *Geophysical Research Letters*, **31**, L20401, doi:10.1029/2004GL020379.

Kirkbride, M.P. and Spedding, N. (1996), The influence of englacial drainage on sediment-transport pathways and till texture of temperate valley glaciers, *Annals of Glaciology*, **22**, 160-166.

Knight, J. (2002), Bedform patterns, subglacial meltwater events, and late Devensian ice sheet dynamics in north-central Ireland, *Global and Planetary Change*, **35**, 237-253.

Knudsen, Ó. (1995), Concertina eskers, Brúarjökull, Iceland: an indicator of surge-type glacier behaviour, *Quaternary Science Reviews*, **14**, 487-493.

Koteff, C. (1974), The morphological sequence concept and deglaciation of southern New England, *In*: Coates, D.R. (Ed.), *Glacial Geomorphology*, Binghampton, New York, State University of New York, Publications in Geomorphology, 121-144.

Krüger, J. (1983), Glacial morphology and deposits in Denmark, *In*: Ehlers, J., (Ed.), Glacial deposits in north-west Europe: Rotterdam, The Netherlands, A.A. Balkema, 181-192.

Lewis, W.V. (1949), An esker in process of formation: Boverbreen, Jotunheimen, *Journal of Glaciology*, **1**, 314-319.

Lindström, E. (1985), The Uppsala esker: the Asby-Dralinge exposures, *Striae*, **22**, 27-32.

Lindström, E. (1993), Esker enlargements in northern Sweden, *Geografiska Annaler*, **75A**(3), 95-110.

Lingle, C.S., Post, A., Herzfeld, U.C., Molnia, B.F., Krimmel, R.M. and Roush, J.J. (1993), Bering Glacier surge and iceberg-calving mechanism at Vitus Lake, Alaska, U.S.A, *Journal of Glaciology*, **39**(133), 722-727.

Lliboutry, L. (1968), General theory of subglacial cavitation and sliding of temperate glaciers, *Journal of Glaciology*, **7**, 21-58.

Lliboutry, L. (1983), Modifications of the theory of intraglacial waterways for the case of subglacial ones, *Journal of Glaciology*, **29**, 216-226.

Lønne, I. and Lauritsen, T. (1996), The architecture of a modern push-moraine at Svalbard as inferred from ground-penetrating radar measurements, *Arctic and Alpine Research*, **28**, 488-495.

Lønne, I., Nemec, W., Blikra, L.H. and Lauritsen, T. (2001), Sedimentary architecture and dynamic stratigraphy of a marine ice-contact system, *Journal of Sedimentary Research*, **28**, 488-495.

Lundqvist, J. (1979), Morphogenic classification of glaciofluvial deposits, *Sveriges Geologiska Undersökning*, Series C, **73**(8), 72.

Lundqvist, J. (1999a), Scandinavian eskers, global climatic relationships, and solar forcing, *Geological Quarterly*, **43**, 149-152.

Lundqvist, J. (1999b), Periodical sedimentation in Scandinavian eskers, *GFF*, **121**, 175-181.

Mäkinen, J. (2003), Time-transgressive deposits of repeated depositional sequences within interlobate glaciofluvial (esker) sediments in Köyliö, SW Finland, *Sedimentology*, **50**, 327-360.

Mäkinen, J. and Artimo, A.P. (2007), Sedimentology and 3-D modelling of aquifer properties of the Säkylänharju-Virttaankangas interlobate esker in SW Finland, *Geological Society of America Abstracts with programs*, **39**(6), 118.

Mäkinen, J. and Räsänen, M. (2003), Early Holocene regressive split-platform and nearshore sedimentation on a glaciofluvial complex during the Yodia Sea and Ancylus Lake phases of the Baltic Basin, SW Finland, *Sedimentary Geology*, **158**, 25-56.

Maria, A., Carey, S., Sigurðsson, H. and Kincaid, C. (2000), Source and dispersal of jökulhlaup sediments discharged to the sea following the 1996 Vatnajökull eruption, *Geological Society of America Bulletin*, **112**, 1507-1521.

Marren, P.M. (2005), Magnitude and Frequency in proglacial rivers: a geomorphological and sedimentological perspective, *Earth-Science Reviews*, **70**, 203-251.

McDonald, B.C. and Shilts, W.W. (1975), Interpretation of faults in glaciofluvial sediments, *In*: Jopling, A.V., McDonald, B.C., (Eds.), *Glaciofluvial and Glaciolacustrine Sedimentation*, Society of Economic Palaeonologists and Mineralogists, Special Publication, **23**, 123-131.

Meier, M.F. and Post, A. (1969), What are glacier surges?, *Canadian Journal of Earth Sciences*, **6** (4), 807-817.

Meier, M., Lundstrom, S., Stone, D., Kamb, B., Engelhardt, H., Humphrey, N., Dunlap, W.W., Fahnestock, F., Krimmel, R.M. and Walters, R. (1994), Mechanical and hydrological basis for the rapid motion of a large tidewater glacier, *Journal of Geophysical Research*, **99**(B8), 15,219-15,229.

Meigs, A. and Sauber, J. (2000), Southern Alaska as an example of the long-term consequences of mountain building under the influence of glaciers, *Quaternary Science Reviews*, **19**, 1543-1562.

Merrand, Y. and Hallet, B. (1996), Water and sediment discharge from a large surging glacier: Bering Glacier, Alaska, U.S.A., summer 1994, *Annals of* Glaciology, **22**, 233-240.

Miller, J.R., Tracy, M.W., Fleisher, P.J., Bailey, P.K. and Natel, E.M. (2006), Retreat, downwasting and englacial discharge, eastern sector, Bering Glacier, Alaska, *Geological Society of America Abstracts with Programs*, **38**(2), 13.

Mokhtari Fard, A. (2001), Morphology of subglacial conduit deposits: control by bedrock topography, discharge flow variation, or both? A cautionary case study: Axelsberg, Nynäshamn, south central Sweden, *Global and Planetary Change*, **28**, 145-161.

Mokhtari Fard, A. (2002), Large dead-ice depressions in flat-topped eskers: evidence of a Preboreal jökulhlaup in the Stockholm area, Sweden, *Global and Planetary Change*, **35**, 273-295.

Mokhtari Fard, A. and Gruszka, B. (2007), Subglacial conditions in a branching Saalian esker in north-central Poland, *Sedimentary Geology*, **193**, 33-46.

Mokhtari Fard, A. and Ringberg, B. (2001), Sedimentological evidence of a meandering Younger Dryas subglacial conduit: Horn, SE central Sweden, *Global and Planetary Change*, **28**, 255-265.

Molnia, B.F. (1993), Major surge of the Bering Glacier, *EOS*, **72**(29), 322.

Molnia, B.F. (2005), Repeated rapid retreats of Bering Glacier by disarticulation – The cyclic dynamic response of an Alaskan glacier system, *American Geophysical Union*, Fall Meeting 2005, Reston, Abstract C42A-03.

Molnia, B.F., Post, A. and Carlson, P.R. (1996), 20$^{th}$-century glacial marine sedimentation in Vitus Lake, Bering Glacier, Alaska, U.S.A., *Annals of Glaciology*, **22**, 205-210.

Muller, E.H. and Fleisher, P.J. (1995), Surging history and potential for renewed retreat: Bering Glacier, Alaska, *Arctic and Alpine Research*, **27**, 81-88.

Murray, T., Gooch, D.L. and Stuart, G.W. (1997), Structures within the surge-front of Bakaninbreen, Svalbard, *Annals of Glaciology*, **24**, 122-129.

Murray, T., Stuart, G.W., Fry, M., Gamble N.H. and Crabtree, M.D. (2000b), Englacial water distribution in a temperate glacier from surface and borehole radar velocity analysis, *Journal of Glaciology*, **46**(154), 389-398.

Murray, T., Stuart, G.W., Miller, P.J., Woodward, J., Smith, A.M., Porter, P.R. and Jiskoot, H. (2000a), Glacier surge propagation by thermal evolution at the bed, *Journal of Geophysical Research*, **105**, 13491-13507.

Neal, A. (2004), Ground-penetrating radar and its use in sedimentology: principles, problems and progress, *Earth-Science Reviews*, **66**, 261-330.

Nienow, P., Sharp, M. and Willis, I. (1996), Temporal switching between englacial and subglacial drainage pathways: dye tracer evidence from the Haut Glacier d'Arolla, Switzerland, *Geografiska Annaler*, **78A**, 51-60.

Nobes, D.C. (1994), Ground-penetrating radar profiles of rubble-covered temperate glaciers: Results from the Tasman and Mueller glaciers of the Southern Alps of New Zealand, Expanded Abstracts, *Annual meeting of the Society of Exploration Geophysicists*, **64**, 826-829.

Nye, J.F. (1973), Water at the bed of a glacier, Symposium on the hydrology of glaciers, *International Association of Hydrological Sciences*, Cambridge, **95**, 189-194.

Nye, J.F. (1976), Water flow in glaciers; jökulhlaups, tunnels and veins, *Journal of Glaciology*, **17**, 181-207.

Nye, J.F. and Frank, F.C. (1973), Hydrology of the intergranular veins in a temperate glacier, *In*: Glen, J.W., Adie, R.J. and Johnson, D.M. (eds.), Symposium on the Hydrology of Glaciers, *International Association of Hydrological Sciences*, Special Publication, **95**, 157-161.

Paterson, W.S.B. (1994), *The physics of glaciers*, (3rd Edition), Pergammon Press, p 480.

Pohjola, V.A. (1994), TV-video observation of englacial voids in Storglaciären, Sweden, *Journal of Glaciology*, **40**, 231-240.

Post, A.S. (1969), Distribution of surging glaciers in western North America, *Journal of Glaciology*, **8**(53), 2229-240.

Post, A.S. (1972), Periodic surge origin folded medial moraines on Bering piedmont glacier, Alaska, *Journal of Glaciology*, **11** (62), 219-226.

Price, R.J. (1966), Eskers near the Casement glacier, Alaska, *Geografiska Annaler*, **48**, 111-125.

Price, R.J. (1969) Moraines, sandur, Kames and eskers near Breiðamerkurjökull, Iceland, *Transactions of the Institute of British Geographers*, **46**, 17-43.

Punkari, M. (1997), Glacial and glaciofluvial deposits in the interlobate areas of the Scandinavian Ice Sheet, *Quaternary Science Reviews*, **16**, 741-753.

Retzlaff, R. and Bentley, C.R. (1993), Timing of stagnation of Ice Stream C, West Antarctica, from short-pulse radar studies of buried surface crevasses, *Journal of Glaciology*, **39**(133), 553-561.

Ringberg, B. (1984), Cyclic lamination in proximal varves reflecting the length of summers during Late Weischel in southernmost Sweden, In: Mörner, N. A. and Karlén, W. (eds.), *Climatic Changes on a Yearly to Millennial Basis*, D. Riedel Publishing Company, 57-62.

Roberts, M.J. (2002), Controls on supraglacial outlet development during glacial outburst floods, *Ph.D. Thesis*, Staffordshire University, U.K.

Roberts, M.J. (2005), Jökulhlaups: A reassessment of floodwater flow through glaciers, *Reviews of Geophysics*, **43**(1), RG1002.

Roberts, M.J., Russell, A.J., Tweed, F.S. and Knudsen, Ó. (2000a), Rapid sediment entrainment and englacial deposition during jökulhlaups, *Journal of Glaciology*, **153**, 349-351.

Roberts, M.J., Russell, A.J., Tweed, F.S. and Knudsen, Ó. (2000b), Ice fracturing during jökulhlaups: implications for englacial floodwater routing and outlet development, *Earth Surface Processes and Landforms*, **25**, 1429-1446.

Roberts, M.J., Russell, A.J., Tweed, F.S. and Knudsen, Ó. (2001), Controls on englacial sediment deposition during the November 1996 jökulhlaup, Skeiðarárjökull, Iceland, *Earth Surface Processes and Landforms*, **26**, 935-952.

Roberts, M.J., Russell, A.J., Tweed, F.S. and Knudsen, Ó. (2002), Controls on the development of supraglacial floodwater outlets during jökulhlaups, *In*: Snorassion, Á. (Ed.), *Proceedings of the Extremes of the Extremes: Extraordinary Floods* (Proceedings of s symposium held in Reykjavík, Iceland, July 2000), Special Publication 271, International Association of Hydrological Sciences, 71-76.

Roberts, M.J., Pálsson, F., Gudmundsson, M.T., Björnsson, H. and Tweed, F.S. (2005), Ice-water interactions during floods from Grænalón glacier-dammed lake, Iceland, *Annals of Glaciology*, **40**, 1, 133-138.

Röthlisberger, H. (1972), Water pressure in intra- and subglacial channels, *Journal of Glaciology*, **11**, 177-203.

Roush, J.L., Lingle, C.S., Guritz, R.M. and Fatland, D.R. (2003), Surge-front propagation and velocities during the early-1993-95 surge of Bering Glacier, Alaska, U.S.A., from sequential SAR imagery, *Annals of Glaciology*, **36**, 37-44.

Russell, A.J. (1994), Subglacial jökulhlaup deposition, Jotunheimen, Norway, *Sedimentary Geology*, **40**, 1091-1111.

Russell, A.J. and Knudsen, Ó. (1999a), Controls on the sedimentology of November 1996 Jökulhlaup deposits, Skeiðarársandur, Iceland, *In*: Smith, N.D. and Rogers J. (Eds.),

*Fluvial Sedimentology VI*, International Association of Sedimentologists, Special Publication, **28**, 315-329,.

Russell, A.J. and Knudsen, Ó. (1999b), An ice-contact rythmite (turbidite) succession deposited during the November 1996 catastrophic outburst flood (jökulhlaup), Skeiðarárjökull, Iceland, *Sedimentary Geology*, **127**, 1-10.

Russell, A.J., Knight, P.G., Van Dijk, T.A.G.P. (2001b), Glacier surging as a control on the development of proglacial, fluvial landforms and deposits, Skeiðarársandur, Iceland, *Global and Planetary Change*, **28**, 163-174.

Russell, A.J., Fay, H., Marren, P.M., Tweed, F.S. and Knudsen, Ó. (2005), Icelandic jökulhlaup impacts, *In*: Caseldine, C., Russell, A., Harðardóttir, J. and Knudsen, Ó. (Eds.), *Iceland – Modern Processes and Past Environments*, Developments in Quaternary Science, **5**, 153-203.

Russell, A.J., Gregory, A.R., Large, A.R.G., Fleisher, P.J. and Harris, T.D. (2007b), Tunnel channel formation during the November 1996 jökulhlaup, Skeiðarárjökull, Iceland, *Annals of Glaciology*, **45**, 95-103.

Russell, A.J., Knudsen, Ó., Fay, H., Marren, P.M., Heinz, J. and Tronicke, J. (2001a), Morphology and sedimentology of a giant supraglacial, ice-walled, Jökulhlaup channel Skeiðarárjökull, Iceland: implications for esker genesis, *Global and Planetary Change*, **28**, 193-216.

Russell, A.J., Roberts, M.J., Fay, H., Marren, P.M., Cassidy, N.J., Tweed, F.S. and Harris, T. (2006), Icelandic jökulhlaup impacts: implications for ice-sheet hydrology, sediment transfer and geomorphology, *Geomorphology*, **75**, 33-64.

Russell, A.J., Burke, M.J., Woodward, J., Fleisher, P.J., Gregory, A., Bailey, P.K., Blauvelt, D. and Large, A. (2007a), Controls on the morphology and sedimentology of a jökulhlaup esker, Skeiðarárjökull, Iceland, *Geological Society of America Abstracts with programs*, **39**(6), 117.

Sambrook Smith, G.H., Ashworth, P.J., Best, J.L., Woodward, J. and Simpson, C.J. (2006), The sedimentology and alluvial architecture of the sandy braided South Saskatchewan River, Canada, *Sedimentology*, **53**, 413-434.

Sandmeier, K.J. (2006), *REFLEXW (Version 4.2) Processing program for seismic, acoustic and electromagnetic reflection, refraction and transmission data*, K.J. Sandmeier, Karlsruhe, Germany.

Sauber, J.M. and Molnia, B.F. (2004), Glacier fluctuations and fault instability in tectonically active southern Alaska, *Global Planetary Change*, **42**, 279-293.

Saunderson, H.C. (1975), Sedimentology of the Brampton Esker and its associated drainage: an empirical test of theory, *In*: Jopling, A.V. and McDonald, B.C. (Eds.), *Glaciofluvial and glaciolacustrine sedimentation.* Tulsa: Society of Economic Palaeontologists and Mineralogists, Special Publication, **23**, 155-176.

Saunderson, H.C. (1977), The sliding bed facies in esker sands and gravels: a criterion for full-pipe (tunnel) flow?, *Sedimentology*, **24**, 623-638.

Sharp, M.J. (1985a), "Crevasse-fill" ridges – a landform type characteristic of surging glaciers?, *Geografiska Annaler*, **67A**(3-4), 213-220.

Sharp, M.J. (1985b), Sedimentation and stratigraphy at Eyjabakkajökull – an Icelandic surging glacier, *Quaternary Research*, **24**(3), 268-284.

Sharp, M.J. (1988), Surging glaciers: geomorphic effects, *Progress in Physical Geography*, **12**, 533-559.

Shaw, J. (1972), Sedimentation in the ice-contact environment with examples from Shropshire (England), *Sedimentology*, **18**, 23-62.

Shilts, W.W. (1984), Esker sedimentation models, Deep Rose Lake map area, District of Keewatin, *Geological Survey of Canada Paper*, **84-1B**, 217-222.

Shreve, R.L. (1972), Movement of water in glaciers, *Journal of Glaciology*, **11**, 205-214.

Shreve, R.L. (1985), Esker Characteristics in terms of glacier physics, Katahdin esker system, Maine, *Geological Society of America Bulletin*, **96**, 639-646.

Shulmeister, J. (1989), Flood deposits in the Tweed Esker (southern Ontario, Canada), *Sedimentary Geology*, **65**, 153-163.

Sigurðsson, O. (2005), Variations of termini of glaciers in Iceland in recent centuries and their connection with climate, *In*: Caseldine, C., Russell, A., Harðardóttir, J. and

Jnudsen, Ó (eds.), *Iceland – Modern Processes and Past Environments*. Developments in Quaternary Science, **5**, 241-255.

Sjogren, D.B., Brennand, T.A. and Moorman, B.J. (2007), Esker morpho-sedimentary relationships in Southern Alberta, Canada, *Geological Society of America Abstracts with programs*, **39**(6), 117.

Smith, L.C., Alsdorf, D.E., Magilligan, F.J., Gomez, B., Mertes, L.A.K., Smith, N.D. and Garvin, J.B. (2000), Estimation of erosion, deposition and net volumetric change caused by the 1996 Skeiðarársandur jökulhlaup, Iceland, from synthetic aperture radar interferometry, *Water Resources Research*, **36**, 1583-1594.

Smith, L.C., Sheng, Y., Magilligan, F.J., Smith, N.D., Gomez, B., Mertes, L.A.K., Krabill, W.B. and Garvin, J.B. (2006), Geomorphic impact and subsequent recovery from the 1996 Skeiðarársandur jökulhlaups, Iceland, measured with multi-year airborne lidar, *Geomorphology*, **75**, 65-75.

Snorrason, Á., Jónsson, P., Pálsson, S., Árnason, S., Víkingsson, S. and Kaldal, I. (2002), November 1996 jökulhlaup on Skeiðarársandur outwash plain, Iceland, *In*: Martini, I.P., Baker, V.R., Garzón, G. (Eds.), Flood and megaflood processes and deposits: recent and ancient examples, *Special Publication of the International Association of Sedimentologists*, **32**, 55-65.

Spring, U. and Hutter, K. (1981), Numerical studies of jökulhlaups, *Cold Region Science and Technology*, **4**, 221-244.

Steenson, B.O. (1951), Radar methods for the exploration of glaciers, *Ph.D. Thesis*, Californian Institute of Technology, Pasedena, USA.

Stenborg, T. (1969), Studies of the internal drainage of glaciers, *Geografiska Annaler*, **51**A, 13-41.

Stenborg, T. (1973), Some viewpoints on the interna drainage of glaciers, *In*: Glen, J.W., Adie, R.J. and Johnsson, D.M. (Eds.), *Symposium on the Hydrology of Glaciers*, International Association of Hydrological Sciences, Special Publication, **95**, 117-129.

Stokes, J.C. (1958), An esker-like ridge in the process of formation, Flatisen, Norway, *Journal of Glaciology*, **3**, 286-289.

Syverson, K.M., Gaffield, S.J. and Mickelson, C.D.M. (1994), Comparison of esker morphology and sedimentology, Burroughs Glacier, Alaska, *Geological Society of America Bulletin*, **106**, 1130-1142.

Szilder, K. and Lozowski, E.P. (1997), Stability of quasi-steady flow in an englacial conduit, *Hydrological Processes*, **11**, 1737-1746.

Teller, J.T., Leverington, D.W. and Mann, J.D. (2002), Freshwater outbursts to the oceans from glacial Lake Agassiz and their role in climate change during the last deglaciation, *Quaternary Science Reviews*, **21**, 879-887.

Theakstone, W.H. (2001), Fracturing and sediment deposition at the glacier surface by jökulhlaups: a common occurrence, *Journal of Glaciology*, **47** (158), 517-518.

Thomas, G.S.P. and Chiverrell, R.C. (2006), A model of subaqueous sedimentation at the margin of the Late Midlandian Irish Ice Sheet, Conemara, Ireland, and its implications for regionally high isostatic sea-levels, *Quaternary Science Reviews*, **25**, 2868-2893.

Thomas, G.S.P. and Montague, E. (1997), The morphology, stratigraphy and Sedimentology of the Carstairs Esker, Scotland, U.K., *Quaternary Science Reviews*, **16**, 661-674.

Thomas, G.S.P., Huddart, D. and Bennett, M.R. (2007), The Newbigging esker system, Lanarkshire, Southern Scotland: a model for tunnel, subaqueous fan and supraglacial esker sedimentation, *Geological Society of America Abstracts with programs*, **39**(6), 118.

Þórarinsson, S. (1943), Vatnajökull: scientific results of the Swedish-Icelandic investigations 1936-37-38, oscillations of the Icelandic glaciers in the last 250 years, *Geografiska Annaler*, **1-2**, 1-54.

Tweed, F.S. and Russell, A.J. (1999), Controls on the formation and sudden drainage of glacier-impounded lakes: implications for jökulhlaup characteristics, *Progress in Physical Geography*, **23**, 79-110.

van Dijk, T.A.G.P. (2002), Glacier surges as a control on the development of proglacial fluvial landforms and deposits, *Ph.D. Thesis*, Keele University, U.K.

Vieli, A., Jania, J., Blatter, H. and Funk, M. (2004), Short-term velocity variations on Hansbreen, a tidewater glacier in Spitsbergen, *Journal of Glaciology*, **50**(170), 389-398.

Walder, J.S. (1982), Stability of sheet flow of water beneath temperate glaciers and its implications for glacier surging, *Journal of Glaciology*, **28** (99), 273-293.

Walder, J.S. (1986), Hydraulics of subglacial cavities, *Journal of Glaciology*, **32**, 439-445.

Walder, J.S. and Fowler, A.C. (1994), Channelized aubglacial drainage over a deformable bed, *Journal of Glaciology*, **40**, 3-15.

Waller, R.I., Russell, A.J., van Dijk, T.A.G.P. and Knudsen, Ó. (2001), Jökulhlaup related ice fracture and the supraglacial routing of water and sediment, Skeiðarárjökull, Iceland, *Geografiska Annaler*, **83**A, 29-38.

Warren, W.P. and Ashley, G.M. (1994), Origins of the ice contact stratified ridges (eskers) of Ireland, *Journal of Sedimentary Research*, **A64**, 433-449.

Watts, R.D. and England, A.W. (1976), Radio-echo sounding of temperate glaciers: ice properties and sounder design criteria, *Journal of Glaciology*, **17**(75), 39-48.

Weertman, J. (1957), On the sliding of glaciers, *Journal of Glaciology*, **3**, 33-38.

Weertman, J. (1964), The theory of glacier sliding, *Journal of Glaciology*, **5**(39), 287-303.

Weertman, J. (1972), General theory of water flow at the base of a glacier or ice sheet, *Reviews of Geophysics and Space Physics*, **10**, 287-333.

White, W.B. (1988), *Geomorphology and Hydrology of Karst Terrains*, Oxford University Press, Oxford.

Wiles, G.C., Post, A., Muller, E.H. and Molnia, B. (1999), Dechronology and late Holocene History of Bering Piedmont Glacier, Alaska, *Quaternary Research*, **52**, 185-195.

Wingham, D.J., Siegert, M.J., Shepherd, A. and Muir, A. (2006), Rapid discharge connects Antarctic subglacial lakes, *Nature*, **440**, 1033-1036.

Woodward, J. (1999), Structural glaciology of Kongsvegen, Svalbard, using ground-penetrating radar, *Ph.D. Thesis*, Division of Geography, University of Leeds.

Woodward, J. and Burke, M.J. (2007), Applications of ground-penetrating radar to glacial and frozen materials, *Journal of Environmental and Engineering Geophysics*, **12**(1), 69-85.

Woodward, J., Murray, T. and McCaig, A. (2002), Formation and reorientation of structure in the surge-type glacier Kongsvegen, Svalbard, *Journal of Quaternary Science*, **17**, 201-209.

Woodward, J., Burke, M.J., Tinsley, R. and Russell, A.J. (2008), Investigating reworking of proglacial sediments using GPR: Skeiðarárjökull, Iceland, *Proceedings of the 12th International Conference on Ground Penetrating Radar*, 16-19th June 2008, University of Birmingham, U.K.

Woodward, J., Murray, T., Clark, R.A. and Stuart, G.W. (2003a), Glacier surge mechanisms inferred from ground-penetrating radar: Kongsvegen, Svalbard, *Journal of Glaciology*, **49**(167), 473-480.

Woodward, J., Ashworth, P.J., Best, J.L., Smith, G.H.S. and Simpson, C.J. (2003b), The use and application of GPR in sandy fluvial environments: methodological considerations, *In*: Bristow, C.S. and Jol, H.M. (Eds.), *Ground Penetrating Radar in Sediments,* Geological Society, London, Special Publications, **211**, 127-142.

# Appendix 1

## Published Papers by M.J. Burke Based on the Findings of this Thesis

**Co-Authors' Involvement with Publications Pertaining to this Project**

Below are details of the role of each author in the research and publication of papers associated with this research. Articles are listed in chronological order.

**Woodward, J. and Burke, M.J. (2007), Applications of ground-penetrating radar to glacial and frozen materials, *Journal of Environmental and Engineering Geophysics*, 12(1), 69-85.**

**Woodward, J.**

- Responsible for reviewing relevant literature
- Devised the concept behind the article
- Responsible for the writing of the manuscript and liaising with the journal editor

**Burke, M.J.**

- Wrote initial sections concerning glacial/glaciofluvial landforms, permafrost and rock glaciers
- Produced figures for the article
- Assisted with article editing

**Burke, M.J., Fleisher, P.J., Woodward, J., Bailey, P.K., Natel, E. and Russell, A.J. (2008a), GPR investigations of subglacially deformed fossil tree horizons: Bering Glacier, Alaska, *Proceedings of the 12th International Conference on Ground Penetrating Radar*, 16th-19th June 2008, University of Birmingham, U.K.**

**Burke, M.J.**

- Designed the project
- Devised the concept behind the article
- Led data collection, processing and interpretation
- Responsible for the writing of the manuscript and liaising with the journal editor

**Fleisher, P.J.**

- Research funding and logistical support (Earthwatch Insitute)
- Assisted with data collection
- Assisted with data interpretation
- Assisted with article editing

**Woodward, J.**

- Principle supervisor of research
- Assisted with data processing and interpretation
- Assisted with article structure and editing

**Bailey, P.K.**

- Assisted with data collection
- Assisted with data interpretation
- Assisted with article editing

**Natel, E.**

- Assisted with data collection

**Russell, A.J.**

- Secondary supervisor of research
- Assisted with article editing

**Woodward, J., Burke, M.J., Tinsely, R. and Russell, A.J. (2008b), Investigating reworking of proglacial sediments using GPR: Skeiðarárjökull, Iceland, *Proceedings of the 12th International Conference on Ground Penetrating Radar*, 16th-19th June 2008, University of Birmingham, U.K.**

**Woodward, J.**

- Designed the project
- Devised the concept behind the article
- Led data interpretation
- Responsible for the writing of the manuscript and liaising with the journal editor

**Burke, M.J.**

- Led data collection
- Aided data interpretation
- Produced initial versions of the manuscript figures
- Assisted with article editing

**Tinsley, R.**

- Assisted with data collection
- Aided data interpretation

**Russell, A.J.**

- Research funding and logistical support (Earthwatch Institute)
- Assisted with article editing

**Burke, M.J., Woodward, J., Russell, A.J., Fleisher, P.J. and Bailey, P.K. (2008c), Controls on the sedimentary architecture of a single event englacial esker: Skeiðarárjökull, Iceland, *Quaternary Science Reviews*, In press.**

**Burke, M.J.**

- Designed the project
- Responsible for reviewing relevant literature and identifying research gap
- Devised the concept behind the article
- Led data collection, processing and interpretation
- Responsible for the writing of the manuscript and liaising with the journal editor

**Woodward, J.**

- Principle supervisor of research
- Assisted data collection in the field
- Assisted with data processing and interpretation
- Assisted with article structure and editing

**Russell, A.J.**
- Secondary supervisor of research
- Research funding and logistical support (Earthwatch Institute)
- Assisted with data collection and provided sedimentological expertise
- Assisted with article structure and editing

**Fleisher, P.J.**
- Assisted with data collection
- Provided discussions that were helpful to initial data interpretation
- Assisted with article editing

**Bailey, P.K.**
- Assisted with data collection
- Provided discussions that were helpful to initial data interpretation
- Assisted with article editing

**Burke, M.J., Woodward, J., Russell, A.J. and Fleisher, P.J. (Submitted), Structural controls on englacial proto-esker sedimentation: Skeiðarárjökull, Iceland, *Annals of Glaciology*.**

**Burke, M.J.**
- Designed the project
- Responsible for reviewing relevant literature and identifying research gap
- Devised the concept behind the article
- Led data collection, processing and interpretation
- Responsible for the writing of the manuscript and liaising with the journal editor

**Woodward, J.**
- Principle supervisor of research
- Assisted data collection in the field
- Assisted with data processing and interpretation
- Assisted with article structure and editing

**Russell, A.J.**
- Secondary supervisor of research
- Research funding and logistical support (Earthwatch Institute)
- Provided field assistance
- Assisted with article editing

**Fleisher, P.J.**
- Provided field assistance
- Assisted with article editing

# Appendix 2

**GPR lines collected on the ice surface of Skeiðarárjökull. The GPR lines (Grid 2), processed following the sequence presented in Figure 4.14, are positioned above the line interpretations.**

**GRID 2**

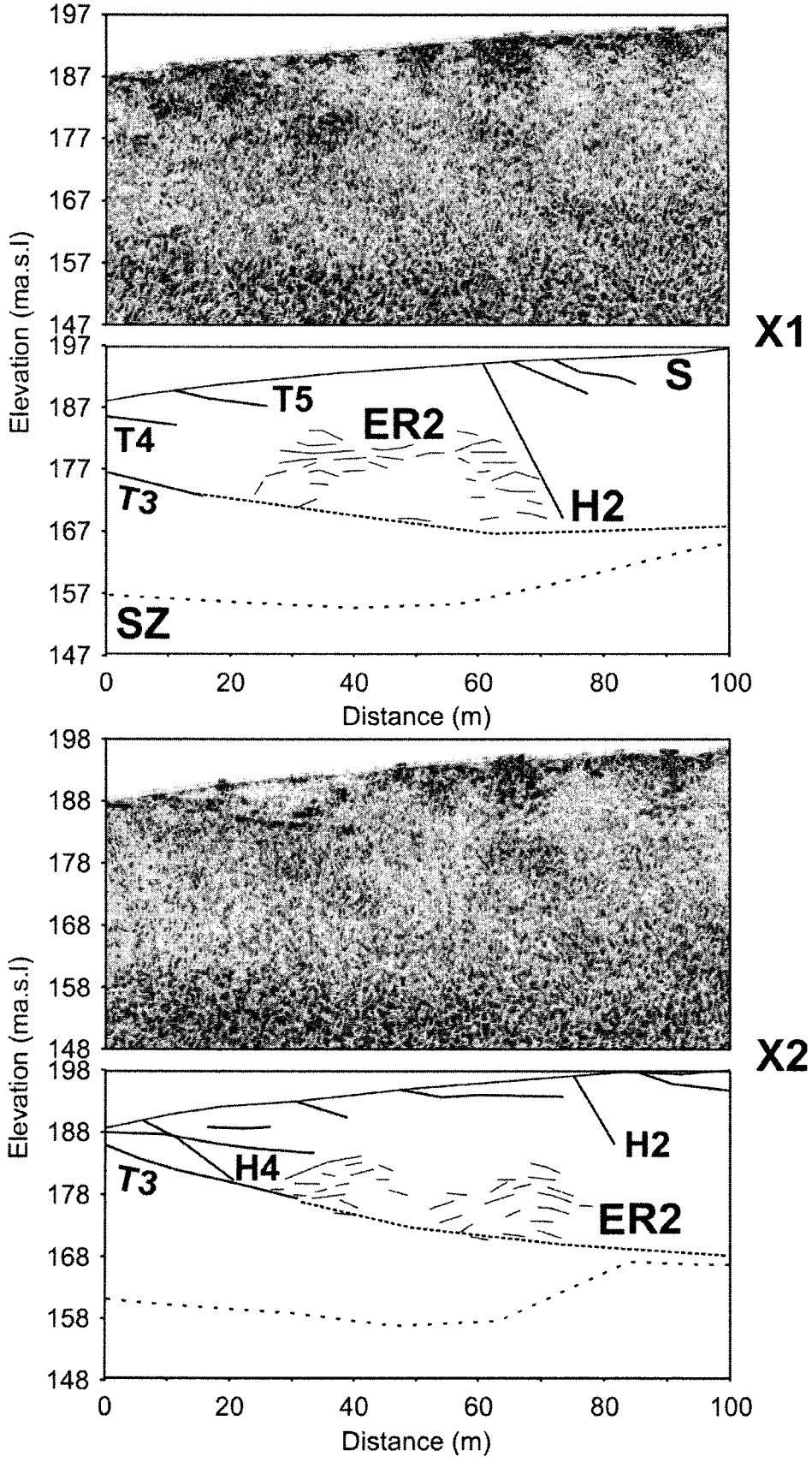
197
187
177
167
157
147
Elevation (ma.s.l)
X1
T5
S
T4
ER2
T3
H2
SZ
0
20
40
60
80
100
Distance (m)
198
188
178
168
158
148
Elevation (ma.s.l)
X2
H2
H4
T3
ER2
0
20
40
60
80
100
Distance (m)

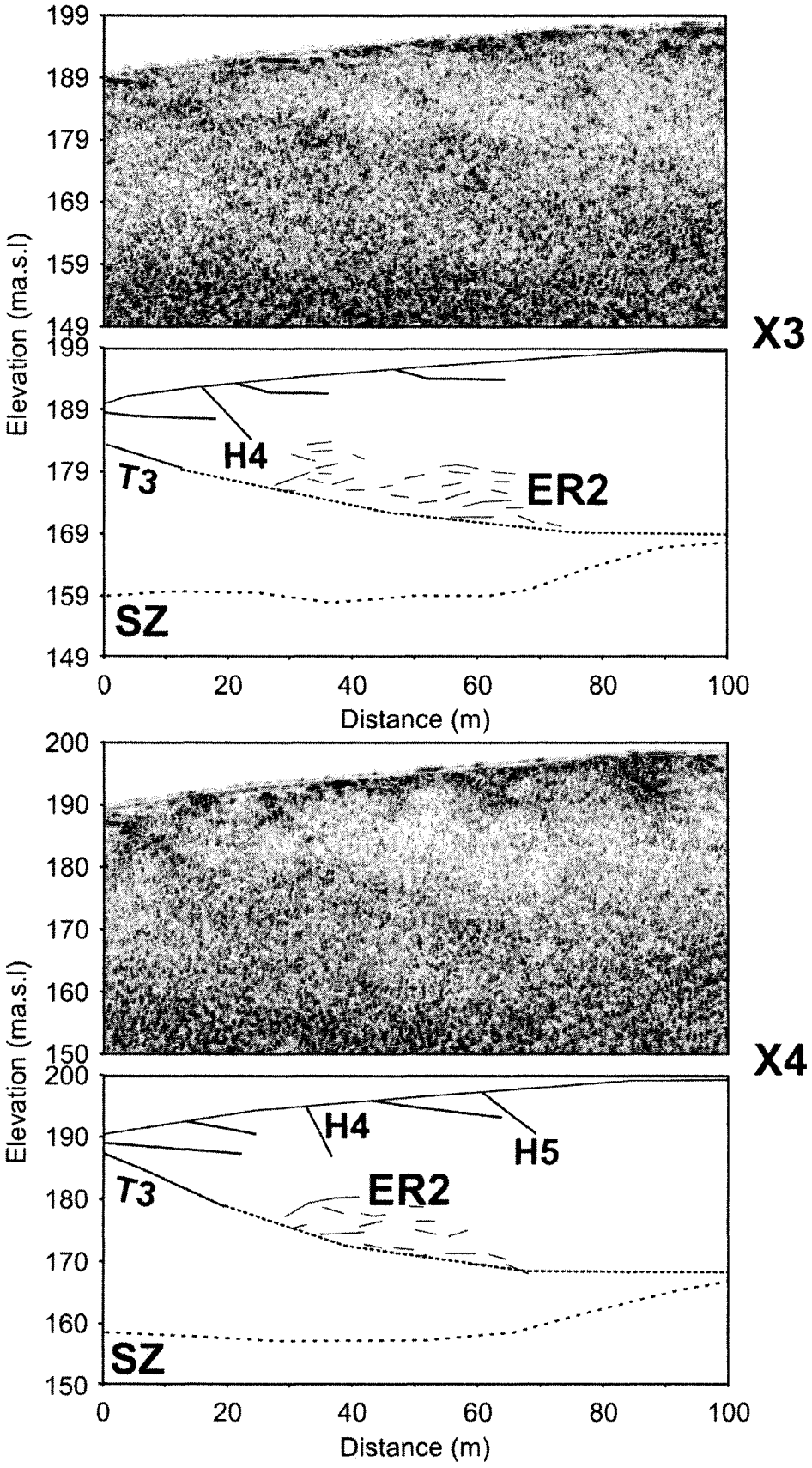
199
189
179
169
159
149
X3
199
189
179
169
159
149
Elevation (ma.s.l)
H4
T3
ER2
SZ
0
20
40
60
80
100
Distance (m)
200
190
180
170
160
150
X4
200
190
180
170
160
150
Elevation (ma.s.l)
H4
H5
T3
ER2
SZ
0
20
40
60
80
100
Distance (m)

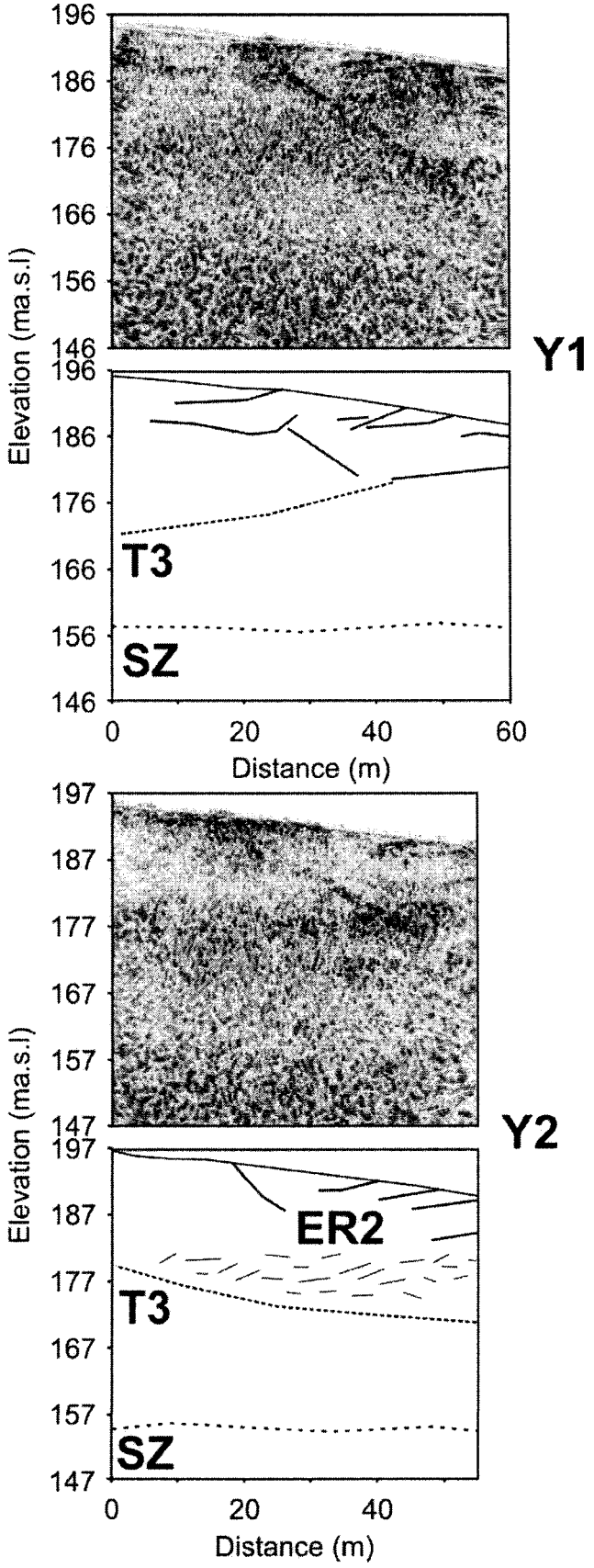
196
186
176
166
156
146
Elevation (ma.s.l)
Y1
T3
SZ
0
20
40
60
Distance (m)
197
187
177
167
157
147
Y2
ER2
T3
SZ
0
20
40
Distance (m)

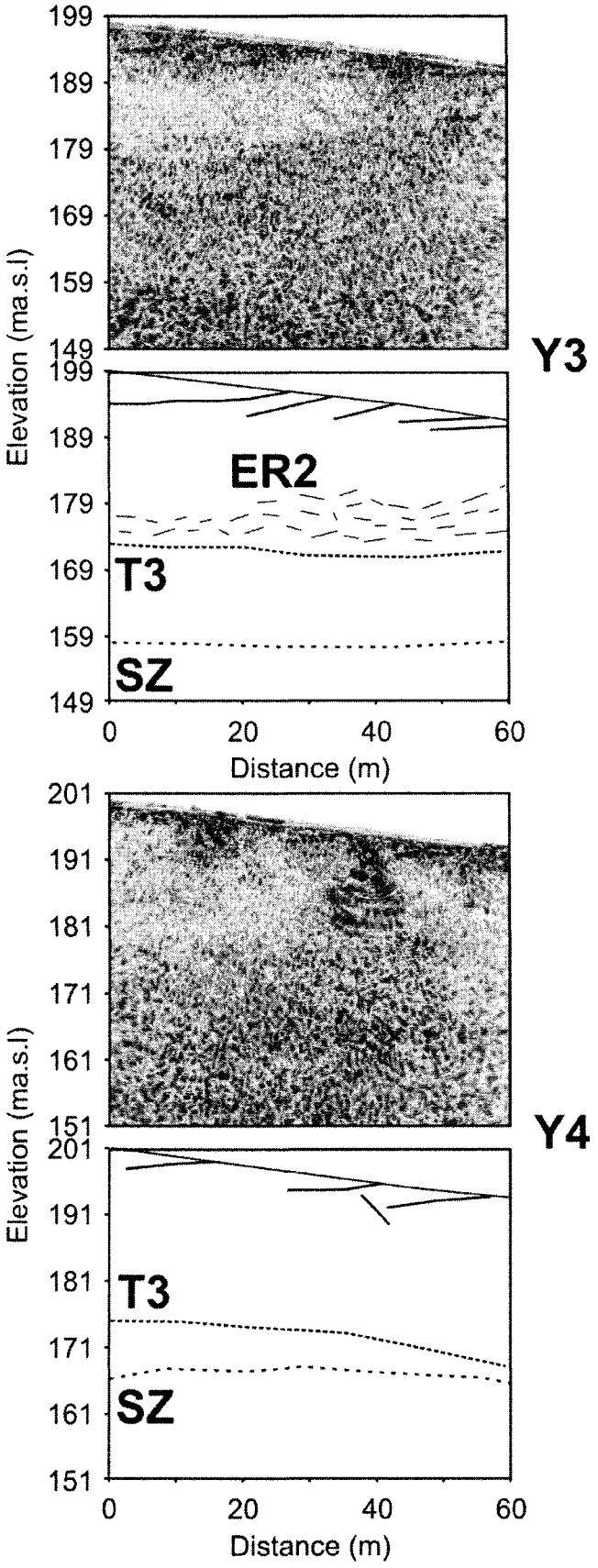
Y3
ER2
T3
SZ
Elevation (ma.s.l)
199
189
179
169
159
149
0
20
40
60
Distance (m)
Y4
T3
SZ
Elevation (ma.s.l)
201
191
181
171
161
151
0
20
40
60
Distance (m)

# Appendix 3

**GPR lines collected on the esker and ice-walled canyon fill at Skeiðarárjökull. The GPR lines, processed following the sequence presented in Figure 4.15, are positioned above the line interpretations. Colour coding corresponds to the radar facies scheme presented in Figure 6.1.**

**GRID 1**

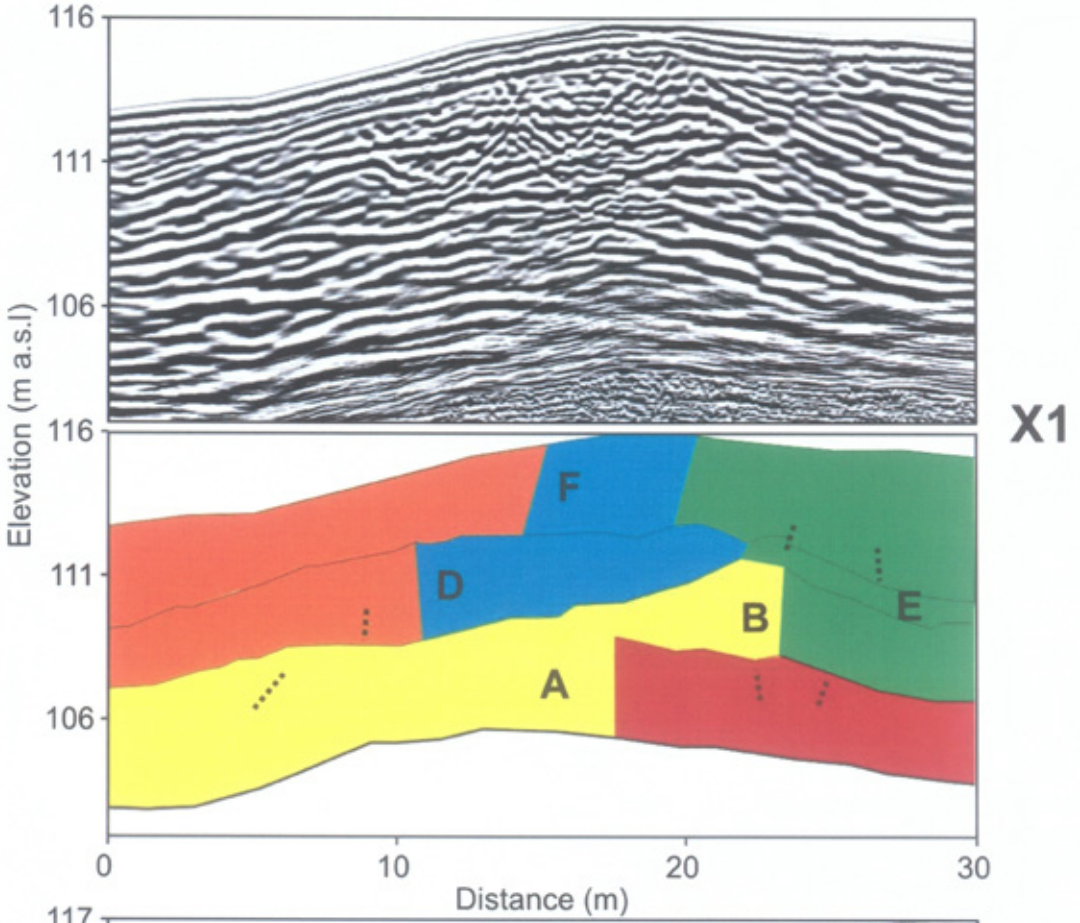
116
111
106
Elevation (m a.s.l)
X1
116
111
106
F
D
B
E
A
0
10
20
30
Distance (m)

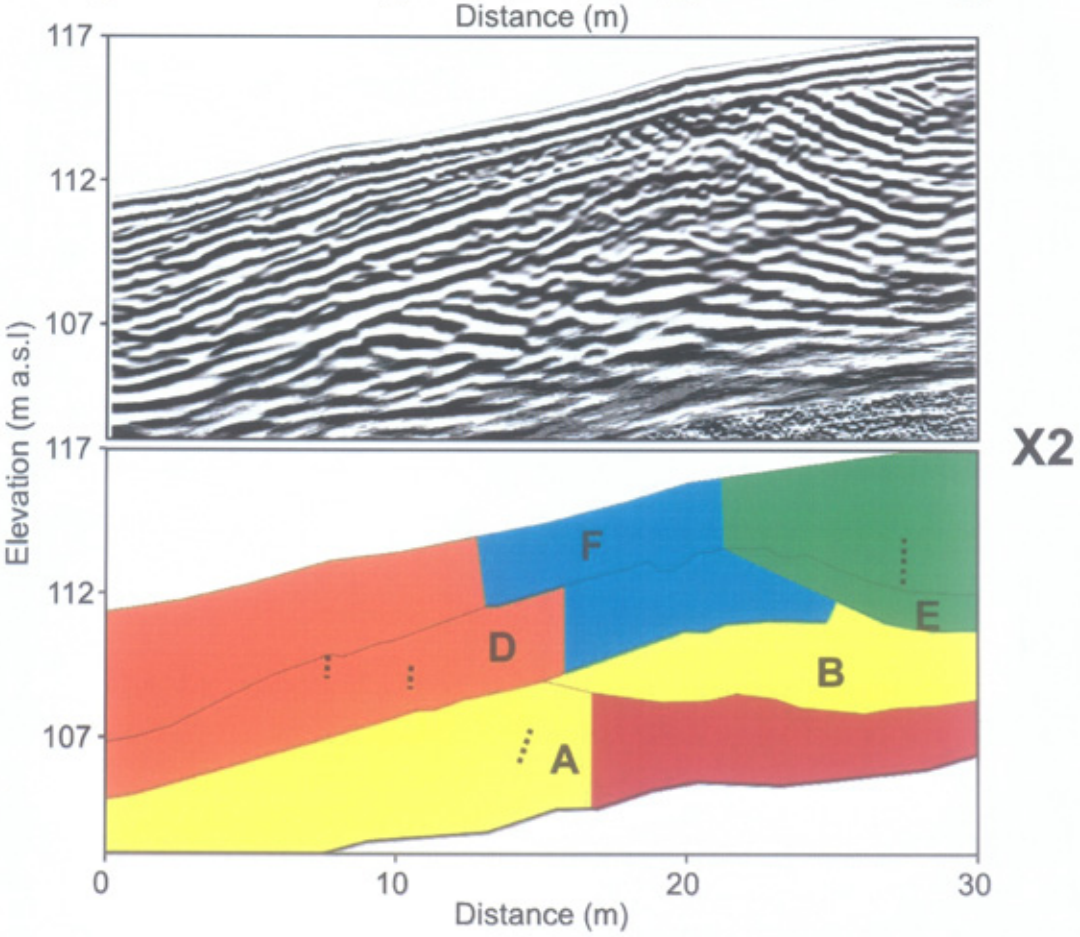
117
112
107
Elevation (m a.s.l)
X2
117
112
107
F
D
E
B
A
0
10
20
30
Distance (m)

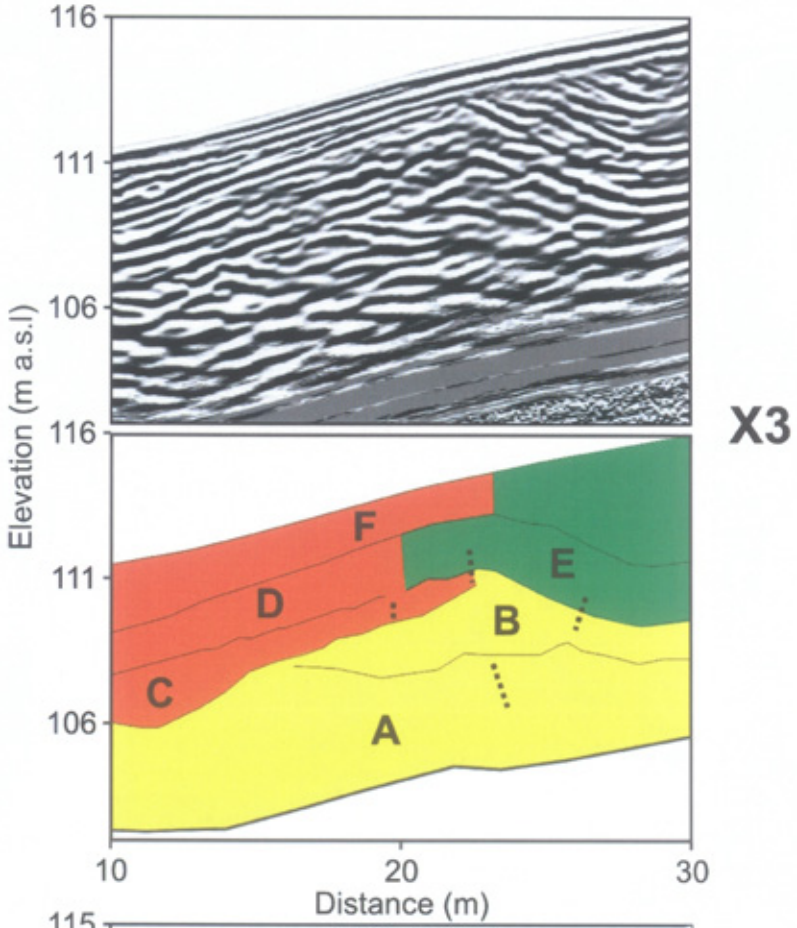
116
111
106
116
111
106
Elevation (m a.s.l)
F
E
D
B
C
A
10
20
30
Distance (m)

X3

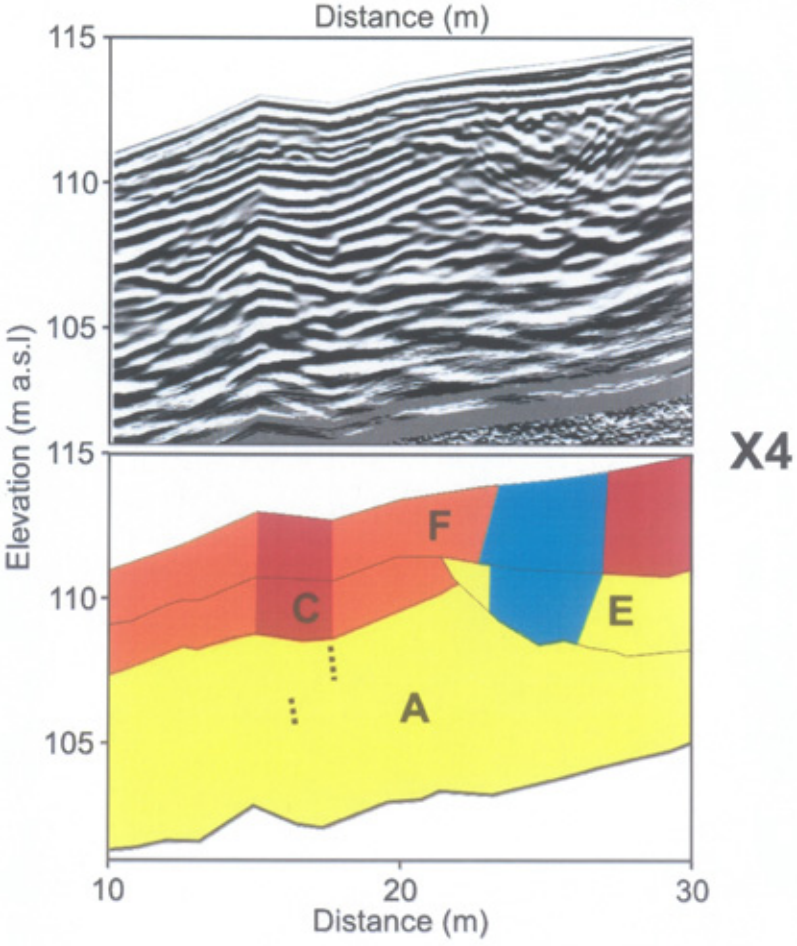
115
110
105
115
110
105
Elevation (m a.s.l)
F
C
E
A
10
20
30
Distance (m)

X4

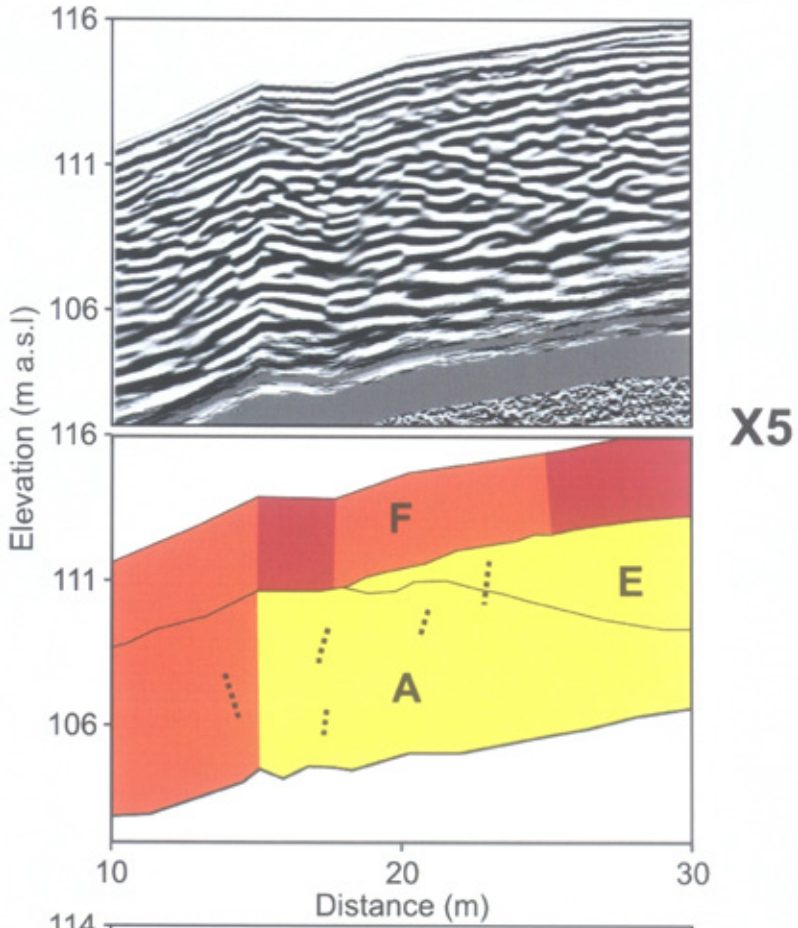
116
111
106
Elevation (m a.s.l)
X5
F
E
A
10
20
30
Distance (m)

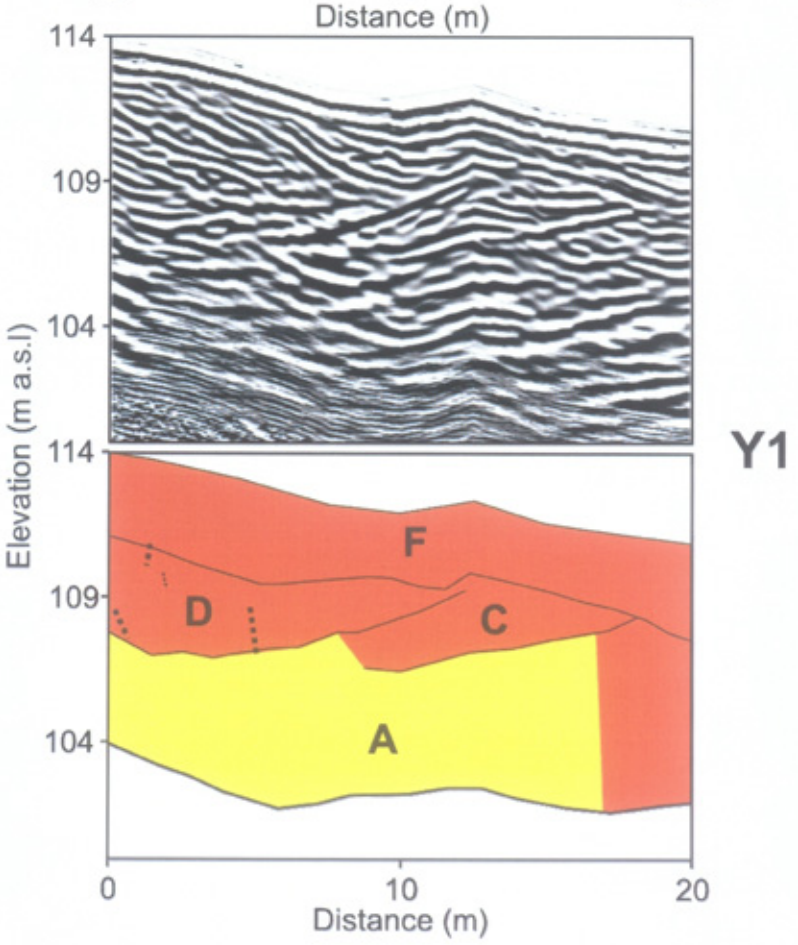
114
109
104
Elevation (m a.s.l)
Y1
F
D
C
A
0
10
20
Distance (m)

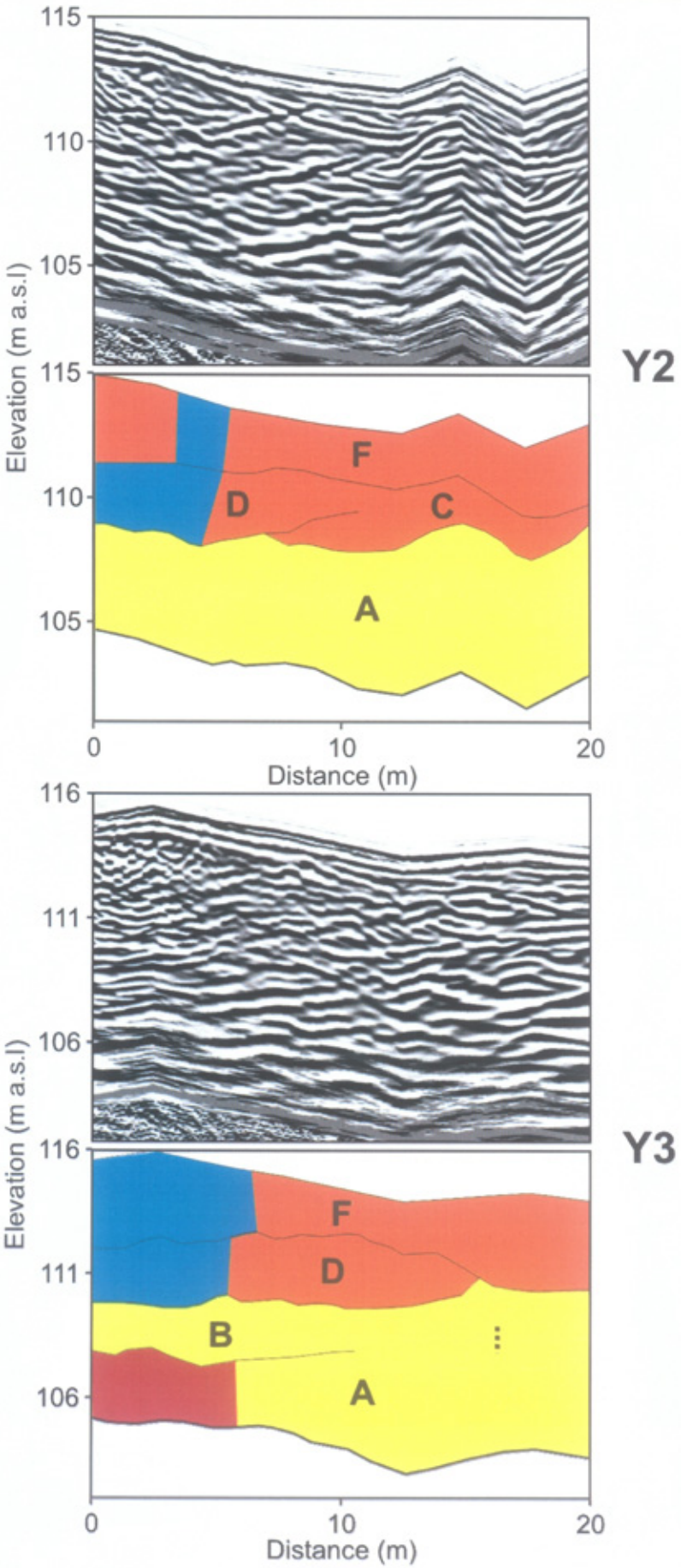
115
110
105
Elevation (m a.s.l)
115
110
105
F
D
C
A
0
10
20
Distance (m)
Y2
116
111
106
Elevation (m a.s.l)
116
111
106
F
D
B
A
0
10
20
Distance (m)
Y3

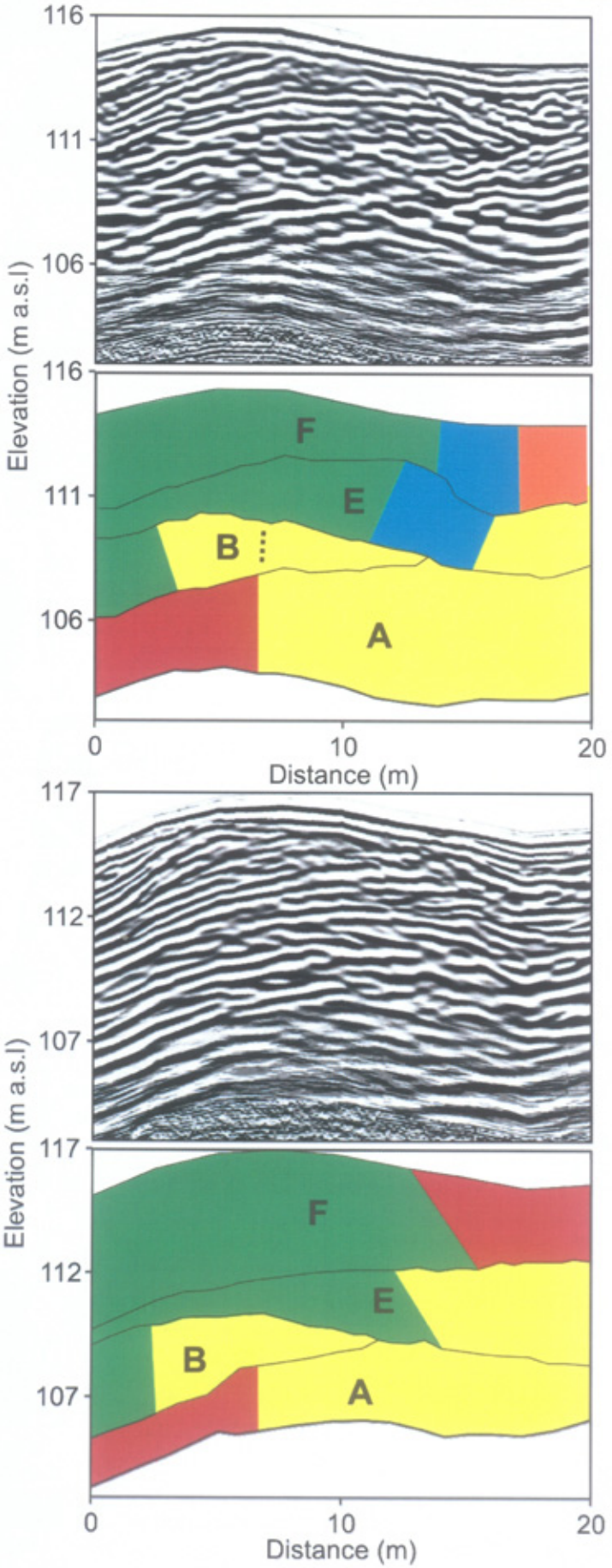
116
111
106
Elevation (m a.s.l)
Y4
F
E
B
A
0
10
20
Distance (m)
117
112
107
Y5

**GRID 2**

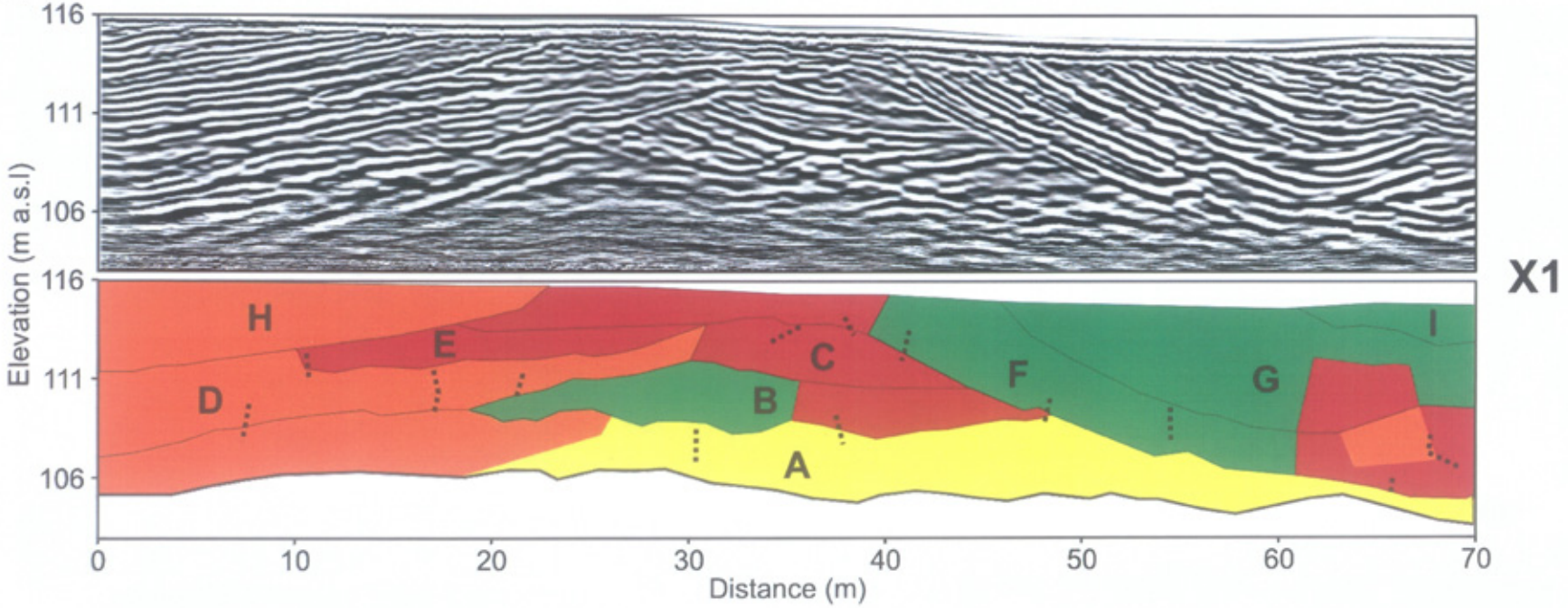
116
111
106
Elevation (m a.s.l)
H
E
C
I
D
B
F
G
A
0
10
20
30
40
50
60
70
Distance (m)

**X1**

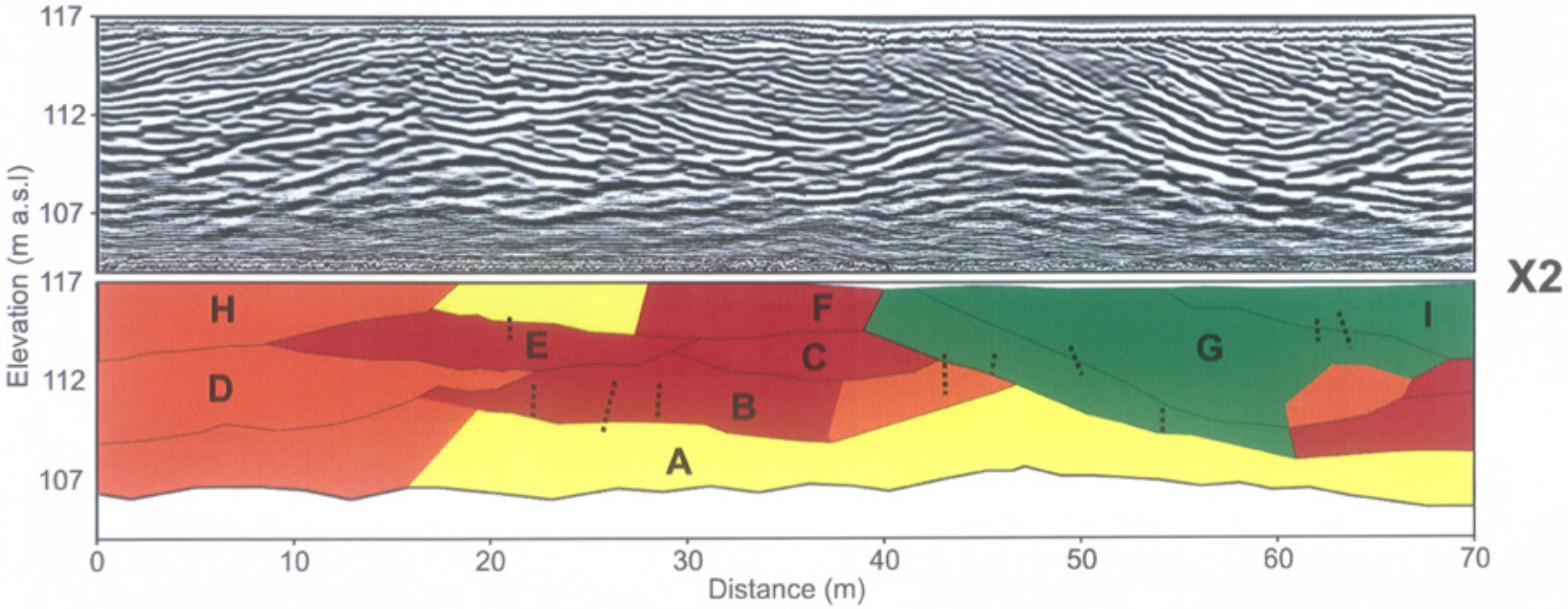
117
112
107
Elevation (m a.s.l)
117
112
107
H
D
E
F
C
B
A
G
I
0
10
20
30
40
50
60
70
Distance (m)
X2

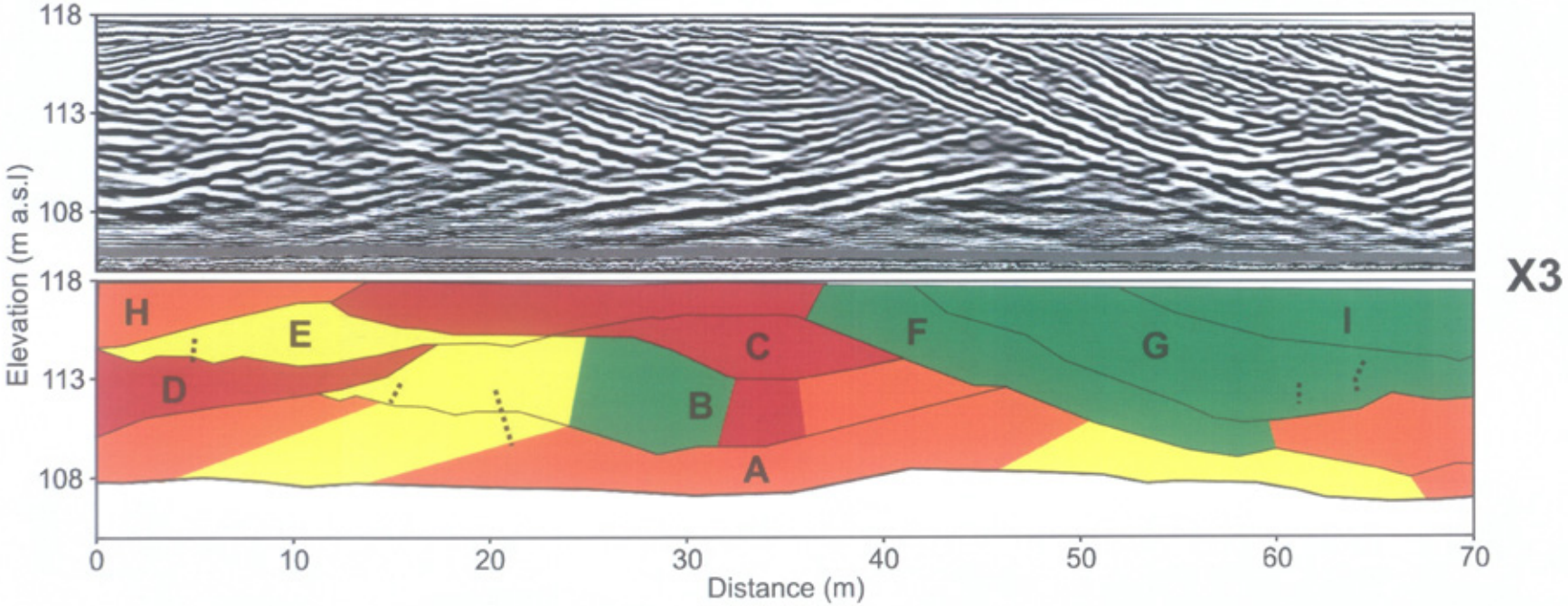
118
113
108
Elevation (m a.s.l)
H
E
D
C
B
A
F
G
I
0
10
20
30
40
50
60
70
Distance (m)

X3

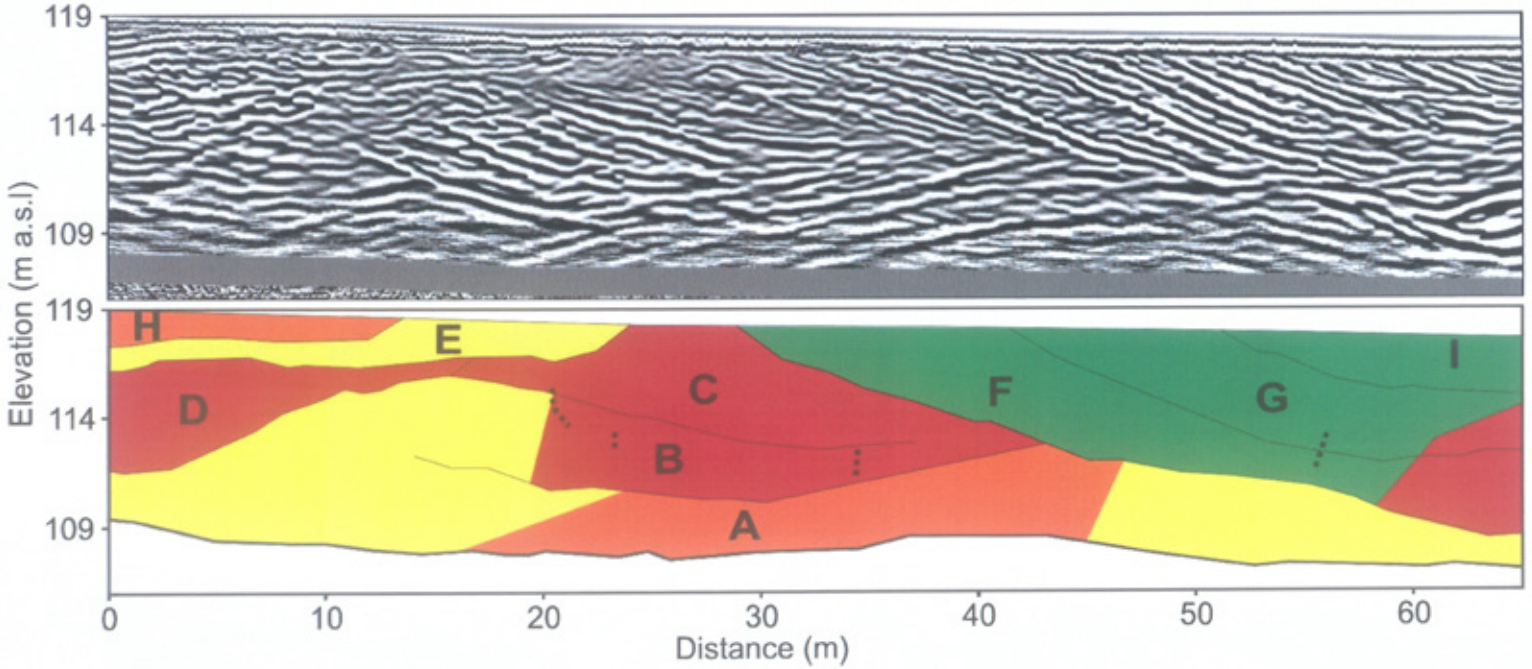
119
114
109
119
114
109
Elevation (m a.s.l)
H
E
D
C
F
G
I
B
A
0
10
20
30
40
50
60
Distance (m)

X4

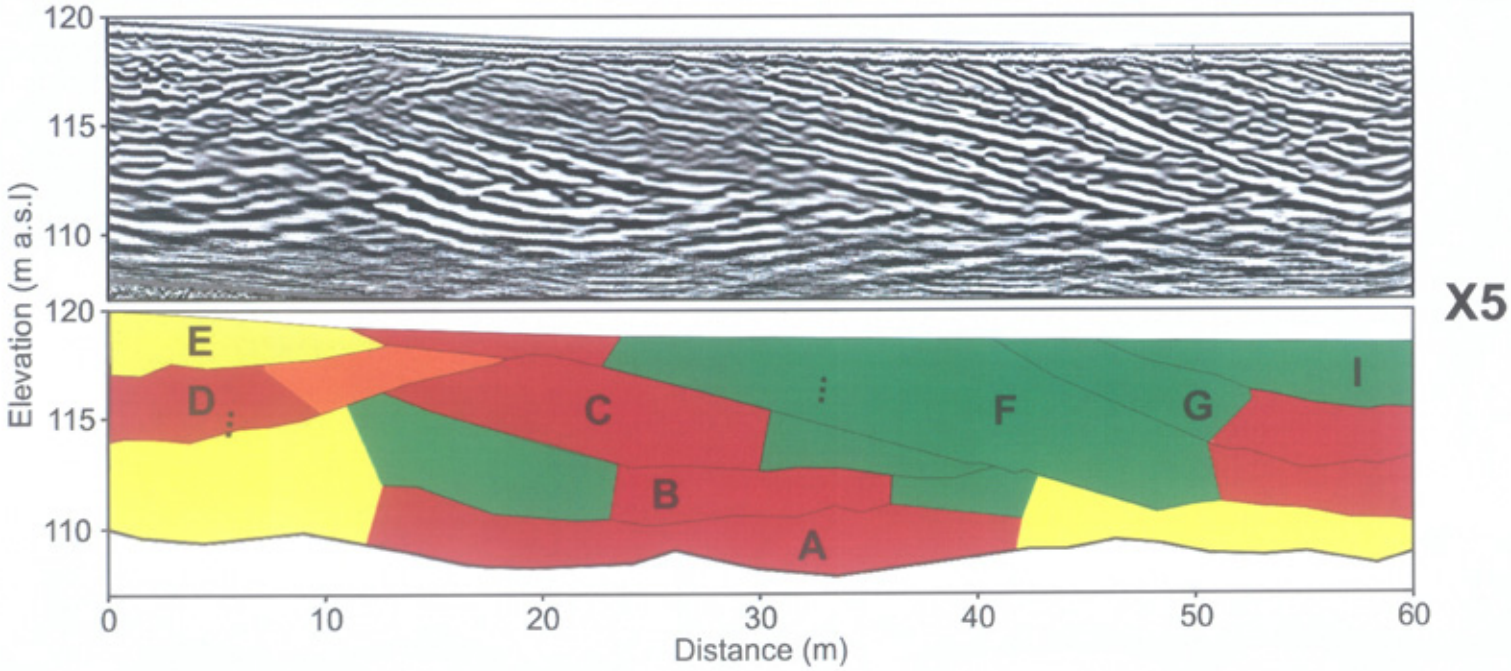
120
115
110
120
115
110
Elevation (m a.s.l)
E
D
C
B
A
F
G
I
0
10
20
30
40
50
60
Distance (m)
X5

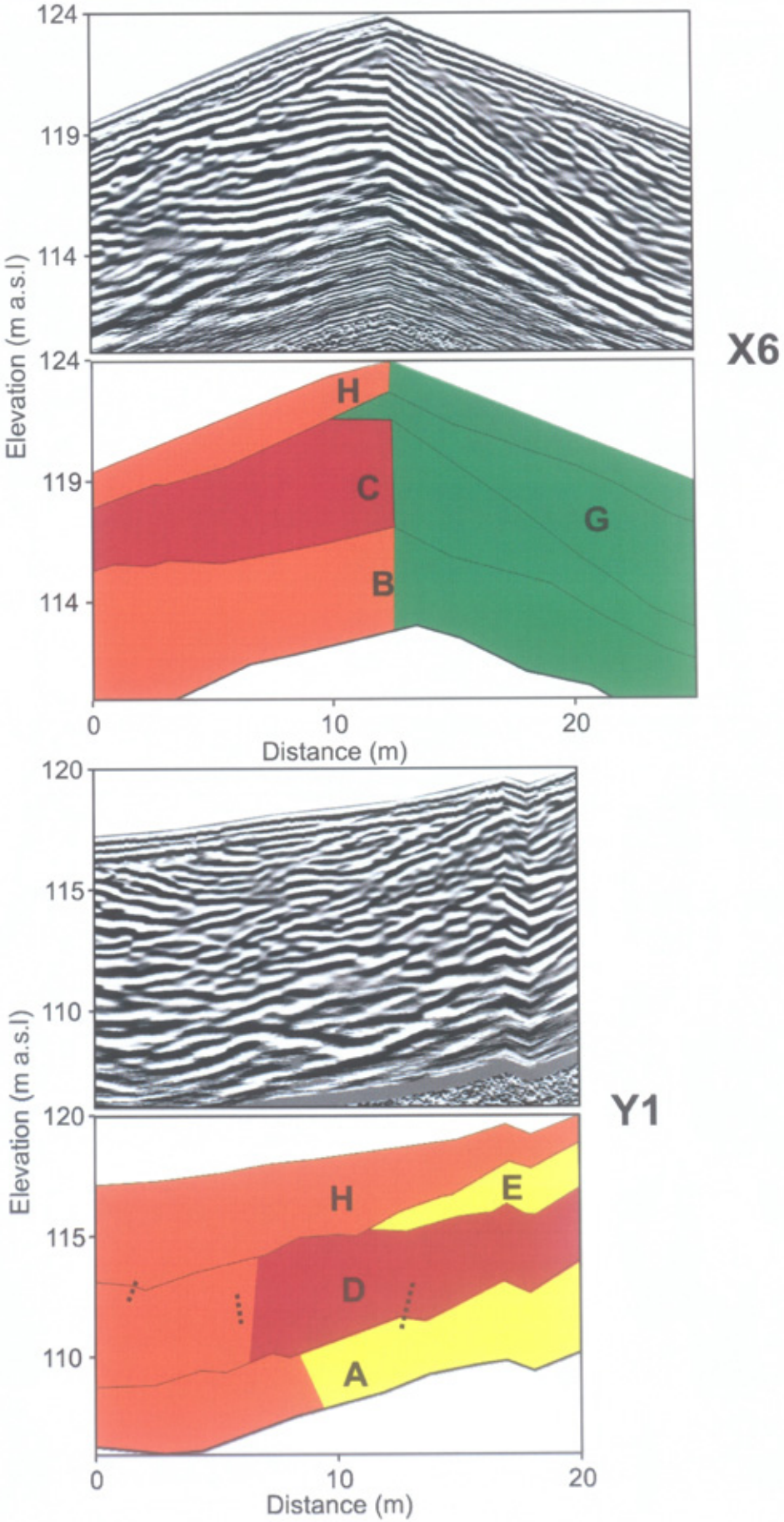
124
119
114
Elevation (m a.s.l)
X6
H
C
G
B
0
10
20
Distance (m)
120
115
110
Y1
E
D
A

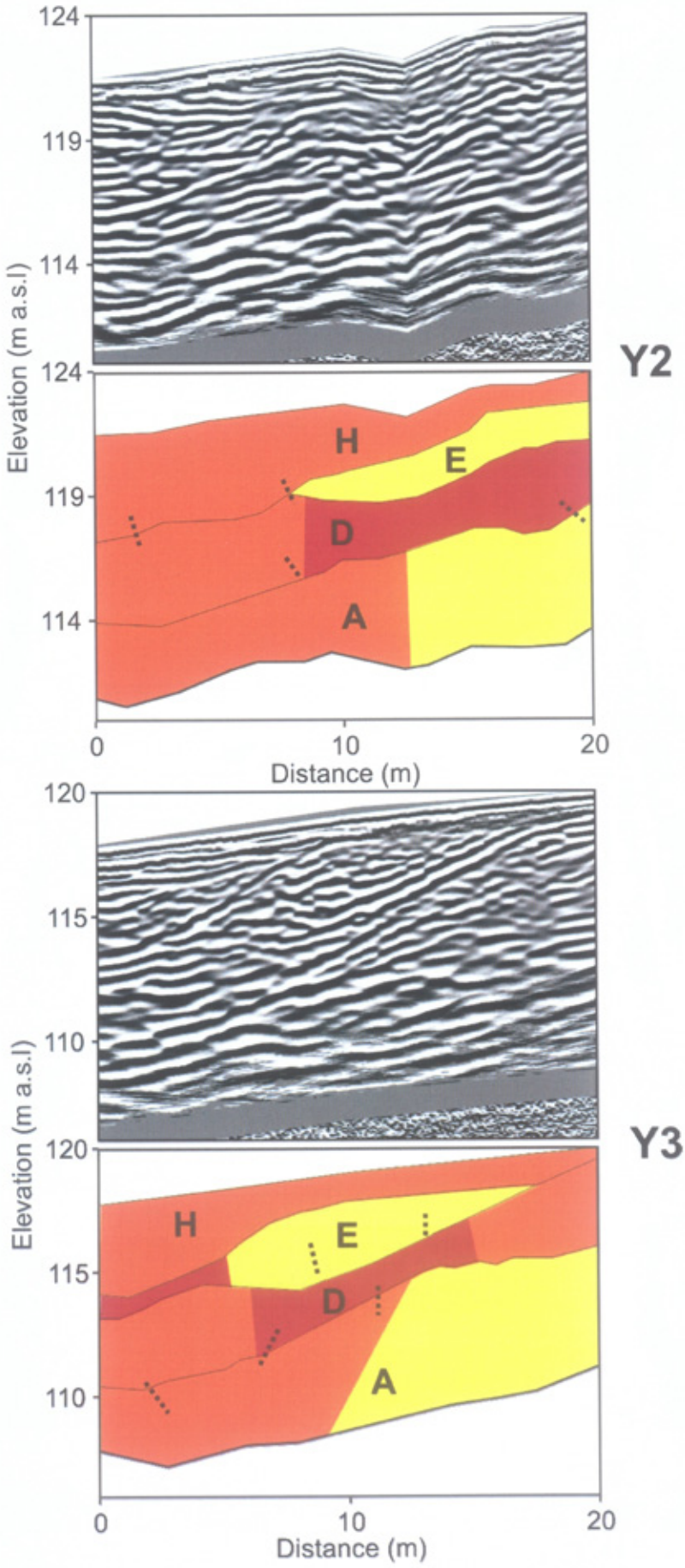
124
119
114
Elevation (m a.s.l)
Y2
H
E
D
A
0
10
20
Distance (m)
120
115
110
Y3
H
E
D
A

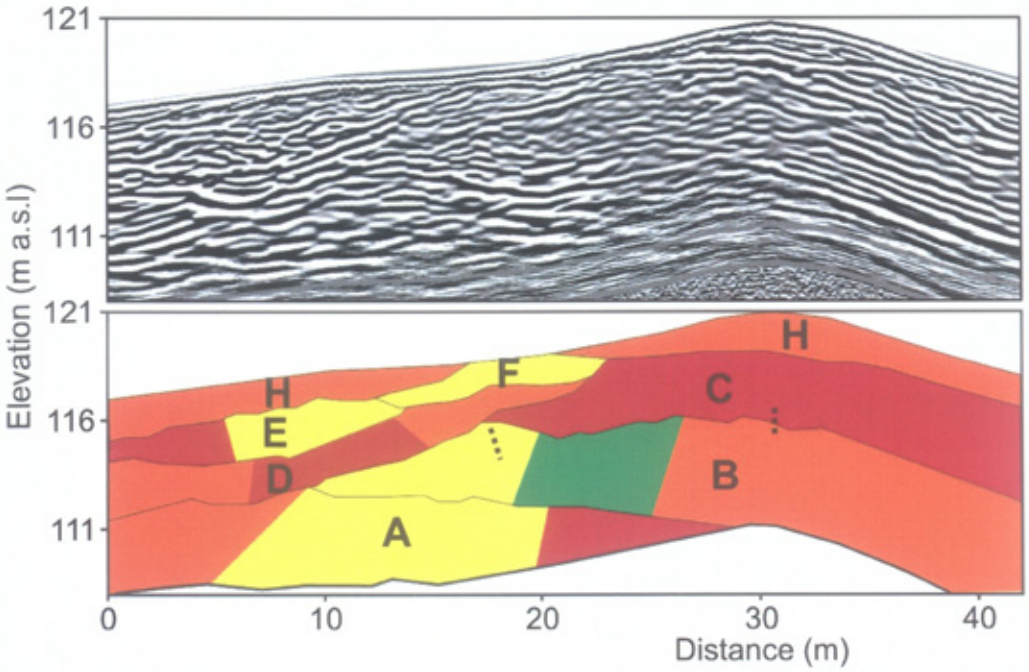
121
116
111
Elevation (m a.s.l)
121
116
111
H
F
C
H
E
D
B
A
0
10
20
30
40
Distance (m)

Y4

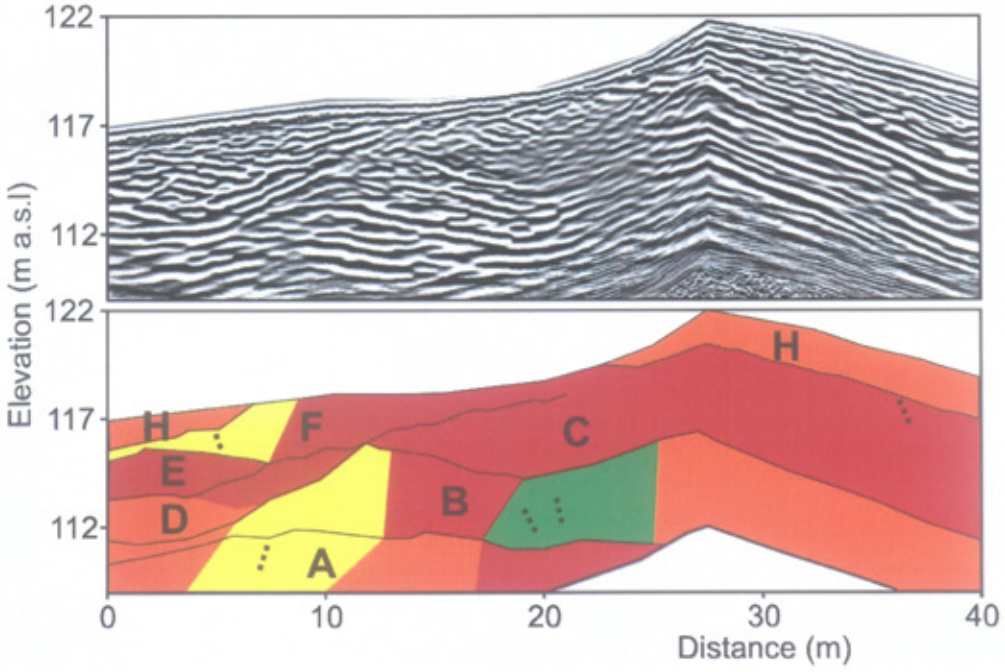
122
117
112
Elevation (m a.s.l)
122
117
112
H
H
F
C
E
D
B
A
0
10
20
30
40
Distance (m)

Y5

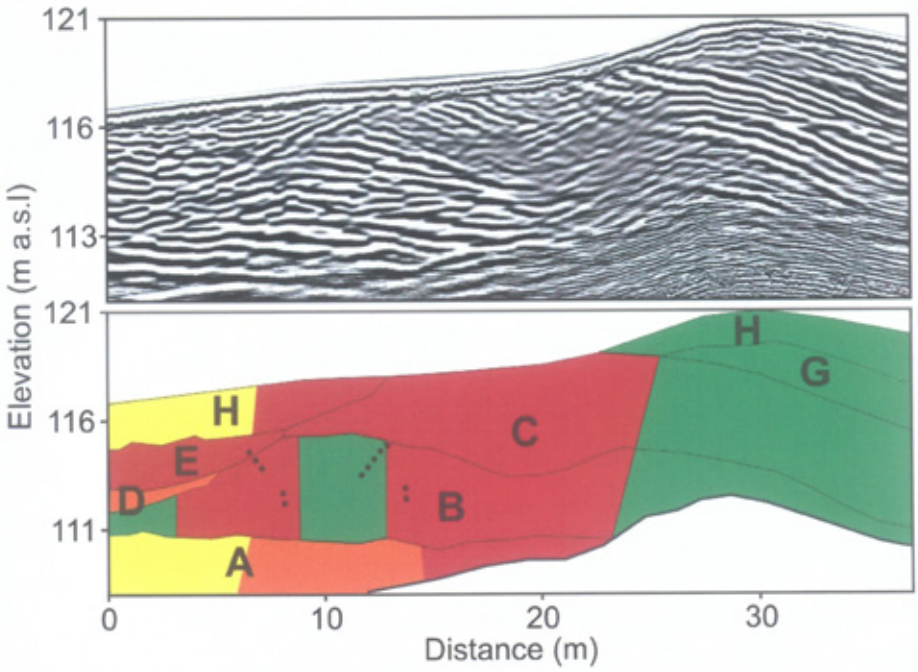
121
116
113
121
116
111
Elevation (m a.s.l)
H
G
H
C
E
D
B
A
0
10
20
30
Distance (m)

Y6

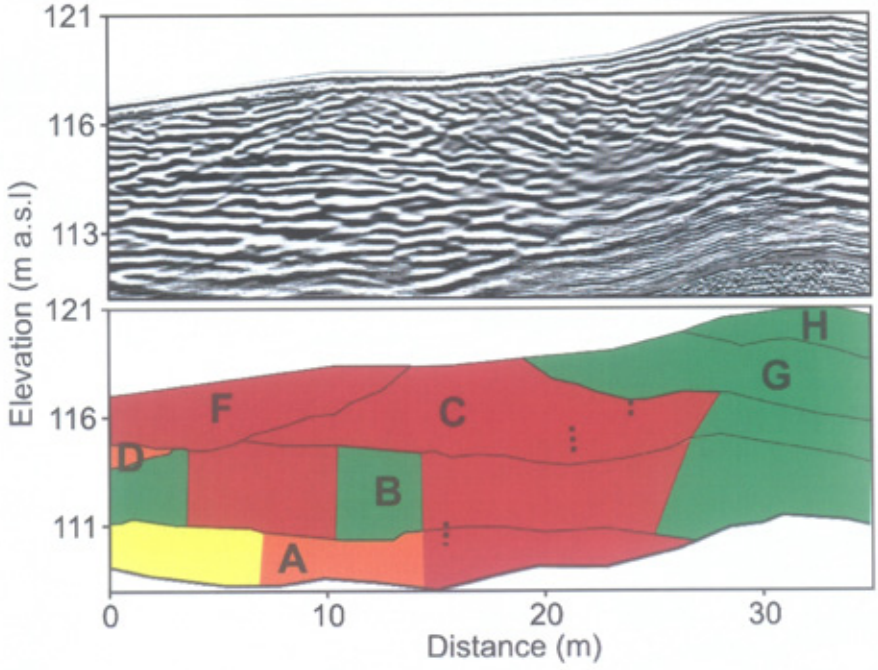
121
116
113
121
116
111
Elevation (m a.s.l)
H
G
F
C
D
B
A
0
10
20
30
Distance (m)

Y7

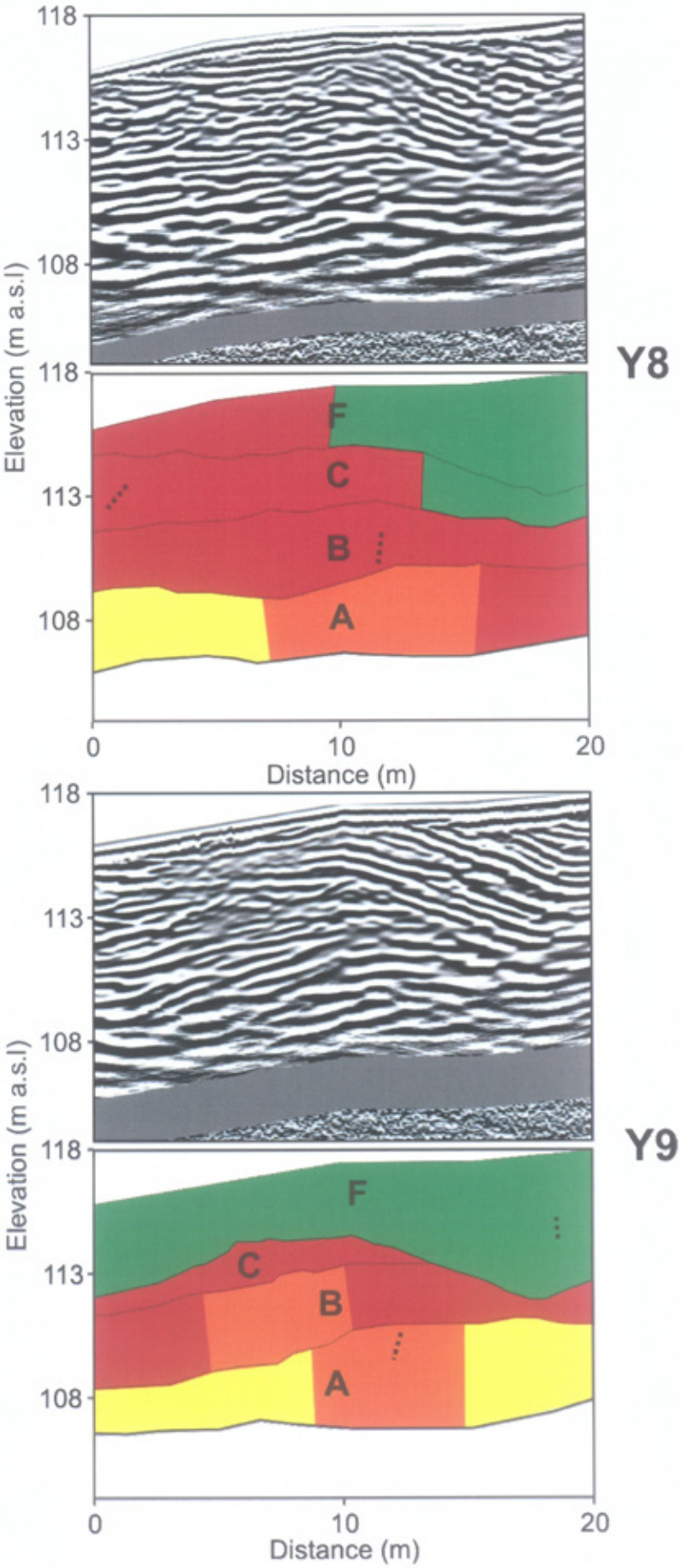
118
113
108
Elevation (m a.s.l)
Y8
F
C
B
A
0
10
20
Distance (m)
Y9

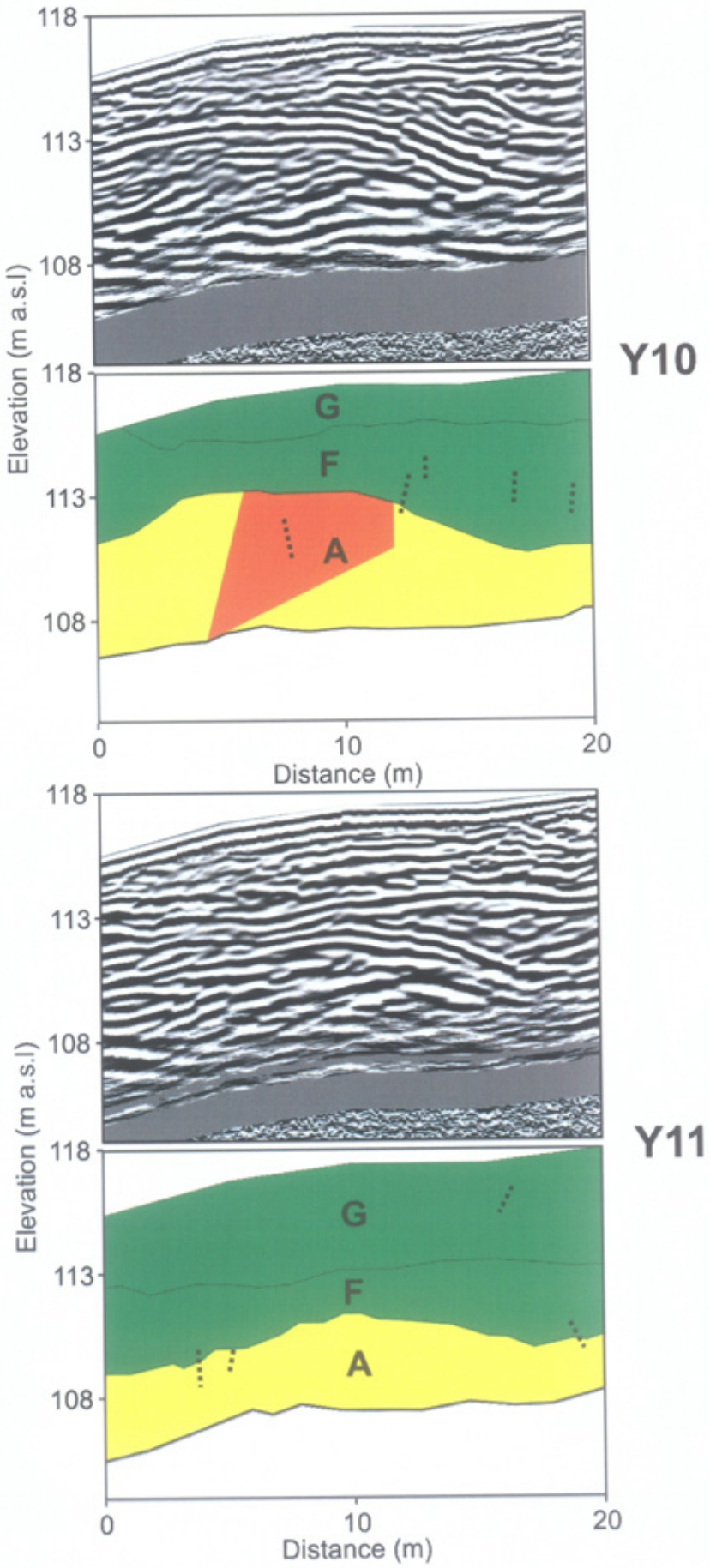
118
113
108
Elevation (m a.s.l)
Y10
G
F
A
0
10
20
Distance (m)
Y11

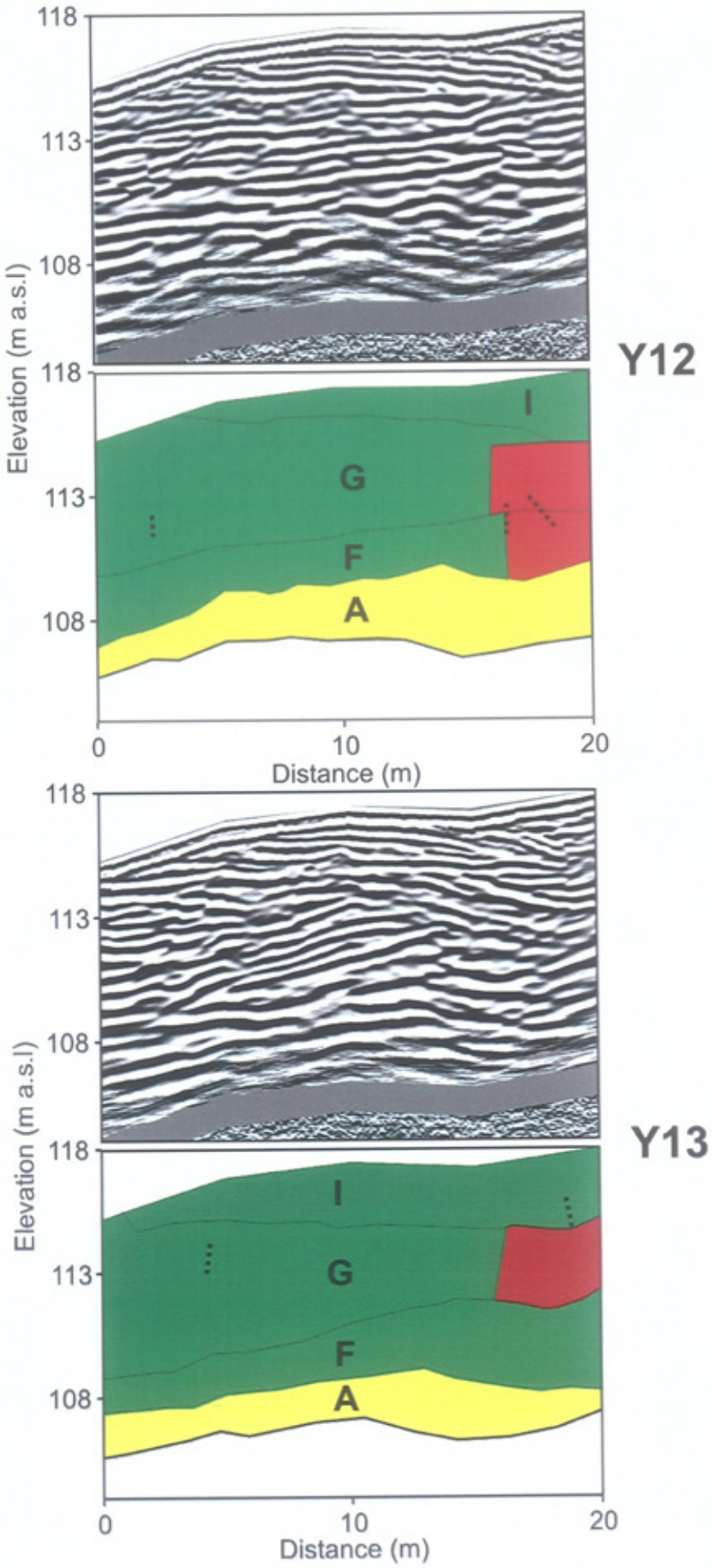
118
113
108
Elevation (m a.s.l)
Y12
I
G
F
A
0
10
20
Distance (m)
Y13

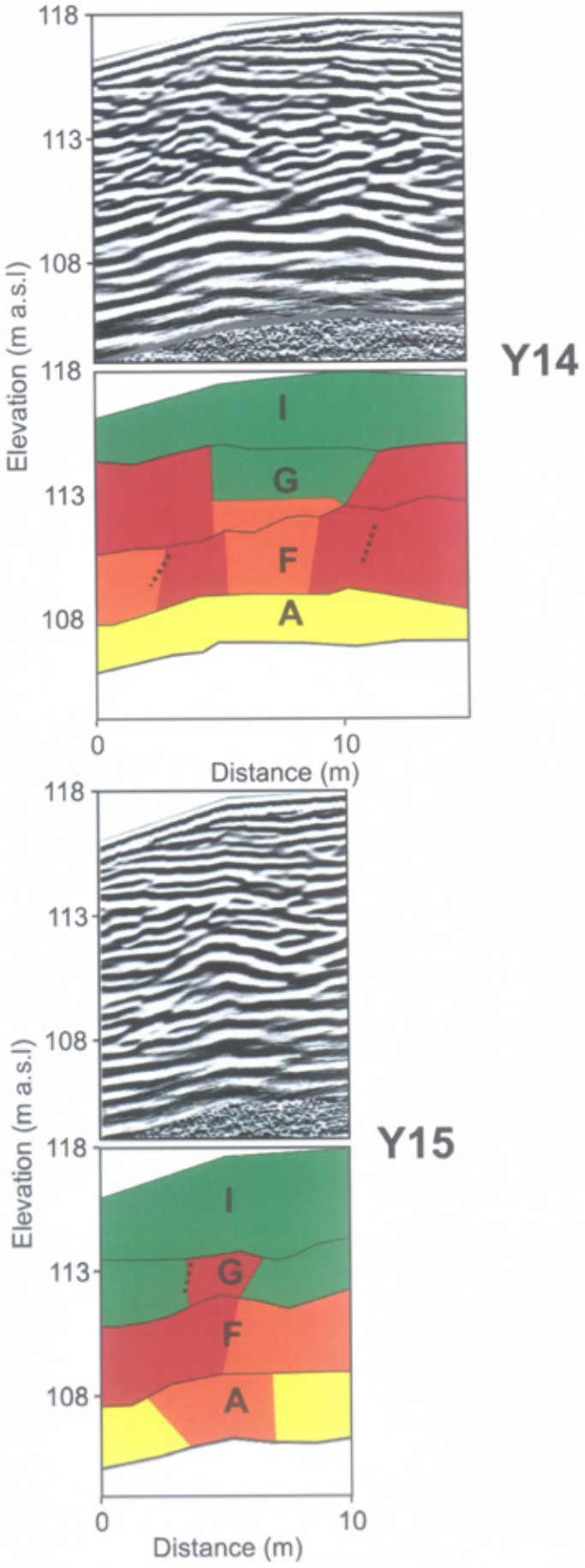
118
113
108
Elevation (m a.s.l)
Y14
I
G
F
A
0
10
Distance (m)
Y15

**SUB-GRID 3a**

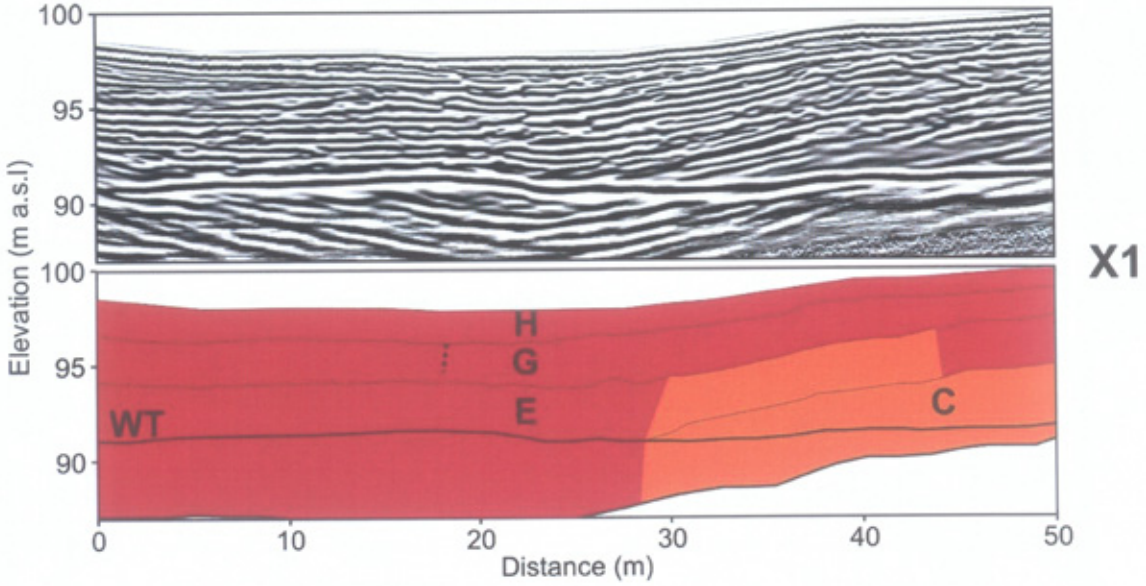
100
95
90
Elevation (m a.s.l)
X1
H
G
E
C
WT
0
10
20
30
40
50
Distance (m)

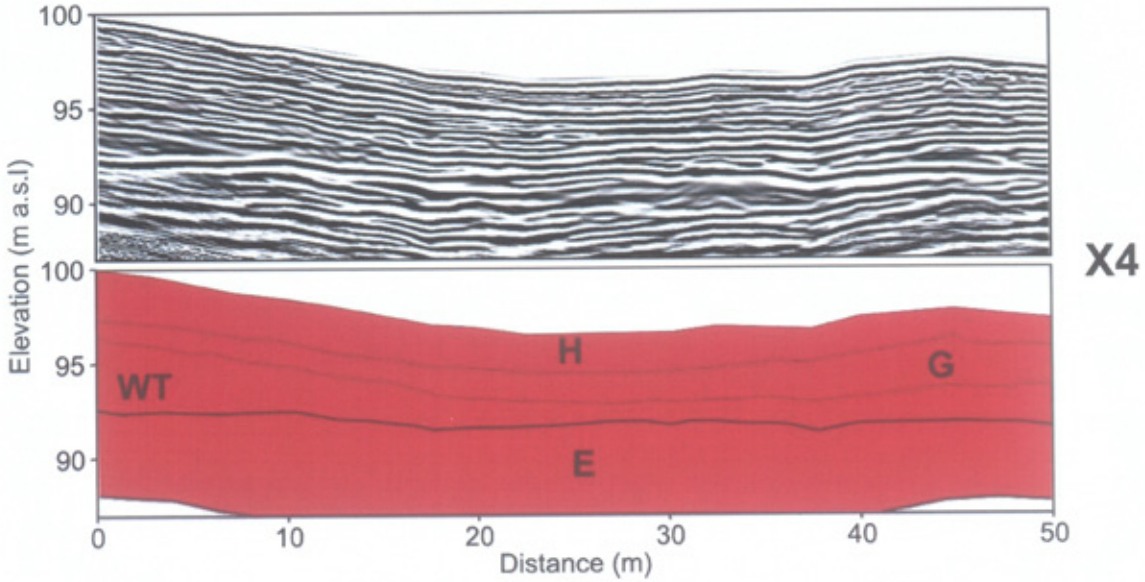
100
95
90
Elevation (m a.s.l)
X4
H
G
WT
E
0
10
20
30
40
50
Distance (m)

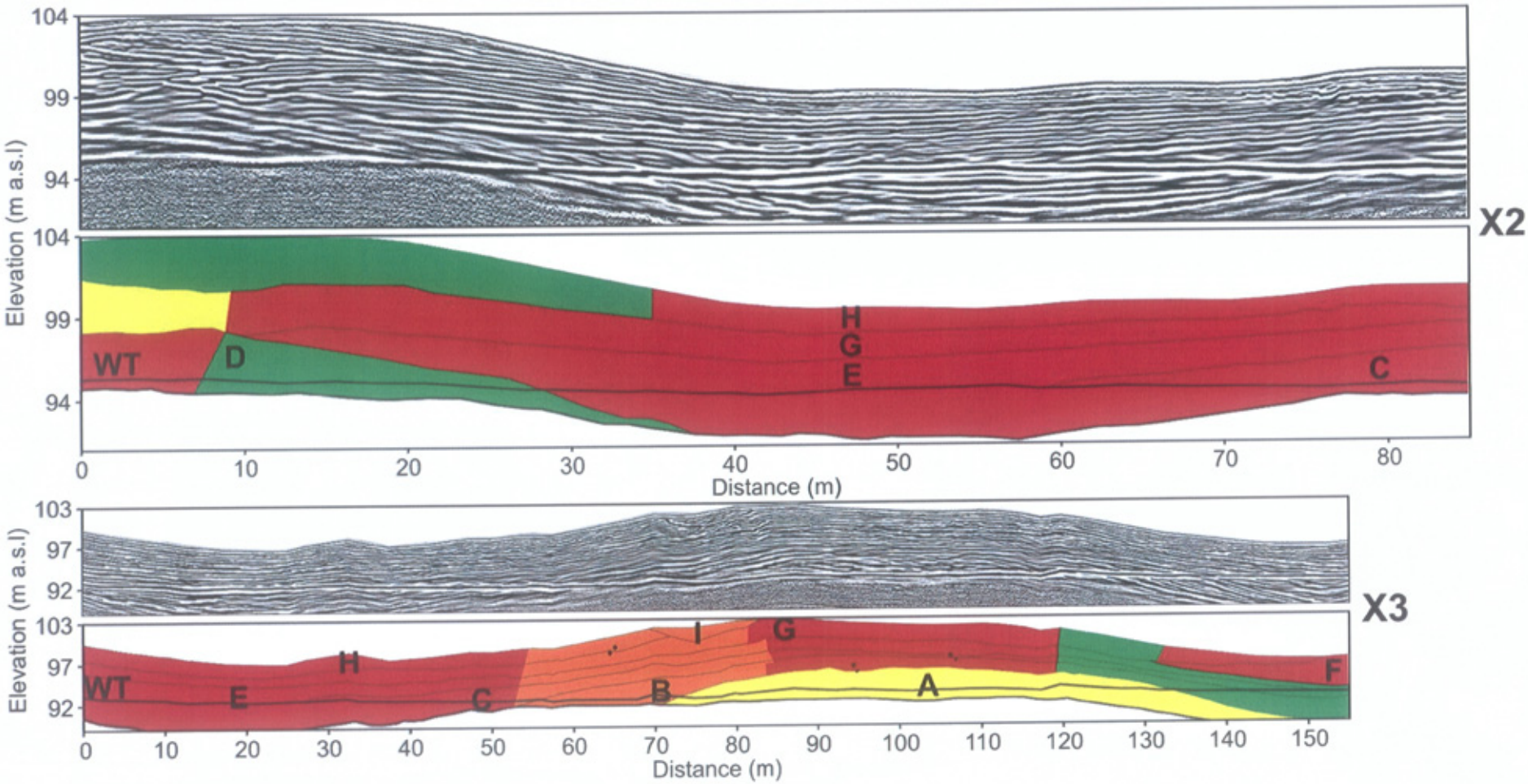
104
99
94
Elevation (m a.s.l)
X2
WT
D
H
G
E
C
0
10
20
30
40
50
60
70
80
Distance (m)
103
97
92
X3
I
G
H
WT
E
C
B
A
F
90
100
110
120
130
140
150

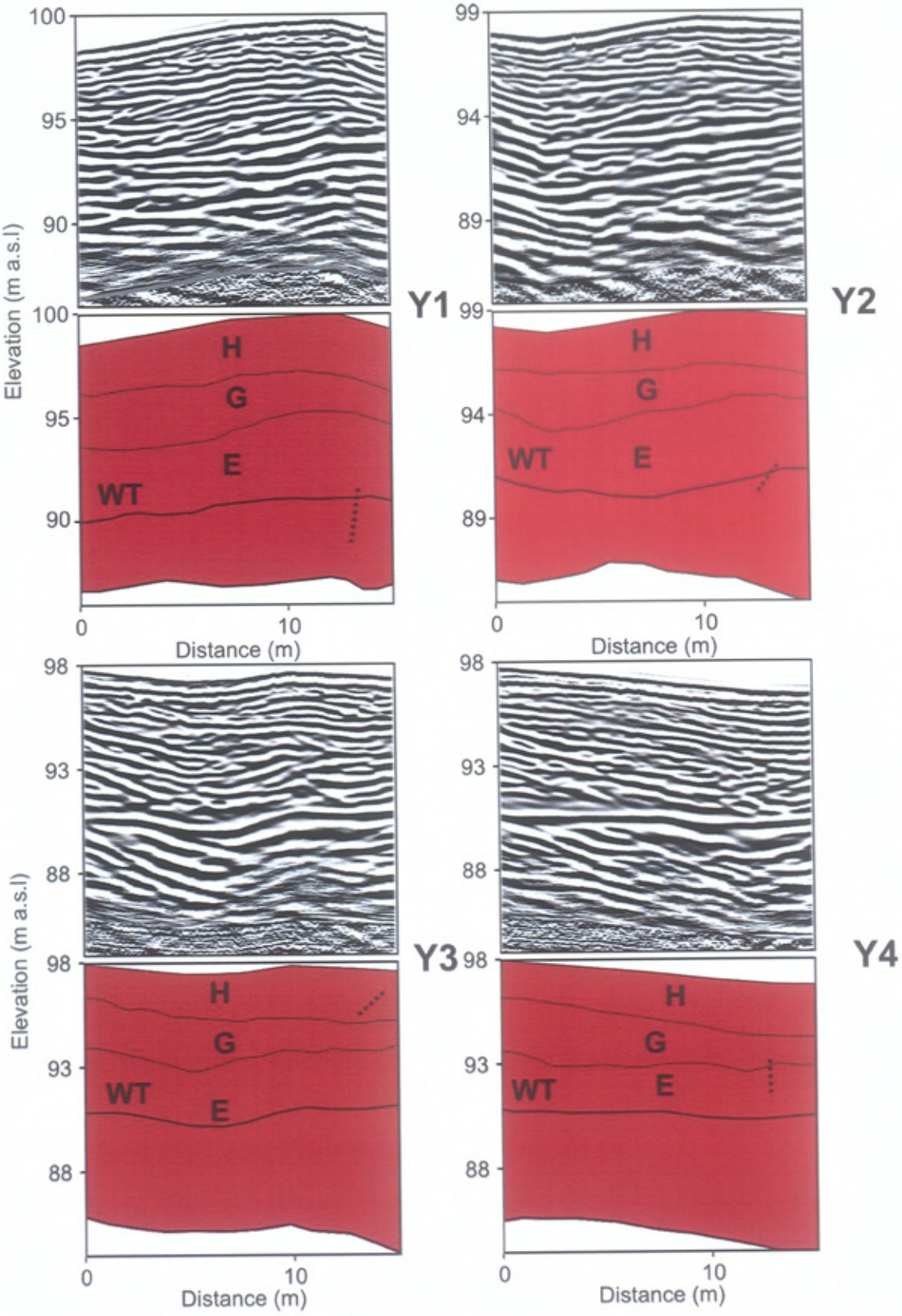
Y1
Y2
Y3
Y4
Elevation (m a.s.l)
Distance (m)
H
G
E
WT
100
95
90
99
94
89
98
93
88
0
10

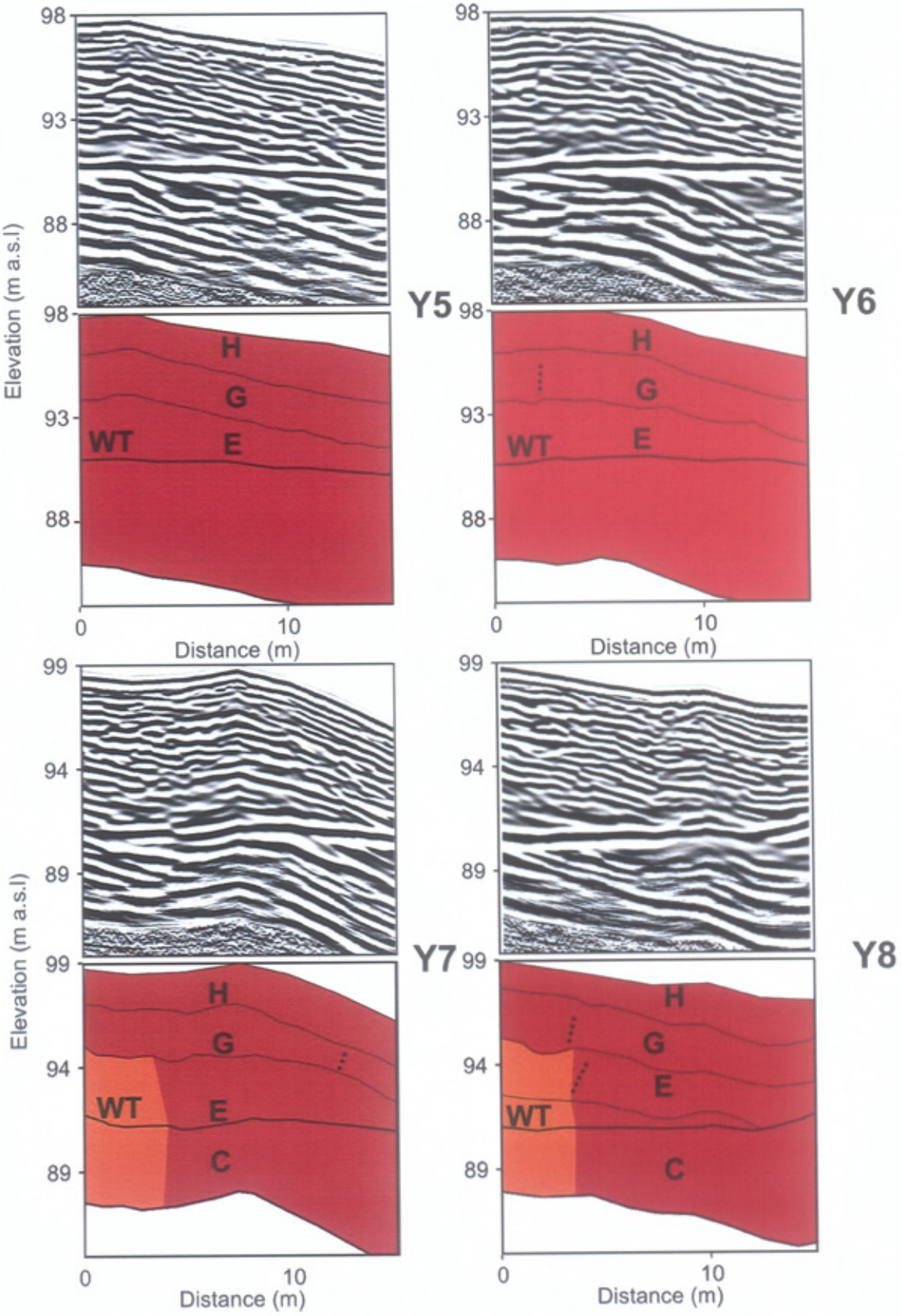
Y5
Y6
Y7
Y8
Elevation (m a.s.l)
Distance (m)
H
G
E
C
WT
98
93
88
99
94
89
0
10

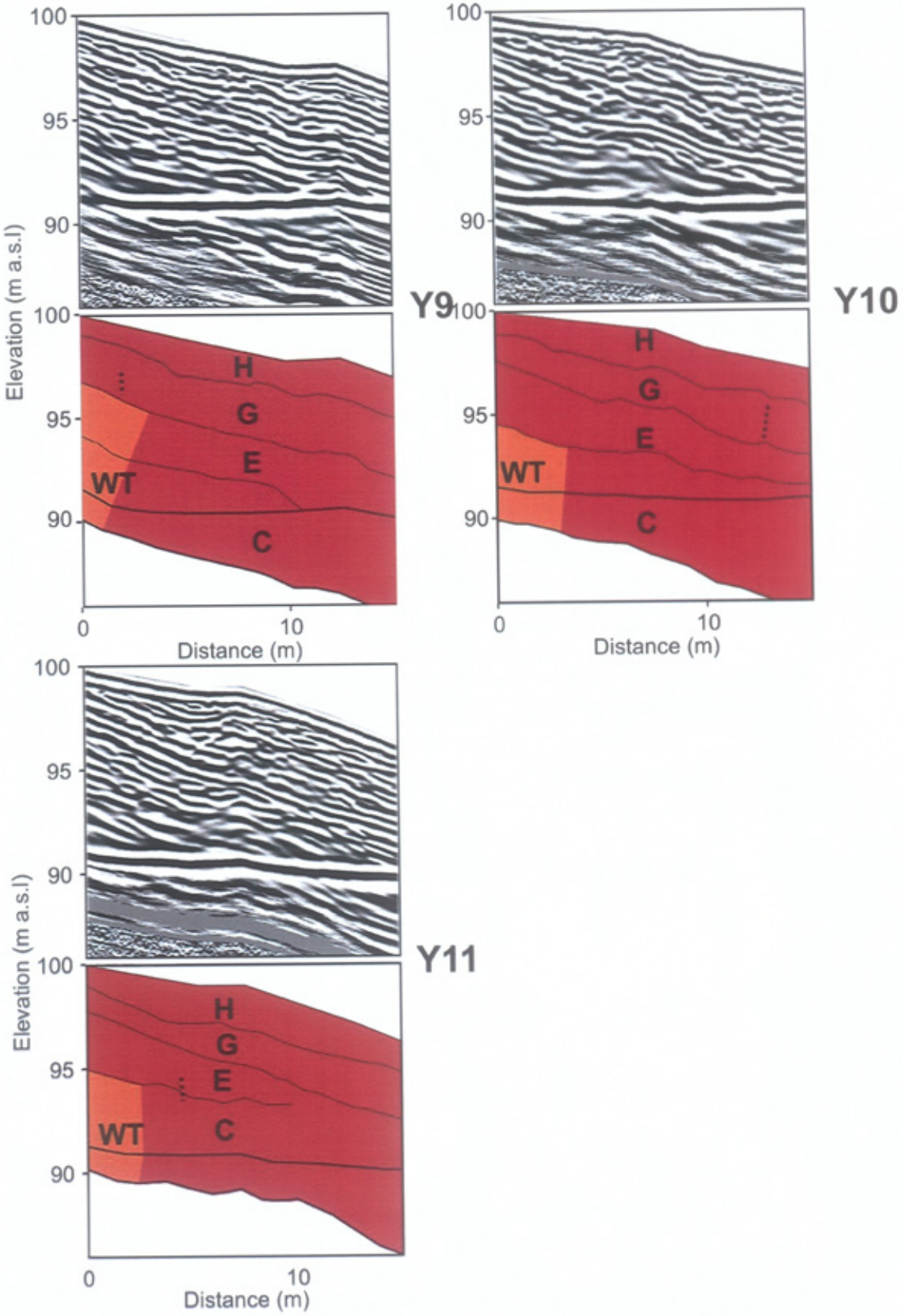
Y9
Y10
Y11
Elevation (m a.s.l)
Distance (m)
100
95
90
0
10
H
G
E
C
WT

**SUB-GRID 3b**

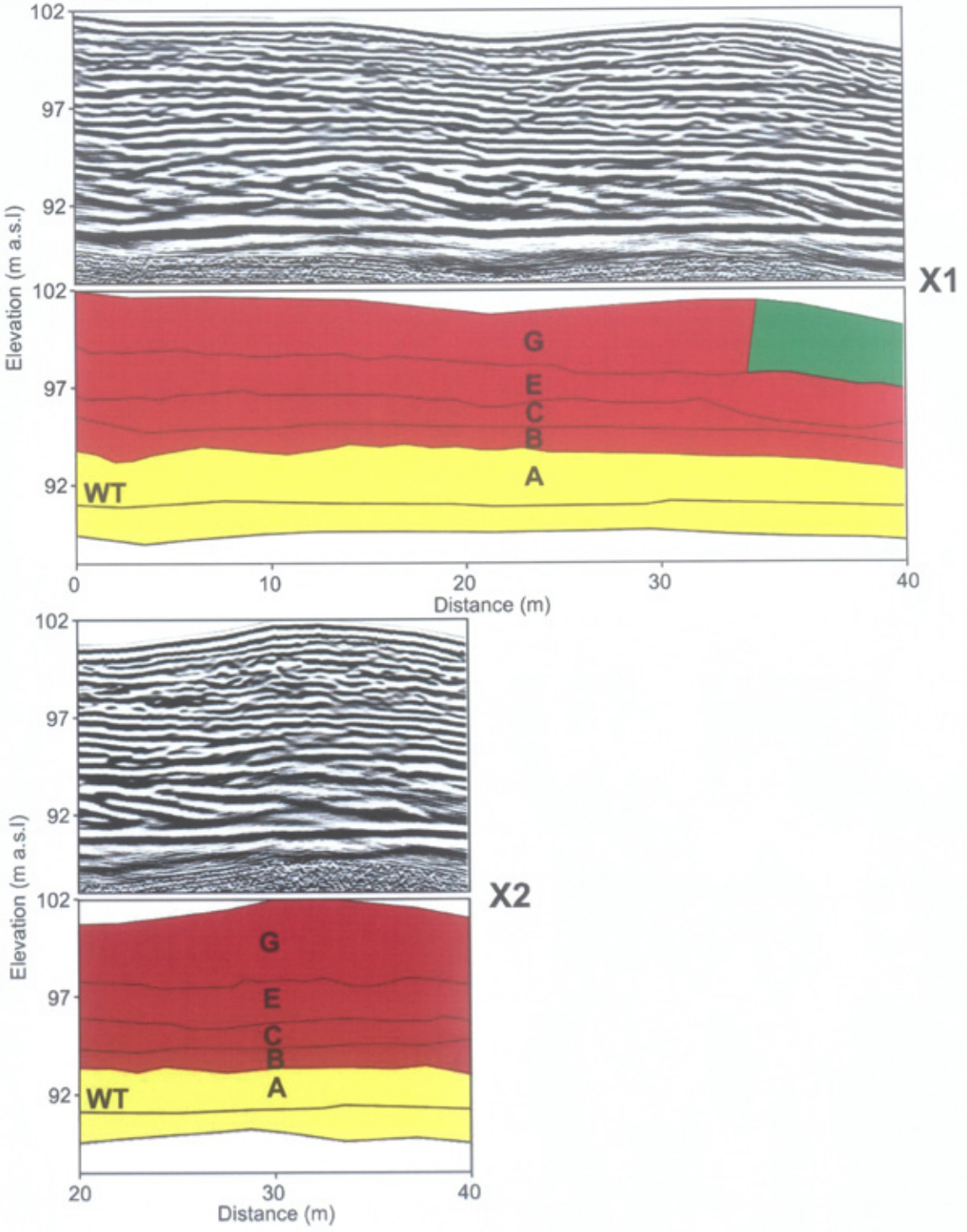
102
97
92
Elevation (m a.s.l)
X1
G
E
C
B
A
WT
0
10
20
30
40
Distance (m)
X2
20
30
40
Distance (m)

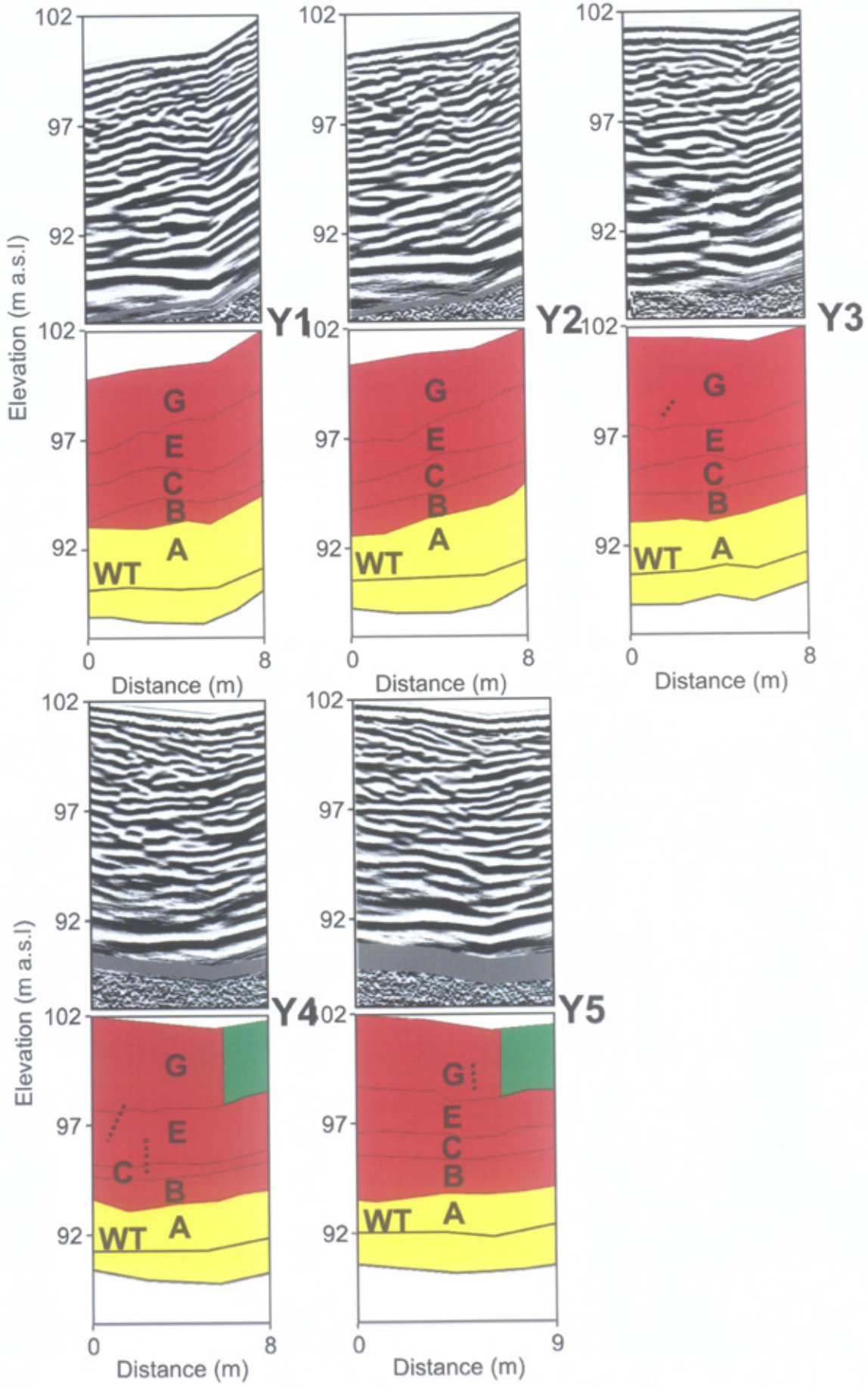
Elevation (m a.s.l)
102
97
92
Y1
Y2
Y3
Y4
Y5
G
E
C
B
A
WT
0
8
9
Distance (m)

**SUB-GRID 3c**

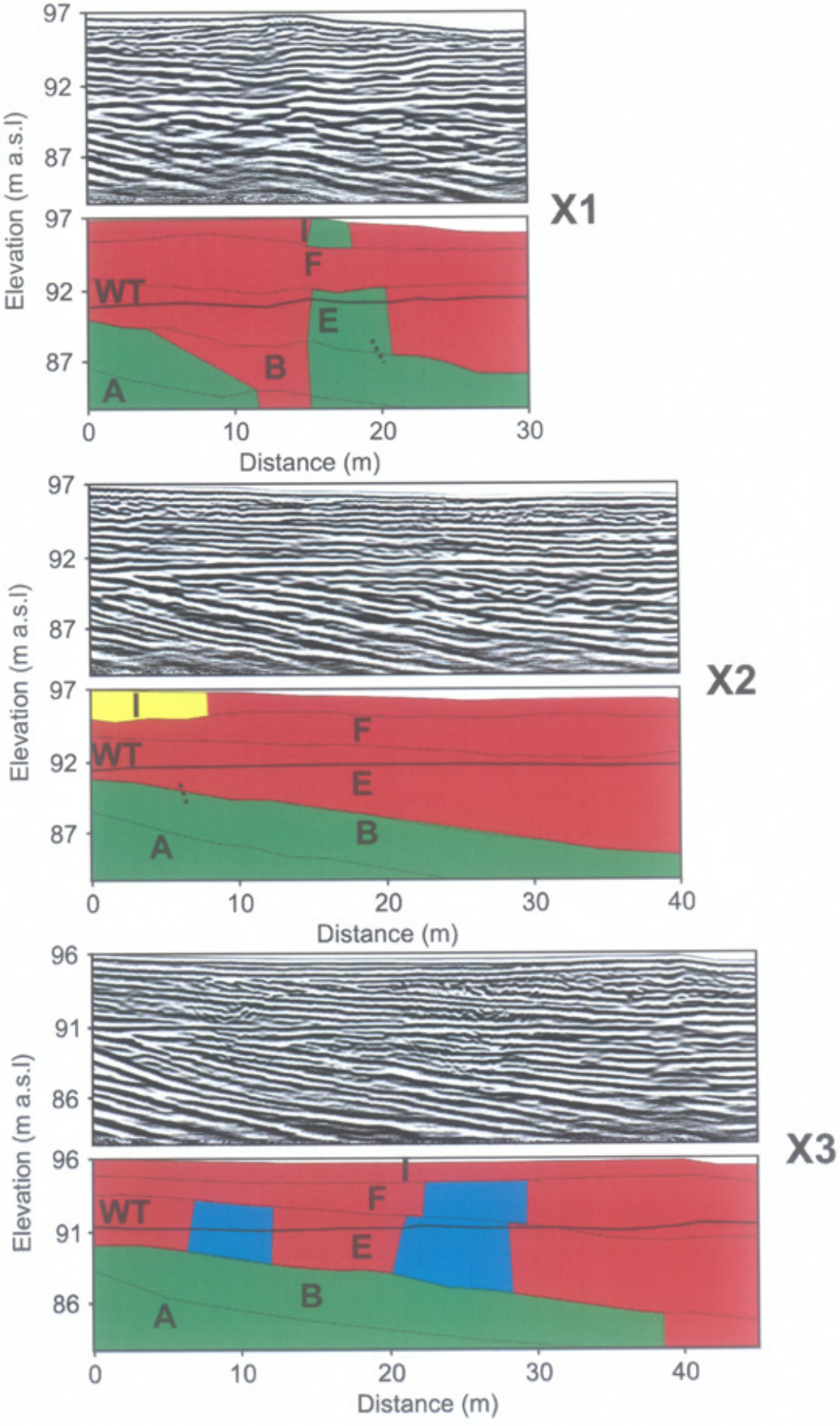

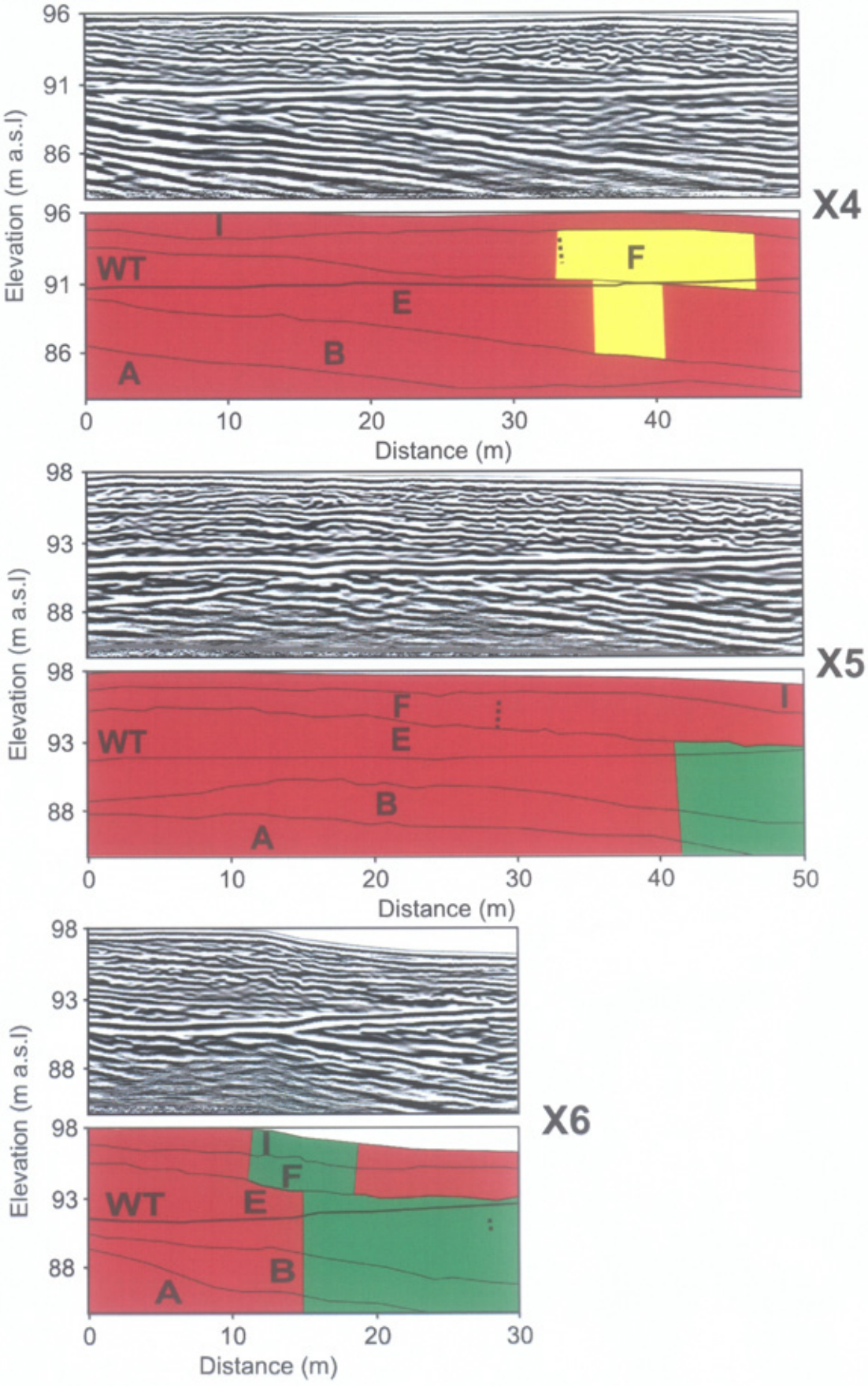
96
91
86
Elevation (m a.s.l)
X4
I
WT
F
E
B
A
0
10
20
30
40
Distance (m)
98
93
88
X5
I
F
E
WT
B
A
50
X6

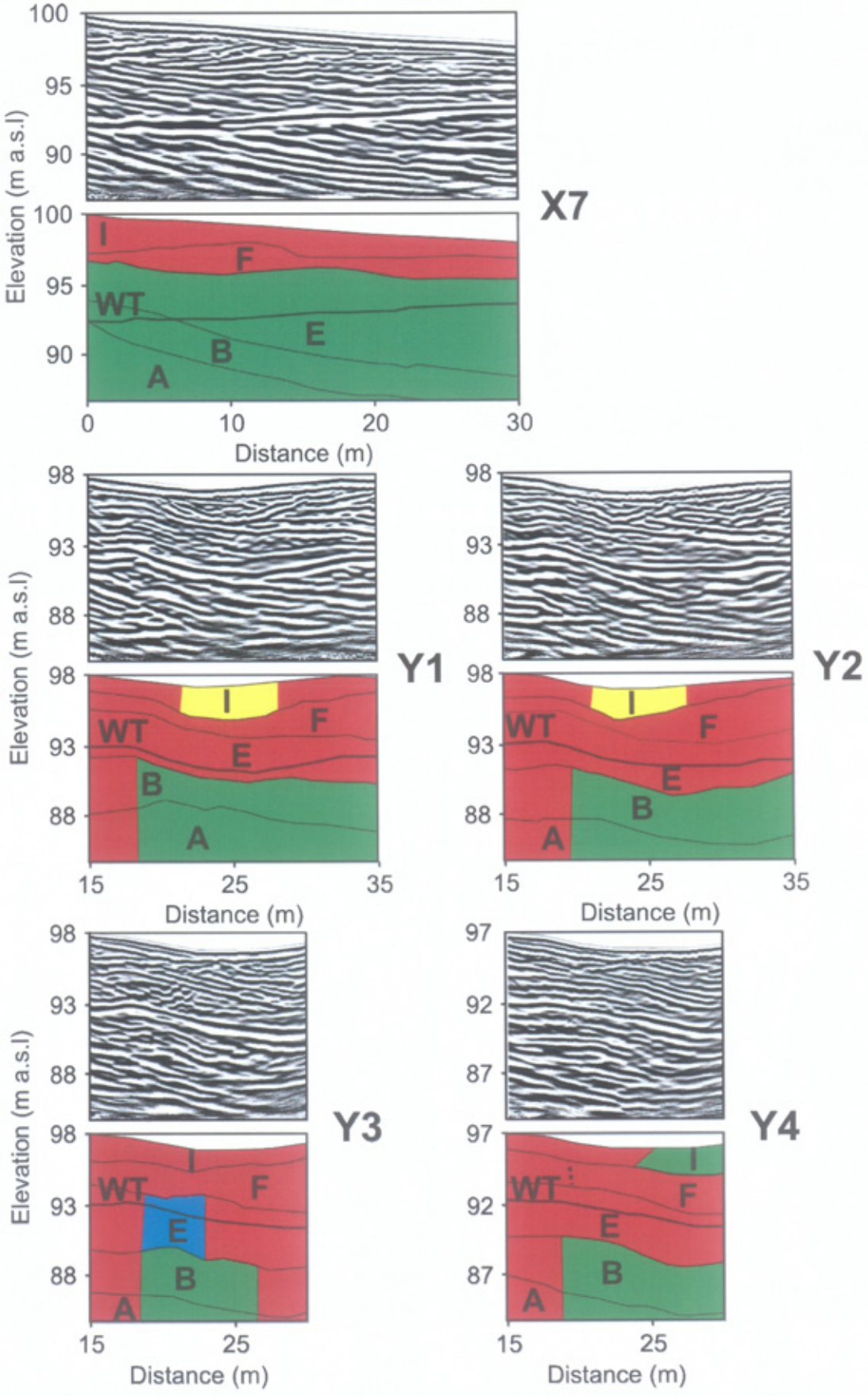
X7
Elevation (m a.s.l)
100
95
90
I
F
WT
E
B
A
0
10
20
30
Distance (m)
Y1
98
93
88
15
25
35
Y2
Y3
97
92
87
Y4

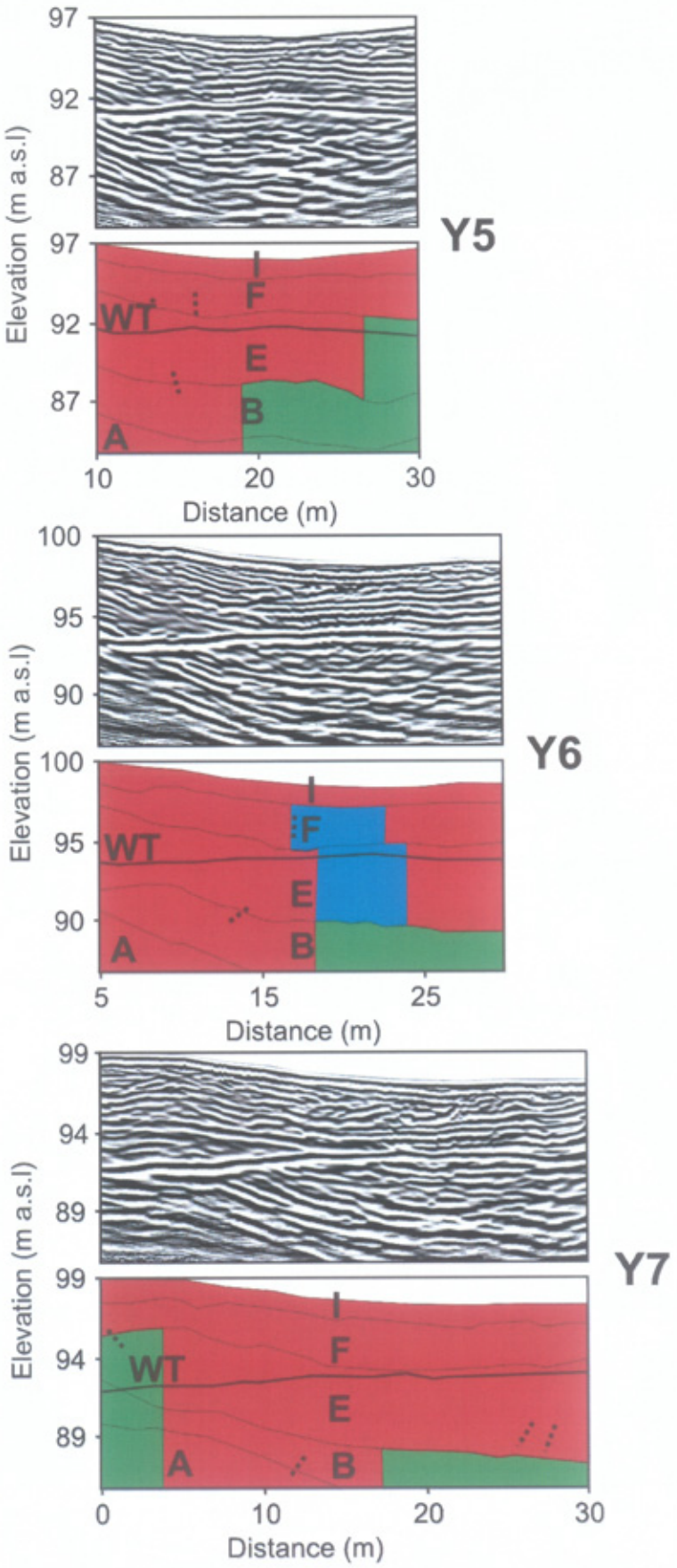
Y5
Elevation (m a.s.l)
97
92
87
WT
F
E
B
A
10
20
30
Distance (m)
Y6
100
95
90
5
15
25
Y7
99
94
89
0

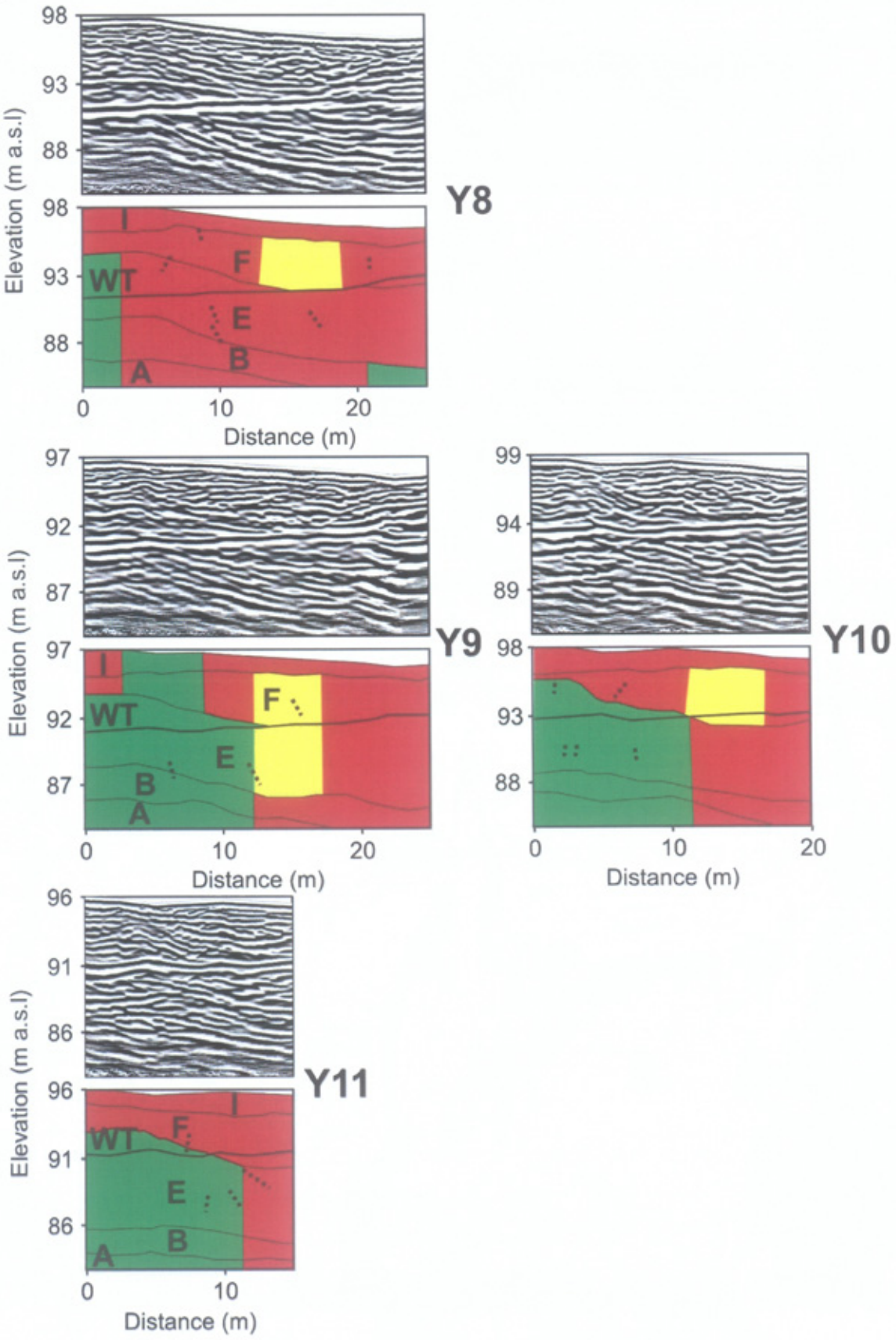
Y8
Y9
Y10
Y11
Elevation (m a.s.l)
Distance (m)
WT
I
F
E
B
A

**SUB-GRID 4a**

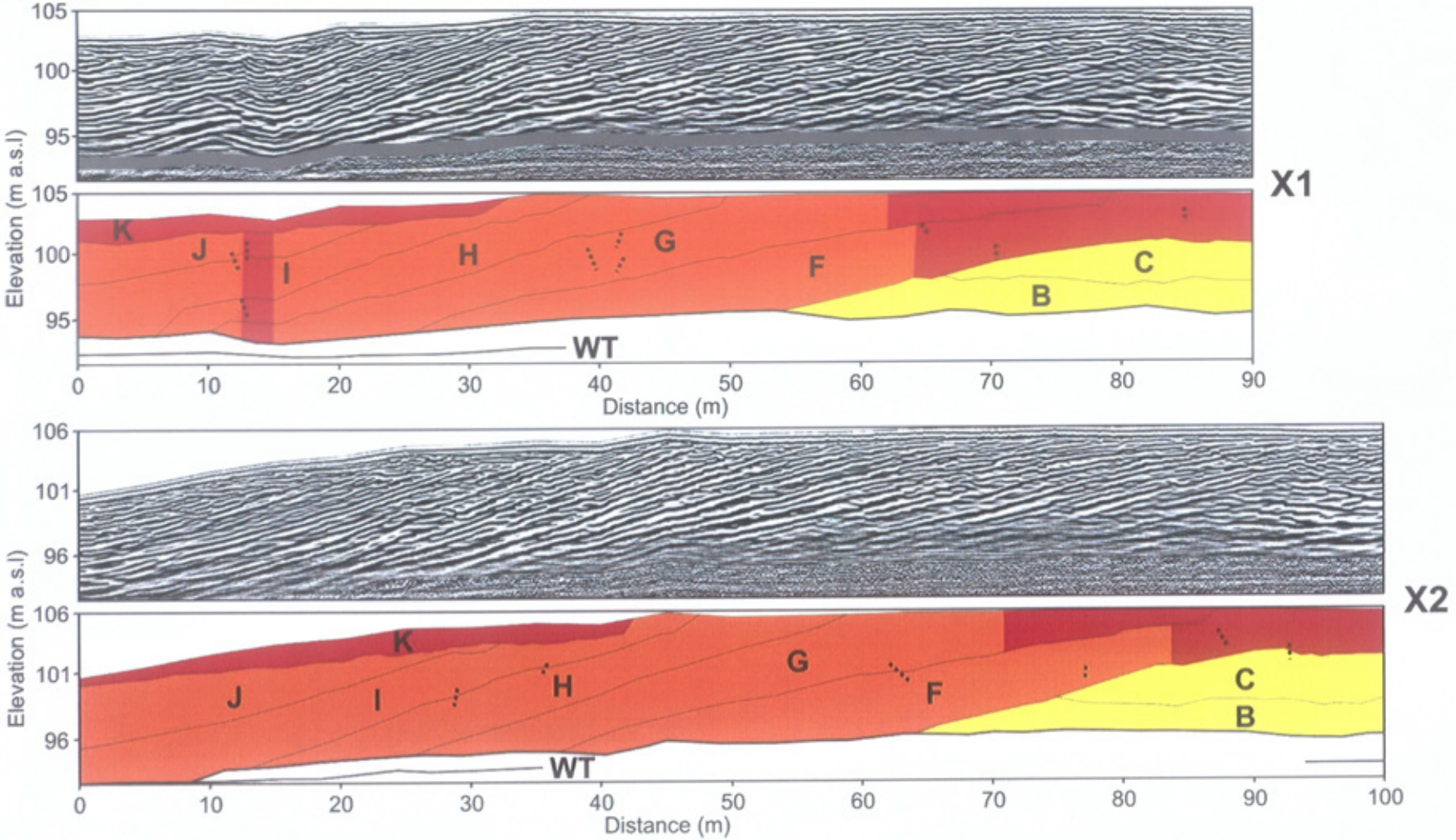
X1
Elevation (m a.s.l)
105
100
95
K
J
I
H
G
F
C
B
WT
0
10
20
30
40
50
60
70
80
90
Distance (m)
X2
Elevation (m a.s.l)
106
101
96
K
J
I
H
G
F
C
B
WT
0
10
20
30
40
50
60
70
80
90
100
Distance (m)

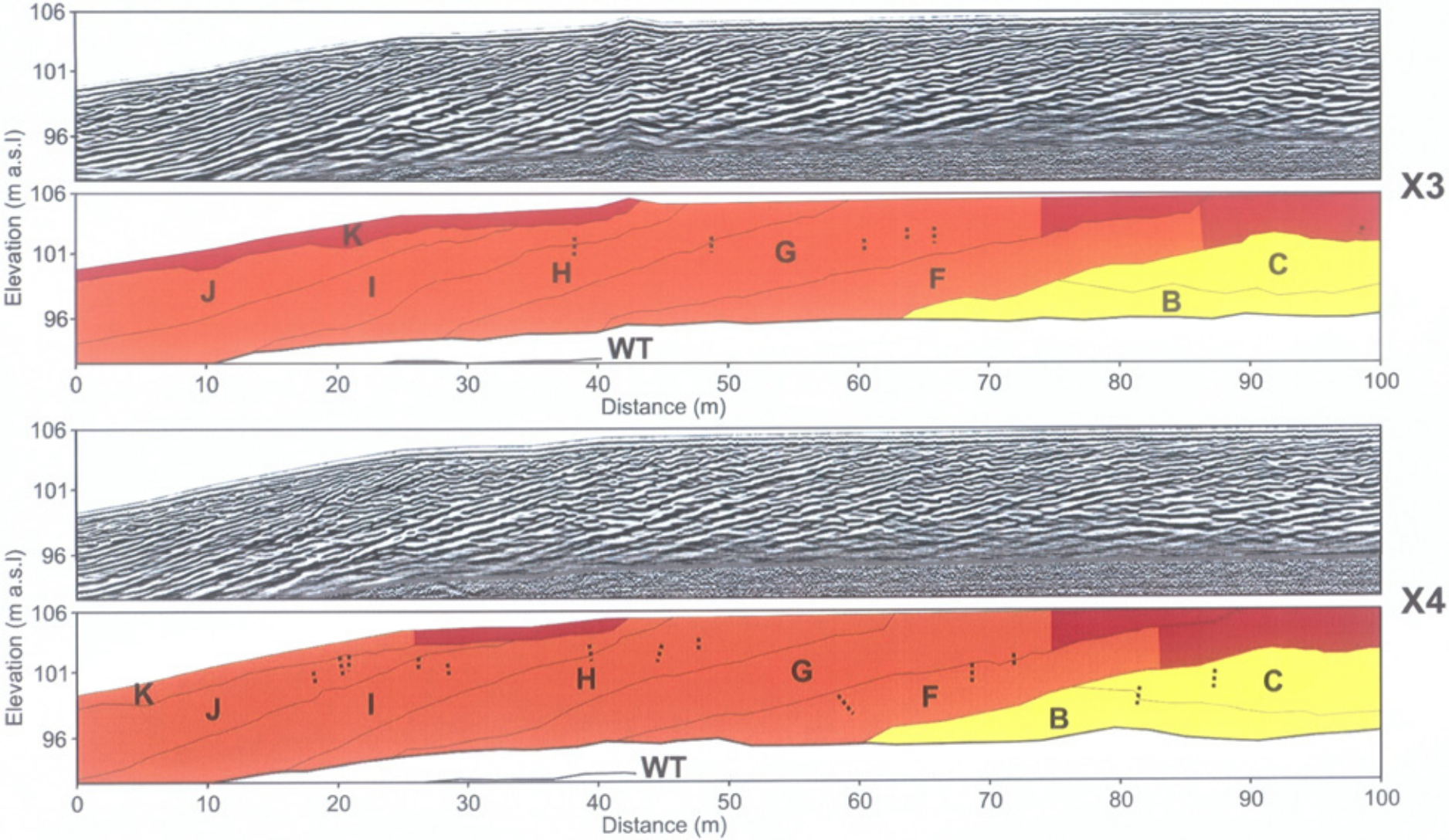
X3
X4
Elevation (m a.s.l)
106
101
96
K
J
I
H
G
F
C
B
WT
0
10
20
30
40
50
60
70
80
90
100
Distance (m)

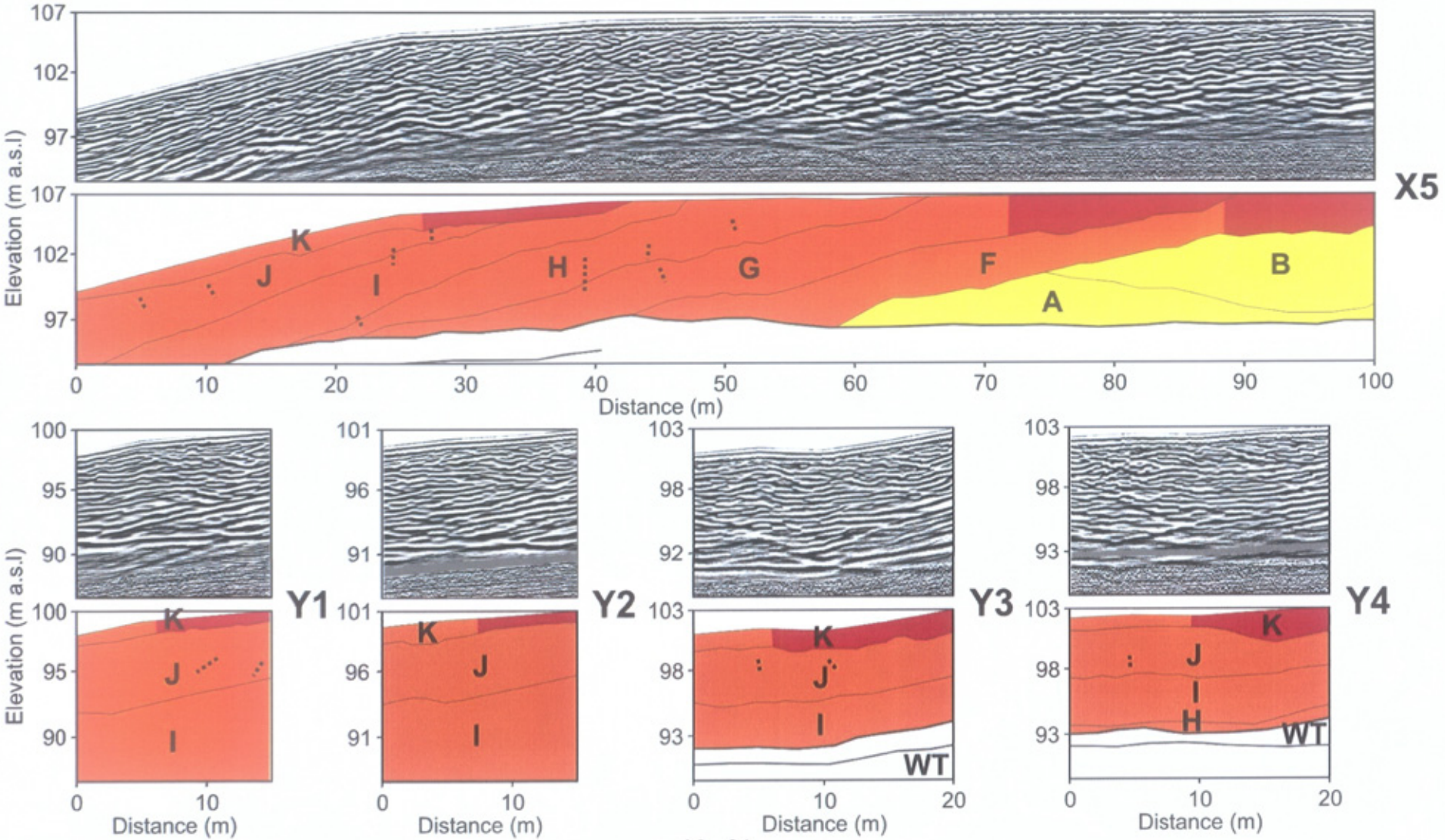
X5
Elevation (m a.s.l)
Distance (m)
K
J
I
H
G
F
A
B
Y1
Y2
Y3
Y4
WT

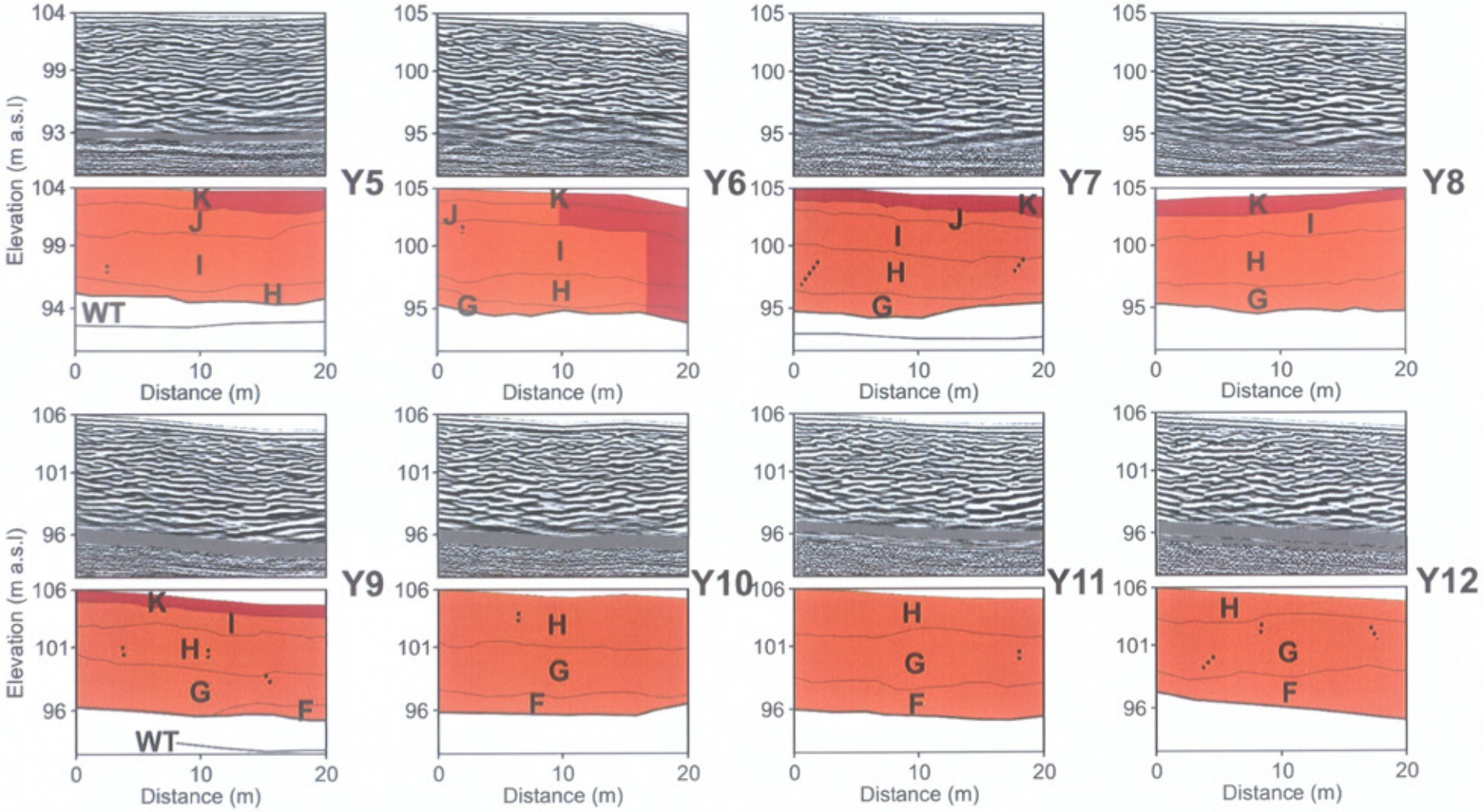
Y5
Y6
Y7
Y8
Y9
Y10
Y11
Y12
Elevation (m a.s.l)
Distance (m)
WT
K
J
I
H
G
F

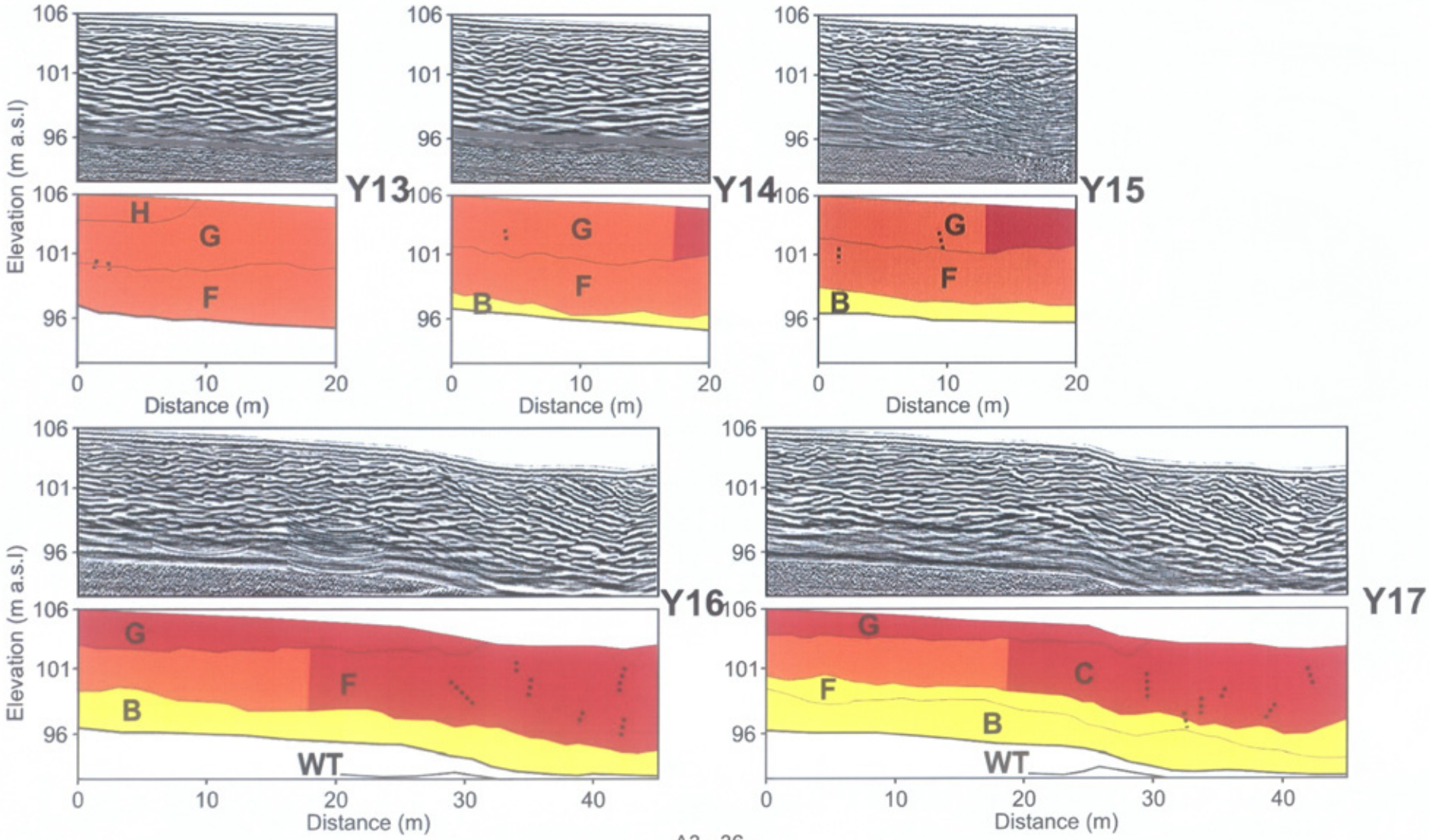
Y13
Y14
Y15
Y16
Y17
Elevation (m a.s.l)
Distance (m)
106
101
96
H
G
F
B
C
WT
0
10
20
30
40

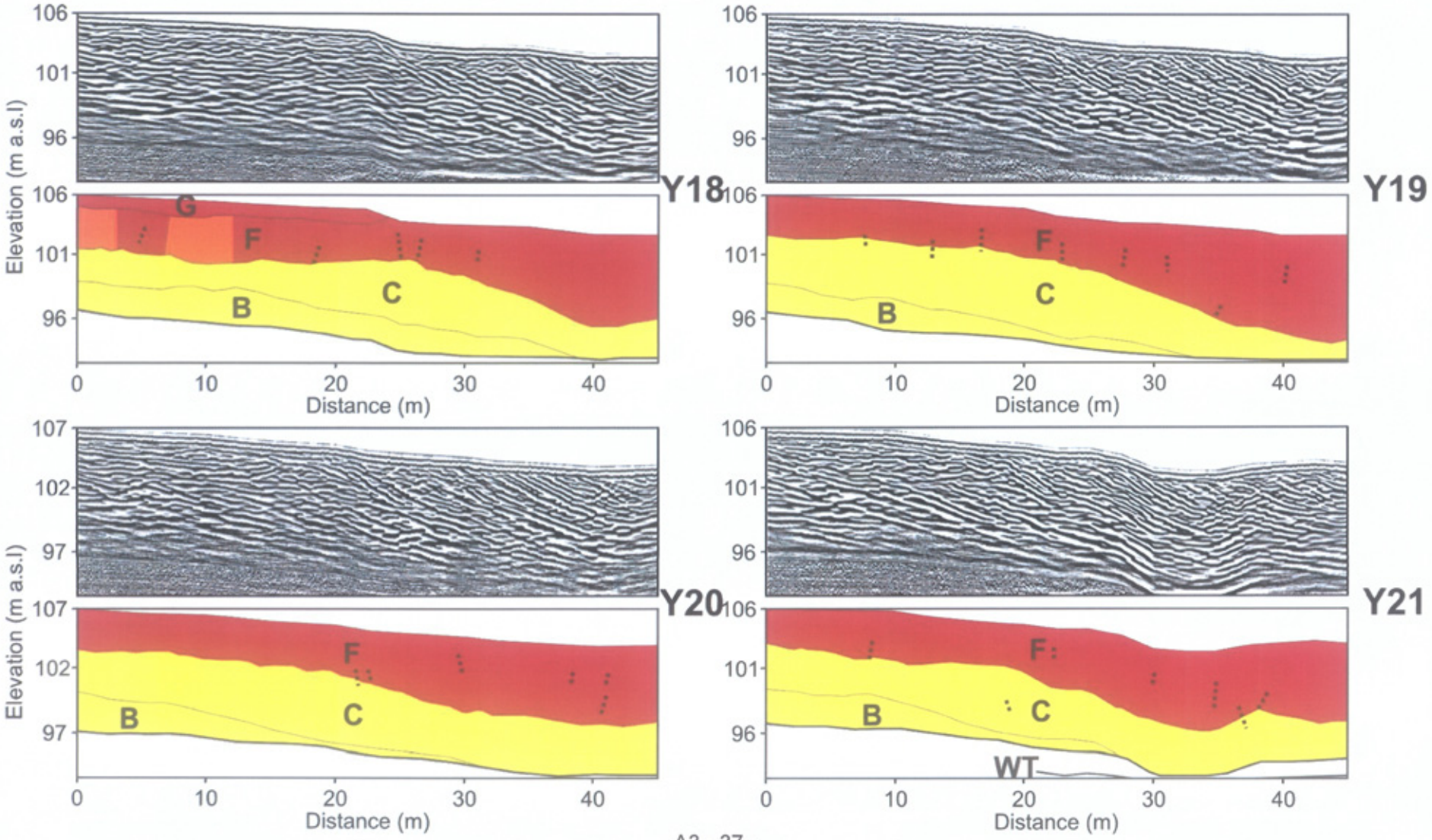
Y18
Y19
Y20
Y21
Elevation (m a.s.l)
Distance (m)
G
F
C
B
WT
106
101
96
107
102
97
0
10
20
30
40

**SUB-GRID 4b**

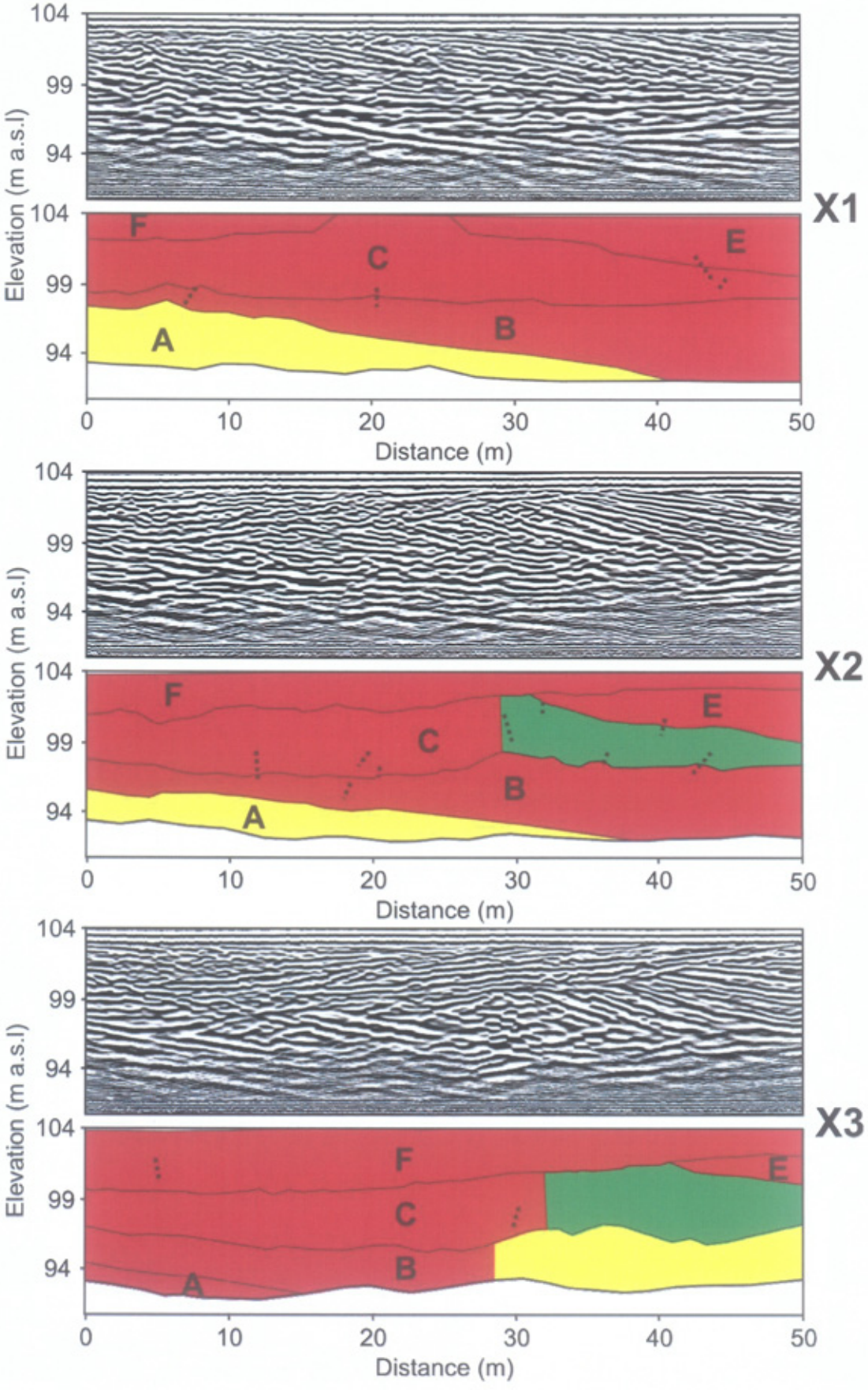
104
99
94
Elevation (m a.s.l)
X1
F
C
E
A
B
0
10
20
30
40
50
Distance (m)
X2
X3

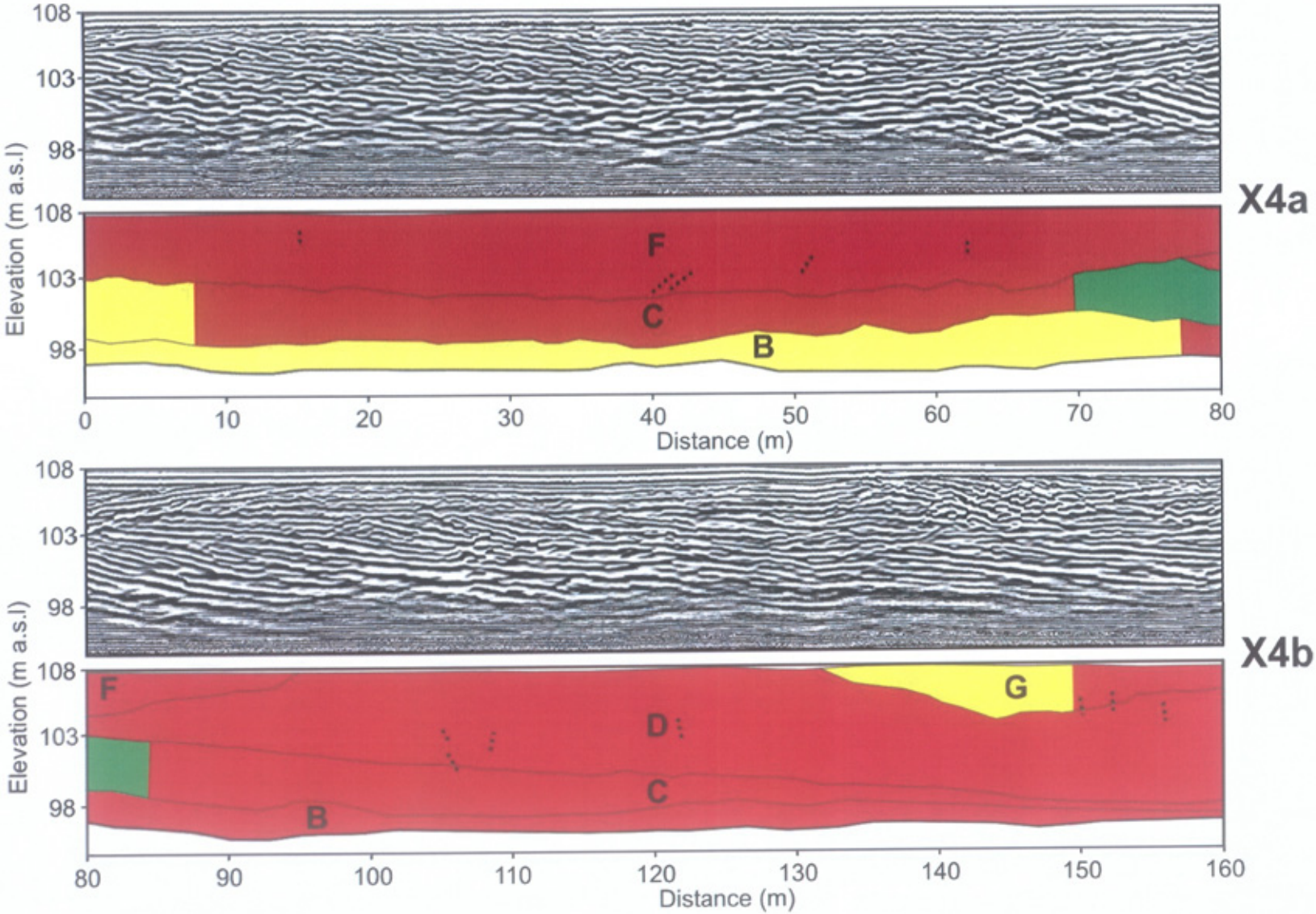
X4a
Elevation (m a.s.l)
108
103
98
F
C
B
0
10
20
30
40
50
60
70
80
Distance (m)
X4b
Elevation (m a.s.l)
108
103
98
F
G
D
C
B
80
90
100
110
120
130
140
150
160
Distance (m)

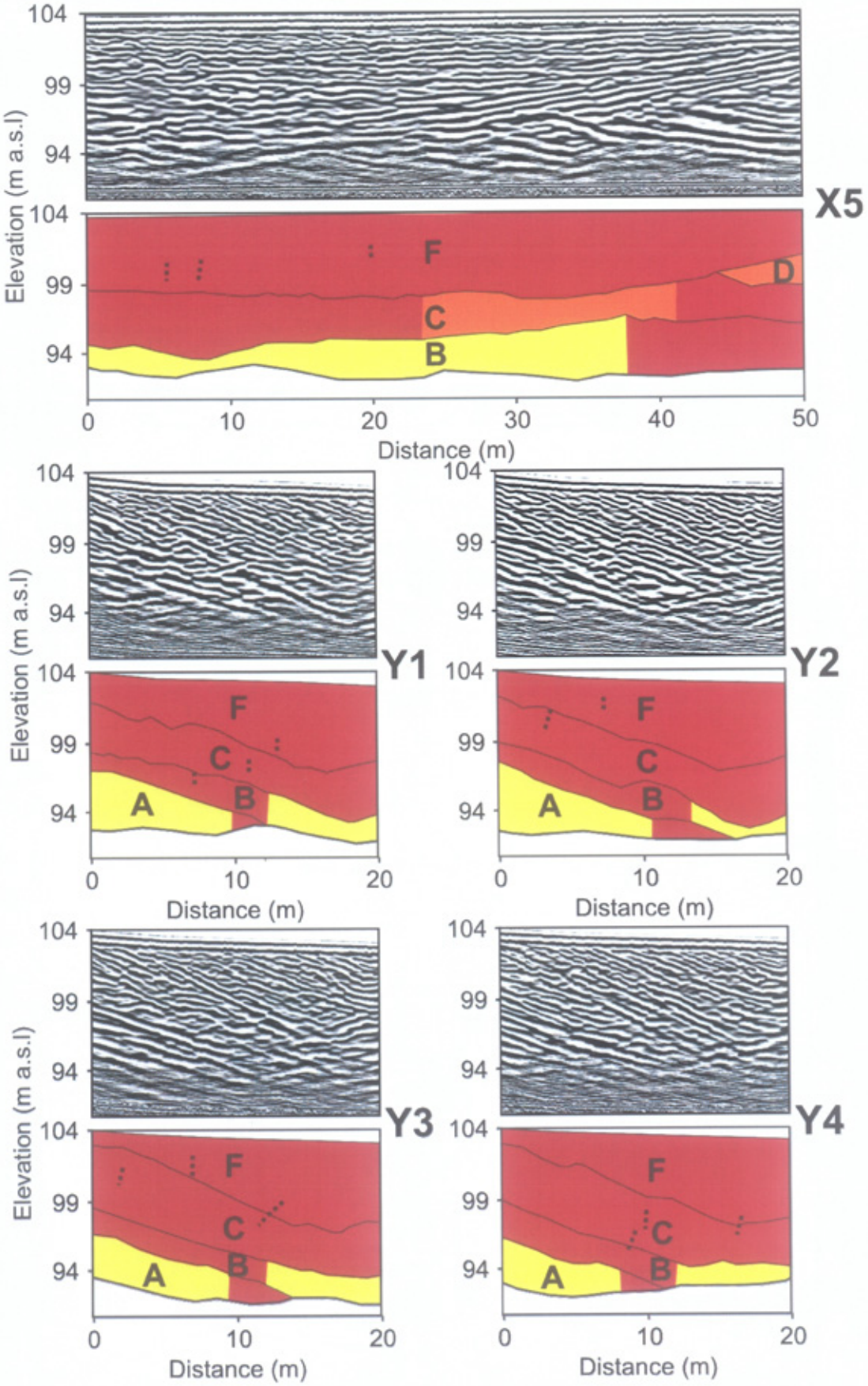
X5
Y1
Y2
Y3
Y4
Elevation (m a.s.l)
Distance (m)
104
99
94
0
10
20
30
40
50
A
B
C
D
F

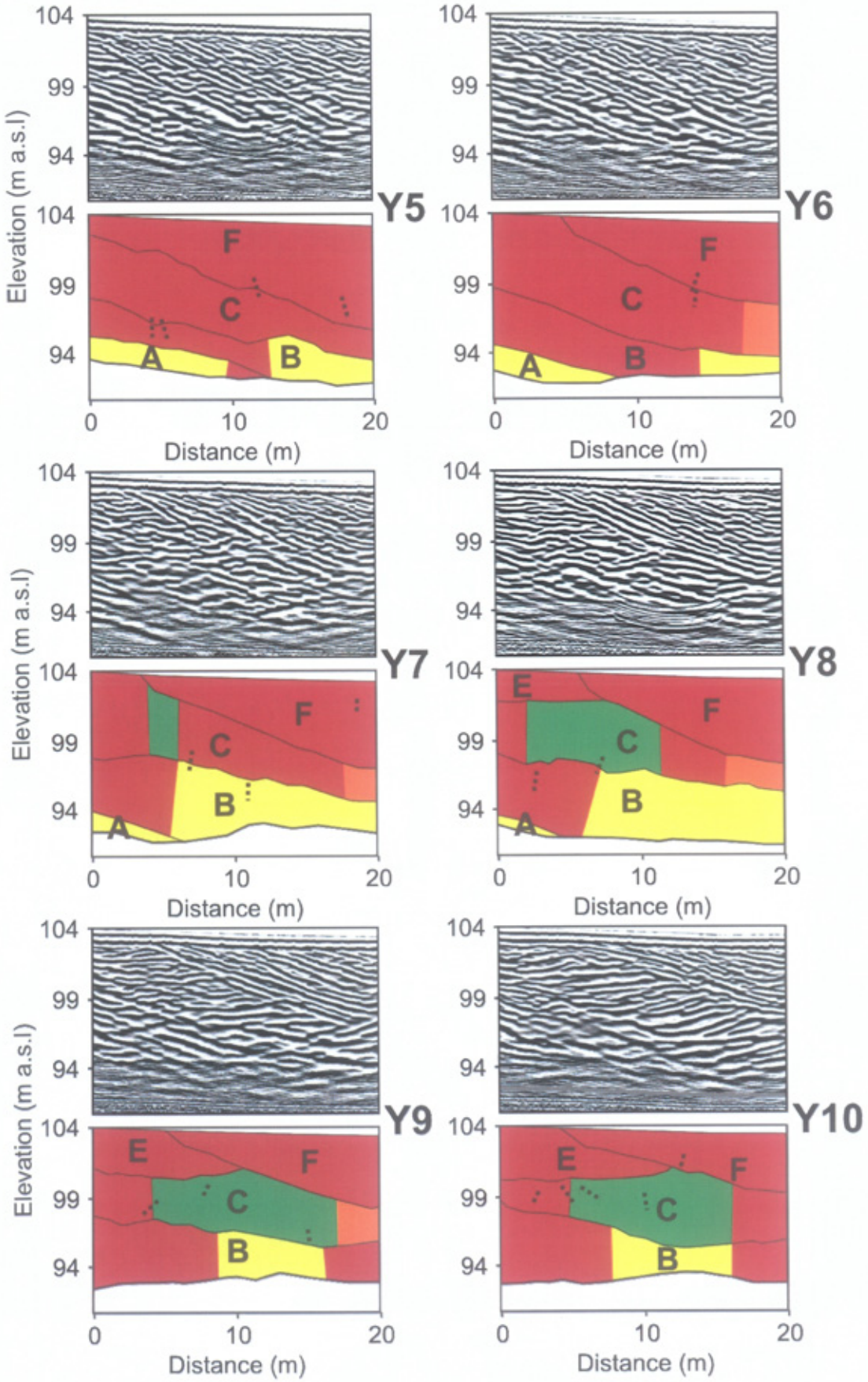
Y5
Y6
Y7
Y8
Y9
Y10
Elevation (m a.s.l)
Distance (m)
104
99
94
0
10
20
A
B
C
E
F

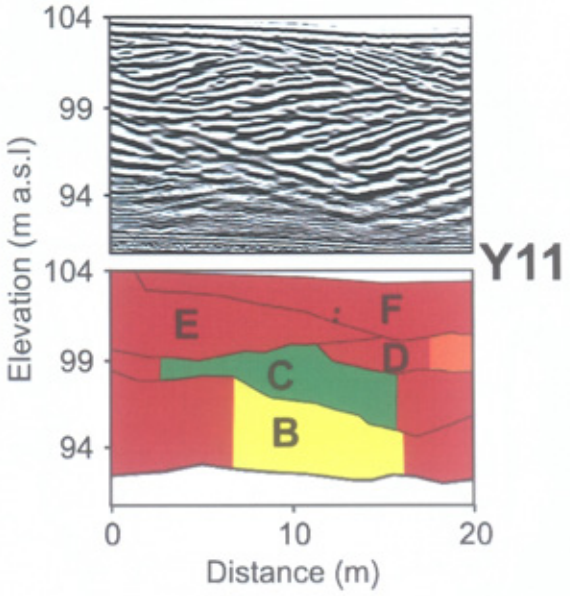
104
99
94
Y11
104
99
94
Elevation (m a.s.l)
E
F
D
C
B
0
10
20
Distance (m)

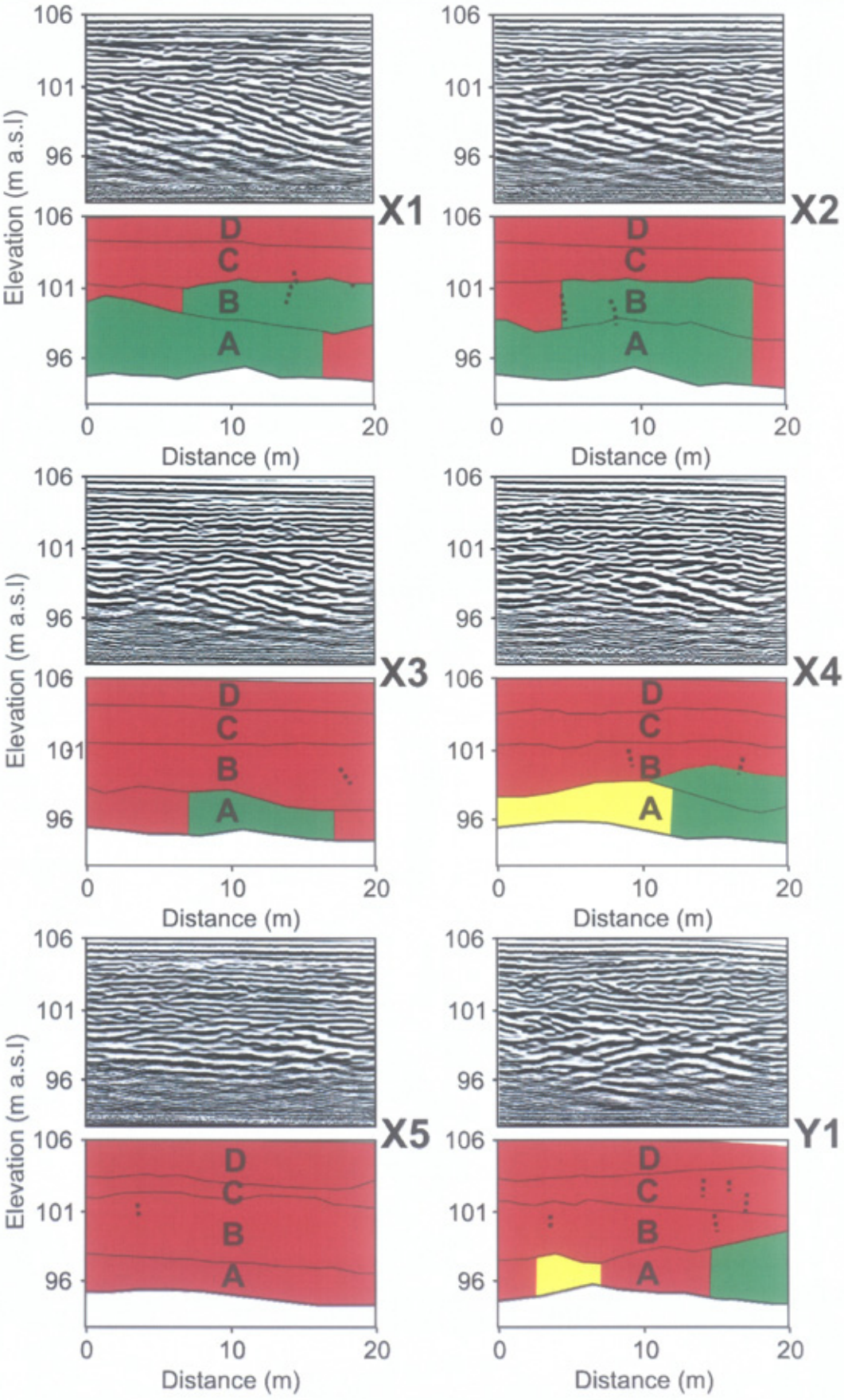
X1
X2
X3
X4
X5
Y1
Elevation (m a.s.l)
Distance (m)
106
101
96
0
10
20
A
B
C
D

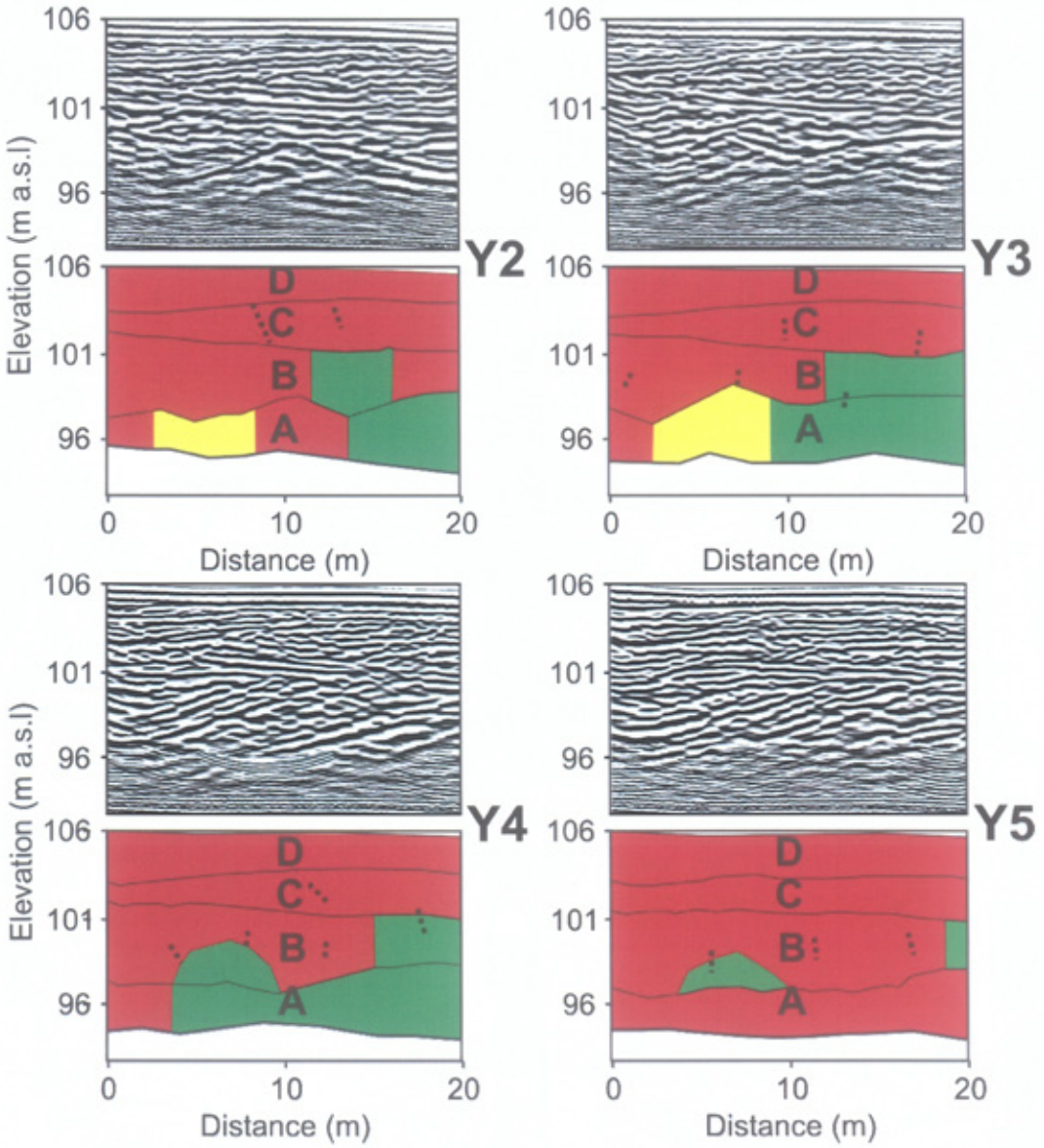
Y2
Y3
Y4
Y5
Elevation (m a.s.l)
106
101
96
D
C
B
A
0
10
20
Distance (m)

# Appendix 4

**GPR lines collected on the esker and ice-walled canyon fill at Bering Glacier. The GPR lines, processed following the sequence presented in Figure 4.16, are positioned above the line interpretations. Colour coding corresponds to the radar facies scheme presented in Figure 7.1.**

**GRID 1**

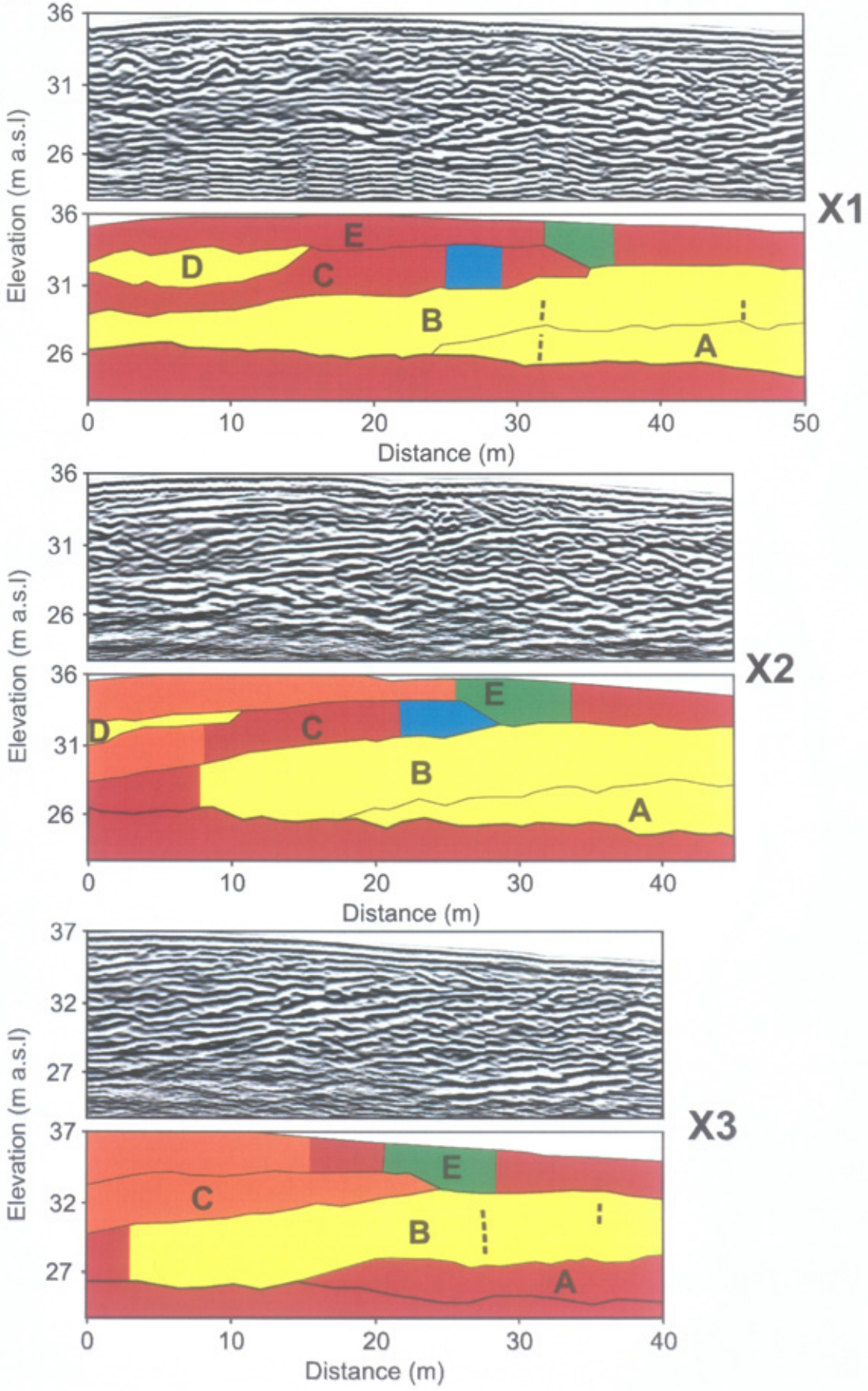
X1
Elevation (m a.s.l)
36
31
26
E
D
C
B
A
0
10
20
30
40
50
Distance (m)
X2
Elevation (m a.s.l)
36
31
26
E
D
C
B
A
0
10
20
30
40
Distance (m)
X3
Elevation (m a.s.l)
37
32
27
E
C
B
A
0
10
20
30
40
Distance (m)

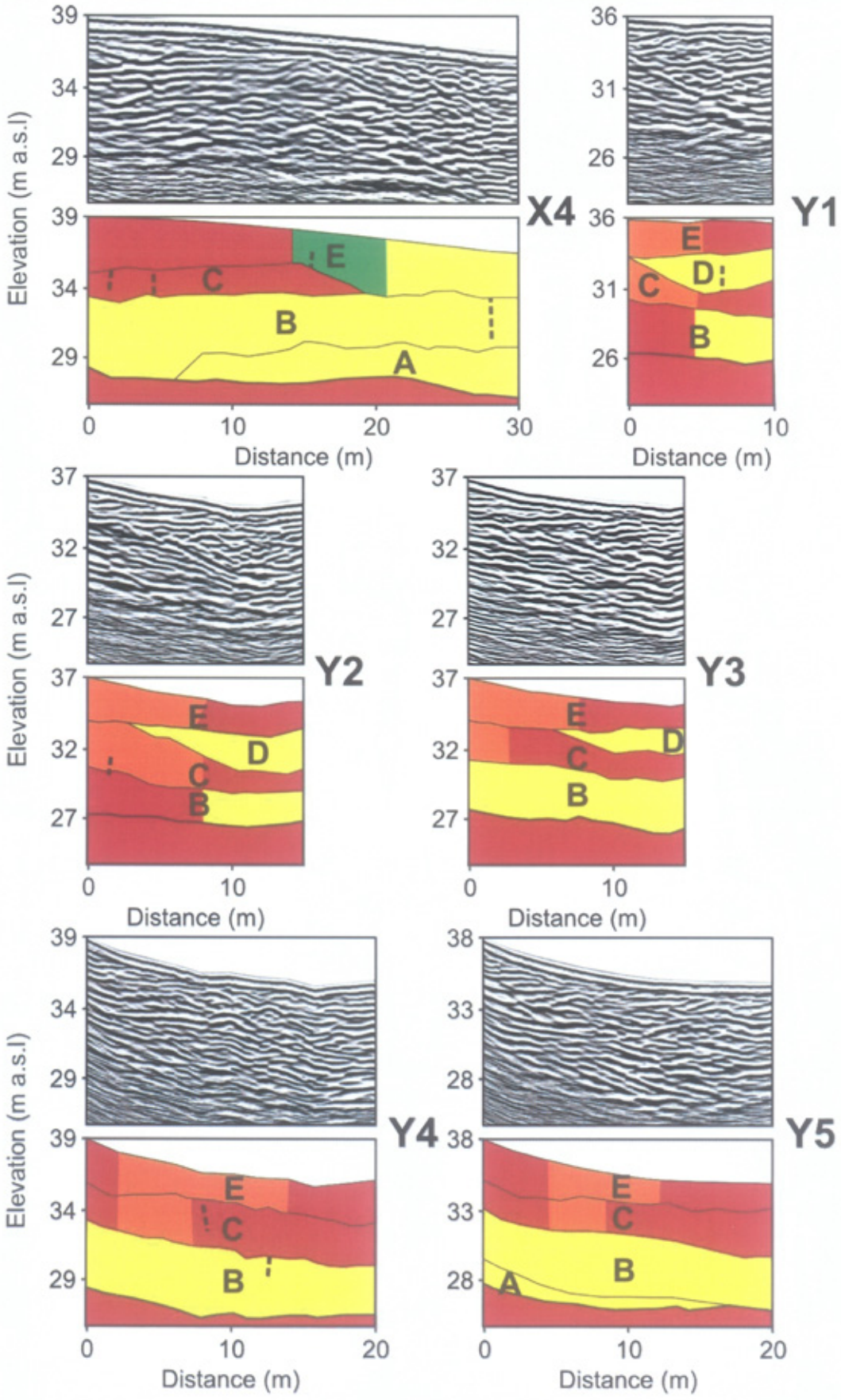
X4
Y1
Y2
Y3
Y4
Y5
Elevation (m a.s.l)
Distance (m)
A
B
C
D
E

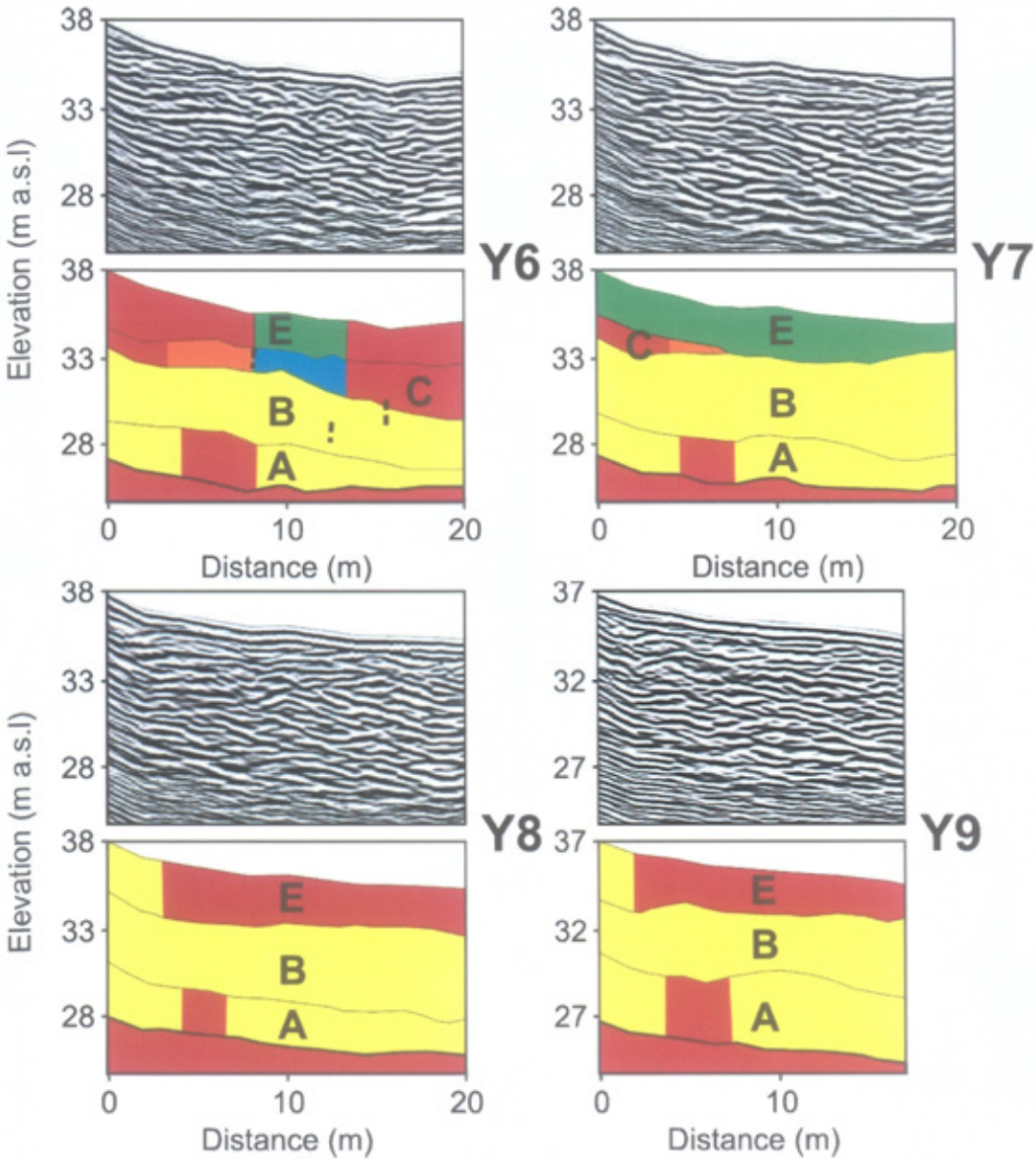
Elevation (m a.s.l)
38
33
28
Y6
E
C
B
A
0
10
20
Distance (m)
Y7
C
E
B
A
Y8
Y9
37
32
27

**GRID 2**

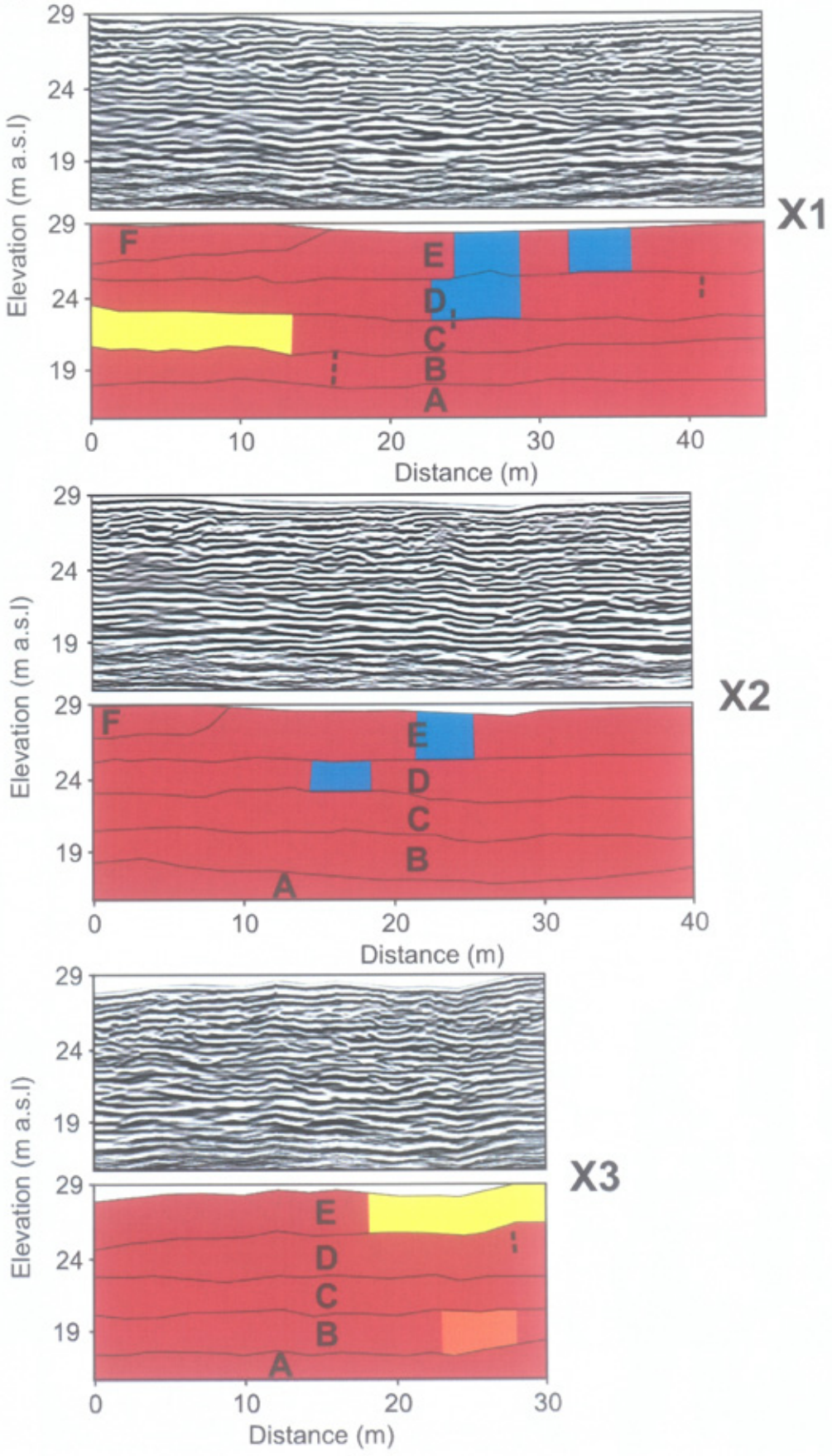

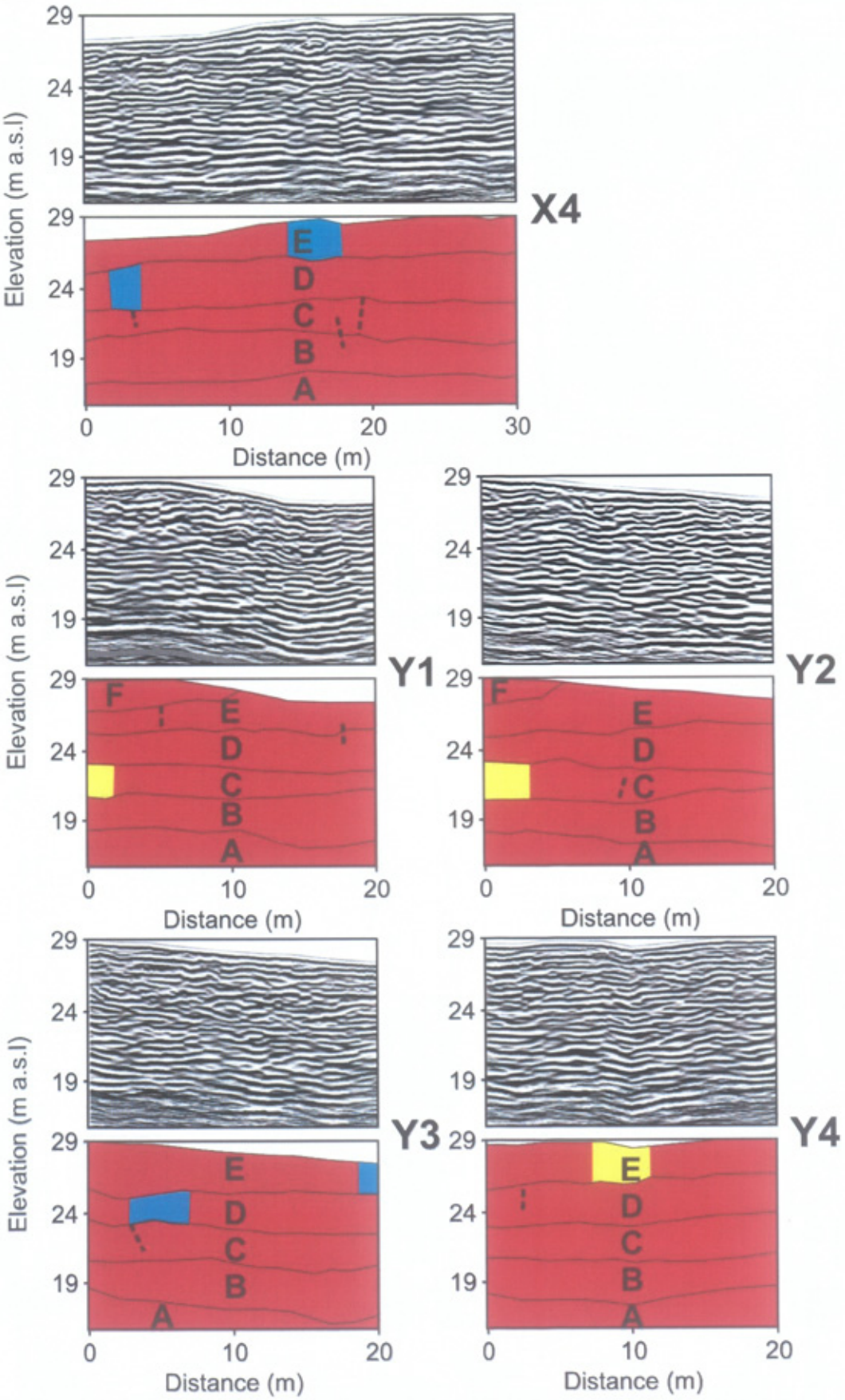
X4
Y1
Y2
Y3
Y4
Elevation (m a.s.l)
Distance (m)
29
24
19
0
10
20
30
A
B
C
D
E
F

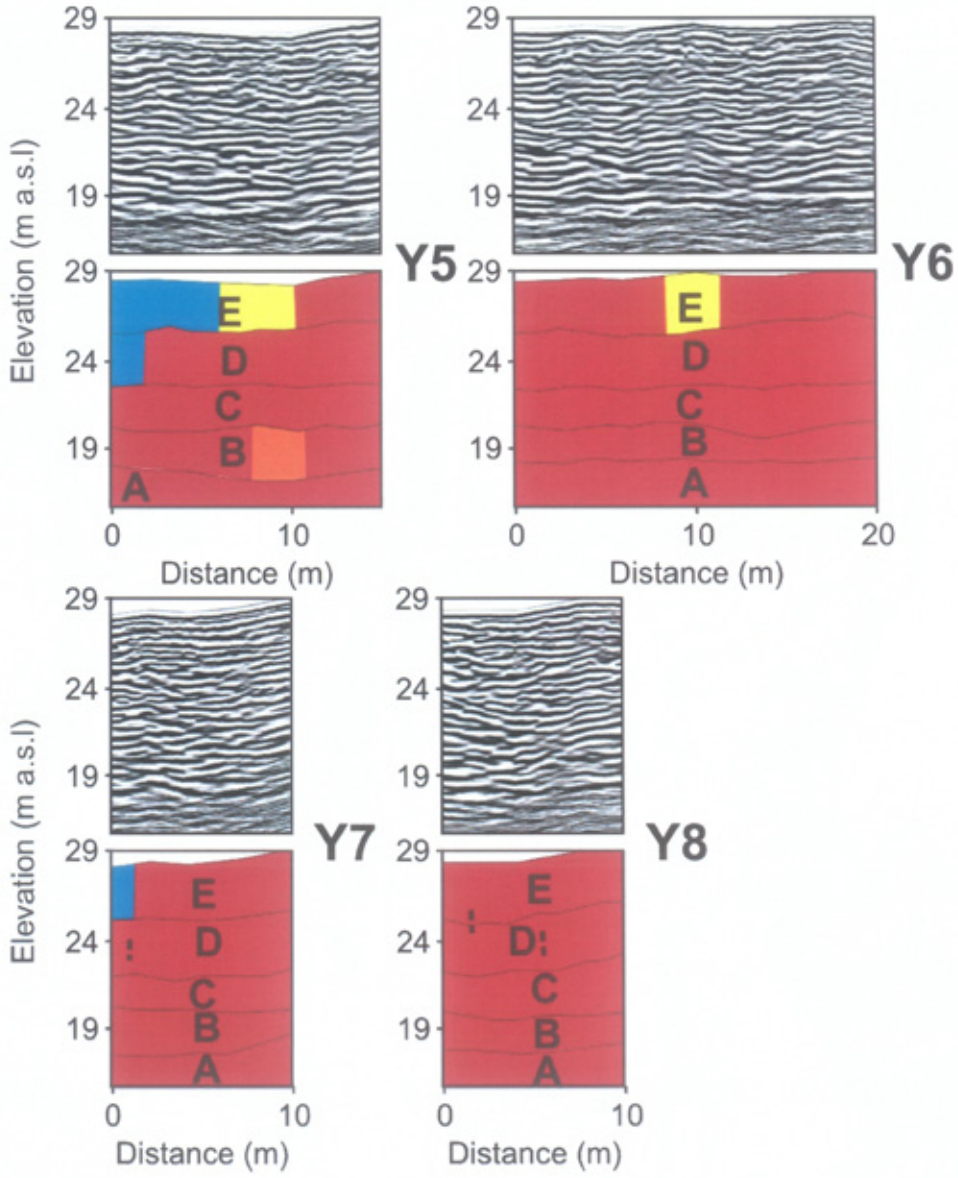
Elevation (m a.s.l)
29
24
19
Y5
E
D
C
B
A
0
10
Distance (m)
Y6
20
Y7
Y8

**GRID 3**

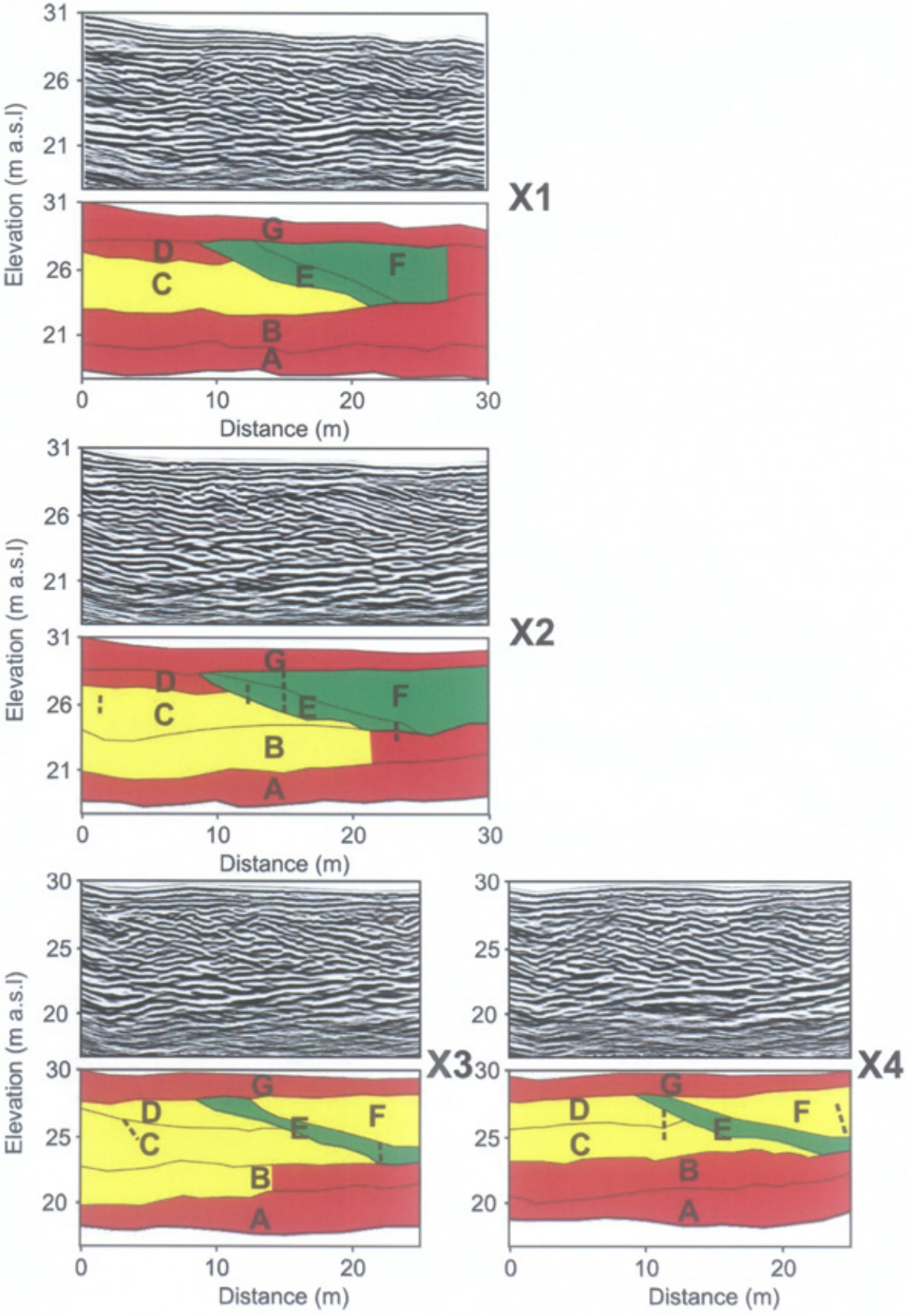

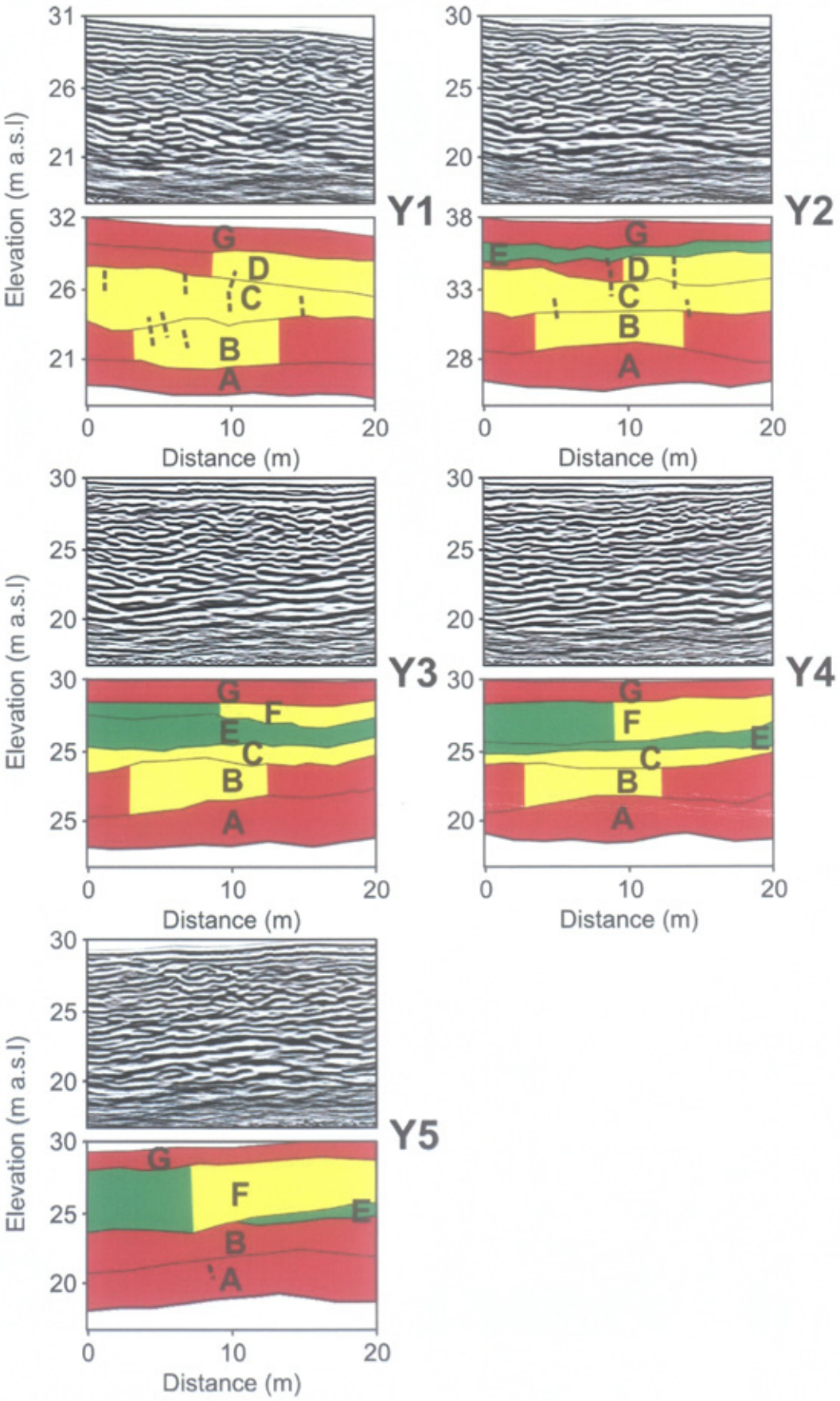
Y1
Y2
Y3
Y4
Y5
Elevation (m a.s.l)
Distance (m)
A
B
C
D
E
F
G